Studies of the Thermal Rearrangements of

dispiro-1,2,4-Trioxanes

Benjamin J. Taylor

Submitted for the degree of Doctor of Philosophy

Heriot-Watt University

School of Engineering and Physical Sciences

July 2009

ABSTRACT

A series of α-alkoxy-3,6-*dispiro*-1,2,4-trioxanes have been synthesised by acid-catalysed perhydrolyses of α-alkoxy methylenecyclohexane oxides (provides ring **A**) to give selectively the corresponding 1-hydroperoxy-1-(hydroxymethyl)cyclohexanes followed by acid-catalysed condensation with an appropriate cycloalkanone (provides ring **C**). Analogous perhydrolyses catalysed by $MoO_2(acac)_2$ afforded mixtures of regioisomeric β-hydroxy hydroperoxides, albeit in overall increased yields. The resulting 1-(hydroperoxymethyl)-1-hydroxycyclohexanes allowed entry to the isomeric 3,5-*dispiro*-1,2,4-trioxanes. X-ray crystallographic analysis of the isomeric *dispiro*-1,2,4-trioxanes revealed that (a) they originate from different diastereoisomers of the epoxide substrates, and (b) the 1,2,4-trioxane rings of the 3,5-isomers adopt distorted half-chair rather than chair conformations as a consequence of intramolecular 1,3-diaxial steric interactions. Modelling studies of the perhydrolysis process are in broad agreement with the regioselectivity of the acid-catalysed reactions, but suggest that the α-alkoxy-substituted epoxides can act as bidentate ligands which can adopt different binding modes to the Mo catalyst and hence provide alternative reaction pathways.

Thermolysis of dilute solutions of the α-alkoxy-3,6-*dispiro*-1,2,4-trioxanes in decane afforded a variety of 13-, 14-, 15- and 20-membered fully ring-expanded keto lactones in high yield via stepwise, β-scission/radical recombination reactions in contrast to the partially ring-expanded oxalactones obtained previously from other 3,6-*dispiro*-1,2,4-trioxane derivatives.

An investigation of substituent effects on the thermal rearrangement mechanisms of 3,6-*dispiro*-1,2,4-trioxanes using DFT calculations indicated that, after the initial O-O bond homolysis to form the corresponding oxy biradical, ring **C** generally opens significantly faster than the unsubstituted ring **A** because of the greater delocalisation of radical character into ring **C**. In these cases, the lowest rearrangement energy barrier links directly to the partially ring-expanded oxalactone product as observed experimentally. Methyl or methoxy substituents at the α-position of ring **A** render its ring opening by β-scission increasingly more competitive to that of ring **C** due to increased delocalisation of radical character onto the α-substituent, consistent with the 'α-effect'. Methoxy-substituents are also noted to engage in close range interactions with the 1,2,4-trioxane ring. Since the energy barrier for ring **A** opening falls below that of ring **C** in the methoxy model, formation of the fully ring-expanded keto lactone becomes favoured.

ACKNOWLEDGEMENTS

Name*:*	BENJAMIN JOHN TAYLOR		
School/PGI:	EPS/ CHEMISTRY		
Version: *(i.e. First, Resubmission, Final)*	FINAL	Degree Sought (Award **and** Subject area)	PhD

Declaration

In accordance with the appropriate regulations I hereby submit my thesis and I declare that:

1) the thesis embodies the results of my own work and has been composed by myself
2) where appropriate, I have made acknowledgement of the work of others and have made reference to work carried out in collaboration with other persons
3) the thesis is the correct version of the thesis for submission and is the same version as any electronic versions submitted*.
4) my thesis for the award referred to, deposited in the Heriot-Watt University Library, should be made available for loan or photocopying and be available via the Institutional Repository, subject to such conditions as the Librarian may require
5) I understand that as a student of the University I am required to abide by the Regulations of the University and to conform to its discipline.

* *Please note that it is the responsibility of the candidate to ensure that the correct version of the thesis is submitted.*

Signature of Candidate*:*		Date:	

Submission

Submitted By *(name in capitals):*	
Signature of Individual Submitting:	
Date Submitted:	

For Completion in Academic Registry

Received in the Academic Registry by *(name in capitals):*			
Method of Submission (Handed in to Academic Registry; posted through internal/external mail):			
*E-thesis Submitted (**mandatory for final theses from January 2009**)*			
Signature:		Date:	

iv

CONTENTS

Chapter One

Synthesis of *Dispiro*-1,2,4-Trioxanes

Chapter Two

Thermolysis of *Dispiro*-1,2,4-Trioxanes

Chapter Three

DFT studies for the thermal rearrangement of *dispiro*-1,2,4-trioxanes

ix

Publication

Model Studies of the β-scission Ring-Opening Reactions of Cyclohexyloxy Radicals: Applacation to Thermal Rearrangement of Dispiro-1,2,4-Trioxanes, S. Erhardt, S. A. Macgregor, K. J. McCullough, K. Savill, and B. J. Taylor, *Org Lett.*, 2007, **9**, 5569-5572

Chapter One

Synthesis of *Dispiro*-1,2,4-trioxanes

Cyclic peroxides have been found as substructural units in many naturally occurring compounds isolated from a variety of marine sponges and plants.[1,2] Various examples include the 1,2,4-trioxane in artemisinin (**1**),[3] the 1,2-dioxane in yingzhaosu A (**2**)[4] and yingzhaosu C (**3**),[5] and the 1,2-dioxolane in **4**.[6] These peroxide-containing compounds have been shown to possess a range of pharmacological properties,[7] in particular antimalarial activity, with the peroxide bond being the key pharmacophore.[3]

1 Artemisinin   **2 Yingzhaosu A**

$R= C_{11}H_{23}, C_{12}H_{25}, C_{13}H_{27}, C_{14}H_{29}, C_{15}H_{31}$

3 Yingzhaosu C   **4**
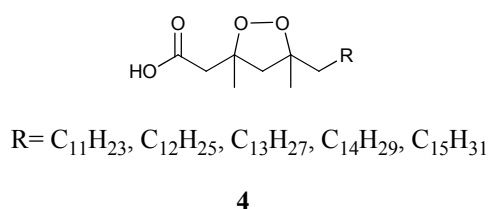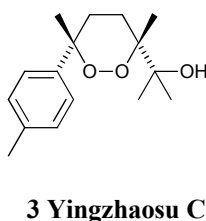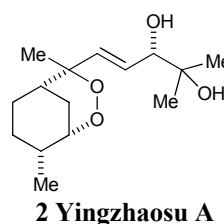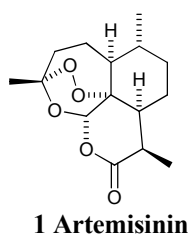
Over the last thirty years, 1,2,4-trioxane synthesis has come to particular prominence because of the antimalarial properties of naturally occurring artemisinin (**1**) (IC$_{50}$= 9.7 nM). Artemisinin was identified as the active component of *qinghaosu* which has been used for centuries in China as a herbal medicine for the treatment of malaria. Although artemisinin (**1**) was originally characterised as an ozonide, the presence of the 1,2,4-trioxane ring was determined unambiguously by X-ray crystallography. The presence of the 1,2,4-trioxane ring in a natural product was considered unusual at the time.[3]

The treatment of malaria strain *P. falciparum* is becoming increasingly difficult due to its widespread resistance to the traditional cheap and readily available quinine- and-chloroquinine-related therapies. This strain of malaria can be fatal and is estimated to affect up to 200 million people,[8] Artemisinin (**1**) exhibits potent pharmalogical activity against chloroquinine-resistant strains of malaria, and in particular *P. falciparum*. There have been no reports of any drug resistance to artemisinin-based compounds.[9]

The 1,2,4-trioxane ring contains a relatively weak peroxide bond, which on cleavage, can form highly reactive oxy radicals. This characteristic is the basis of the useful properties of the 1,2,4-trioxanes. Catalytic hydrogenation of artemisinin (**1**) affords the acetal **5** which is completely inactive against the malaria parasite,[10] confirming that the 1,2,4-trioxane moiety and particularly the endoperoxide bridge is the active pharmacophore. Although artemisinin (**1**) has been used successfully in the treatment of malaria due to its high potency, low toxicity and rapid action against malaria, poor bioavailability has led to the development of several semi-synthetic analogues. Thus, artemether (**6**), arteether (**7**) and artesunic acid (**8**), which have the basic artemisinin structure, have been shown to hold greater potency and bioavailability and are now also used routinely in the clinical treatment of malaria.[11] Further derivatives including modifications at the C10 position have shown better solubility and stability.[12] Although none of these new derivatives are in commercial production, artemisone (**9**) shows particular promise.[13] The artemisinin-based family of compounds however do suffer from limited availability because of erratic supply and high cost. A recently announced collaboration between OneWorld Health, Amyris Biotechnologies, and Sanofi-Aventis aims to introduce a low-cost, semisynthetic artemisinin into the supply chain.[14]

5   **6 R=Me, Artemether**   **8 Artesunic acid**   **9 Artemisone**
                   7 R=Et, Arteether
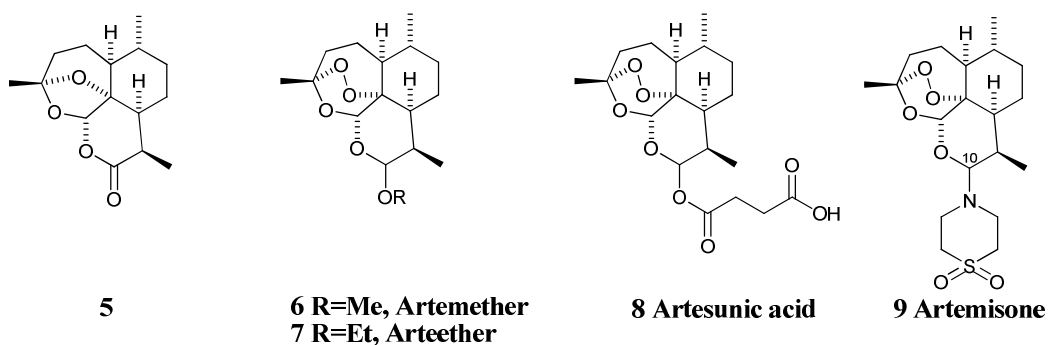
The search for a new potent anti-malarial based on artemisinin continues. This has led to the synthesis of artemisinin dimers. The artemisinin dimer **10**, connected through an ether linkage was noted to have similar potency to arteether.[15] Further studies suggested that dimer **11** is likely to be a reduction metabolite of arteether itself.[16] The synthesis[17] and biological activity[18,19] of artemisinin dimers based on **12** (IC$_{50}$= 0.59-0.91 nM) demonstrate a *ca.* 10-fold increase in antimalarial potency *in vitro* compared to artemisinin, suggesting a benefit in having two trioxane rings in the same molecule. Although, the biological activity of artemisinin-based dimers depends on the nature of

the linker between the artemisinin type moieties, in general they show increased potency.[20,21] Additionally, some artemisinin dimers show high *in vivo* anticancer activity.[22]

10   **11**

12a, X=⟨structure with OH⟩ **12b**, X=⟨structure with OH⟩ **12c**, X=⟨structure with O⟩
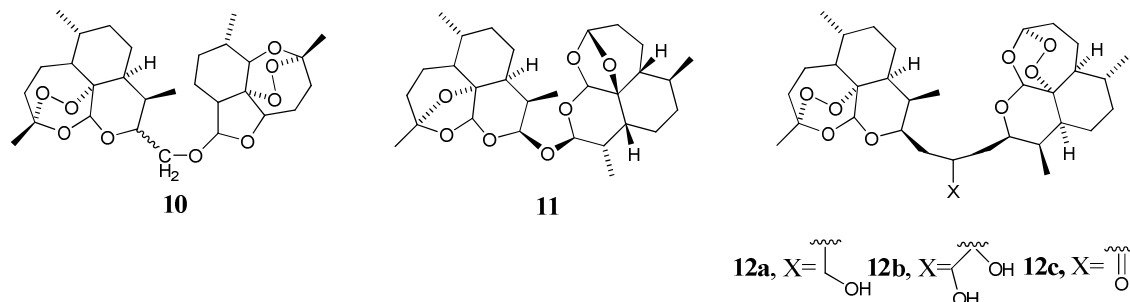
Trioxaquines **13**, which are hybrid molecules made up of a 1,2,4-trioxane bonded through a linker to a quinoline, have been identified as potential antimalarial drug targets. [23] This gives the drug two pharmacophores which are able to interact with the heme target. Although the individual pharmacophores have limited biological effect in isolation, trioxaquines are found to be highly active against drug-resistant *P. falciparum* strains of malaria[24] and are able to alkylate heme as efficiently as artemisinin and its derivatives.[25,26]

13

Quinoline ⟨~~~Linker~~~⟩ Trioxane
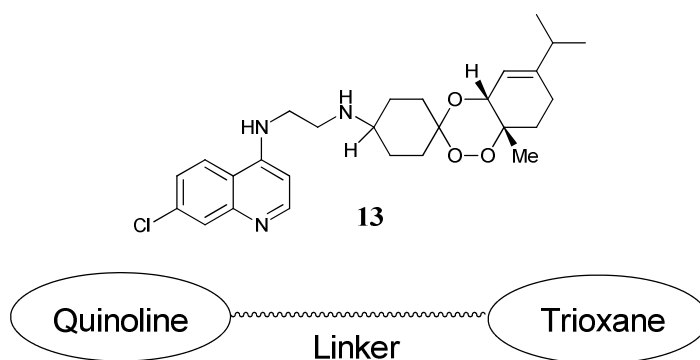
Promising biological activity has been found for 1,2,4-trioxolanes **14**,[27] 1,2,4-trioxepanes **15**,[28] 1,2,4,5-tetroxanes **16**[29] and 1,2,4,5-tetraoxanes **17**[30]. Although no synthetic peroxide antimalarial drugs have yet been identified from these classes of compounds, the ozonide OZ277 (**14**) is currently in phase II clinical trials.[31] These compounds have the advantage of being cheaper to make due to their easily accessible starting materials and short synthetic routes.

14   **15**   **16**   **17**
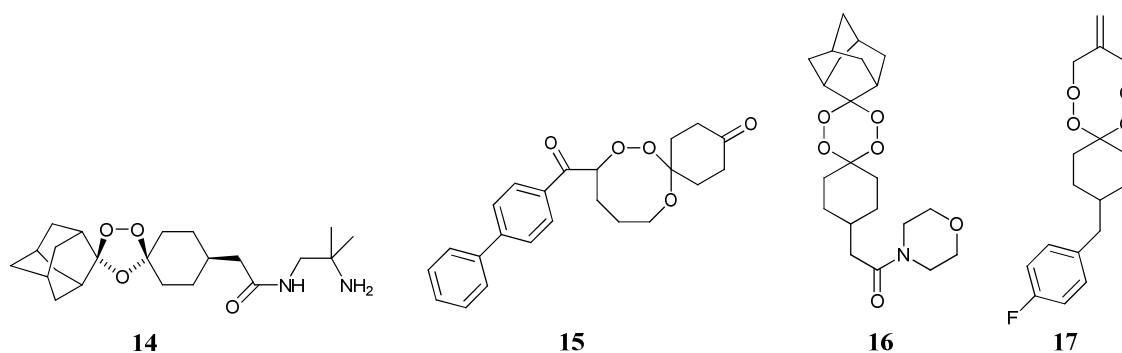
Additionally, 1,2,4-trioxanes are found to be useful in the treatment of schistosomiasis which is a parasitic disease caused by several species of fluke of the genus *Schistosoma.* Schistosomiasis is the second-most socioeconomically devastating disease after malaria. Schistosomes ingest hemoglobin and aggregate the release of heme as a dark pigment similar to the hemozoin produced by *P. falciparum* in the malaria infection. Praziquantel (**18**), synthesised as a racemate with only one of the enantiomers biologically active, is the current drug of choice for the treatment of schistosomiasis and has been used successfully for many years. However, recently signs of resistance to praziquantel have been reported.[32] Although artemisinin (**1**) has low but real effects on schistosomicide activity, a new class of hybrid molecules called trioxaquantels **19,** made up of a praziquantel (**18**) linked to a 1,2,4-trioxane, have been developed.[33]

18 Praziquantel   **19 Trioxaquantel**
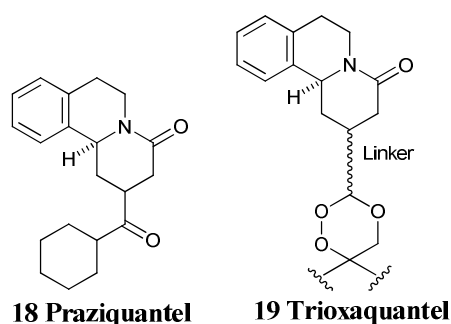
There have been further reports into another natural product containing a 1,2,4-trioxane ring. Two previously reported 1,2,4-trioxanes **20** and **20a**[34] and one new 1,2,4-trioxane **21** have been isolated from the roots of *J. integerrima*. Although the medicinal properties of **20, 20a** and **21** are as yet unexplored, it is known that the leaves of the *J. integerrima* are very toxic.[35]

5

20, R= H, R¹= CH₃   **20a**

21, R= CH₃, R¹= CH₃
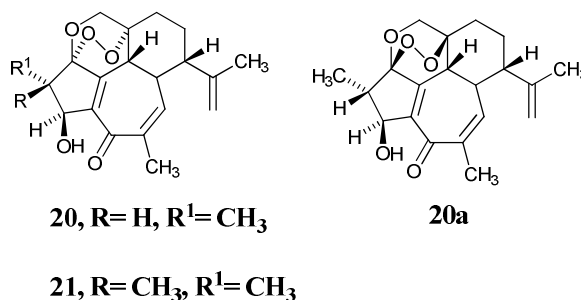
Artemisinin and related peroxides: Mechanism of therapeutic effects

There have been a number of reviews discussing how artemisinin provides its anti-malarial effect.[36,37,38,39] The mechanism of action was first proposed to involve a heme-mediated oxidative stress leading to the destruction of the parasite.[40] Heme was found to catalyse the reductive decomposition of artemisinin and dihydroartemisinin *in vitro*. Since these conclusions were based on tests involving dose concentrations far higher than pharmacological drug concentrations, it was concluded that parasite death was not due to heme-mediated oxidative stress.[41]

Artemisinin was found to react with hemin in aqueous solutions to form an adduct with a high molecular weight and identical physical and chemical properties as the parasite-derived product. It was suggested that the formation of the adduct was by alkylation of hemin by organic free radicals. The hemin-rich internal environment of the malaria parasite therefore may account for the selectivity of the drugs toxicity.[42] This notion was further supported when artemisinin was shown to be >50 times less effective than chloroquine-resistant *P.berghei* strain which lacks hemozoin.[43]

In 1992, it was shown that ferrous iron triggers the cleavage of the peroxide bond in artemisinin and the oxygen radicals rearrange to form carbon-centred radicals.[44] This was concluded after subjecting an ^{18}O-labelled trioxane **22** to the effects of ferrous and non-ferrous reducing agents *(Scheme 1)*.
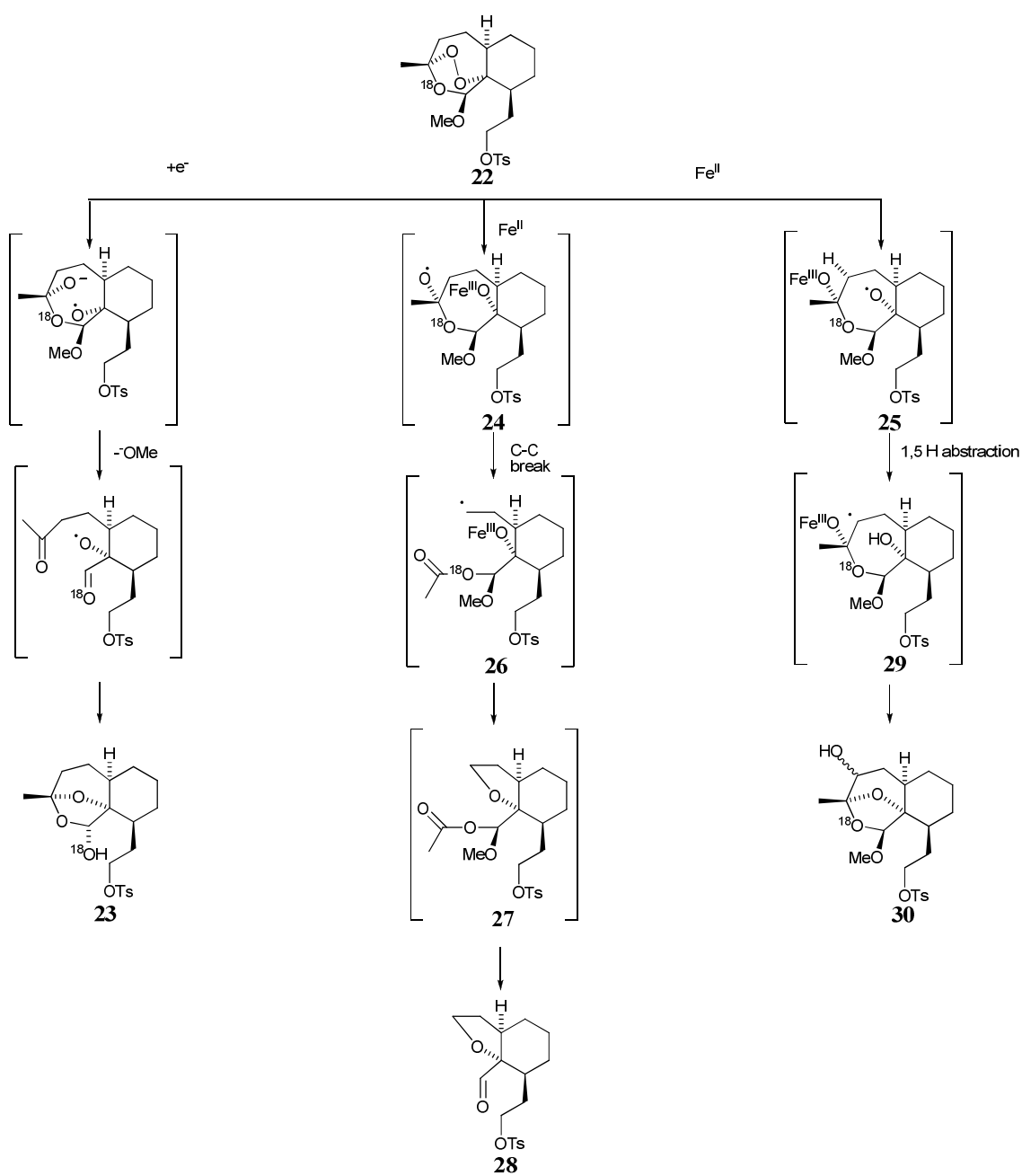
Scheme 1

The products isolated from the two experiments were different indicating that the ferrous iron cleavage follows a different mechanistic course to that of non-ferrous cleavage. The reductive cleavage of trioxane **22** using either samarium diiodide, or zinc metal, or trityllithium produce dioxolane **23** involving the release of methoxide ion. ^{13}C NMR spectroscopic analysis confirmed the ^{18}O-labelled oxygen was located entirely in the exocyclic hemiacetal position of dioxolane **23**. The reductive cleavage of trioxane **22**, in the presence of ferrous salts or heme, produces dioxolane products **28** and **30**. Iron(II)-induced cleavage of the peroxide bond in **22** produces two distinct oxy-radical intermediates **24** and **25.** Each intermediate can then proceed via two separate reaction mechanisms. Oxy-radical **24** undergoes β-scission producing primary carbon-centred intermediate **26** before ring contraction to form the furan ring in **27** with the ^{18}O located in the acetoxy group (confirmed by mass spectrometry). A subsequent loss of the acetoxy group then forms the non-^{18}O labelled **28**. Oxy-radical **25** performs an intramolecular 1,5-hydrogen abstraction to produce the more stable C4-carbon radical **29** and then ultimately forming dioxolane **30** as a mixture of two diastereoisomers with the ^{18}O-labelled atom not being observed on the methoxy group (confirmed by mass spectrometry).

Following this, the antimalarial activity of arteether (**6**) was shown to be antagonised by two iron chelators, pyridoxal benzoylhydrazone and 1,2-dimethyl-3-hydroxypyrid-4-one, demonstrating that iron plays a role in the mechanisms of action and toxicity of artemisinin.[45] Further to this the hemozoin isolated from [^{14}C] artemisinin-treated parasites demonstrated hemozoin-associated radioactivity in HPLC and TLC experiments indicating that artemisinin was covalently bonded to heme in malarial hemozoin.[46]

In a study designed to evaluate the importance of the carbon-centred radicals, the potency of different 4-methylated analogues of the artemisinin skeleton was tested against both chloroquinine-susceptible and chloroquinin-resistant strains of *P. falciparium* malaria parasites.[47] The results demonstrated a direct relationship between the ease of the intermediate oxy radicals performing an intermolecular-1,5-hydrogen abstraction and the anti-malarial activity of the compound *(Table 1)*.

31a, R^1= H, R^2= Me

31b, R^1= Me, R^2= H

31c, R^1= Me, R^2= Me
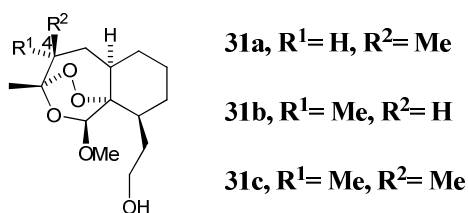
Compound	IC50 (ng/mL)	
	W-2 iodochina clone	D-6 African clone
31a	4.5	3.5
31b	>500	>500
31c	>500	>500
Artemisinin (1)	8	8

Table 1: Potency against P. falciparum malarial strain/ ng/mL

Compound **31a** is around 100 times more potent than either **31b** or **31c**. Of the three compounds, only **31a** has the ability to undergo intermolecular-1,5-hydrogen abstraction to produce the C-4 radical. This suggests the creation of a C-4 radical is linked to the antimalarial activity.

The Haynes group have also suggested that iron may act as a Lewis acid to facilitate an ionic rather than radical activation of antimalarial trioxanes.[48,49] In this proposal, heterolysis of one of the C-O bonds induced by Lewis acid iron salts produces oxygen-stabilised carbocation **32**. This then forms an unsaturated alkyl hydroperoxide **33** which can act as a source of cytotoxic, reactive oxygen species *(Scheme 2).* [50]
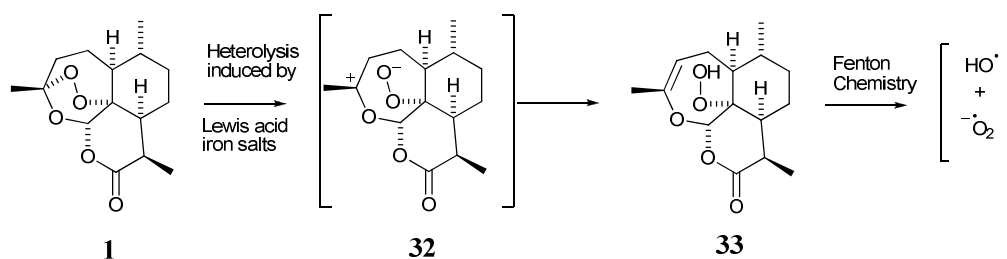
Scheme 2

It has been argued that although the concentration of 'free' iron in living cells is very low, free heme is produced as a waste product of the consumption of haemoglobin by

the parasite. This free heme induces the cleavage of the O-O bond in artemisinin to give oxy radicals which rearrange by β-scission giving a C4 radical capable of alkylating the *meso*-position of heme. Alternatively, the C4 radical could alkylate a nearby parasite causing its death. Meunier *et. al.* reported the first covalent adduct **34** between artemisinin and a heme model obtained using a synthetic manganese metalloporphyrin and involved the alkylation by artemisinin of the β-pyrrolic position on the macrocycle.[51]

34
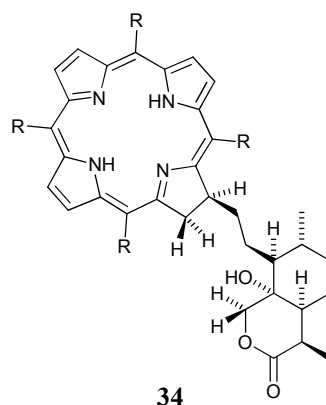
Evidence for the existence of the carbon-centred radicals during ferrous-mediated peroxide cleavage was provided by electron paramagnetic resonance (EPR) spin-trapping studies, in which the trapped primary and secondary carbon-centred radicals of artemisinin were identified.[52,53] The reaction of artemether (**6**) with catalytic amounts of ferrous iron in the presence of excess cysteine produced two adducts of cysteine **35** and **36**, derived from the primary and secondary radicals, in the aqueous phase in addition to the expected observable products *(Scheme 3)*.[54]
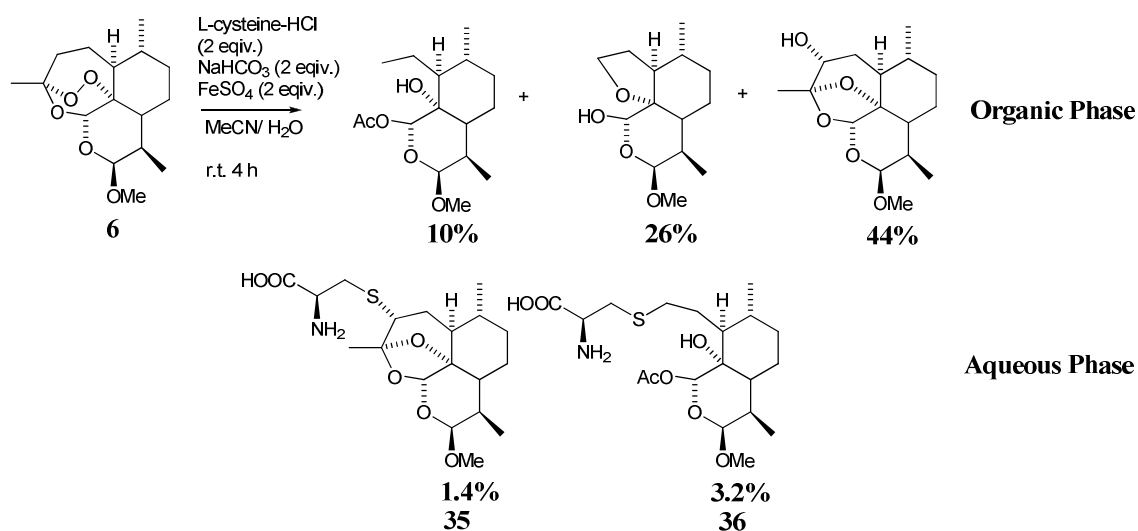
Scheme 3

In a further study, the isolation of hydroxyl epoxide **38** was achieved in low yield through the iron-induced cleavage of artemisinin *(Scheme 4)*.[51] It was first proposed by Posner *et. al.* that **38** could be the intermediate in the decomposition pathway between **37** and **39**.[55] The hydroxy epoxide **38** can be produced through two mechanistic routes: first by the direct intramolecular ring closure, and second by β-scission of Fe(IV)=O followed by rebound epoxidation from intermediate vinyl ether **40**. The highly electrophilic epoxide **38** is now a potent alkylating agent and potentially cytotoxic. Epoxide **38** would be expected to rearrange though an S_N1 mechanism making use of its free hydroxide to form the dioxolane intermediate **39**. However there is debate about the intermediacy and importance of high-valent iron-oxo species. Arguments from Meunier *et. al.* suggest that the formation of all characterised products can be explained by route **A**, *Scheme 4* alone.[56]
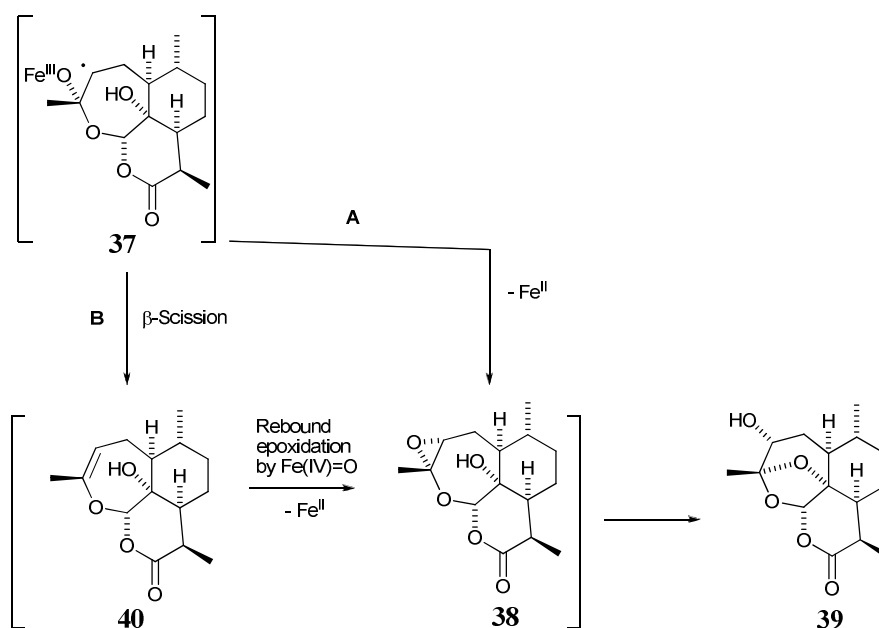
Scheme 4

The alkylation of heme by artemisinin was reported in 2001.[57] This involved the alkylation of heme at one of its four *meso*-positions by the carbon-centred radical derived from the β-scission of oxy radicals after the heme-mediated reductive activation of artemisinin *(Scheme 5)*. This behaviour was repeated using artemisinin derivatives and mimics of the active 1,2,4-trioxane ring.[58,59]
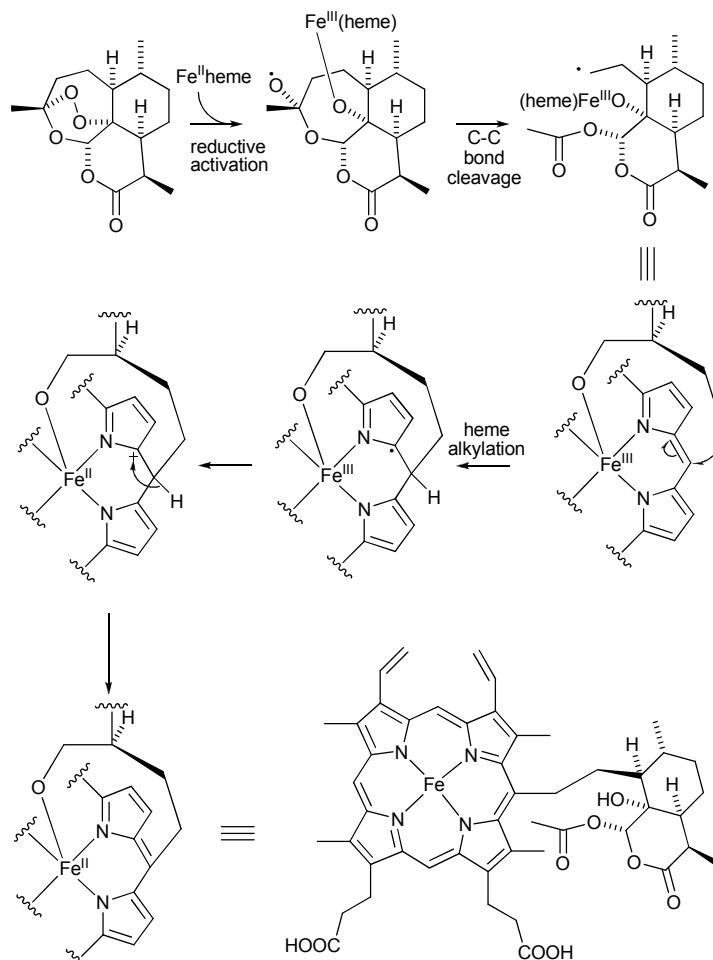
Scheme 5

Additionally, artemisinin and its analogues, but not chloroquine or quinine, were shown to inhibit the sarco/endoplasmic reticulum Ca^{2+}-ATPase (SERCA) orthologues (PfATP6) of *P. falciparum*. This provided evidence of the molecular target for artemisinins and suggested that artemisinin acted by inhibiting PfATP6 outside the food vacuole after activation by iron. Artemisinin shows inhibiting properties similar to thaigarin, a well known inhibitor of SERCA. Artemisinin was shown to inhibit SERCA with high specificity, leaving other Ca^{2+}-ATPases like PfATP4 unaffected. There is almost a perfect correlation between the antimalarial activity of 1,2,4-trioxanes and their ability to active PfATP6. Desoxyartemisinin was also shown not to inhibit PfATP6 even at high concentrations confirming that the endoperoxide bridge is essential for the inhibition. It was therefore hypothesised that artemisinins produce carbon-centred free radicals in the presence of catalytic quantities of Fe^{2+} with the selective targeting of PfATP6.[60]

It has also been noted that the accessibility of the peroxide bond has an effect on the antimalarial activity of the compound *(Scheme 6)*. If the peroxide bond is crowded by bulky alkyl groups, homolysis of the peroxide bond is inhibited and consequently antimalarial potency is low.[61] Therefore a close interaction between the metal centre and the endoperoxide bridge is necessary in order to facilitate the inner-sphere electron transfer and that the ability to alkylate heme is crucial for the antimalarial activity of 1,2,4-trioxane molecules.[41]
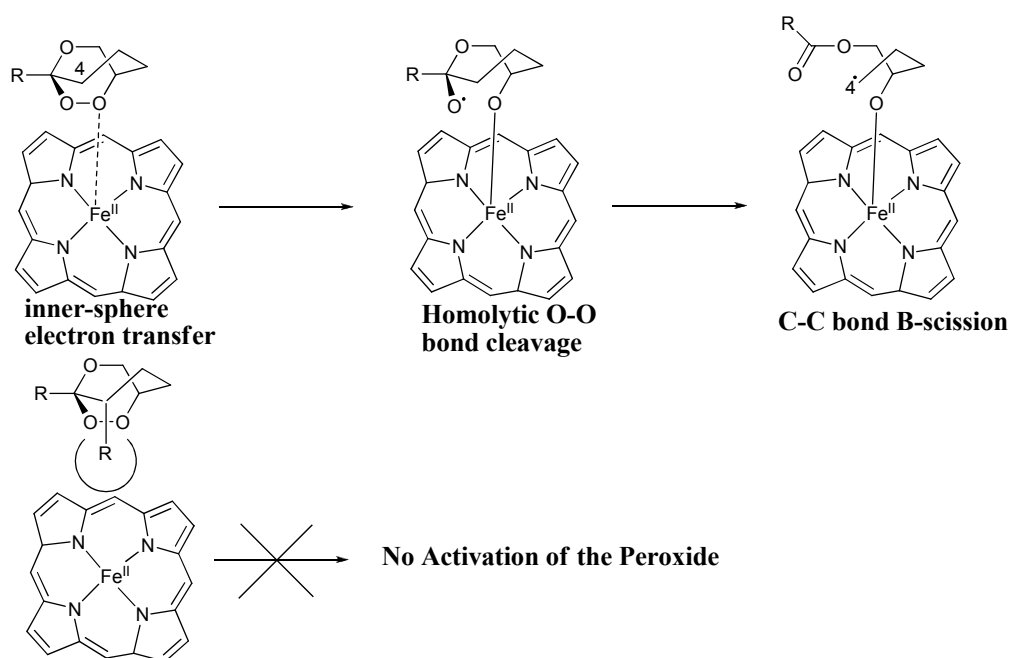
Scheme 6

A similar explanation was proposed for the low potency of some methyl-substituted 1,2,4,5-tetroxanes. Compounds **41** and **42** demonstrated very low potency (>1000nM) as antimalarials whilst the less-substituted model **40** (55 nM) had a similar potency to that of **43** (38 nM).[62] It was suggested that steric hinderence about the peroxide bonds of **41** and **42** substantually reduced their antimalarial activity. Similar patterns of activity have been observed for a series of 1,2,4,5,7,8-hexaoxonanes.[63]
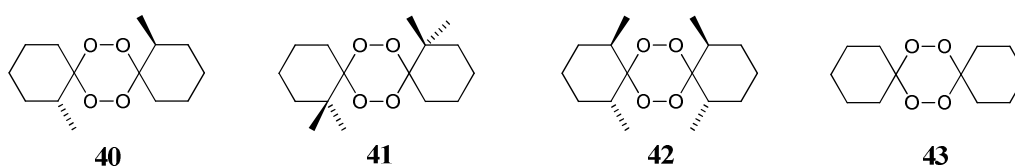
Within red blood cells, the malaria parasite consumes haemoglobin as a source of amino acids. This consumption releases free heme and ferriprotoporphyrin which are toxic to the malaria parasite. The heme remains toxic to the parasite until its conversion to hemozoin, which is harmless. It had previously been thought that the hemozoin was made up of polymeric chains of heme[64] however the X-ray analysis proved that it had crystalline properties.[65] Crystallization experiments confirmed that β-hemozoin crystal growth in the presence of chloroquine took longer and the shape seemed tapered at each end of the needle-like crystals. Thus, it was proposed that the prevention of the crystallisation of β-hemozoin is what kills the parasite and is the mode of action of antimalarial agents.[66]

In a study of potent antimalarial compounds, a marked antagonism was observed for all compounds in combination with the iron chelators desferrioxamine (DFO) (**44**) and deferipone (DFP) (**45**). A more marked antagonism was seen for artemesone (**9**) with DFP than with DFO and in a short experiment the sensitivity of the parasites to artemisone (**9**) and artesunate (**8**) was decreased significantly by 10-fold and five-fold respectively. This strongly suggests that none-heme, chelatable free-iron activation is essential for the activity of both compounds. A further experiment using labelled artemisinin with a fluorescent probe demonstrated the selective build-up of drug at the infected erythrocytes in the parasite cytoplasm with exclusion from the digestive vacuole. Significantly, the drug is completely washed out of the cell in the presence of DFO, whilst it remains irreversibly bound when the iron chelator is absent. Thus the labelled compounds were being accumulated by the parasite and then activated by the iron to form stable covalent adducts with the parasite.[67]
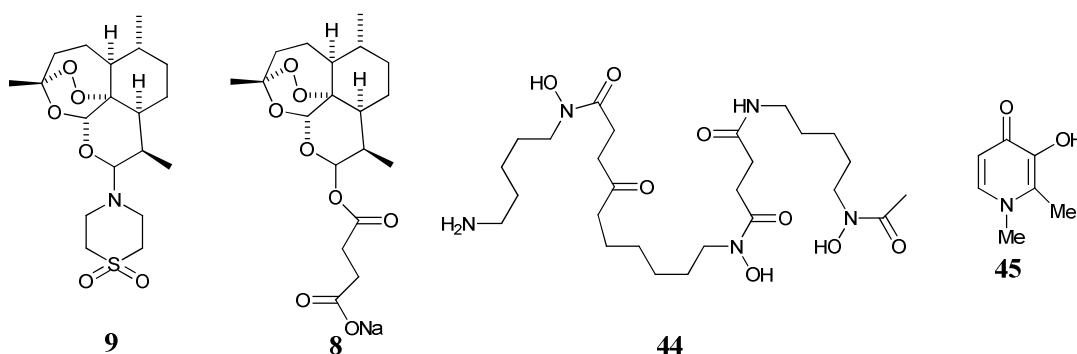
Synthetic routes to 1,2,4-trioxanes

Preparation of β-Hydroxy hydroperoxides via epoxide ring opening with anhydrous hydrogen peroxide

Although there has been a number of different approaches to the synthesis of 1,2,4-trioxanes, most synthetic routes proceed through the formation of a β-hydroxy hydroperoxide intermediate.[68,69] The first synthesis of a 1,2,4-trioxane derivative **49** was reported by Payne and Smith in 1957.[70] The addition of excess hydrogen peroxide and tungstic acid catalyst to cyclohexene (**46**) formed β-hydroxy hydroperoxide **48** *in situ*. Although no evidence was found, the production of the β-hydroxy hydroperoxide was thought to proceed though epoxide **47**. The addition of excess hydrogen peroxide and subsequent condensation with acetone yields the bicyclic 1,2,4-trioxane **49** which has been form via the key β-hydroxy hydroperoxide intermediate **48** *(Scheme 7)*.
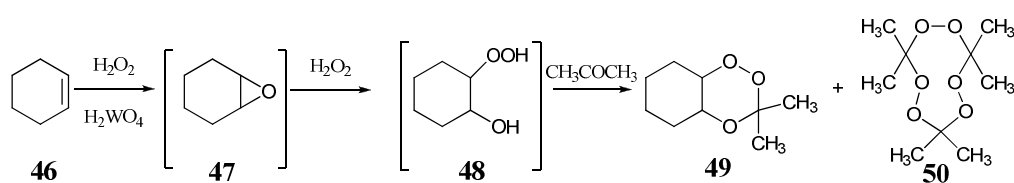
Scheme 7

It was noted that the percentage yield of **49** varied with the concentration of hydrogen peroxide. Increasing the concentration of hydrogen peroxide from 34% to 90% increased the yield from 23% to 49% of **49**. This route however produces quantities of the extremely explosive triacetone triperoxide (**50**) upon addition of acetone to the excess hydrogen peroxide. Although this method is not generally used in the synthesis of 1,2,4-trioxanes, it showed that the perhydrolysis of epoxides to β-hydroxy hydroperoxides could be used as a synthetic method in the formation of 1,2,4-trioxane rings.

Ring-opening reactions of epoxides are normally enhanced by a catalyst. Under neutral and basic conditions, nucleophilic attack occurs at the sterically less-hindered carbon centre by a classic S_N2 mechanism. In contrast, the acid-catalysed ring openings of epoxides are considerably accelerated and nucleophilic attack proceeds via an S_N2 type reaction mechanism at the more substituted side of the epoxide. The reagent tends to sit

further away from the position of attack and the driving force of the reaction is said to be more a transfer of electron density from the carbon centre to the epoxide oxygen than from reagent to carbon. This S_N2 reaction is referred to as a 'borderline S_N2'.[71,72]

An apparently uncatalysed epoxide ring-opening using 98% hydrogen peroxide reported an encouraging 70% yield of the β-hydroxy hydroperoxide **51** *(Scheme 8)*.[73] However this method required extended reaction times of 14 days and the product was contaminated with diol **52**, produced from reagent and product decomposition. The β-hydroxy hydroperoxide **53** was subsequently condensed with acetone using anhydrous cupric sulfate to give the 1,2,4-trioxane **53** in up to 50% yield.
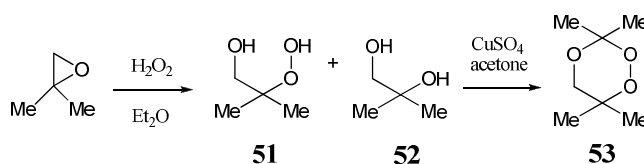
Scheme 8

Perchloric acid-catalysed epoxide ring openings using a five-fold excess of 98% hydrogen peroxide for 2 hours at 0-5°C gave 55-95% yields of the β-hydroxy hydroperoxides **54** *(Scheme 9)*.[74] Although unsymmetrical epoxides could open either way, NMR spectroscopic analysis showed only one product arising from attack at the more substituted carbon was formed. Subsequent acid-catalysed ring openings of *spiro*-epoxides result in the same selectivity for the attack of hydrogen peroxide.[75,76] Base-catalysed perhydrolysis reactions yielded no isolable products, with either steric hindrance or insufficient nucleophilicity of HOO⁻ being deemed responsible for recovery of starting material even after extended reaction times of 24 hours.[74]
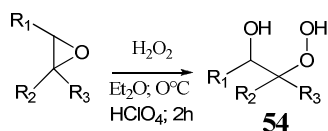
54a $R_1 = R_2 = H$, $R_3 = Ph$
54b $R_1 = R_2 = R_3 = Me$
54c $R_1 = PhCH_2CH_2$, $R_2 = R_3 = Me$

Scheme 9

Molybdenyl acetylacetonate has been shown to catalyse the production of isobutylene oxide by reaction of isobutene **55b** and hydrogen peroxide. In the proposed mechanism

outlined in *Scheme 10,* the epoxide **56**, when formed, would continue reacting with excess hydrogen peroxide producing a β-hydroxy hydroperoxide intermediate **57**. Subsequent reaction between the β-hydroxy hydroperoxide **57** and the alkene **55b** produces the observable epoxide **56** and diol impurity **58**.[77]

55a, R=H, R$_1$= Me
55b, R=Me, R$_1$= Me
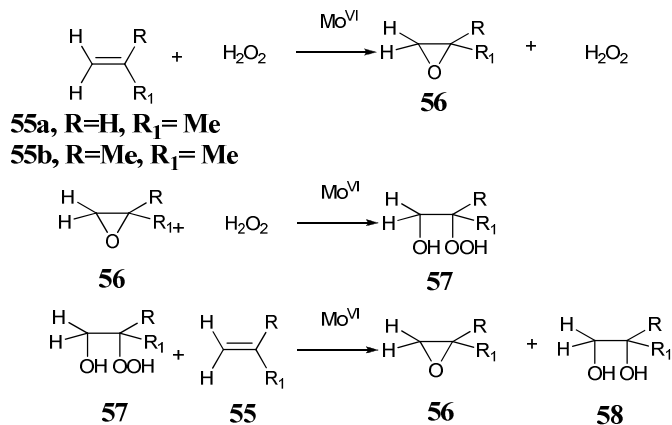
Scheme 10

The existence of a β-hydroxy hydroperoxide **57** is an important observation as it demonstrates the potential of the molybdenum catalyst to promote the formation of the key intermediate in 1,2,4-trioxane synthesis. To confirm the presence of the β-hydroxy hydroperoxide **57**, isobutylene oxide **56** was reacted in isolation with hydrogen peroxide. The reaction produced the β-hydroxy hydroperoxide **57** in an exothermic and very fast reaction which only occurred in the presence of the molybdenum catalyst. It was noted that the selectivity of the reaction gave rise to a hydroperoxide group at the more substituted carbon centre. These results were repeated in the reaction of propene (**55a**).
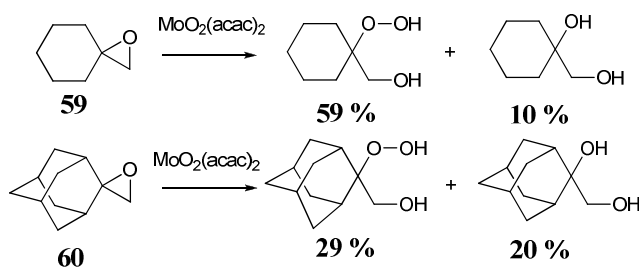
Scheme 11

The catalytic production of β-hydroxy hydroperoxide using molybdenyl acetylacetonate was used effectively in the synthesis of 1,2,4-trioxanes.[78] Thus perhydrolyses of epoxides **59** and **60**, using a 10-fold excess of 50% H_2O_2 pretreated with anhydrous

MgSO$_4$, were catalysed with 5% molybdenyl acetylacetonate *(Scheme 11)*. When the reaction time was extended to 18 hours (compared to 2 hours for acid-catalysed reactions) increased yields of β-hydroxy hydroperoxide were reported. Attempted perhydrolyses of epoxide **59** with acid catalysis and different solvents (ether, acetonitrile and 2-propanol) produced a higher ratio of diol to β-hydroxy hydroperoxide. Furthermore under similar conditions, epoxide **60** produced no isolable products.

Allylic alcohols as precursors of 1,2,4-trioxanes

There are major advantages in designing syntheses of 1,2,4-trioxanes that do not require a high concentration of hydrogen peroxide. There have been several different methods of synthesising the 1,2,4-trioxane ring via β-hydroxy hydroperoxide obtained from the 'ene' reaction of singlet molecular oxygen with allylic alcohols. [79] These synthetic methods proceed under milder conditions which may be more appealing when scaling up 1,2,4-trioxane synthesis.

The photo-oxygenation reaction of allylic alcohol **61** in ethanol in the presence of a photosensitizer, methylene blue (MB), at 0-10°C produced the β-hydroxy hydroperoxide **62** in 37-55% yield after 16 hours.[80] Following acid-catalysed condensations of β-hydroxy hydroperoxide **62** with cyclopentanone and cyclohexanone, a range of *spiro*-1,2,4-trioxanes **63** were produced, generally in good yield *(Scheme 12)*.[81]

61

a X= H, R= H   e X= Me, R= H
b X= F, R= H   f X= H, R= Me
c X= Cl, R= H   g X= Cl, R= Me
d X= OMe, R= H
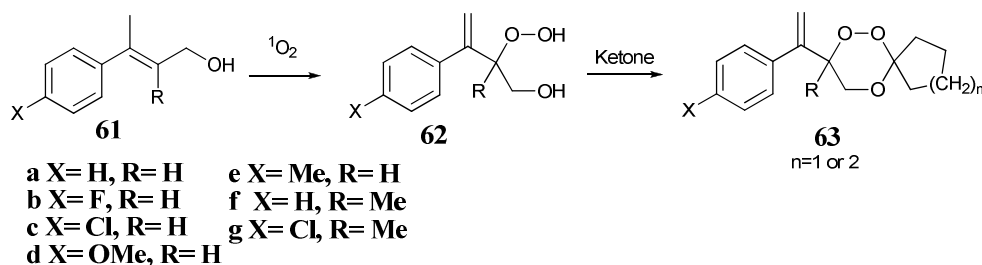
Scheme 12

The photo-oxygenation of allylic alcohols becomes complicated when there are several sites for the 'ene' reaction to take place. This problem was highlighted when geraniol (**64**) was investigated as a potential precursor to antimalarial trioxanes *(Scheme 13)*.[82] The photo-oxygenation of geraniol produced four products (**65a-d**). It was beneficial for

the synthesis of 1,2,4-trioxanes that the mixture was separated into hydroxy *bis* hydroperoxides **65c,d** and the hydroxy monohydroperoxides **65a,b**. Subsequent acid-catalysed condensation of **65c,d** with acetone followed by reduction with NaBH$_4$ in methanol produced mixtures of trioxanes **66a** and **66b** which were separated by flash column chromatography on silica gel. Although 1,2,4-trioxane **66a** was thought to be synthesised as a mixture of two diastereoisomers no evidence was found by either TLC, or spectroscopic analysis. Similar 1,2,4-trioxanes were obtained from acid-catalysed condensations with cyclopentanone, cyclohexanone and 2-adamantanone.
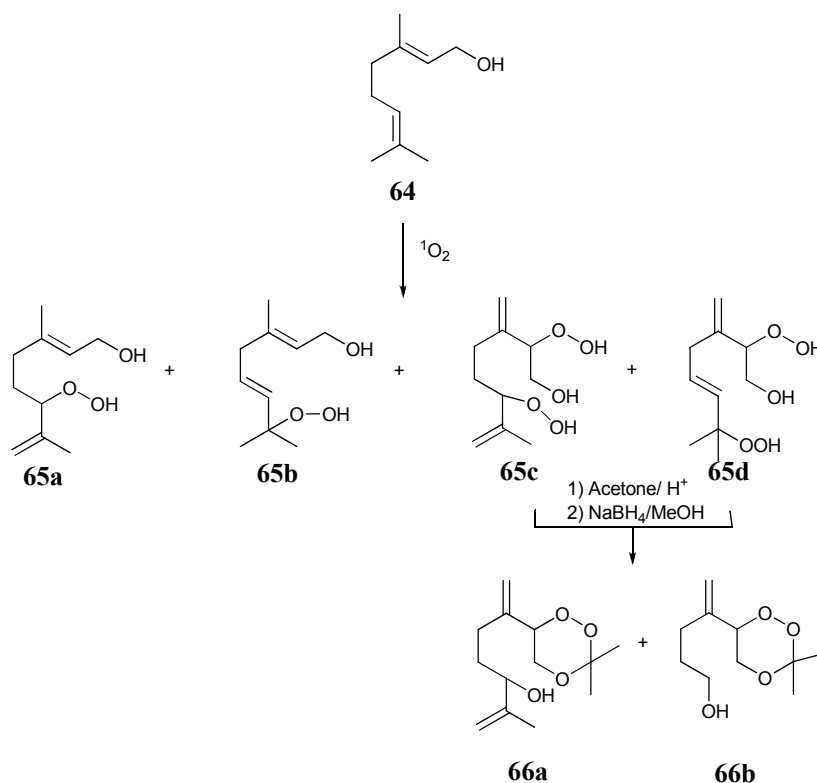
Scheme 13

The hydroxyl group in **66a,b** offers a useful functional group for further elaboration to produce a series of new 1,2,4-trioxane derivatives. However problems with the low yielding 'ene' reactions producing a mixture of products, as indicated above, prompted the investigation of the photo-oxidation of **67** which is readily available in three steps from commercially available geranyl acetate.[83] Thus Methylene Blue-sensitized photo-oxygenation of allylic alcohol **67** in MeCN gave β-hydroxy hydroperoxide **68** in 30-45% yield as inseparable mixtures of diastereoisomers. A range of 1,2,4-trioxanes **69** were reported from **68** by acid-catalysed condensation with cyclohexanone, cyclopentanone, and 2-adamantanone *(Scheme 14)*.
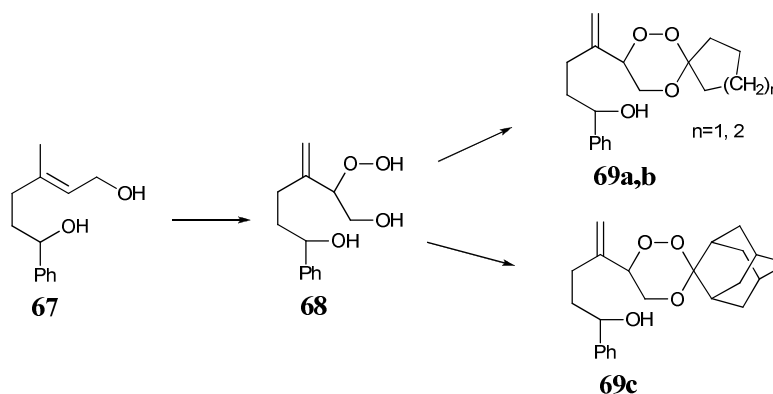
Scheme 14

The β-hydroxy hydroperoxide **71** was synthesized by the standard method from **70** and was then reacted *in situ* with 1,4-cyclohexanedione to produce 1,2,4-trioxane **72** in overall 40-50% yield. Subsequent reductive amination of **72** afforded the antimalarial trioxaquine **73**, which, when converted into its dicitrate salt **74**, becomes more stable and soluble in water *(Scheme 16)*.[84]
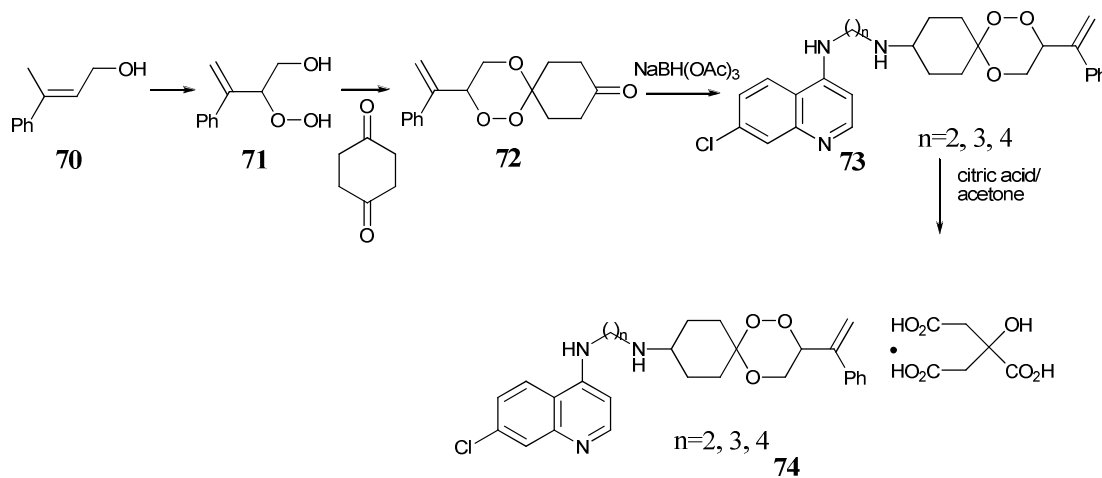
Scheme 16

Application of this method to cyclic allylic alcohols allowed access to the bicyclic 1,2,4-trioxanes **76** *(Scheme 17)*.[85] There have been a few reports of the photo-oxygenation of cyclohexenols and only one isolated a hydroperoxide.[86] Using normal photo-oxygenation conditions, hydroxy hydroperoxide **75** was obtained in 22-35 % yield and then, following acid-catalysed condensation with cyclohexanone,

cyclopentanone and 2-adamantanone, produced the corresponding 1,2,4-trioxanes **76** in 12-37% yield.
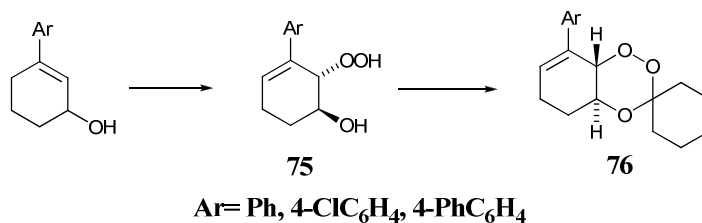
Scheme 17

1,2,4-Trioxanes and 1,2,4-trioxolanes containing the adamantylidene substituent show an increase in antimalarial activity when compared to other structurally related compounds.[87,88] Since the economic cost of having an adamantylidene substituent in the structure is high, the replacement of the adamantane ring with a steroidal unit has been investigated.[89] A range of steroid-derived *spiro*-1,2,4-trioxanes **79** were synthesised by the photo-oxygenation of allylic alcohols **77** to give the corresponding β-hydroxy hydroperoxide **78** followed by condensation with 3,20-pregnanedione to yield 1,2,4-trioxanes **79** in 40-87% overall yield *(Scheme 18)*. 1,2,4-Trioxane **79** showed encouraging results in testing against *P. yoelii* in mice. However, the analogous steroidal 1,2,4-trioxanes derived from cholestanone **80** (23-69% yield) and a tigogenine **81** (35-55% yield) showed weak activity in the treatment of *P. yoelii* in mice.
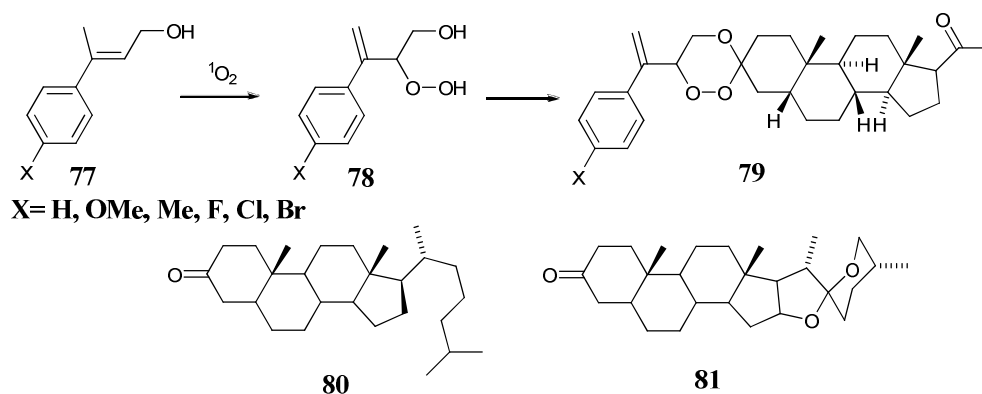
Scheme 18

Photo-oxygenation of chiral allylic alcohols

The 'ene' reactions with substrate **82** react selectively to form **83a** and **83b** in a 93:7 ratio when using non-polar solvents, e.g. CCl$_4$ *(Scheme 19)*. The selectivity drops when performed in protic solvents, e.g. MeOH, suggesting an important role for hydrogen-bonding interactions.[90] The use of a polystyrene microcontainer photo-oxidation also provides a similar selectivity to MeOH.[91] Formation of the 1,2,4-trioxane **84** from the **83a**:**83b**, 93:7, mixture was achieved by condensation with acetone. No product from the *erythro* isomer was apparent. Condensation of the **83a**:**83b**, 73:27, mixture gave both diastereoisomers with analysis of the ^{1}H NMR specra proving that the major product was the *threo* isomer **84**.[92] A selection of diastereotopically pure 1,2,4-trioxanes have been synthesised using this method.[93,94]
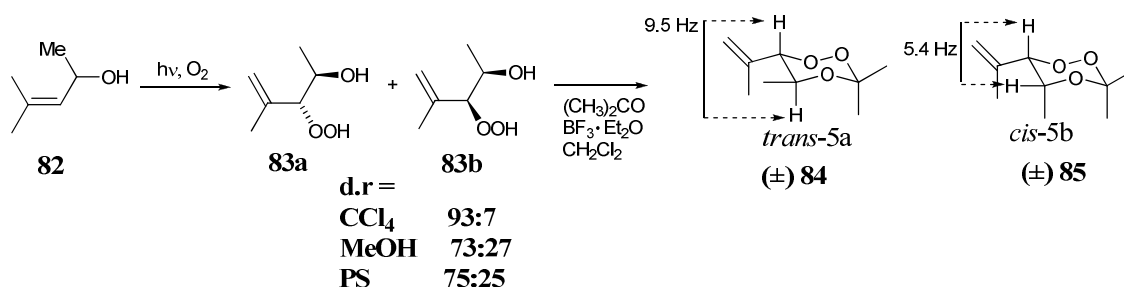
Scheme 19

1,2,4-Trioxanes from the hydroperoxysilylation of allylic alcohols

Using conditions developed by Mukaiyama and Isayama[95,96] [Co(acac)$_2$, Et$_3$SiH, O$_2$], 2-methyl-2-propen-ol **86** was readily converted at room temperature into a peroxysilyl alcohol **87** (40-60% yield). The method takes advantage of the implied regioselective 'Markovnikov' addition of molecular oxygen to the alkene to give the peroxysilyl alcohol **87**. Additionally, a significant increased yield of **87** (75-85%) was observed when using the Co(thd) complex (**90**) instead of Co(acac)$_2$ (**89**). [97,98] After purification, peroxysilyl alcohol **87** has been condensed with a range of aldehydes and ketones under acid catalysis to give the corresponding 1,2,4-trioxanes, **88,** in moderate to good yield [40-90%]. It has been found that purification of the intermediate peroxysilyl alcohol **87** is not always nessessary *(Scheme 20)*.[99]
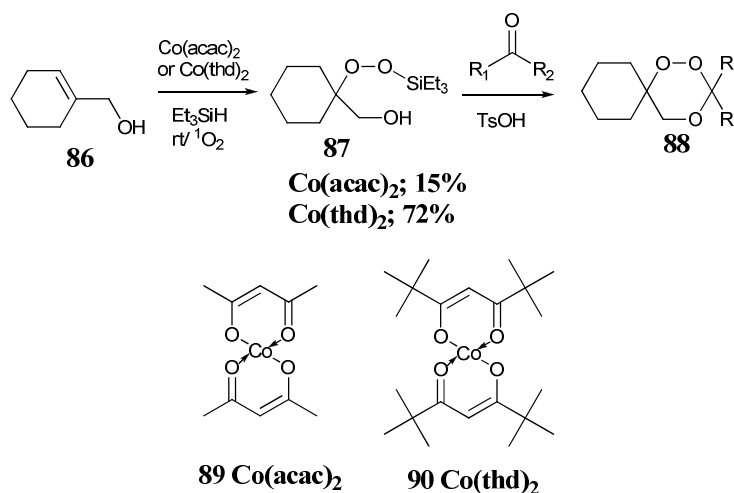
Scheme 20

The mechanism for the hydroperoxysilylation of alkenes was elucidated by Nojima *et. al.* as outlined in *Scheme 21.*[100,101] It was proposed that the first step involves the insertion of the alkene into the H-Co bond of the Co^{III}-hydride to give a Co^{III}-alkyl complex, **91**. The second step was the homolytic cleavage of the Co^{II}-C bond followed by the reaction of molecular oxygen to produce a Co^{III}-alkylperoxo complex **92**. The triethylsilyl peroxide is then produced by transmetallation with Et$_3$SiH, accompanied with the regeneration of the Co^{III}-H complex.
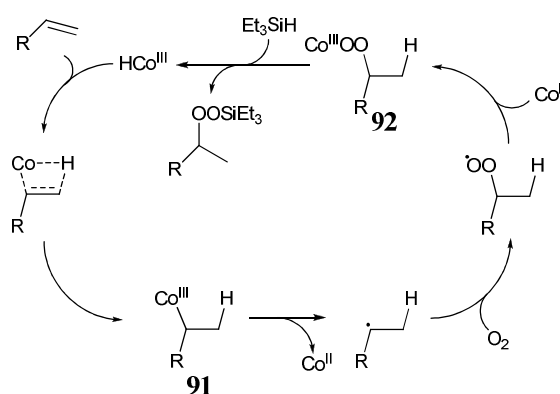
Scheme 21

The hydroperoxysilylation of allylic alcohols has also been used in the synthesis of trioxaquantels. As observed in previous hydroperoxysilylations during the synthesis of 1,2,4-trioxepanes,[102] the silylperoxidation step is 6-8 times slower in dichloromethane than in alcohol whilst an increased yield was observed with the vigorous stirring of the mixture, allowing more oxygen to dissolve. Reductive amination of **93** with

praziquanamine and sodium triacetoxyborohydride in dichloromethane at room temperature afforded the trioxaquentel **94** in 47-70% overall yield *(Scheme 22)*.[33] The complex pattern of multiplets (for position *) in the ^{1}H NMR spectrum of trioxaquentel **94** was consistent with its formation as a mixture of two diastereoisomers **94a** and **94b**, estimated to be in the ratio 70:30 respectively by HPLC analysis.
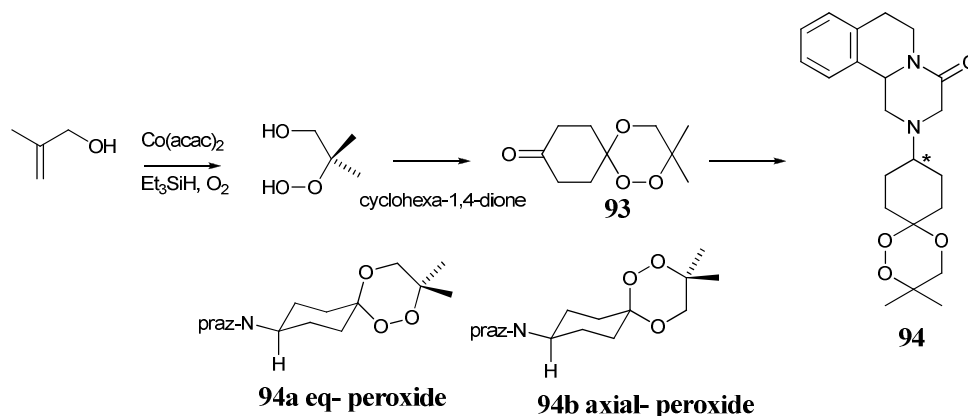
Scheme 22

All four possible isomers of **97**, have been synthesised individually from trioxane **96** via **95** *(Scheme 23)*. Although the activities of the diastereoisomers of **97** as antischistosomiasis and antimalarial agents were moderate in each case, significant differences in activity between the diasteoisomers were apparent.[33]
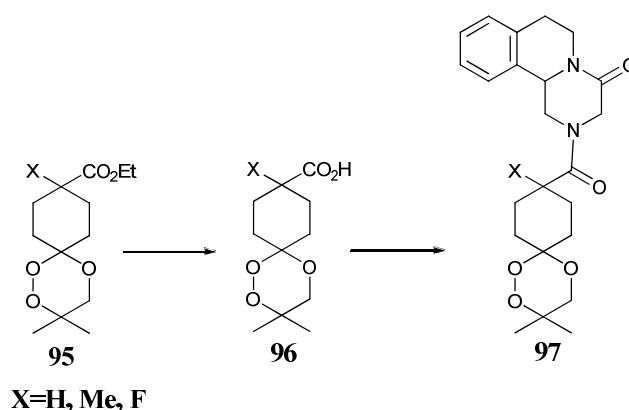
Scheme 23

The synthesis of 1,2,4-trioxanes from the thiol-oxygen co-oxidation (TOCO) of allylic alcohols

The thio-oxygen co-oxidation (TOCO) of olefins provides an efficient route into hydroperoxy sulfides **98c** via a three-step chain propagation sequence *(Scheme 24).*[103] In step one, the addition of thiyl radicals will add regioselectively to the less hindered side of the olefinic bond.
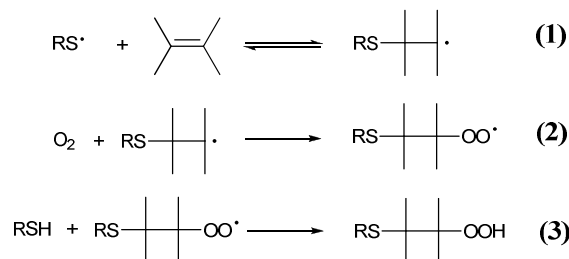
Scheme 24

This procedure has been used successfully in the synthesis of analogues of the anti-malarial bicyclic dioxane, yingzhaosu A (**2**) *(Scheme 25).*[104,105]

2 Yingzhaosu A
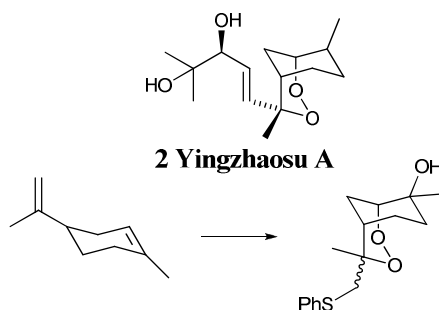
Scheme 25

A further extension of the TOCO reaction was reported using substituted allylic alcohols **98** to produce α-hydroxyperoxides **98c** *(Scheme 26).* These α-hydroxyperoxides were then condensed *in situ* with various ketones to form functionalised 1,2,4-trioxanes **99** in a convenient one-pot synthesis with yields ranging from 40-80%. The resulting sulfur-containing 1,2,4-trioxane derivatives were crystalline and their structures where determined by X-ray crystallographic analysis confirming the structure of the 1,2,4-trioxane ring. The sulfur-containing 1,2,4-trioxanes were reported as having moderate to good biological activity.[106]
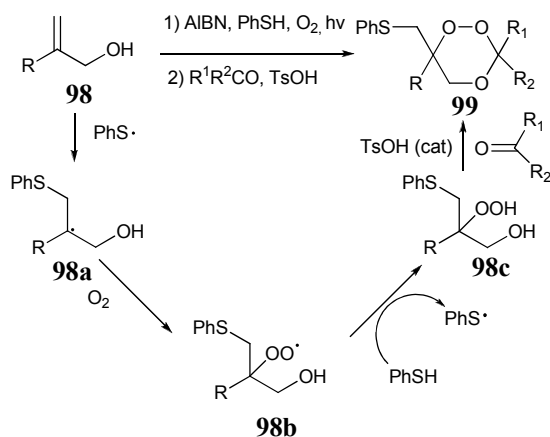
Scheme 26

The side chain can be manipulated via the Pummerer reaction[107,108] to produce a range of new 1,2,4-trioxane derivatives **100**. The carbonyl group in **100** can be elaborated further, e.g. by a Wittig reaction to form **101** *(Scheme 27)*.
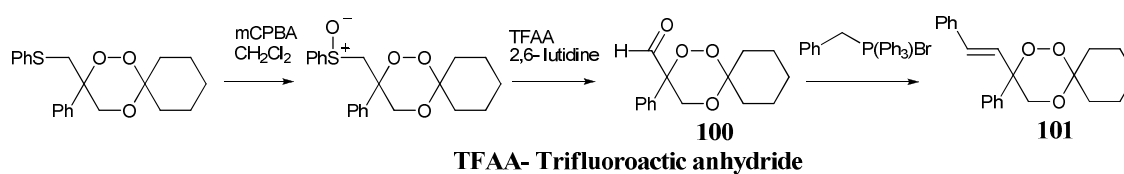
Scheme 27

The TOCO method has been further adapted for the synthesis of 1,2,4-trioxepanes by simply extending the chain of the allylic alcohol *(Scheme 28)*.[109]
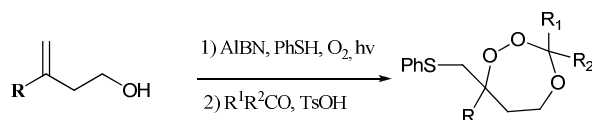
Scheme 28

First Solid-Phase Synthesis of 1,2,4-trioxane
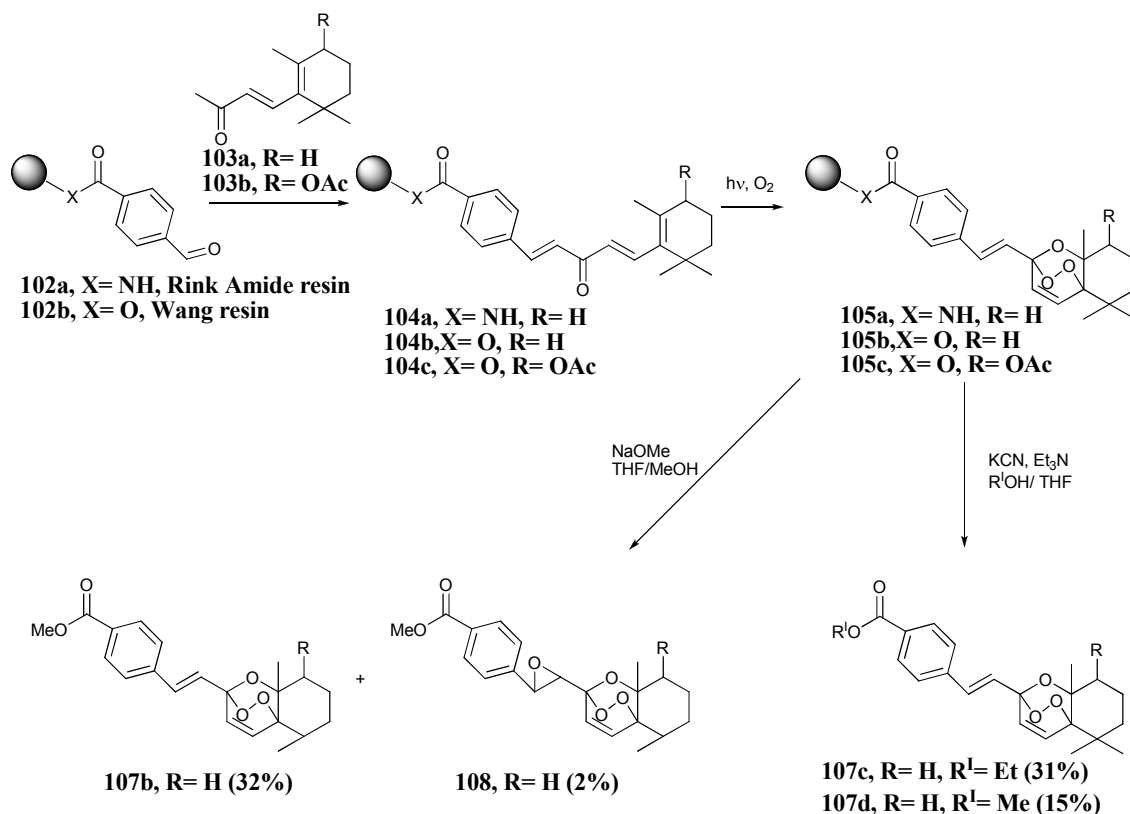
Scheme 29

The synthesis of 1,2,4-trioxanes through the photo-oxygenation of β-ionone **103a** was reported in 1999.[110] In a variation on the route, the β-ionone **103a,b** has been anchored to a polystyrene polymer by Wang and Rink resin linkers in the first solid state synthesis of 1,2,4-trioxanes *(Scheme 29)*.[111] An aldol condensation between **102a,b** and an excess of **103a,b** with LiOH in DME produced the dieone **104a-c**. The 1,2,4-trioxane ring was synthesised by irradiation of **104** in an oxygen atmosphere.
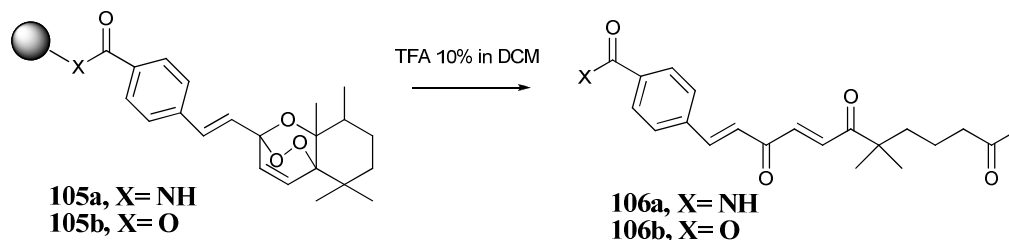
Scheme 30

The release of the solid support was reported to be difficult. Attempts to use an acid treatment yielded no 1,2,4-trioxane and instead produced a triketone from cleavage of the peroxy bond followed by β-scission reaction *(Scheme 30)*. Successful release of the

Wang–resin anchored 1,2,4-trioxane was achieved by the use of 1 equivalent of NaOMe in THF/OMe leading to the methyl ester **107b** and a small quantity of epoxide **108**. Alternatively the use of ethyl alcohol and KCN produced the corresponding ester in moderate yield *(Scheme 29)*.

Synthesis of bridged bicyclic 1,2,4-trioxanes synthesis using UHP (Urea-H$_2$O$_2$ Complex)

Using methods developed for the synthesis of 1,2-dioxanes,[112,113] the peroxide bond has been introduced into the bicyclic-1,2,4-trioxane **111** using UHP, a urea-hydrogen peroxide complex *(Scheme 31)*.[114] The treatment of unsaturated ketone **109** with UHP in the presence of p-TsOH in DME afforded the hydroperoxide **110a,b** in 89% yield as a mixture of isomers (*cis*:*trans*, 1.6:1). The isomers **110a,b** were separated by column chromatography. Under mild base-catalysed conditions the *cis*-hydroperoxide **110a** underwent intramolecular Michael addition to give the bicyclic 1,2,4-trioxane **111.** The *trans*-isomer **110b** cannot form a bicyclic 1,2,4-trioxane.
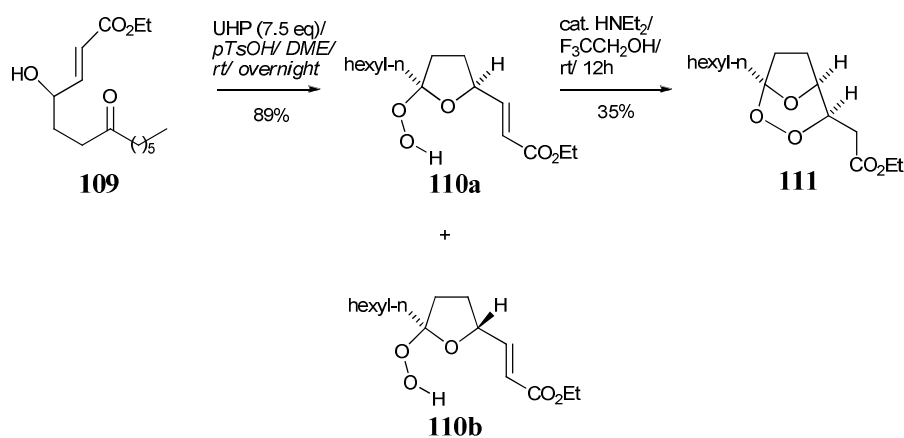
Scheme 31

Attempts to effect the analogous transformation of the unsaturated ketone **112** into the bicyclic 1,2,4-trioxane **113** were unsuccessful even using different catalysts and microwave irridation *(Scheme 32)*.[115] It is likely that 1,3-synaxial interactions required in the formation of the *cis* isomer **112c** render this arrangement energetically unfavourable.
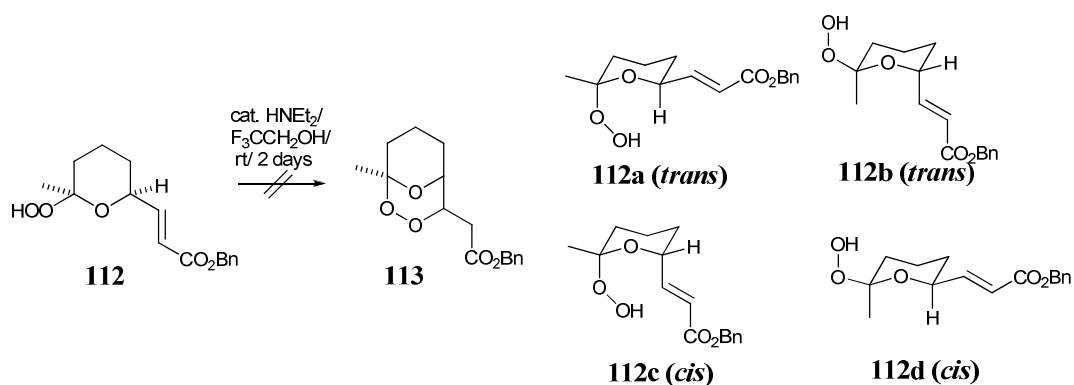
Scheme 32

Structural Analysis of 1,2,4-trioxanes

The structures of ninety-eight molecules containing the 1,2,4-trioxane moiety have been determined by X-ray crystallographic analysis.[116] The majority of the 1,2,4-trioxane structures reported are either related directly to artemisinin (**1**) or are polycyclic systems, because similar monocyclic 1,2,4-trioxane derivatives tend to be low melting solids. This brief review will highlight the following: artemether (**6**),[117] the fused bicyclic 1,2,4-trioxanes **115**[118] and **115**,[119] and the monocyclic 1,2,4-trioxanes including *monospiro* **117**[106], *dispiro* **119**[120], and C5-substituted **118**[121] and **116**[122] 1,2,4-trioxanes.
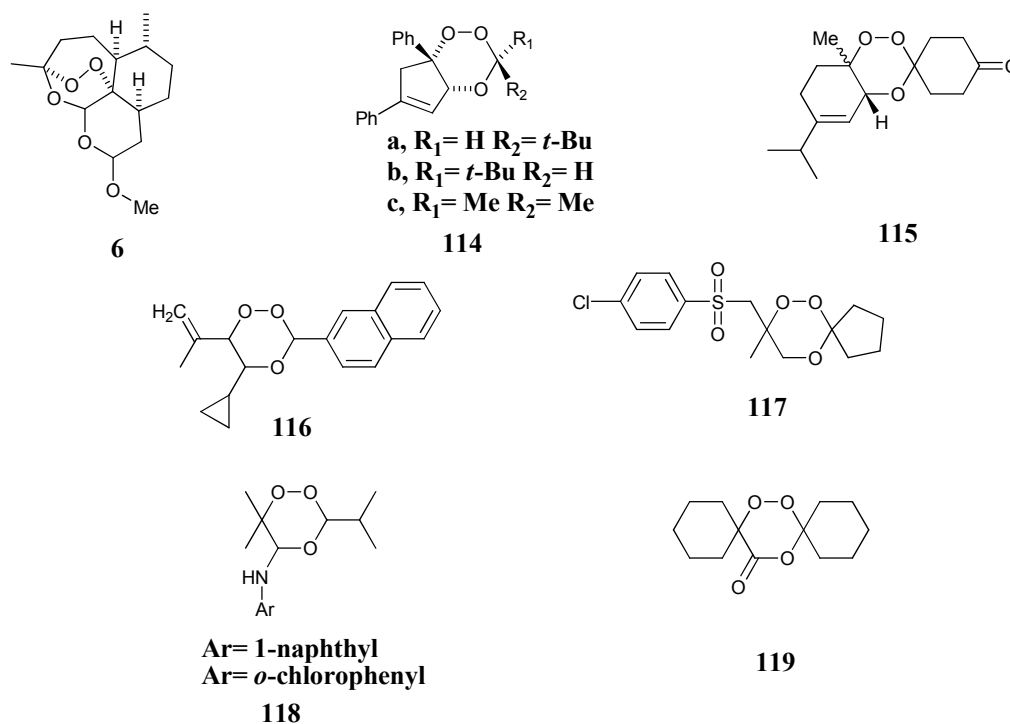
The conformations of the 1,2,4-trioxane rings in these structure vary between a chair or near-chair conformation and a twist-boat. Since polycyclic structures like artemether (**6**) have highly restricted movement, the 1,2,4-trioxane ring tends to be in a twist-boat conformation. Other bicyclic 1,2,4-trioxanes, e.g. **114** and **115**, have similar conformational restrictions on the 1,2,4-trioxane ring. Interestingly, despite the restriction, there is a fine balance between the 1,2,4-trioxane being in a chair or twist-boat conformation in **114**. 1,2,4-Trioxane **114c** is in a twist-boat conformation whereas 1,2,4-trioxanes **114a** and **114b**, which contain a bulky t-butyl group, are in chair conformations. Since the monocyclic 1,2,4-trioxanes **116-119** have no structural restrictions the central 1,2,4-trioxane ring adopts a classical chair conformation in each case. The *dispiro*-1,2,4-trioxan-5-one **119** which contains an sp^2-centre in the 1,2,4-trioxane ring adopts a *pseudo* twist-boat conformation. The orientation of the substituent at the C5 position in 1,2,4-trioxane **118** can also show a change depending on size: **118a** has the 1-naphtyl group in an equatorial position whereas the o-chlorophenyl group in **118b** is in an axial orientation. The O-O bond distance in a 1,2,4-trioxane is around 1.48 Å and is comparable with other peroxide bond distances.[123] The structure of 1,2,4-trioxane rings are further discussed in the results and discussion section.

Thermal decomposition of 1,2,4-trioxanes
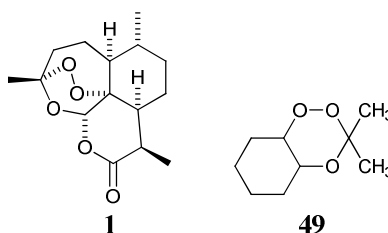
The kinetics of the homolytic cleavage of the peroxide bond has been shown to be first order by monitoring the disappearance of the 1,2,4-trioxane **49** during a thermolysis reaction.[124] The temperature for the decomposition has been shown to be similar for a variety of 1,2,4-trioxanes and independent of their physical form and melting point.[125] The resulting oxy radicals follow a step-wise fragmentation mechanism with β-scission reactions with activation barriers of *ca.* 15-18 kcal mol^{-1} resulting in the formation of carbon-centred radicals *(Scheme 33)*.[126]
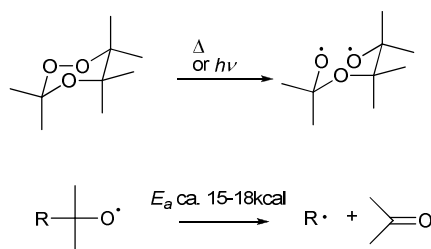
Scheme 33

The thermolysis of 1,2,4-trioxane **49** took place in octane at 160-189°C via a first order reaction.[127] Two products were isolated from the reaction and were determined to be acetone (**121**) and adipaldehyde (**122**). The oxygen diradical formed from the initial bond cleavage, **120,** can further react by either cleavage of bond **A** or bond **B** or 1,5-hydrogen abstraction before forming the products isolated *(Scheme 34).*
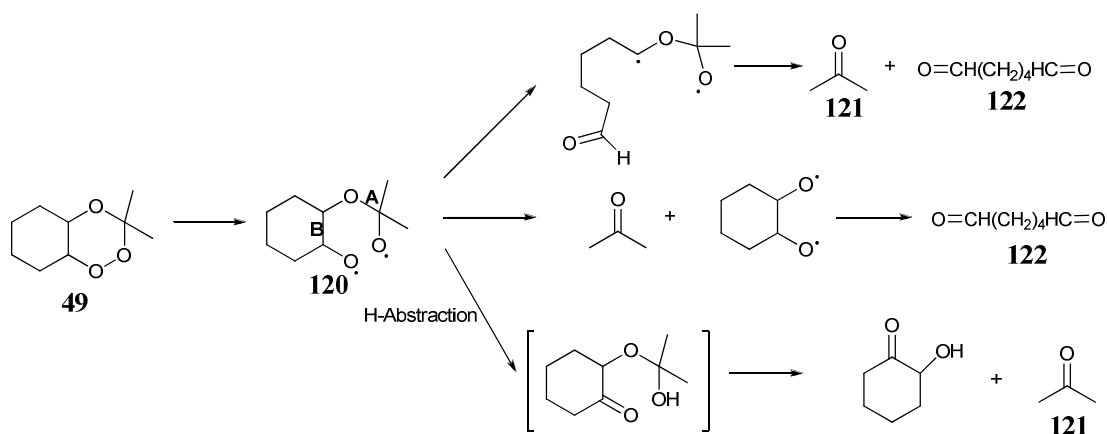
Scheme 34

In a similar study, the thermolysis of 1,2,4-trioxane **123** gave rise to the formation of three carbonyl compounds **124-126** in almost quantative amounts by different β-scission reactions prompting the fragmentation of the molecule (*Scheme 35).*[128]

	124	**125**	**126**
R= Me	68%	91%	84%
R= Ph	83%	66%	71%
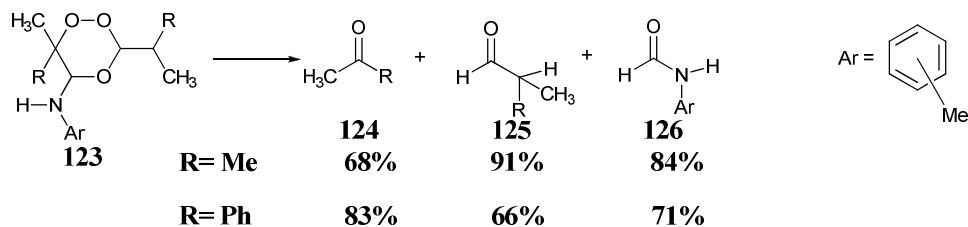
Scheme 35

Artemisinin (**1**) was shown to decompose at temperatures of 190°C, with no artemisinin detected after 10 minutes, producing a mixture of **127, 128** and **5** from a radical

31

rearrangement process *(Scheme 36)*.[129] Compounds **127**, **128** and **5** were separated on a silica gel column and fully characterised by NMR spectroscopy and X-Ray crystallography. Similar products have been observed in other thermolyses of artemisinin (**1**).[130] The thermolysis of dihydroartemisinin (**129**) produced two products, **5** and **130,** in 30% and 50% yield respectively.[131] The formation of the major product **130** from **129** was consistent with the fragmentation of the molecule by a series of β-scission reactions after the initial cleavage of the peroxide bond.
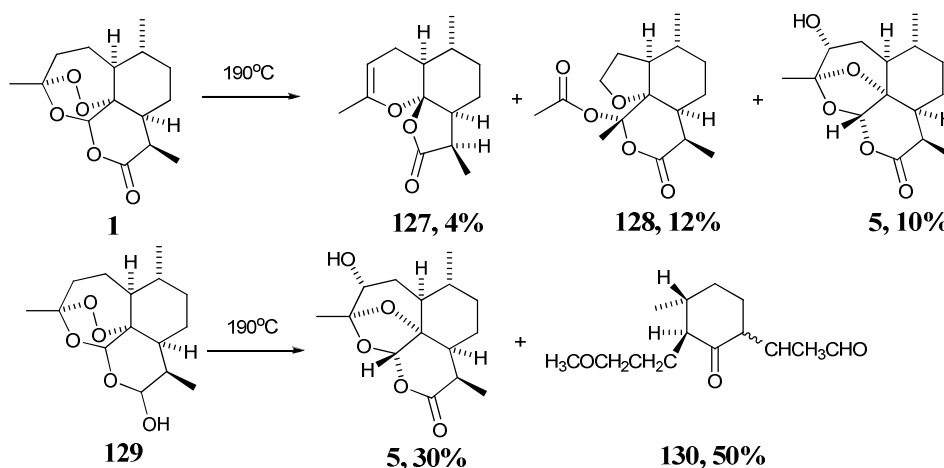
Scheme 36

In addition to aldehydes and ketones from the fragmentation of the whole molecule, the thermolysis of 1,2,4-trioxane **131** formed benzoic acid and deoxybenzoin. This is consistent with 1,2-hydrogen- and 1,2-phenyl-shifts occurring in the mechanism. The thermolysis of **132** also formed **134** by an intramolecular hydrogen abstraction *(Scheme 37)*.[132]
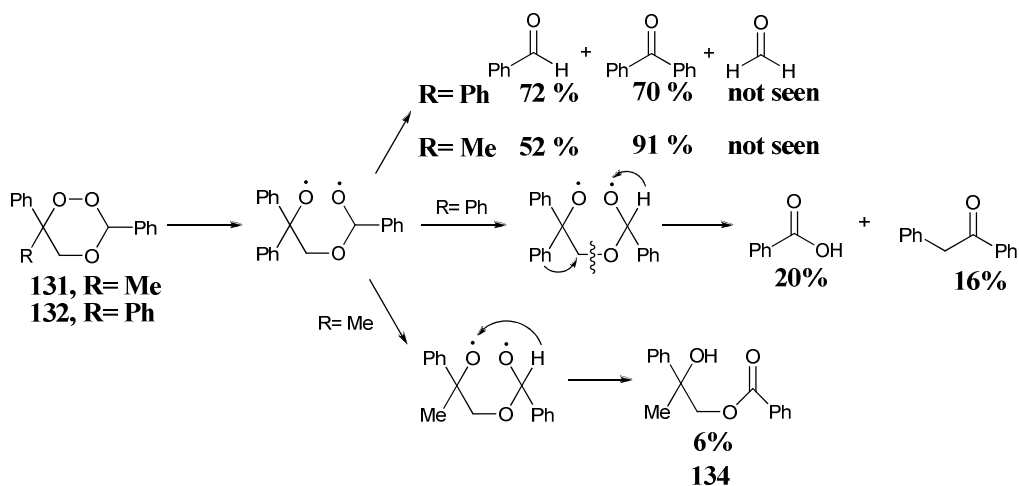
Scheme 37

Before 1,2,4-trioxan-5-ones had actually been synthesised,[133,134] it was believed that such trioxanes would spontaneously decompose to produce carbon dioxide and its two component carbonyl compounds. In reality, 1,2,4-trioxan-5-ones were found to be stable at room temperature forming crystalline solids.[120] Initial experiments using capillary column gas chromatography showed that 1,2,4-trioxan-5-ones were stable at temperatures below 180°C. At temperatures above 210 °C they underwent complete fragmentation. Additionally heating 1,2,4-trioxanes **134-136** at 189°C for 2-3 hours in boiling decalin under argon, resulted in complete fragmentation. However fragmentation of **138** and **139** was only observed after extended reaction times of 3-5 hours. Using flash-vacuum thermolysis, the 1,2,4-trioxanes **135** and **136** survived temperatures up to 300°C before fragmenting at 350-400°C.[135]

134 R= t-butyl   136
135 R= 1-adamantyl   137
138
139
140
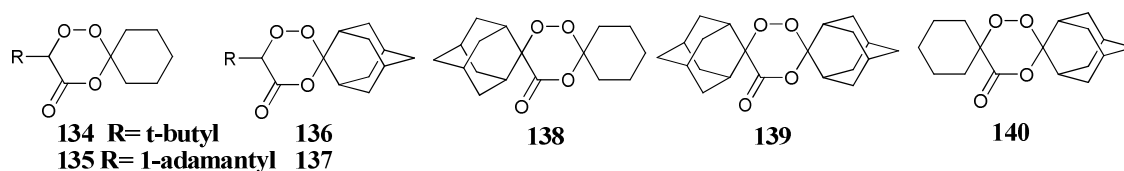
The chemiluminescence quantum yields (Φ_{cl}) of 1,2,4-trioxan-5-ones **139** and **140** were shown to be the same within experimental error at 200°C. The (Φ_{cl}) of 1,2,4-trioxan-5-ones **138** was shown to be significantly lower than that seen for either **139** or **140**. This suggests that a concerted fragmentation is not possible, since both **138** and **140** would produce the same fragmentation. Consequently a stepwise process where cleavage of one side of the 1,2,4-trioxan-5-one ring happened first was suggested *(Scheme 38).*[136]
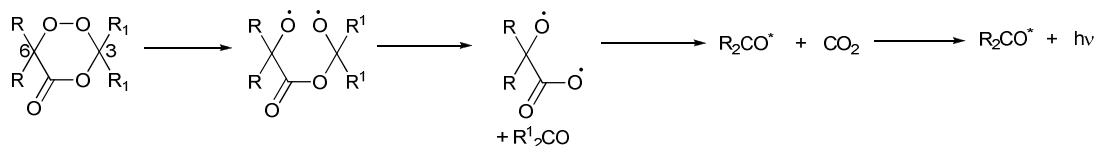
Scheme 38

GC-MS analysis of the crude product from the thermolysis of 1,2,4-trioxanes **141** and **142** identified 12 and 11 different products respectively. The products were derived from the homolytic cleavage of the peroxide bond followed by several different step-wise mechanisms.[137] Analysis of the reaction rate noted that no effect was evident for the decomposition by adding a hydroxyl group in **142**.[138] This was due to the homolytic cleavage being the rate determining step and the substituents being relatively far away

from the peroxide bond. Although the expected activation energy for the homolytic cleavage of a peroxide bond is 33 kcal mol^{-1} [139] the value obtained for 1,2,4-trioxanes **143** differs slightly from this whereas the other values for the 1,2,4-trioxanes are closer to the expected value. The similar $\Delta H^{\ddagger}$ values observed for 1,2,4-trioxanes **141** and **142** reflect the fact the influential changes to the molecule are far away from the peroxide bond. The rate constant values for the cleavage increase as the polarity of the solvent increases with a faster reaction rate seen for the decomposition of **141** in methanol than that in n-hexane.[140] A faster reaction rate (1.6 times greater) for the thermolysis of *cis*-fused 1,2,4-trioxane **144** has been observed by varying the solvent from benzene to methanol, whilst the reaction rate for **143** was less affected by changing the solvent.[141] The reaction rate for **144** measured in the same solvent was also faster than that for **143**. This difference was said to be due to additional shielding effects of one side of the peroxide bond in **144**. The measurement of the entropy of activation also helped determine the mechanism for the reaction. The entropy of activation $\Delta S^{\ddagger}$ was measured to be between -3.0 to 30.2 cal mol^{-1} K^{-1} for 1,2,4-trioxanes **141-144** in methanol *(Table 2)*. For a concerted pericyclic process in which bond breaking in the transition state is partly compensated by bond making, the experimentally measured $\Delta S^{\ddagger}$ would be expected to be heavily negative. This therefore supports the step-wise homolytic cleavage of the peroxide bond.[142]
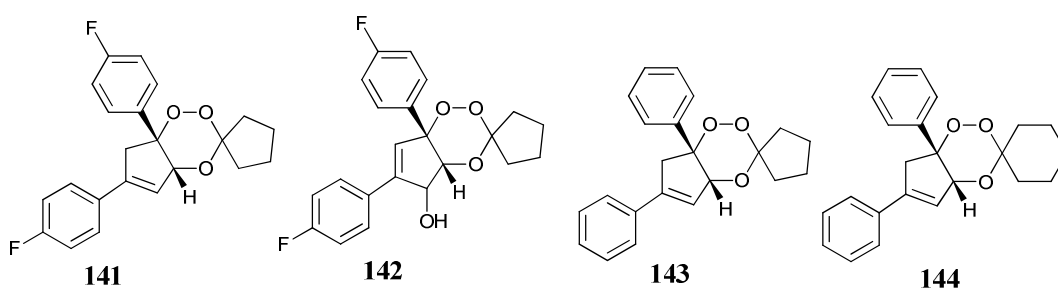
1,2,4-Trioxane	$\Delta H^{\ddagger}$/ kcal mol^{-1}	$\Delta S^{\ddagger}$/ cal mol^{-1} K^{-1}	$\Delta G^{\ddagger}$/ kcal mol^{-1}
141	28.2 ± 0.7	-3.0 ± 1.3	28.9 ± 0.7
142	29.0 ± 0.9	0.4 ± 2.1	30.9 ± 0.9
143	20.2 ± 0.6	0.1 ± 1.6	20.2 ± 0.6
144	39.6 ± 0.6	30.2 ± 1.6	28.8 ± 0.7

*Table 2: Kinetic information for thermolysis of 1,2,4-trioxanes **141-144** in methanol*

Synthetic routes to *dispiro*-1,2,4-trioxanes

A retrosynthetic analysis of the 1,2,4-trioxane structure would suggest a few routes to synthesise the 1,2,4-trioxane ring *(Scheme 39)*.
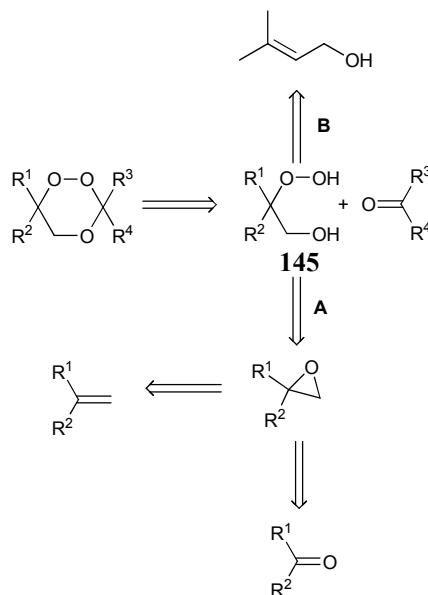
Scheme 39

It is apparent from the retrosynthetic analysis that the production of the β-hydroxy hydroperoxide **145** is a key intermediate in the synthesis of 1,2,4-trioxanes. There are two possible strategies for the production of the β-hydroxy hydroperoxide:

    (i)   Epoxide ring opening with anhydrous hydrogen peroxide (route **A**)

    (ii)   Addition of singlet molecular oxygen to an allylic alcohol (route **B**)

Due to the *dispiro*- nature of the desired 1,2,4-trioxane derivatives, route **A** starting from a cyclic ketone has been preferred. Acid-catalysed condensation of another ketone into the β-hydroxy hydroperoxide then produces the 1,2,4-trioxane *(Scheme 40)*.
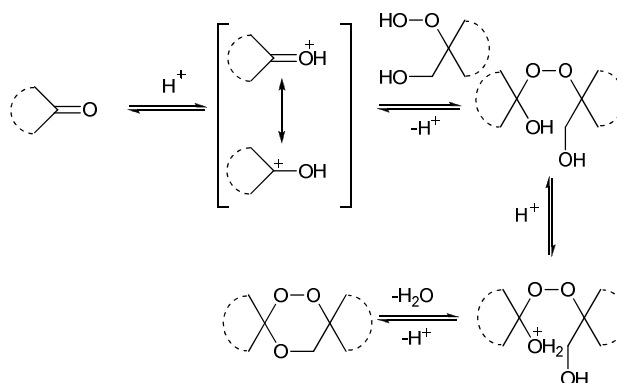
Scheme 40

The synthesis of *dispiro*-1,2,4-trioxanes

It was proposed to synthesise a family of methoxy- or ethoxy- substituted *dispiro*-1,2,4-trioxanes **149** using a 3-step route from **146a,b** as outlined in *Scheme 41*. Thus the reaction of cyclohexanones with dimethyloxosulfonium methylide (**151**) forms epoxide **147a,b**. Subsequent acid- or $MoO_2(acac)_2$-catalysed ring opening of epoxide **147a,b** in the presence of excess hydrogen peroxide gave a β-hydroxy hydroperoxides **148a,b**. The *dispiro*-1,2,4-trioxanes **149** were obtained via acid-catalysed condensations of β-hydroxy hydroperoxides **148** with the appropriate cyclic ketone.

146a, R= OMe
146b, R= OEt
146c, R= Me
146d, R= H

147a, R= OMe
147b, R= OEt
147c, R=Me
147d, R= H

H_2O_2 (ca. 98 %);
Ether; $Mo(acac)_2$
or H^+(cat);
RT; 18 hours

149a, R= OMe
149b, R= OEt
149c, R= Me
149d, R= H

148a, R= OMe
148b, R= OEt
148c, R= Me
148d, R= H

$R^1, R^2=$ a= -$(CH_2)_5$-
b= -$(CH_2)_4$-
c= -$(CH_2)_6$-
d= -$(CH_2)_{11}$-

e= -$(CH_2)_2CO(CH_2)_2$-
f= 1,4-dioxaspiro[4.5]decylidene
g= indanylidene

Scheme 41

36
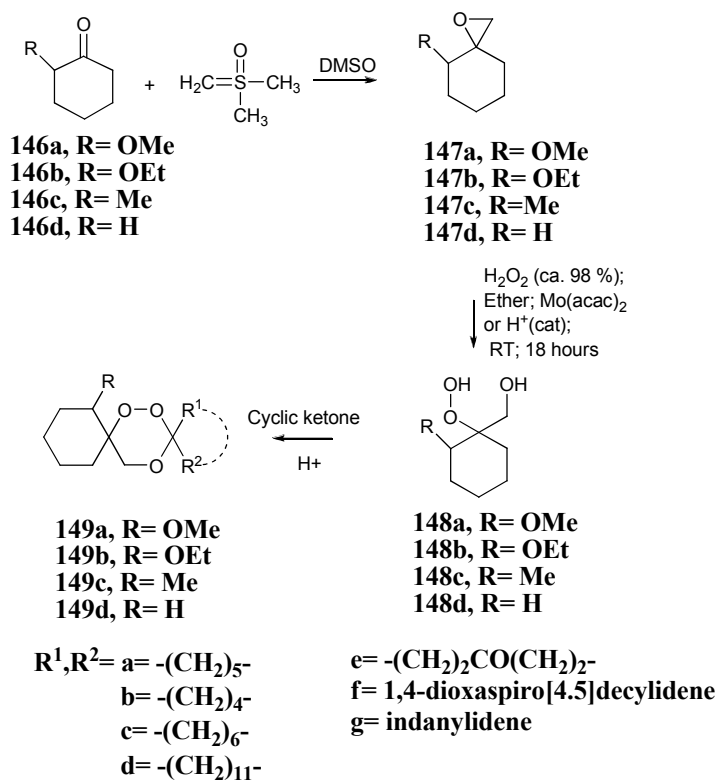
Preparation of Epoxides

The required epoxides were readily prepared from the reaction of the cyclohexanones
146a,b with the stabilized sulfur ylide, dimethyloxosulfonium methylide (**151**) which
was conveniently generated *in situ* by the sodium hydride-mediated deprotonation (in
DMSO) of the sulfoxonium salt **150** *(Scheme 42)*. [143,144]
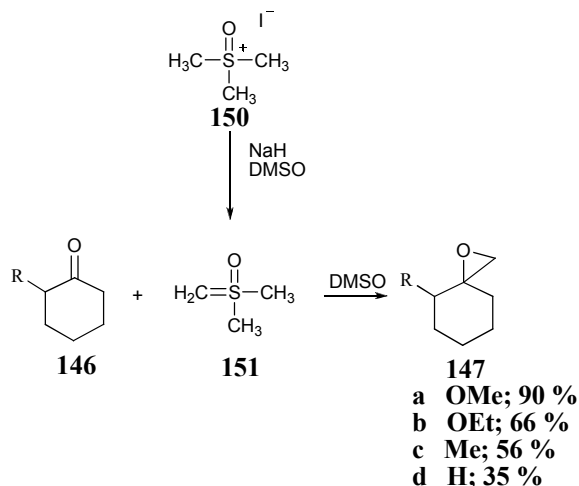
Scheme 42

In previous syntheses of **147a** it was noted that heating of the reaction mixture after
addition of the ketone caused epoxide-ring opening and low yields of product were
obtained.[145] When the reaction was carried out at room temperature, the yields of **147a**
improved significantly, usually in the range 60-90%. The revised procedure was also
used in the synthesis of **147b** giving around 65% yields. The epoxides **147a,b** were
isolated from the crude mixture by distillation under reduced pressure. Careful removal
of DMSO during the reaction work-up was required to avoid contamination of the
distilled product.
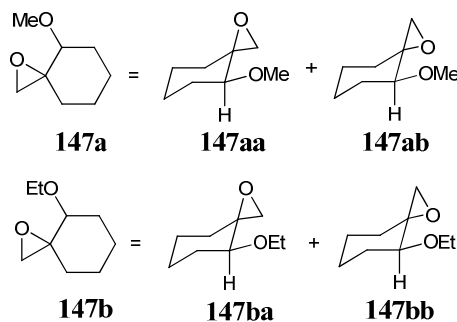
Scheme 43

Unlike epoxide **147c**,[146] epoxides **147a,b** were obtained as a mixture of diastereoisomers (**147aa,ab,** ratio= 60:40), (**147ba,bb,** ratio= 70:30) *(Scheme 43)*. Both diastereoisomers were observed by ^{13}C NMR spectroscopic analysis of the product. The ^{13}C NMR spectrum of **147aa,ab** and **147ba,bb** showed 16 and 18 signals representing two peaks for each carbon atom *(Figure 1a,b)*. Analysis of epoxide **147a** by ^{1}H NMR spectroscopy clearly showed two methyl signals at δ3.30 and δ3.35 for both the diastereoisomers *(Figure 2a)*. Additionally, four doublets with coupling constants of 5.0 *Hz* (major) and 5.1 *Hz* (minor) where present at δ2.47, δ2.53, δ2.61 and δ2.83 consistent with the CH_2 group of the epoxide. By analysis of the integrations and COSY ^{1}H NMR spectroscopy, the peaks for the major isomer **147aa** were at δ2.47 and δ2.61 whilst those of the minor diastereoisomer **147ab** were positioned at δ2.53 and δ2.83. The signal at δ2.61 was further split into a doublet of doublets by a long range ^4J coupling with the CH group *(Figure 2a)*. NOESY ^{1}H NMR spectroscopy showed two further long range interactions in the major diastereoisomer. Similar analysis of the minor diastereoisomer showed that only one of these interactions was present.

147aa   **147ab**
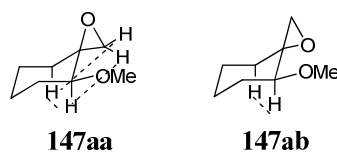
Although analysis of the ethoxy substituted epoxide was more difficult due to further overlapping signals, two triplets for the ethoxy methyl at 1.12 ppm and 1.15 ppm for **147ba,bb** are seen. Additionally, the same pattern of signals was seen for the epoxide CH_2 group confirming the same major diastereoisomer was formed *(Figure 2b)*. The conformation of the major diastereoisomer isomer is consistent with the delivery of the methylene group by the sulfur ylide to the equatorial position of the epoxide,[143] however, the formation of both diastereoisomers of **147a,b** proves that the dimethyloxosulfonium methylide is not particularly facially selective.
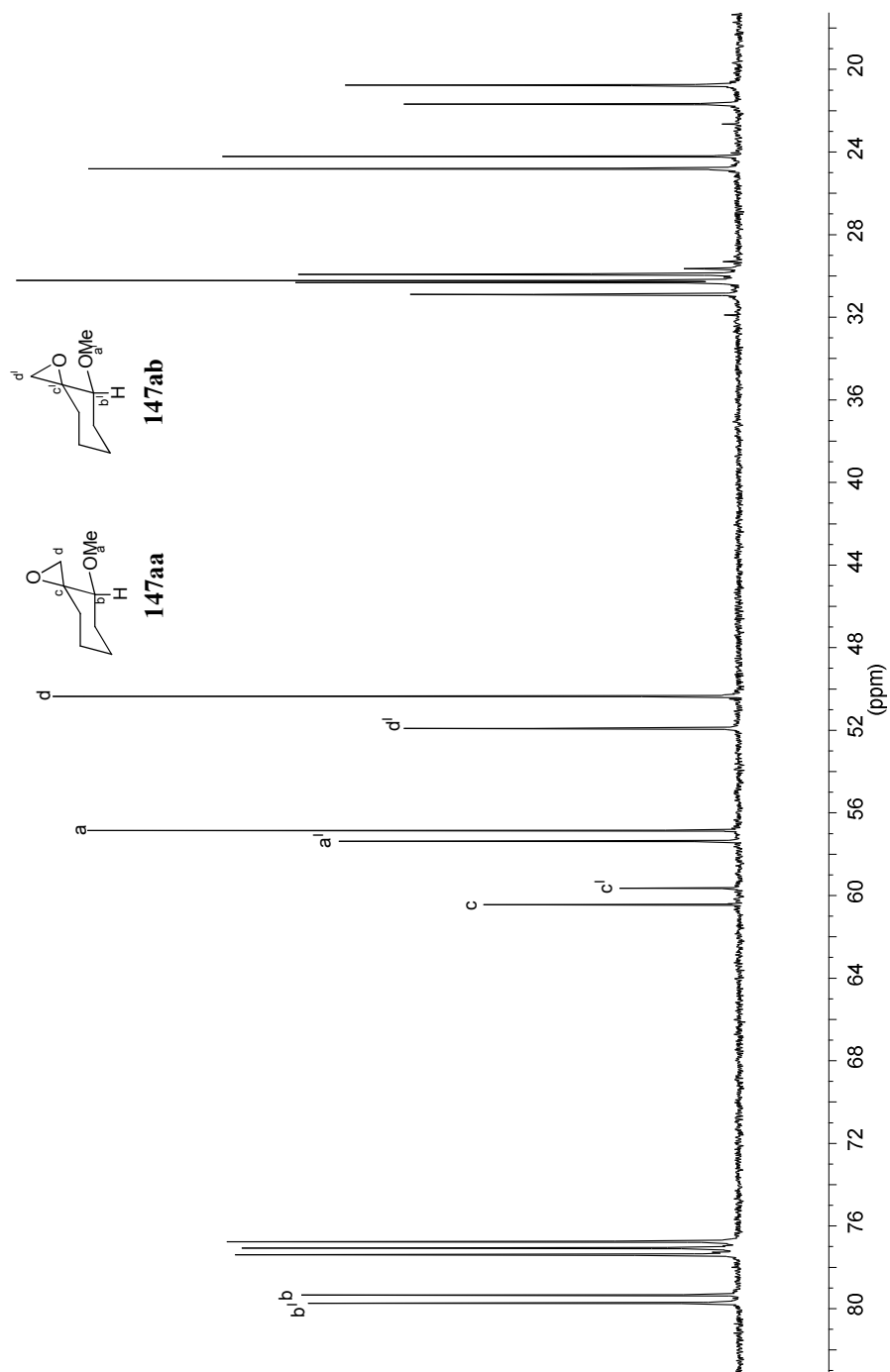
*Figure 1a: ^{13}C NMR spectra for mixture of epoxides **147aa**, **147ab***
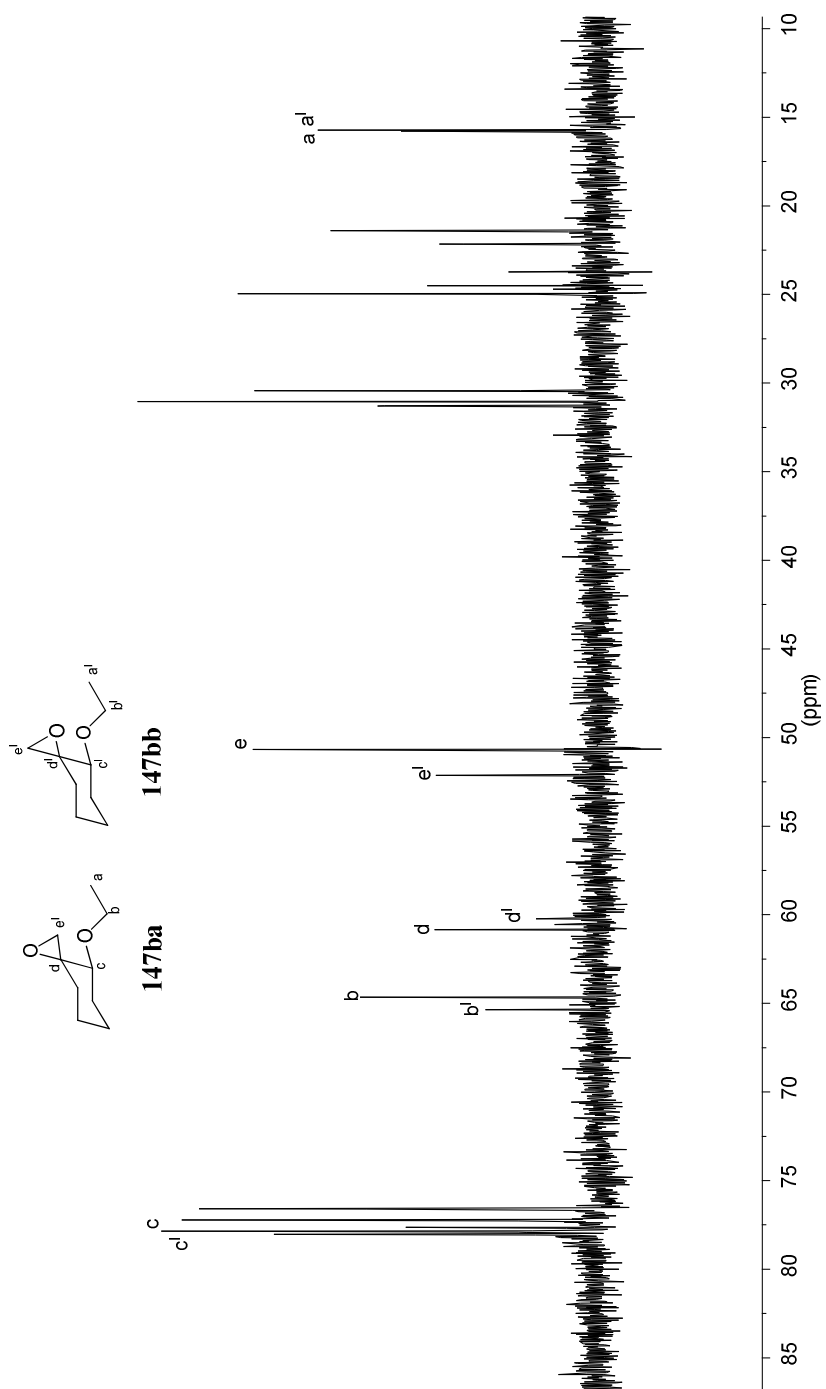
*Figure 1b: ^{13}C NMR spectra for mixture of epoxides **147ba**, **147bb***
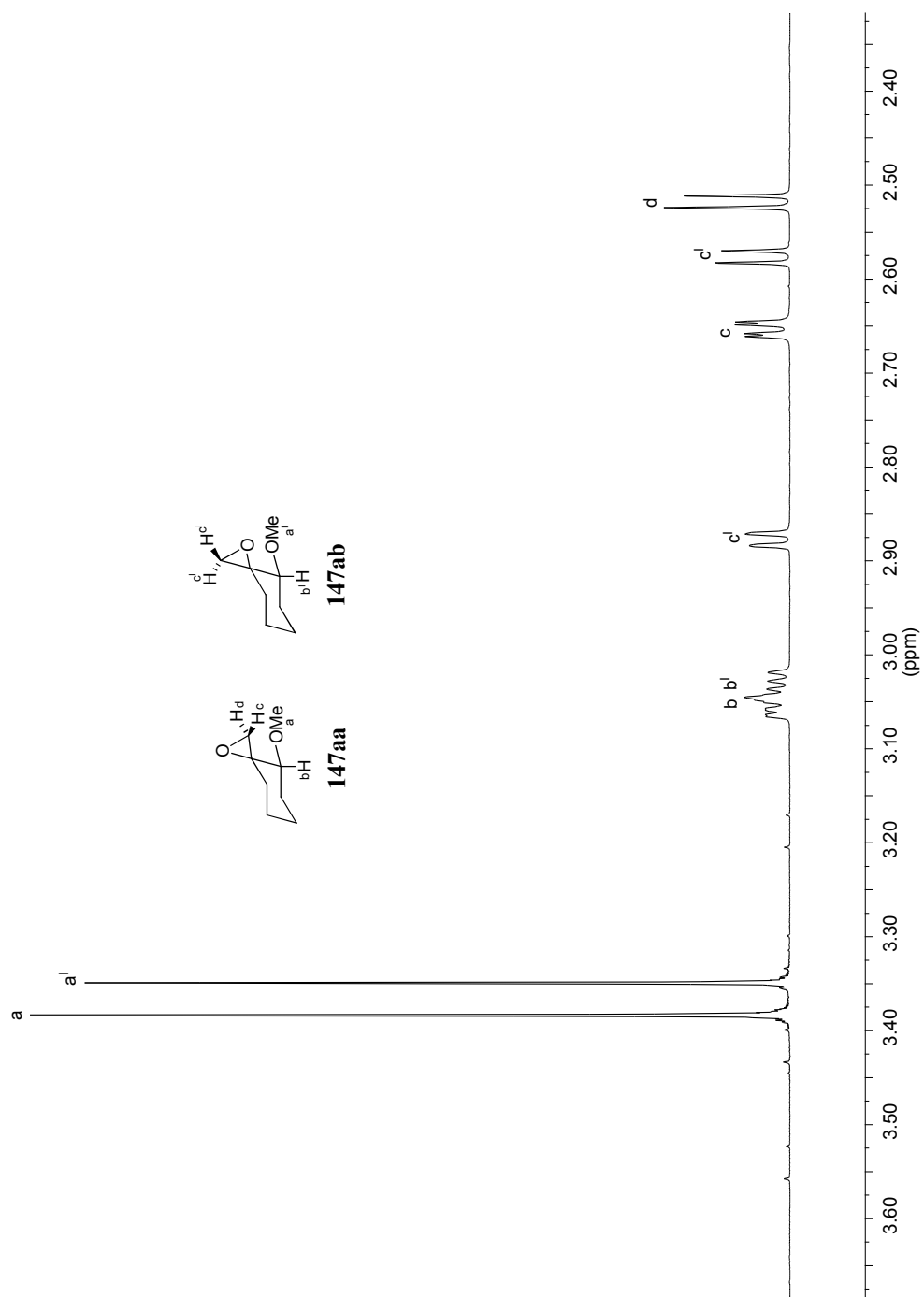
*Figure 2a: ^{1}H NMR spectra for mixture of epoxides **147aa**, **147ab***
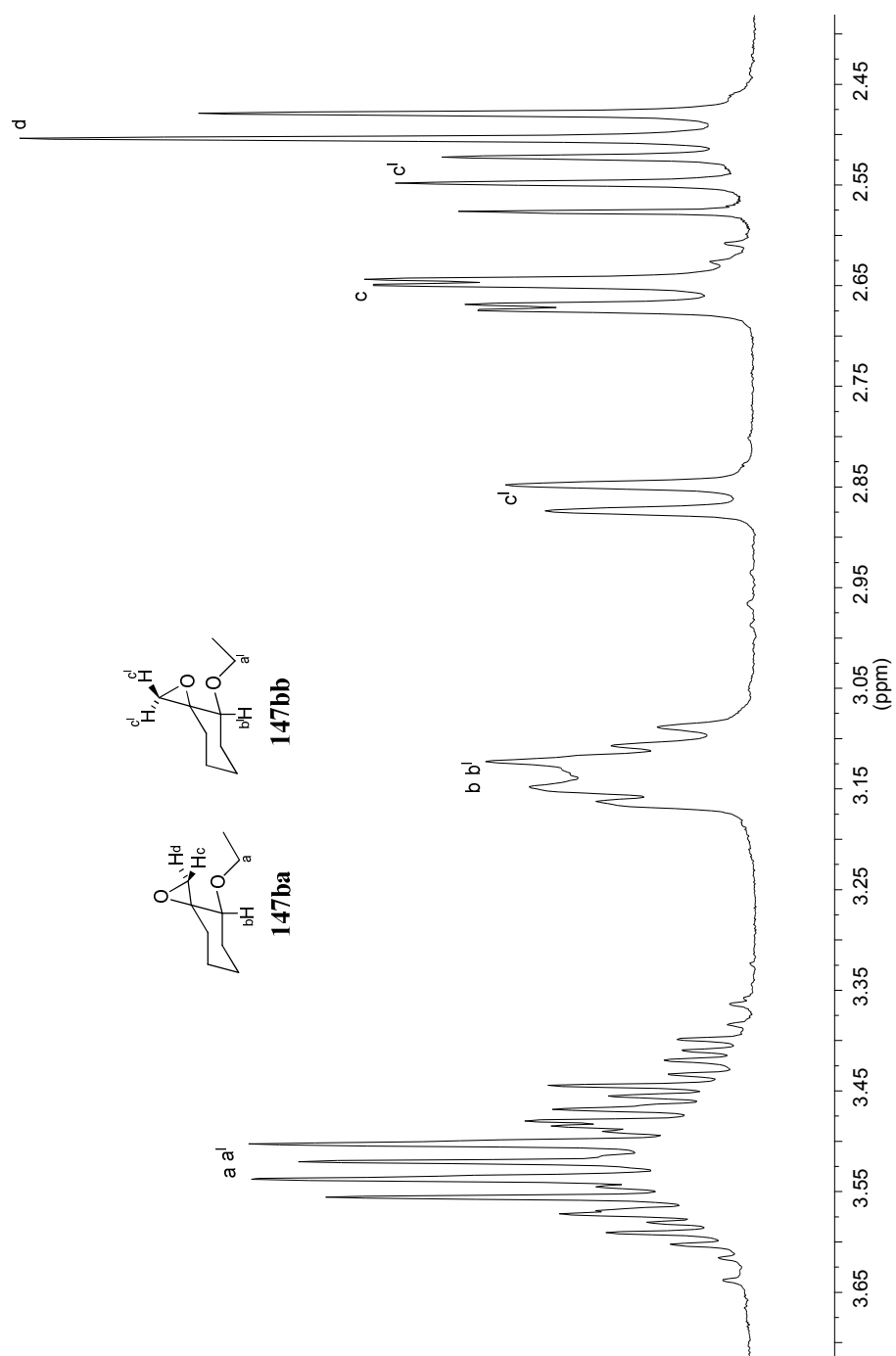
*Figure 2b: ¹H NMR spectra for mixture of epoxides **147ba**, **147bb***

Synthesis of β-hydroxyhydroperoxides by perhydrolysis of epoxides

As outlined in *Scheme 39,* the β-hydroxyhydroperoxides required in this study were most conveniently made by the perhydrolysis of the epoxide **147**. In previous syntheses of β-hydroxyhydroperoxides, it was noted that anhydrous conditions and a five-fold excess of hydrogen peroxide were the optimum reaction conditions and prevented the formation of a diols like **152** *(Scheme 44).*[146] Commercially available 60% v/v hydrogen peroxide was dried using a combination of calcium chloride and phosphorus pentoxide in dry ether at -78°C and the resultant anhydrous hydrogen peroxide solution was used immediately.[147] Since the reaction of phosphorus pentoxide with water is exothermic, external cooling was required to prevent the possible decomposition of the hydrogen peroxide. Alternative drying methods for hydrogen peroxide using magnesium sulfate as the dehydrating agent at 0°C have also been reported.[78]
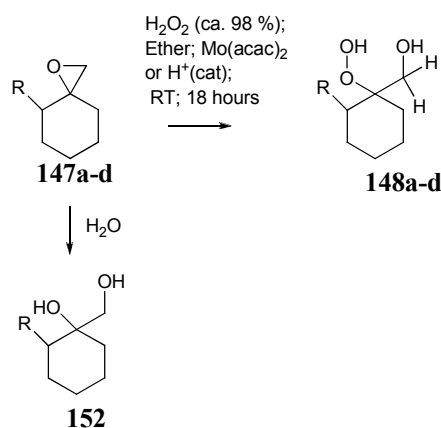
Scheme 44

Although sulfuric acid has been successfully used to catalyse the ring opening of epoxides, the reaction of epoxide **147a** produced only low yields of β-hydroxy hydroperoxide **148a**. Isolation of the product after 45 minutes and 2 hours showed no significant increase in the yield of **148a**. Although analysis of the crude reaction mixture by thin layer chromatography (tlc) showed unreacted starting material, it was assumed therefore that the reaction would not proceed any further. The reaction was stopped to avoid potential decomposition of the product in acidic conditions. The ¹H NMR spectrum of the isolated β-hydroxy hydroperoxide **148a** contained a single methoxy signal at δ3.35 indicating it had been formed as a single diastereoisomer.

It is well known that epoxide ring opening in acidic conditions occurs via an S_N2-type mechanism where attack of the nucleophile takes place at the most hindered carbon centre.[71] By way of explanation, it has been suggested that the attack of hydrogen peroxide on the epoxide ring is restricted by steric interactions with axial hydrogen interactions as indicated *(Scheme 45)*. Epoxide **147ab** is not set up favourably for an S_N2 reaction. With the oxygen of the epoxide positioned equatorial, attack of the hydrogen peroxide by its preferred linear approach is hindered by axial hydrogens. Epoxide **147aa** is better set up for an S_N2 reaction. With the oxygen of the epoxide positioned axial the attack of the hydrogen peroxide is less sterically hindered.

147aa

147ab
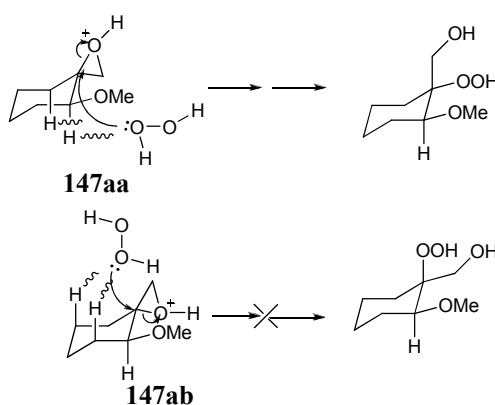
Scheme 45

As an alternative to the use of sulfuric acid, it has been reported that the complex $MoO_2(acac)_2$ can catalyse the perhydrolysis of unsubstituted *spiro*-epoxides giving the β-hydroxy hydroperoxide in good yields.[78] In an attempt to increase the yield of β-hydroxyhydroperoxide **148a**, $MoO_2(acac)_2$ was used as a catalyst in the perhydrolysis of epoxide **147a**. $MoO_2(acac)_2$ catalyst was used at the 5 mol% level with extended reaction times of 16-18 hours. Similar to the acid-catalysed epoxide ring opening, the reaction involves the use of a five-fold excess of hydrogen peroxide. By this method, three products were formed from epoxide **147a** at R_f 0.80, 0.46, and 0.40 on tlc analysis.

Each of the components was separated using column chromatography on silica gel. The component at R_f 0.80 was collected by elution with 1:1 ethyl acetate: light petroleum. Since this component had a similar R_f to epoxide **147a** it was initially thought to correspond to unchanged starting material, however, the component gave a positive result in a peroxide test (produced a pink spot on treatment with a peroxide detector spray).[148] The ^1H NMR spectrum showed additional prominent signals at δ1.60, δ2.48

and δ8.90 which corresponded to an additional product. On removal of solvent, the resulting oil partially crystallised as colourless plates on prolonged storage at 0°C. A suitable crystal was picked out and subjected to X-ray crystallographic analysis which revealed surprisingly that the solid was the *bis*-hydroperoxy peroxide **153** *(Figure 3)*. The synthesis of *bis*-hydroperoxy peroxide **153** had already been reported by the acid-catalysed reaction between acetylacetone and hydrogen peroxide.[149]
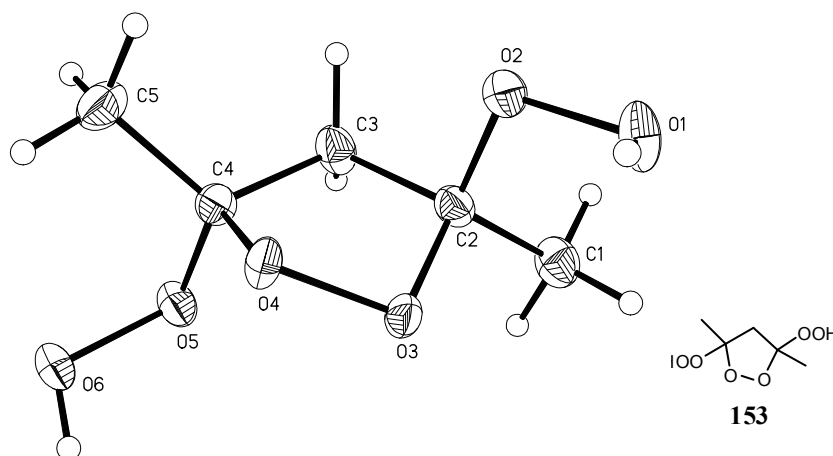
*Figure 3: X-ray crystal structure of **153** (Ortep, 50% probability ellipsoids for non hydrogen atoms)*[150]

The additional signals in the ^{1}H NMR spectrum can now be attributed to a CH_3 group at δ1.60, a CH_2 at δ2.48 and hydroperoxy hydrogen at δ8.90 in *bis*-hydroperoxy peroxide **153**. This suggests that an acac ligand from the Mo catalyst must have been displaced at some point during the reaction. *Bis*-hydroperoxy peroxide **153** would then have been formed through reaction with three molecules of hydrogen peroxide. The structure of **153** shows C_2 symmetry and confirms the *trans*-relationship between the hydroperoxy groups. Due to the unstable nature of the *bis*-hydroperoxy peroxide **153,** the sample was immediately destroyed after isolation.

Further elution of the column with 1:1 ethyl acetate: light petroleum yielded the component at R_f 0.46. Complete separation of the components at R_f 0.46 and 0.40 was not always possible. Mixed fractions of both components could be resolved by further column chromatography. The component at R_f 0.46 gave a positive result from a peroxide test and was at first thought to be the alternative diastereoisomer of **148a**. Although the ^{1}H and ^{13}C NMR spectra showed all the signals associated with β-hydroxy hydroperoxide **148a**, the chemical shifts were significantly different to those observed for **148a**. In particular, large differences in the chemical shifts of the quaternary carbon

and the -CH$_2$O- group suggested that they were in completely different chemical environments from the corresponding positions on **148a**. Detailed analysis of the ^{1}H and ^{13}C NMR spectra indicates that the regioisomer **154a** has been formed in 8% yield from the epoxide **147a** instead of the other diastereoisomers of **148a**.

148   **154**
R= H, Me, OMe, OEt   **R= OMe, OEt**
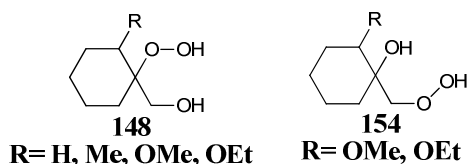
Further elution with 1:1 ethyl acetate: light petroleum yielded the component at R$_f$ 0.40. The component gave a positive result in a peroxide test and came at the same R$_f$ as the β-hydroxy hydroperoxide **148a** synthesised using sulfuric acid catalysis. On removal of solvent and isolation of the product, spectroscopic analysis confirmed the formation of β-hydroxy hydroperoxide **148a** in 34% yield. As previously observed with sulfuric acid-catalysed epoxide ring opening, the β-hydroxy hydroperoxide **148a** was obtained as a single diastereoisomer. The reaction yield was possibly higher because of the appearance of an additional band *ca.* R$_f$= 0.20 which was probably diol from the decomposition of **148a** and **154a** during the reaction work-up and purification.

On monitoring the Mo-catalysed perhydrolysis reaction by tlc, it was found that both isomers are formed simultaneously after *ca.* one hour. Although it has been expected that MoO$_2$(acac)$_2$ was acting as a Lewis acid promoting regioselective attack at the most hindered carbon centre, the synthesis of **154a** indicates that the epoxide ring has also been opened at the least hindered carbon centre. This had never been observed with perhydrolysis reactions catalysed by H$_2$SO$_4$.

This alternative acid-catalysed epoxide ring opening is not without further examples. The unsubstituted epoxide **147d** reacted in deuterated chloroform, which is known to contain small quantities of deuterated hydrochloric acid, over a long period to form large clear glass-like crystals *(Scheme 46)*. A suitable crystal was picked out and subjected to X-ray crystallographic analysis which revealed that the solid was halohydrin **155** *(Figure 4)*. The X-ray crystal structure confirmed that chloride had opened the ring at the least hindered position and mass spectrometry confirms the presence of deuterium and chlorine in the molecule.
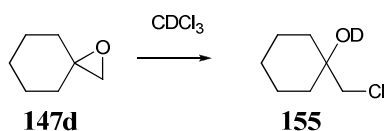
Scheme 46
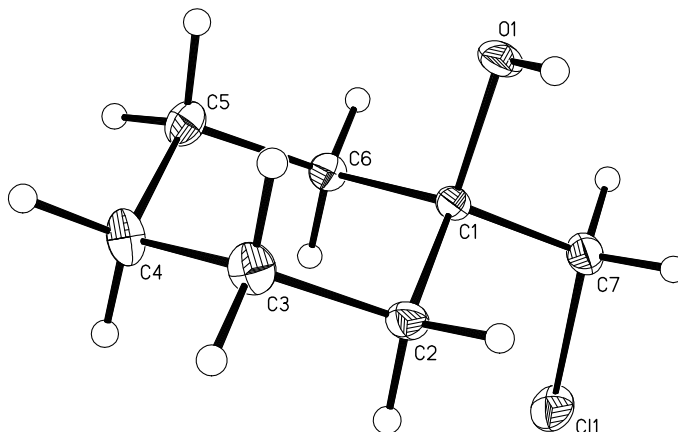
*Figure 4: X-ray crystal structure of **155** (Ortep, 50% probability ellipsoids for non hydrogen atoms)[150]*

To try to further understand the reasons for the formation of the unexpected products **154a** and **153,** the reaction of epoxides **147b,c,d** with excess hydrogen peroxide in the presence of $MoO_2(acac)_2$ was further investigated. The reaction of epoxide **147b** forms three products at R_f 0.80, 0.55, and 0.50 on tlc. Each of the components was separated using column chromatography on silica gel. The component at R_f 0.8 gave a positive peroxide test and when collected by elution with 1:1 ethyl acetate: light petroleum was again shown to be *bis*-hydroperoxy peroxide **153**.

Further elution of the column with 1:1 ethyl acetate: light petroleum yielded the components at R_f 0.55 and 0.50 as a mixture. Although further purification by column chromatography was attempted, the mixture proved to be inseparable. On removal of solvent and isolation of the product the ^1H and ^{13}C NMR spectra showed significant evidence for the formation of both **148b** and **154b**. Although the spectroscopic data was difficult to interpret due to a number of overlapping signals, signals indicative of both compounds, in particular for the -CH_2OH group, were evident in the spectrum.

The Mo-catalysed perhydrolysis of epoxides **147c** and **147d** produced one major component at R_f 0.40 and 0.42 respectively by tlc analysis. There was no indication of

47

the formation of either the *bis*-hydroperoxy peroxide **153** or the alternative regioisomer **154** in either case. These components were purified using column chromatography on silica gel eluting with 1:1 ethyl acetate: light petroleum. On removal of the solvent, spectroscopic analysis confirmed the formation of the known β-hydroxy hydroperoxides **148c** and **148d** in 85% and 73% yield respectively. The ring openings of the epoxides **147a-d** all produce high yields of the corresponding β-hydroxy hydroperoxide **148a-d** in the presence of $MoO_2(acac)_2$ catalyst. The replacement of the sulfuric acid catalyst with $MoO_2(acac)_2$ gives a considerable increase in the yield of β-hydroxy hydroperoxide **147a** and **147c** *(Table 3)*.

	Catalyst	148/ %	154/ %
147a	H_2SO_4	8	0
	$MoO_2(acac)_2$	34	9
147b	$MoO_2(acac)_2$	Inseparable mixture[#]	
147c	H_2SO_4	47[146]	-
	$MoO_2(acac)_2$	85	-
147d	H_2SO_4	64[145]	-
	$MoO_2(acac)_2$	73	-

Table 3: Yields for perhydrolysis reaction using acid and $MoO_2(acac)_2$ catalyst

*# 33.2 % yield for **147b** and **154b**. Doublet at δ4.39, J= 14.1 is indicative of **154b***

As well as a large increase in yield of β-hydroxy hydroperoxide **148c** from epoxide **147c,** the β-hydroxy hydroperoxide **148c** product was also cleaner. In previous syntheses of β-hydroxy hydroperoxide **148c**, using sulfuric acid-catalysed epoxide ring opening, the product was isolated as an oil, whereas using $MoO_2(acac)_2$ catalyst and the same method of purification β-hydroxy hydroperoxide **148c** was isolated as a colourless low melting solid (m.p. 48 °C). Recrystallisation of **148c** from diethyl ether/ light petroleum gave large, plate-shaped, colourless crystals suitable for X-ray crystallographic analysis.

X-ray crystallographic analysis confirmed that the solid was **148c** and interestingly the orientation of both the methyl group and the peroxide oxygens were *trans*-diaxial with the hydroxyl methyl group in a equatorial position *(Figure 5)*.
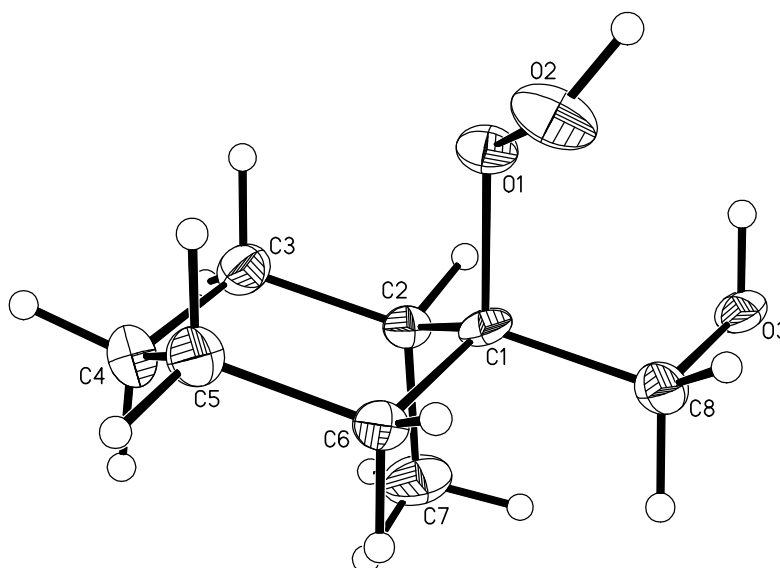
*Figure 5: X-ray crystal structure of **148c** (Ortep, 50% probability ellipsoids for non hydrogen atoms)[150]*

From the structure of **148c**, the stereochemistry of the epoxide **147c**, which has reacted to form β-hydroxy hydroperoxide **148c**, can be definitively assigned as epoxide **147ca**. *(Scheme 47)*. Nucleophilic attack of hydrogen peroxide on **147ca** would be more favourable due to the axial leaving group and the axial hydrogens in **147cb** causing steric hindrance. The β-hydroxy hydroperoxide from this preferred reaction must perform a ring inversion moving the methyl and hydroperoxy groups into axial positions in the solid state.

Scheme 47
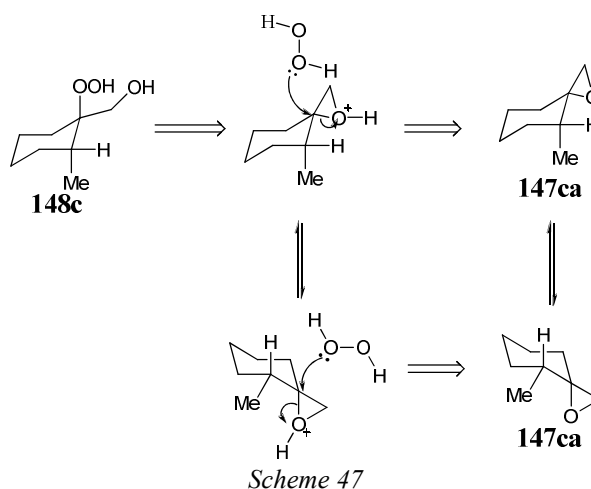
The compound has also crystallised in the uncommon space group of P3(2). This is a three-fold screw axis in which groups of three molecules are held together by a tight network of hydrogen bonding interactions. Each molecule is hydrogen bonded to four other molecules via two short interactions and one long interaction.
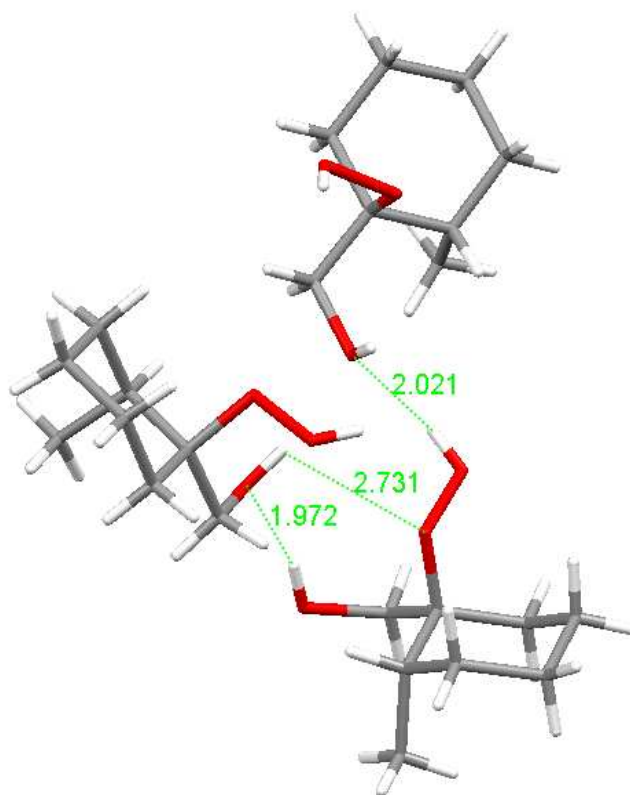
*Figure 6: Crystal packing of **148c** indicating three different H-bonds*

The two short interactions are between OH⋯OH of 1.972 Å (O⋯O= 2.769(5) Å) and OOH⋯OH of 2.021 Å (O⋯O= 2.759(5) Å) and the long interaction is between HOO⋯HO of 2.731 Å (O⋯O= 3.063(10) Å) *(Figure 6)*. Interestingly the methyl substituent is situated at the furthest point away from any of the hydrogen bonding network. Looking down the *c*-axis of the crystal structure at the mosaic pattern of hydrogen bonds demonstrates how the molecules have packed maximising all possible intermolecular interactions allowing the solid structure *(Figure 7)*.
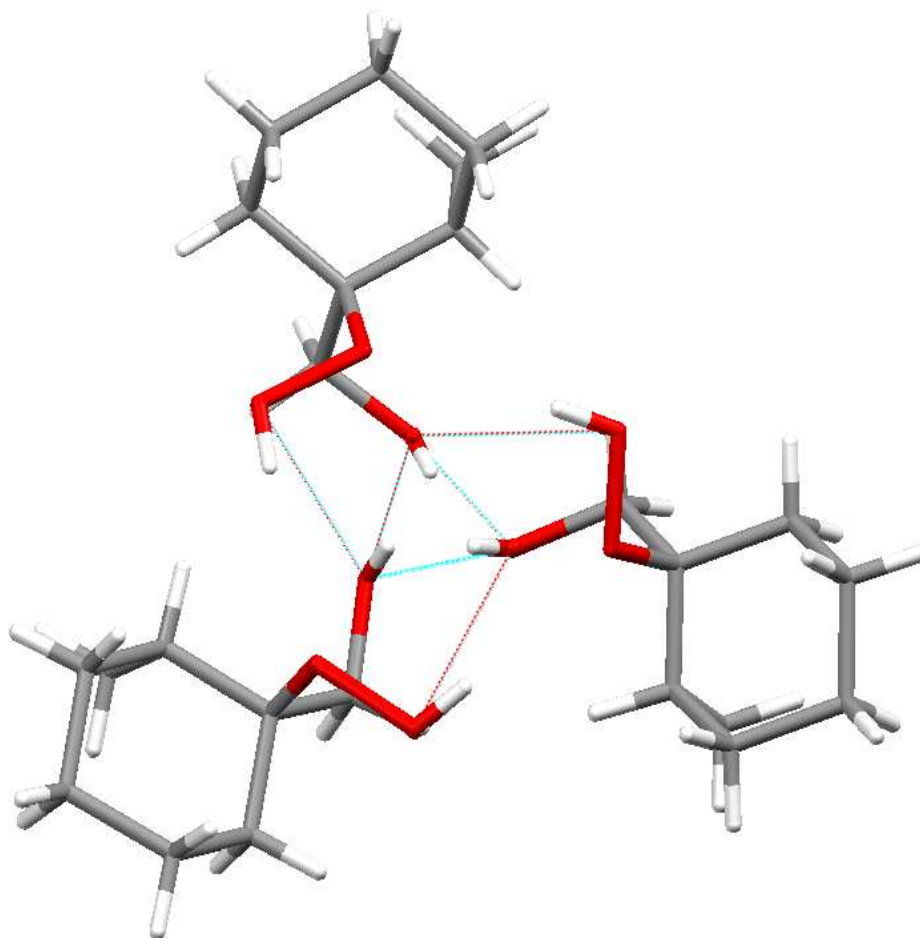
*Figure 7: Crystal packing of **148c** looking down the middle of 3-fold screw axis
showing H-bond network*

It is interesting to note that in the crystal structure of the trisubstituted perhydrate **156**, derived from α-bromocyclohexanone (**157**) and hydrogen peroxide, the molecule adopts a conformation with one axial group and two equatorial groups *(Scheme 48)*.[151] This is expected in order to give the fewest possible axial substituents. It may be that the hydrogen bond network in **140c** overcomes any disadvantages in having two axial substituents and one equatorial.

Scheme 48

51
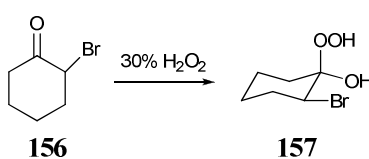
From the nature of the products obtained from the Mo-catalysed perhydrolysis of epoxides **147a-d**, it is clear that different mechanisms are operating. For epoxides **147c,d**, the Mo-catalyst is behaving in a similar manner to the sulfuric acid and promoting the highly regioselective formation of the corresponding β-hydroxy hydroperoxides **148c,d**; the other regioisomers **154c,d** have not been observed or isolated in sufficient quantities. The formation of regioisomer **154a,b** together with the *bis*-hydroperoxy peroxide **153** in the reaction of **147a,b** suggests that the oxygen from the alkoxy substituent plays a vital role in the perhydrolysis leading to **154a,b** *(Scheme 49)*.
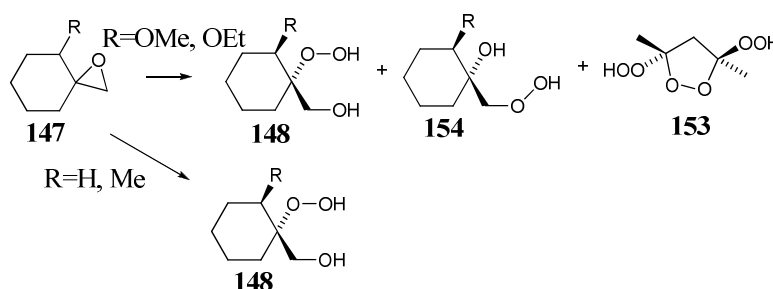
Scheme 49

Since the *bis*-hydroperoxy peroxide **153** is obviously derived from acetylacetone, the oxygen substituent may be responsible for the displacement of one of the acac ligands from the Mo catalyst. Assuming that the acac group is cleaved from the catalyst in the active species, one possible explanation is that the epoxide acts as a bidentate ligand by displacing one of the acac ligands **158** *(Scheme 50)*. This species may then be more susceptible to nucleophilic attack at the least hindered centre. It is not possible at this stage to distinguish which of the diastereoisomers of epoxide **147a,b** react to form each of the β-hydroxy hydroperoxide regioisomers **148a,b** and **154a,b**. X-Ray crystallographic analysis of corresponding *dispiro*-1,2,4-trioxanes will resolve this question (*vide infra*) .
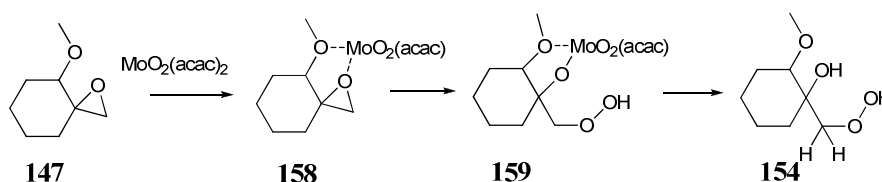
Scheme 50

NMR analysis of β-hydroxy hydroperoxides 148a,b and 154a,b

Previous ^{1}H NMR analysis of β-hydroxy hydroperoxides **148c,d** showed that the most distinguishable signals in the spectrum are for the diastereotopic hydroxymethyl group which gives two doublets at *ca.* δ3.5. It was found that the regeoisomeric β-hydroxy hydroperoxides **148a** and **154a** show enough significant differences in their respective ^{1}H and ^{13}C NMR spectra to unambiguously assign which regioisomer has been formed *(Table 4)*. The ^{1}H NMR spectrum of β-hydroxy hydroperoxide **148a** has two sets of doublets at δ3.75 and δ3.95 with a ^2J coupling constant of 12.0 Hz and a carbon signal at δ63.0 in the ^{13}C NMR spectrum for the diasterotopic hydroxymethyl group *(Figure 8)*. In contrast, the ^{1}H NMR spectrum of β-hydroxy hydroperoxide **154a** has a set of two doublets much wider apart, further down-field and a larger ^2J value than that seen in **148a**. The ^{1}H NMR signals at δ3.95 and δ4.45 with ^2J 14.0 Hz and a ^{13}C NMR signal at δ80.0 show that the peroxide group is more highly de-shielding than a hydroxide group *(Figure 9)*. This effect on the chemical shifts in the ^{1}H and ^{13}C NMR spectrum for a hydroxide versus peroxide is documented in the literature.[152]
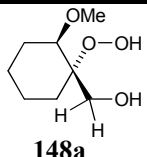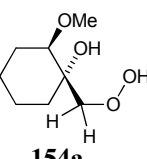
		$CH_2OOH/$ δ	$qC/$ δ	$CH/$ δ	$CH_3/$ δ
OMe O—OH OH H H **148a**	[1]H	3.75, d, J 12.0 3.95, d, J 12.0	-	3.45, m	3.35, s
	[13]C	63.0	84.4	80.1	57.1
OMe OH OH O H H **154a**	[1]H	3.95, d, J 14.0 4.45, d, J 14.0	-	3.20, m	3.45, s
	[13]C	80.0	74.4	84.9	57.7

Table 4: δ values (ppm) and coupling constants (J) for ^{1}H and ^{13}C NMR data of 148a, and 154a

There were similar changes evident for other sections of the molecule by ^{1}H and ^{13}C NMR spectral analysis. Of particular interest is the quaternary carbon shifting up-field from δ84.7 in **148a** to δ74.4 in **154a**. This further highlights the effective difference of a hydroxy to a peroxy substituent. Other smaller differences show a slight downfield shift from δ80.1 in **148a** to δ84.9 in **154a** for the CH group. This is matched in the ^{1}H NMR spectrum where the CH multiplet moves upfield from δ3.45 in **148a** to δ3.20. The signals for the OCH$_3$ group show no change in the chemical shift in the ^{13}C NMR spectrum however there is a slight downfield shift in the ^{1}H spectrum from δ3.35ppm in

148a to δ3.45 in **154b**. Similar but less apparent effects were seen for the mixture of regioisomers **148b** and **154b**. Since β-hydroxy hydroperoxides **148b** and **154b** could not be separated efficiently by conventional column chromatography, definitive ^{1}H and ^{13}C NMR spectra were not obtained for the compounds. However the ^{1}H NMR spectrum of the mixture, an additional doublet at δ4.4, ^2J 14.1, indicated the presence of **154b** *(Figure 10)*. In general, the mixture was reacted further without purification.
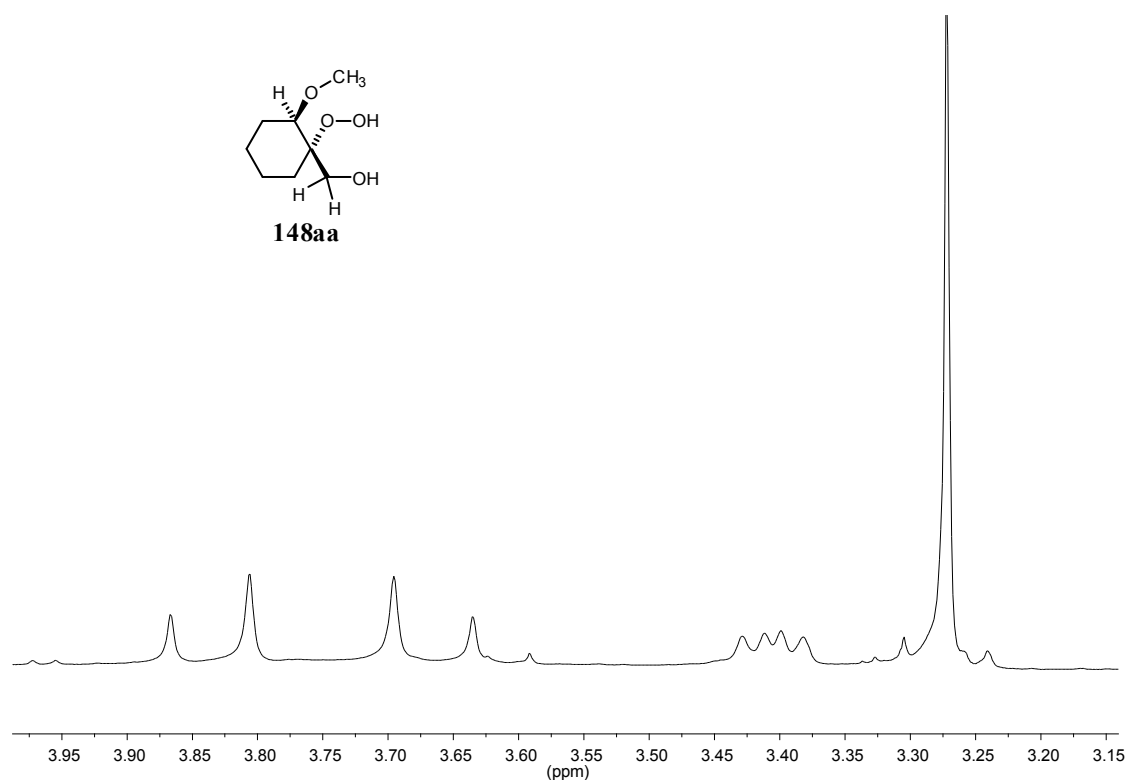
*Figure 8: ^{1}H NMR spectra for **148aa***
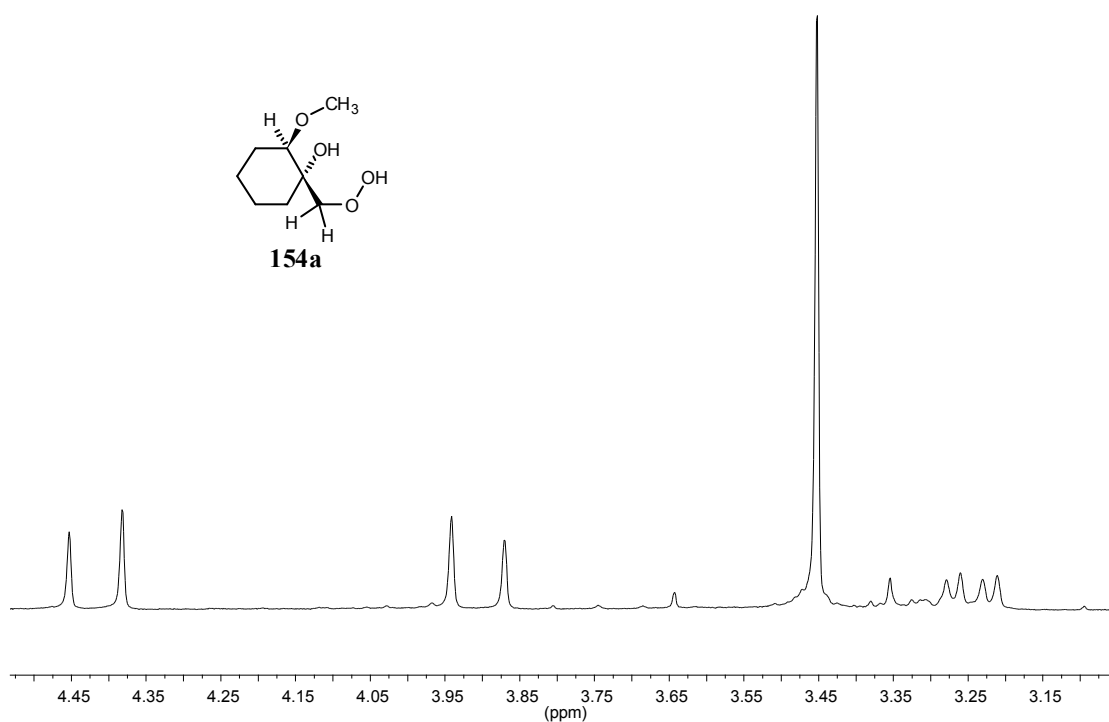
*Figure 9: ¹H NMR spectra for **154a***
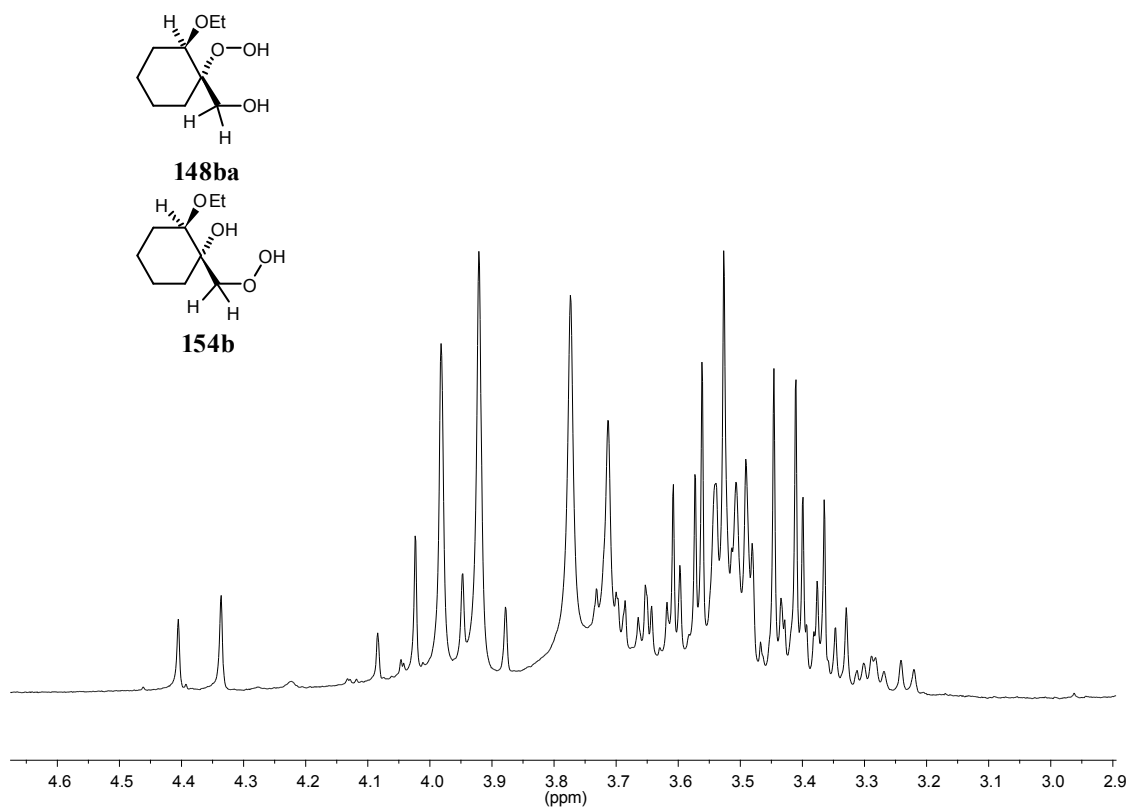
*Figure 10: ¹H NMR spectra for **148ba**, **154b***

55

Dispiro-1,2,4-trioxane synthesis

The final step in the synthesis of *dispiro*-1,2,4-trioxanes is the condensation of an appropriate cyclic ketone into β-hydroxy hydroperoxides **148a,b**. The availability of β-hydroxy hydroperoxides **154a,b** also provided the opportunity to form structurally novel *dispiro*-1,2,4-trioxanes **160a,b** via the same route *(Scheme 51)*.

148a, R= OMe   **149a, R= OMe**
148b, R= OEt   **141b, R= OEt**

154a, R= OMe   **160a, R= OMe**
154b, R= OEt   **160b, R= OEt**

$R^1, R^2=$ a= -$(CH_2)_5$-
b= -$(CH_2)_4$-
c= -$(CH_2)_6$-
d= -$(CH_2)_{11}$-
e= -$(CH_2)_2CO(CH_2)_2$-
f= 1,4-dioxaspiro[4.5]decylidene
g= indanylidene
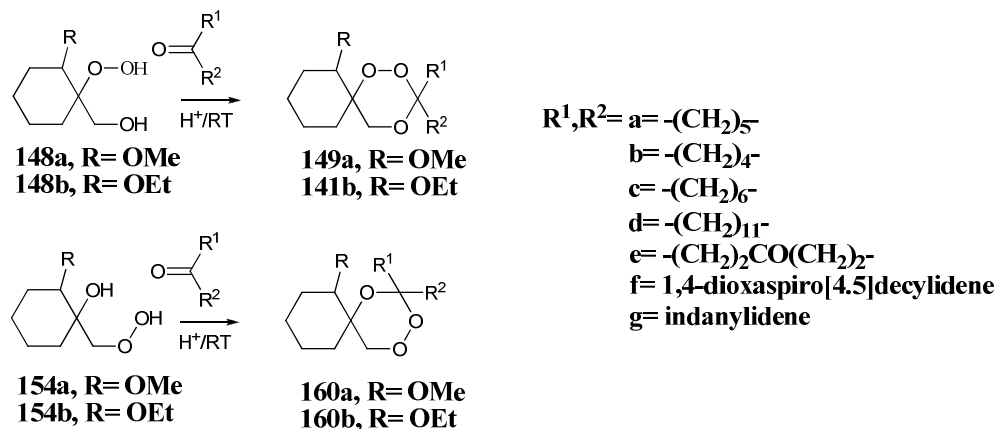
Scheme 51

The condensation reaction takes place with the addition of the relevant cyclic ketone (1.5 eq.) to a cooled solution (-5 °C) of the β-hydroxy hydroperoxide in dry dichloromethane (DCM). The reaction is catalysed by tosic acid and left to stir for 18-20 hours at room temperature. The reaction was monitored by tlc by the disappearance of the low R_f β-hydroxy hydroperoxide fraction on with the simultaneous appearance of a new spot at higher R_f.

Condensation of cyclic ketones with β-hydroxy hydroperoxides 140a and 145a

Although β-hydroxy hydroperoxide **148a** and **154a** could be separated as described above, it was often convenient to carry out the condensation reaction using the mixture. From the condensation reaction with cyclohexanone, two components were obtained with R_f 0.30 and 0.25 by tlc analysis which were both peroxidic. Although the components at R_f 0.30 and 0.25 are close together by tlc analysis, each of the components was separated readily using column chromatography eluting with 1:25 ethyl acetate: light petroleum. Fractions corresponding to component at R_f 0.30 were collected as a viscous oil. Upon storage at 0°C, the collected oil formed a low melting point solid. The melting point was thought to be around room temperature because it

melted on prolonged exposure to ambient temperatures. The position of the –CH$_2$O-signal in the ^{1}H NMR spectrum was similar to that seen for β-hydroxy hydroperoxide **154a** indicating the product was derived from this regioisomer. The solid was recrystallised from ethanol to form crystals suitable for X-ray crystallography. Careful handling of the crystals was required in order to prevent the melting of the crystals during transportation and before being positioned in the cooled (160 K) N$_2$ gas stream of the X-ray diffractometer. Following data collection and refinement X-ray crystallographic analysis of the crystals revealed the formation of *dispiro*-1,2,4-trioxane **160aa** as illustrated in *Figure 11*. To our knowledge this is this first reported trioxane of this type. It is clear that this particular *dispiro*-1,2,4-trioxane is derived from β-hydroxy hydroperoxide **154a** rather than **148a**. The overall yield of **160aa** was 4.4% from epoxide **147a**.
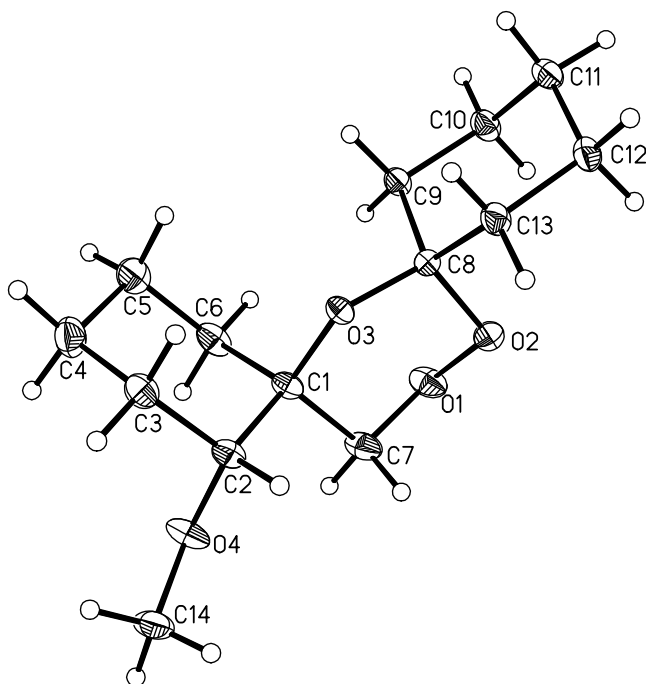
*Figure 11: X-ray crystal structure of **160aa** (Ortep, 50% probability ellipsoids for non hydrogen atoms)[150]*

After removal of solvent from the fractions corresponding to R$_f$ 0.25 the component was obtained as an oil. The position of the –CH$_2$O- signal in the ^{1}H NMR spectrum was similar to that seen for β-hydroxy hydroperoxide **148a** indicating the product was derived from this regioisomer. Detailed analysis of the ^{1}H and ^{13}C NMR spectra showed that *dispiro*-1,2,4-trioxane **149aa** had been obtained. The overall yield was 9.4% from the epoxide **147a**.

Similarly the condensation of cyclopentanone with the mixture of β-hydroxy hydroperoxide **148a** and **154a** resulted in two peroxide containing components at R$_f$ 0.30 and 0.25 respectively by tlc. Each of the components was separated readily using column chromatography on silica gel eluting with 1:25 ethyl acetate: light petroleum. Following the removal of solvent the fraction at R$_f$ 0.30 was isolated as an oil. Upon storage at 0°C the collected oil formed a low melting point solid. The solid was recrystallised using ethanol to form crystals suitable for X-ray crystallography. X-ray crystallographic analysis of the crystals revealed the formation of *dispiro*-1,2,4-trioxane **160ab** as illustrated in *Figure 12*. The overall yield of **160ab** was 7.1% from epoxide **147a**.
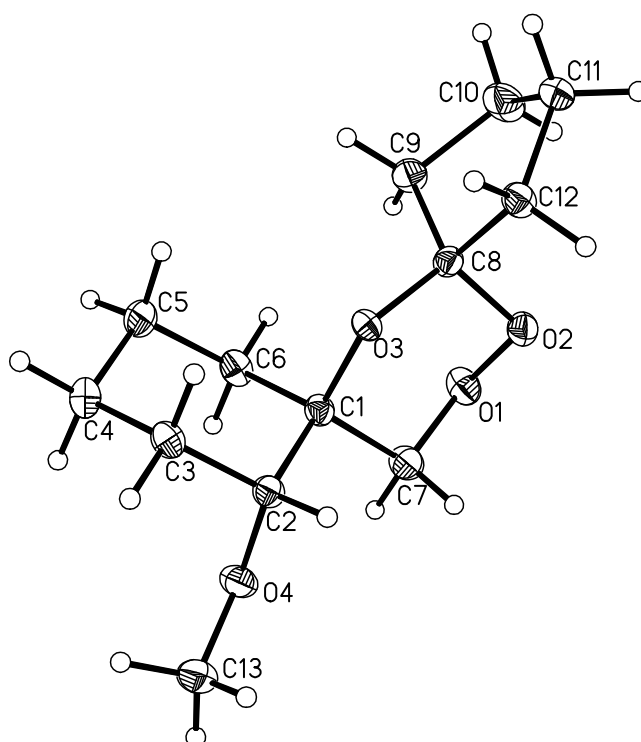
*Figure 12: X-ray crystal structure of **160ab** (Ortep, 50% probability ellipsoids for non hydrogen atoms)[150]*

The fractions corresponding to the component at R$_f$ 0.25 were collected and upon removal of the solvent gave an oil. Detailed analysis of the ^{1}H and ^{13}C NMR spectra was consistent with the formation of *dispiro*-1,2,4-trioxane **149ab** (10.5% yield from the epoxide **147a**).

The reaction of cycloheptanone with the mixture of β-hydroxy hydroperoxide **148a** and **154a** resulted in the formation of only one component with R$_f$ 0.30 by tlc. The component purified using column chromatography on silica gel eluting with 1:25 ethyl

acetate: light petroleum and isolated as an oil. Detailed analysis of the ^{1}H and ^{13}C NMR spectra indicates that *dispiro*-1,2,4-trioxane **149ac** has been formed (7.4% yield form the epoxide **147a**). No isolatable quantities of product derived from the reaction of regioisomer **154a** were obtained.

Subsequent attempts to condense ring sizes greater than six into pure samples of β-hydroxy hydroperoxides **154a,b** yielded none of the expected *dispiro*-1,2,4-trioxane **160ac**. Previous work had reported difficulties in condensing cyclooctanone into β-hydroxy hydroperoxides.[146]

Further condensation to form methoxy-substituted *dispiro*-1,2,4-trioxanes involved β-hydroxy hydroperoxides which had been separated into regioisomers **148a** and **154a**. Using the same method described above, cyclododecanone was successfully condensed with β-hydroxy hydroperoxide **148a** to produce *dispiro*-1,2,4-trioxane **149ad** in 7.3% overall yield from the epoxide.

Unfortunately attempts to purify *dispiro*-1,2,4-trioxane **149ag** following the condensation of a 2-indanone into the β-hydroxy hydroperoxide **148a** were unsuccessful. Although the expected signals for the *dispiro*-1,2,4-trioxane were present, extra signals in the ^{13}C NMR spectra demonstrated that it was impure. As purification of **149ag** was unsuccessful, the *dispiro*-1,2,4-trioxane was reacted further without characterisation.

In early condensation reactions, other products had also been isolated from the reaction of cyclohexanone, cyclopentanone and cycloheptanone with a mixture of β-hydroxy hydroperoxide **148a** and **154a**. From the condensation of cyclohexanone with **148a** and **154b** an additional low lying intense component was present at R_f 0.15 by tlc. The fractions corresponding to the component at R_f 0.15 were combined and upon removal of solvent were collected as a colourless semi-solid. Trituration of this semi-solid using light petroleum formed large crystals. A suitable crystal was picked out and subjected to X-ray crystallographic analysis which revealed surprisingly that the solid was *bis* hydroperoxy peroxide **161** *(Figure 13)*. The X-ray crystal structure of **161** had previously been reported by P. Groth *et. al.* using less accurate photographic collection methods.[153] The new X-ray crystal structure shows some differences in intramolecular and intermolecular hydrogen bonds involving the peroxy groups.
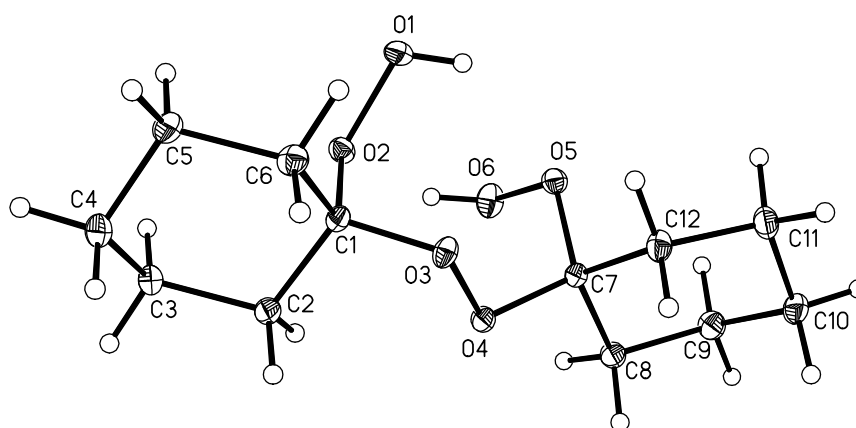
*Figure 13: X-ray crystal structure of **161** (Ortep, 50% probability ellipsoids for non hydrogen atoms)[150]*

The synthesis of **161** indicates that hydrogen peroxide has been collected alongside the β-hydroxy hydroperoxide in the isolation of **148a**. The residual hydrogen peroxide has reacted with an excess of cyclohexanone to form **161**. Similar products were also formed through the condensation of the contaminated β-hydroxy hydroperoxide **148a** and **154a** mixture with cyclopentanone and cycloheptanone. These products were again titrated with light petroleum to give crystals suitable for X-ray crystallography. Similar to the structure of **161** the product derived from cyclopentanone was shown to be *bis* hydroperoxy peroxide **162** *(Figure 14)* whilst the product derived from cycloheptanone was shown to be *dispiro*-1,2,4,5-tetroxane **163** *(Figure 15).* The crystal structure of **163** had previously been determined by P. Groth *et. al.* using photographic collection methods.[154]
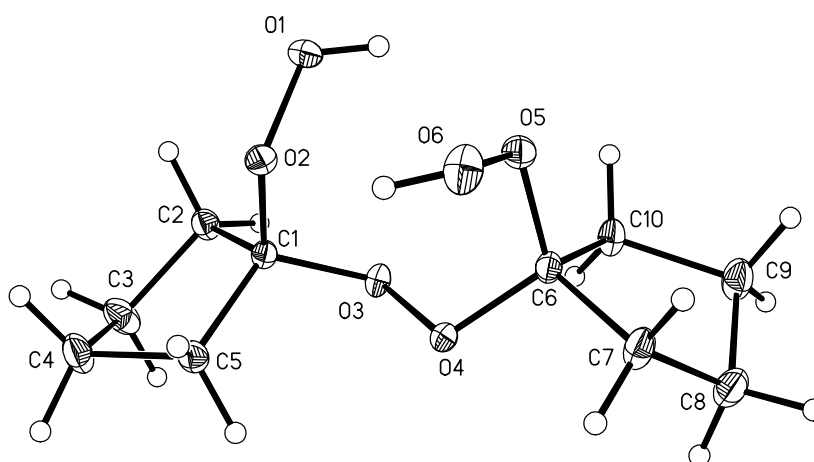
*Figure 14: X-ray crystal structure of **162** (Ortep, 50% probability ellipsoids for non hydrogen atoms)[150]*
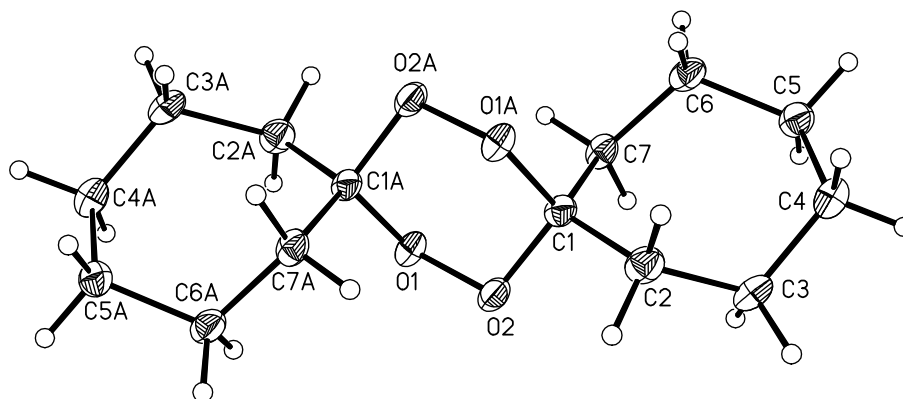
*Figure 15: X-ray crystal structure of **163** (Ortep, 50% probability ellipsoids for non hydrogen atoms)[150]*

More care was taken in future isolation of the β-hydroxy hydroperoxides with more extensive washing of the product to remove any unreacted hydrogen peroxide. Future condensation using non-contaminated β-hydroxy hydroperoxides **148a** and **148b** gave no isolable quantities of compounds like **161-163**.

Condensation of cyclic ketones with β-hydroxy hydroperoxides 148b and 154b

Since β-hydroxy hydroperoxides **148b**, **154b** could not be readily separated the condensation reactions were carried out using a mixture. Thus the β-hydroxy hydroperoxide **148b**, **154b** were reacted by acid-catalysed condensation using a series of cyclic ketones which formed *dispiro*-1,2,4-trioxanes which were more readily separable. The condensation of cyclohexanone with β-hydroxy hydroperoxides **148b**, **154b** formed two peroxidic components which were very close together by tlc analysis with R_f 0.30 and 0.27. Although attempts to separate the components using column chromatography on silica gel were at first unsuccessful, successive band shaving of the fractions provided a pure samples of *dispiro*-1,2,4-trioxane **149ba** (R_f 0.27) in 7.9% yield from the epoxide **147b**. Similarly isolation of the fraction at R_f 0.30 isolated a product in 4.3% yield from epoxide **147b**. Detailed NMR analysis of this fraction indicated that *dispiro*-1,2,4-trioxane **160ba** was contaminated by small amounts of *dispiro*-1,2,4-trioxane **148ba.** Repeated column chromatography did not significantly improve the purity of this trioxane.

Although separation of regioisomers **149ba** and **160ba** was not completely successful, the regioisomers from the condensation of cyclopentanone and β-hydroxy

61

hydroperoxides **148b** and **154b** were readily separated. Thus by careful combination of appropriate column fractions, pure samples of both regioisomers **149bb** (R_f 0.30) and **160bb** (R_f 0.35) were obtained as oils in 13.4% and 1.0 % yields from their corresponding epoxides.

The acid-catalysed reaction of cycloheptanone with the mixture of β-hydroxy hydroperoxides **148b** and **154b** resulted in the formation of only one component at R_f 0.30 by tlc. The component at R_f 0.30 was collected by elution with 1:50 ethyl acetate: light petroleum initially as an oil in 9.8% yield from epoxide **147a**. Trituration of the oil using light petroleum afforded crystals of the product which were suitable for X-Ray crystallography. X-Ray crystallographic analysis confirmed that the structure of the solid product was the expected *dispiro*-1,2,4-trioxane **149bc** rather than the regioisomer **160bc** *(Figure 16).*
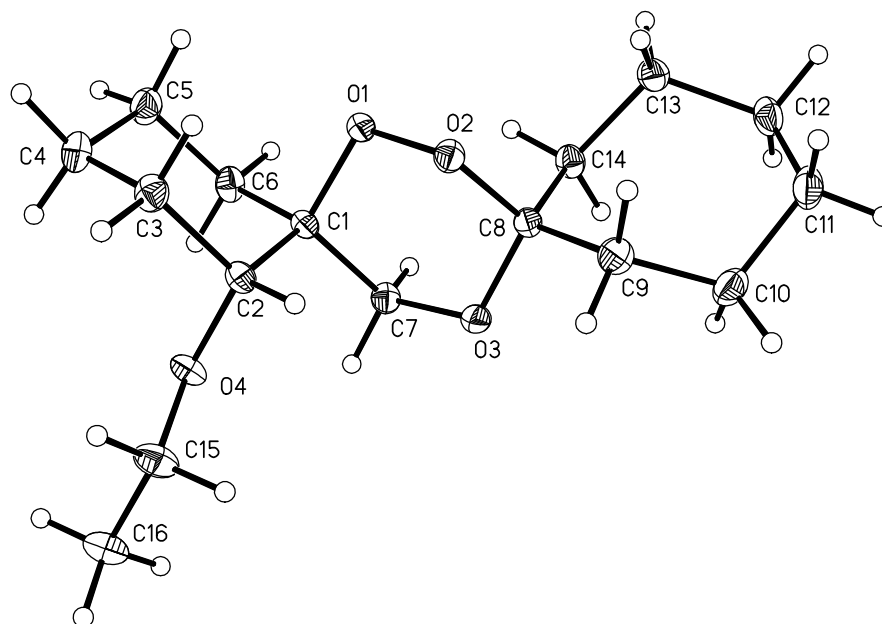
*Figure 16: X-ray crystal structure of **149bc** (Ortep, 50% probability ellipsoids for non hydrogen atoms)[150]*

Since no isolatable quantities of *dispiro*-1,2,4-trioxane **160bc,** derived from the reaction of regioisomer **154b** with cycloheptanone, were obtained, this reinforced the conclusion that cyclic rings with ring sizes greater than six are incapable of reacting with β-hydroxy hydroperoxide **154a,b**.

Using the same method described above, cyclododecanone was successfully condensed with β-hydroxy hydroperoxide **148b** to produce *dispiro*-1,2,4-trioxane **149ad** in 2.9% yield from the epoxide **147a**.

In contrast to the reaction of β-hydroxy hydroperoxide **148a** with 2-indanone which gave an impure product, the condensation of 2-indanone with **148b** formed the *dispiro*-1,2,4-trioxane **149bg** cleanly in 1.7% yield from epoxide **147a**. Although *dispiro*-1,2,4-trioxane **149bg** was initially isolated as an oil, trituration with light petroleum gave the *dispiro*-1,2,4-trioxane **149bg** as a crystalline solid. Crystals suitable for X-ray crystallographic analysis were grown using a diethyl ether: light petroleum mixture. X-Ray crystallographic analysis confirmed the formation of the expected *dispiro*-1,2,4-trioxane **149bg** as illustrated in *Figure 17*.
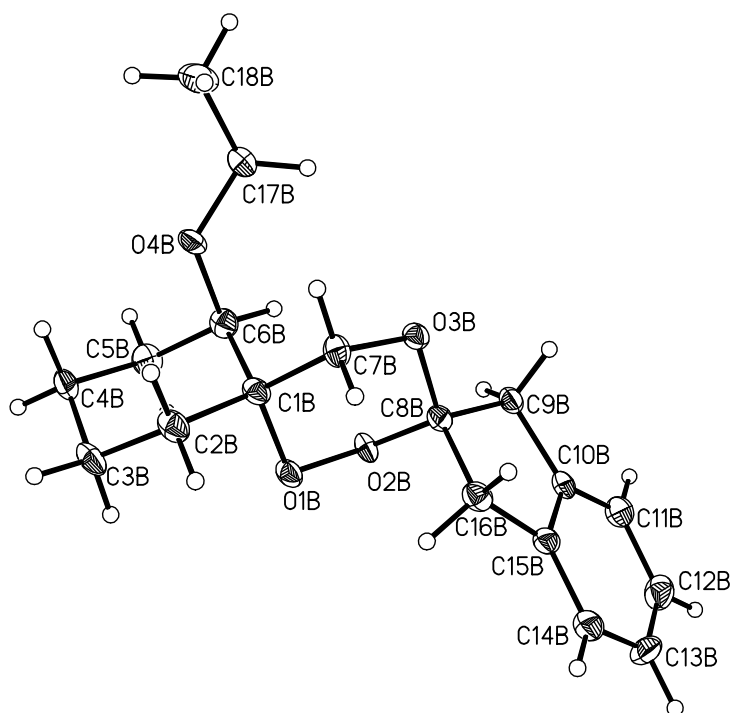
*Figure 17: X-ray crystal structure of **149bg** (Ortep, 50% probability ellipsoids for non hydrogen atoms)[150]*

Condensation of cyclohexane-1,4-dione with β-hydroxy hydroperoxide 140a,b and 145a,b

The *dispiro*-1,2,4-trioxane **149af,bf** derived from the condensation of cyclohexane-1,4-dione with β-hydroxy hydroperoxide **148a,b** was a further synthetic target. The additional functionality provides the opportunity to synthesise a more fuctionalised keto lactone from the thermolysis of *dispiro*-1,2,4-trioxane **149af,bf**. Despite previous successful condensation reactions of cyclohexane-1,4-dione with β-hydroxy hydroperoxide **148c**,[145] the corresponding reactions with β-hydroxy hydroperoxides **148a,b** and **154a,b** did not produce the desired *dispiro*-1,2,4-trioxane. As an alternative

approach, the condensation of β-hydroxy hydroperoxides **148a,b** and **154a,b** with the protected derivative 1,4-dioxa*spiro*[4,5]decan-8-one (**164**) followed by an acid-catalysed hydrolysis in acetone was investigated *(Scheme 52)*.
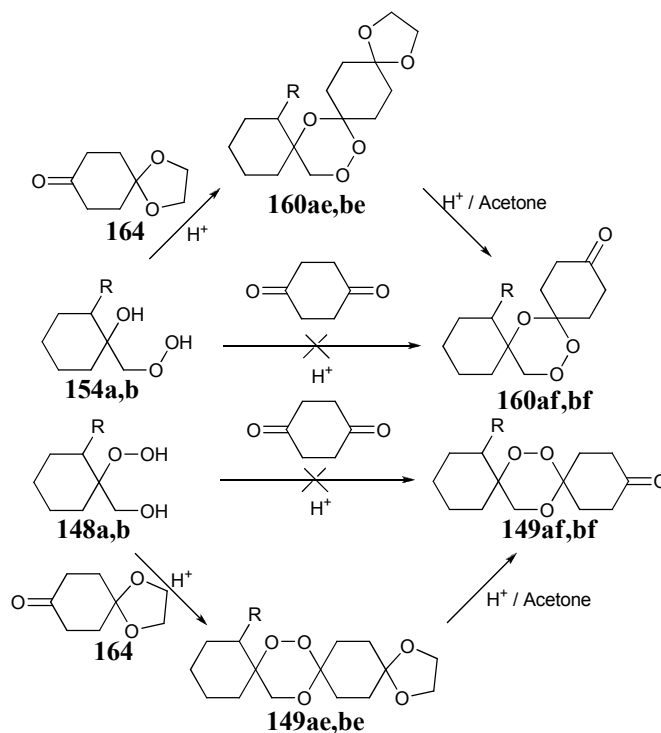
Scheme 52

The condensation reaction of 1,4-dioxa*spiro*[4,5]decan-8-one (**164**) with β-hydroxy hydroperoxide **148a** successfully produced the *dispiro*-1,2,4-trioxane **149ae** in 3.9 % yield from the epoxide. Since the *dispiro*-1,2,4-trioxane **149ae** was considerably more polar, it required a more polar solvent system e.g. 1:5 ethyl acetate: light petroleum for tlc analysis and column chromatography.

The condensation reaction of semi-protected diketone **164** with β-hydroxy hydroperoxide **154a** surprisingly gave a 5:2 mixture of the protected **160ae** and de-protected **160af**. In the ¹H NMR spectrum of the crude product mixture, two sets of two sharp doublets (δ3.89 and δ4.26 **160ae,** δ3.97 and δ4.35 **160af**) were observed for the trioxane methylene group and in the ¹³C NMR spectrum, there was a carbonyl signal at δ210 which would correspond to the carbonyl group carbon of **160af**. The formation of both **160ae** and **160af** suggests that reaction conditions used for the condensation reaction are favourable for the partial removal of the ketal group in **160ae**.

The condensation reaction of semi-protected ketone **164** with β-hydroxy hydroperoxide regioisomers **148b** and **154b** formed two components at R_f 0.40 and 0.29 by tlc. Both components were separated using column chromatography on silica gel eluting with 1:5 ethyl acetate: light petroleum. Following solvent removal, the component was collected as an oil. The ^{1}H NMR spectrum of the oil contained two sets of two sharp doublets (δ3.90 and δ4.28 **160be,** δ3.98 and δ4.37 **160bf**) for the trioxane methylene and in the ^{13}C NMR spectrum there was seen a carbonyl signal at δ210 which would correspond to the formation of **160bf**. This is consistent with the formation of a mixture of the *dispiro*-1,2,4-trioxane regioisomers **160be** and **160bf**. On further elution of the column the component at R_f 0.29 was collected as an oil. Although ^{1}H NMR spectroscopic analysis was not conclusive in the determination of the products, a carbonyl signal at δ210 in the ^{13}C NMR spectrum demonstrated the formation of **149be** and **149bf** as a mixture.

The complete de-protection of the *dispiro*-1,2,4-trioxanes **149be** and **160ae,be** was attempted using a tosic acid-acetone mixture with continuous stirring for 24 hours. However following the work-up of the reaction, **149be** and **160ae,be** were still present in each of their respective reactions indicating the difficulty of the hydrolysis. Further treatment with tosic acid in acetone for 24 hours produced the product in most cases however a mixture still existed in the case of **149bf.** Unfortunately the conditions used for the de-protection of the *dispiro*-1,2,4-trioxane **149ae** caused the complete degradation of the sample. To avoid further loss of **149ae** the *dispiro*-1,2,4-trioxane was reacted further without de-protecting the ketone.

The yields of all the *dispiro*-1,2,4-trioxanes synthesised are listed in *Table 5*. Although some of the *dispiro*-1,2,4-trioxanes were necessarily synthesised from mixtures of β-hydroxy hydroperoxides **148** and **154** rather than the pure β-hydroxy hydroperoxide, all the yields are reported from their corresponding epoxide **147a,b**. Yields for both the methoxy- and ethoxy- substituted *dispiro*-1,2,4-trioxanes were generally around the same with a small increase seen for the ethoxy compounds. The reaction yields for condensations involving **148a,b** are lower than previous condensations using **148c,d**. *(Table 5)*.[75,76] Lower yields for the reaction of **148a,b** may be due to steric restrictions associated with the alkoxy group preventing efficient condensation. None the less the formation of the methoxy- and ethoxy-substituted *dispiro*-1,2,4-trioxanes **149a,b** were adequate for thermolysis studies.

Compound	R= OMe		R= OEt	
	149aa	9.4	**149ba**	7.9
	149ab	10.5	**149bb**	13.4
	149ac	7.4	**149bc**	9.8
	149ad	2.5 (7.3)	**149bd**	2.9
	149ae	3.9 (11.7)	**149be**	6.0#
	149af	-	**149bf**	4.7*
	149ag	*	**149bg**	1.7
	160aa	4.4	**160ba**	4.3*
	160ab	7.1	**160bb**	1.0
	160ac	2.1# (22.4)	**160bc**	1.1#
	160ad	2.0	**160bd**	0.7

Table 5: Yield of dispiro-1,2,4-trioxanes from corresponding epoxide

Number in brackets for yield directly from purified β-hydroxy hydroperoxide

 # Product mixed with deprotected impurity

* Not fully characterised due to impurity. Reacted further with impurity where appropriate

Structure analysis of *dispiro*-1,2,4-trioxanes via X-Ray crystallography

Generally *dispiro*-1,2,4-trioxanes are isolated as viscous oils or low melting solids. As reported above, a small number of *dispiro*-1,2,4-trioxanes derived from the condensation reactions of cyclic ketones and β-hydroxy hydroperoxides **148b** and **154a** have been isolated as solids which on recrystallisation gave crystals suitable for a X-ray crystallographic study.

The solid state structures of *dispiro*-1,2,4-trioxanes **160aa,ab** *(Figure 11 and 12)* demonstrate they are unambiguously derived from the condensation of cyclohexanone or cyclopentanone respectively with the β-hydroxy hydroperoxide regioisomer **154a**. The central 1,2,4-trioxane ring in **160aa,ab** is distorted significantly from the classical chair conformation *(Figure 18)*. Steric interactions between the 1,3-diaxial methylene groups in the *spiro*-substituents flatten the trioxane ring out of the chair conformation and into a half chair. The flattening of the 1,2,4-trioxane ring allows the 1,3-diaxial methylene groups to move away from each other. The extent of the distortion can be appreciated by comparing the interatomic distance between the *spiro*-carbons in **160aa,ab** (ca. 2.45 Å) with that between the diaxial methylene groups (*ca.* 3.30 Å) *(Figure 19)*.

The bond lengths associated with the 1,2,4-trioxane rings in **160aa,ab** are normal and similar to those reported previously reported *(See Table 8 and references there in)*. The bond angles however deviate significantly from the tetrahedral angle of 109°. The O-C-C bond shows significant expansion of the angle to almost 120° whilst the O-O-C angle shows compression to around 103° *(Table 9)*.
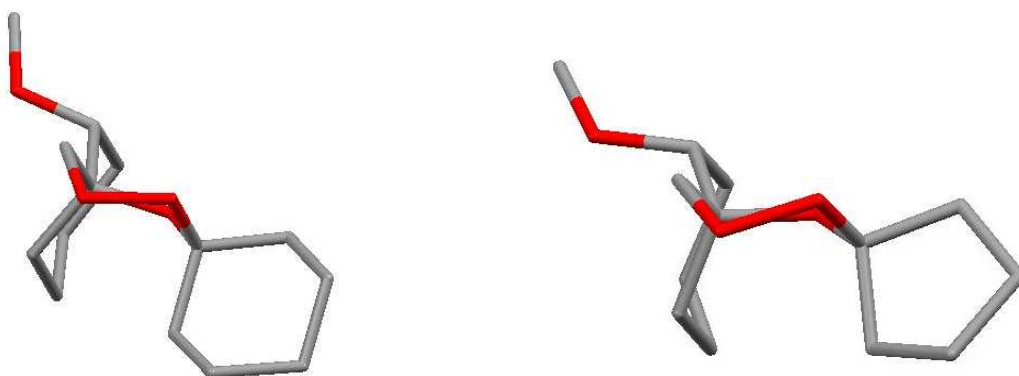
*Figure 18: **160aa** and **160ab** from showing distortion out of chair-like conformation.*
Hydrogens have been removed for clarity.
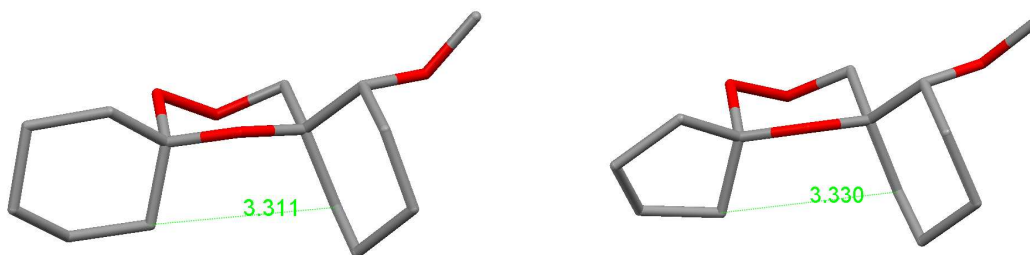
*Figure 19:**160aa** and **160ab** showing 1,3-diaxial interaction. Distances in Å. Hydrogens have been removed for clarity.*

This would suggest these structures are very rigid and would not easily take up alternative conformations. The general features of the X-ray crystal structures are readily reproducible by DFT calculations using a B3LYP hybrid functional and 6-31G** basis set. Optimisation of the structure gave bond lengths and angles comparative to the structures of **160aa,ab** *(Figure 20) (Tables 6 and 7)*. Like the structures of **160aa,ab** the O-C-C bond shows significant expansion to *ca*. 120° whilst the O-O-C similarly shows a compression to *ca*. 103°. This results in the 1,2,4-trioxane ring being in a similar half chair conformation seen for **160aa,ab** and the 1,3-diaxial methylene groups being *ca*. 3.30 Å apart.

Surprisingly it was found that the acid-catalysed reaction between cycloheptanone and β-hydroxy hydroperoxide **154b** did not give the expected trioxane **160ac**. This could be due to one of two reasons: either there are additional steric restrictions which prevent the formation of **160ac**, or the product has excessive intramolecular steric restrictions meaning the product is thermodynamically unstable. Initial computational analysis of *dispiro*-1,2,4-trioxane **160ac** indicates the former of the two possibilities is more likely. It is therefore thought that steric restrictions in the condensation reaction prevents in cycloheptanone from reacting with the β–hydroxyhydroperoxide **154a**.
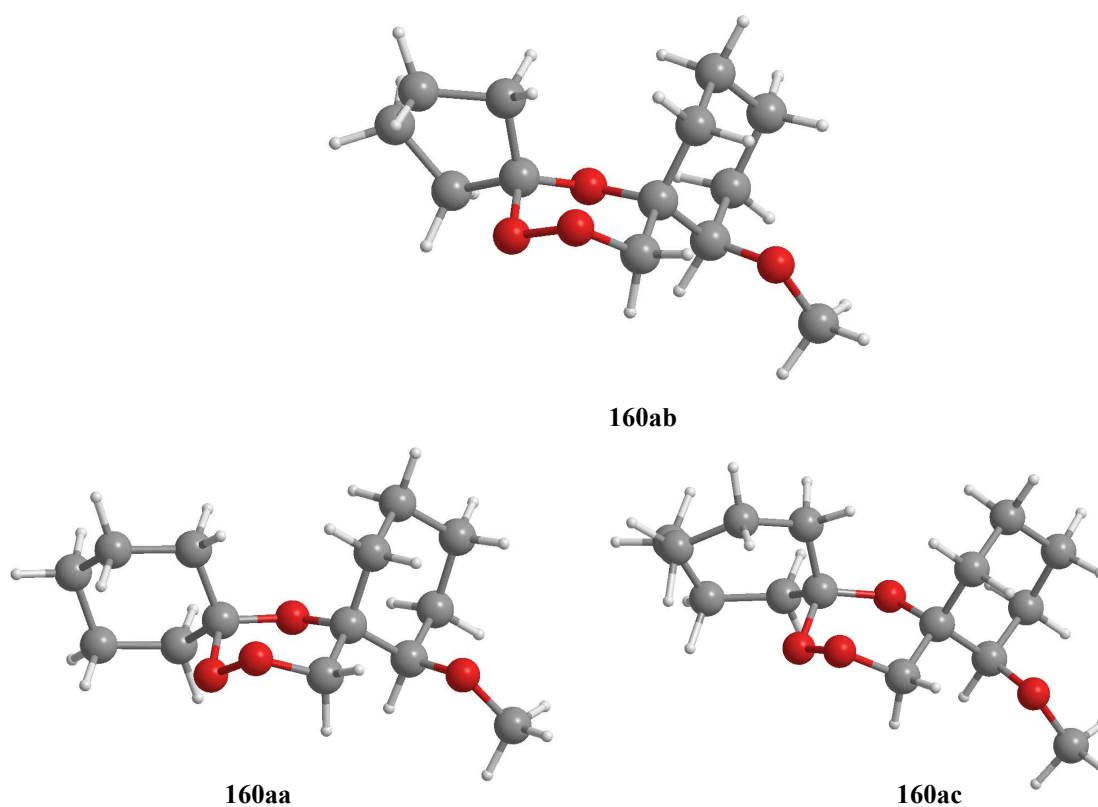
160ab

160aa   **160ac**

*Figure 20:**160ac**, **160aa** and **160ab** optimised structure using DFT calculations.*

B3LYP hybrid functional and 6-31G** basis set
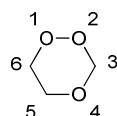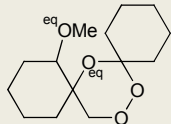
Compound	O1-O2	O2-C3	C3-O4	O4-C5	C5-C6	C6-O1
160aa	1.462	1.420	1.428	1.446	1.538	1.424
160ab	1.463	1.427	1.420	1.446	1.537	1.425
160ac	1.463	1.420	1.435	1.446	1.538	1.424
	1.461	1.425	1.429	1.449	1.538	1.427

*Table 6: Bond lengths associated with optimised structures of **160aa** and **160ac***
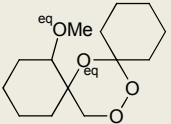
Compound	6-1-2	1-2-3	2-3-4	3-4-5	4-5-6	5-6-1	6123
160aa	104.36	107.44	110.64	120.05	109.74	110.53	-75.03
160ab	104.84	107.30	110.36	118.65	109.04	110.36	-73.30
160ac	104.03	107.22	110.57	120.68	109.99	110.14	-76.47
	104.49	107.41	110.55	120.43	108.80	110.11	-74.73

*Table 7: Angles associated with optimised structures of **160aa** and **160ac***

The preferred orientation of the methoxy group in **160aa,ab** is axial with respect to ring A with a *trans*-relationship (torsion angle 173.3° and 170.9° respectively) to the ether oxygen at the 4-position of the 1,2,4-trioxane ring. At first sight this arrangement looks unfavourable as the methoxy group would be expected to be equatorial in order to minimise 1,3-diaxial interactions. But from modelling studies it appears that the alternative conformation where the –OMe group and the ether oxygen are in an equatorial positions on ring **A**, obtained by a ring inversion in ring **A**, bring the –OMe hydrogens into close contact with the ether oxygen *(Figure 21)*. Additional gauche interactions between the methoxy oxygen and the methylene carbon and the ether oxygen of the 1,2,4-trioxane ring destabilise the molecule. As the energy of this conformation is *ca.* 2.5 kcal mol^{-1} higher than the optimised crystal structure the gauche interactions must destabilise the structure more than the methoxy group being in an axial position.
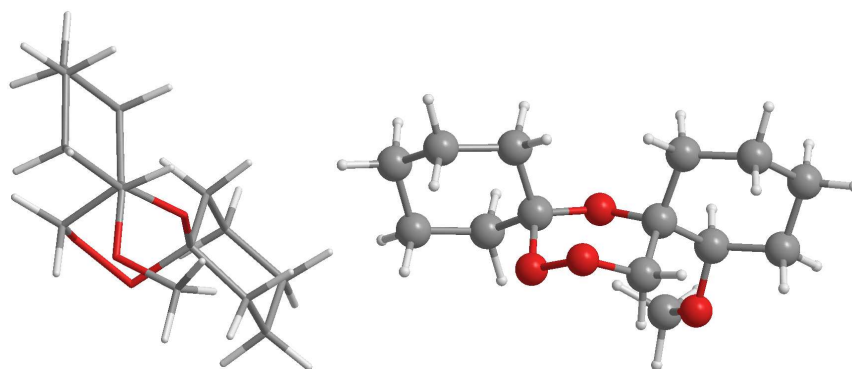
*Figure 21: **160ac***

B3LYP hybrid functional and 6-31G** basis set

A retrosynthetic analysis of the structures for **160aa,ab** confirms that the *dispiro*-1,2,4-trioxane ring must have been formed in each case from epoxide **147ab** via β-hydroxy hydroperoxide **154ab** *(Scheme 53)*. Thus the Mo-mediated perhydrolysis occurs via the nucleophilic attack at the least hindered carbon-centre of the minor epoxide **147ab**. In contrast epoxide **147c** was formed as a single diastereoisomer which on Mo-mediated perhydrolysis gives exclusively ring opening at the most substituted carbon centre. Therefore this suggests that methyl-substituted 1,2,4-trioxanes of the type **160ca** cannot be formed due to epoxide **147cb** not being present.
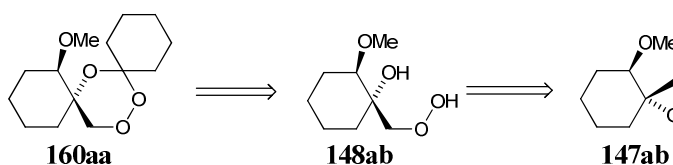
Scheme 53

The condensation reaction of cyclododecanone into β-hydroxy hydroperoxide **148c** gave *dispiro*-1,2,4-trioxane **149cd** as a colourless solid which on recrystallisation from ethanol gave crystal suitable for X-ray crystallography.[155] X-ray crystallographic analysis confirmed the formation of the expected *dispiro*-1,2,4-trioxane **149cd** as illustrated in *Figure 22*. As expected **149cd,** retains the same *trans*-relationship between the methyl group and the peroxide group observed in the crystal structure of β-hydroxy hydroperoxide **148c** *(See Figure 5)*. Similar to the structure of the β-hydroxy hydroperoxide **148c**, the methyl group is in the axial position. The 12-membered ring is in a [3333] conformation and is similar to that observed in previous X-ray structures.[156,157] Unlike the structures of **160aa,ab,** the central 1,2,4-trioxane ring adopts a near-classical chair conformation.
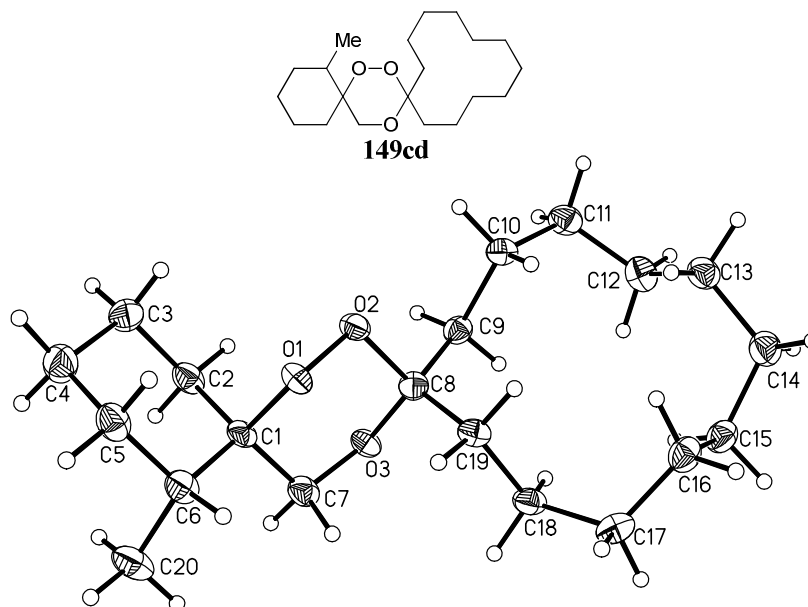
*Figure 22: X-ray crystal structure of **149cd** (Ortep, 50% probability ellipsoids for non hydrogen atoms)[150]*

The crystal structure of *dispiro*-1,2,4-trioxane **149bc** demonstrates very similar characteristics to that of **149cd** *(See Figure 16)*. The ethoxy group in **149bc** lies axial with a *trans*-relationship to the peroxide group and the central 1,2,4-trioxane ring is in a chair-like conformation. Although the *spiro*-seven-membered ring has two possible low

lying conformations,[158] which often leads to disorder in crystal structures, in this case it has adopted a well defined twist-chair conformation.

Following data collection and structure refinement *dispiro*-1,2,4-trioxane **149bg** was shown to have crystallised as two crystallographically independent molecules with both the R,S and S,R enantiomers present in the crystal *(Figure 23)*. When the structures are overlaid on each other (one structure inverted), the major structural differences between the enantiomers are in the orientation of the ethoxy groups and a slight distortion of the indanylidene group *(Figure 24)*. Despite the presence of the aromatic rings there is no π-stacking or significantly short intramolecular interactions in the crystal. The ethoxy group in **149bg** is again situated axial and *trans* to the peroxide bond and the central 1,2,4-trioxane rings are in the expected chair conformation.
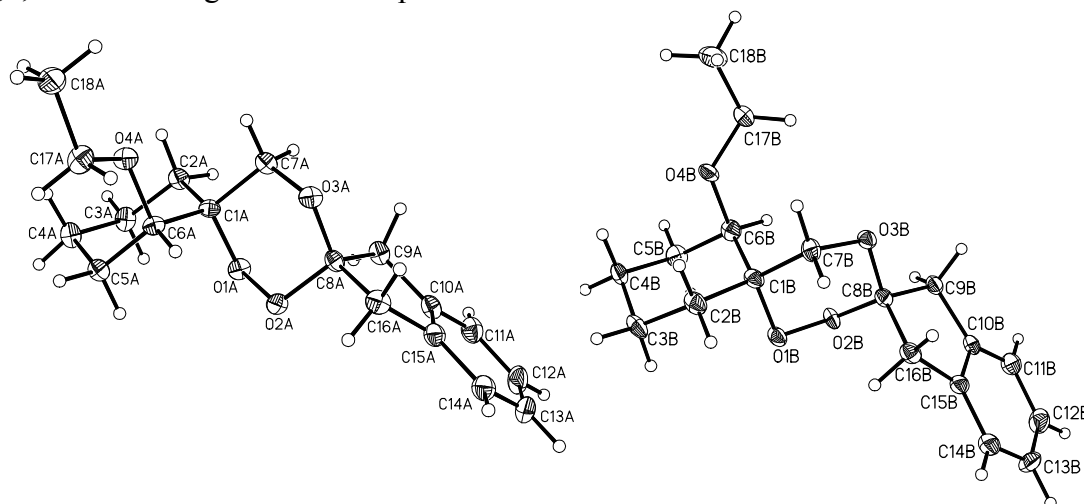
*Figure 23: X-ray crystal structure of R,S and S,R enatiomers of **149bg** (Ortep, 50% probability ellipsoids for non hydrogen atoms)[150]*
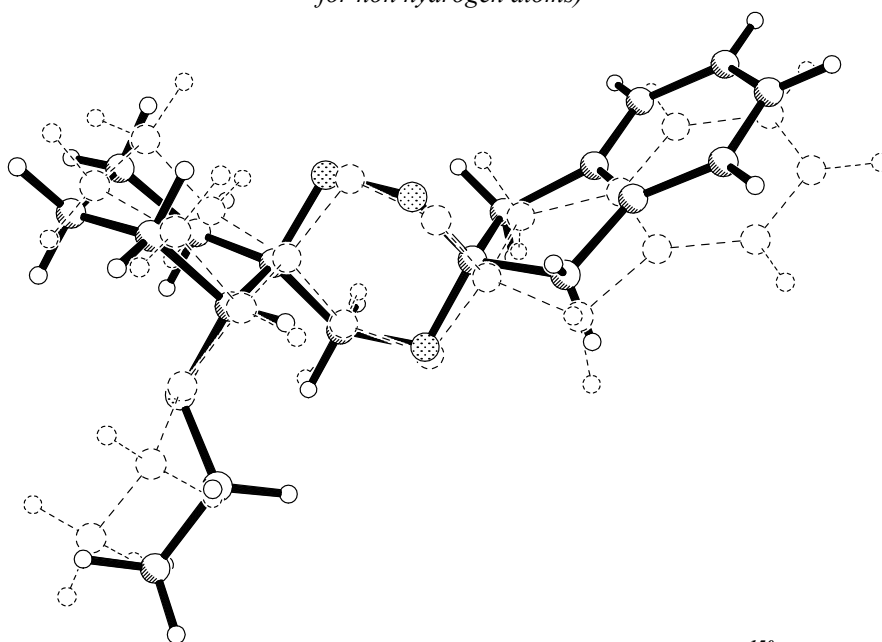
*Figure 24: Overlay of R,S and S,R enatiomers of **149bg**[150]*

The centre 1,2,4-trioxane ring contained within the *dispiro*-1,2,4-trioxanes **149bc,bg** and **149d** is in a near-perfect chair conformation. This is the expected conformation of the 1,2,4-trioxane ring and is in contrast to the ring seen for **160aa,ab**. An overlap of the 1,2,4-trioxane rings in **149bg** onto **160aa** demonstrates the distortion associate with the position of O4. The structures shown in *Figure 25* clearly illustrate the flattening of the ring at the O4 position.
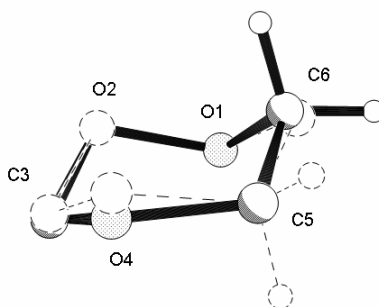
*Figure 25: 1,2,4-trioxane ring of **141bg**(Dotted line) superimposed onto **160aa** (Dark line)*

A retrosynthetic analysis of the structures for **149bc,bg** confirms that the *dispiro*-1,2,4-trioxane ring must have been formed in each case from epoxide **147ba** via β-hydroxy hydroperoxide **148ba** *(Scheme 54).* Thus the Mo-mediated perhydrolysis occurs via the nucleophilic attack of the most substituted carbon-centre of the major epoxide **147ba**.
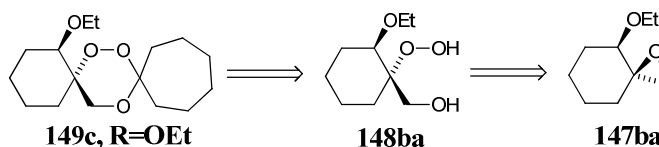
Scheme 54

It is therefore apparent that the formation of regioisomers **148a,b** and **154a,b** occur from the reaction of two different diastereoisomers of epoxide **147a,b**. There is no evidence for these reactions occurring on the opposite epoxide diastereoisomer indicating that the reaction of each epoxide diastereoisomer is taking place with a high degree of selectivity.

The bond lengths around the central 1,2,4-trioxane ring of these novel *dispiro*-1,2,4-trioxanes are listed in *Table 8* and are compared to previously obtained crystal structures of 1,2,4-trioxanes and 1,2,4,5-tetroxanes. The observed O-O bond distances of around 1.48 Å are comparable to that previously reported for a peroxide bond

distance.[123] The acetalic C-O bonds O2-C3 and C3-O4 lie between 1.41 Å and 1.44 Å with the length of O2-C3 being slightly longer in most cases. These lengths are similar to previously reported acetal C-O bond lengths.[159] The lengths of O5-C5 and C6-O1 are longer than the acetal C-O bonds and are consistent with literature values for C-O bond lengths.

The bond angles around the peroxide bond for these new *dispiro*-1,2,4-trioxanes are listed in *Table 9* and are compared to previously obtained crystal structures of 1,2,4-trioxanes and 1,2,4,5-tetroxanes. The bond angles associated with the 1,2,4-trioxane varied dramatically depending upon the nature of the *dispiro*-linkages. Where the *spiro*-linkages is at positions 3 and 6 angles of around 107-108° are seen for *dispiro*-1,2,4-trioxanes **149bc,bg** and **149cd** around the peroxide bond. Further bond angles around the 1,2,4-trioxane do not significantly vary from 109°. This is similar to previously reported structures of *dispiro*-1,2,4-trioxanes (**165**, **166** and **167**) and close to the angles associated with 1,2,4,5-tetroxane **163**. Angles of *ca.* 109° around the ring are indicative of a chair conformation.

119   **165**

166   **167**
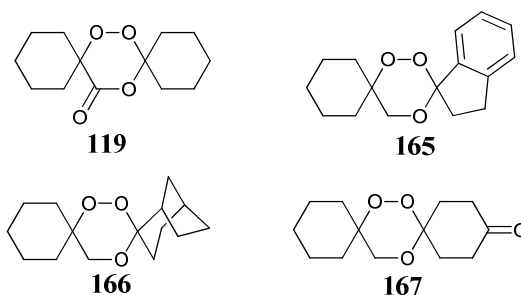
Dispiro-1,2,4-trioxanes **160aa,ab** have a compressed O1-O2-C3 angle of(103.96(6)° for **160aa** and 103.37(11)° for **160ab** as well as an expanded O4-C5-C6 bond angle (118.65(6)° for **160aa** and 117.50(11)° for **160ab** consistent with a flattening of one side of a chair conformation to give a half-chair. The magnitude of the O4-C5-C6 angles for **160aa,ab** is close to that in 1,2,4-trioxanone **119** (*ca.* 120°) which contains an sp^2-centre at C5.

The torsion angle C6-O1-O2-C3 for **149bc,bg** and **149cd** is similar in size to previously reported *dispiro*-1,2,4-trioxanes and 1,2,4,5-tetroxanes. 1,2,4-Trioxanes **160aa,ab** have a much bigger torsion angle for C6-O1-O2-C3 closer to that in the 1,2,4-triox-5-one **119** (*Table 9*).

The clear differences in the central 1,2,4-trioxane ring of **149bc,bg,cd** and **160aa,ab** exemplify the different conformations associated with the 1,2,4-trioxane ring. Although the half-chair conformation in **160aa,ab** was unexpected, it is seen that 1,3-diaxial interactions between *spiro*-methylene groups seem to distort the 1,2,4-trioxane ring by flattening out the angles associated with O4 in the ring. The absence of the 1,3-diaxial interaction in **149bc,bg,cd** enables the 1,2,4-trioxane ring to adopt a chair-like conformation with all the angles associated with the 1,2,4-trioxane ring being more tetrahedral-like.
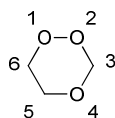
Ref		O1-O2	O2-C3	C3-O4	O4-C5	C5-C6	C6-O1
	160aa	1.4709(10)	1.4240(10)	1.4232(10)	1.4423(9)	1.5222(12	1.4266(10)
	160ab	1.4734(17)	1.4283(18)	1.4152(19)	1.4520(18)	1.518(2)	1.433(2)
	149bc	1.47480(8)	1.4410(9)	1.4271(9)	1.4325(9)	1.5303(10)	1.4492(9)
	149bg	1.481(3)	1.431(4)	1.410(4)	1.438(4)	1.515(4)	1.449(4)
	149bg	1.487(3)	1.432(4)	1.409(4)	1.429(4)	1.513(4)	1.450(4)
	149cd	1.479(2)	1.438(3)	1.430(3)	1.427(3)	1.520(4)	1.462(3)
[118]	**119**	1.436	1.430	1.485	1.336	1.494	1.442
[146]	**165**	1.477	1.436	1.405	1.426	1.513	1.452
[146]	**166**	1.471	1.434	1.425	1.422	1.520	1.449
[145]	**167**	1.471	1.427	1.419	1.433	1.518	1.454
	163	1.473(2)	1.441(3)	1.429(3)	1.473(2)	1.441(3)	1.429(2)

Table 8: Selected bond lengths of dispiro-1,2,4-trioxane ring structures

Ref		6-1-2	1-2-3	2-3-4	3-4-5	4-5-6	5-6-1	6123
	160aa	103.96(6)	107.18(6)	110.42(6)	118.65(6)	109.23(7)	109.62(7)	-74.03(7)
	160ab	103.37(11)	107.37(11)	110.33(12)	117.50(11)	108.87(13)	109.52(13)	-73.43(14)
	149bc	108.67(5)	108.55(5)	108.74(6)	113.26(6)	111.34(6)	107.84(6)	66.76(6)
	149bg	108.3(2)	108.4(2)	109.6(3)	110.5(2)	110.8(3)	108.1(3)	64.17(3)
	149bg	108.0(2)	107.1(2)	109.2(3)	112.1(2)	111.5(3)	107.9(3)	-66.90(3)
	149cd	107.71(16)	108.02(16)	108.83(19)	113.35(18)	112.0(2)	106.54(19)	-68.7(2)
[118]	**119**	106.43	106.98	107.50	121.68	120.08	110.27	-79.68
[146]	**165**	108.34	107.49	108.66	111.59	111.29	107.11	-66.42
[146]	**166**	107.94	107.67	107.96	113.45	112.39	107.29	-69.52
[145]	**167**	107.64	107.59	108.79	112.98	111.93	106.80	69.54
	163	108.26(17)	107.51(19)	107.51(19)	108.28(17)	107.31(19)	107.51(19)	-64.22(2)

Table 9: Selected bond angles and torsion angles of dispiro-1,2,4-trioxane ring structures

Structure determination of *dispiro*-1,2,4-trioxanes 149a,b via ¹H and ¹³C NMR spectroscopy

Although several 1,2,4-trioxane structures have been analysed using X-ray crystallography, most 1,2,4-trioxanes were isolated as low melting solids or oils which were unsuitable for X-ray crystallography. Analysis of 1,2,4-trioxanes by NMR spectroscopy at room temperature is difficult because like other saturated six-membered ring heterocycles, the three *spiro*-rings readily undergo ring inversion.

The main characteristic signals in the ¹H NMR spectrum are the two doublets at δ3.0-4.0 corresponding to the 1,2,4-trioxane methylene group at C5. The asymmetrical nature of the *dispiro*-1,2,4-trioxane plus the dynamic chair-to-chair interconversions of each of the rings results in the doublets being broadened or not fully resolved at room temperature. The room temperature ¹H and ¹³C NMR spectra of *dispiro*-1,2,4-trioxanes **149ab** gave unresolved signals demonstrating the dynamic changes in the conformation of the molecule. At this temperature the ¹H NMR showed one broadened doublet at δ3.94 for the equatorial hydrogen atom at C5 plus a very broad unresolved signal at δ3.39 for the axial hydrogen. In addition a sharp singlet at δ3.30 was present for the OCH₃ group with a broad signal at δ4.10 for the CH group *(Figure 26a)*. The ¹³C NMR signals were generally broad apart from the acetal *spiro*-carbon at δ114 and the methylene CH₂ in the C5 position at δ64 *(Figure 27a)*.

On lowering the temperature to -55 °C, the ¹H and ¹³C NMR spectra of **149ab** become resolved as the conformation begins to lock. The ¹H NMR spectra now shows two clear doublets for the methylene C5 group at δ3.94 and δ3.39 with a ²*J* coupling constant of 11.5 Hz *(Figure 26b)*. The methoxy group remains unaffected by the low temperature and still shows its characteristic singlet at δ3.33; however, the CH group is now a broad singlet at -55°C. The ¹³C NMR spectra at -55 °C of 1,2,4-trioxane **149ab** shows sharp signals for each of the carbon atoms *(Figure 27b)*. Through a combination of ¹³C NMR DEPT experiments and C–H correlation experiments *(Figure 28)*, the spectra were assigned to show the methoxy carbon at δ57, the methylene group C5 of the 1,2,4-trioxane ring at δ64, the CH at δ73 and the two *spiro* carbons at δ78 and δ114 (*spiro*-acetal). The difference in the chemical shifts for the *spiro*-carbons is due to the inductive effect of a further oxygen atom adjacent to the carbon.
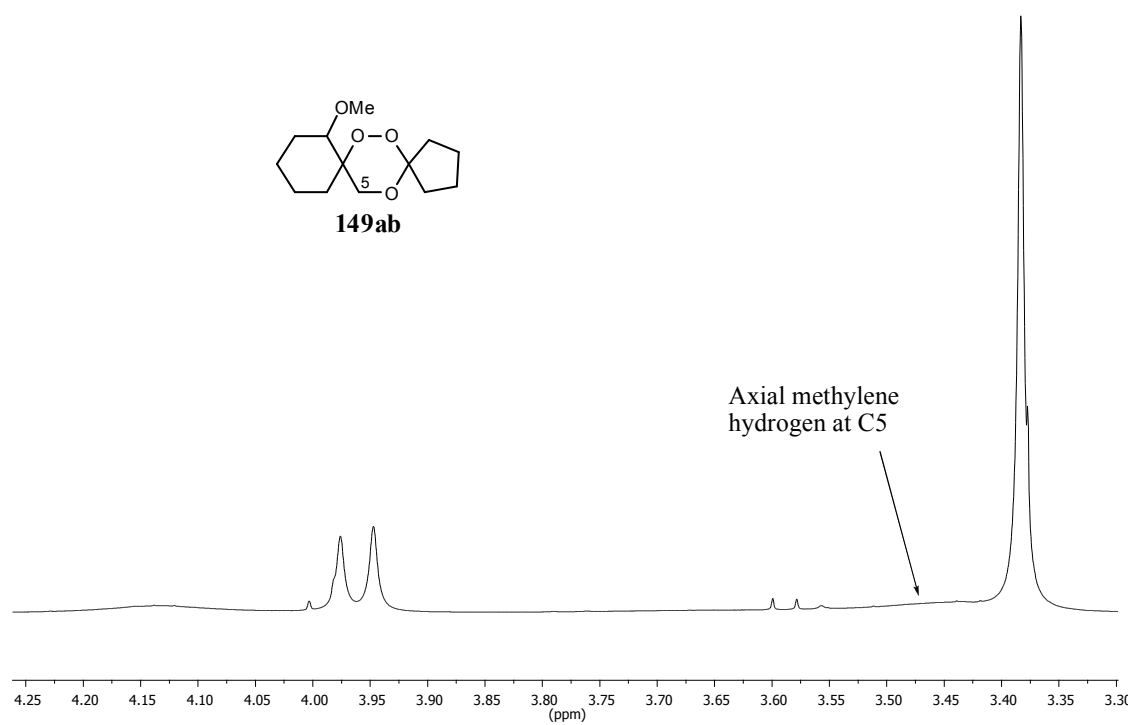
*Figure 26a: ^{1}H NMR spectrum of characteristic chemical shifts of **149ab** at room temperature*
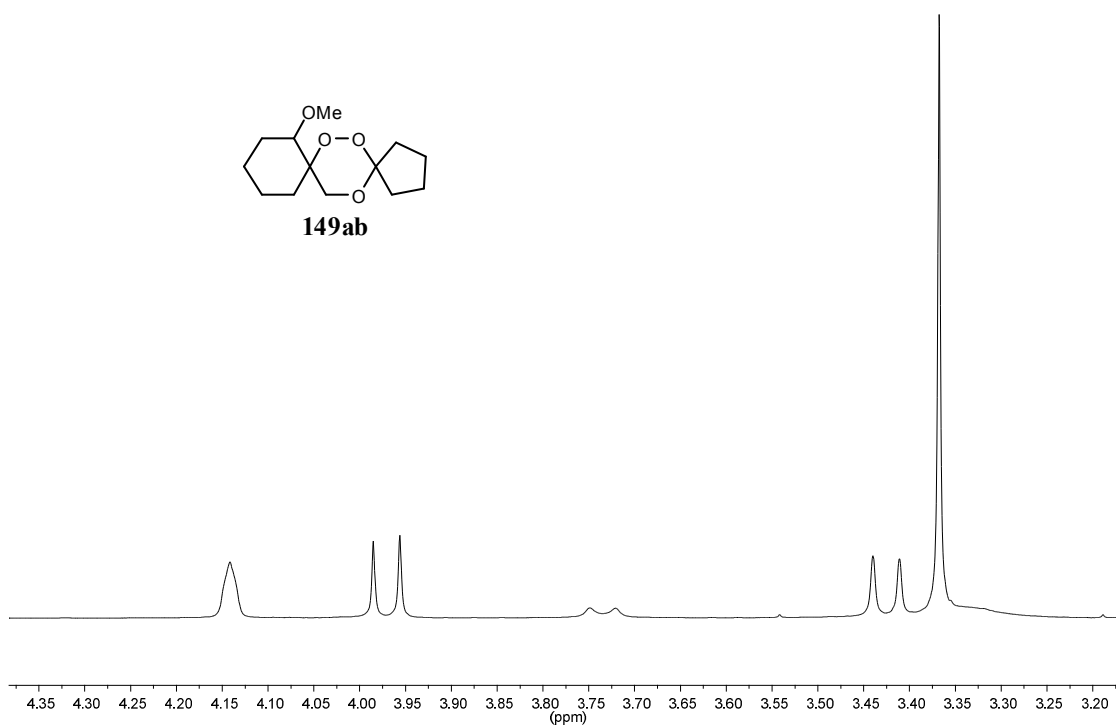
*Figure 26b: ^{1}H NMR spectrum of characteristic chemical shifts of **149ab** at -55°C*
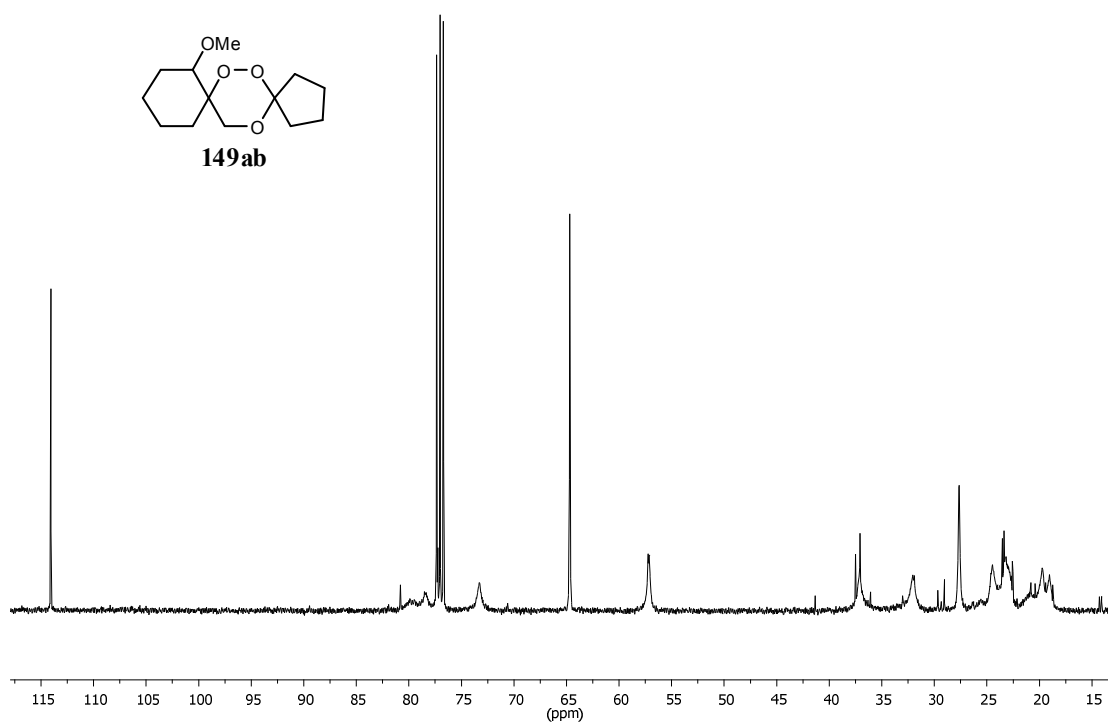
*Figure 27a: ^{13}C NMR spectrum of **149ab** at room temperature*
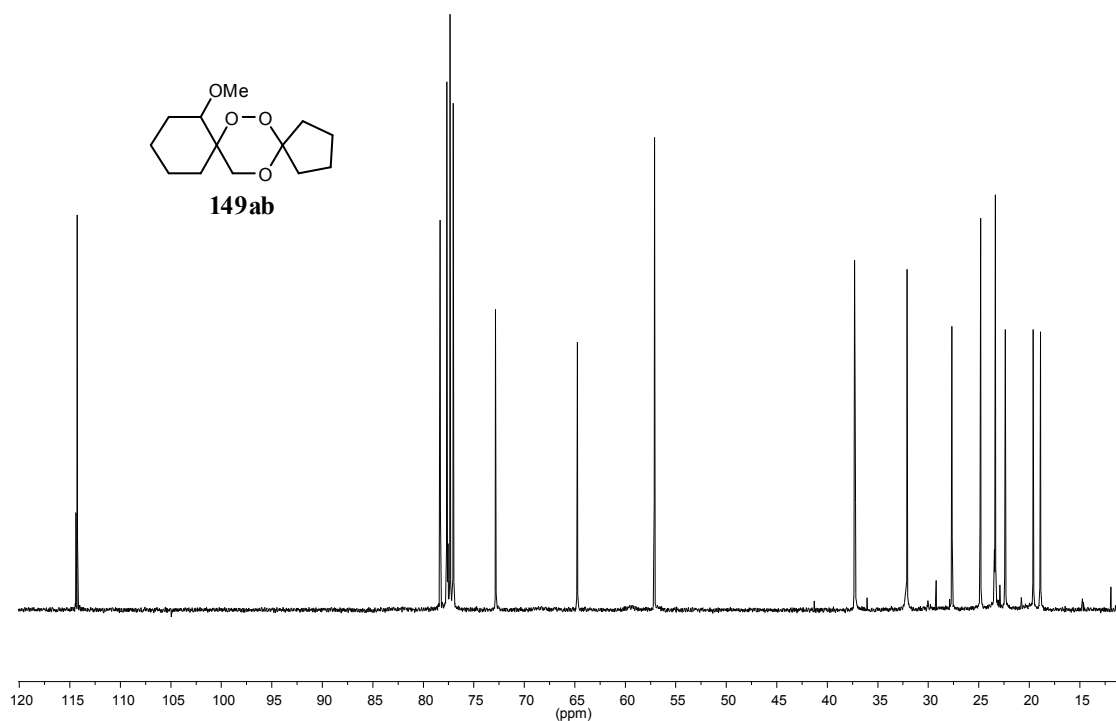
*Figure 27b: ^{13}C NMR spectrum of **149ab** at -55°C*
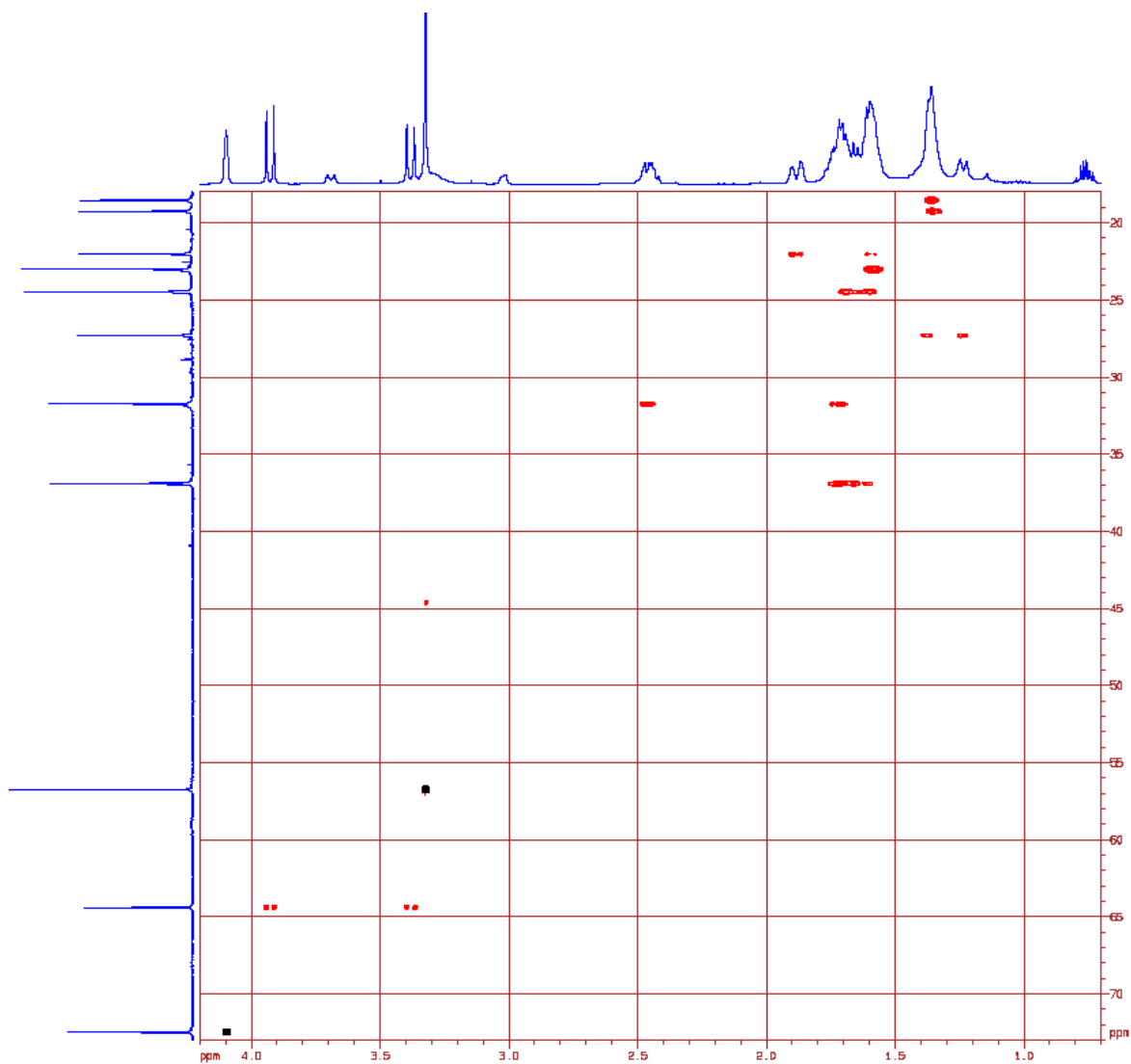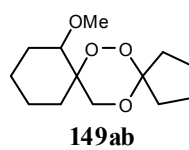
*Figure 28: C – H correlation spectrum for dispiro-1,2,4-trioxane **149ab***

Despite the structure of **149ab** being locked out at -55 °C, it is apparent from the ^{1}H NMR spectrum of **149aa** that the molecule is still fluxional because the doublet associated with the methylene group at C5 in the 1,2,4-trioxane ring was not resolved. This was confirmed by the ^{13}C NMR spectrum which showed broad signals for some signals in particular between δ10-40 which indicate that some parts of the molecule were not yet rigid even at -55 °C.

The room temperature NMR spectra of ethoxy-substituted 1,2,4-trioxanes **149b** did not contain sufficient information to determine their structures and seemed to indicate that a more dynamic chair-to-chair interconversion was occurring than in the corresponding methoxy-substituted cases *(Figure 29a)*. Both the ^{1}H and ^{13}C NMR spectra showed generally broad undefined signals which could not be interpreted. High temperature NMR spectra for ethoxy-substituted 1,2,4-trioxanes give first order spectra which could be more readily correlated with structure. At these temperatures the doublets for the C5-methylene group of the 1,2,4-trioxane ring could be clearly observed in all cases *(Figure 29b)*. The high temperature ^{1}H NMR spectrum of the ethoxy-substituted 1,2,4-trioxanes also split the CH_2 of the ethoxy group into two clear doublet of quartets for each of the hydrogens.

The position of the doublets for the 1,2,4-trioxane methylene group in *dispiro*-1,2,4-trioxanes **149a,b** vary only slightly throughout the series analysed *(Table 10)*. The doublets situated at ca. δ3.90 and ca. δ3.50 for all *dispiro*-1,2,4-trioxanes have a germinal coupling constant which varies between 11.8 Hz for methoxy substituted *dispiro*-1,2,4-trioxanes and 11.5 Hz for ethoxy substituted *dispiro*-1,2,4-trioxanes. Assuming the signals is consistent with substituted cyclohexanes the proton with the lower chemical shift is in the axial position due to diamagnetic anisotropic effects.[158]

Overall, the order in which the carbons appear in the ^{13}C NMR spectrum does not change in any *dispiro*-1,2,4-trioxane **149a,b**. Equally the chemical shifts associated with the ^{13}C NMR vary only slightly over the series of *dispiro*-1,2,4-trioxanes **149a,b** except the position of the acetal *spiro*-C3 which seems to vary depending on the size of the ring bonded to the carbon. In general, values of δ100-102 were recorded for six membered rings, δ106 for 12-membered rings, δ106-107 for 7-membered rings and δ112-114 for 5-membered rings *(Table 11)*.[160]
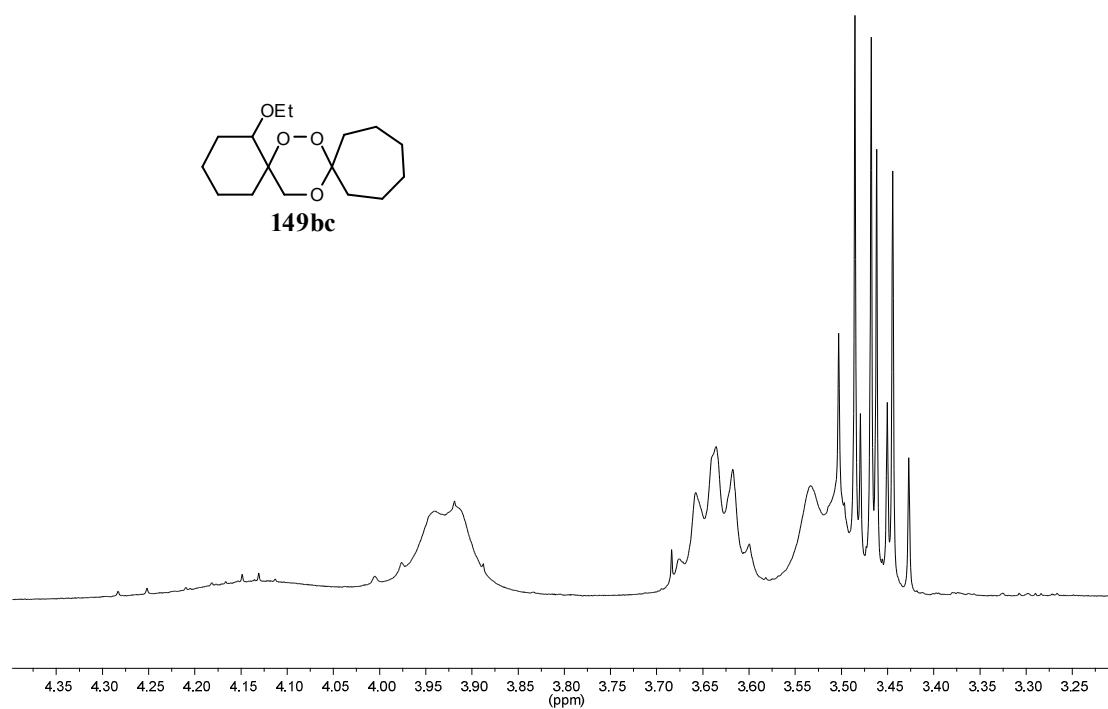
*Figure 29a: ¹H NMR spectrum of characteristic chemical shifts of **149bc** at room temperature*
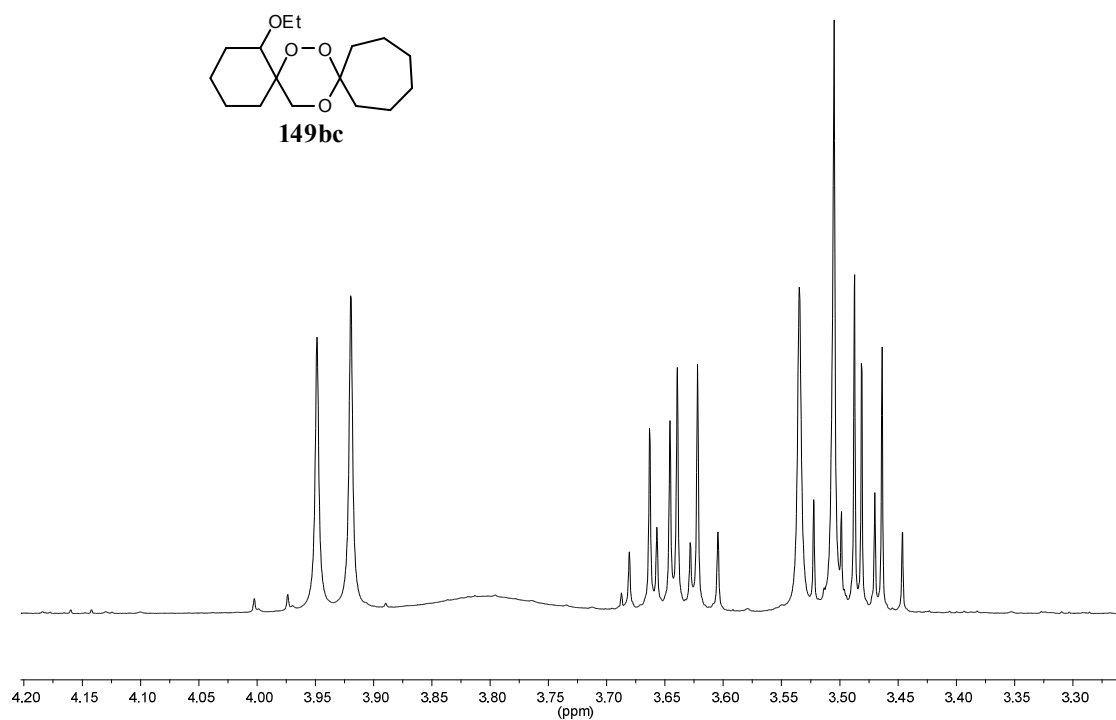
*Figure 29b: ¹H NMR spectrum of characteristic chemical shifts of **149bc** at 60°C*

Compound	Temp	δH_{eq}	δH_{ax}	Coupling constant J/ Hz
149aa	-50°C	3.86	3.56	11.8
149ba	60°C	3.92	3.52	11.5
149ab	-50°C	3.94	3.39	11.8
149bb	60°C	3.95	3.50	11.5
149ac	-50°C	3.84	3.48	11.8
149bc	60°C	3.90	3.48	11.5
149ad	-30°C	3.80	3.43	11.8
149bd	60°C	3.91	3.48	11.5
149ae	-50°C	3.92	3.51	11.8
149bf	60°C	4.02	3.57	11.8
149bg	55°C	4.08	3.55	11.8

Table 10: δ values (ppm) and coupling constants (J) for methylene group of trioxane rings
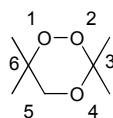
Compound	Temp	C3	C5	C6	Sub	CH
149aa	-50°C	102.0	61.7	78.0	56.8	72.6
149ba	60°C	102.1	62.3	79.4	15.5 64.5	74.1
149ab	-50°C	113.9	64.4	78.0	56.8	72.5
149bb	60°C	114.1	64.8	79.2	15.6 65.0	74.0
149ac	-50°C	107.2	62.2	78.0	56.9	72.9
149bc	60°C	106.7	62.5	79.3	15.5 64.0	74.2
149ad	-30°C	106.1	62.5	78.2	57.1	73.4
149bd	60°C	106.2	62.5	79.2	15.6 65.1	74.2
149ae	-50°C	101.5 108.5	62.6	79.5	57.2	81.3
149bf	60°C	100.7	62.9	79.8	15.4 64.9	73.8
149bg	55°C	112.8	64.8	79.4	15.6 65.1	79.1

Table 11: δ values (ppm) for ^{13}C NMR signals of dispiro-1,2,4-trioxanes

Structure determination of *dispiro*-1,2,4-trioxanes 160a,b via ^{1}H and ^{13}C NMR spectroscopy

In contrast to the NMR spectra of *dispiro*-1,2,4-trioxanes **149a,b**, the ^{1}H NMR and ^{13}C NMR spectra of 1,2,4-trioxanes **160** are completely resolved at room temperature *(Figure 30)*. The ring methylene group exhibits sharp doublets at *ca.* δ3.9 and δ4.5 for all *dispiro*-1,2,4-trioxanes **160** *(Table 12)*. The doublets lie further upfield and are further apart than the corresponding signals for *dispiro*-1,2,4-trioxanes **149a,b**. Additionally they have a larger ^2J coupling constant of 12.6 Hz in all cases. This is around 1 Hz higher than the coupling constant for *dispiro*-1,2,4-trioxanes **149** and demonstrates further the difference in the conformation of the 1,2,4-trioxane ring. A slight 0.3 Hz splitting of each peak in the doublet also suggests microfine coupling between the methylene CH$_2$ group and other parts of the molecule. With the exception of a haystack of signals between δ1.2 and δ2.0 the remaining signals in each of the spectra are completely resolved at room temperature with no variable temperature analysis required.

The chemical shifts for the ^{13}C NMR spectroscopy of **160a,b** follow the same trend as was seen for the *dispiro*-1,2,4-trioxanes **149a,b** *(Figure 31)*. Through a combination of ^{13}C NMR DEPT experiments and C – H correlation experiments the signals were assigned to show the 1,2,4-trioxane methylene group at *ca.* δ77, the CH at *ca.* δ80 and the two *spiro*-carbons at *ca.* δ77 and *ca.* δ100-115 (*spiro*-acetal) (*Table 13*). Although the chemical shifts of the *spiro*-carbon and the methylene group have changed, this is only because the *spiro*-carbon position has changed to C5 in the trioxane ring and is now next to the ether oxygen rather than the peroxide oxygens.

The clarity of the spectra at room temperature further demonstrates the central 1,2,4-trioxane ring is not undergoing chair-to-chair interconversion because of the 1,3-diaxial interactions between the CH$_2$ group in the *spiro*-rings.

Compound	δH ax	δH eq	Coupling constant J/ Hz
160aa	4.25	3.87	12.6
160ba	4.27	3.88	12.6
160ab	4.25	3.88	12.6
160bb	4.27	3.90	12.6
160af	4.34	3.97	12.6
160bf	4.37	3.98	12.6

Table 12: δ values (ppm) and coupling constants (J) for methylene group of trioxane rings
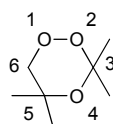
Compound	C3	C5	C6	Sub	CH
160aa	102.0	70.9	76.3	56.9	80.9
160ba	102.1	71.0	76.3	15.5, 62.0	79.0
160ab	113.0	71.3	76.6	56.9	79.6
160bb	112.3	71.3	77.7	15.6, 64.5	77.8
160af	100.7	71.6	76.5	56.3	80.7
160bf	100.6	71.7	76.4	15.6, 64.4	78.8

Table 13: Selected ^{13}C NMR δ values (ppm) of dipiro-1,2,4-trioxanes
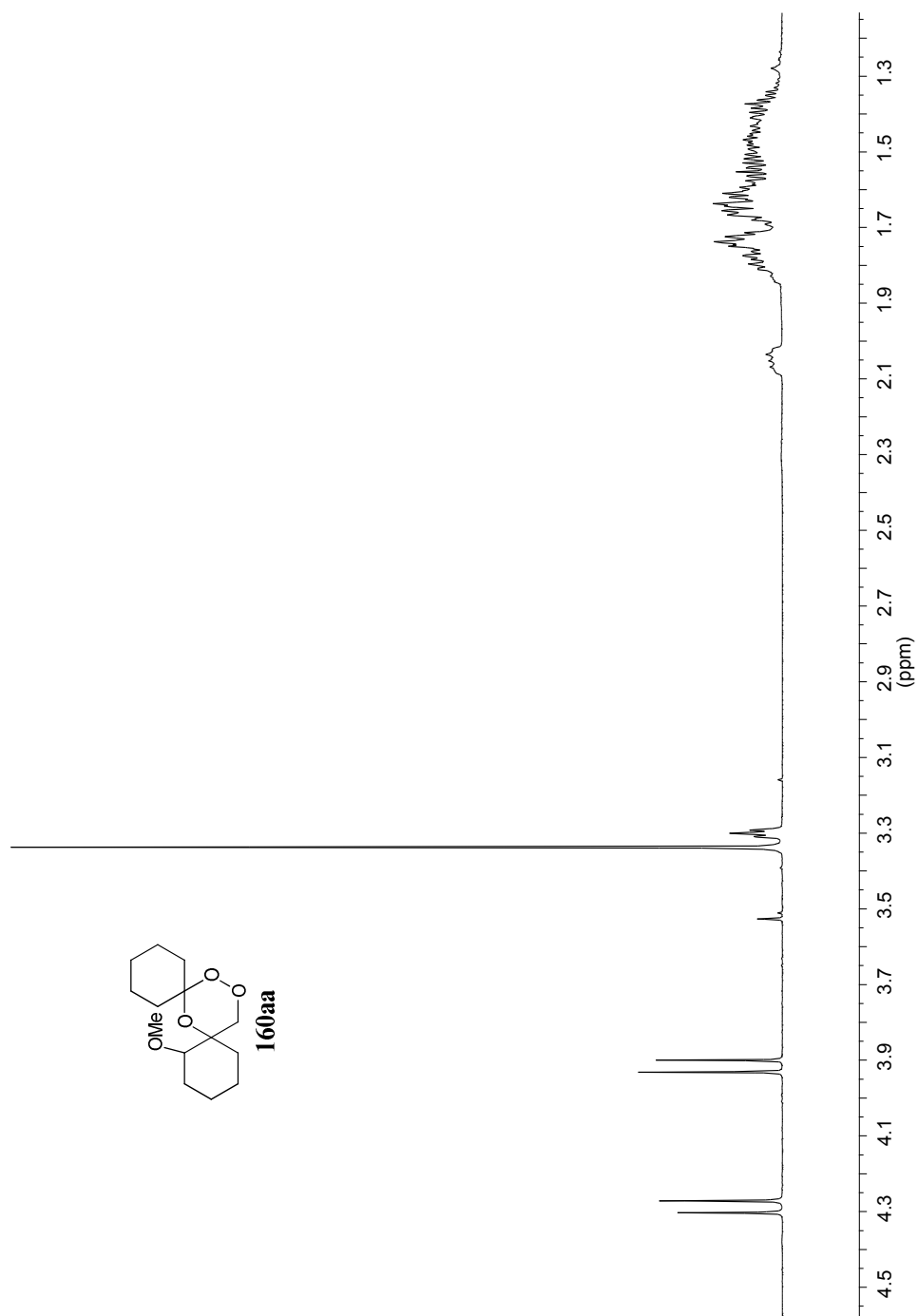
*Figure 30: ^{1}H NMR of **160aa***
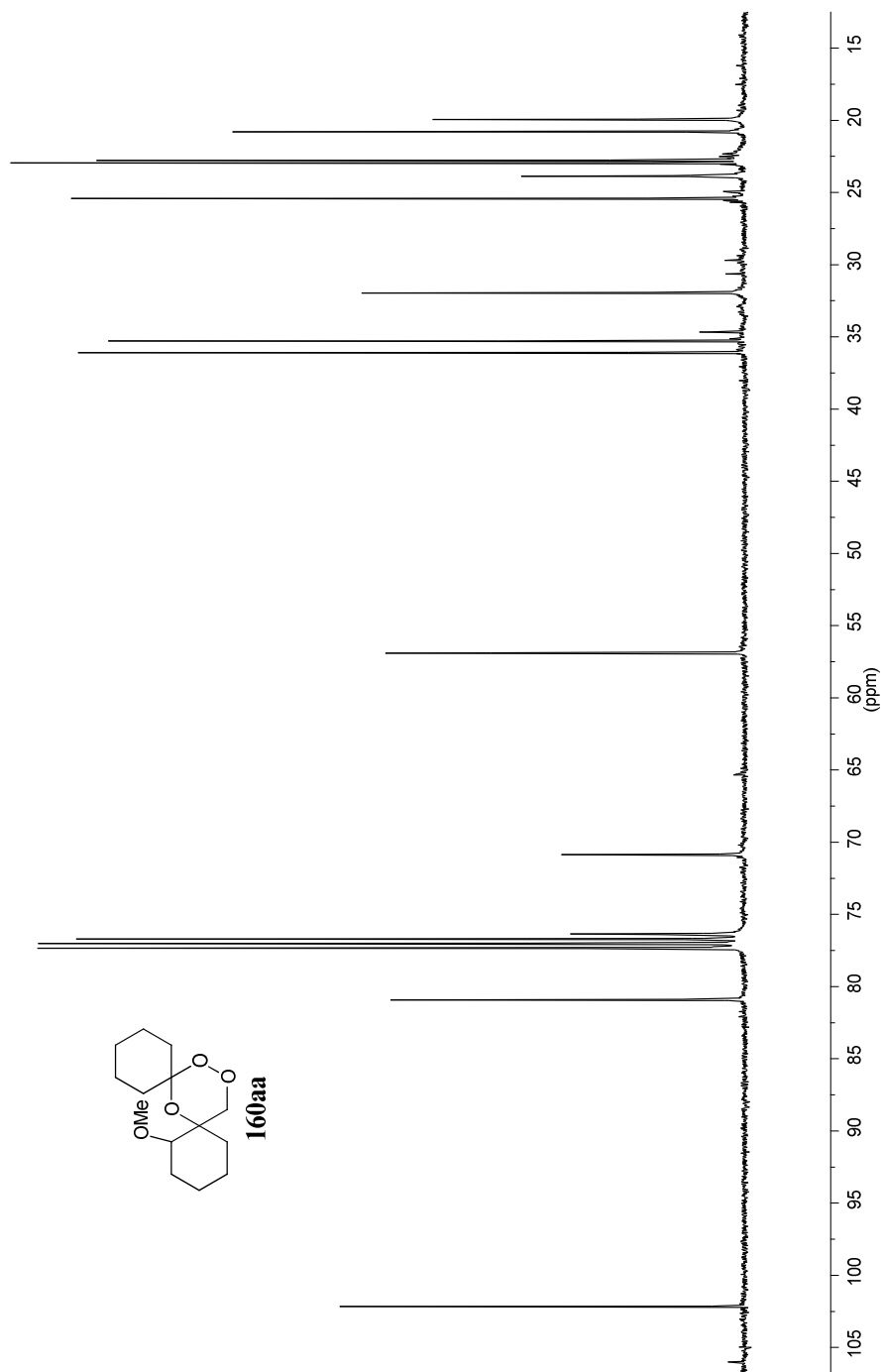
*Figure 31: ^{13}C NMR of **160aa***

Computational analysis of acid-catalysed perhydrolysis

The acid-catalysed perhydrolysis of simple non-substituted and methyl-substituted *spiro* epoxides **147c** and **147d** has been shown to give good overall reaction yields of the corresponding β-hydroxy hydroperoxides **148c** and **148d** respectively. In contrast, the perhydrolysis of the methoxy-substituted derivatives **147a** only gave low isolable yields of β-hydroxy hydroperoxide **148a**. Moreover, unlike the synthesis of the methyl-substituted *spiro*-epoxide **147c**, the methoxy-substituted epoxide **147a** was obtained as a mixture of diastereoisomers **147aa** and **147ab,** which upon acid-catalysed perhydrolysis only produced β-hydroxy hydroperoxide **148aa**. No product derived from **147ab** was isolated indicating that epoxide **147aa** is significantly more reactive than its diastereoisomer **147ab** *(Scheme 55)*. Computer modelling of this system sought to investigate, (i) the energies of the transition states involved in the perhydrolysis process and (ii) the greater reactivity of **147aa** over **147ab** in the methoxy-substituted example.

147aa=R=OMe
c=R=Me
d=R=H

148

147ab

148ab
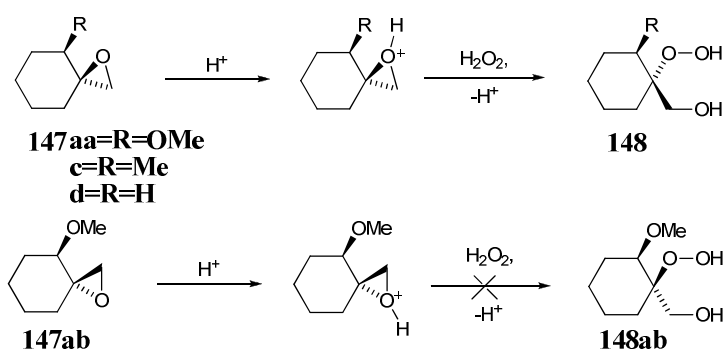
Scheme 55

Computational Details

The calculations contained within this section have been carried out using the MP2[161] method deploying a 6-31G** basis set. MP2 calculations were used to describe the geometry of protonated epoxides because DFT methods fail to accurately describe the epoxide C(*spiro*)-O bond distance. Previous reports noted large differences in the C-O bond distance by varying the density functional employed including an elongation of 0.4Å to an almost completely open structure.[162] The use of either MP2 or CCSD or newly developed methods such as M05 and M05-2X better describe the structure.[163] However due to the extra cost of computer time in running CCSD and the inaccessibility of M05 and M05-2X, MP2 calculations were used.

To carry out the calculations, the distance between the hydrogen peroxide nucleophile and the *spiro*-carbon of the protonated epoxide was scanned until the energy associated with the system reaches a maximum. This point served as a guess geometry for the subsequent location for the S_N2 transition state. During the scan, the angle of the oxygen nucleophile to the C(*spiro*)-O(epoxide) was fixed to a 180° angle to best mimic the S_N2 reaction. In the transition state optimisation, this angle was allowed to vary with no restriction. During the scanning process the C(*spiro*)-O bond length increased steadily as would be anticipated for an S_N2 reaction. Similar scans, allowing the hydrogen peroxide to approach the least-hindered carbon centre on the epoxide ring, showed no elongation of the least hindered C(epoxide)-O(epoxide) bond. There was instead a dramatic increase in the energy of the system implying the alternative S_N2 reaction was not likely to occur. All the energies quoted in this section are with respect to the protonated reactant with the epoxide oxygen in its preferred conformation in each model.

Ring opening of unsubstituted epoxide 147d

The protonated unsubstituted epoxide **147d+H$^+$** can form two conformational isomers, of similar energy, which are linked by a chair-to-chair interconversion. Both conformations contain elongated C(*spiro*)-O bonds of 1.61 Å and 1.62 Å which are consistent with the low energy barriers (4.6 and 6.2 kcal mol^{-1}) and the overall exothermic reaction calculated for the perhydrolysis reaction *(Figure 32)*. The results demonstrate a kinetic preference for the oxygen leaving group being in an axial position on the ring. Distances of 2.35 Å and 2.48 Å between the hydrogen peroxide and the *spiro*-carbon in the transition state demonstrate the long-range influence of the nucleophile in the S_N2 reaction of epoxides as speculated in early literature for epoxide ring opening.[71] This is consistent for all the transition states of epoxide ring openings.
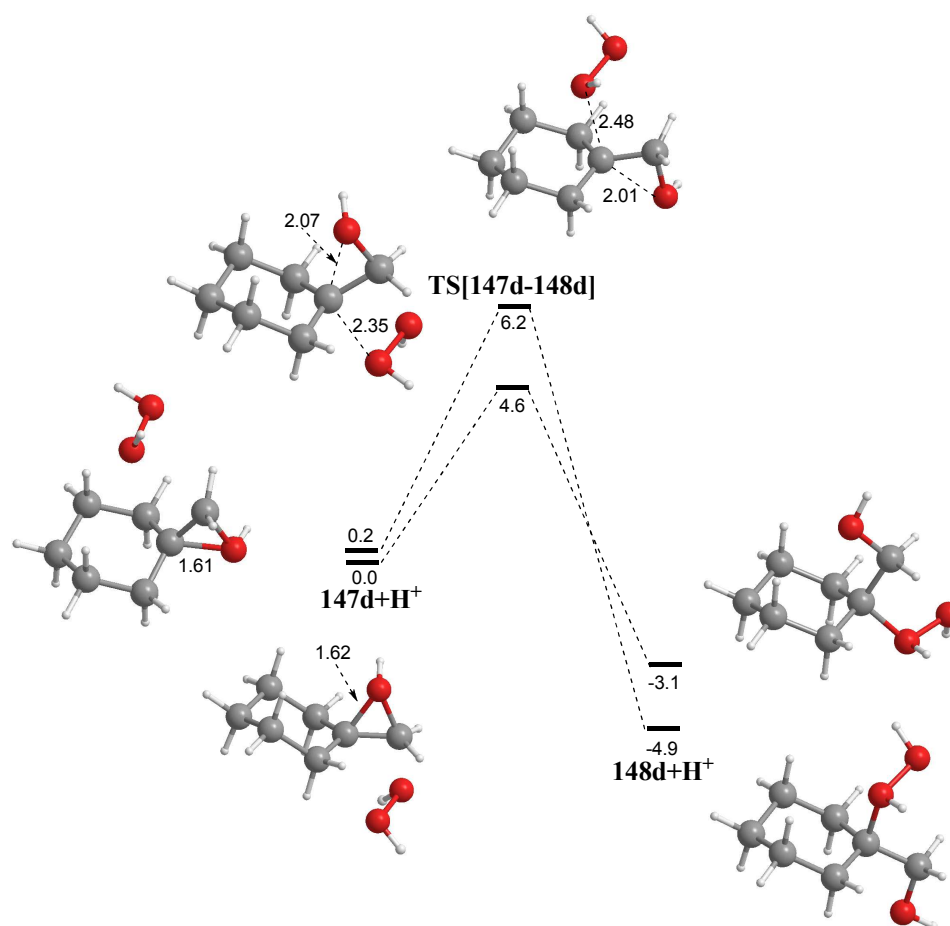
*Figure 32: Reaction profile for the acid-catalysed perhydrolysis of epoxide **147d**. Energies are in kcal mol^{-1} and relative to lowest energy conformation. Bond distances are given in Å.*

Ring opening of methyl-substituted epoxide 147c

The methyl-substituted epoxide was synthesised as a single diastereoisomer **147ca** in which the epoxide oxygen and the methyl group are *cis* to each other. The protonated epoxide **147c** again can form two conformational isomers of similar energy linked by a chair-to-chair interconversion. In principle, two different positions of the proton could also be considered where the proton is positioned towards or away from the methyl. However since, this only caused a small energy difference, it was deemed not to be an important factor. Both conformations contain elongated C(*spiro*)-O bonds of 1.61 Å and 1.62 Å within the epoxide ring consistent with favourable nucleophilic attack at the *spiro*-carbon. The activation energies associated with the ring opening of epoxide **147ca** (3.9 and 6.5 kcal mol^{-1}) were comparable to those seen for the unsubstituted epoxide **147d** and are consistent with the high yields achieved in both reactions. The conformer which gave the lowest barrier was again corresponding to the displacement of the axial oxygen leaving group *(Figure 33)*.
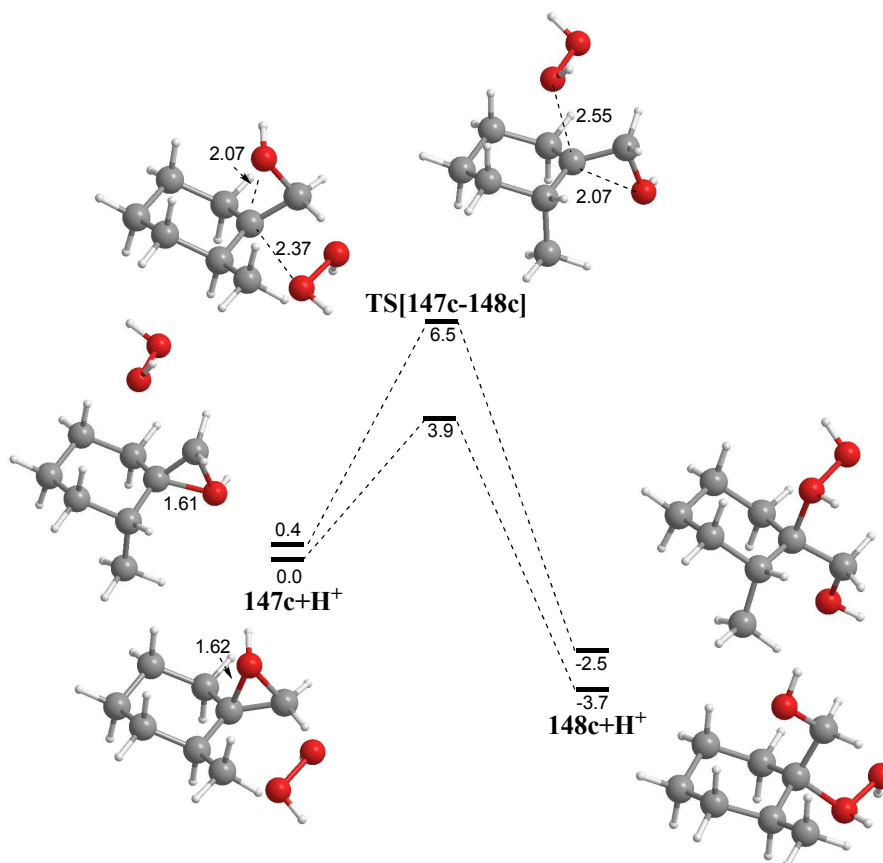
*Figure 33: Reaction profile for the acid-catalysed perhydrolysis of epoxide **147c**. Energies are in kcal mol^{-1} and relative to lowest energy conformation. Bond distances are given in Å.*

Ring opening of methoxy-substituted epoxide 147aa and 147ab

Although the methoxy-substituted epoxide was synthesised as the two possible diastereoisomers **147aa** and **147ab**, the acid-catalysed perhydrolysis afforded only the β-hydroxy hydroperoxide **148a** in generally low yield, implying that epoxide **147ab** was less reactive to acid-catalysed perhydrolysis. The introduction of the methoxy-substituent provides a potential hydrogen bond between the proton situated on the epoxide oxygen and the methoxy oxygen. The proton on the epoxide oxygen can either be situated towards the methoxy oxygen or away from it meaning four possible conformations of the epoxide needed to be considered. The four conformations **147aa(1)-(4)** are illustrated in *Figure 34* and show a 8.8 kcal mol^{-1} energy difference between conformer **147aa(1)**, which contains the hydrogen bond, and conformer **147aa(2)**. The remaining two conformations, **147aa(3)** and **147aa(4)**, where the methoxy-substituent is axial with respect to the ring are even higher in energy at 9.0 and 9.9 kcal mol^{-1} respectively. It is clear therefore that the most abundant conformation in

solution is going to be **147aa(1)**. The methoxy-substituted epoxide **147aa(1)** contains a hydrogen bond of 1.73 Å between the proton on the epoxide oxygen and the methoxy oxygen which creates a *pseudo* 5-membered ring. This causes the C(*spiro*)-O bond distance to contract from 1.60 Å in **147aa(2)** to 1.57 Å in **147aa(1)**. A complete reaction profile from the ring opening of conformations **147aa(1)** and **147aa(3)** is detailed below *(Figure 35)*. Protonated epoxides **147aa(1)** and **147aa(3)** were considered because they represent the lowest energy conformations in which the epoxide oxygen is positioned axial or equatorial.

0.0   **8.8**   **9.0**   **9.9**
147aa(1)   **147aa(2)**   **147aa(3)**   **147aa(4)**
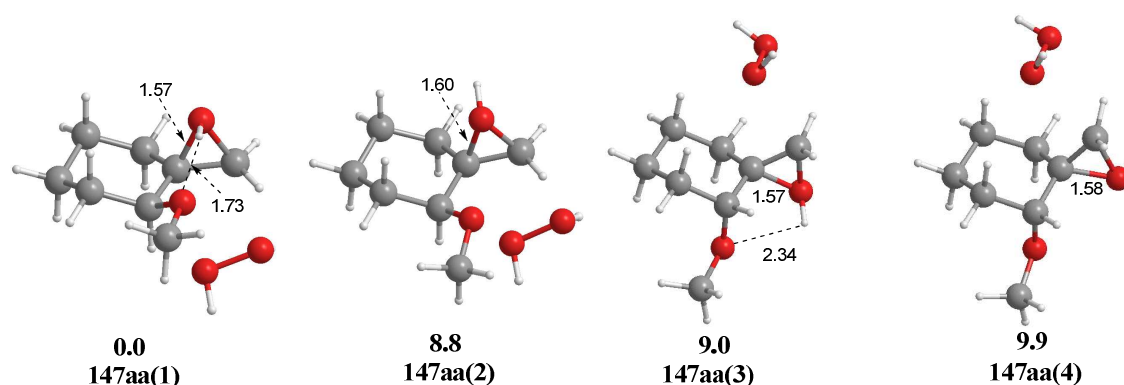
*Figure 34: Four conformations of the acidified epoxide **147aa** showing crucial C-O bond distances and close range H-bonding interactions (Å). Energies are in kcal mol^{-1} and relative to lowest energy conformation.*

Consistent with the shortened C(*spiro*)-O bond in **147aa(1)**, the calculated barrier for the opening of the epoxide bond by nucleophilic attack of hydrogen peroxide is 10.8 kcal mol^{-1} which is considerably higher than for the unsubstituted **147d** or methyl-substituted epoxides **147c** *(Figure 35)*. The transition state for the opening of **147aa(3)** is only 8.8 kcal mol^{-1} but as the conformer is unlikely to form in solution as it is 9.0 kcal mol^{-1} higher in energy than **147aa(1)** this transition state is unlikely to be observed. As a consequence of the shortened C(*spiro*)-O bond the hydrogen peroxide has to be considerably closer to the *spiro*-carbon (2.21 Å and 2.23 Å) to open the epoxide ring than was calculated for the unsubstituted and methyl-substituted epoxide models.

Although the reaction of **147aa+H$^+$** is very exothermic, as a proton has transferred to the methoxy oxygen, it is concluded that the reaction is under kinetic rather than thermodynamic control. This is supported by the larger yield of β-hydroxy hydroperoxide **148aa** achieved when using an alternative catalyst i.e. MoO$_2$(acac)$_2$ which suggested the energy barrier and not the energy of the product is determining the low yields isolated in the acid-catalysed reaction. Although the activation energy for the

opening of **147aa(1)** is relatively low for a room temperature reaction, the higher energy transition states due to the stabilisation of one conformation are consistent with the lower yields of β-hydroxy hydroperoxide **148a**.
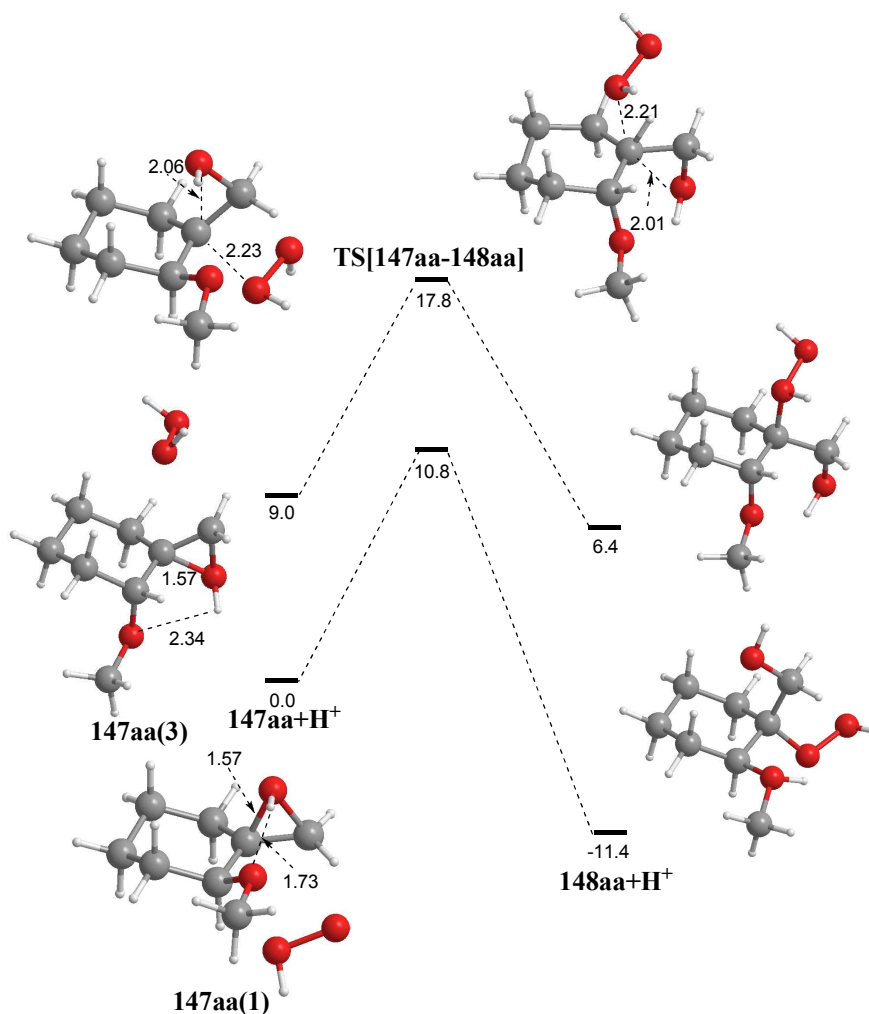
*Figure 35: Reaction profile for the acid-catalysed perhydrolysis of epoxide **147aa**. Energies are in kcal mol^{-1} and relative to lowest energy conformation. Bond distances are given in Å.*

No products were isolated from the acid-catalysed perhydrolysis of epoxide **147ab** implying that there is a larger energy barrier associated with its perhydrolysis reaction than epoxide **147aa**. Like epoxide **147aa, 147ab** can accommodate an additional hydrogen bond between the proton on the epoxide oxygen and the methoxy group. The four conformations considered in this study **147ab(1)-(4)** are illustrated in *Figure 36* and show a 5.5 kcal mol^{-1} energy difference between conformer **147ab(1)** and **147ab(2)**. Both of these conformations have the additional hydrogen bond and are considerably stabilised by 8.4 kcal mol^{-1} and 7.2 kcal mol^{-1} respectively compared to **147ab(3)** and **147ab(4)**. It is again clear that conformer **147ab(1)** is going to be the most abundant in solution.
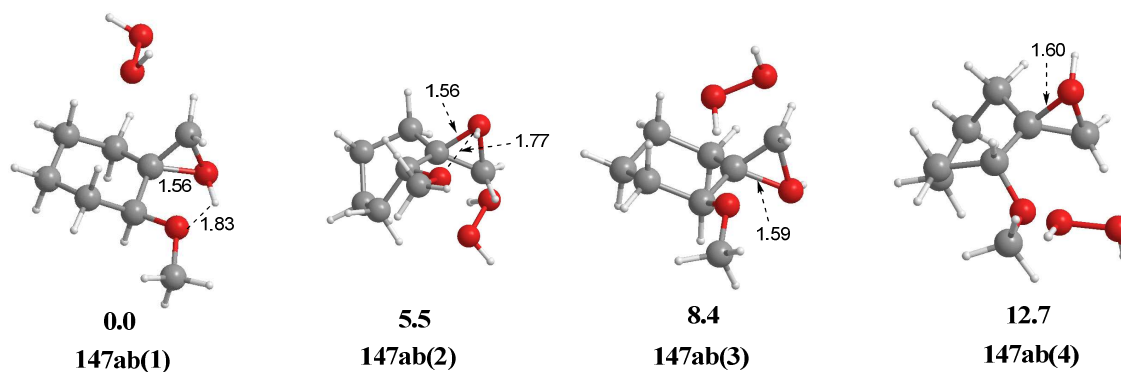
*Figure 36: Four conformations of the acidified epoxide **147ab** showing crucial C-O bond distances and close range H-bonding interactions (Å). Energies are in kcal mol^{-1} and relative to lowest energy conformation.*
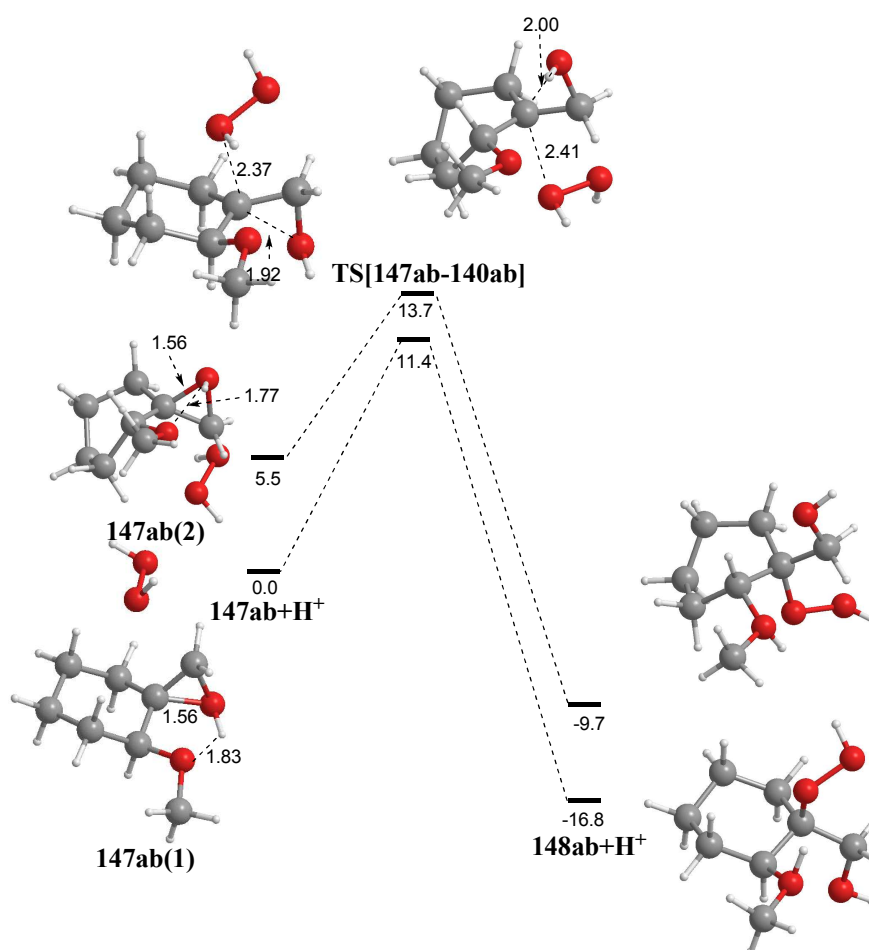
*Figure 37: Reaction profile for the acid-catalysed perhydrolysis of epoxide **147ab**. Energies are in kcal mol^{-1} and relative to lowest energy conformation. Bond distances are given in Å.*

In the same way as was explained for epoxide **147aa**, the hydrogen bond contracts the C-O bond to 1.56 Å in **147ab(1)** making the bond harder to break. Accordingly the energy barrier for the opening of **147ab(1)** was calculated to be 11.4 kcal mol^{-1} *(Figure 37)*. Although this transition state for the opening of epoxide **147ab(1)** is slightly higher

in energy than epoxide **147aa(1)** the difference is only 0.6 kcal mol^{-1} and therefore does not give a clear reason for the apparent unreactive nature of **147ab** to acid-catalysed perhydrolysis. The energies are however still substantially higher than the methyl–substituted epoxide ring openings and consistent with a more difficult ring opening. Although the transition state for the opening of **147ab(2)** is only 8.2 kcal mol^{-1} the conformer is unlikely to form in solution as it is 5.5 kcal mol^{-1} higher in energy than **147ab(1)** again indicating that the reactivity of **147ab** is dictated by the stability of one of its conformations.

Computational studies into the MoO$_2$(acac)$_2$-catalysed methoxy-substitueted epoxide ring opening reaction

The perhydrolysis of methoxy-substituted epoxides **147aa** and **147ab** using a MoO$_2$(acac)$_2$ catalyst gave increased yields of the β-hydroxy hydroperoxide **148aa**, but surprisingly, also gave β-hydroxy hydroperoxide **154a**. The isolated β-hydroxy hydroperoxides **148a** and **154a** are derived from the diastereoisomeric epoxides **147aa** and **147ab** via Mo-mediated ring openings at the most hindered or the least hindered carbon centre respectively *(Scheme 56)*.
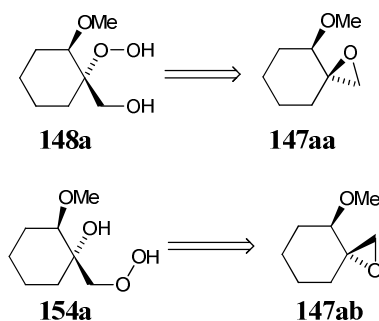
Scheme 56

The calculations discussed within this section have been carried out using density functional theory (DFT) using a B3LYP functional, a 6-31G** basis set and a pseudopotential representing the core electrons of the molybdenum. The calculations sought to investigate the stability of possible epoxide-molybdenum catalyst complexes to determine if the stability of one reactant may correlate with the outcome of the reaction. To do this a series of docking studies have been carried out in order to assess the geometry of the epoxide and the preferred binding orientation at the Mo metal centre. These calculations assume that an acac ligand has been cleaved from the Mo centre allowing the epoxide to bind in a bidentate manner. All energies reported in this section are relative to the most stable Mo-epoxide complex. It is noted however, that

94

other studies of Mo catalysts have made reference to possible seven co-ordinate Mo catalysts where the nucleophile is first bound to the Mo centre as the seventh ligand.[164] Unfortunately attempts to carry out reaction profiles for ring opening reactions were unsuccessful due to unrealistic side reactions between the opened epoxide and the oxo ligands on the catalyst.

The optimised geometry of $MoO_2(acac)_2$ is illustrated in *Figure 38* and shows the preferred *cis*-arrangement between the oxo ligands. The oxo ligand has a *trans*-influence on the acac ligand which means the Mo-O bond *trans* to the oxo ligand is 0.22 Å longer than the Mo-O bond *trans* to the other acac ligand. In this study, the methoxy-substituted epoxides replace an acac ligand meaning the epoxide oxygen can be positioned either *cis* or *trans* to the oxo groups giving a short or long interaction with the molybdenum.
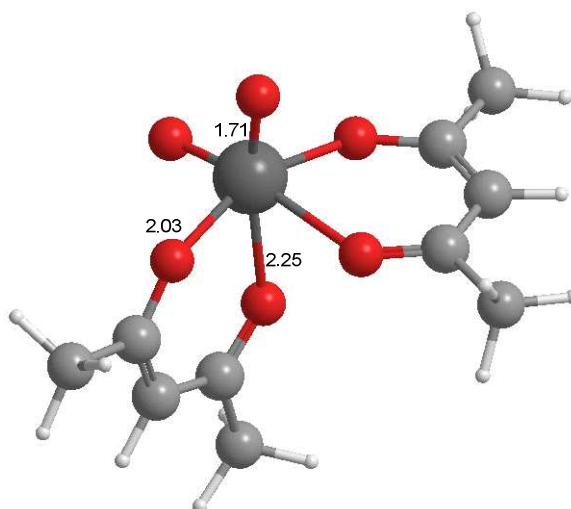
Figure 38: Optimised geometry of $MoO_2(acac)_2$. Distances in Å.

The ring opening of epoxide **147aa** has been shown to produce **148a** via the nucleophilic attack at the *spiro*-carbon by hydrogen peroxide. Epoxide **147aa** can take up two low energy conformations by having the methoxy group or the epoxide oxygen axial in the six-membered ring. The two conformations are related by chair-to-chair interconversion. In either conformation, the epoxide oxygen can be bound to the molybdenum complex *cis* or *trans* to the oxo ligand as illustrated in structures **168-171**.

In each of the four possible arrangements, the epoxide **147aa** is interacting with the molybdenum via both the epoxide oxygen and the methoxy oxygen. A range of distances between the epoxide and the molybdenum are observed depending on the

conformation of the epoxide. In general, the epoxide oxygen is more strongly bound to the molybdenum than the oxygen of the methoxy group with the distance dependant on if the epoxide is *trans* to the oxo or acac ligand. Where the epoxide oxygen is *trans* to the acac ligand there is a short bond of *ca.* 2.16 Å to the molybdenum whilst *trans* to the oxo ligand is slightly longer (2.31-2.39 Å).

The energy of the complexes show a clear preference for **168** and **169** where the epoxide oxygen is in an axial position. The conformations of **168** and **169** look favourable for the nucleophilic attack at the most substituted carbon centre as the epoxide oxygen is in an axial position, which have been shown to be preferred during acid-catalysed reactions. The preferred binding site for epoxide **147aa** looks to be where the epoxide oxygen is *cis* with respect to the oxo ligand in **168**. In this arrangement, a short epoxide oxygen Mo-bond distance of 2.16 Å is accompanied by a longer MeO···Mo bond distance of 2.39 Å. A slight elongation of the C(*spiro*)-O to 1.51 Å in **168** is also observed which is consistent with the site of opening required to produce β-hydroxy hydroperoxide **148a**.
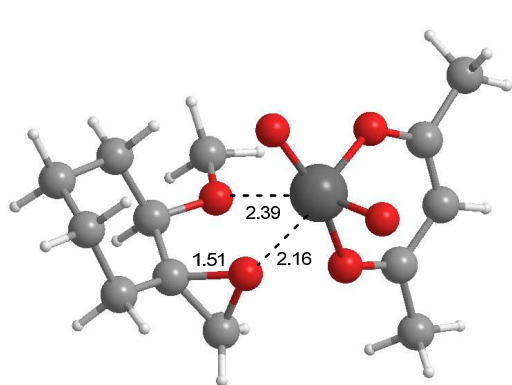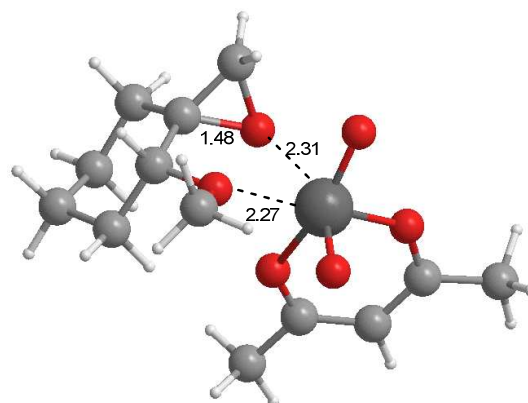
168 (1.02 kcal mol⁻¹)   **169 (1.21 kcal mol⁻¹)**
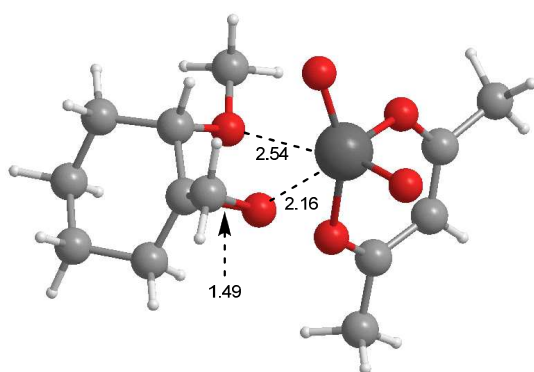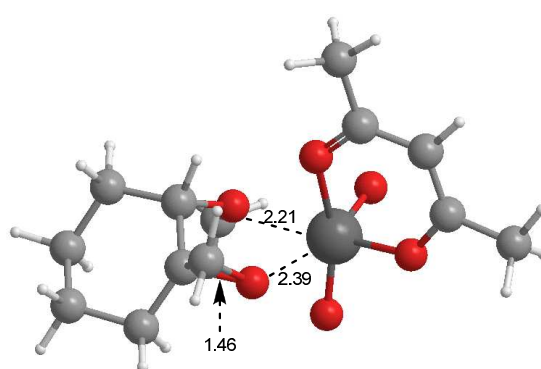
170 (3.37 kcal mol⁻¹)   **171 (6.96 kcal mol⁻¹)**

The ring opening of epoxide **147ab** has been shown to produce **154a** in preference to **148ab** via the nucleophilic attack at the least substituted carbon of the epoxide. Like epoxide **147aa**, epoxide **147ab** can take up two low energy conformations, however in this case the oxygen substituents would either be diaxial or diequatorial. In the arrangement in which the methoxy group and the epoxide oxygen are diaxial the epoxide failed to coordinate to the Mo complex as a bidentate ligand as shown in **172-173**. Due to the gap between the epoxide oxygen and the methoxy group being too large, the epoxide binds by the epoxide oxygen alone leaving the molybdenum atom in a trigonal bipyramidal arrangement. The relative energy levels of **172** and **173** are substantially higher than any other arrangement investigated. It is therefore assumed these complexes would not exist during the reaction.

172 (10.24 kcal mol^{-1})   **173 (7.98 kcal mol^{-1})**
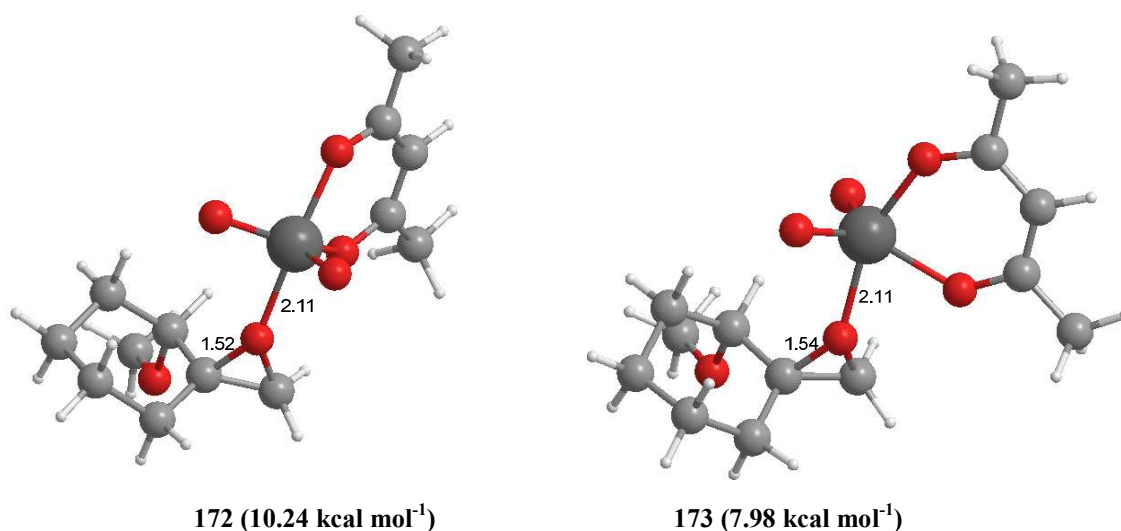
In contrast, the alternative conformers **174-175**, where the oxygens are both equatorial, can form complexes in which both the epoxide oxygen and methoxy oxygen are interacting with the molybdenum. The energy associated with both of these arrangements of epoxide **147ab (174** and **175)** are comparable to the lowest energy form of the diastereoisomer **147aa (168** and **169)**. The preferred binding site for epoxide **147ab** looks to be where the epoxide oxygen is *cis* with respect to the remaining acac ligand (**175**) giving a complex with two similar Mo-O bond distances of *ca*. 2.30 Å to epoxide **147ab**. This is different to epoxide **147aa** which showed preferred binding of the epoxide oxygen *trans* to the remaining acac ligand. In **175** the epoxide shows a shortened C(*spiro*)-O bond of 1.47 Å which implies that nucleophilic attack at the *spiro*-carbon would be more difficult than the corresponding reaction of epoxide

147aa. The shorter C(*spiro*)-O bond in the most stable conformation (**175**) therefore may allow for nucleophilic attack of the least hindered carbon-centre giving **154a**.
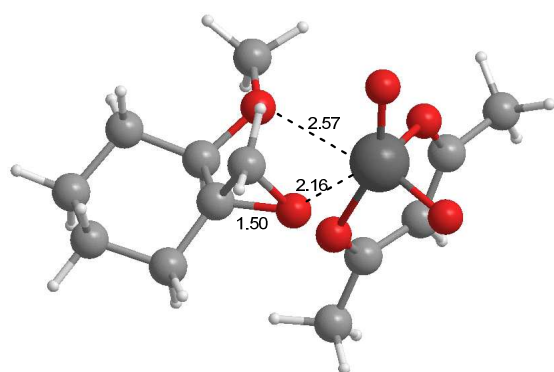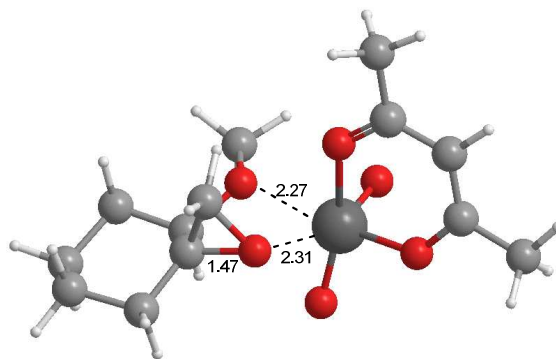
174 (1.69 kcal mol^{-1})   **175 (0.00 kcal mol^{-1})**

General Experimental

Analytical thin layer chromatography was carried out using aluminium backed plates coated with Merck Kieselgel 60 GF254 (Art. 05554). Developed plates were visualised using UV light, molybdic acid spray and a peroxide active spray.[148] Flash chromatography was performed using DAVISIL® silica (60 Å; 35-70 μm) from Fisher (cat. S/0693/60). Fully characterised compounds were chromatographically homogeneous.

Melting points were determined using a Stuart Scientific SMP10 apparatus and are uncorrected. IR spectra were recorded on a Perkin Elmer 1600 FT IR spectrometer as films between sodium chloride plates or as solutions in $CHCl_3$. Mass spectra were obtained on a Kratos Concept IS EI (electron impact) spectrometer at Heriot-Watt University, Finnigan MAT 900 XLT (electron impact and electrospray) at the EPSRC National Mass Spectrometry Service Centre in Swansea and Kratos MS50 (electron impact) at the University of Edinburgh. Elemental analyses were carried out by the analytical service of the Chemistry Department at Heriot-Watt University using an Exeter CE-440 Elemental Analyser. Purity of thermolysis mixtures were checked using Gas chromatatography using a Perkin Elmer 8310 gas chromatography.

^{1}H NMR spectra were recorded at 200 and 400 MHz on Bruker AC200 and DPX400 spectrometers; ^{13}C NMR spectra were recorded at 50 and 100 MHz on the same instruments. Chemical shifts are recorded in parts per million (δ in ppm) and are referenced against solvent signals (δC 77.16 for chloroform) for ^{13}C NMR spectra and solvent residual resonances (δH 7.26 for chloroform) for ^{1}H NMR spectra. Chemical shift values are accurate to ±0.01 ppm and ±0.1 ppm respectively. *J* values are given in Hz. Multiplicity designations used are: s, d, t, q, quint and m for singlet, doublet, triplet, quartet, quintet and multiplet respectively. In ^{13}C NMR spectra, signals corresponding to CH, CH_2, or CH_3 groups are assigned from DEPT.

Commercially available cyclic ketones were purchased from Aldrich, Lancaster, and Fluorochem chemical companies and were generally used as supplied without further purification. Hydrogen peroxide was purchased as a 60% w/v aqueous solution and

dried using calcium chloride and phosphorus pentoxide.[147] Dichloromethane, dimethyl sulphoxide and diethyl ether were pre-dried using activated molecular sieves. 'Light petroleum' refers to the fraction boiling between 40 °C and 60 °C.

Crystallographic Data Collection

Single crystals suitable for X-ray diffraction were mounted in inert oil on a glass fibre and cooled to 100K by an Oxford Cryostream. Data were collected on a Bruker X8 APEX2 diffractometer,[165] employing graphite-monochromated Mo-K$_\alpha$ X-radiation (λ = 0.71069 Å) and were corrected for absorption semi-empirically from symmetry-equivalent and repeated reflectons. Structures were solved by direct and difference ourier methods and refined by full-matrix least squares against F^2 using SHELXTL program suite.[150] Refinement was completed with all non-hydrogen atoms assigned anisotropic displacement parameters. Geometry measurements were made using Mercury.[166]

Preparation of Epoxides

Preparation of 1-oxa*spiro*[2.5]octane (147d)[143,144]

Dried dimethyl sulfoxide (160 mL) was added with stirring to sodium hydride (60% oil dispersion, 5.86 g; 146.3 mmol), which had been washed with light petroleum (2 x 100 mL). Under a constant flow of nitrogen trimethylsulfoxonium iodide (37.13 g; 168.7 mmol) was added slowly over 15 minutes with constant stirring. The mixture was then stirred continuously for an additional 30 minutes until all the hydrogen gas had evolved. Cyclohexanone (8.07 g; 82.3 mmol) was added dropwise over *ca.* 5 minutes. The reaction was left to stir for *ca.* 15 minutes at room temperature then 30 minutes at *ca.* 55°C. The reaction mixture was poured into water (500 mL) and the product extracted using diethyl ether (3 x 100 mL). The organic extract was washed with water (50 ml) and sat. sodium bicarbonate (50 mL) and dried over magnesium sulfate. The solvent was distilled off before 1-oxa*spiro*octane (3.19 g, 28.4 mmol, 34.5%) (b.p. 42°C at 90mm Hg) was collected by distillation under reduced pressure as a clear, colourless liquid: δ_H (200MHz, CDCl$_3$); 1.3-1.8(10 H, m, CH$_2$), 2.5 (2 H, s CH$_2$O), δ_C (50MHz, CDCl$_3$); 24.7, 25.0, 33.4 (CH$_2$), 54.3 (CH$_2$O), 58.8 (qC).

C$_7$H$_{12}$O
112.17 gmol^{-1}
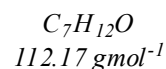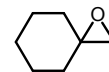
Preparation of 1-(chloroethyl)cyclohexanol (155)

1-*O*xa*spiro*[2.5]octane formed large glass like crystals of 1-(chloroethyl)cyclohexanol **155** when left in deuterated chloroform in the freezer for an extended period: δ_H (200MHz, CDCl$_3$); 1.00-1.70 (10 H, m), 3.43 (2 H, s, CH$_2$Cl), δ_C (50MHz, CDCl$_3$); 21.4, 25.1, 34.5 (CH$_2$), 54.9 (CH$_2$Cl), 70.1 (qC), *m/z* 149 (M$^+$)

C$_7$H$_{12}$DOCl
149.64 gmol^{-1}
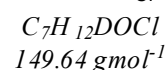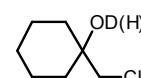
Preparation of 4-methyl-1-oxa*spiro*[2.5]octane (147c)[143,144]

Dried dimethyl sulfoxide (160 mL) was added with stirring to sodium hydride (60% oil dispersion, 5.14 g; 128.4 mmol), which had been washed with light petroleum (2 x 100 mL). Under a constant flow of nitrogen trimethylsulfoxonium iodide (31.27 g; 142.1 mmol) was added slowly over 15 minutes with constant stirring. The mixture was then stirred continuously for an additional 30 minutes until all the

C$_8$H$_{14}$O
126.20 gmol^{-1}
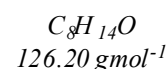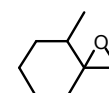
hydrogen gas had evolved. 2-Methylcyclohexanone **146d** (8.00 g; 71.3 mmol) was added dropwise over *ca*. 5 minutes. The reaction was left to stir for *ca*. 15 minutes at room temperature then 30 minutes at *ca*. 55°C. The reaction mixture was poured into water (500 mL) and the product extracted using diethyl ether (3 x 100 mL). The organic extract was washed with water (50 ml) and sat. sodium bicarbonate (50 mL) and dried over magnesium sulfate. The solvent was distilled off before 4-methyl-1-oxa*spiro*octane **147c** (5.07 g, 40.2 mmol, 56.4%) (b.p. 54°C at 80mm Hg) was collected by distillation under reduced pressure as a clear, colourless liquid: δ_H (200MHz, CDCl$_3$); 0.8 (3 H, d, *J* 13.5, CH$_3$), 1.0-1.8 (9 H, m, CH$_2$), 2.6 (2 H, d, *J* 10.4, CH$_2$O), δ_C (50MHz, CDCl$_3$); 13.9 (CH$_3$), 23.5, 24.2, 32.1, 32.4 (CH$_2$), 34.0 (CH), 52.1 (CH$_2$O), 60.5 (qC).

Preparation of 4-methoxy-1-oxa-*spiro*-octane (147a) [143,144]

Dried dimethyl sulfoxide (150 mL) was added with stirring to sodium hydride (60% oil dispersion, 6.13 g; 153.1 mmol), which had been washed with light petrolum (2 x 100 mL). Under a constant flow of nitrogen trimethylsulfoxonium iodide (34.40 g; 156.3 mmol) was added slowly over 15 minutes with constant stirring. The mixture was then stirred continuously for an additional 30 minutes until all the hydrogen gas had evolved. 1-Methoxycyclohexanone (10.04g; 78.3 mmol) was added dropwise over *ca*. 5 minutes. The reaction was left to stir for *ca*. 45 minutes. The reaction mixture was poured into water (500 mL) and the product extracted using diethyl ether (3 x 100 mL). The organic extract was washed with water (50 ml) and sat. sodium chloride (50 mL) and dried over magnesium sulfate. The solvent was distilled off before 4-methoxy-1-oxa*spiro*octane was collected by distillation under reduced pressure as a clear, colourless liquid (10.00 g; 70.3 mmol; 89.8 % yield, 60:40 mixture of diastereoisomers) (b.p. 67°C at 80mm Hg): δ_H (200 MHz CDCl$_3$); 1.1-2.0 (12 H, m), 2.47 (major) (1 H, d, *J* 5.0, CH$_2$O), 2.53 (minor) (1 H, d, *J* 5.1, CH$_2$O), 2.61 (major) (1 H, dd, *J* 5.0 and 1.3, CH$_2$O), 2.83 (minor) (1 H, d, *J* 5.1, CH$_2$O), 3.0 (1 H, m, CH) 3.30 (minor) (3 H, s, OCH$_3$), 3.35 (major) (3 H, s, OCH$_3$), δ_C(50 MHz, CDCl$_3$); 20.8, 21.9, 24.0, 24.9, 29.5, 30.0, 30.2, 30.8 (CH$_2$), 50.4, 51.8 (CH$_2$O), 56.8,57.2 (OCH$_3$), 59.7, 60.2 (qC) 78.9, 79.7 (CH).

$C_8H_{14}O_2$
$142.20 \, gmol^{-1}$
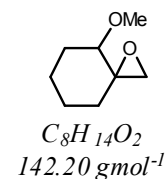
Preparation of 4-ethoxy-1-oxa-*spiro*-octane (147b)[143,144]

Dried dimethyl sulfoxide (180 mL) was added with stirring to sodium hydride (60% oil dispersion, 5.65 g; 141.1 mmol), which had been washed with light petroleum (2 x 100 mL). Under a constant flow of nitrogen trimethylsulfoxonium iodide (31.02 g; 141.0 mmol) was added slowly over 15 minutes with constant stirring. The mixture was then stirred continuously for an additional 30 minutes until all the hydrogen gas had evolved. 2-Ethoxycyclohexanone (10.00 g; 70.3 mmol) was added dropwise over *ca*. 5 minutes. The reaction was left to stir for *ca*. 45 minutes. The reaction mixture was poured into water (500 mL) and the product extracted using diethyl ether (3 x 100 mL). The organic extract was washed with water (50 ml) and sat. sodium bicarbonate (50 mL) and dried over magnesium sulfate. The solvent was distilled off before 4-ethoxy-1-oxa*spiro*octane was collected by distillation under reduced pressure as a clear, yellow liquid (7.75 g; 46.1 mmol; 65.6%, 70:30 mixture of diastereoisomers) (b.p. 70°C at 80mm Hg): δ_H(200 MHz CDCl$_3$); 1.12 (minor), 1.15 (major) (3 H, t, *J* 8.0, CH$_3$), 1.2-2.0 (8 H, m), 2.47 (major) (1 H, d, *J* 5.2, CH$_2$O), 2.52 (minor) (1 H, d, *J* 5.2, CH$_2$O), 2.64 (major) (1 H, dd, *J* 5.0 and 1.1, CH$_2$O), 2.84 (minor) (1 H, d, *J* 5.2, CH$_2$O), 3.1 (1 H, m, CH), 3.5 (2 H, m, OCH$_2$), δ_C(50 MHz, CDCl$_3$); 15.2, 15.3 (CH$_3$), 20.9, 21.7, 24.0, 24.5, 29.9, 30.6, 30.8 (CH$_2$), 50.2, 51.6 (CH$_2$O), 59.7, 60.3, 59.7 (qC), 64.2, 64.9 (OCH$_3$) 77.5, 77.2 (CH)
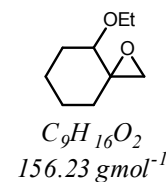
Perhydrolysis of epoxides

General Procedure for the drying of hydrogen peroxide[147]

Hydrogen peroxide (60 %; 12.1 mL; 0.214 mol) was added with stirring to dry diethyl ether (100 mL), at *ca*. -78°C in a thick walled, flat bottomed vessel. Anhydrous calcium chloride (*ca*. 5 g) was added and the reaction mixture and stirred for 10 minutes. Phosphorus pentoxide (*ca*. 5 g) was then slowly added in small portions over 15 minutes with careful monitoring of reaction temperature in order to minimise the exothermicity. The ethereal solution of hydrogen peroxide was decanted into a pre-cooled reaction vessel (-78°C) and used immediately.

Preparation of 1-hydroperoxy-1-hydroxymethylcyclohexanone using Mo(acac)₂ catalyst (148d)

A solution of 1-oxa*spiro*[2.5]octane **147d** (1.55 g, 13.8 mmol) in dry diethyl ether (5 mL) was added dropwise to the anhydrous hydrogen peroxide solution (*ca.* 35 mL) at 0°C and stirred for 24 hours along with molybdenyl acetylacetonate (0.25g; 0.75 mmol). The reaction mixture was poured into water (50 mL) and extracted using diethyl ether (3 x 30 mL). The organic extracts were washed with sat. sodium bicarbonate (30 mL), water (30 mL) and sat. sodium chloride (30mL). The solvent was removed under reduced pressure to yield a yellow oil which was purified collected by flash column chromatography on silica gel eluting with 1:1 light petroleum/ ethyl acetate. 1-Hydroperoxy-1-hydroxymethylcyclohexanone R_f = 0.42 was collected as a viscous oil (1.50 g, 10.3 mmol, 72.8%): δ_H (200MHz, CDCl₃); 1.1-1.9 (10 H, m, CH₂), 3.6 (2 H, s, CH₂O) δ_C (50MHz, CDCl₃); 21.7, 25.9, 29.7 (CH₂), 66.7 (CH₂O), 83.5 (qC)
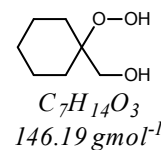
Preparation of 1-hydroperoxy-1-hydroxymethyl-2-methylcyclohexanone using Mo(acac)₂ catalyst (148c)

A solution of 4-methyl-1-oxa*spiro*[2.5]octane **147c** (2.59 g, 20.5 mmol) in dry diethyl ether (5 mL) was added dropwise to the anhydrous hydrogen peroxide solution (*ca.* 50 mL) at 0°C and stirred for 24 hours along with molybdenyl acetylacetonate (0.33 g; 1.0 mmol). The reaction mixture was poured into water (50 mL) and extracted using diethyl ether (3 x 30 mL). The organic extracts were washed with sat. sodium bicarbonate (30 mL), water (30 mL) and sat. sodium chloride (30mL). The solvent was removed under reduced pressure to yield a yellow oil which was purified collected by flash column chromatography on silica gel eluting with 1:1 light petroleum/ ethyl acetate. 1-Hydroperoxy-1-hydroxymethyl-2-methylcyclohexanone R_f = 0.40 was collected as a viscous oil (2.81 g, 17.5 mmol, 85.4%) as a crystalline solid: m.p. 48 °C from diethyl ether/light petroleum, δ_H (200MHz, CDCl₃); 0.9 (3 H, d, *J* 15.6, CH₃), 1.1-2.0 (9 H, m, CH₂), 2.9 (1 H, *b*s, OH), 3.6 (1 H, d, *J* 12.0, CH₂O), 3.7 (1 H, d, *J* 12.0, CH₂O), 8.8 (1 H, *b*s, 1H, OOH) δ_C (50MHz, CDCl₃); 15.5 (CH₃), 21.8, 22.0, 26.5, 29.7 (CH₂), 32.0 (CH), 64.1 (CH₂O), 86.6 (qC), $C_8H_{16}O_3$ requires C 60.0% H 10.1%, found C 59.6% H 10.2%.
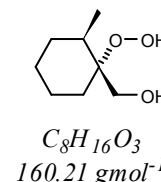
Preparation of 1-hydroperoxy-1-hydroxymethyl-2-methoxycyclohexanone using acid catalyst (148a)

A solution of 4-methoxy-1-oxa*spiro*octane **147a** (6.04 g; 42.8 mmol) in dry diethyl ether (5 mL) was added dropwise to the anhydrous hydrogen peroxide solution (*ca.* 100 mL) at 0°C. Sulfuric acid was added (2 drops, *ca.* 50 mg) and the mixture was stirred for 2 hours.

$C_8H_{16}O_4$
$176.21\,gmol^{-1}$
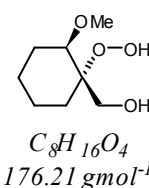
The reaction mixture was poured into water (50 mL) and extracted using diethyl ether (3 x 20 mL). The organic extracts were washed with sat. sodium bicarbonate (30 mL), water (30 mL) and sat. sodium chloride (30mL). The solvent was removed under reduced pressure to yield a yellow oil which was purified collected by flash column chromatography on silica gel eluting with 1:1 light petroleum/ ethyl acetate at R_f = 0.40 as a viscous oil (0.59 g; 3.3 mmol; 7.9%): δ_H(200 MHz CDCl$_3$); 1.1-1.8 (8 H, m), 3.35 (3 H, s, OCH$_3$), 3.45 (1 H, m, CH), 3.7 (1 H, d, *J* 12.0, OCH$_2$), 3.9 (1 H, d, *J* 12.0, OCH$_2$), δ_C(50 MHz, CDCl$_3$); 21.2, 21.3, 24.8, 28.1 (CH$_2$), 57.1 (CH$_3$), 63.0 (CH$_2$OH), 80.1 (CH), 84.7 (COOH)

Preparation of 1-hydroperoxy-1-hydroxymethyl-2-methoxycyclohexanone (148a) and 1-(hydroperoxymethyl)-2-methoxycyclohexanol (154a) using Mo(acac)$_2$ catalyst

A solution of 4-methoxy-1-oxa-*spiro*-octane **147a** (7.99 g; 56.6 mmol) in dry diethyl ether (5 mL) was added dropwise to the anhydrous hydrogen peroxide solution (*ca.* 130 mL) at 0°C and stirred for 24 hours along with molybdenyl acetylacetonate (1.00g; 3.0 mmol). The reaction mixture was poured into water (100 mL) and extracted using diethyl ether (3 x 30 mL). The organic extracts were washed with sat. sodium bicarbonate (30 mL), water (30 mL) and sat. sodium chloride (30mL).

$C_8H_{16}O_4$
$176.21\,gmol^{-1}$

$C_8H_{16}O_4$
$176.21\,gmol^{-1}$
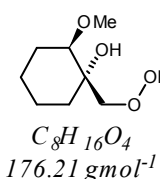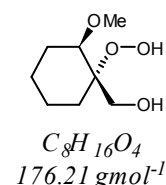
The solvent was removed under reduced pressure to yield a yellow oil which was purified collected by flash column chromatography on silica gel eluting with 1:1 light petroleum/ ethyl acetate. 1-(Hydroperoxymethyl)-2-methoxycyclohexanol R_f = 0.46 was collected as a viscous oil (0.89 g; 5.1 mmol; 9.3% yield): δ_H(200 MHz CDCl$_3$); 1.1-2.0 (8 H, m), 3.20 (1 H, m, CH), 3.45 (3 H, s, CH$_3$), 3.9 (1 H, d, *J* 14.0, OCH$_2$) 4.4 (1 H, d, *J* 14.0, OCH$_2$), 8.2 (1 H, *b*s, OH), 10.5 (1 H, *b*s, OOH), δ_c(50 MHz CDCl$_3$); 22.0, 23.3, 26.0, 33.8 (CH$_2$), 57.7 (CH$_3$), 74.4 (COH), 80.4 (CH$_2$OOH), 84.9 (CH) and

1-hydroperoxy-1-hydroxymethyl-2-methoxycyclohexanone R_f = 0.40 was collected as a viscous yellow oil (3.34 g; 19.0 mmol; 33.7%): δ_H(200 MHz CDCl$_3$); 1.1-1.8 (8 H, m), 3.35 (3 H, s, OCH$_3$), 3.45 (1 H, m, CH), 3.7, (1 H, d, *J* 12.0, OCH$_2$), 3.9 (1 H, d, *J* 12.0 OCH$_2$) δ_C(50 MHz, CDCl$_3$); 21.2, 21.3, 24.8, 28.1 (CH$_2$), 57.1 (CH$_3$), 63.0 (CH$_2$OH), 80.1 (CH), 84.7 (COOH),

Preparation of 1-hydroperoxy-1-hydroxymethyl-2-methoxycyclohexanone (148b) and 1-(hydroperoxymethyl)-2-methoxycyclohexanol (154b) using Mo(acac)$_2$ catalyst.

A solution of 4-ethoxy-1-oxa-*spiro*-octane **147b** (6.00 g; 38.4 mmol) in dry diethyl ether (5 mL) was added dropwise to the anhydrous hydrogen peroxide solution (*ca.* 100 mL) at 0°C and stirred for 24 hours along with molybdenyl acetylacetonate (0.66g; 2.0 mmol). The reaction mixture was poured into water (100 mL) and extracted using diethyl ether (3 x 30 mL). The organic extracts were washed with sat. sodium bicarbonate (30 mL), water (30 mL) and sat. sodium chloride (30mL).

$C_9H_{18}O_4$
190.24 gmol^{-1}

$C_9H_{18}O_4$
190.24 gmol^{-1}
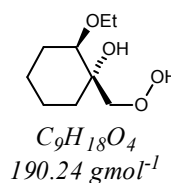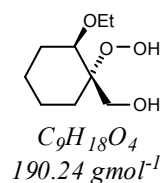
The solvent was removed under reduced pressure to yield a yellow oil which was purified by flash column chromatography on silica gel eluting with 1:1 light petroleum/ ethyl acetate at R_f = 0.55, 0.60 as a viscous yellow oil (2.43g; 12.8 mmol; 33.2%): δ_H(200 MHz CDCl$_3$); 1.13 (t, *J* 7.0, CH$_3$), 1.20-1.90 (m, CH$_2$), 3.30-3.70 (m, CH, CH$_2$O), 3.76, (d, *J* 12.0, OCH$_2$), 3.97 (d, *J* 12.0 OCH$_2$), 4.40 (d, *J* 14.1 OCH$_2$), 9.22 (*b*s), 9.22 (*b*s), 9.57 (*b*s), 10.05 (*b*s), 11.14 (*b*s), δ_c(50 MHz CDCl$_3$); 15.4, 17.5 (CH$_3$), 20.5, 21.1, 21.5, 22.9, 25.8, 26.6, 28.1, 32.7, 33.3 (CH$_2$), 51.2, 62.8, 64.3, 65.2, 65.4 (OCH$_2$), 74.1 (qC), 78.0, 78.6 (CH), 84.5 (qC)

Preparation of *dispiro*-1,2,4-trioxanes

Preparation of 2-(methoxy)cyclohexane-1-*spiro*-3'-(1',2',4'-trioxane)-6'-*spiro*-1''-2''-cyclohexane (149aa) and 2-(Methoxy)cyclohexane-1-*spiro*-3'-(1',2',4'-trioxane)-5'-*spiro*-1''-2''-cyclohexane (160aa)

Cyclohexanone (1.40 g; 14.2 mmol) was added to a cooled (-5°C) solution of 1-hydroperoxy-1-hydroxymethyl-2-methoxycyclohexane oxide **148a** (1.70 g; 9.7 mmol) in dry DCM (30 mL) along with tosic acid (50mg). The mixture was allowed to warm up to room temperature and left to stir for 24 hours. The solution was washed in turn with sat. sodium bicarbonate (30 mL) and water (30 mL) before being extracted into DCM (3 x 30 mL). The combined extracts washed with water (10 mL) and sat. sodium chloride (10 mL) and dried over anhydrous magnesium sulfate before the solvent was removed under vacuum. The crude product was purified by flash column chromatography (1:25 ethyl acetate/ light petroleum) to afford the title compounds. 2-(Methoxy)cyclohexane-1-*spiro*-3'-(1',2',4'-trioxane)-5'-*spiro*-1''-2''-cyclohexane R_f = 0.30 (0.32 g; 1.25 mmol; 4.4% from the epoxide) as a white crystalline solid: υ_{max} (CHCl$_3$)/cm^{-1} 3019, 2939, 2863, 1216; δ_H(400 MHz CD$_2$Cl$_2$) 1.25-1.81 (17H, m, CH$_2$), 2.00 (1 H, m, CH$_2$), 3.26 (1H, t, *J* 3.5, CH), 3.30 (3 H, s, OCH$_3$), 3.87 (1 H, d, *J* 12.6, OCH$_2$), 4.25 (1 H, d, *J* 12.6, OCH$_2$) δ_C (100MHz, CDCl$_3$); 19.9, 20.8, 22.8, 22.9, 25.4, 31.9, 35.3, 36.1 (CH$_2$), 56.9 (CH$_3$), 70.9 (*spiro* C), 76.3 (CH$_2$O), 80.9 (CH), 102.0 (*spiro*-acetal C); *m/z* 256 (M$^+$), accurate mass C$_{14}$H$_{24}$O$_4$ requires 256.16728, found 256.16746; C$_{14}$H$_{24}$O$_4$ requires C 65.6% H 9.4%, found C 65.6% H 9.7% and 2-(methoxy)cyclohexane-1-*spiro*-3'-(1',2',4'-trioxane)-6'-*spiro*-1''-2''-cyclohexane R_f = 0.25 (0.68 g; 2.66 mmol; 9.4% from epoxide) was collected as a yellow viscous oil: υ_{max}/cm^{-1} 2935, 2864, 1448, 1362; δ_H(400 MHz, -50°C CDCl$_3$) 1.15-1.70 (17 H, m), 1.89 (1 H, m, CH$_2$), 3.32 (3 H, s, OCH$_3$), 3.56 (1 H, m, OCH$_2$) , 3.86 (1 H, d, *J* 11.8, OCH$_2$), 4.09 (1 H, s, CH), δ_C(100 MHz, -50°C, CDCl3); 18.5, 19.3, 21.9, 23.7, 24.7, 25.0, 27.4, 27.8 (CH$_2$), 56.8 (CH$_3$), 61.7 (CH$_2$O), 72.6 (CH), 78.0 (*spiro*-C), 102.0 (*spiro*-acetal C); *m/z* 256 (M$^+$), accurate mass C$_{14}$H$_{24}$O$_4$ requires 256.16728, found 256.16746, C$_{14}$H$_{24}$O$_4$ requires C 65.6% H 9.4%, found C 65.3% H 9.6%,

In one reaction 1,1'-peroxybis(1-hydroperoxycyclohexane) (**161**) R_f= 0.15 (0.77 g; 2.94 mmol) was collected as a white crystalline solid: υ_{max} (CHCl$_3$)/cm^{-1} 3420, 3019, 2942, 2866, 1450, δ_H(200 MHz CD$_2$Cl$_2$) 1.40-1.70 (12 H, m, CH$_2$), 1.80-2.00 (8 H, m, CH$_2$), 9.50 (2 H, s, OOH) δ_C (50MHz, CDCl$_3$); 22.0, 24.9, 29.3 (CH$_2$), 110.7 (COOH).

C$_{12}$H$_{22}$O$_6$
262.30 gmol^{-1}
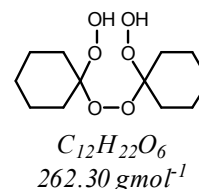
Preparation of 2-(methoxy)cyclohexane-1-*spiro*-3'-(1',2',4'-trioxane)-6'-*spiro*-1''-2''-cyclopentane (149ab) and 2-(methoxy)cyclohexane-1-*spiro*-3'-(1',2',4'-trioxane)-5'-*spiro*-1''-2''-cyclohexane (160ab)

Cyclopentanone (1.22 g; 14.5 mmol) was added to a cooled (-5°C) solution of 1-hydroperoxy-1-(hydroxymethyl)-2-(methoxy)cyclohexane oxide **148a** (1.70 g; 9.7 mmol) in dry DCM (30 mL) along with tosic acid (50 mg). The mixture was allowed to warm up to room temperature and left to stir for 24 hours. The solution was washed in turn with sat. sodium bicarbonate (30 mL) and water (30 mL) before being extracted into DCM (3 x 30 mL). The combined extracts washed with water (10 mL) and sat. sodium chloride (10 mL)

C$_{13}$H$_{22}$O$_4$
242.32 gmol^{-1}

C$_{13}$H$_{22}$O$_4$
242.32 gmol^{-1}

and dried over anhydrous magnesium sulfate before the solvent was removed under vacuum. The crude product was purified by flash column chromatography (1:25 ethyl acetate/ light petroleum) to afford the title compounds. 2-(Methoxy)cyclohexane-1-*spiro*-3'-(1',2',4'-trioxane)-5'-*spiro*-1''-2''-cyclohexane R_f = 0.30 (0.50 g; 2.06 mmol; 7.1% from the epoxide) was obtained as a white crystalline solid: υ_{max} (CHCl$_3$)/cm^{-1} 3019, 2941, 1215 δ_H(400 MHz CD$_2$Cl$_2$) 1.33-1.80 (15 H, m, CH$_2$), 2.25 (1 H, m, CH$_2$), 3.30 (1 H, m, CH), 3.30 (3 H, s, OCH$_3$), 3.88 (1 H, d, *J* 12.6, OCH$_2$), 4.25 (1 H, d, *J* 12.6, OCH$_2$) δ_C (100MHz, CDCl$_3$); 20.0, 20.6, 23.0, 24.1, 29.9, 36.9, 38.0 (CH$_2$), 56.9 (CH$_3$), 71.3 (*spiro* C), 76.6 (CH$_2$O), 79.6 (CH), 113.0 (*spiro*-acetal C)]; *m/z* 242 (M$^+$), accurate mass C$_{12}$H$_{22}$O$_4$ requires 242.15164, found 242.15181; C$_{13}$H$_{22}$O$_4$ requires C 64.45% H 9.2%, found C 64.11% H 9.26%, and 2-(methoxy)cyclohexane-1-*spiro*-3'-(1',2',4'-trioxane)-6'-*spiro*-1''-2''-cyclopentane R_f = 0.25 (0.737 g; 3.04 mmol; 10.5% from epoxide) was collected as a yellow viscous oil: υ_{max}/cm^{-1} 2937, 2868, 1455, 1332; δ_H(400 MHz CDCl$_3$, -50°C) 1.15-1.89 (15 H, m, CH$_2$), 2.46 (1 H, m, CH$_2$), 3.33 (3 H, s, OCH$_3$), 3.39 (1 H, d, *J* 11.5), 3.94 (1 H, d, *J* 11.5), 4.10 (1 H, s, CH) δ_C (100MHz, CDCl3, -50°C); 18.6, 19.3, 22.0, 22.6, 24.5, 27.3, 31.8, 37.0 (CH$_2$), 56.8 (CH$_3$), 64.4 (CH$_2$O), 72.5 (CH), 78.0 (*spiro* C), 113.9 (*spiro*-acetal C); *m/z* 242 (M$^+$), accurate mass

$C_{12}H_{22}O_4$ requires 242.15164, found 242.15181; $C_{13}H_{22}O_4$ requires C 64.45% H 9.15%, found C 64.85% H 9.35%

In one reaction 1,1'-peroxybis(1-hydroperoxycyclopentane) (**162**) R_f = 0.13 (0.21g; 0.88 mmol) was collected as a white crystalline solid: υ_{max} (CHCl$_3$)/cm^{-1} 3426, 3018, 2945, 2876, 1715, 1214, δ_H(200 MHz CD$_2$Cl$_2$) 1.50-1.70 (10 H, m, CH$_2$), 1.80-2.05 (8 H, m, CH$_2$), 9.70 (2 H, s, OOH) δ_C (50MHz, CDCl$_3$); 24.1, 32.8 (CH$_2$), 122.0 (COOH).

$C_{10}H_{20}O_6$
236.26 gmol^{-1}

Preparation of 2-(methoxy)cyclohexane-1-*spiro*-3'-(1',2',4'-trioxane)-6'-*spiro*-1''-2''-cycloheptane (149ac)

Cycloheptanone (0.57 g; 5.1 mmol) was added to a cooled (-5°C) solution of 1-hydroperoxy-1-(hydroxymethyl)-2-(methoxy)cyclohexane oxide **148a** (0.59 g; 3.4 mmol) in dry DCM (40 mL) along with tosic acid (50 mg). The mixture was allowed to warm up to room temperature and left to stir for 24 hours. The solution was washed in turn with sat. sodium bicarbonate (30 mL) and water (30 mL) before being extracted into DCM (3 x 30 mL). The combined extracts washed with water (10 mL) and sat. sodium chloride (10 mL) and dried over anhydrous magnesium sulfate before the solvent was removed under vacuum. The crude product was purified by flash column chromatography (1:25 ethyl acetate/ light petroleum) to afford the title compound. 2-(Methoxy)cyclohexane-1-*spiro*-3'-(1',2',4'-trioxane)-6'-*spiro*-1''-2''-cycloheptane R_f = 0.30 (0.20g; 0.74 mmol; 7.4% from epoxide) was collected as a yellow viscous oil : υ_{max}/cm^{-1} 2931, 1457, 1369; δ_H(400 MHz CDCl$_3$, -50°C) 1.26-1.94 (19 H, m, CH$_2$), 2.48 (1 H, m, CH$_2$), 3.34 (3 H, s, OCH$_3$), 3.48 (1 H, d, *J* 11.8), 3.84 (1 H, d, *J* 11.8) , 4.05 (1 H, s, CH) δ_C (100MHz, CDCl3, -50°C); 18.6, 19.2, 21.8, 21.9 22.0, 27.5, 30.0, 30.1, 30.4, 37.8 (CH$_2$), 56.9 (CH$_3$), 62.2 (CH$_2$O), 72.9 (CH), 78.0 (*spiro* C), 107.2 (*spiro*-acetal C); *m/z* 270 (M$^+$), accurate mass $C_{15}H_{26}O_4$ requires 270.18292, found 270.18311; $C_{15}H_{22}O_4$ requires C 66.7% H 9.7%, found C 66.8% H 9.8%.
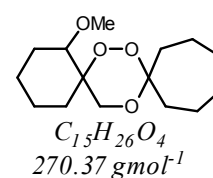
$C_{15}H_{26}O_4$
270.37 gmol^{-1}

In one reaction 3,6-*spiro*-dicycloheptylidene-1,2,4,5-tetraoxacyclohexane (**163**) R_f = 0.42 (180 mg; 0.70 mmol) was collected as a white crystalline solid: υ_{max} (CHCl$_3$)/cm^{-1} 3019,

$C_{14}H_{24}O_4$
256.34 gmol^{-1}

2932, 2856, 1635, 1215, δ_H(200 MHz CDCl$_3$) 1.20-2.00 (20 H, m, CH$_2$), 2.16 (2 H, m, CH$_2$), 2.42 (2 H, m, CH$_2$), δ_C (50MHz, CDCl$_3$, -50°C); 22.74, 29.9, 32.9 (CH$_2$), 112.8 (*spiro*-acetal C)

Preparation of 2-(methoxy)cyclohexane-1-*spiro*-3'-(1',2',4'-trioxane)-6'-*spiro*-1''-2''-cyclododecane (149ad)

Cyclododecanone (1.09 g; 6.0 mmol) was added to a cooled (-5°C) solution of 1-hydroperoxy-1-hydroxymethyl-2-methoxycyclohexane oxide **148a** (0.70 g; 4.0 mmol) in dry DCM (30 mL) along with tosic acid (50 mg). The mixture was allowed to warm up to room temperature and left to stir for *ca.*

$C_{20}H_{36}O_4$
$340.50\ gmol^{-1}$

24 hours. The solution was washed in turn with sat. sodium bicarbonate (30 mL) and water (30 mL) before being extracted into DCM (3 x 30 mL). The combined extracts washed with water (10 mL) and sat. sodium chloride (10 mL) and dried over anhydrous magnesium sulfate before the solvent was removed under vacuum. The crude product was purified by flash column chromatography (2:25 ethyl acetate/ light petroleum) to afford the title compound. 2-(Methoxy)cyclohexane-1-*spiro*-3'-(1',2',4'-trioxane)-6'-*spiro*-1''-2''-cyclododecane R$_f$ = 0.30 (100 mg; 0.29 mmol; 7.3%) was collected as a white solid: m.p 91-93°C from diethyl ether/ light petroleum, υ_{max} (CHCl$_3$)/cm^{-1} 3019, 2936, 1215; δ_H(400 MHz CD$_2$Cl$_2$, -30°C) 1.12-1.67 (28 H, m, CH$_2$), 1.88 (2H, m), 3.32 (3 H, s, OCH$_3$), 3.43 (1H, d, *J* 11.8), 3.80 (1 H, d, *J* 11.8), 4.03 (1 H, s, CH), δ_C (100MHz, CDCl3, -30°C); 18.7, 19.2, 19.5, 19.9 21.4, 21.9, 22.21, 22.26, 22.7, 23.8, 26.0, 26.1, 26.2, 28.0, 31.9 (CH$_2$), 57.1 (CH$_3$), 62.5 (CH$_2$O), 73.4 (CH), 78.2 (*spiro* C), 106.1 (*spiro*-acetal C); *m/z* 270 (M$^+$), accurate mass C$_{20}$H$_{36}$O$_4$ requires 340.26656, found 340.26949; C$_{20}$H$_{36}$O$_4$ requires C 70.6% H 10.7%, found C 70.4% H 10.8%.

Attempted preparation of indane-2-*spiro*-3'1(1',2',4'-trioxane)-6'-*spiro*-1''-2''-methoxycyclohexane (149ag)

2-Indanone (0.37 g; 3.1 mmol) was added to a cooled (-5°C) solution of 1-hydroperoxy-1-hydroxymethyl-2-methoxycyclohexane oxide **148a** (0.54 g; 3.1 mmol) in dry DCM (30 mL) along with tosic acid (*ca.* 50 mg). The mixture
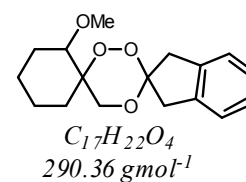
$C_{17}H_{22}O_4$
290.36 gmol^{-1}

was allowed to warm up to room temperature and left to stir for *ca.* 24 hours. The solution was washed in turn with sat. sodium bicarbonate (30 mL) and water (30 mL) before being extracted into DCM (3 x 30 mL). The combined extracts washed with water (10 mL) and sat. sodium chloride (10 mL) and dried over anhydrous magnesium sulfate before the solvent was removed under vacuum. The crude product was purified by flash column chromatography (2:25 ethyl acetate/ light petroleum) to afford a mixture of the title compound and unidentified products R_f= 0.35 (50 mg; 0.17 mmol; 5.5%) was collected as a colourless viscous oil. Observed signals for indane-2-*spiro*-3'1(1',2',4'-trioxane)-6'-*spiro*-1''-2''-methoxycyclohexane **149ag**: δ_H(400 MHz CD$_2$Cl$_2$, -50°C) 1.15-1.77 (m, CH$_2$), 1.93 (m, CH$_2$), 3.02-3.33 (m, CH) 3.38 (s, OCH$_3$), 3.41 (s, CH$_2$), 3.57 (d, *J* 11.8, OCH$_2$), 3.93 (d, *J* 11.8, OCH$_2$), 4.11 (1 H, s, CH), 7.16-7.25 (m, Ar C-H) δ_C (100MHz, CDCl3, -50°C); 18.5, 19.2, 21.9, 27.3, 38.2, 43.3 (CH$_2$), 56.9 (CH$_3$), 62.9 (CH$_2$O), 72.5 (CH), 78.3 (*spiro* C), 101.9 (*spiro*-acetal C), 124.3, 125.0, 129.2, 130.2 (Aromatic CH), 138.0, 139.2 (Aromatic qC)

Preparation of 2-(methoxy)cyclohexane-1-*spiro*-3'-(1',2',4'-trioxane)-6'-*spiro*-1''-2''-1''',4'''-dioxa*spiro*[4.5]decane (149ae)

1,4-Dioxa*spiro*[4.5]decan-8-one (0.41 g; 2.6 mmol) was added to a cooled (-5°C) solution of 1-hydroperoxy-1-hydroxymethyl-2-methoxycyclohexane oxide **148a** (0.45 g; 2.6 mmol) in dry DCM (30 mL) along with tosic acid (50 mg). The mixture was allowed
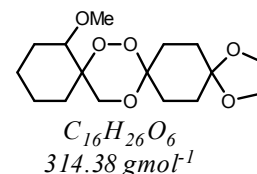
$C_{16}H_{26}O_6$
314.38 gmol^{-1}

to warm up to room temperature and left to stir for *ca.* 24 hours. The solution was washed in turn with sat. sodium bicarbonate (30 mL) and water (30 mL) before being extracted into DCM (3 x 30 mL). The combined extracts washed with water (10 mL) and sat. sodium chloride (10 mL) and dried over anhydrous magnesium sulfate before the solvent was removed under vacuum. The crude product was purified by flash column chromatography (1:3 ethyl acetate/ light petroleum) to afford the title

compound.   2-(Methoxy)cyclohexane-1-*spiro*-3'-(1',2',4'-trioxane)-6'-*spiro*-1''-2''-1''',4'''-dioxa*spiro*[4.5]decane R$_f$ = 0.51 (90 mg; 0.30 mmol; 11.7%) was collected as a white solid: υ$_{max}$ (CHCl$_3$)/cm^{-1} 3015, 2937, 2881, 1375, 1215, 1109; δ$_H$(400 MHz CDCl$_3$, 60°C) 1.18-2.20 (16H, m, CH$_2$), 3.34 (3 H, s, OCH$_3$), 3.51 (1 H, d, *J* 11.5), 3.70 (1 H, *b*s, CH), 3.90 (4 H, s, CH$_2$), 3.92 (1 H, d, *J* 11.5), δ$_C$ (100MHz, CDCl3, -30°C); 20.3, 28.8, 24.1, 28.0, 28.1, 30.8, 30.9, 32.2 (CH$_2$), 57.2 (CH$_3$), 62.6 (CH$_2$O), 64.3 (OCH$_2$CH$_2$O), 79.5 (*spiro* C), 81.3 (CH), 101.5 108.5 (*spiro*-acetal C); *m/z* 314 (M$^+$), accurate mass C$_{16}$H$_{26}$O$_6$ requires 314.17262, found 314.17239.

Attempted preparation of 2-(methoxy)cyclohexane-1-*spiro*-3'-(1',2',4'-trioxane)-5'-*spiro*-1''-2''-1''',4'''-dioxa*spiro*[4.5]decane (160ae)

1,4-Dioxa*spiro*[4.5]decan-8-one (0.30 g; 1.92 mmol) was added to a cooled (-5°C) solution of 1-hydroperoxy-1-hydroxymethyl-2-methoxycyclohexane oxide **154a** (0.28 g; 1.59 mmol) in dry DCM (30 mL) along with tosic acid (*ca.* 50 mg). The mixture was allowed to warm up to room temperature and left to stir for 24 hours. The solution was washed in turn with sat. sodium bicarbonate (30 mL) and water (30 mL) before being extracted into DCM (3 x 30 mL). The combined extracts were washed with water (10 mL) and sat. sodium chloride (10 mL) and dried over anhydrous magnesium sulfat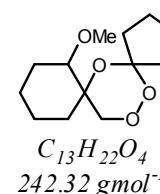e before the solvent was removed under vacuum. The crude product was purified by flash column chromatography (1:5 ethyl acetate/ light petrolum) to afford the title compound. 2-(Methoxy)cyclohexane-1-*spiro*-3'-(1',2',4'-trioxane)-5'-*spiro*-1''-2''-1''',4'''-dioxa*spiro*[4.5]decane R$_f$ = 0.40 (108 mg; 0.34 mmol; 22.4%) was collected as a colourless oil: δ$_H$(400 MHz CDCl$_3$, 25°C) 1.26-2.30 (16 H, m, CH$_2$), 2.48 (2 H, m, CH$_2$), 3.26 (1 H, s, CH), 3.29 (3 H, s, CH$_3$), 3.31 (3 H, s, OCH$_3$), 3.89 (1H, d, *J* 12.6, OCH$_2$), 3.93 (4 H, s, OCH$_2$CH$_2$O), 3.97 (1 H, d, *J* 12.6, OCH$_2$), 4.26 (1 H, d, *J* 12.6, OCH$_2$), 4.35 (1 H, d, *J* 12.6, OCH$_2$), δ$_C$ (100MHz, CDCl$_3$); 19.7, 19.8, 20.7, 20.8, 22.4, 23.7, 23.8, 23.9, 24.2, 31.0, 31.2, 31.6, 31.7, 32.2, 33.2, 33.4, 34.6, 36.8, 37.0 (CH$_2$), 56.7, 56.9 (CH$_3$), 64.2, 64.3 (CH$_2$) 70.9, 71.5 (*spiro* C), 76.5 (CH$_2$O), 80.7 (CH), 100.7, 101.3 (*spiro*-acetal C), 108.2 (*spiro*-acetal C), 210.0 (C=O).

$C_{16}H_{26}O_6$
$314.38 \, gmol^{-1}$

Preparation of cyclohexane-4-one-1-*spiro*-3'-(1',2',4'-trioxane)-5'-*spiro*-1''-2''-methoxycyclohexanone (160af)

2-(Methoxy)cyclohexane-1-*spiro*-3'-(1',2',4'-trioxane)-6'-*spiro*-1''-2''-1''',4'''-dioxa*spiro*[4.5]decane **160ac** (108 mg, 0.34 mmol) in acetone (10 mL) was treated with tosic acid (0.23 g, 1.2 mmol) and continuously stirred overnight at r.t. The product was extracted using ethyl acetate (3 x 20 mL) and the combined extracts were washed with sat. sodium bicarbonate (10 mL) and sat. sodium chloride (10 mL). After drying with magnesium sulfate, the solvent was evaporated. Incomplete reaction meant the reaction was repeated for a further 24 hours. The crude product was purified by flash column chromatography (1:5 ethyl acetate/ light petroleum) to afford the title compound. Cyclohexane-4-one-1-*spiro*-3'-(1',2',4'-trioxane)-5'-*spiro*-1''-2''-methoxycyclohexanone R_f = 0.40 (90 mg; 0.33 mmol; 97.1%) was collected as a colourless oil: υ_{max} (CHCl$_3$)/cm^{-1} 3019, 2938, 2865, 1718, 1215; δ_H(400 MHz CDCl$_3$, -50°C) 1.31-1.79 (10 H, m, CH$_2$), 2.05 (1 H, m, CH$_2$), 2.16 (1 H, m, CH$_2$), 2.43 (4 H, m, CH$_2$), 3.27 (1 H, m, CH), 3.31 (3 H, s, OCH$_3$), 3.97 (1 H, d, *J* 12.0, OCH$_2$), 4.34 (1 H, d, *J* 12.0, OCH$_2$) δ_C (100MHz, CDCl$_3$); 19.9, 20.8, 24.0, 31.7, 33.4, 34.6, 36.9, 37.1 (CH$_2$), 56.9 (CH$_3$), 71.6 (*spiro* C), 76.5 (CH$_2$O), 80.7 (CH), 100.7 (*spiro*-acetal C), 210.0 (C=O); *m/z* 270 (M$^+$), accurate mass C$_{14}$H$_{22}$O$_5$ requires 270.14620, found 270.14618

Preparation of 2-(ethoxy)cyclohexane-1-*spiro*-3'-(1',2',4'-trioxane)-6'-*spiro*-1''-2''-cyclohexane (149ba) and 2-(ethoxy)cyclohexane-1-*spiro*-3'-(1',2',4'-trioxane)-5'-*spiro*-1''-2''-cyclohexane (160ba)

Cyclohexanone (0.78 g; 8.0 mmol) was added to a cooled (-5°C) solution of 1-hydroperoxy-1-hydroxymethyl-2-ethoxycyclohexane oxide **148b** (1.00 g; 5.3 mmol) in dry DCM (30 mL) along with tosic acid (50 mg). The mixture was allowed to warm up to room temperature and left to stir for *ca*. 24 hours. The solution was washed in turn with sat. sodium bicarbonate (30 mL) and water (30 mL) before being extracted into DCM (3 x 30 mL). The combined extracts were wa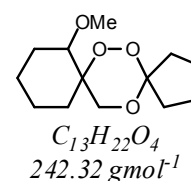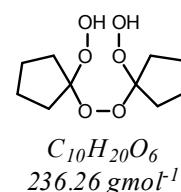shed with water (10 mL) and sat. sodium chloride (10 mL) and dried over anhydrous magnesium sulfate before the solvent was removed under vacuum. The crude product was purified by flash column chromatography (1:50)
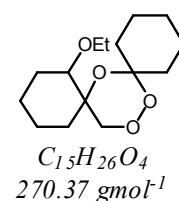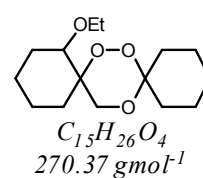
ethyl acetate/ light petroleum) to afford the title compounds. 2-(Ethoxy)cyclohexane-1-*spiro*-3'-(1',2',4'-trioxane)-5'-*spiro*-1''-2''-cyclohexane R_f = 0.30 (0.18 g; 0.67 mmol; 4.3% from the epoxide) as a viscous oil: δ_H(400 MHz CD_2Cl_2) 1.13 (3 H, t, *J* 7.0, CH_3) 1.27-2.01 (18H, m, CH_2), 3.35 (1 H, m, CH), 3.44 (1 H, m, CH_2CH_3), 3.58 (1 H, dq, *J* 7.0, 7.0, 7.0 and 9.4, CH_2CH_3) 3.88 (1 H, d, *J* 12.6, OCH_2), 4.27 (1 H, d, *J* 12.6, OCH_2) δ_C (100MHz, $CDCl_3$); 15.5, 20.2, 20.4, 22.4, 22.5, 22.8, 25.1, 25.7, 28.0, 30.8, 32.6 (CH_2), 62.0 (OCH_2CH_3), 64.5 (OCH_2), 71.0 (*spiro*-C) 79.0 (CH), 102.1 (*spiro*-acetal C) and 2-(ethoxy)cyclohexane-1-*spiro*-3'-(1',2',4'-trioxane)-6'-*spiro*-1''-2''-cyclohexane R_f = 0.27 (0.34 g; 1.25 mmol; 7.9% from epoxide) was collected as a colourless viscous oil: υ_{max} ($CHCl_3$)/cm^{-1} 2935, 2864, 1448, 1362; δ_H(400 MHz, 60°C $CDCl_3$) 1.16 (3 H, t, *J* 8.0, CH_3) 1.30-2.03 (18 H, m, CH_2), 3.44 (1 H, dq, *J* 7.0 and 9.5, CH_2CH_3), 3.52 (1 H, d, *J* 11.5, CH_2O), 3.60 (1 H, dq, *J* 7.0, 7.0, 7.0 and 9.5, CH_2CH_3), 3.80 (1 H, bs, CH), 3.92 (1 H, d, *J* 11.5 CH_2O), δ_C(100 MHz, 60°C, $CDCl_3$); 15.5 (CH_3) 20.2, 20.4, 22.4, 22.5, 22.8, 25.1, 25.7, 28.0, 30.8, 32.6 (CH_2), 62.3 (OCH_2), 64.5 (OCH_2CH_3), 74.1 (CH), 79.4 (*spiro*-C), 102.1 (*spiro*-acetal C); *m/z* 270 (M^+), accurate mass $[C_{15}H_{26}O_4NH_4]^+$ requires 288.2169, found 288.2171; $C_{15}H_{26}O_4$ requires C 66.6% H 9.7%, found C 66.6% H 9.9%.

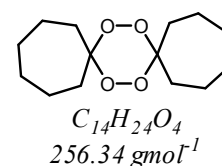**Preparation of 2-(ethoxy)cyclohexane-1-*spiro*-3'-(1',2',4'-trioxane)-6'-*spiro*-1''-2''-cyclopentane (149bb) and 2-(Ethoxy)cyclohexane-1-*spiro*-3'-(1',2',4'-trioxane)-5'-*spiro*-1''-2''-cyclopentane (160bb)**

Cyclopentanone (0.67 g; 8.0 mmol) was added to a cooled (-5°C) solution of 1-hydroperoxy-1-hydroxymethyl-2-ethoxycyclohexane oxide **148b** (1.00 g; 5.3 mmol) in dry DCM (30 mL) along with tosic acid (50 mg). The mixture was allowed to warm up to room temperature and left to stir for *ca*. 24 hours. The solution was washed in turn with sat. sodium bicarbonate (30 mL) and water (30 mL) before being extracted into DCM (3 x 30 mL). The combined extracts were washed with water (10 mL) and sat. sodium chloride (10 mL) and dried over anhydrous magnesium sulfate before the solvent was removed under vacuum. The crude product was purified by flash column chromatography (1:**25)** ethyl acetate/ light petroleum 40-60°C) to afford the title compounds. 2-(Ethoxy)cyclohexane-1-*spiro*-3'-(1',2',4'-trioxane)-5'-*spiro*-1''-2''-cyclopentane R_f = 0.33 (13 mg; 0.05 mmol; 1.0% from the epoxide) as a colourless oil: υ_{max}/cm^{-1} 3019, 1521, 1424, 1214 δ_H(400 MHz CD_2Cl_2) 1.14 (3 H, t, *J* 7.0, CH_3) 1.33-1.85 (14 H, m,

$C_{14}H_{24}O_4$
256.36 gmol⁻¹

$C_{14}H_{24}O_4$
256.36 gmol⁻¹

CH$_2$), 1.97 (1 H, m, CH$_2$), 2.25 (1 H, m, CH$_2$), 3.34 (1 H, m, CH$_2$CH$_3$), 3.41 (1 H, t, *J* 3.5, CH) 3.58 (1 H, dq, *J* 7.0, 7.0, 7.0 and 9.4, CH$_2$CH$_3$) 3.90 (1 H, d, *J* 12.6, OCH$_2$), 4.27 (1 H, d, *J* 12.6, OCH$_2$) δ_C (100MHz, CDCl$_3$); 15.6 (CH$_3$), 20.2, 20.6, 23.1, 23.9, 24.1, 30.0, 37.0, 38.0 (CH$_2$), 64.5 (OCH$_2$CH$_3$), 71.3 (*spiro*-C), 77.8 (CH), 77.7 (OCH$_2$), 112.3 (*spiro*-acetal C); *m/z* 256 (M$^+$), accurate mass C$_{15}$H$_{22}$O$_4$ requires 254.15181 , found 254.15181 and 2-(ethoxy)cyclohexane-1-*spiro*-3'-(1',2',4'-trioxane)-6'-*spiro*-1''-2''-cyclopenane R$_f$ = 0.50 (0.54 g; 2.12 mmol; 13.4% from epoxide) was collected as a colourless viscous oil: υ_{max} (CHCl$_3$)/cm^{-1} 3019, 2940, 2866, 1214; δ_H(400 MHz, 60°C, CDCl$_3$) 1.16 (3 H, t, *J* 7.0, CH$_3$) 1.23-2.27 (16 H, m, CH$_2$), 3.45 (1 H, m, CH$_2$CH$_3$), 3.50 (1 H, d, *J* 11.8, CH$_2$O), 3.61 (1 H, dq, *J* 7.0 and 9.5, CH$_2$CH$_3$), 3.85 (1 H, bs, CH), 3.95 (1 H, d, *J* 11.8 CH$_2$O), δ_C(100 MHz, 60°C, CDCl$_3$); 15.6 (CH$_3$) 20.3, 23.7, 24.1, 25.1, 27.9, 34.0, 36.0 (CH$_2$), 64.8 (OCH$_2$), 65.0 (OCH$_2$CH$_3$), 74.0 (CH), 79.2 (*spiro*-C), 114.1 (*spiro*-acetal C); *m/z* 256 (M$^+$), accurate mass C$_{15}$H$_{26}$O$_4$ requires 256.1675, found 256.1732; C$_{14}$H$_{24}$O$_4$ requires C 65.6% H 9.4%, found C 65.0% H 9.6%.

Preparation of 2-(ethoxy)cyclohexane-1-*spiro*-3'-(1',2',4'-trioxane)-6'-*spiro*-1''-2''-cycloheptane (149bc)

Cycloheptanone (0.89g; 7.9 mmol) was added to a cooled (-5°C) solution of 1-hydroperoxy-1-hydroxymethyl-2-ethoxycyclohexane oxide **148b** (1.00 g; 5.3 mmol) in dry DCM (30 mL) along with tosic acid (50 mg). The mixture was allowed to warm up to room

<div align="right">

OEt
O—O

$C_{16}H_{28}O_4$
$284.40\ gmol^{-1}$

</div>

temperature and left to stir for *ca*. 24 hours. The solution was washed in turn with sat. sodium bicarbonate (30 mL) and water (30 mL) before being extracted into DCM (3 x 30 mL). The combined extracts washed with water (10 mL) and sat. sodium chloride (10 mL) and dried over anhydrous magnesium sulfate before the solvent was removed under vacuum. The crude product was purified by flash column chromatography (1:25) ethyl acetate/ light petroleum) to afford the title compounds. 2-(Ethoxy)cyclohexane-1-*spiro*-3'-(1',2',4'-trioxane)-6'-*spiro*-1''-2''-cycloheptane R$_f$ = 0.30 (0.44 g; 1.55 mmol; 9.8% from epoxide) was collected as a white solid: υ_{max} (CHCl$_3$)/cm^{-1} 3019, 2935, 2864, 1217; δ_H(400 MHz, 60°C CDCl$_3$) 1.16 (3 H, t, *J* 7.0, CH$_3$) 1.31-2.12 (20 H, m, CH$_2$), 3.45 (1 H, m, CH$_2$CH$_3$), 3.48 (1 H, d, *J* 11.5, CH$_2$O), 3.60 (1 H, dq, *J* 7.0 and 9.5, CH$_2$CH$_3$), 3.80 (1 H, bs, CH), 3.90 (1 H, d, *J* 11.5 CH$_2$O), δ_C(100 MHz, 60°C, CDCl$_3$); 15.5 (CH$_3$) 20.1, 20.3, 22.2, 25.1, 28.0, 29.5, 29.6, 33.5, 35.5 (CH$_2$), 62.5 (OCH$_2$), 64.0 (OCH$_2$CH$_3$), 74.2 (CH), 79.3 (*spiro*-C), 106.7 (*spiro*-acetal C); *m/z* 284 (M$^+$), accurate

mass $C_{16}H_{28}O_4$ requires 284.19812, found 284.19821; $C_{14}H_{24}O_4$ requires C 67.7% H 9.9%, found C 67.4% H 10.0%.

Preparation of 2-(ethoxy)cyclohexane-1-*spiro*-3'-(1',2',4'-trioxane)-6'-*spiro*-1''-2''-cyclododecane (149bd)

Cyclododecanone (0.77g; 4.2 mmol) was added to a cooled (-5°C) solution of 1-hydroperoxy-1-hydroxymethyl-2-ethoxycyclohexane oxide **148b** (0.80 g; 4.2 mmol) in dry DCM (30 mL) along with tosic acid (50 mg). The mixture

$C_{21}H_{38}O_4$
$354.53\ gmol^{-1}$

was allowed to warm up to room temperature and left to stir for *ca*. 24 hours. The solution was washed in turn with sat. sodium bicarbonate (30 mL) and water (30 mL) before being extracted into DCM (3 x 30 mL). The combined extracts washed with water (10 mL) and sat. sodium chloride (10 mL) and dried over anhydrous magnesium sulfate before the solvent was removed under vacuum. The crude product was purified by flash column chromatography (1:25) ethyl acetate/ light petroleum) to afford the title compounds. 2-(Ethoxy)cyclohexane-1-*spiro*-3'-(1',2',4'-trioxane)-6'-*spiro*-1''-2''-cyclododecane R_f = 0.45 (130 mg; 0.37 mmol; 2.9% from epoxide) was collected as a colourless viscous oil: υ_{max}/cm^{-1} 2932, 2863, 1710, 1449, 1362; δ_H(400 MHz, 60°C CDCl$_3$) 1.17 (3 H, t, *J* 7.0, CH$_3$) 1.24-2.00 (30 H, m, CH$_2$), 3.46 (1 H, m, CH$_2$CH$_3$), 3.48 (1 H, d, *J* 11.5, CH$_2$O), 3.61 (1 H, dq, *J* 7.0 and 9.5, CH$_2$CH$_3$), 3.78 (1 H, bs, CH), 3.91 (1 H, d, *J* 11.5, CH$_2$O), δ_C(100 MHz, 60°C, CDCl$_3$); 15.6 (CH$_3$) 19.2, 19.4, 20.3, 20.4, 22.3, 22.5, 22.7, 25.2, 26.2, 26.3, 28.1, 29.7 (CH$_2$), 62.5 (OCH$_2$), 65.1 (OCH$_2$CH$_3$), 74.2 (CH), 79.2 (*spiro*-C), 106.2 (*spiro*-acetal C); *m/z* 354 (M$^+$), accurate mass [C$_{21}$H$_{38}$O$_4$NH$_4$]$^+$ requires 372.3108, found 372.3113.

Preparation of indane-2-*spiro*-3'1(1',2',4'-trioxane)-6'-*spiro*-1''-2''-ethoxycyclohexane (149bg)

2-Indanone (0.51g; 4.24 mmol) was added to a cooled (-5°C) solution of 1-hydroperoxy-1-hydroxymethyl-2-ethoxycyclohexane oxide **148b** (0.80 g; 4.21 mmol) in dry DCM
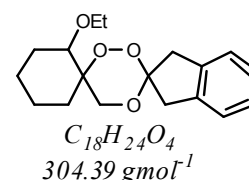
$C_{18}H_{24}O_4$
$304.39\ gmol^{-1}$

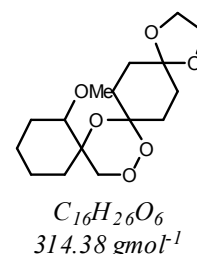(30 mL) along with tosic acid (50 mg). The mixture was allowed to warm up to room temperature and left to stir for *ca*. 24 hours. The solution was washed in turn with sat. sodium bicarbonate (30 mL) and water (30 mL) before being extracted into DCM (3 x 30 mL). The combined extracts washed with water (10 mL) and sat. sodium chloride

(10 mL) and dried over anhydrous magnesium sulfate before the solvent was removed under vacuum. The crude product was purified by flash column chromatography (1:25) ethyl acetate/ light petroleum) to afford the title compounds. Indane-2-*spiro*-3'1(1',2',4'-trioxane)-6'-*spiro*-1''-2''-ethoxycyclohexane R_f = .26 (66 mg; 0.22 mmol; 1.7% from epoxide) was collected as a colourless viscous oil: υ_{max}/cm^{-1} 2935, 2864, 1448, 1362; δ_H(400 MHz, 55°C, CDCl$_3$) 1.25 (3 H, t, J 7.0, CH$_3$) 1.3-2.0 (8 H, m, CH$_2$), 3.26 (4 H, m, CH$_2$Ph), 3.50 (1 H, dq, *J* 7.0and 9.5, CH$_2$CH$_3$), 3.55 (1 H, m, CH$_2$O), 3.60 (1 H, m, CH$_2$CH$_3$), 3.65 (1 H, bs, CH), 4.08 (1 H, d, *J* 11.8, CH$_2$O), 7.15 (4 H, m, Ph-H), δ_C(100 MHz, 55°C, CDCl$_3$); 15.6 (CH$_3$) 20.3, 24.8, 27.9, 29.7, 44.6, 45.1 (CH$_2$), 64.8 (OCH$_2$), 65.1 (OCH$_2$CH$_3$), 79.1 (CH), 79.4 (*spiro*-C), 112.8 (*spiro*-acetal C) 124.6, 124.8 (Ph-H), 138.9, 139.5 (Ph, *q*C); *m/z* 304 (M$^+$), accurate mass [C$_{18}$H$_{24}$O$_4$NH$_4$]$^+$ requires 322.2013, found 322.2011; C$_{18}$H$_{24}$O$_4$ requires C 71.0% H 7.9%, found C 70.7% H 8.4%.

Attempted preparation of 2-(ethoxy)cyclohexane-1-*spiro*-3'-(1',2',4'-trioxane)-6'-*spiro*-1''-2''-1''',4'''-dioxa*spiro*[4.5]decane (149be) and 2-(ethoxy)cyclohexane-1-*spiro*-3'-(1',2',4'-trioxane)-5'-*spiro*-1''-2''-1''',4'''-dioxa*spiro*[4.5]decane (160be)
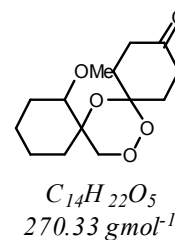
1,4-Dioxa*spiro*[4.5]decan-8-one (0.79 g; 4.2 mmol) was added to a cooled (-5°C) solution of 1-hydroperoxy-1-hydroxymethyl-2-ethoxycyclohexane oxide **148b** (0.80 g; 4.2 mmol) in dry DCM (30 mL) along with tosic acid (50 mg). The mixture was allowed to warm up to room temperature and left to stir for *ca.* 24 hours. The solution was washed in turn with sat. sodium bicarbonate (30 mL) and water (30 mL) before being extracted into DCM (3 x 30 mL). The combined extracts were washed with water (10 mL) and sat. sodium chloride (10 mL) and dried over anhydrous

$C_{17}H_{28}O_6$
328.41 gmol^{-1}

$C_{17}H_{28}O_6$
328.41 gmol^{-1}

magnesium sulfate before the solvent was removed under vacuum. The crude product was purified by flash column chromatography (1:5, ethyl acetate/ light petroleum) to afford the title compounds. 2-(Ethoxy)cyclohexane-1-*spiro*-3'-(1',2',4'-trioxane)-5'-*spiro*-1''-2''-1''',4'''-dioxa*spiro*[4.5]decane R_f = 0.40 (45 mg; 0.14 mmol; 1.1% from the epoxide) as a colourless viscous oil: δ_H(400 MHz, CDCl$_3$) 1.13 (3H, t, *J* 8.0, CH$_3$) 1.22-2.22 (16 H, m, CH$_2$), 2.42 (4 H, m, CH$_2$), 3.35 (1 H, m, CH), 3.43 (1 H, m, CH$_2$CH$_3$), 3.61 (1 H, m, CH$_2$CH$_3$), 3.90 (1, H, d, *J* 12.6, OCH$_2$), 3.93 (4 H, s, OCH$_2$CH$_2$O), 3.98 (1 H, d, *J* 12.6, OCH$_2$), 4.28 (1 H, d, *J* 12.6, OCH$_2$) 4.37 (1 H, d, *J*

12.6, OCH$_2$) δ_C (100MHz, CDCl$_3$); 15.5 (CH$_3$) 19.0, 19.4, 23.7, 25.3, 25.5, 27.6, 27.8, 30.6, 30.7, 30.8, 36.4, 36.5 (CH$_2$), 62.4, 62.7, 64.2, 64.3, 64.8, 64.8 (CH$_2$) 76.5, 76.7 (CH), 78.3, 78.8 (*spiro*-C), 108.3, 108.2, 101.3, 100.6, 130 (qC) 210.1 (C=O) and 2-(ethoxy)cyclohexane-1-*spiro*-3'-(1',2',4'-trioxane)-6'-*spiro*-1''-2''-1''',4'''-dioxa*spiro*[4.5]decane R$_f$ = 0.29 (0.25 g; 0.76 mmol; 6.0% from epoxide) was collected as a colourless viscous oil: δ_H(400 MHz, CDCl$_3$) 1.15 (3 H, t, *J* 7.0, CH$_3$) 1.22-1.82 (16 H, m, CH$_2$), 2.41 (4 H, m, CH$_2$), 3.35-3.69 (6 H, m), 3.92 (4 H, s, OCH$_2$CH$_2$O), 4.03 (1 H, d, *J* 12.0, CH$_2$O), δ_C(100 MHz, CDCl$_3$); 15.5 (CH$_3$) 19.0, 19.4, 23.7, 25.3, 25.5, 27.6, 27.8, 30.6, 30.7, 30.8, 36.4, 36.5 (CH$_2$), 62.4, 62.7, 64.2, 64.3, 64.8, 64.8 (CH$_2$) 74.1 (CH), 79.2 (*spiro*-C), 108.3, 101.2, 100.5 (qC) 209.8 (C=O).

Preparation of cyclohexane-4-one-1-*spiro*-3'-(1',2',4'-trioxane)-6'-*spiro*-1''-(2''-ethoxycyclohexaneone (149bf)

2-(Ethoxy)cyclohexane-1-*spiro*-3'-(1',2',4'-trioxane)-6'-*spiro*-1''-2''-1''',4'''-dioxa*spiro*[4.5]decane **148bf** (251 mg, 0.88 mmol) in acetone (10 mL) was treated with tosic acid (0.52 g, 2.70 mmol) and continuously stirred overnight at r.t. The product was extracted
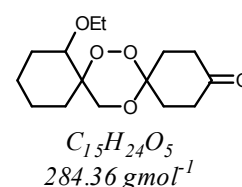
OEt

$C_{15}H_{24}O_5$
$284.36\,g\,mol^{-1}$

using ethyl acetate (3 x 20 mL) and the combined extracts were washed with sat. sodium bicarbonate (10mL) and sat. sodium chloride (10 mL). After drying with magnesium sulfate, the solvent was evaporated. Incomplete reaction meant the reaction was repeated for a further 24 hours. The crude product was purified by flash column chromatography (1:5 ethyl acetate/ light petroleum) to afford the title compound. Cyclohexane-4-one-1-*spiro*-3'-(1',2',4'-trioxane)-6'-*spiro*-1''-(2''-ethoxycyclohexaneone R$_f$ = 0.30 (88 mg; 0.31 mmol; 35.2%) was collected as a colourless viscous oil: δ_H(400 MHz, 60°C, CDCl$_3$) 1.26 (3 H, t, *J* 7.0, CH$_3$) 1.33-1.82 (10 H, m, CH$_2$), 2.16 (2 H, m, CH$_2$), 2.40 (4 H, m, CH$_2$), 3.44 (1 H, dq, *J* 7.0, 7.0, 7.0 and 9.5, CH$_2$CH$_3$), 3.57 (1H, d, *J* 11.8, CH$_2$O), 3.62 (1H, m, CH$_2$CH$_3$), 4.02 (1H, d, *J* 11.8 CH$_2$O), δ_C(100 MHz, 60°C, CDCl$_3$); 15.4 (CH$_3$), 19.1, 19.5, 20.1, 20.3, 25.0, 27.9, 36.4, 36.4 (CH$_2$), 62.9 (CH$_2$O), 64.9 (CH$_2$), 73.8 (CH), 79.8 (*spiro* C) 100.7 (*spiro*-acetal C), 209.3 (C=O).

Preparation of cyclohexane-4-one-1-*spiro*-3'-(1',2',4'-trioxane)-5'-*spiro*-1''-(2''-ethoxycyclohexanone (160bf)

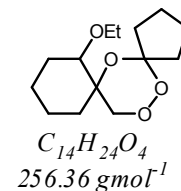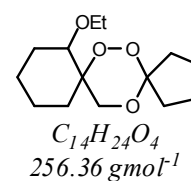2-(Ethoxy)cyclohexane-1-*spiro*-3'-(1',2',4'-trioxane)-5'-*spiro*-1''-2''-1''',4'''-dioxa*spiro*[4.5]decane **160bc** (45 mg, 0.16 mmol) in acetone (10 mL) was treated with tosic acid (0.12g, 0.6 mmol) and continuously stirred overnight at r.t. The product was extracted using ethyl acetate (3 x 20 mL) and the combined extracts were washed with

$C_{15}H_{24}O_5$
$284.36 \ gmol^{-1}$

sat. sodium bicarbonate (10mL) and sat. sodium chloride (10 mL). After drying with magnesium sulfate, the solvent was evaporated. Incomplete reaction meant the reaction was repeated for a further 24 hours. The crude product was purified by flash column chromatography (1:5 ethyl acetate/ light petroleum) to afford the title compound. Cyclohexane-4-one-1-*spiro*-3'-(1',2',4'-trioxane)-5'-*spiro*-1''-(2''-ethoxycyclohexanone R_f = 0.50 (25 mg; 0.88 mmol; 64.1%) was collected as a colourless oil: υ_{max} (CHCl$_3$)/cm^{-1} 3019, 1214, 1716 δ_H(400 MHz CDCl$_3$) 1.15 (3 H, t, J 7.0, CH$_3$) 1.19-1.77 (10 H, m, CH$_2$), 2.04 (1 H, m, CH$_2$), 2.16 (1 H, m, CH$_2$), 2.42 (4 H, m, CH$_2$), 3.35 (1 H, m, CH), 3.37 (1 H, m, CH$_2$CH$_3$), 3.59 (1 H, dq, J 7.0, 7.0, 7.0, 9.3 CH$_2$CH$_3$), 3.98 (1 H, d, J 12.7, OCH$_2$), 4.37 (1 H, d, J 12.7, OCH$_2$) δ_C (100MHz, CDCl$_3$); 15.6 (CH$_3$), 20.1, 20.9, 24.9, 31.8, 33.5, 34.6, 36.9, 37.1, 37.2 (CH$_2$), 64.6 (CH$_2$), 71.7 (*spiro* C), 76.4 (CH$_2$O), 78.8 (CH), 100.6 (*spiro*-acetal C), 210.2 (C=O); m/z 284 (M$^+$), accurate mass C$_{15}$H$_{24}$O$_5$ requires 284.16181, found 284.16183

[1] D. A. Casteel, *Nat. Prod. Rep.*, 1992, **9**, 289-311

[2] D. A. Casteel, *Nat. Prod. Rep.*, 1999, **16**, 55-73

[3] D. Klayman, *Science*, 1985, **228**, 1049-1055

[4] J. N. Cummin, P. Ploypradith, G. H. Posner, *Advances in Pharmacology*, 1997, **37**, 253-297

[5] X. X. Xu, H. Q. J. Dong, *J. Org. Chem.*, 1995, **60**, 3039-3044

[6] A. D. Patil, PCT Int. Appl. US Patent: 86-825920, 1987

[7] V. M. Dembitsky, T. A. Gloriozova, and V. Poroikov, *Mini-Rev. Med. Chem.*, 2007, **7**, 571-589

[8] H. Jomaa, J. Wiesner, S. Sutherland, B. Altincicek, C. Weidemeyer, M Hintz, I. Tubachova, M. Eberl, J. Zeider, H.K. Liechtenthaler, D. Soldati and E. Beck, *Science,* 1999, **28**, 1573-1576

[9] N. J. White, *Phil. Trans. T. Soc. Lond. B.*, 1999, **354**, 739-749

[10] C-C. Shen, and L-G. Zhuang, *Med. Res. Rev.* 1984, **4**, 47-86

[11] C. Singh, H. Malik and S.K. Puri, *Biorg. and Med. Chem. Lett.*, 2005, **15**, 4484-4487

[12] R. K. Haynes, W-Y. Ho, H-Q. Chan, B. Fugmann, J. Stetter, S. L. Croft, L. Vivas, W. Peters, and B. L. Robinson, *Angew. Chem. Int. Ed.*, 2004, **43**, 1381-1385

[13] R. K. Haynes, B. Fugmann, J. Stetter, K. Rieckmann, H-D. Heilmann, H-W. Chan, M-K. Cheung, W-L. Lam, H-N. Wong, S. L Croft, L. Vivas, L. Rattray, L. Stewart, W. Peters, B. L. Robinson, M. D. Edstein, B. Kotecka, D. E. Kyle, B. Beckermann, M. Gerisch, M. Rodtke, G. Schmuck, W. Steinke, U. Wollborn, K. Schmeer, and A. Römer, *Angew. Chem. Int. Ed.*, 2006, **45**, 2082-2088

[14] www.Oneworldhealth.org, press release 03.03.2008

[15] B. Venugopalen, C. P. Bapat, P. J. Karnik, D. K. Chatterjee, N. Iyer, and D. Lepcha, *J. Med. Chem.*, 1995, **38** 1922-1927

[16] A. M. Galal, M. Shamim Ahmad, and E El-Feraly, *J. Nat. Prod.*, 1996, **59**, 917-920

[17] G. H. Posner, I-H. Paik, S. Sur, A. J. Rimmer, K. Borstnik, S. Xie, and T. A. Shapiro, *J. Med. Chem.*, 2003, **46**, 1060-1065

[18] G. H. Posner, W. Chang, L. Hess, L. Woodward, S. Sinishtaj, A. R. Usera, W. Maio, A. S. Rosenthal, A. S. Kalinda, J. G. D'Angelo, K. S. Peterson, R. Stoher, J. Chollet, J. Santo-Tomas, C. Snyder, M. Rottmann, S. Wittlin, R. Brun, and T. A. Shapiro, *J. Med. Chem.*, 2008, **51**, 1035-1042

[19] G. H. Posner, I-H. Paik, W. Chang, K. Borstnik, S. Sinishtaj, A. S. Rosenthal, and T. A. Shapiro, *J. Med. Chem*., 2007, **50**, 2516-2519

[20] G. Posner, P. Ploypradith, W. Hapangama, D. Wang, J. N. Cumming, P. Dolan, T. W. Kensler, D. Klinedinst, T. A. Shapiro, Q. Y. Zheng, C. K. Murray, L. G. Pilkington, L. R. Jayasinghe, J. F. Bray, R. Daughenbaugh, *Bioorg. Med. Chem*.,1997, **5**, 1257-1265

[21] G. Posner, P. Ploypradith, M. H. Parker, H. O'Dowd, S-H. Woo, J. Northrop, M. Krasavin, P. Dolan, T. W. Kensler, S. Xie, and T. A. Shapiro, *J. Med. Chem*.,1999, **21**, 1275-1280

[22] G. H. Posner, P. Ploypradith, M. H. Parker, H. O'Dowd, S-H Woo, J. Northrop, M. Krasavin, P. Dolan, T. W. Kensler, S. Xie and T. A. Shapiro*, J. Med. Chem.,* 1999, **42**, 4275-4280

[23] O. Dechy-Cabaret, F. Benoit-Vical, A. Robert, and B. Meunier, *ChemBioChem*, 2000, **4**, 281-283

[24] B. Meunier, *Acc. Chem. Res.,* 2008, **41**, 69-77

[25] A. Robert, C. Bonduelle, S. A.-L. Laurent, and B. Meunier; *J. Phys. Org. Chem*., 2006, **19**, 562-569

[26] S. A.–L. Laurent, C. Loup, S. Mourgues, A. Robert, and B. Meunier, *ChemBioChem*, 2005, **6**, 653-658

[27] J. L. Vennerstrom, S. Arbe-Barnes, R. Brun, S. A. Charman, F. C. K. Chiu. J. Chollet, Y. Dong, A. Dorn, D. Hunzikert, H. Matile, K. MacIntosh, M. Padmanilayam, J. S. Tomas, C. Scheurer, B. Scorneaux, Y. Tang, H. Urwyler, S. Wittlin, and W. N. Charman, *Nature,* 2004, **340**, 900-904

[28] C. Singh, S. Pandey, M. Sharma, and S. K. Puri, *Biorg. Med. Chem,* 2008, **16**, 1816-1821

[29] R. Amewu, A. V. Stachulski, S. A. Ward, N. G. Berry, P. G. Bray, J. Davis, G. Labat, L. Vivas, and P. M. O'Neill, *Org. Biomol. Chem.* 2006, **4**, 4431-4436

[30] G. L. Ellis, R. Amewu, C. Hall, K. Rimmer, S. A. Ward, and P. M. O'Neill, *Bioorg. Med. Chem. Lett,* 2008, **18***, 1720-1724*

[31] L. Zhou, A. Alker, A. Ruf, X. Wang, F. C. K. Chiu, J. Morizzi, S. A. Charman, W. N. Charman, C. Scheurer, S. Witten, Y. Dong, D. Hunzilker, and J. L. Vennerstrom, *Bioorg. Med. Chem. Lett*., 2008, **18**, 1555-1558

[32] D. Alonso, J. Muňoz, J. Gascón, M. E. Valls, and M. Corachan, *Am. J. Trop. Med. Hyg.,* 2006, **74**, 342-344

[33] S. A.–L. Laurent, J. Boissier, F. Coslédan, H. Gornitzka, A. Robert, and B. Meunier, *Eur. J. Org. Chem.*, 2008, **5**, 895-913

[34] J. Jakupovic, M. Grenz, and G. Schmeda-Hirschmann, *Phytochemistry*, 1988, **27**, 2997-2998

[35] S. Sutthivaiyakit, W. Mongkolvisut, P. Ponsitipiboon, S. Prabpai, P. Kongsaeree, S. Ruchirawat and C. Mahidol, *Tetrahedron Lett.*, 2003, **44**, 3637-3640

[36] C. W. Jefford, *Curr. Med. Chem.*, 2001, **8**, 1803-1826

[37] W-M Wu, *Acc. Chem. Res.*, 2002, **5**, 255-258

[38] S. Krishna, A-C. Uhlemann, R. K. Haynes, *Drug Res. Updates*, 2004, **7**, 233-244

[39] P. M. O'Neill, G. H. Posner, *J. Med. Chem.*, 2004, **46**, 2945-2964

[40] M. D. Scott, S.R. Meshnick, R. A. Williams, D. T. –Y. Chiu, H. C. Pan, B. H. Lubin, F. A. Kuypers, *J. Lab. Clin. Med.*, 1989, **114**, 401-406

[41] A. Robert, F Benoit-Vical, B. Meunier, *Coord. Chem. Rev.*, 2005, **249**, 1927-1938

[42] S. R. Meshinik, A. Thomas, A. Ranz, C-M. Xu, and H-Z. Pan, *Mol. Biochem. Paracitol.*, 1991, **49**, 181-190

[43] W. Peters, L. Ze-Lin, B. L. Robinson, *Ann. Trop. Med. Parasitol.*, 1986, **80**, 483-489

[44] G. H. Posner, C. H. Oh, *J. Am. Chem. Soc.*, 1992, **114**, 8328-8329

[45] S. R. Meshinik, Y-Z. Yang, V. Lima, F. Kuypers, S. Kamchonwongpaisan, and Y. Yuthavong, *Antimicrob. Agents Chem.*, 1993, **37**, 1108-1114

[46] Y-L. Hong, Y-Z. Yang, S. R. Meshnick, *Mol. Biochem. Parasitol.,* 1994, **63**, 121-128

[47] G. H. Posner, C. H. Oh, D. S. Wang, L. Gerena, W. K .Milhous, S. R. Meshnich and W. Asawamahasadka, *J. Am. Chem. Soc.*, 1994, **37**, 1256-1258

[48] R. K. Haynes, and S. C. Vonwiller, *Tetrahedron Lett.*, 1996, **37**, 253-256

[49] R. K. Haynes, and S. C. Vonwiller, *Tetrahedron Lett.*, 1996, **37**, 257-260

[50] R. K. Haynes, H. H-O. Pai, and A. Voerste, *Tetrahedron Lett.*, 1999, **40**, 4715-4718

[51] A. Robert and B. Meunier, *J. Am. Chem. Soc.*, 1997, **119**, 5968-5969

[52] W-M Wu, Y. Wu, Y-L. Wu, Z-J Yao, C-M. Zhou, Y. Li, and F. Shan, *J. Am. Chem. Soc.*, 1998, **120**, 3316-3325

[53] P. M. O'Neill, L. P. D. Bishop, N. L. Searle, J. L. Maggs, R. C. Storr, S. A. Ward, B. K. Parks, and F. Mabbs, *J. Org. Chem*, 2000, **65**, 1578-1582

[54] W-M. Wu, Y-L. Chen, Z. Zhai, S-H. Xiao, and Y-L. Wu, *Bioorg. Med. Chem. Lett.,* 2003, **13**, 1645-1647

[55] G. H. Posner, J. N. Cummings, P. Ploypradith, H. O. Chang, *J. Am. Chem. Soc.*, 1995, **117**, 885-5886

[56] A. Robert, and B. Meunier, *Chem. Soc. Rev.*, 1998, **27**, 273-279

[57] A. Robert. J. Cazelles, and B. Meunier, *Angew. Chem. Int. Ed.*, 2001, **40**, 1954-1957

[58] S. A. -L. Laurent, A. Robert and B Meunier, *Angew. Chem. Int. Ed.*, 2005, **44**, 2060-2063

[59] J. Cazelles, A. Robert, B. Meunier, *J. Org. Chem.*, 2002, **67**, 609-619

[60] U. Eckstein-Lunwig, R. J. Webb, I. D. a. Van Goethem, J. M. East, A. G. Lee, M. Kimura, P. M. O'Neill, P. G. Bray, S. A. Ward, and S. Krishna, *Nature*, 2003, **424**, 957-961

[61] A. Robert, and B. Meunier, *Chem. Eur. J.*, 1998, **4**, 1287-1296

[62] K. J. McCullough, J. K. Woods, A. K. Bhattacharjee, Y. Dong, D. E. Kyle, W. K. Milhous, and J. L. Vennerstrom*, J. Med. Chem.,* 2000, **43**, 1246-1249

[63] Y. Dong, D. Creek, J. Chollet, H. Matile, S. A. Charman, S. Witten, J. K. Wood, and J. L. Vennerstrom, *Antimicrob. Agents Chem.*, 2007, **51**, 3033-3035

[64] A. F. G. Slater, W. J. Swiggard, B. R. Orton, W. D. Flitter, D. E. Goldberg, A. Cerami, and G. B. Henderson, *Proc. Natl. Acad. Sci. U.S.A.,* 1991, **88**, 325-329

[65] D. Pagola, P. W. Stephens, D. S. Bohle, A. D. Kosar, and S. K. Madsen, *Nature*, 2000, **404**, 307-310

[66] I. Solomonov, M. Osipova, Y. Feldman, C. Baehtz, K. Kjaer, I. K. Robinson, G. T. Webster, D. McNaughton, B. R. Wood, I. Weissbuch, and L. Leiderowitz, *J. Am. Chem. Soc.*, 2007, **129**, 2615-2627

[67] P. A. Stocks, P. G. Bray, V. E. Barton, M. Al-Helal, M. Jones, N. C. Araujo, S. A. Ward, R. H. Hughes, G. A. Biagini, J. Davies, R. Amewu, A. E. Mercer, G. Ellis, and P. O'Neill, *Agnew. Chem. Int. Ed.*, 2007, **46**, 6278-6283

[68] K. J. McCullough*, J. Cont. Org. Synth.*, 1995, 225-249

[69] K. J. McCullough, and M. Nojima, *Curr. Org. Chem.*, 2001, **5**, 601-636

[70] G. Payne and C. Smith, *J. Org. Chem.*, 1957, **22**, 1682-1685

[71] R. E. Parker, and N. S. Issacs, *Chem. Rev.*, 1959, **59**, 738-799

[72] J. G. Smith, *Synthesis,* 1984, 629-656

[73] W. Adam, and A. Rios, *J. Chem. Soc. Chem. Commun.*, 1971, 822-823

[74] V. Subramanyam, C. L. Brizuela, and A. H. Soloway, *J. Chem. Soc. Chem. Commun.*, 1976, 508-509

[75] B. Kerr, and K. J. McCullough, *J. Chem. Soc. Chem. Commun.*, 1985, 590-591

[76] A. Haq, B. Kerr, and K. J. McCullough, *J. Chem. Soc. Chem. Commun.*, 1993, 1076-1078

[77] A. M. Mattucci, and A. Santambrogio, *J. Chem. Soc. Chem Comm.*, 1970, 1198-1199

[78] Y. Tang, Y. Dong, X. Wang, K. Sriraghaven, J. K. Woods, and J. L. Vennerstrom, *J. Org. Chem*, 2005, **70**, 5103-5110

[79] A. Nickon, and W. L. Mendelson, *J. Am. Chem. Soc.*, 1965, **17**, 3921-3928

[80] C. Singh, *Tetrahedron Lett.*, 1990, **31**, 6901-6902

[81] C. Singh, D. Misra, G. Saxena, and S. Chandra, *Bioorg. & Med. Chem. Lett.,* 1995, **5**, 1913-1916

[82] C. Singh, N. Gupta, and S. K. Puri, *Bioorg. Med. Chem. Lett.,* 2002*, 12, 1913-1916*

[83] D. S. Dodd, A. C. Oehlschlager, N. H. Georgopapadakou, A. –M. Polok, P. G. Hartman, *J. Org. Chem.*, 1992, **57**, 7226-7234

[84] C. Singh, H. Malik, and S. K. Puri, *Bioorg. Med. Chem. Lett.* 2004, **12**, 1177-1182

[85] C. Singh, N. Gupta, and S. K. Puri, *Tetrahedron Lett.*, 2005, **46**, 205-207

[86] M. Prein, and W. Adam, *Angew. Chem. Engl. Ed.*, 1996, **35**, 477-494

[87] Y. Dong, J. Chollet, H. Matile, S. A. Charman, F. C. K. Chiu, W. N. Charman, B. Scorneaux, H. Urwyler, J. S. Tomas, C. Scheurer, C. Snyder, A. Dorn, X. Wang, J. M. Karle, Y. Tang, S. Wittlin, R. Brun, and J. L. Vennerstrom, *J. Med. Chem*, 2006, **48**, 4953-4961

[88] A. G. Griesbeck, T. T. El-Idreesy, L. –O. Höinck, J. Lex, R. Brun, *Bioorg. Med. Chem. Lett.*, 2005, **15**, 595-597

[89] C. Singh, U. Sharma, G. Saxena, and S. K. Puri, *Bioorg. Med. Chem Lett.*, 2007, **17**, 4097-4101

[90] A. G. Griesbeck, A. Bartoschek, T. T. El-Idreesy, O. Höinck, and C. Miara, *J. Mol. Catal. A: Chem.*, 2006, **251**, 41-48

[91] A. G. Griesbeck, and A Bartoschek, *Chem. Commun.*, 2002, **346**, 1594-1595

[92] A. G. Griesbeck, T. T. El-Idreesy, M. Fiege, R. Brun, *Org. Lett.*, 2002, **4**, 4193-4195

[93] A. G. Griesbeck, T. T. El-Idreesy, J. Lex, *Tetrahedron*, 2006, **62**, 10615-10622

[94] A. G. Griesbeck, L. –O. Höinck, J. Lex, *Lett. Org. Chem.*, 2006, **3**, 247-249

[95] S. Isayama, T. Mukaiyama, *Chem. Lett.*, 1989, **11**, 573-576

[96] S. Isayama, *Bull. Chem. Soc. Jpn.*, 1990, **63**, 1305-1310

[97] P. M. O'Neill, S. Hindley, M. D. Pugh, J. Davis, P. G. Bray, B. K. Park, D. S. Kapu, S. A. Ward and P. A. Stocks, *Tetrahedron Lett.*, 2003, **44**, 8135-8138

[98] A. A. Patel, Heriot-Watt University, MPhil thesis, 2002

[99] P. M. O'Neill, M. Pugh. J. Jervis, S. A. Ward and B. K. Park, *Tetrahedron Lett.*, 2001, **42**, 4569-4571

[100] T. Tokuyasu, S. Kunikawa, A. Masuyama and M. Nojima, *Org. Lett.*, 2002, **4**, 3595

[101] T. Tokuyasu, S. Kunikawa, K. J. McCullough, A. Masuyama and M. Nojima, *J. Org. Chem.*, 2005, **70**, 251-260

[102] C. H. Oh, and J. H. Kang, *Tetrahedron Lett.*, 1998, **39**, 2771-2774

[103] A. L. J. Beckweith, and R. D. Wagner, *J. Org. Chem.*, 1982, **46**, 3638-3645

[104] M. D. Bachi, and E. E. Korshin, *Synlett,* 1998, 122-124

[105] E. E. Korshin, R. Hoos, A. M. Szpilman, L. Konstantinovski, G. H. Posner, and M. D. Bachi, *Tetrahedron*, 2002, **58**, 2449-2469

[106] P. M. O'Neill, A. Mukhtar, S. A. Ward, J. F. Bickley, J. Davis, M.D. Bachi and P. A. Stocks, *Org. Lett.*, 2004, **6**, 3035-3038

[107] Y. Arroyo-Gómez, J. F. Rodriguez-Amo, M. Santos-Garciá, and M. A. Sanz-Tejedor, *Tetrahedron.: Asym.*, 2000, **11**, 789-796

[108] M. D. Bachi, E. E. Korshin, R. Hoos,, and A. M. Szpilman, *J. Heterocyclic Chem.*, 2000, **37**, 639-646

[109] R. Amewu, A. V. Stachulski, N. G. Berry, S. A. Ward, J. Davies, G. Labat, J-F. Rossingnol, and P. M .O'Neill, *Bioorgan. & Med. Chem. Lett.*, 2006, **16**, 6124-6130

[110] M. P. Mischne, S. N, Huber, and J. Zinczuk, *Can. J. Chem*, 1999, **77**, 237-242

[111] A. La-Venia, E. G. Mata, and M. P. Mischne, *J. Comb. Chem.*, 2008, **10**, 504-506

[112] N. Murakami, M. Kawanishi, S. Itagaki, T. Horii, and M. Kobayashi, *Tetrahedron Lett.*, 2001, **42**, 7281-7285

[113] N. Murakami, M. Kawanishi, S. Itagaki, T. Horii, and M. Kobayashi, *Bioorg. Med. Chem. Lett.*, 2002, **12**, 69-72

[114] Q. Zhang, H. –X. Jin, and Y. Wu, *Tetrahedron*, 2006, **62**, 11627-11634

[115] Q. Zhang, and Y. Wu, *Tetrahedron*, 2007, **63**, 10189-10201

[116] F. H. Allen, *Acta Cryst.*, 2002, B**58**, 380-388

[117] X-D. Luo, H. J. C. Yeh, and A. Brossi, *Helv. Chim. Acta*, 1984, **67**, 1515-1522

[118] C. W. Jefford, D-J. Jin, J-C. Rossier, S. Kohmoto, and G. Bernardinelli, *Heterocycles*, 1997, **44**, 367-387

[119] O. Dechy-Cabaret, F. Benoit-Vical, C. Loup, A. Robert, H. Gornitzka, H. Vial, J-F. Magnaval, J-P. Séguéla, B Meunier*, Chem. Eur. J.*, 2004, **10**, 1625-1636

[120] G. Bergnardinelli, C. W. Jefford, G. D. Richardson, and J. C. Rossier, *Acta Cryst.*, 1991, **C47**, 388-392

[121] H. Yamamoto, I. Nakai, C. Kashima, Y. Omote, and M. Akutagawa, *Bull. Chem. Soc. Jpn.*, 1983, 1841-1844

[122] A. Bartoschek, T. T. El-Idreesy, A. G. Griesbeck, L-O. Höinck, L. Lex, C. Miara, J. M. Neudörfl, *Synthesis*, 2005, **14**, 2433-2444

[123] J. D. Dunitz, *X-Ray analysis and structure of organic molecules*, Cornell University Press, 1979, 338

[124] P. D. Bartlett, and J. E. Leffler*, J. Am. Chem. Soc.*, 1950, **72**, 3030-3035

[125] C. W. Jefford, A. Jaber, J. Boukouvalas, and P. Tissot, *Therm. Chim. Acta.*, 1991, **188**, 337-342

[126] W. Adam, *Acc. Chem. Res.*, 1979, **12**, 390-396

[127] G. B. Schuster, and L. A. Bryant, *J. Org. Chem*, 1978, **43**, 521-522

[128] T. Fujisaka, M. Miura, M. Nojima, and S. Kusabayashi, *J. Chem. Soc., Perkin Trans. 1*, 1989, 1031- 1039

[129] A. J. Lin, D. L. Klayman, and J. M. Hoch, *J. Org. Chem.*, 1985, **50**, 4504-4508

[130] X, -D. Luo, H. J. C. Yeh, and A. Brossi, *Heterocycles*, 1985, **23**, 881-887

[131] A. J. Lin, A. D. Theoharides, and D. L. Klayman, *Tetrahedron,* 1986, **42**, 2181-2184

[132] H. Yamamoto, M. Akutagawa, and H. Aoyama, *J. Chem. Soc., Perkin Trans. 1*, 1980, 2300-2303

[133] C. W. Jefford, J. –C. Rossier, and G. D. Richardson, *J. Chem. Soc. Chem. Commun.*, 1993, 1064-1065

[134] C. W. Jefford, J. Currie, G. D. Richardson, and J. –C Rossier, *Helv. Chim. Acta.*, 1991, **74**, 1239-1246

[135] C. W. Jefford, and G. H. Vicente, *Heterocycles*, 1993, **2**, 725-729

[136] C. W. Jefford, M. C. Josso, M. H. Vicente, H. R. Hagemann, D. Lovy, and H. Bill, *Helv. Chim. Acta.*, 1994, **77**, 1851-1860

[137] R. S. Rimada, P. E. Allegretti, J. J. P. Furlong, L. F. R. Cafferata, *J. High Resol. Chromotogr.,* 1999, **22**, 67-69

[138] L. F. R. Cafferata, C. W. Jefford, and R. S. Rimada*, Int. J. Chem. Kin.*, 2000, **32**, 523-528

[139] L. F. R. Cafferata, R. Jeandupeux, G. P. Romanelli, C. M. Matteo, *Afinidad*, 2003, **60**, 206-211

[140] L. F. R. Cafferata, G. N. Eyler, A. I. Caňizo, C. M. Mateo, and R. S. Rimada, *Molecules*, 2000, **5**, 362-364

[141] L. F. R. Cafferata, and C. W. Jefford, *Molecules*, 2001, **6**, 699-709

[142] L. F. R. Cafferata, and R. S. Rimada, *Molecules*, 2003, **8**, 655-662

[143] E. J. Corey, M. Chaykovsky, *J. Am. Chem. Soc.*, 1965, **87**, 1353-1364

[144] E. J. Corey, M. Chaykovsky, *Organic Synthesis*, Collective Vol. **5**, 755

[145] K. Savill, PhD thesis, Heriot-Watt University, 1993

[146] B. Kerr, PhD thesis, Heriot-Watt University, 1989

[147] M. Schmidt, P. Bornmann, *Zeit. Anorgan. Allgemeine Chem.*, 1964, **330**, 309-310

[148] R. A. Johnson, E. G. Nidy, *J. Org Chem*, 1975, **40**, 1680-1681

[149] A. Rieche and C. Bischhoff, *Ber. Dtsch. Chem. Ges.,* 1962, **95**, 77-82

[150] G. M. Sheldrick, *ShelXTL PC (vers. 5.1)*; Bruker AXS: Madison, WI, 1997

[151] A. J. Carnell, W. Clegg, R. A. W. Johnstone, C. C. Parsy, and W. R. Sanderson, *Tetrahedron*, 2000, **56**, 6571-6575

[152] H. Meerwein, (Houben-Weyl) 4th ed. 1952–, 1965, **6/3**, 1422-1452

[153] P. Groth, *Acta. Chem. Scand.*, **1969**, 2277-2293

[154] P. Groth, *Acta. Chem. Scand.*, **1967**, 2631-2646

[155] Compound Synthesised by S. McIlwaigne, 2008, 4th Year BSc (*Hons*) project, Heriot-Watt University, Crystallised and X-Ray Crystallographic data by B. J. Taylor

[156] K. J. McCullough, H. Tokuhara, A. Masuyama, and M. Nojima, *Org. Biomol. Chem*, 2003, **1**, 1522-1527

[157] K. J. McCullough, T. Ito, T. Tokuyasu, A. Masuyama, and M. Nojima, *Tetrahedron. Lett.*, 2001, **42**, 5529-5532

[158] E. L. Eliel, S. H. Wilen, *Stereochemistry of Organic Compounds, J. Wiley & Sons, Inc*, 1994

[159] F. H. Allan, and A.J. Kirby, *J. Am Chem. Soc.*, 1984, **106**, 6197

[160] J. G. Buchanan, A. R. Edgar, D. I. Rawson, P. Shahidi, R. H. Wightman, *Carbohydrate Research*, 1982, **100**, 75-86

[161] C. Møller and M. S.Plesset, *Phys. Rev.*, 1934, **46**, 618-622

[162] P. R. Carlier, N. Deora, and T. D. Crawford, *J. Org. Chem.*, 2006, **71**, 1592-1597

[163] Y. Zhou, and D. G. Truhlar, *J. Org. Chem.*, 2007, **72**, 295-298

[164] L. F. Veiros, Â. Prazeres, P. J. Costa, C. C. Romão, F. E. Kühn, and M. J. Calhorda, *J. Chem. Soc. Dalton Trans.*, 2006, 1383-1389

[165] *Bruker* AXS APEX 2, V1.0-8, Bruker –AXS, Madison, WI, USA, 2003

[166] *Mercury*, version 1.4.2, Cambridge Crystallographic Data Centre, Cambridge, UK, 2006

Chapter Two

Thermolysis of *Dispiro*-1,2,4-Trioxanes

In this review a number of different synthetic routes to macrocyclic lactones will be outlined, including ring closure, ring contraction and ring expansion reactions. Particular emphasis will be given to the synthesis of macrolides through radical processes.

The term macrocycle refers to medium to large ring structures of greater than 9 atoms. Macrocycles which contain one or more ester linkages are generally referred to as macrolides or macrocyclic lactones. Macrolides occur widely in nature and have been seen to exhibit a wide range of pharmaceutical applications.[1,2] They have been used as antibiotics since the 1950s after isolation of the first macrolide antibiotic, picromycin (**1**), from an *actinomyces* culture.[3] Macrocylic lactones erythromycin (**2**) and oleandomycin (**3**) are still used as antibiotics, and also have also been reported to have other therapeutic benefits including anti-tumour and more significantly, anti-HIV properties.[1,2] The natural product, racicol (**4**), has also shown good anti-tumour properties and a derivative of radicicol is currently in phase II clinical trials.[2] There have been extensive reviews on the synthesis of antibiotic macrolides particularly derivatives of erythromycin and the total synthesis of macrolide natural products.[4,5,6]

1 Picromycin   **2 Erythromycin**   **3 Oleandomycin**

4 Radicicol   **5 Exaltolide**   **6 Ambrettolide**
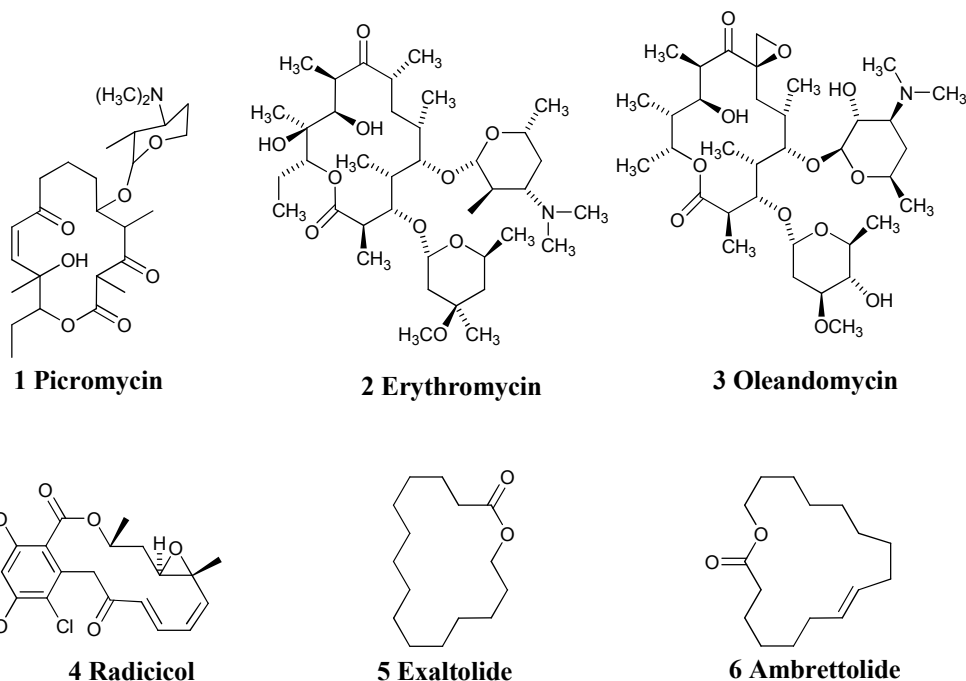
As well as pharmaceutical applications, macrolides exaltolide (**5**) and ambrettolide (**6**), first isolated from angelica root and ambrette seed oil respectively, have been used as components of musks or fragrances.[7] Although macrolides were one of the first

examples of macrocyclic musks, their limited availability from natural sources plus the cost of manufacture meant that they were rarely used as a component in musks. The use of macrocycles as musks however is a growing market. In 1998 around only 25% of all musks or fragrances contained a macrocycle. This figure is expected to rise to around 65%.[8]

Synthetic routes to macrolides

Since the synthesis of macrocyclic lactones has been extensively researched,[9,10,11] this review is only intended to give a short overview of selected synthetic methods of macrocyclic lactones.

There are three basic principles by which macrolides are formed;

  i)   ring closure
  ii)   ring contraction
  iii)   ring expansion

By far the most commom route for macrolide synthesis is by ring closure of a long chain either to form the ester linkage in an intramolecular estertification or with a pre-formed ester linkage e.g. by ring closure metathesis or Diels-Alder reaction. Routes involving intramolecular Diels-Alder reactions and ring contraction metathesis have been used to form the required macrolides from larger ringed compounds. Ring expansion reactions can also be used to synthesise macrolides. Ring expansion by thermolysis or oxidation reactions has allowed macrolides to be produced from fused bicyclic and smaller ringed compounds. Alternatively, the production of oxygen-centred radicals by either thermolysis or pyrolysis, or the use of hypervalent iodine has enabled the production of macrolides via radical mechanisms.

i) Ring closure
Ring closure to macrolides through esterification

The most widely used method for macrolide synthesis is intramolecular esterification of a long-chained hydroxyl carboxylic acid **7** *(Scheme 1).* On its own, this approach is insufficient for the synthesis of macrolides with high temperatures and very dilute solutions required to prevent condensation polymerization. Although activation of the

functional groups promotes the reaction producing the macrolide **8**, most activated systems still form varying yields of cyclic dimer even when using very dilute reaction conditions.

Scheme 1

The activation of both the carboxyl group and the alcohol group greatly improves the esterification, e.g the Corey double activation macrolactonization is outlined in *Scheme 2*. In this example, 2,2'-dipyridyl disulfide (**10**) is used as the activating agent to form the thionyl ester **11** from **9**. After proton transfer from the hydroxyl group to the pyridine ring, nucleophilic attack of the oxygen anion on the carbonyl group carbon results in cyclisation of **12** to **13** without further need for either acid or base catalysts. The hydrogen bond between the carbonyl group and the pyridinium hydrogen atom creates a rigid *pseudo*-6-membered ring in **12** which allows the oxygen anion greater access for nucleophilic attack in the carbonyl group. This method was demonstrated by the synthesis of 12-, 13-, 14-, and 16-membered marolides in 47-80% isolable yield. [12]
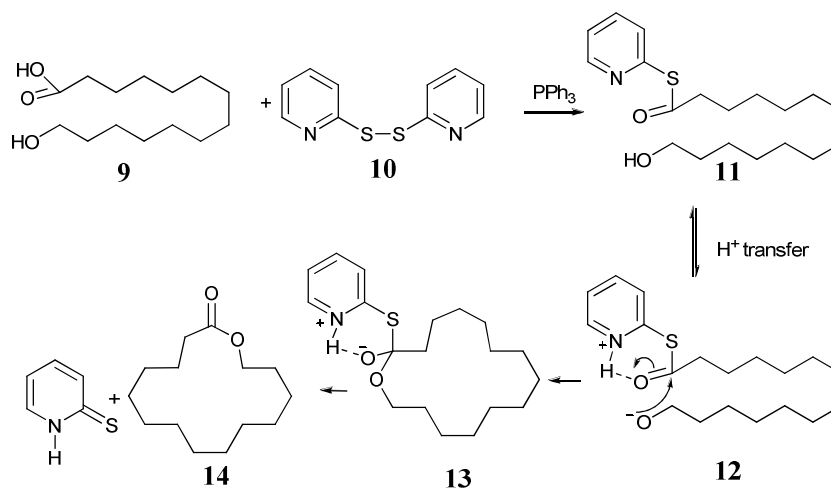
Scheme 2

The addition of 1-methyl-2-chloro-pyridinium iodide (**15**) to the ω-hydroxycarboxylic acid in the presence of triethylamine does a similar job of activating the carboxylic acid *(Scheme 3)*. Thus **15** reacts with the substrate to produce 12- (n= 10), 13- (n=11) and 16-membered (n=14) macrolides in 61%, 69% and 84% yield respectively.[13]
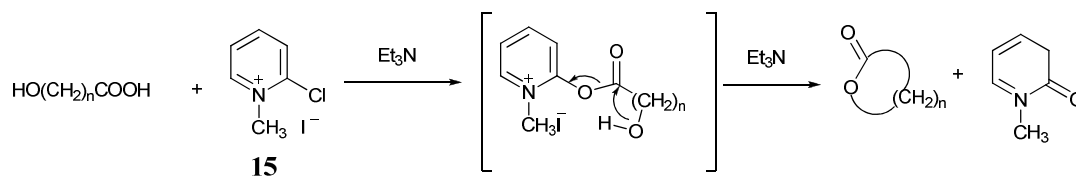
Scheme 3

The Mitsunobu lactonization reaction uses the activation of the hydroxy group of the ω-hydroxycarboxylic acid by the formation of a dipolar alkoxylphosphonium salt (**16**) *(Scheme 4)*. This is achieved through reaction of the hydroxy acid, Ph_3P, and diethyl azodicaroxylate (DEAD) which brings the two reaction sites closer together and enables an S_N2 displacement giving the lactone product **17** with inversion of configuration at the alcohol. Although the reaction takes up to 2 days to go to completion and requires high dilution conditions, the reaction is generally milder with no heating required. This procedure was used to make the 13-membered (n= 11) macrolide in 63% yield.[14]
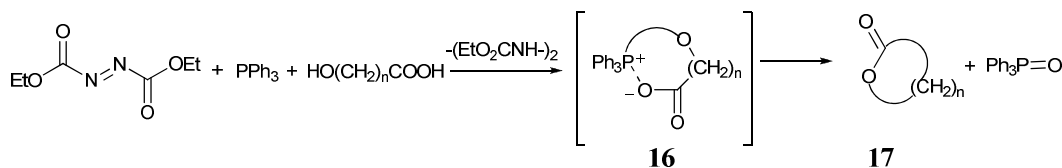
Scheme 4

Mixed anhydrides generated *in situ* from the carboxyl group have also been used as intermediates in the synthesis of macrocyclic lactones. The anhydride reacts with the hydroxyl group under base catalysis leading to lactonization as outlined in *Scheme 5*. One such method is the Yamaguchi lactonization where the esterification consists of two steps: the formation of the mixed anhydride **18**, and the intramolecular alcoholysis of the anhydride to form macrolide **17**. Following a test of different mixed anhydrides, 2,4,6-trichlorobenzoyl chloride (**19**) proved to be the most efficient with a fast reaction rate and almost quantitative conversion to the lactone after 150 minutes. Further to this, it acts as a good leaving group and is sterically hindered towards nucleophilic attack. This reaction was used to form 9- (n= 7), 12- (n= 10) and 13-membered (n= 11) in 36, 48 and 67% yield respectively.[15]

Scheme 5
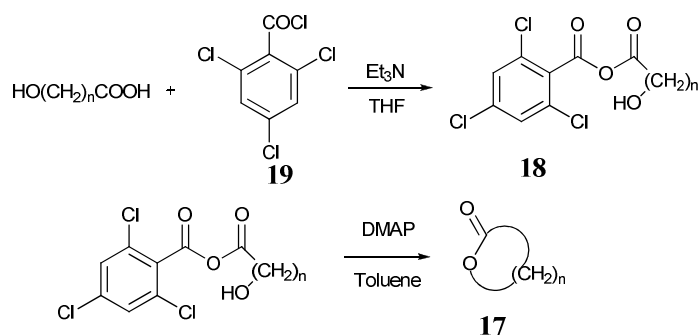
A variety of further routes exist where the activation of either the hydroxyl group or the carboxylic acid promotes the formation of macrocyclic lactones, e.g. 4-(trifluoromethyl)benzoic anhydride,[16] or scandium triflate,[17] or di-2-thienyl carbonate.[18]

Ring closure to macrolides through ring closure metathesis (RCM)

Ring closure metathesis (RCM) has also been adapted for the synthesis of macrolides.[19] RCM is simply an intramolecular olefin metathesis of a long chain bis-unsaturated compound. If the long chain contains an ester group, the product would be a macrolide. RCM uses a ruthenium-based catalyst, Grubbs' catalyst **21**, or similar. *Scheme 6* outlines the catalytic cycle by which it creates a new bond whilst regenerating the catalyst.[20]
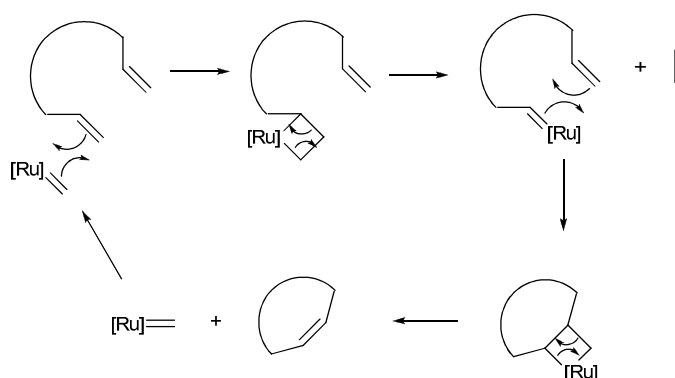
Scheme 6

The musks, exaltolide (**5**) and ambrettolide (**6**) have been prepared by RCM *(Scheme 7)*. For example, exaltolide (**5**) was obtained by the metathesis of the diene ester **20** using a ruthenium catalyst **21**. This produces the unsaturated macrolide **22** (E/Z 46:53) which is hydrogenated to produce exaltolide (**5**). Exaltolide is now a widely used musk and is produced in upwards of 200 tonnes per year.[21]
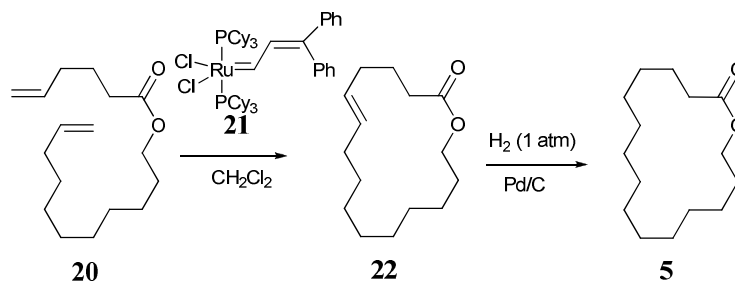
Scheme 7

RCM was proposed as a possible synthetic route to the natural product e.g. amphildinolide W (**25**). Although the substrate looks like a good candidate RCM to a 12-membered ring the reaction was competing with another RCM to form a 17-membered ring exclusively *(Scheme 8).*[22] This reaction was said to be more favourable due to entropic factors and the ring strain dictating that the formation of 12-membered rings is less favourable than the 17- membered ring.
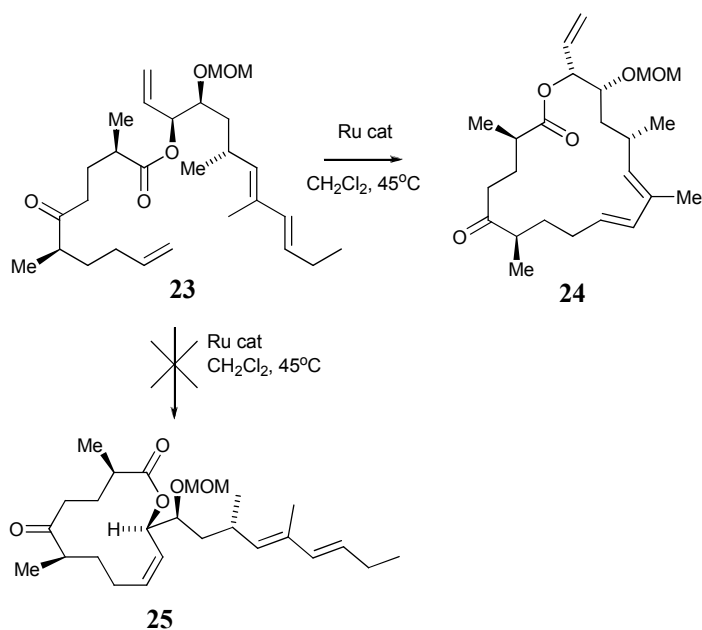
Scheme 8

Both first- and second-generation Grubbs' catalysts have been used in *Scheme 8*. The addition of the first-generation catalyst **20** required Ti(O^{i}Pr)$_4$ as a Lewis acid to produce **24** in a 60% yield. When no additive was used, no reaction took place. Addition of the second-generation catalyst **26** required no additives and increased the yield of **24** to 82%.

20
1st generation

26
2nd generation
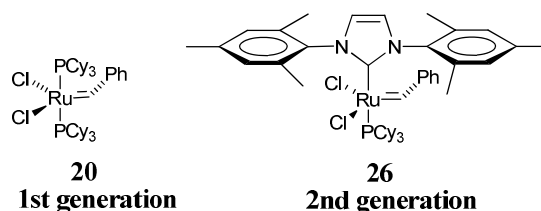
RCM has been used successfully in the key cyclisation step in the synthesis of salicylihalamide **(29)**, a potential antitumour compound *(Scheme 9)*. RCM is more effective than other methods because it provides an effective way of locating the alkene functionality in **28**. The RCM proceeds in varying yields with *E-:Z-* selectivity depending on the nature of R. When the phenolic OH group is protected by a methyl ether, the reaction proceeds in 89% yield with a *E/Z* ratio of 18:1. However in the unprotected model the yield falls to 41% and the *E/Z* ration changes to 1:3 in favour of the unwanted *Z* isomer. Although the reaction gives a lower yield, further investigation into the influences of protecting groups at the second alcohol group showed that the unprotected alcohol gives a 29:1 *E/Z* ratio.[23]

27

28

29
Salicylihalamide
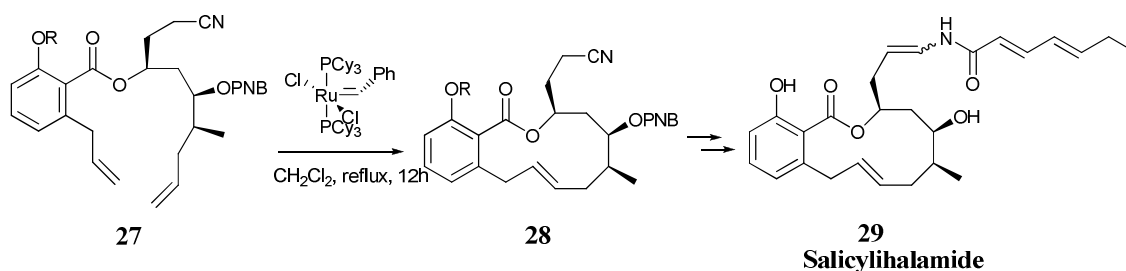
Scheme 9

Ring closure via Diels-Alder reaction

An intramolecular Diels-Alder reaction which in turn ring closes a large chain can also be used in the synthesis of large-ringed lactones. The synthesis of the basic ring structure of cytohalasans, a group of fungal metabolites, has been achieved. Although a 5% yield of the regioisomer **32** was also formed in the reaction of **30**, the intramolecular cycloadduct containing the basic structure of cyctohalsan B **31** was isolated in 27% yield *(Scheme 10)*.[24]
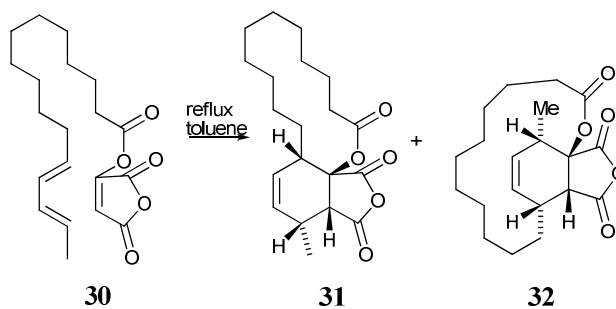
Scheme 10

In a more selective intramolecular cycloaddition reaction, some 11-membered lactones have been formed as illustrated in *Scheme 11*. The reaction of **33** via an intramolecular Diels-Alder reaction produced **34** in high *exo-/endo-* selectivity whilst isomer **35** is not isolated in any measurable quantity form the reaction. Replacement of the methyl group with an isopropyl group or tert-butyl group sees the selectivity decrease. Subsequent reaction with NaOMe to open the more strained lactone group at the bridge-head produced the 11-membered lactone **36**.[25,26]

	34	**35**	
R=Me	100	0	68% yield
R= isopropyl	88	12	64% yield
R= tert-butyl	80	20	61 % yield
		all endo/exo 100:0	
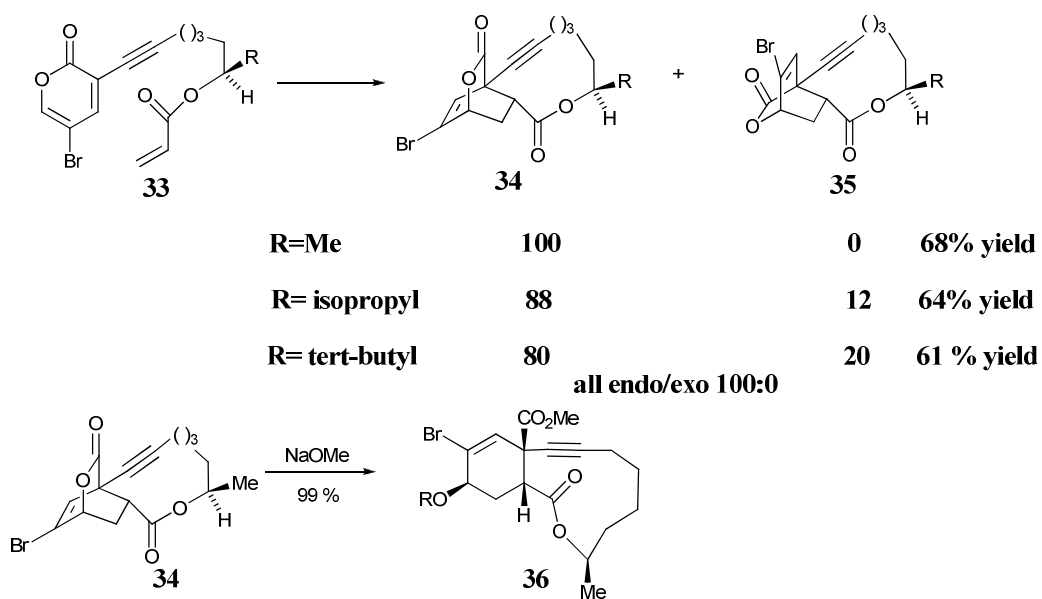
Scheme 11

ii) Ring contraction

Ring contraction to yield macrolides

The use of ring contraction to yield macrolides is relatively rare as they would require larger ringed precursors. Early ring contractions focused on the production of 10- to 13-membered macrolides from the treatment of erythromycin with either acid or base.[27,28]

Recently, ring contraction has been achieved using ring-opening-ring-closing metathesis of conjugated dienes via the removal of a C_2H_2 unit.[29] Treatment of the 16-membered macrolide, josamycin (**37**), with Grubbs' second-generation catalyst[30] in 1-hexene afforded the corresponding ring-contracted macrolide **38** in high yield *(Scheme 12)* *(Table 1)*. Although transformations using Grubbs first-generation catalyst were unsuccessful, the procedure offers a synthetic route from larger ring structures containing a conjugated dienyl system to new antibiotics, several of which exhibited similar biological effects to **37**.
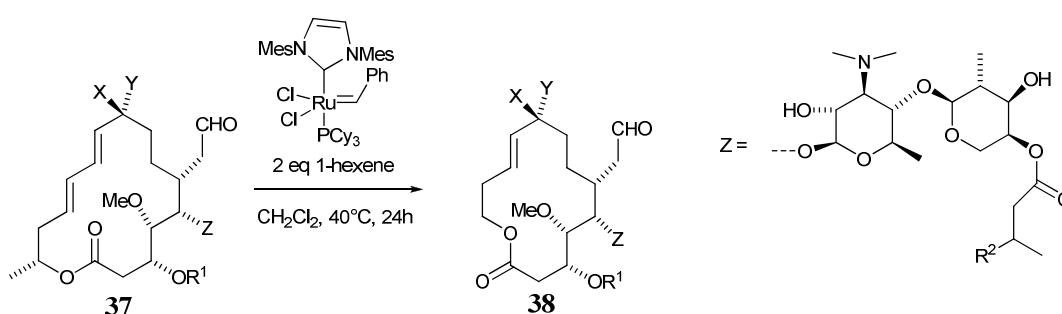
Scheme 12

X	Y	R^1	R^2	Yield
H	OH	COMe	Me	78%
H	OH	H	H	65%
OH	H	COMe	Me	42%

Table 1: Percentage yields for ring-opening-ring-closing metathesis in Scheme 12

Additionally, 14- and 16-membered macrolides were shown to contract via a five-centre, five-electron transition state yielding 13- and 15- membered macrolides via the β-(alcyloxy)alkyl migration of the ester group.[31] The macrolide undergoes tin hydride mediated dehalogenation to produce the carbon-centred radical required for the migration *(Scheme 13)*.
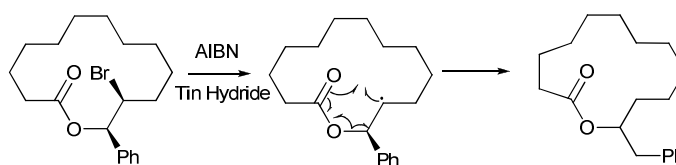
Scheme 13

Intramolecular Diels-Alder reactions have also been shown to be useful for the contraction of large-ringed macrolides.[32] Macrolactonization of **39** produced three products, the expected 18-membered ring **40** and two additional 10-membered ring products **41, 41a** *(Scheme 14)*. The lower yield of isomer **41a** demonstrates the stereoselectivity of the intramolecular Diels-Alder process and is further highlighted when, under forcing conditions, **40** further reacts via the intramolecular Diel-Alder reaction to form **41** in good yield as the sole product. In a further extension to this work the intramolecular Diels-Alder ring contraction has been used in the synthesis of (+)-Superstolide[33] and (-)-Spinosyn A.[34]
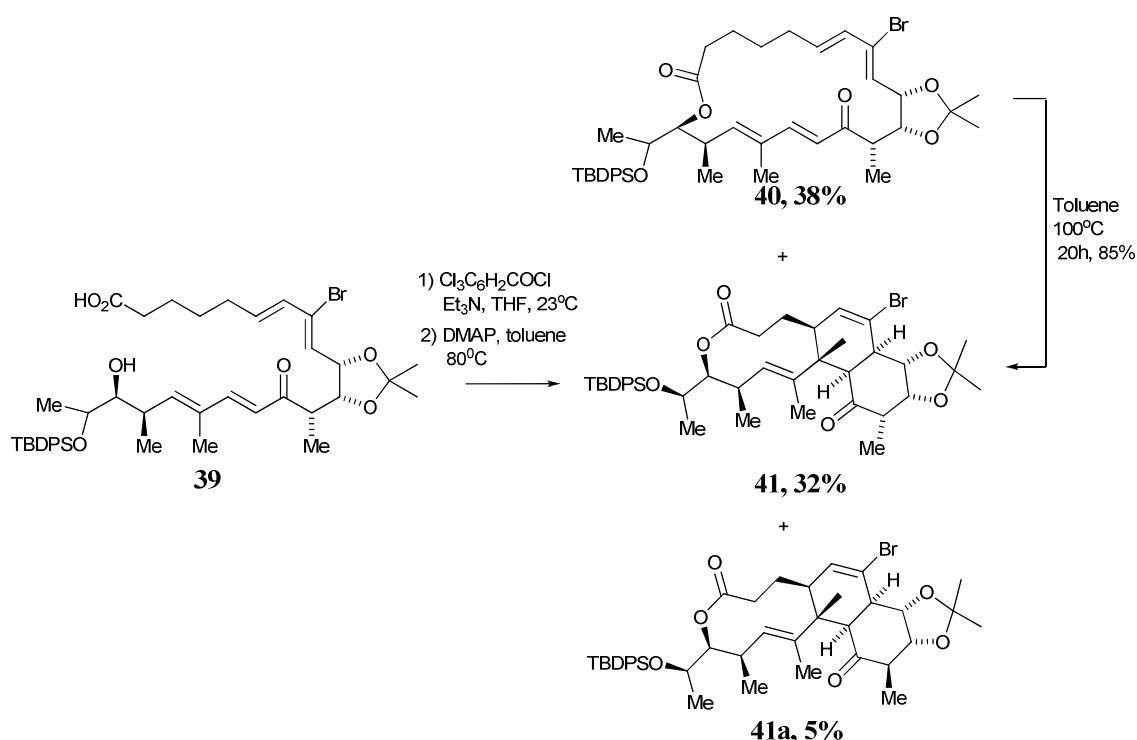
Scheme 14

iii) Ring expansion
Ring expansion to macrolides

One of the more obvious ring expansion routes to large macrolides is via a Baeyer-Villiger oxidation of large cyclic ketones as outlined in *Scheme 15*. There are recent examples of the synthesis of (R)-12-methyltridecanolide (**44**) and (S)-muscolide (**47**) by the Baeyer-Villiger oxidation of macrocyclic ketones **43** and **46** respectively. The reaction however formed two regioisomers of each product in a 70:30 **44:45**, 86% yield ((R)-12-methyltridecanolide (**44**)) and 80:20 **47:48**, 80% yield ((S)-muscolide (**47**)).[35]
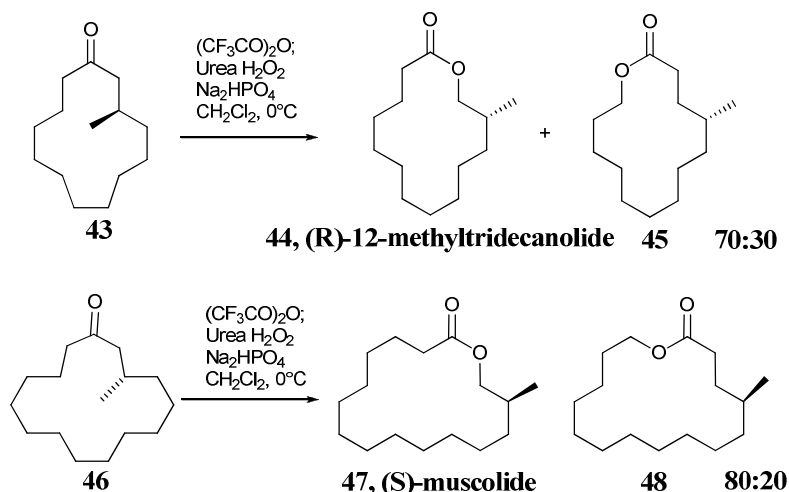
Scheme 15

Thermolysis of a neat sample of the 12-membered ring macrolide isomigrastatin (**49**) yielded the 14-membered ring macrolide migrastatin (**50**) via a [3,3]-sigmatropic rearrangement *(Scheme 16)*. Attempts to carry out the reaction in various solvents (such as toluene, DMF, DMSO, and mineral oil) gave a complex mixture of products. The scope of the reaction was demonstrated with six further examples of the rearrangement.[36]

49	(R=R^2, R^1=OCH$_3$)	**50**
49a	(R=R^2, R^1=OH)	**50a**
49b	(R=R^2, R^1=H)	**50b**
49c	(R=R^3, R^1=OCH$_3$)	**50c**
49d	(R=R^3, R^1=OH)	**50d**
49e	(R=R^3, R^1=H)	**50e**
49f	(R=R^4, R^1=OCH$_3$)	**50f**
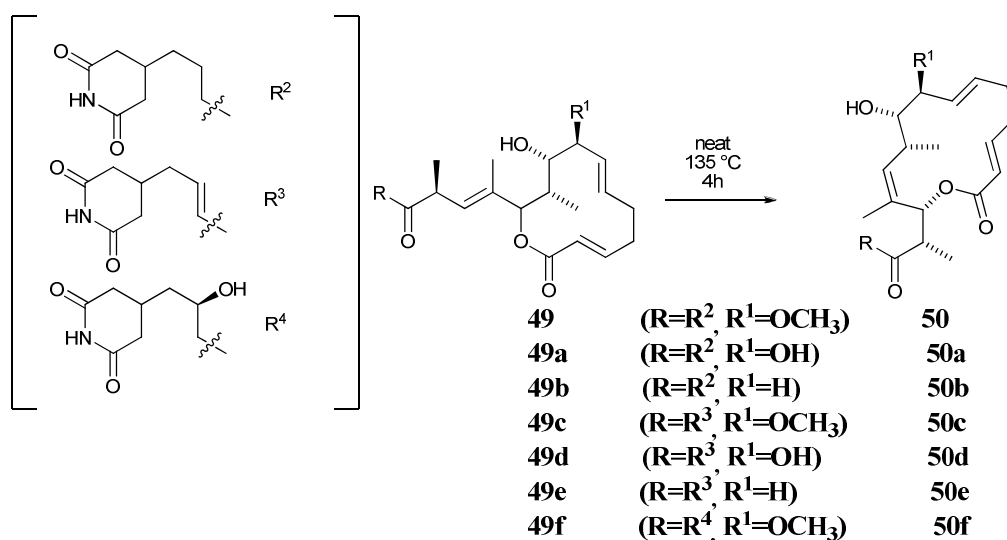
Scheme 16

Macrolides can be formed in moderate yield by a 4-step route from either cyclopentanone (**51**) or cyclohexanone *(Scheme 17)*.[37] A series of ring expansion reactions takes place from **52** to ultimately produce large-ringed macrolide **55**. Oxidative cleavage of **53** using ceric ammonium nitrate creates the 9-membered

macrolide **54** which on subsequent catalytic hydrogenation followed by intramolecular *trans* esterification produces the 11-membered macrolide **55** in moderate yield. This method has been used to create a series of macrolides with ring sizes ranging from 9- to 12-member.
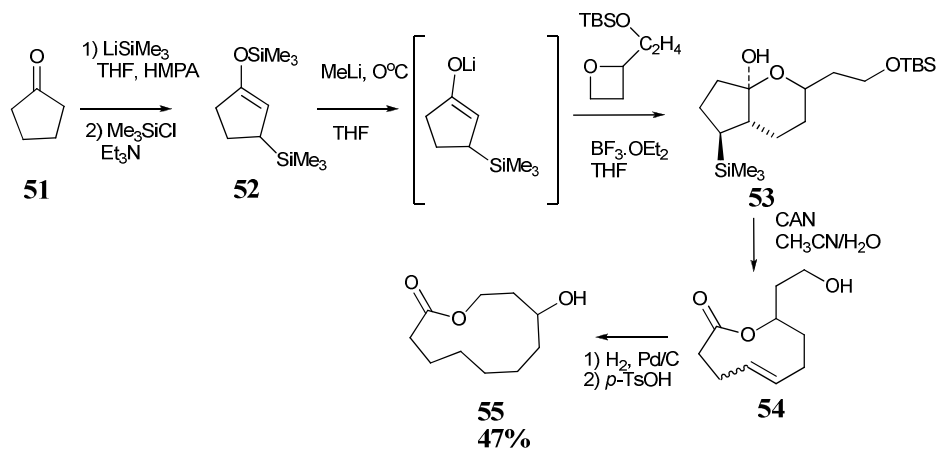
Scheme 17

Another ring-expansion procedure utilizes the oxidative cleavage of an enol ether double bond by ruthenium tetroxide *(Scheme 18).*[38] Following the alkylation of cyclononanone (**56**) and acid-catalysed cyclization to the enol ether (R)-**57**, oxidative cleavage of the enol ether double bond with ruthenium tetroxide/ sodium periodate gives the 13-membered keto lactone **58** (80% yield) which was then reduced to the target compound (R)-**59**. Investigations of (R)-**59** noted a more intense smell than previously analysed (S)-**59** demonstrating that the enantiomers of musks hold different the sensory properties.
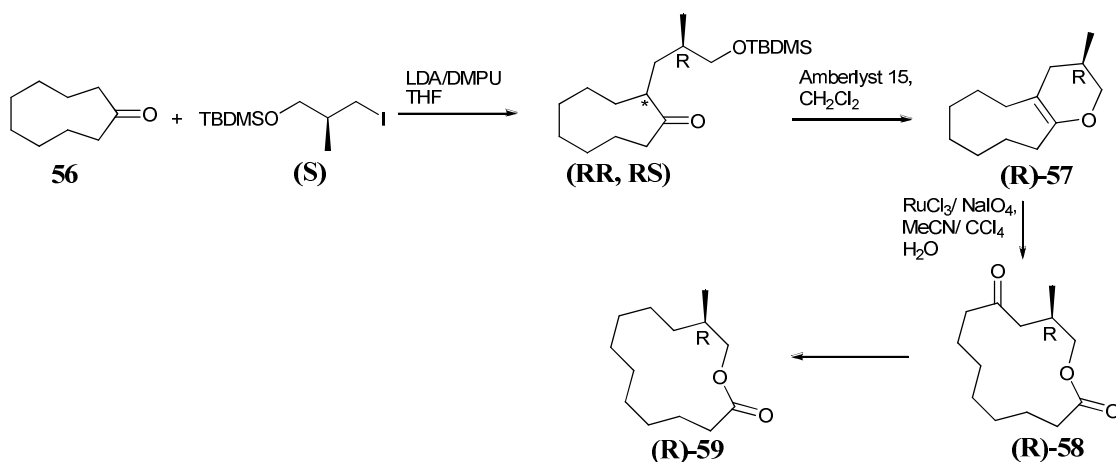
Scheme 18

Macrocyclic lactones via radical ring expansion

Macrolides may also be obtained by intramolecular cyclisation of radicals derived from the unsaturated hydroperoxy acetals (**61**) *(Scheme 19)*. Hydroperoxy acetal **61**, synthesised via the ozonolysis of vinyl ether **60**, was treated with iron(II) sulfate and copper(II) chloride to give macrolide **63**, R=H in 49% yield. From **61**, R=Me the macrolide was obtained in 35% yield. The formation of the macrolide suggests that the intermediate oxy radical undergoes β-scission of the six-membered ring followed by an intramolecular radical cyclisation and chlorination by CuCl$_2$ to give macrolide **63**. In the absence of copper (II) chloride, significant quantities of the dimeric macrolides **64** were obtained instead.[39]
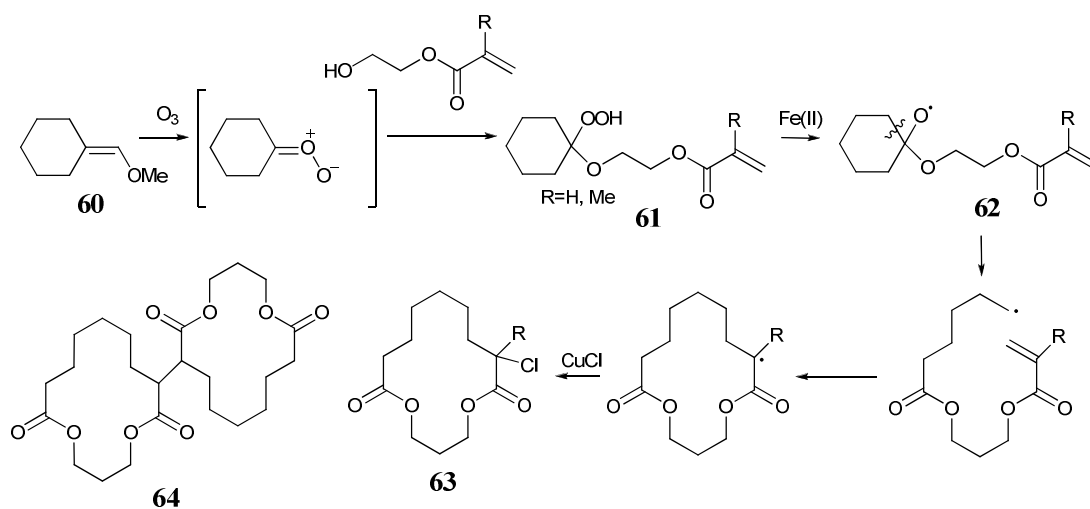
Scheme 19

In an alternative approach, hypervalent iodine compounds have been reacted with hemiacetals to generate oxy radicals. The photolysis of hemiacetals **65** and **68** using visible light with a small excess of DIB (diacetoxyiodobenzene) in the presence of stoichiometric quantities iodine (I$_2$) produced 9- and 10-membered lactones *(Scheme 20)*. The iodine was deemed essential since no reaction was observed when in the absence of iodine whereas a catalytic quantity of iodine produced only 30% conversion after 2 hours *(Table 2)*.[40]
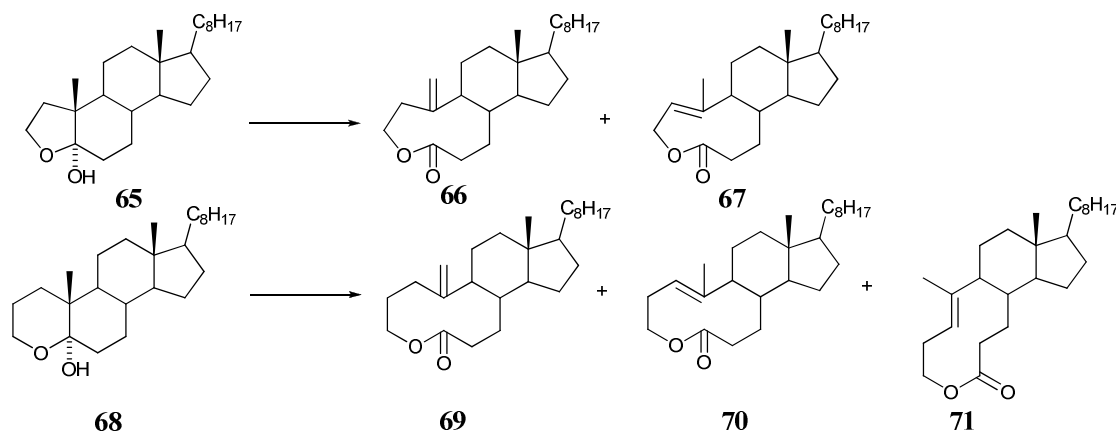
Scheme 20

Hemiacetal	DIB/ mmol	Iodine/ mmol	Products
65	1.1	1	**66** (45%), **67** (40%)
65	1.1	0	No reaction
65	1.1	0.1	**66** (13%), **67** (12%), **65** (70%)
68	1.2	1.4	**69** (33%), **70** (17 %), **71** (33 %)

Table 2: Percentage yields of products derived form 65 and 68

The photolysis of the steroidal alcohol **72** with a protected side chain in the presence of HgO/I_2 gave the 10-membered ring ketone **73** in 85% yield *(Scheme 21)*. In contrast, the use of DIB/I_2 in this reaction produced no product. Hydrolysis of acetate **72** with saturated methanolic solution of $NaHCO_3$ at 0°C gave the hemiacetal **73a** in 99% yield. Subsequent photolysis of the hemiacetal **73b** using HgO/I_2 afforded a mixture of macrolides **74** in 30% yield. Catalytic hydrogenation of the mixture over PtO_2 gave the 13-membered ring macrolide **75** in 75% yield.[41]
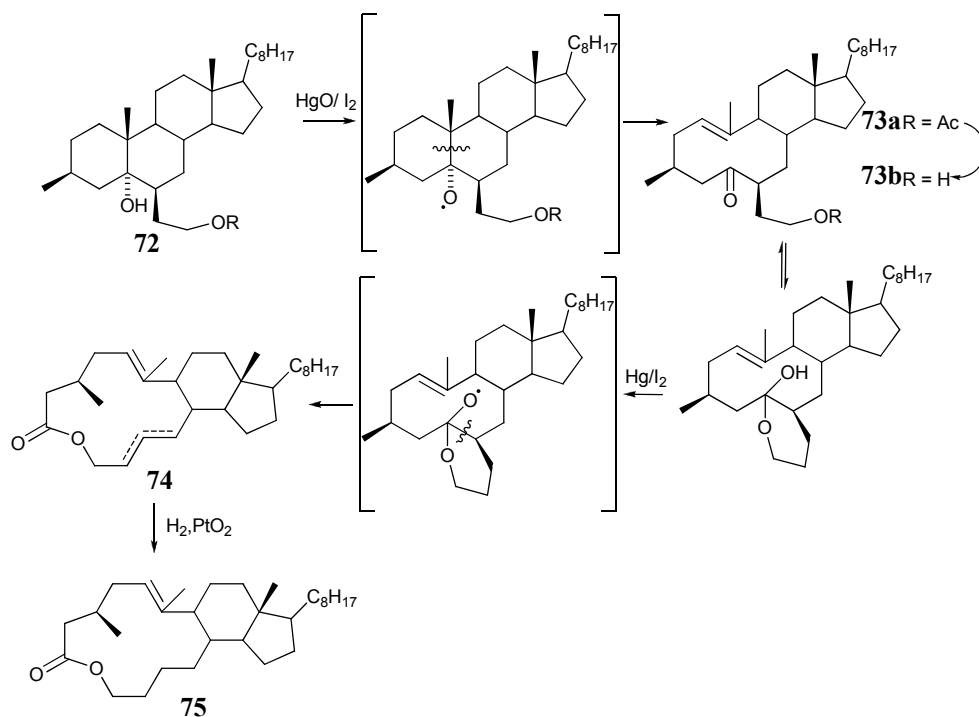
Scheme 21

Macrocylic lactones from *dispiro*-1,2,4,5-tetroxanes

The thermolysis of dimeric and trimeric cyclic peroxides derived from cyclic ketones has been shown to be a quick synthetic route to macrocyclic lactones *(Scheme 22)*.[42] Symmetrical *dispiro*-1,2,4,5-tetroxanes such as **77** were synthesised by the acid-catalysed reaction of the appropriate cyclic ketone with hydrogen peroxide.[43] The thermolysis of **77** at 150°C for 30 minutes afforded a mixture of cyclododecane (**78**) (44%), undecanolide (**79**) (23%) and cyclohexanone (**76**) (21%).[44] The reaction produced better yields when the peroxide was dissolved in a high boiling hydrocarbon solvent at a concentration of 5-10 wt%. At higher concentrations, lower yields of macrolide were obtained due to the formation of polymeric material.[45]
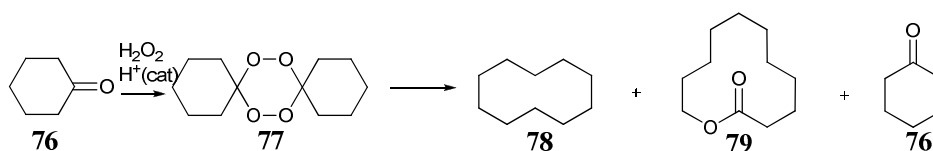
Scheme 22

Tricyclohexylidene triperoxide (**80**) has also been shown to decompose on thermolysis at 180 °C to give a mixture of cyclopentadecane (**81**), 16-hexadecanolide (**82**), cyclohexanone (**76**) and a small amount of the isomeric dilactones *(Scheme 23)*.[44]
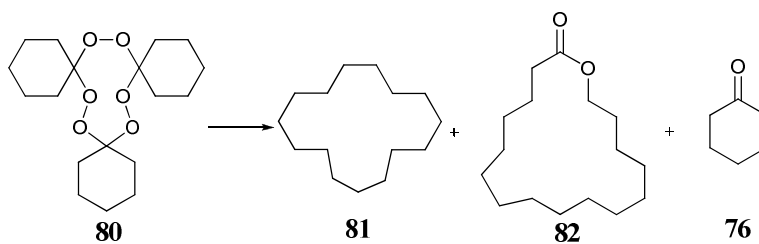
Scheme 23

The synthetic usefulness of this reaction is heavily dependant on the availability of the required 1,2,4,5-tetroxane. However, different 1,2,4,5-tetroxane derivatives may decompose to give the same product. Thus synthesis of unsymmetrical and even substituted[46] diperoxides and triperoxides allowed access into a range of macrocycles C8 to C33.[47]

The mechanism for the decomposition of *dispiro*-1,2,4,5-tetroxanes proceeds via the homolytic cleavage of the O-O bond producing the oxy bi radical **83** *(Scheme 24)*. Concerted double β-scission of the C-C bonds produce alkyl biradical **84** which undergoes radical recombination to produce the cyclic diacyl peroxide **85**. Further decomposition via homolytic cleavage of the O-O bond in **85** followed by loss of one or two molecules of carbon dioxide produced **78** and **79** respectively. The regeneration of the cyclohexanone (**76**) can be explained via a double β-scission of the C-O bonds in **83** to release oxygen molecule plus two molecules of ketone **76**. The decomposition of **80** proceeds in a similar fashion.
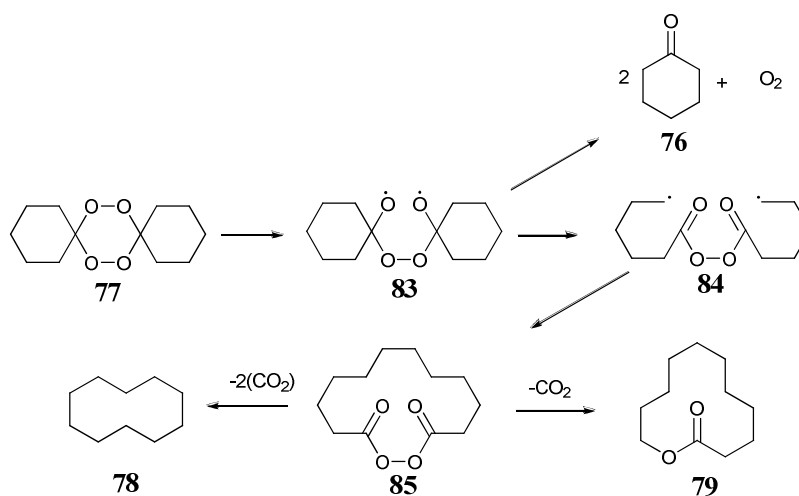
Scheme 24

Macrocyclic lactones from *dispiro*-1,2,4-trioxanes

By analogy with the decomposition of *dispiro*-1,2,4,5-tetroxanes, it was anticipated that the thermal decomposition of *dispiro*-1,2,4-trioxanes **86** could provide macrocyclic compounds. With only one peroxide bond further decomposition of any cyclic intermediates releasing carbon dioxide to form cyclic alkanes would be prevented. In addition, the cyclic keto lactones **90** have additional functionality which would allow further manipulation e.g the keto group. Additionally the ability to synthesise unsymmetrical *dispiro*-1,2,4-trioxanes allows access to a wider range of ring systems.
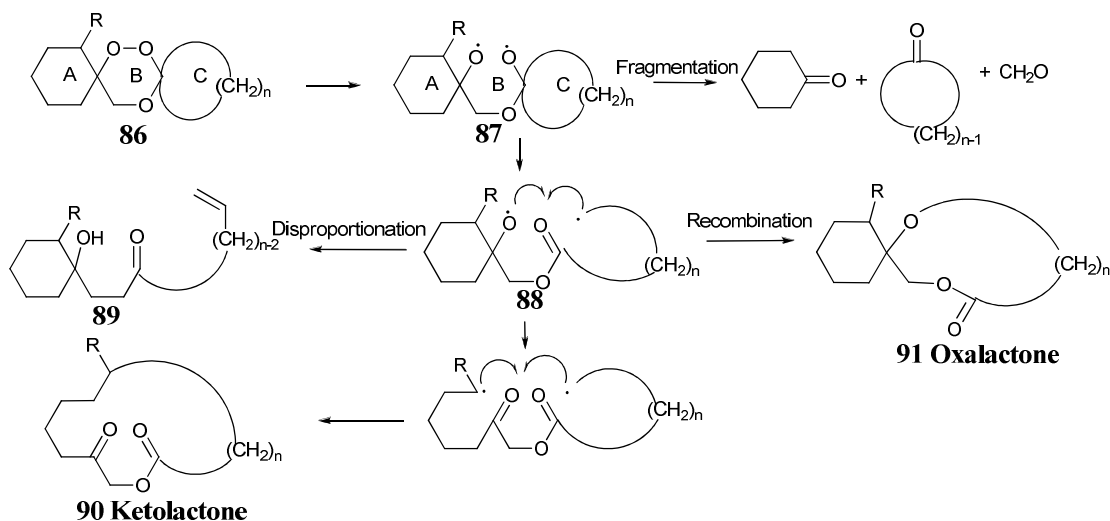
Scheme 25

Although the initial step is the homolytic cleavage of the peroxide bond in **86** to form an oxy-biradical **87**, the reaction products obtained seem to be indicate that the ring opening of ring **C** is occurring without the ring opening of ring **A**. Thus as well as the production of the desired macrocyclic keto lactone **90,** there is also the production of the oxolactone **91** *(Scheme 25) (Table 3).*[48] The formation of the oxalactone **91** suggests that the β-scission of rings **A** and **C** is stepwise rather than simultaneous thus the β-scission of ring **C** forming **88** and recombination with the oxy radical is occurring faster than the β-scission of ring **A**. The relative quantities of keto lactone and oxalactone vary with the nature of the α-substituent on ring **A** indicating it must have an effect on the rate of opening of ring **A**. When R= H, the keto lactone **90** is only obtained when ring **C** is a 12-membered ring. This is thought to be due to the size and flexibility of the ring preventing efficient recombination and giving the system time to undergo the β-scission

of ring **A**. When R=H and ring **C** is 5-, 6-, or 7-membered, only oxolactone **91** and the fragmentation products are formed. In contrast, when R is a methyl group, there is a move to increasing yields of keto lactone **90** indicating that the opening of ring **A** is more competitive with that of **C**. The formation of oxalactone **91** for methyl-substituted *dispiro*-1,2,4-trioxanes is still the preferred reaction route. In fact the thermolysis of a methyl-substituted *dispiro*-1,2,4-trioxane with an indanylidene ring **C** formed the exclusive formation of the corresponding oxalactone **91**.[49] The unsaturated hydroxyl ester **89** has also been isolated from the thermolysis of methyl-substituted cases and is thought to be due to a intramolecular 1,8-hydrogen abstraction process. Similar to *dispiro*-1,2,4,5-tetroxanes, the thermolysis of *dispiro*-1,2,4-trioxanes results in some total fragmentation into the corresponding ketones and formaldehyde as judged by GC analysis of the thermolysate.
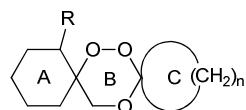
86a, R= H   **a, n= 5**
86b, R= Me   **b, n= 4**
86c, R=OMe   **c, n= 6**
                  d, n= 11

	R	**n**	**Keto lactone**	**Oxalactone**	**Alkene**
			Yields of each product/ %		
86ab	H	5	-	25	-
86aa	H	6	-	24	-
86ac	H	7	-	26	-
86ad	H	12	18	-	-
86bb	Me	5	15	15	20
86ba	Me	6	15	22	-
86bc	Me	7	15	25	6

Table 3: Percentage yields of products derived from the thermolysis of unsubstituted and methyl-substituted dispiro-1,2,4-trioxanes

Structure of macrocyclic lactones

Large ringed macrolides can adopt a variety of different conformations depending on the substitution patterns of the ring themselves. This is due to the many degrees of freedom each structure possesses resulting in many different conformations being close in energy.

This review will concentrate on the structure and conformations of 13- to 15-membered ring structures. The structural studies of 14-membered rings have been extensively covered due to many naturally occurring macrocycles being 14-membered rings and the 'diamond-like' packing of the rings. In contrast odd-numbered 13- and 15-membered cyclic systems rings have been studied less with very few X-ray crystal structures having been determined. [50]

Early structural studies of macrocycles by X-ray crystallography, NMR experiments and semi-empirical molecular mechanics suggest the large rings try to avoid as much torsion strain (Pitzer strain) by opening certain CCC bond angles even at the expense of the increase angle strain (Baeyer strain). Whilst studying large ringed structures, Dale found that a completely strain-free conformation is possible for 14-membered rings[51] whilst 13- and 15-membered rings were never formed without some strain. Investigation of the conformational energies of large rings suggested that the lower energy conformations have as many torsion angles close to 180° with *gauche* interactions also required to form corners. From the initial studies of the conformation of 14-membered rings, Dale proposed that the conformations would be superimposable on a diamond lattice framework, such as a [4343] conformation.[52] NMR studies also suggested that a 14-membered ring was in a [4343] rectangular conformation. This conformation has four chemically individual carbons A-D in a 1:2:2:2 ratio *(Figure 1)*.
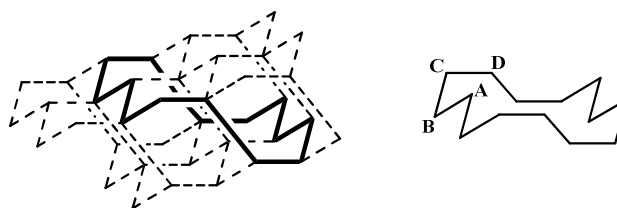
Figure 1: Conformation of a 14-membered ring indicating 4 chemically different carbons

Although room temperature ^{13}C NMR spectrum of cyclotetradecane consisted of a single signal, the ^{13}C NMR spectrum at -132°C contained 3 lines in approximate ratio of 4:1:2. It was suggested that two of the signals had such a small chemical shift difference that they had overlapped.[53]

Dale also proposed that whilst 14-membered cycloalkanes have rectangular conformations, 13- and 15- membered homologues have more strained quintangular conformations. The calculated favoured conformation for simple 13-15 membered cycloalkanes are listed in *Table 4*.[54] In this study, Dale also found two low-energy 14-membered ring conformations which were not based on the diamond lattice. These were [4433] conformations, with a strain energy of 1.1 kcal mol^{-1} and 2.4 kcal mol^{-1} relative to the [4343] conformation. These conformations proved to be lower in energy than any other diamond-lattice based 14-membered ring with the exception of [4343]. The most stable conformation of a 14-membered ring was confirmed as a rectangular [4343] by analysis of the X-ray crystal structures of cyclotetradecane[55] and cyclotetradecanone.[56]

Cycloalkane	Conformation
Cyclotridecane	[12433]
Cycletetradecane	[3434]
Cyclopentadecane	[33333]

Table 4: The conformations are represented by a shorthand notation first used by Dale where the numbers in the brackets represent the number of atoms between the corners of the molecule.[57]

Force field calculations showed that there were major differences in the energies of the possible conformations of cyclotridecane with the [13333] conformation being the lowest in energy *(Figure 2)*.[58] In the same study, however, the conformation of the 15-membered ring was confirmed as [33333]. X-Ray crystal structure determinations of a 13-membered nitrogen-containing macrocycle[59] as well as a 13-membered ring macrolide[39] confirm the preference for [13333] over [12433]. However, other 13-membered ring structures have also been reported as adopting [337] triangular conformations.[60,61,62] Although the lowest energy form of cyclopentadecane was calculated as the quinquangular conformation [33333], X-ray structural determination has indicated the presence of a quadrangular form [3444][63] not investigated by Dale in his original study. Further 15-membered ring structures have also been reported as [13353][64] and [12345][65] conformations. The different conformations observed for these

structures are consistent with the flexibility of their macrocyclic systems and hence many local minima are possible.
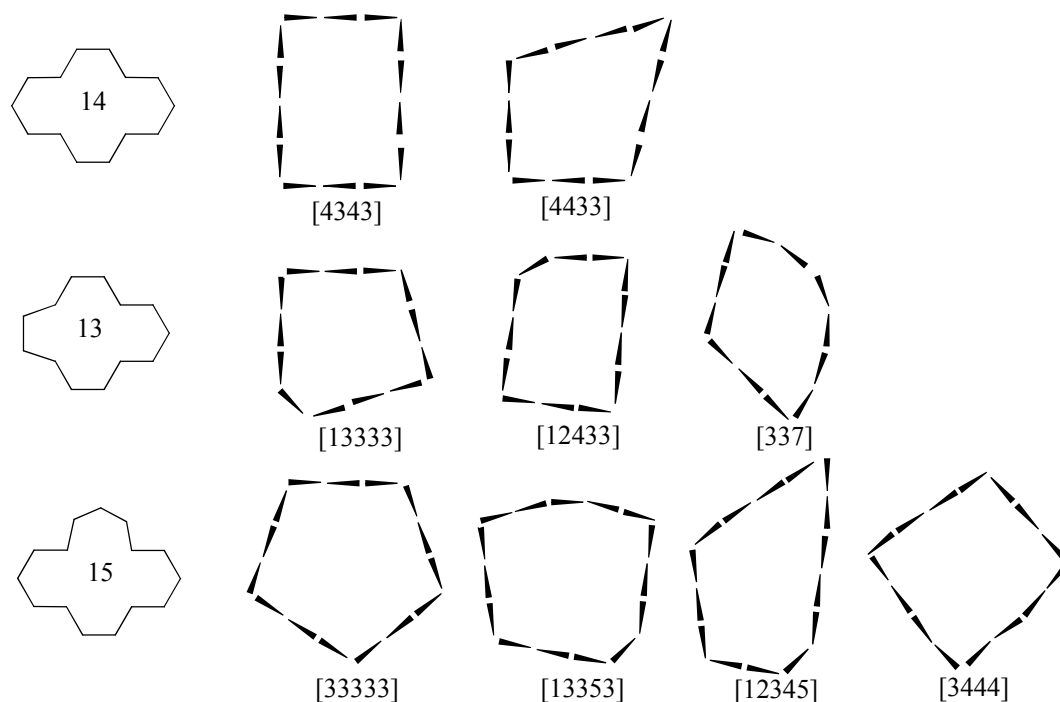
Figure 2: Conformations of 13-, 14-, and 15-membered rings using Dales numencleture[57]

The replacement of one of the ring CH_2 groups in a cycloalkane with oxygen, nitrogen or a carbonyl group has little effect on the conformation of the rings.[53] Generally sp^2-carbonyl group carbons are located at facial rather than corner positions,[66] because this helps to reduce repulsive gauche interactions between methylene groups.[67] This is highlighted by the [4343] conformation of 1,3,8,10-tetraoxacyclotetradecane in which the carbonyl groups are in facial positions *(Figure 3)*.[68]

MM2 calculations also clearly indicated that the oxygen atom in 14-membered macrocyclic ethers tend to prefer a position in the middle of a face in the structure. The structural simulation also identified four other conformations within 2 kcal mol^{-1} of the [4343] global minima. These local minima included a [4433] conformation at 0.99 kcal mol^{-1} in which the oxygen atom was located in the centre of a face *(Figure 3)*.[69]

1,3,8,10-Tetraoxacyclotetradecane

0.00 kcal mol^{-1}
[4343]

0.99 kcal mol^{-1}
[4433]

0.00 kcal mol^{-1}
[22334]

0.41 kcal mol^{-1}
[22244]

1.97 kcal mol^{-1}
[4343]
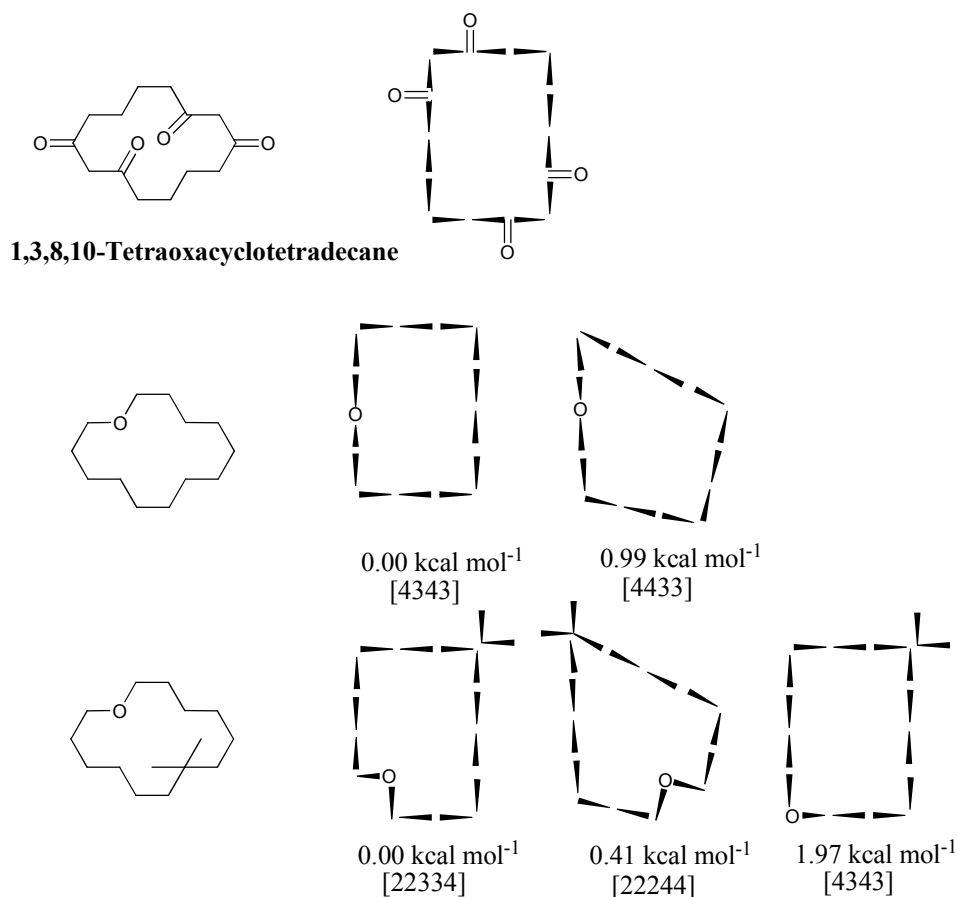
Figure 3: Conformations of ether containing 14-membered rings using Dales numencleture[57]

Moreover, the substituents e.g. alkyl groups, on a large ring can only occupy an exterior position of the face to avoid transangular interactions.[70] However, the introduction of a geminally substituted ring atom forces the molecule to adopt a conformation where the di substituted ring atom occupies a corner position *(Figure 3)* because this is the only part of the structure where both substituents occupy an exterior position and consequently do not experience severe transannular interactions.[71,72] Depending on the rest of the molecule, this can force the large ring into otherwise unfavoured conformations. For example, introducing a geminally substituted carbon atom into the 14-membered ring ether would affect the conformation of the molecule where the spacing between the ether oxygen and the geminally substituted carbon is either 4 or 7 atoms apart. This would mean that both geminally substituted carbon and ether oxygen atom would be located at corner positions. In this case, molecular mechanics calculations found that the lowest conformation was [22334] whilst the [22244] and [3344] conformations where within 0.7 kcal mol^{-1}. The [3434] diamond lattice conformations were much higher in energy at 1.97 kcal mol^{-1}.[73]

In a similar study into the conformation of macrolide (12R)-12-methyl-13-tridecanolide, the global minimum was shown to be a [3434] conformation with the methyl in the corner position *(Figure 4)*. Interestingly the closest [3344] conformation was only 0.43 kcal mol^{-1} higher in energy with the methyl group in the same place. Only a small change in the ring conformation is required for the interconversion of their conformations.[74]

0.00 kcalmol^{-1}
[4343]

0.43 kcalmol^{-1}
[4433]
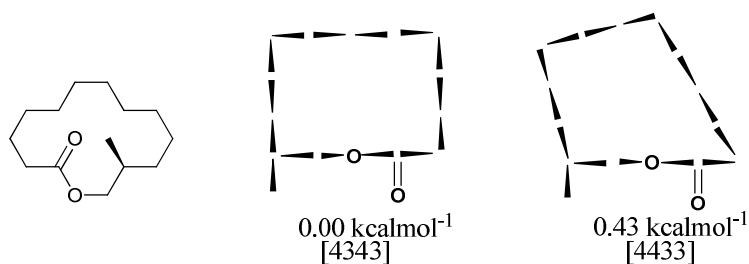
Figure 4: Conformations of a 14-membered macrolide using Dales nomenclature[57]

Thermolysis of *dispiro*-1,2,4-trioxane as a route to macrocyclic compounds

As found previously,[48,49] the thermolysis of *dispiro*-1,2,4-trioxanes **86aa-ac** and **86ba-bc** showed a preference for the production of oxalactones **91a,b** via radical rearrangement reactions. The formation of oxalactone demonstrates that β-scission of ring **A** is less favourable than β-scission of ring **C** for unsubstituted *dispiro*-1,2,4-trioxanes **86a**. Although the corresponding oxalactones **91b** remained the major product, the thermolysis of methyl-substituted *dispiro*-1,2,4-trioxanes **86ba-bc** also produced some of the desired fully ring expanded keto lactones **90b**. A preliminary investigation into the thermolysis of methoxy-substituted *dispiro*-1,2,4-trioxane **86ca** indicated that significant amounts of the fully ring expanded keto lactone **90c** had been obtained.[75]

As described in *Chapter 1,* a series of methoxy- and ethoxy-substituted *dispiro*-1,2,4-trioxanes **86ca-86cd** and **86da-86dd** have been synthesised. In this chapter these new compounds have been thermolysed to investigate in detail the effect of the alkoxy substituent on the rearrangement reaction. By changing the size of ring **C**, it was hoped that the thermolysis of *dispiro*-1,2,4-trioxanes **86ca-86cd** and **86da-86dd** would form a range of substituted 13-, 14-, 15, and 20-membered macrolides **90c,d** *(Scheme 26)*.

86a, R= H	**a, n= 5**
86b, R= Me	**b, n= 4**
86c, R=OMe	**c, n= 6**
86d, R=OEt	**d, n= 11**

91a, R= H
91b, R= Me

90b, R= Me
90c, R= OMe
90d, R= OEt
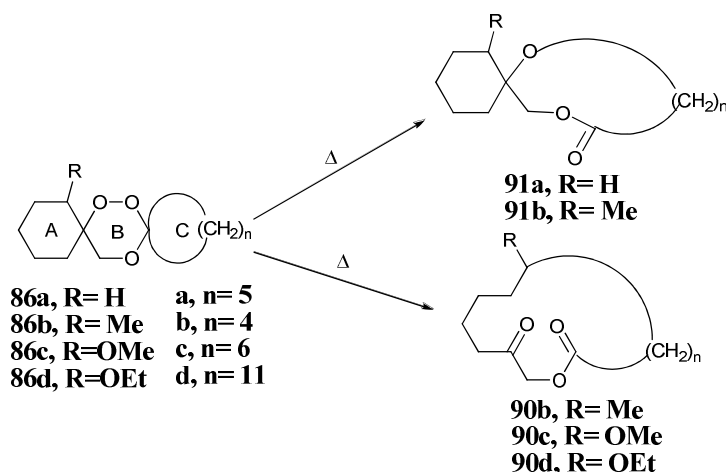
Scheme 26

The thermolysis reactions were carried out using a modified procedure using thick-walled Schlenk tubes rather than single-use sealed glass tubes.[75] This allowed the Schlenk tubes to be recycled and the thermolysis reactions to be carried out on a large scale. Samples of the *dispiro*-1,2,4-trioxane *ca.* 100-200 mg were dissolved in decane

ca. 10-15 mL (ca. 1-1.5% w/v) and carefully transferred to the Schlenk tubes via a pipette. Following the degassing of the solutions using three "freeze-pump-thaw" cycles, the reaction vessels were immersed in a temperature-controlled silicone oil bath and heated at 185 °C for *ca.* 16 hours.

Thus, the thermolysis of the methoxy-substituted *dispiro*-1,2,4-trioxane **86ca** at 185°C produced a clean thermolysate which on analysis by TLC seemed to give a single component at R_f 0.46. Subsequent analysis of the thermolysate by gas chromatography gave a chromatogram which contained one large peak with a retention time (t_r) of 6.93 min and two small signals with t_r 3.53 min and as a shoulder of the main peak as illustrate in *Figure 5*. The identities of the two small signals were confirmed to be cyclohexanone and 2-methoxycyclohexanone respectively by comparison with authentic samples by GC.

RT	AREA	BC	AREA %
2.98	0.0426	T	0.0163
3.53	0.4296	V	0.1644
4.10	0.1770	V	0.0677
5.07	0.0408	T	0.0156
5.93	0.1254	T	0.0480
6.17	0.0750	T	0.0287
6.93	83.0878	T	31.8052
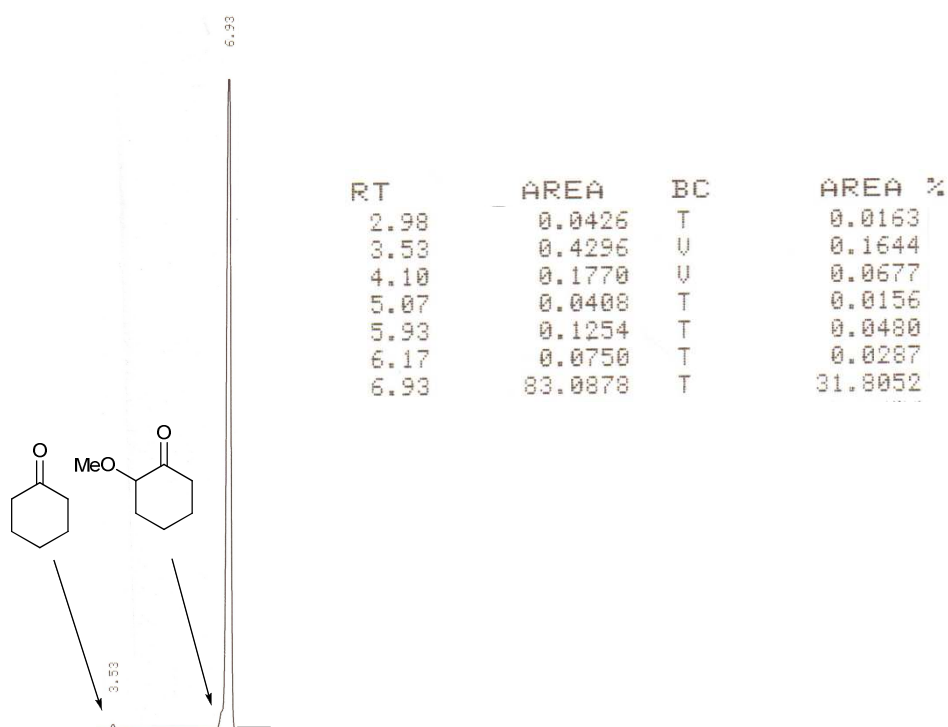
*Figure 5: GC spectrum of thermolysate from thermolysis of **86ca** demonstrating single large peak and two small peaks for cyclohexanone and 2-methoxycyclohexanone*

In previous methods for the isolation of the thermolysis products, it was customary to remove the decane solvent by distillation before separation and isolation of the non-volatile products using flash column chromatography. Using this method, it was found

that, the major product also co-distilled with the decane. TLC analysis of the decane distillate showed that the component at R_f 0.46 was present therefore implying that the use of this method of isolation would result in reduced yields of the product. It was found that the most convenient way of isolating the product was to load the whole thermolysate onto the column and then by eluting with ethyl acetate/ light petroleum, the non-polar decane would run close to the solvent front and be collected in the early fractions before the more polar macrolides had migrated through the column.

The major non-volatile component from the thermolysis of *dispiro*-1,2,4-trioxane **86ca**, corresponding to the fraction at R_f 0.46 was collected by elution with ethyl acetate: light petroleum 1:3 as a crystalline solid in 67% yield with a melting point of 57°C. The mass spectrum of the solid showed a molecular ion peak at m/z 256 with an accurate mass of 256.16746. Given that this mass was the same as that of *dispiro*-1,2,4-trioxane **86ca**, this component must be a rearrangement product. The ^{1}H NMR spectrum of this component showed the two doublets at δ4.3 and δ4.7 with ^2J 16.0 Hz corresponding to the two methylene group hydrogen atoms situated next to the ester group. The ^{13}C NMR spectrum showed two carbonyl group carbon signals at δ173 and δ207 corresponding to an ester and a ketone carbonyl group respectively. These signals corresponded to the spectral data reported previously for macrolide **90ca**.[75] The rearrangement of *dispiro*-1,2,4-trioxane **86ca** to give macrolide **90ca** in an increased yield of 67% is a significant improvement in the selective formation of macrolides from *dispiro*-1,2,4-trioxanes *(Scheme 27)*.
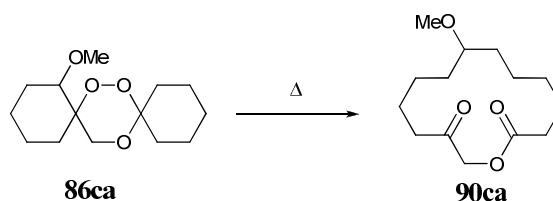
Scheme 27

The crude **90ca** was recrystallised from light petroleum/ diethyl ether mixed solvent and upon slow evaporation crystals suitable for X-ray crystallography were obtained. Following data collection, structural solution and refinement, X-ray crystallographic analysis of the crystals revealed the structure to be the desired methoxy-substituted 14-membered macrolide **90ca** as illustrated in *Figure 6*.
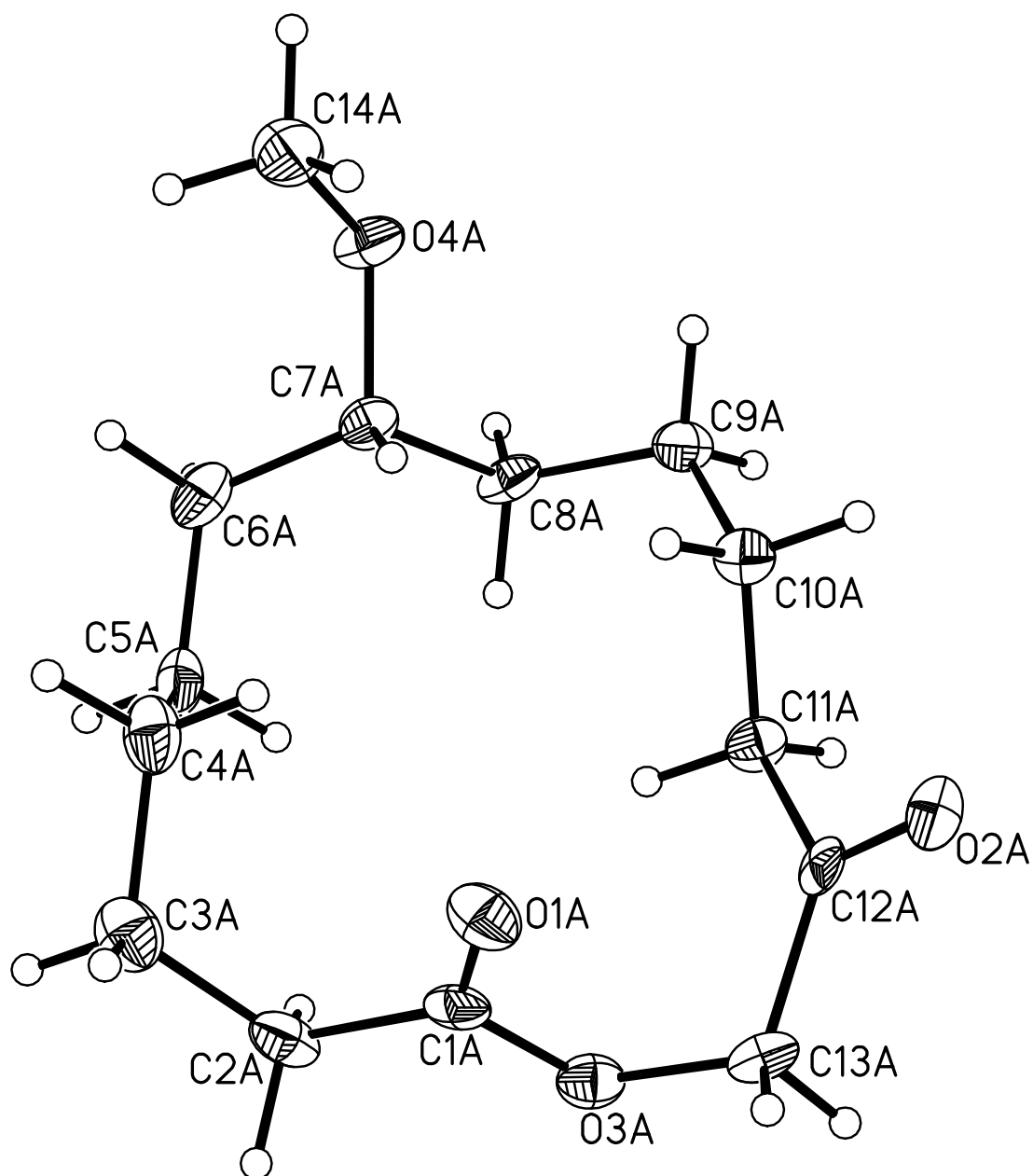
*Figure 6: X-ray crystal structure of **90ca***

(Ortep, 50% probability ellipsoids for non hydrogen atoms)[76]

The structure of macrolide **90ca** shows that the 14-membered ring is not in the classic square [4343] conformation observed for other 14-membered rings.[55,56] Instead the structure forms a [4433] conformation with the keto lactone functionality being located at the corner of the [44] sides. Interestingly the two carbonyl groups on the ring are situated on the same face of the molecule with the ester carbonyl pointing into the centre of the ring and the ketone carbonyl pointing toward the outside of the ring. As expected, the methoxy substituent is situated in a *pseudo*-equatorial position to minimise steric interactions with other hydrogen atoms pointing into the centre of the ring.

Analysis of the packing of the molecules in the crystal structure shows that a number of weak C-H···O close interactions exist between the molecules *(Figure 7)*.[76] Two of these close interactions measure 2.480 Å (C···O = 3.255(9) Å) and 2.439 Å (C···O = 3.192(8) Å) and are between the ketone oxygen and one of the hydrogen atoms of the methylene located between the ketone and ester functionalities. Additionally there is a longer interaction of 2.720 Å between the ketone oxygen and another ring methylene group hydrogen atom. Surprisingly there are no close range interactions involving the methoxy substituent.
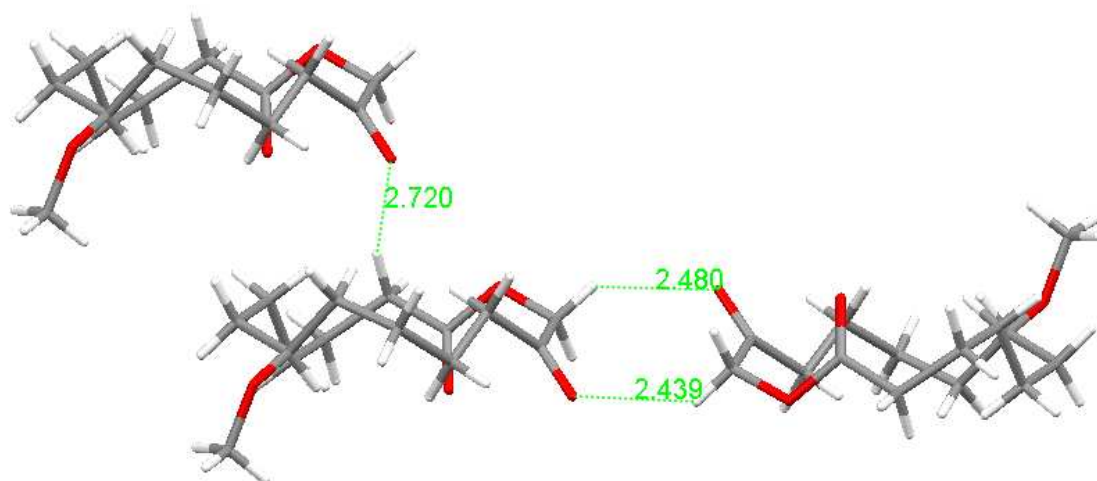
*Figure 7: Selected molecules within the crystal structure of **90ca** highlighting close interactions*

The macrolide **90ca** crystallised in the centrosymmetric monoclinic space group P2$_1$ with two crystallographically independent molecules per asymmetric unit. When the structures of the crystallographically independant molecules are overlaid on each other (one structure inverted), there were no significant structural differences between them *(Figure 8)*.

[4433]

Weighted R.M.S Deviation= 0.0098 Å
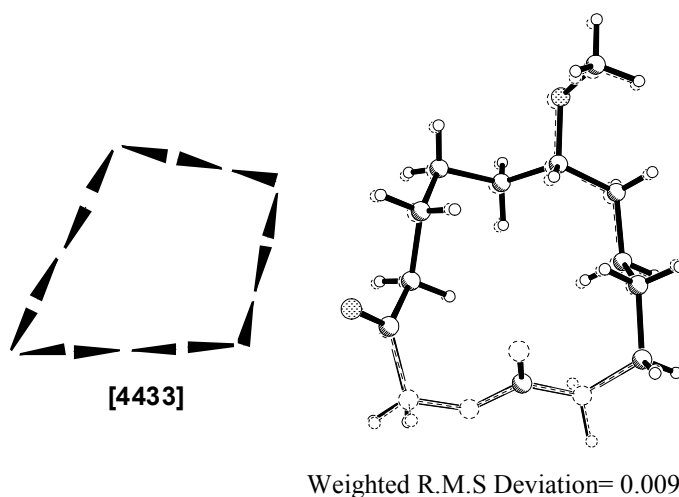
*Figure 8: Overlaid structures of enantiomers of macrolide **90ca** and pictorial representation of the [4433] conformation.[76]*

The infrared spectrum of **90ca** showed a clear band for the carbonyl group stretching frequency. Although both the IR bands from the two carbonyl groups were not resolved, there was a broad signal indicating more than a one carbonyl environment *(Figure 9)*. The C=O stretching frequency for the ester is expected to be the higher than the stretching frequency for the ketone.
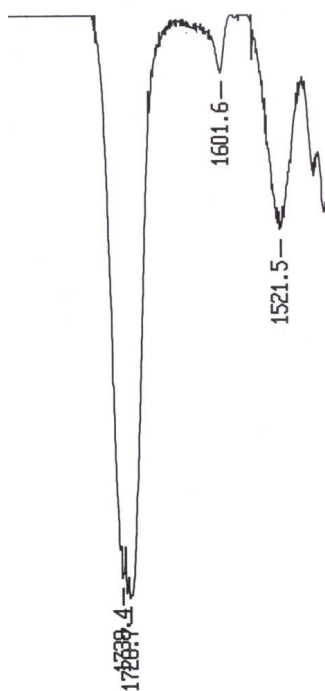
*Figure 9: IR spectrum of X demonstrating broad C=O stretching band for macrolide **90ca***

It is important that any new method for the formation of macrolides can be adapted to produce a number of different ring sizes. Whilst keeping the apparent beneficial effect of the methoxy substituent in ring **A**, the most convenient way of testing this idea is to

158

vary the size of ring **C**. The thermolysis of a series of 1,2,4-trioxanes with ring **C** sizes of 5, 7, and 12 were investigated as an entry to obtaining 13-, 15- and 20-membered macrolides.

Under the standard conditions detailed above, the thermolysis of *dispiro*-1,2,4-trioxane **86cc** resulted in the formation of a single component at R$_f$ 0.30 by TLC. The component was collected by column chromatography, eluting with ethyl acetate: light petroleum 1:3, as a viscous oil in 59% yield from the *dispiro*-1,2,4-trioxane **86cc**. The mass spectrum of the product showed a molecular ion peak at m/z 270 with an accurate mass of 270.18292 confirming that the component was derived from the rearrangement of *dispiro*-1,2,4-trioxane **86cc**. The pattern of signals in the ^{1}H NMR spectrum was similar to that observed for macrolide **90ca**. Like **90ca,** the ^{13}C NMR spectrum of the product contained two signals at δ173.3 and δ207.0 as expected for the keto lactone **90cc** rather than the alternative oxalactone *(Scheme 28)*.

86cc   **90cc**
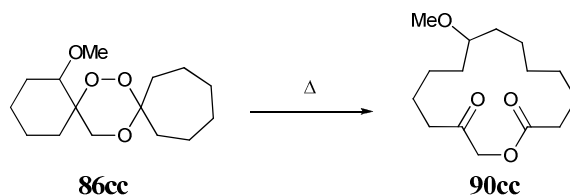
Scheme 28

Upon prolonged storage at 0 °C, the oil obtained directly from column chromatography formed a low melting solid which had a melting point around room temperature (25 °C). The solid was recrystallised from a mixture of light petroleum/diethyl ether and following slow evaporation gave crystals suitable for X-ray crystallography. Careful handling of the crystals was required in order to prevent the crystal melting during transfer into the N$_2$ (160K) gas stream of the X-ray diffractometer.

Following X-ray crystallographic analysis, this structure was revealed to be the 15-membered methoxy-substituted macrolide **90cc** as illustrated in *Figure 10*. The structure demonstrates a [4443] tetragonal conformation in which the keto lactone functionality is situated in a similar corner position of the structure as in the corresponding 14-membered keto lactone **90ca**. A mapping of the 15-membered macrolide **90cc** onto the 14-membered macrolide **90ca** shows the conformation adopted by the keto lactone functionality is similar in each case *(Figure 11)*.
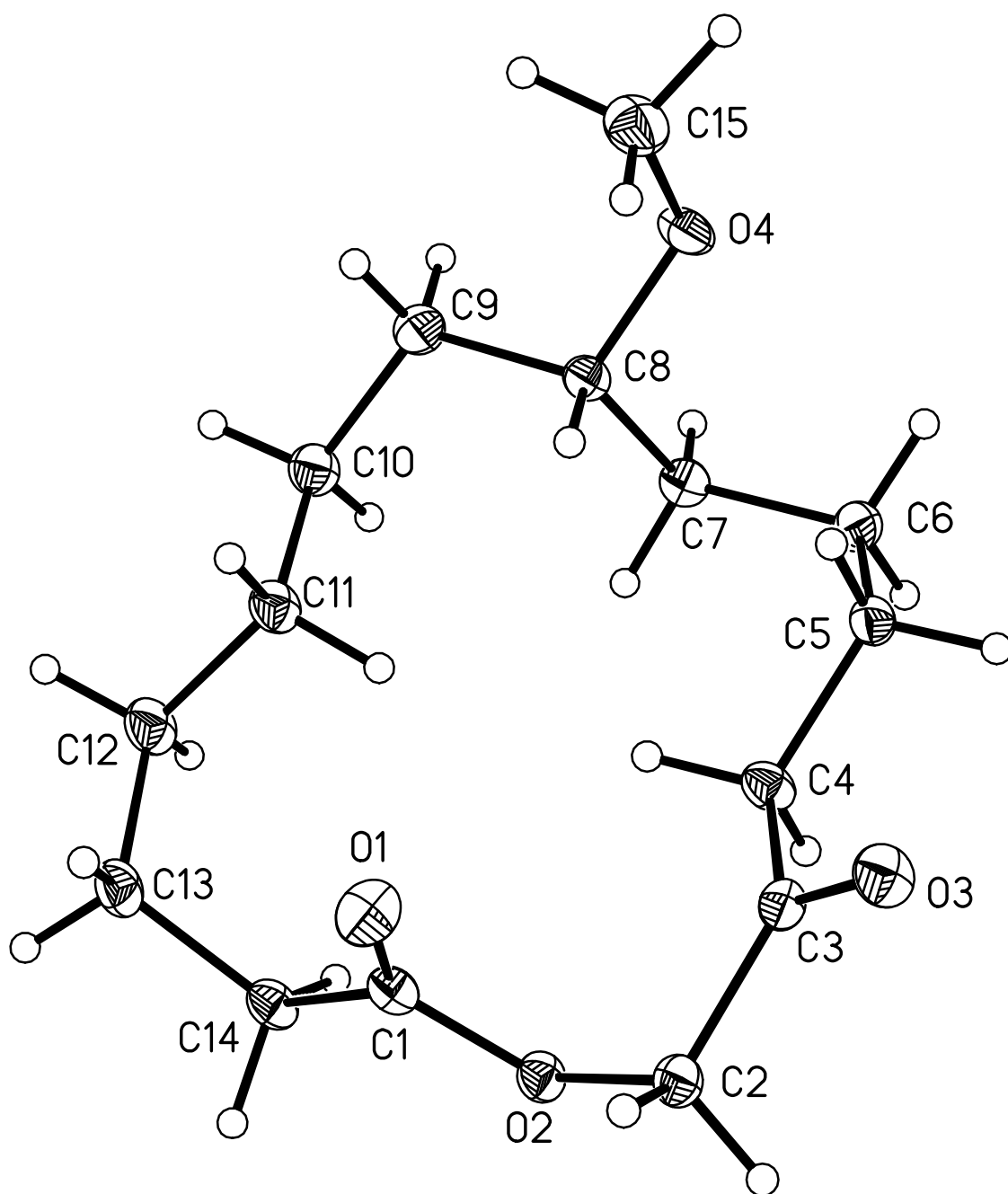
*Figure 10: X-ray crystal structure of **90cc***

(Ortep, 50% probability ellipsoids for non hydrogen atoms)[76]
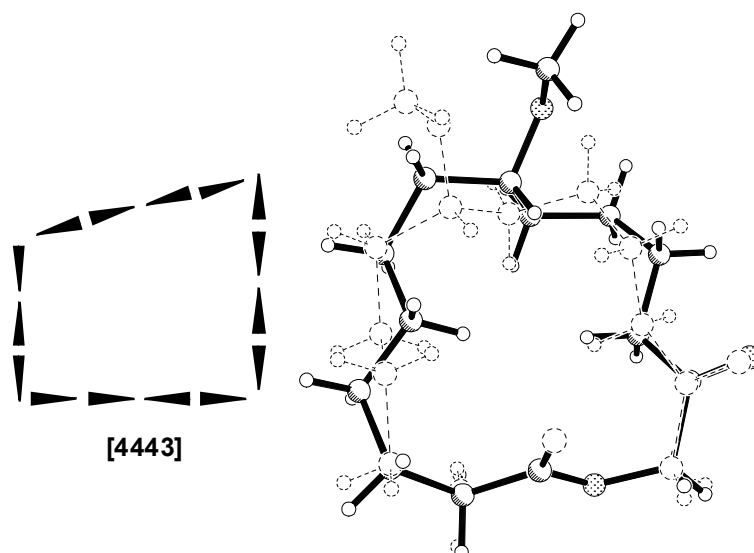
*Figure 11: Overlaid structures of **90ca** (dotted line) onto **90cc** (solid line) and pictorial representation of the [4433] conformation[76]*

Similar to the structure of **90ca** macrolide **90cc** also contains weak C-H···O close range interactions involving the ketone oxygen *(Figure 12)*.[77] The shortest of these is a 2.571 Å (C···O = 3.2504(18) Å) interaction between the ketone oxygen and one of the methylene hydrogens between the ketone and the ester. A further C-H···O close range interactions of 2.556 Å (C···O = 3.3051(18) Å) also exists between the ester carbonyl oxygen and a methylene hydrogen within the ring.
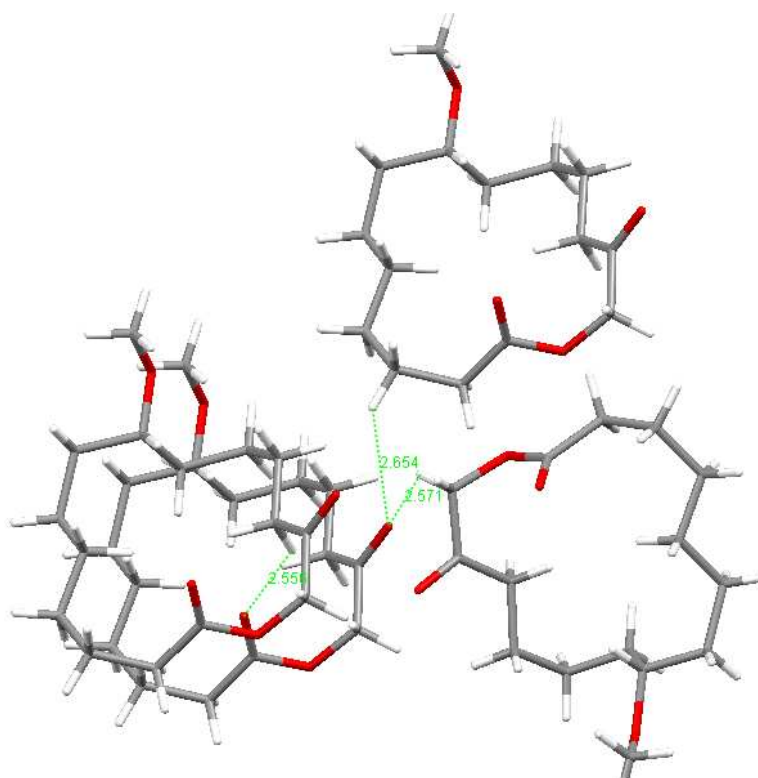
*Figure 12: Selected molecules within the crystal structure of **90cc** highlighting close interactions*

Unlike the crystal structure of macrolide **90ca**, there is a C-H⋯O close range interaction of 2.588 Å (C⋯O = 3.2807(19) Å) between the methoxy oxygen of one molecule of **90ca** and one of the hydrogen atoms on the methoxy group of another *(Figure 13)*.
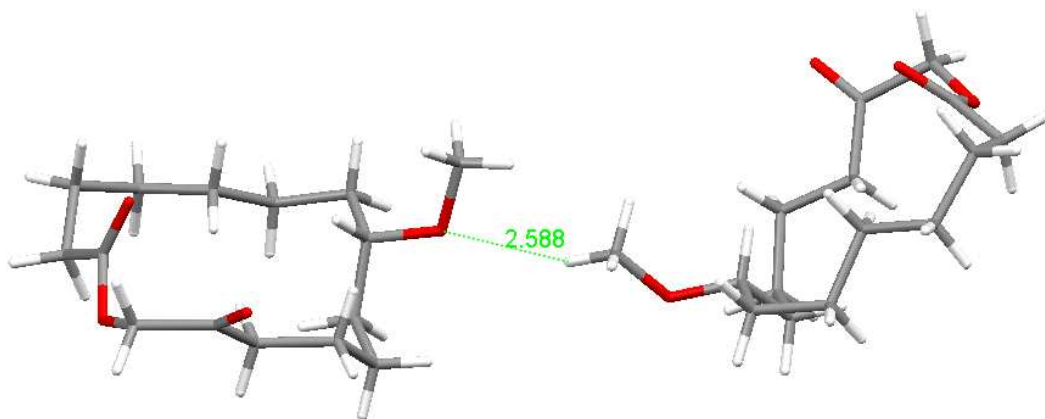
*Figure 13: Selected molecules within the crystal structure of **90cc** highlighting close interactions*

Thermolysis of *dispiro*-1,2,4-trioxanes **86cb** gave a single component at R_f 0.2. Isolation of the appropriate fractions by column chromatography as described above gave the 13-membered macrolide **90cb** in 67% yield as an oil *(Scheme 29)*. Unlike the corresponding 14- and 15-membered macrolides, there was no indication that this product would solidify at ambient temperatures. Although under prolonged storage in the freezer, the product showed signs that some of the mixture was solidifying, unfortunately it quickly melted on removal from the refrigerator. This precluded determination of the structure of 13-membered ring compound **90cb** by X-ray crystallography.

86cb   **90cb**
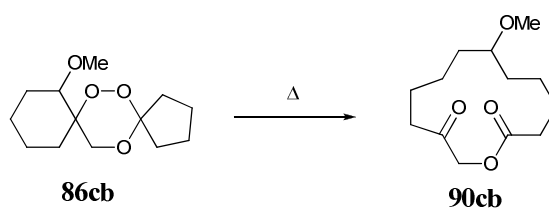
Scheme 29

A previous thermolysis of unsubstituted *dispiro*-1,2,4-trioxane **86ad** afforded the 20-membered ring keto lactone in 18% yield.[78] This was different from the products obtained from other unsubstituted *dispiro*-1,2,4-trioxanes which were exclusively oxalactone. Once β-scission has occurred in the 12-membered ring **C**, the carbon centred radical has more degrees of freedom thus giving the system enough time to open ring **A** before the recombination with the oxy radical. Thermolysis of methoxy-

substituted *dispiro*-1,2,4-trioxane **86cd** gave a single component at R$_f$ 0.53. Upon isolation by column chromatography eluting with light petroleum: ethyl acetate 3:1 the component was isolated as an oil in 50% yield from *dispiro*-1,2,4-trioxane **86cd**. The mass spectrum of the product showed a molecular ion peak at m/z 340 with an accurate mass of 340.26245 confirming that the component was derived from the rearrangement of *dispiro*-1,2,4-trioxane **86cc**. Although all the characteristic signals for macrolide **90cd** were present in the ^{1}H and ^{13}C NMR spectra there were some differences from other analysed methoxy-substituted macrolides in the ^{1}H NMR spectra. The two doublets corresponding to the methylene group between the ester group and the ketone almost overlapped with a chemical shift difference of only 0.05 ppm. However the presence of the two carbonyl groups at δ173.0 and δ204.6 in the ^{13}C NMR spectra confirmed the formation of the 20-membered ring methoxy-substituted keto lactone **90cd** *(Scheme 30)*. The isolated yield of the 20-membered keto lactone **90cd** is significantly greater than that of **90ad**.
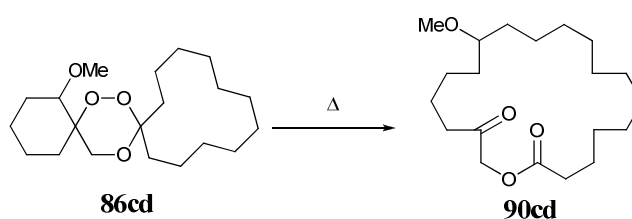
Scheme 30

In summary, the yields of 13-, 14-, 15- and 20-membered methoxy-substituted macrolides **90ca-cd** from the corresponding series of methoxy-substituted *dispiro*-1,2,4-trioxanes **86ca-cd** were in the range of 50-70%, after column chromatography. This represents a major increase in previously isolated yields of macrolides from other *dispiro*-1,2,4-trioxanes. Importantly, the thermolyses did not produce the corresponding oxalactones in isolable quantities showing that the rearrangement reaction producing the fully ring-expanded keto lactone predominates. To investigate further the influence of alkoxy substituents on the selective rearrangement reaction, the thermolyses of the ethoxy-substituted *dispiro*-1,2,4-trioxanes **86d** were undertaken.

Since, as described in *Chapter 1,* the mixture of regiomeric 1,2,4-trioxanes **86da** and **92** (*ca.* 9:1) could not be readily separated, it was pragmatic to carry out the thermolysis reactions on the isomeric mixture under the usual conditions. Nonetheless, a fairly clean thermolysate was obtained which on analysis by TLC gave a single component at

R_f 0.30. Isolation of this fraction using column chromatography eluting with 1:5 ethyl acetate: light petroleum gave the product as a viscous oil in 60% yield. The mass spectrum of the product contained a molecular ion peak at m/z 270. The mass spectrial data on their own do not indicate definitively the origin (**86ca** or **92**) of the product. The ^{1}H NMR spectrum of the product contained two doublets at δ4.3 and δ4.7 with a ^2J of 16.0 *Hz* corresponding to the methylene group situated next to the ester group whilst the ^{13}C NMR spectra contained two carbonyl group carbon signals at δ173 and δ208 corresponding to an ester and ketone carbonyl group carbons respectively. The ^{1}H and ^{13}C NMR spectra were very similar to those of the methoxy-substituted macrolide **90ca** with additional signals at δ3.38 and δ3.48 for the ethoxy CH_2 group thus confirming the formation of macrolide **90da** *(Scheme 31)*. The rearrangement of the mixture of compounds to give only one macrolide demonstrates that the thermolysis of regioisomer **92** does not appear to give significant quantities of macrocyclic products. It is therefore suggested that the regioisomer **92** undergoes complete fragmentation of the 1,2,4-trioxane ring to produce ketones. The rearrangement of *dispiro*-1,2,4-trioxane **86da** to give macrolide **90da** in 67% shows the significance of the alkoxy substituent in the determination of the product and demonstrates that the highly selective formation of macrolides is reproducible.
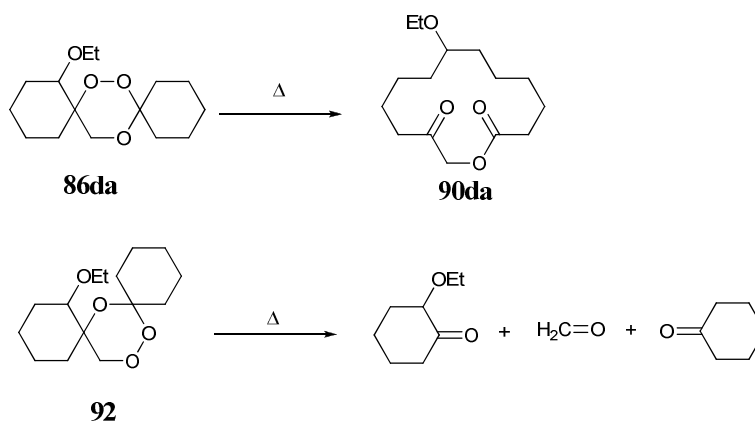
Scheme 31

After storage at 0°C, the viscous oil solidified into small crystals. The crystals were re-grown from light petroleum/diethyl ether mixed solvent and following slow evaporation gave crystals suitable for X-ray crystallography. X-ray crystallographic analysis of the crystals revealed the formation of the ethoxy-substituted macrolide **90da** as illustrated in *Figure 14*.
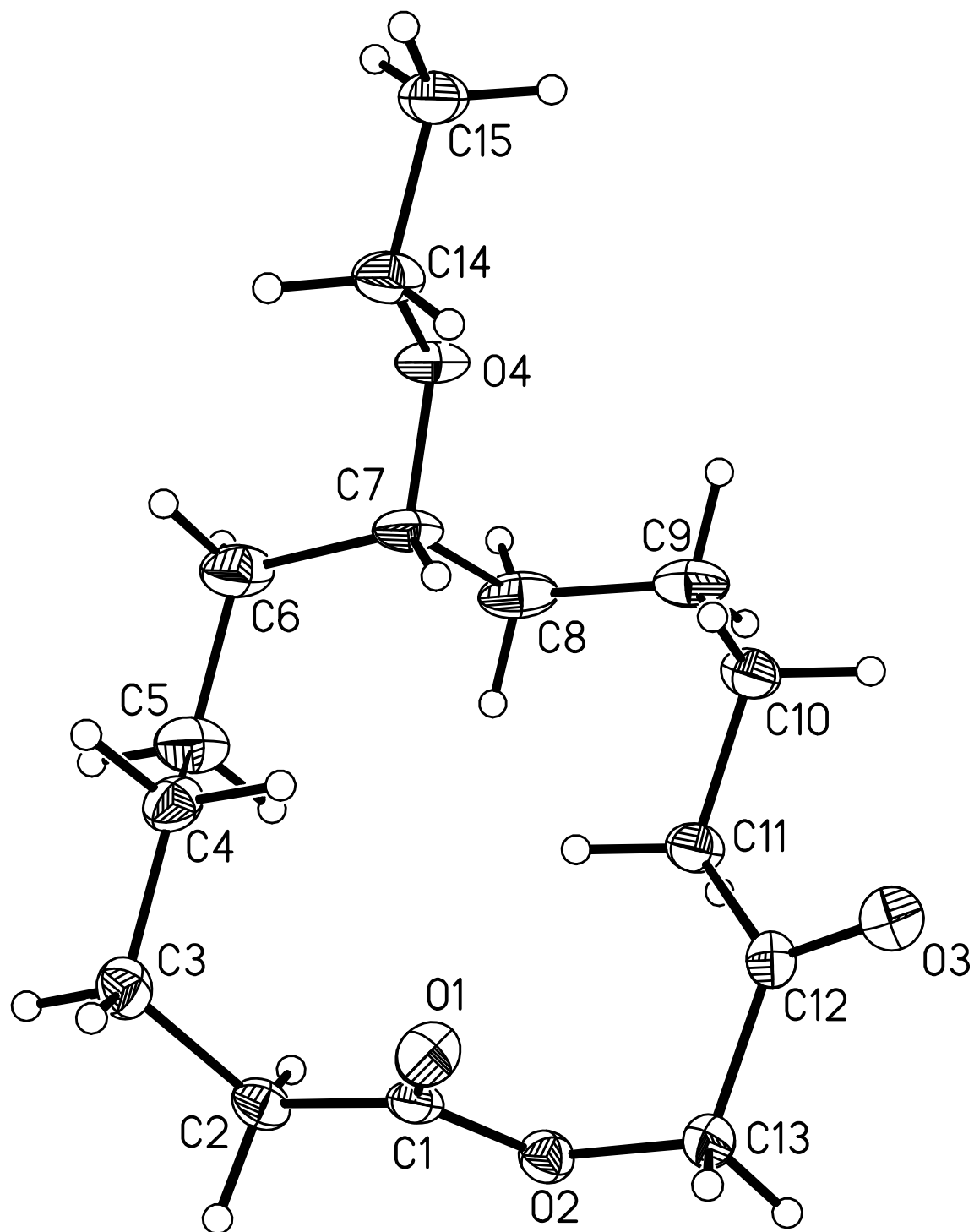
*Figure 14: X-ray crystal structure of **90da***

(Ortep, 50% probability ellipsoids for non hydrogen atoms)[76]

As observed for the X-ray crystal structure of macrolide **90ca**, the 14-membered ring of **90da** also forms a [4433] conformation with the keto lactone functionality forming around the corner of the [44] sides. Mapping the structure of macrolide **90da** onto **90ca** shows only small differences exist between the 14-membered rings and alkoxy substituent *(Figure 15)*.
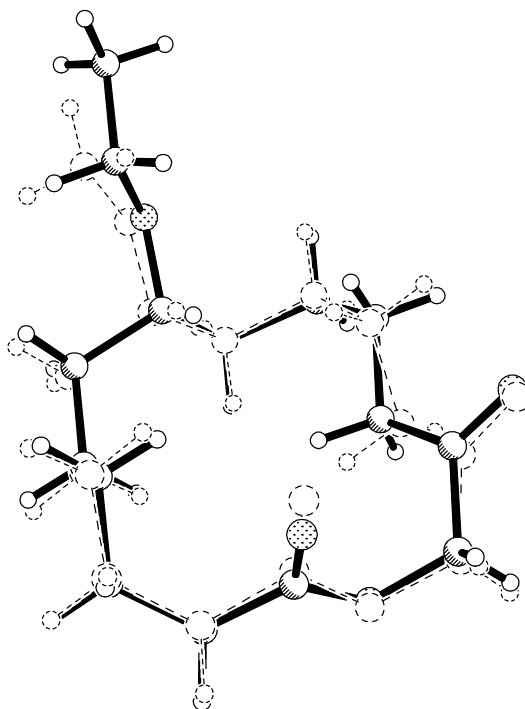
Weighted R.M.S Deviation= 0.2277 Å

*Figure 15: Overlaid structures of **90ca** (dotted line) onto **90da** (solid line)*[76]

Similar to the structure of macrolide **90ca**, the packing of the molecules in the crystal gives rise to a number of weak C-H⋯O close interactions *(Figure 16)*.[76] In this case, there are again close interactions between the ketone oxygen and methylene groups between neighbouring molecules. The shortest of these is again the 2.476 Å (C⋯O= 3.185(2) Å) gap between the ketone oxygen and one of the methylene hydrogens in between the ester and the ketone. Additionally, like the structure of **90ac** close interactions also exists between the ester carbonyl oxygen and a methylene hydrogen within the ring. In this case there are two separate close interactions of 2.552 Å (C⋯O= 3.458(2) Å) and 2.692 Å (C⋯O= 3.405(8) Å) between the ester oxygen and two methylene hydrogens situated in remote positions on the ring. There are again no close-range intermolecular interactions involving the ethoxy-substituents.
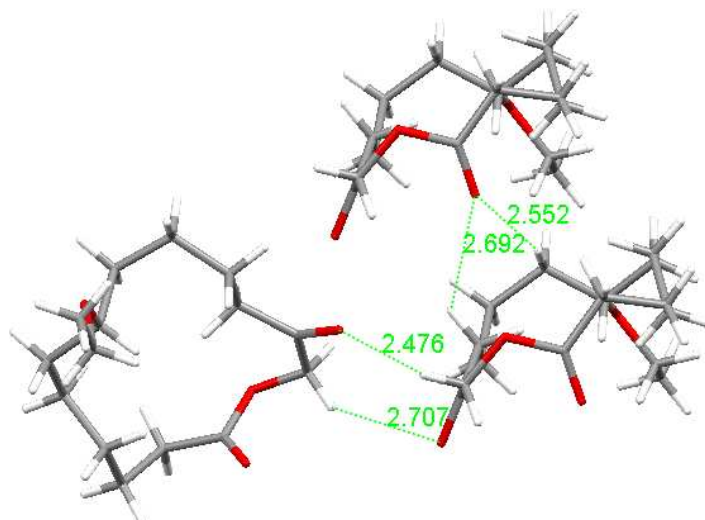
*Figure 16: Selected molecules within the crystal structure of **90da** highlighting close interactions*

The thermolysis of ethoxy-substituted *dispiro*-1,2,4-trioxane **86db** was also carried out using the *ca.* 9:1 mixture of regioisomers. Similar to the thermolysis of *dispiro*-1,2,4-trioxane **86da,** the mixture formed a clean thermolysate with a single component at R_f 0.42. The component was isolated from the rest of the themolysate by column chromatography eluting with ethyl acetate: light petroleum 1:5 and the fraction corresponding to the component at R_f 0.42 was obtained as a viscous oil in 72% yield from the *dispiro*-1,2,4-trioxane **86db**. Mass spectrometric analysis confirmed that the fraction was a rearrangement product from either *dispiro*-1,2,4-trioxane **86da** and/or **93**. The ^{1}H and ^{13}C NMR spectra confirmed the presence of keto lactone **90db** with no trace of any other macrocyclic products derived from *dispiro*-1,2,4-trioxane **93** *(Scheme 32)*. This observation is consistent with **93** undergoing total fragmentation similar to the thermolysis of *dispiro*-1,2,4-trioxane **92**.
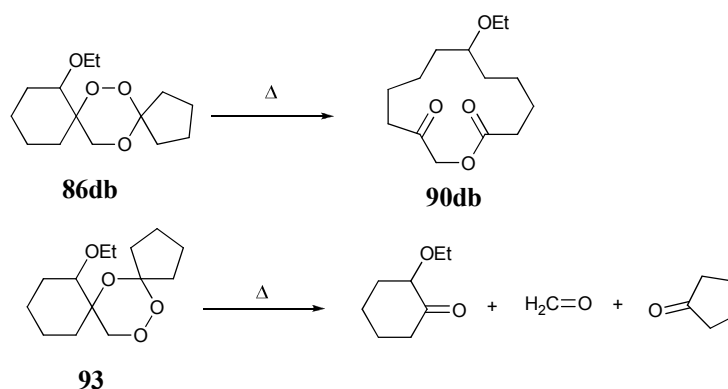
Scheme 32

The thermolysis of the *dispiro*-1,2,4-trioxane **86dc** was carried out using a pure sample. Like the other examples, the reaction gave a thermolysate which consisted of essentially

one component at R_f 0.57. Isolation of the fraction corresponding to the component at R_f 0.57 using the same method described above gave the product as a colourless semi-solid in 52% yield from *dispiro*-1,2,4-trioxane **86dc**. ^{1}H and ^{13}C NMR analysis confirmed the formation of ethoxy-substituted macrolide **90dc** *(Scheme 33)*. Although on storage at 0°C the macrolide formed a solid, subsequent attempts to grow crystals suitable for X-ray crystallography using a number of different solvent systems were unsuccessful.

86dc   **90dc**
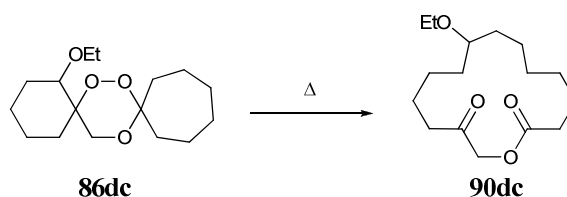
Scheme 33

The thermolysis of ethoxy-substituted *dispiro*-1,2,4-trioxane **86dd** gave a single component at R_f 0.35. Upon isolation by column chromatography eluting with light petroleum: ethyl acetate 5:1 the component was isolated as an oil in 26% yield from *dispiro*-1,2,4-trioxane **86dd**. The ^{1}H and ^{13}C NMR spectra showed similar characteristics to those seen for macrolide **90cd** confirming the formation of macrolide **90dd** *(Scheme 34)*. Although the reaction successfully formed the desired macrolide selectively without the formation of oxalactone or other rearrangement products the yield was significantly lower than for the methoxy-substituted 20-membered ring and other isolated macrolides. The yield was closer to the 18% yield of macrolide **90ad** achieved from the thermolysis of unsubstituted *dispiro*-1,2,4-trioxane **86ad**. Additional thermolysis reactions are required to verify the optimum yield possible from the thermolysis of **86dd**.

86dd   **90dd**
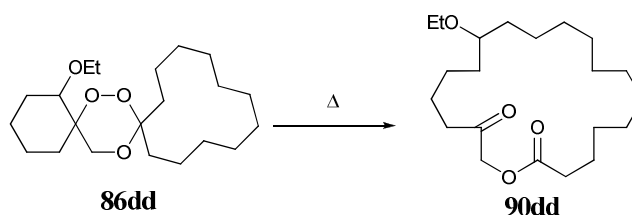
Scheme 34

Overall it has been shown that the thermolysis of alkoxy-substituted *dispiro*-1,2,4-trioxanes is an efficient route into the selective formation of 13-, 14-, 15- and 20-membered rings. In most cases the high yields (between 50-70% after purification) of keto lactone show that the rearrangement reaction is highly selective.

Synthesis of more highly functionalised keto lactones from *dispiro*-1,2,4-trioxanes

To investigate further the scope of this procedure, the thermolysis of more functionalised *dispiro*-1,2,4-trioxanes was undertaken. Complex macrolides like picromycin (**1**), erythromycin (**2**) and oleandomycin (**3**) discussed above, all contain a 14-membered ring core with several functional groups. For example picromycin (**1**)[3] contain a 14-membered ring with a number of ketone groups in selected positions throughout the structure. *Dispiro*-1,2,4-trioxanes with an additional ketone functional group in one of the rings could be a useful precursor to keto lactones related to **1**.

1 Picromycin   **86df**   **86ce**
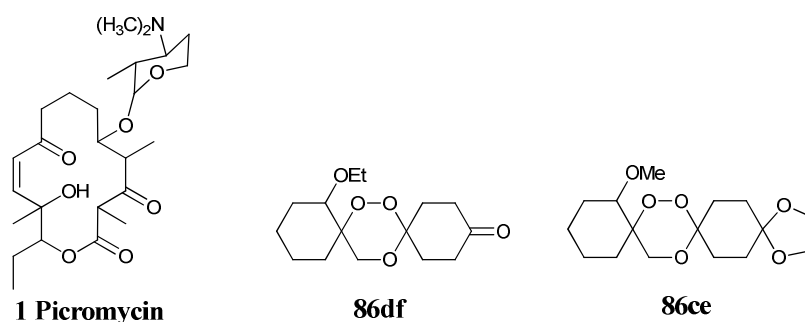
To investigate the selective positioning of the ketone group on a 14-membered macrolide there were two possible routes attempted via the thermolysis of *dispiro*-1,2,4-trioxanes: this first involved the thermolysis of a *dispiro*-1,2,4-trioxanes which already contains the ketone group. The second route requires the thermolysis of a *dispiro*-1,2,4-trioxane which contains a protected ketone group followed by the hydrolysis to unprotect the ketone. The syntheses of **86cf** and **86df** were carried out as discussed in *Chapter 1* and their respective thermolyses have been investigated as a potential entry into providing highly functionalised keto lactones.

Thermolysis of the unsubstituted *dispiro*-1,2,4-trioxane **86af** resulted in the selective formation of the corresponding oxalactone.[78] However, since thermolyses of methoxy- and ethoxy-substituted *dispiro*-1,2,4-trioxanes formed the fully ring-expanded keto

lactones, it was anticipated that a similar shift from the formation of oxalactone to keto lactone would be seen.

The thermolysis of *dispiro*-1,2,4-trioxane **86ce** gave a single component at R_f 0.40 which upon isolation by column chromatography gave the product as an oil in 43% yield. Analysis of the product by mass spectrometry confirmed that the molecular ion was at m/z 314 with an accurate mass of 314.17239. This confirmed that the product was a rearrangement product from **86ce** and indicated that the protecting group remained intact throughout the thermolysis process. The ^{1}H NMR spectrum showed an additional multiplet at $\delta3.9$ which corresponded to the CH_2 groups of the protecting group. The ^{13}C NMR spectrum also showed additional signals at $\delta64.9$ and $\delta64.7$ for the CH_2 groups and a quaternary carbon at $\delta111$. In addition, the two carbonyl carbon signals at $\delta172.5$ and $\delta207.7$ in the ^{13}C NMR spectrum plus the two doublets at $\delta4.3$ and $\delta4.7$ in the ^{1}H NMR spectrum confirmed the rearrangement had formed the keto lactone **90ce** *(Scheme 35)*. Although the deprotection of the acetal group was not attempted, it has been noted that similar acetal containing keto lactones have been deprotected under mild conditions in high yield.[79]
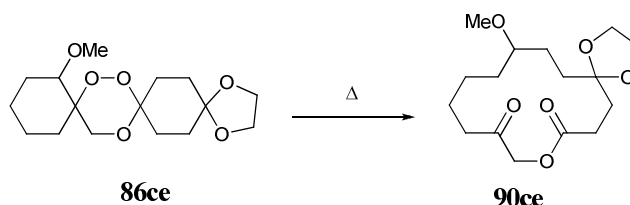
Scheme 35

The thermolysis of *dispiro*-1,2,4-trioxane **86df** gave a single component at R_f 0.40 which upon isolation by column chromatography gave the product as an oil in 21% yield. The mass spectrum of the product contained a molecular ion was present at m/z 284 with an accurate mass of 284.16183 confirming that the fraction was a rearrangement product of *dispiro*-1,2,4-trioxane **86df**. The ^{13}C NMR spectrum of the product showed signals for the three carbonyl groups were present situated at $\delta172$, $\delta207$ and $\delta209$ confirming the product was the diketo macrolide **90df** *(Scheme 36)*.

86df   **90df**
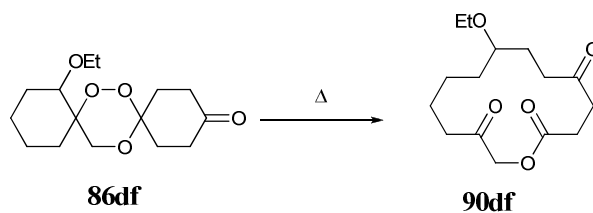
Scheme 36

The exclusive isolation of macrolides **90ce** and **90df** from the thermolysis of *dispiro*-1,2,4-trioxane **86ce** and **86df** demonstrates that introducing extra functionality into a remote position in ring **C** does not perturb the radical rearrangement reaction significantly. The formation of macrolides **90ce** and **90df** represents a significant advance in the synthesis of multi-substituted macrolides from the thermolysis of *dispiro*-1,2,4-trioxanes.

Further examples of a highly functionalised macrolides are the salicycylhalamides A and B (**94a,b**), isolated from the marine sponge *Haliclona*,[80] which contain a 12-membered macrolide with a fused benzo-ring. *Dispiro*-1,2,4-trioxanes with a fused benzo-ring, such as the indanylidene-containing *dispiro*-1,2,4-trioxanes **86cg** and **86dg**, could be useful precursors to macrolide analogues of **94a,b**.
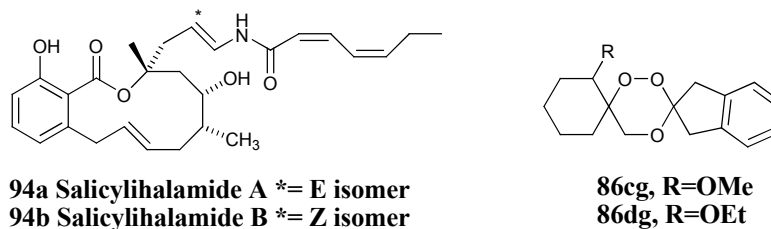
94a Salicylihalamide A *= E isomer   **86cg, R=OMe**
94b Salicylihalamide B *= Z isomer   **86dg, R=OEt**

Previous thermolysis of the methyl-substituted indanylidene-containing *dispiro*-1,2,4-trioxane **86bg** afforded the corresponding oxalactone as a crystalline solid in high yield.[49] It was concluded that following β-scission of the indanylidene ring the carbon-centred radical rapidly cyclises by recombination with the adjacent oxy radical to form the oxalactone. It was hoped that the presence of the methoxy- or ethoxy-substituent could make the β-scission of ring **A** more competitive with the β-scission of the indanylidene ring.

The thermolysis of *dispiro*-1,2,4-trioxane **86cg** afforded a clean thermolysate with only one apparent component at R_f 0.25 by TLC. The appropriate fractions were isolated by

column chromatography to give the product as a viscous oil in 41% yield. The ^{1}H NMR spectrum of the isolated product seemed to show there was a mixture of at least two components present. Subsequent attempts to further purify the mixture by column chromatography using a variety of solvent systems were unsuccessful. Despite this, a number of key signals can be picked out from the ^{1}H and ^{13}C NMR spectra which suggest that the macrolide **90cg** is the major component of the mixture *(Scheme 37)*.

86cg,dg   **90cg,dg**
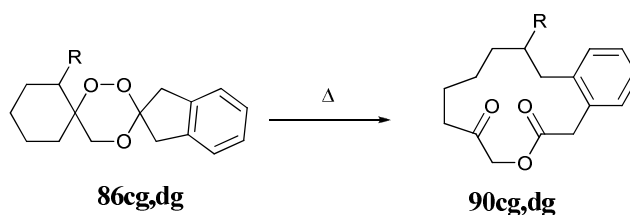
Scheme 37

The ^{1}H NMR spectrum shows characteristic signals which could be assigned to **90cg** including the two doublets for the methylene next to the lactone at δ4.4 and δ4.8 with ^2J germinal coupling constant of 16.8 Hz. The ^{13}C NMR spectrum also showed signals corresponding to an ester and ketone carbonyl carbon at δ174 and δ208 respectively.

There is no evidence that any of the other component(s) in the mixture being the corresponding oxalactone which had been seen as the major product from the thermolysis of indanylidene containing *dispiro*-1,2,4-trioxanes.[49] There is however a number of underlying signals in the aliphatic and aromatic parts of the ^{1}H and ^{13}C NMR spectra and even a extra carbonyl signal at δ171. Additionally there are a number of extra doublet signals between δ4.0-5.0 in a 5:1 ratio with the macrolide hydrogens in the ^{1}H NMR specrum.

Similarly the thermolysis of *dispiro*-1,2,4-trioxane **86dg** also seemed to produce a clean thermolysate with a single component at R$_f$ 0.21. Isolation of the relevant fractions by column chromatography eluting with 1:5 ethyl acetate: light petroleum gave the product as an oil in 29% yield. The ^{1}H and ^{13}C NMR spectra again showed that additional products were present. Further column chromatography of the crude mixture eluting with 1:5 ethyl acetate: light petroleum isolated the macrolide without the majority of the impurities seen for macrolide **90dg**. Although the macrolide was still not isolated as a pure component the impurity corresponding to the additional doublets at *ca.* δ4.0-5.0 were absent from the isolated compound. While the ^{1}H and ^{13}C NMR spectra of the

172

isolated component shows all the signals associated with macrolide **90dg** additional signals at δ1.6, δ2.7 and δ8.4 in the ^{1}H NMR specrum in addition to δ14.1 (CH$_3$), δ17.6 (CH$_3$), δ22.7, δ29.3, δ29.7, δ31.9 (CH$_2$), δ51.2 (CH$_2$) and δ112.9 (*q*C) in the ^{13}C NMR spectrum demonstrates again at least one extra unidentified component is present.

Overall, it is clear that the 13-membered aromatic containing macrolides have been produced however the structures of the impurities are unclear. This demonstrates a change from previous thermolysis of previously studied indanylidene containing *dispiro*-1,2,4-trioxanes which have produced oxalactones in high yield.[49] The formation of the extra product(s) in the thermolysis of *dispiro*-1,2,4-trioxanes **86cg** and **86dg** suggests that additional competitive rearrangement processes are occurring.

Structure determination of macrolides 90a,b via ^{1}H and ^{13}C NMR spectroscopy

Although several of the macrolides have been identified using X-ray crystallography, most macrolides were isolated as low melting solids or oils which were unsuitable for X-ray crystallography.

The ^{1}H NMR spectrum of macrolide **90ca** contained two doublets at δ4.3 and δ4.7 and a germinal ^2J coupling constant of 16.0 Hz for the methylene group next to the ester *(Figure 17)*. A sharp singlet for the methoxy group at δ3.3 and a multiplet for the CH at δ3.1 confirmed the alkoxy substituent was present. Four further multiplets between δ2.2 and δ2.7 were also present for the two further methylenes next to the carbonyl groups. The formation of oxalactone would only show signals for two hydrogens in this region of the spectra therefore confirming the formation of the keto lactone.[75]

Importantly the ^{13}C NMR spectra of macrolide **90ca** contained two signals at δ 173 and δ 208 consistant with the formation of an ester and ketone carbonyl groups respectively *(Figure 18)*. By a combination of ^{13}C NMR DEPT experiments and C – H correlation experiments *(Figure 19)*, all the signals in the ^{13}C NMR spectrum was assigned. In particular, the methoxy carbon signal at δ56, the signal for the methylene group between the ester and the ketone at δ68 and the CH group signal at δ78. The formation of oxalactone would have only shown a signal for the ester carbonyl at *ca.* δ170 plus an additional *spiro*-carbon at *ca.* δ80. The lack of either of these signals show that no oxalactone was present.[75]
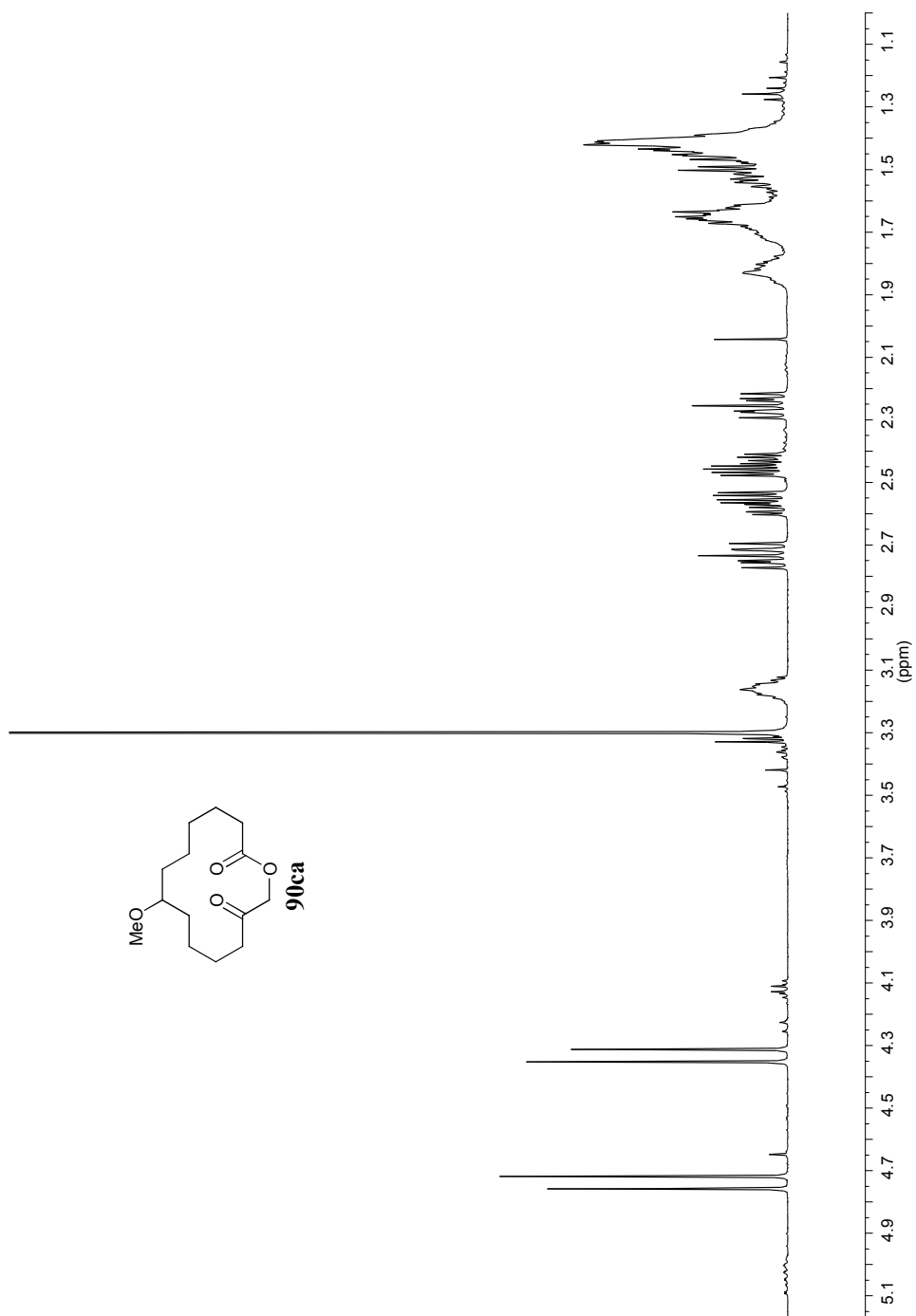
*Figure 17: ^{1}H NMR spectrum of macrolide **90ca***
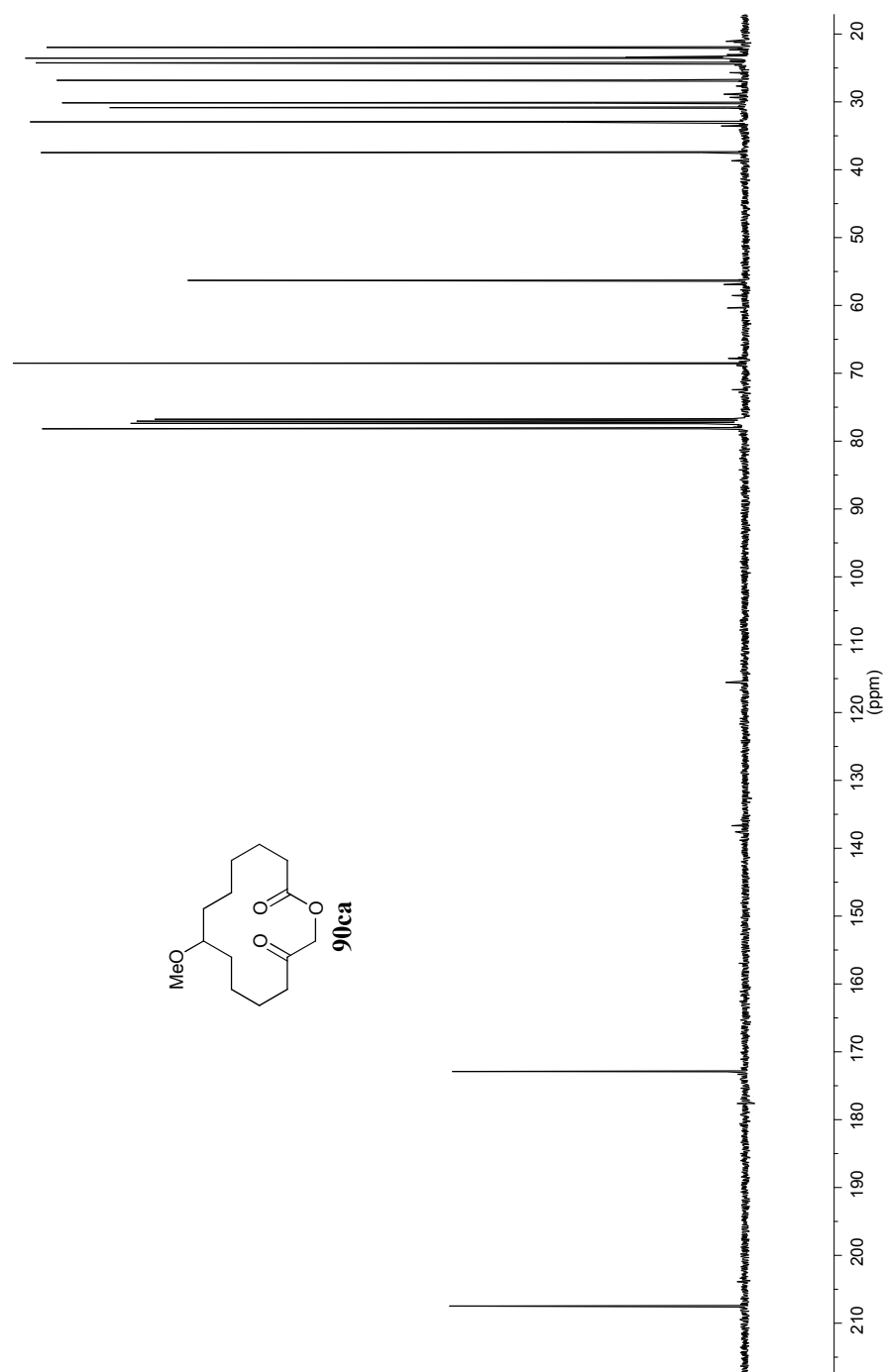
Figure 18:^{13}C NMR spectrum of macrolide **90ca**
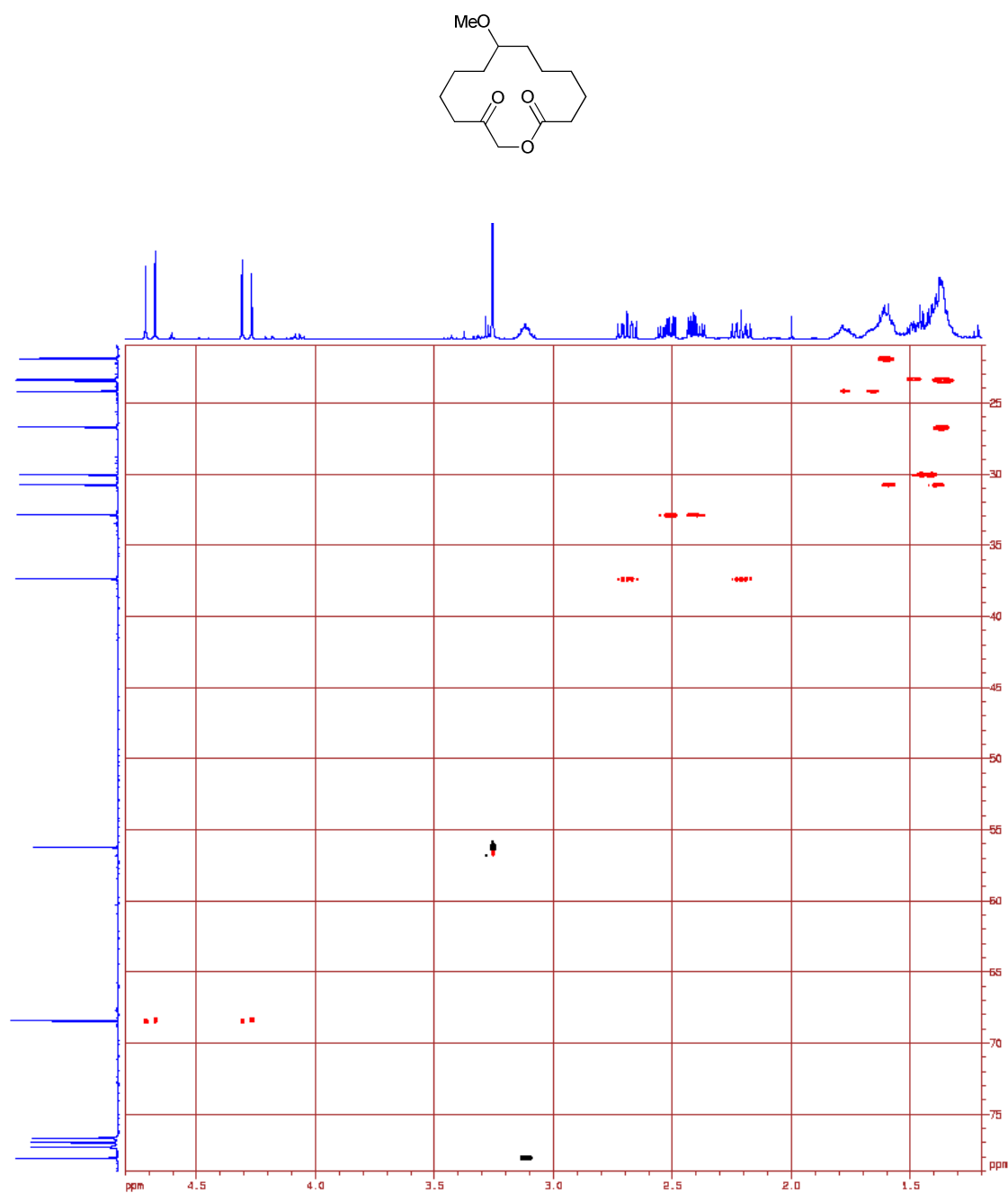
*Figure 19: C-H correlation of ^{1}H and ^{13}C NMR spectra of macrolide **90ca***

The main characteristic of the ^{1}H NMR spectra for all macrolides are the two doublets observed between δ4.0-5.0 corresponding to the methylene group between the ester and ketone groups *(Table 5)*. This is a downfield shift of the corresponding methylene group in the *dispiro*-1,2,4-trioxane which are between δ3.5-4.0. The positions of the doublets vary significantly with changing ring size with the difference in chemical shifts of the doublets being *ca.* 0.4 ppm for the 14-membered ring, 0.2 ppm for the 13-membered ring, 0.1 ppm for the 15-membered ring and 0.05 ppm for the 20-membered ring. The germinal coupling constant of the methylene also changes with increasing ring size with the ^2J of 15.4 Hz, 16.0 Hz, 16.1 Hz and 16.6 Hz for the 13-, 14-, 15- and 20-membered rings respectively.

Other significant signals in the ^{1}H NMR specrum are for the α-methylene groups on either side of the carbonyl groups. The electron-withdrawing influence of the carbonyl shifts the signals downfield away from the remainder of the aliphatic methylene groups which are between δ1.0-2.0, to δ2.0-3.0. The signals for these four hydrogens are differently distributed depending on the size of ring. Each proton is expected to form ddd multiplets in the ^{1}H NMR spectrum. This splitting pattern is apparent in 14-membered whilst two ddd and a 2H multiplet is seen for 13-membered rings. As the ring size increases to the 15- and 20- membered rings, the signals merge together forming a complex multiplet integrating to four hydrogen atoms.

The chemical shifts of the ^{1}H NMR signals for the substituents ($CHOCH_3$ and $CHOCH_2CH_3$) and the CH groups seems unaffected by ring size with chemical shifts only varying randomly by up to 0.1 ppm. The chemical shift of the methoxy OCH_3 and the C-H group remains constant at *ca.* δ3.3 and δ3.1-3.2 respectively. Like the *dispiro*-1,2,4-trioxanes the signals for the ethoxy OCH_2 group give two individual signals which are expected to be doublets of quartets. These signals remain constant between δ3.3-3.5 in all but one macrolides displaying two doublets of quartets. The 20-membered ring macrolide **90bd** however formed a complex multiplet where the two signals have overlapped.

The main signals contained in the ^{13}C NMR spectra which confirm the formation of the keto lactone are the two carbonyl carbon signals for the ketone and the ester groups. The keto carbonyl carbon signal is very important because it provides evidence for the opening of ring **A** via a β-scission reaction. In every case, there are signals at *ca.* δ173

for the lactone carbonyl carbon and *ca.* δ207 for the ketone carbonyl carbon *(Table 6)*. The chemical shift of the keto carbonyl carbon signal for the 20-membered rings differs by approx. 2.0 ppm from the other ring sizes showing the signal at δ204.6 and δ204.7 for **90ad** and **90bd** respectively. The formation of oxalactone would be indicated by a *spiro*-C signal at *ca.* δ80 but this was not observed in the spectra of any isolated product. Overall the ^{13}C NMR spectra of the macrolides show very little differences indicating that each of these distinctive carbons are in similar chemical environments and that ring size has little effect on the ^{13}C NMR spectra.

13 membered: n= 2
14 membered: n= 3
15 membered: n= 4
20 membered: n= 9
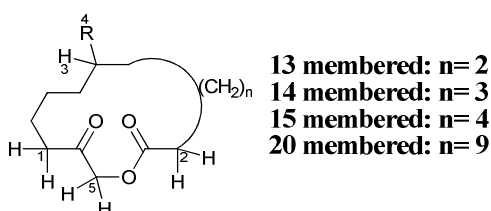
Compound	R	Position			
		1 and 2	**3**	**4**	**5**
R (structure)	OMe **90ca**	2.21, 1H 2.41, 1H 2.52, 1H 2.69, 1H	m, 3.12	s, 3.26	d, 4.29, 4.70, *J* 16.0
	OEt **90da**	2.21, 1H 2.42, 1H 2.55, 1H 2.72, 1H	m, 3.23	t, 1.15 3.38, 3.48	d, 4.30, 4.73, *J* 16.0
R (structure)	OMe **90cb**	2.27, 1H 2.43, 1H 2.55, 2H	m, 3.20	s, 3.29	d, 4.45, 4.63, *J* 15.4
	OEt **90db**	2.24, 1H 2.41, 1H 2.54, 2H	m, 3.28	t, 1.15 3.40, 3.47	d, 4.43, 4.62, *J* 15.4
R (structure)	OMe **90cc**	2.31-2.58, 4H	m, 3.16	s, 3.28	d, 4.50, 4.58, *J* 16.1
	OEt **90dc**	2.35-2.58, 4H	m, 3.26	t, 1.15 3.26, 3.45	d, 4.50, 4.59, *J* 16.1
R (structure)	OMe **90cd**	2.42, 4H	m, 3.15	s, 3.29	d, 4.56, 4.61, *J* 16.6
	OEt **90dd**	2.41, 4H	m, 3.23	t, 1.15 3.45	d, 4.56, 4.61, *J* 16.6

*Table 5: Selected ^{1}H NMR signals of macrolides **90c** and **90d***

13 membered: n= 2
14 membered: n= 3
15 membered: n= 4
20 membered: n= 9
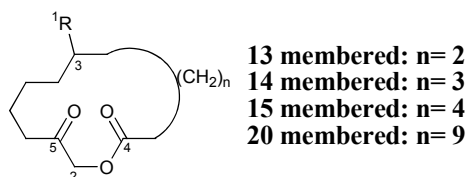
Compound	R	Position				
		1	2	3	4	5
	OMe **90ca**	56.3	68.4	78.1	172.8	207.4
	OEt **90da**	15.6 64.0	68.5	76.2	172.9	207.5
	OMe **90cb**	56.2	68.5	79.1	172.7	207.6
	OEt **90db**	15.6 63.8	68.4	77.1	173.3	207.1
	OMe **90cc**	56.1	68.4	78.9	173.3	207.0
	OEt **90dc**	15.6 63.7	68.5	77.0	172.7	207.7
	OMe **90cd**	56.3	68.1	80.2	173.0	204.6
	OEt **90dd**	15.7 63.8	68.1	78.5	173.1	204.7

*Table 6: Selected ^{13}C NMR signals of macrolides **90c** and **90d***

The introduction of additional substituents into the macrolide rings simplifies the ^{1}H NMR spectra in most cases. Although the sections of the structure which are similar to macrolides **90ca-d,da-d** give a similar pattern of signals, there are additional signals which demonstrate the presence of the further functionality on the keto lactone. The influence of the new functionalities to adjacent methylene groups has resulted in a clearer spectrum due to less overlapping of signals in the region δ1.0-2.0. The most prominent separation has occurred in the ^{1}H NMR spectrum of **90df** where almost all hydrogens can be seen individually or as a CH$_2$ group *(Figure 20)*. The ^{1}H NMR spectrum of **90ce** shows an additional multiplet for the acetal group at δ3.9 whilst the ^{1}H NMR spectrum of **90dg** shows aromatic hydrogens at *ca.* δ7.2 *(Table 7)*.

Figure 20: ^{1}H NMR specrum of macrolide **90df**

13 membered: n= 2
14 membered: n= 3
15 membered: n= 4
20 membered: n= 9
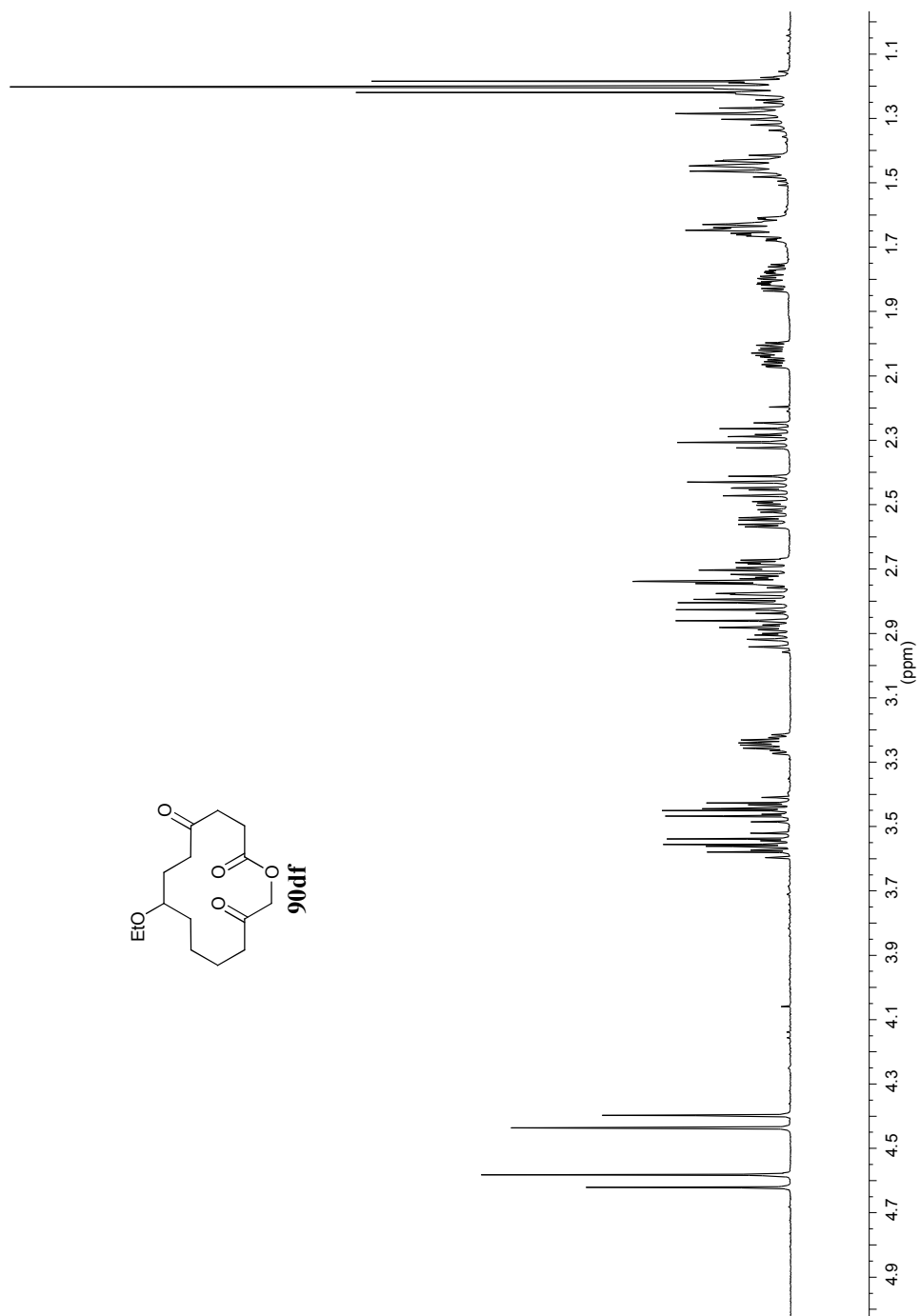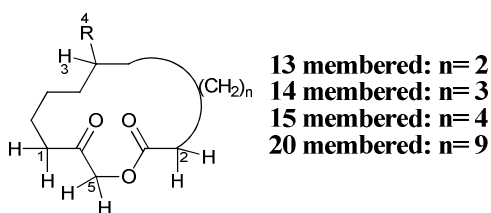
Compound	Position			
	1 and 2	**3**	**4**	**5**
	1.24, 2H 1.40, 2H 1.60, 2H 1.75, 1H 1.99, 1H 2.24, 1H 2.41, 1H 2.49, 1H 2.62-2.92, 5H	m, 3.21	1.16 3.41, 3.51	d, 4.39, 4.56, *J* 15.6
	2.00, 1H 2.15, 1H 2.36, 1H 2.48, 2H 2.78, 1H	m, 3.36	3.29	d, 4.31, 4.66, *J* 16.2
	1.80, 2H 2.27, 1H 2.58, 1H 3.77, 1H 3.83, 1H	m, 3.35	1.15 3.30	d, 4.29, 4.78, *J* 16.6

*Table 7: Selected ^1H NMR signals of macrolides **90c** and **90d***

The ^{13}C NMR spectra of the more functionalised macrolides **90ce,cg** and **90dg** have additional distinguishable signals. Macrolide **90df** has a carbonyl carbon signal for the additional keto functionality lying slightly downfield from the other keto carbonyl carbon signal at δ209. Further to this, additional CH_2 signals between δ30-40 are indicative of groups next to a carbonyl groups *(Table 8)*.

Macrolide **90ce** has a *spiro*-carbon which is observed along with additional CH_2 groups at δ64.7 and δ64.9 at position 7 which have split into two individual signals and moved slightly downfield from the original *dispiro*-1,2,4-trioxane *(Table 8)*.

181

Macrolide **90df** has two additional quaternary carbon signals in the aromatic region of the spectrum at δ131.3 and δ132.0 as well as 4 additional aromatic CH signals δ127.1, δ127.7, δ131.3 and δ132.0 *(Table 8)*.
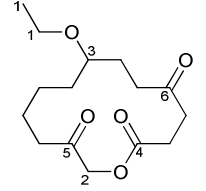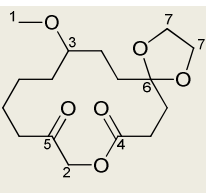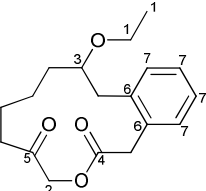
Compound	Position						
	1	2	3	4	5	6	7
(structure)	15.6 63.9	69.0	76.7	172.2	207.2	209.0	-
(structure)	56.3	68.6	78.7	172.5	207.7	111.1	64.7 64.9
(structure)	15.7 64.8	68.0	76.7	170.8	208.3	131.3 137.3	127.1 127.7 131.3 132.0

*Table 8: Selected ^{13}C NMR signals of macrolides **90c** and **90d***

Mechanism for the selective formation of macrolides from *dispiro*-1,2,4-trioxanes

Thermolysis of a series of methoxy- and ethoxy-containing *dispiro*-1,2,4-trioxanes under standard conditions selectively formed the corresponding 13-, 14-, 15- and 20-membered keto lactones in good overall yield without any isolable quantities of either oxalactone or alkene products *(Table 9)*.

The yields for the macrolides obtained by the rearrangement of *dispiro*-1,2,4-trioxanes where ring **C** is a simple 5-, 6- or 7-membered ring are consistently high, in the range *ca.* 60-70 %. Although the rearrangement of other *dispiro*-1,2,4-trioxanes produced the keto lactone as the only isolable product, the overall yield was lower, in the range *ca.* 20-50%. The reasons for the lower isolated yields of highly functionalised keto lactones are unclear. The 21% yield for ketolactone **90df** may be due to the rigidity of the sp^2 carbonyl carbon centre on ring **C** which would reduce the flexibility of the radical intermediates making the recombination more difficult.

1,2,4-Trioxane	Macrolide	R=OMe Yield/ %	R=OEt Yield/ %
		67	60
		67	72
		60	52
		50	26
		43	-
		-	21
		#	29*

Table 9: Percentage yield of isolated macrolide compounds

 # Keto lactone present but isolated as a complex mixture of compounds

**Keto lactone 90dg isolated with unknown impurity*

Overall the thermolysis of methoxy- and ethoxy-substituted *dispiro*-1,2,4-trioxanes **86c,d** signifies a major shift toward the selective synthesis of fully ring expanded keto lactones. Whilst no oxalactone is isolated from the thermolysis of methoxy- and ethoxy-substituted *dispiro*-1,2,4-trioxanes **86c,d**, it is the preferred product from unsubstituted and methyl-substituted *dispiro*-1,2,4-trioxanes **86a,b**. In the methyl-substituted cases, the isolation of some of the macrolide in addition to the oxalactone suggests the methyl

group is having an effect on the barrier of β-scission of ring **A**. The exclusive formation of keto lactone **90c,d** from the thermolysis of methoxy- and ethoxy-substituted *dispiro*-1,2,4-trioxanes **86c,d** suggests the alkoxy substituent further lowers the energy barrier of β-scission of ring **A**. Since no oxalactone **91c,d** is formed in the reaction, the energy barrier for the β-scission of ring **A** must be directly competitive with that of ring **C** *(Scheme 38)*. Although the exact preference is unclear from the thermolysis experiments, the lack of any alternative rearrangement products like **95** from the β-scission of ring **A** and not ring **C** indicates the β-scission of rings **A** and **C** are close in energy.
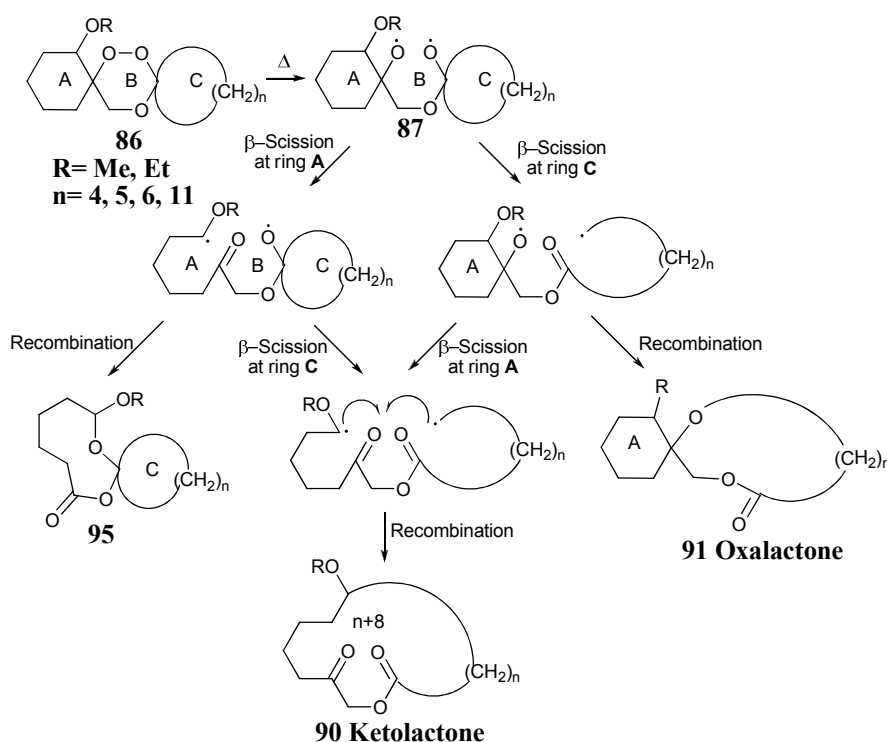
Scheme 38

Although the alkoxy group does not seem to affect the alternative β-scission reaction which facilitate the fragmentation of the molecule into formaldehyde (not observed) and the *dispiro*-1,2,4-trioxane component ketones (identified by gas chromatography) this accounts for only a small portion of the product with the major product in most cases being the ketolactone. Additionally, the increased steric bulk of the ethoxy substituent seems to have little effect on the yield of the product demonstrating the important effect of the oxygen on the β-scission.

The notable exception to the selective formation of macrolides from the thermolysis of *dispiro*-1,2,4-trioxanes is when ring **C** is an indanylidene group. Although for the first

time the thermolysis of an indanylidene containing *dispiro*-1,2,4-trioxane **86cg** and **86dg** formed the fully ring-expanded keto lactone **90cg** and **90dg**, the thermolysis formed a number of unidentified products. This impurity seemed to account for 20% of the isolated product and could not be separated in the case of macrolide **90cg**. However the isolation of macrolide **90dg** was slightly more successful with less of the impurities apparent by ^{1}H and ^{13}C NMR spectra. Despite the formation of keto lactone without any signs of oxalactone, the formation of unidentified product(s) suggest the indanylidene containing *dispiro*-1,2,4-trioxane is behaving differently from the other compounds.

The synthesis of a number of regioisomeric *dispiro*-1,2,4-trioxanes like **92** were described in *Chapter 1*. In the thermolysis of the ethoxy-substituted *dispiro*-1,2,4-trioxane **86da** and **86db** the regioisomers **92** and **93** were also thermolysed. No macrocyclic products derived from the *dispiro*-1,2,4-trioxane regioisomer **92** or **93** were isolated from the thermolysis. The apparent production of cyclic ketones from the thermolysis of *dispiro*-1,2,4-trioxanes **92** and **93** is consistent with the total ring fragmentations reported for other *dispiro*-1,2,4-trioxanes.[81,82] It is therefore concluded that on cleavage of the peroxide bond, the structure would twist to reduce the energy associated with the 1,3-diaxial interaction and therefore rapidly cleave the C-O to fragment the molecule *(Scheme 39)*. Importantly this suggests that purification of *dispiro*-1,2,4-trioxanes prior to the thermolysis is not necessary for the success of the rearrangement reaction to the fully ring expanded keto lactone. The thermolysis of other regioisomeric *dispiro*-1,2,4-trioxanes was not attempted.
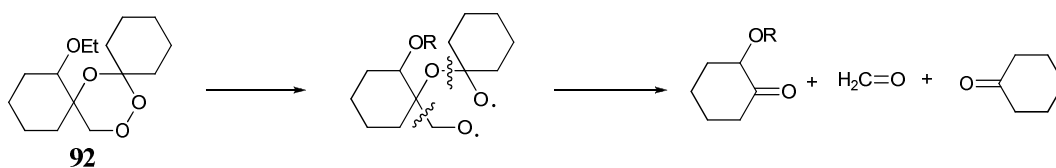
Scheme 39

From the results of the thermolysis reactions undertaken, the exact effect that the different substituents were having on the rearrangement reaction was unclear. Some previous studies outlined a stabilising effect of an oxygen atom on a carbon-centred radical.[83,84] This stabilising effect, known as the "α-effect" may act to lower the energy barrier to the formation of the carbon-centred radicals by the β-scission. In order to investigate the effect of the α-substituent on the rearrangement reaction, a detailed theoretical study of the decomposition mechanism was carried out and the results will be discussed in *Chapter 3*.

Thermolysis of *dispiro*-1,2,4-trioxane

General Procedure

The thermolysis tubes of dimensions 30mm (diameter) x 1550mm (length) were constructed from thick pyrex glass fitted with a Rotaflo tab to enable the tubes to be sealed and recycled. The solvent used for the thermolysis was decane. The *dispiro*-1,2,4-trioxane was dissolved in an appropriate amount of decane and pipetted into the thermolysis tube. The thermolysis tube was connected to a vacuum line and two freeze-pump-thaw cycles were carried out using liquid nitrogen (-196°C). The tube was then placed in a temperature-controlled silicone oil bath at 180 °C for 16 hours. Thermolysis products were isolated using column chromatography on 'flash' silica gel.

Preparation of 8-methoxyoxacyclotetradecane-2,13-dione (90ca)

Cyclohexane-1-*spiro*-3'-(1'-2'-4'-trioxane)-6'-*spiro*-1'',2''-methoxy cyclohexane (**86ca**) (300 mg; 11.67 mmol) was divided into 3 equal portions, each portion was dissolved in decane (10 mL) and pipetted into a thermolysis tube. The solutions were then degassed and the tubes sealed, as stated, before being immersed in a silicone oil bath

$C_{14}H_{24}O_4$
$256.34 \ gmol^{-1}$
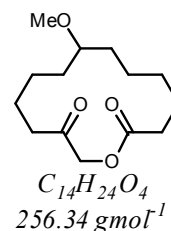
at 180 °C for 16 hours. Qualitative GC analysis of the thermolysate indicated one major product and two minor products. The two minor products were identified as cyclohexanone and 2-methoxycyclohexanone by comparison of the retention times with those of authentic samples. The crude product was purified by flash column chromatography (1:3 ethyl acetate/ light petroleum) to afford the title compound R_f = 0.46 (200 mg; 7.78 mmol; 66.7%) as a white solid: mp 57°C from light petroleum/ diethyl ether, υ_{max} (CHCl$_3$) /cm^{-1} 1728, 1738; δ_H(400 MHz, CDCl$_3$) 1.27-1.71 (13 H, m), 1.78 (1 H, m), 2.21 (1 H, ddd, *J* 6.6, 8.8 and 15.3), 2.41 (1 H, ddd, *J* 3.8, 8.2 and 15.2), 2.52 (1 H, ddd, *J* 3.8, 8.2 and 15.2), 2.69 (1 H, ddd, *J* 6.9, 8.7 and 15.5), 3.12 (1 H, m, CH), 3.26 (3 H, s, OCH$_3$), 4.29 (1 H, d, *J* 16.0, CH$_2$O), 4.70 (1 H, d, *J* 16.0, CH$_2$O) δc(100 MHz, CDCl$_3$); 21.9, 23.4, 23.5, 24.2, 26.7, 30.0, 30.8, 32.9, 37.4 (CH$_2$), 56.3 (OCH$_3$), 68.4 (CH$_2$), 78.1 (CH), 172.8, 207.4 (C=O); *m/z* 256 (M$^+$), accurate mass C$_{14}$H$_{24}$O$_4$ requires 256.16728, found 256.16746.

Preparation of 7-methoxyoxacyclotridecane-2,12-dione (90cb)

Cyclohexane-1-*spiro*-3'-(1'-2'-4'-trioxane)-6'-*spiro*-1'',2''-methoxy cyclopentane (**86cb**) (420 mg; 164.1 mmol) was divided into 2 equal portions, each portion was dissolved in decane (10 mL) and pipetted into a thermolysis tube. The solutions were then degassed and the tubes sealed, as stated, before being immersed in a silicone oil bath at 180 °C for 16 hours. The crude product was purified by flash column chromatography (1:3 ethyl acetate/ light petroleum) to afford the title compound R_f = 0.20 (250 mg; 9.77 mmol; 59.5%) as a colourless oil: υ_{max} (CHCl$_3$) /cm^{-1} 1722, 1732; δ_H(400 MHz, CDCl$_3$) 1.21-1.89 (12 H, m), 2.27 (1 H, ddd, *J* 6.6, 9.3 and 13.7), 2.43 (1 H, ddd, *J* 3.5, 10.0 and 15.1), 2.55 (2 H, m), 3.20 (1 H, m, CH), 3.29 (3 H, s, OCH$_3$), 4.45 (1 H, d, *J* 15.4, CH$_2$O), 4.63 (1 H, d, *J* 15.4, CH$_2$O) δ_C(100 MHz, CDCl$_3$) 23.0, 23.2, 23.3, 24.1, 29.1, 30.5, 33.7, 38.7 (CH$_2$), 56.2 (OCH$_3$), 68.5 (CH$_2$), 79.1 (CH), 172.7, 207.6 (C=O); *m/z* 242 (M$^+$), accurate mass C$_{13}$H$_{22}$O$_4$ requires 242.15164, found 242.15181. C$_{13}$H$_{22}$O$_4$ requires C 64.4% H 9.2%, found C 64.0% H 9.3%.
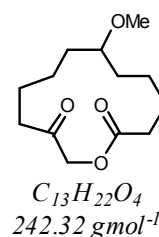
Preparation of 9-methoxyoxacyclopentadecane-2,14-dione (90cc)

Cyclohexane-1-*spiro*-3'-(1'-2'-4'-trioxane)-6'-*spiro*-1'',2''-methoxy cycloheptane (**86cc**) (495 mg; 183.3 mmol) was divided into 2 equal portions, each portion was dissolved in decane (10 mL) and pipetted into a thermolysis tube. The solutions were then degassed and the tubes sealed, as stated, before being immersed in a silicone oil bath at 180 °C for 16 hours. The crude product was purified by flash column chromatography (1:3 ethyl acetate/ light petroleum) to afford the title compound R_f = 0.25 (332 mg; 12.3 mmol; 67.0%) as a semi-solid: υ_{max} (CHCl$_3$) /cm^{-1} 1715, 1739; δ_H(400 MHz, CDCl$_3$) 1.21-1.79 (16 H, m), 2.31-2.58 (4 H, m), 3.16 (1 H, p, *J* 5.7, CH), 3.28 (3 H, s, OCH$_3$), 4.50 (1 H, d, *J* 16.1, CH$_2$O), 4.58 (1 H, d, *J* 16.1, CH$_2$O) δ_C(100 MHz, CDCl$_3$) 22.4, 23.2, 23.6, 24.0, 26.9, 27.6, 30.6, 30.8, 33.5, 38.9 (CH$_2$), 56.1 (OCH$_3$), 68.4 (CH$_2$), 78.9 (CH), 173.3, 207.0 (C=O); *m/z* 270 (M$^+$), accurate mass C$_{15}$H$_{26}$O$_4$ requires 270.18292, found 270.18311.
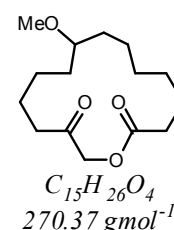
Preparation of 14-methoxyoxacycloicosane-2,19-dione (90cd)

2-(Methoxy)cyclohexane-1-*spiro*-3'-(1',2',4'-trioxane)-6'-*spiro*-1''-2''-cyclododecane (**86cd**) (50 mg; 1.47 mmol) was dissolved in decane (10 mL) and pipetted into a thermolysis tube. The solutions were then degassed and the tubes sealed, as stated, before being immersed in a silicone oil bath at 180 °C for 16 hours. The crude product was purified by flash column chromatography (1:3

$C_{20}H_{36}O_4$
340.50 g mol^{-1}
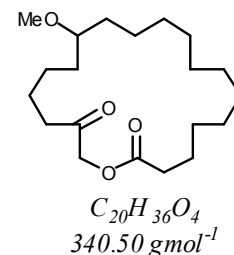
ethyl acetate/ light petroleum) to afford the title compound R_f = 0.53 (25 mg; 0.073 mmol; 50.0%) as a yellow viscous oil: υ_{max} (CHCl$_3$) /cm^{-1} 1732, 1741; δ_H(400 MHz, CDCl$_3$) 1.21-1.73 (26 H, m), 2.42 (4 H, m), 3.15 (1 H, m, CH), 3.29 (3 H, s, OCH$_3$), 4.56 (1 H, d, *J* 16.6, CH$_2$O), 4.61 (1 H, d, *J* 16.6, CH$_2$O), δc(100 MHz, CDCl$_3$) 23.1, 23.7, 24.2, 24.4, 27.6, 278, 27.9, 28.0, 28.1, 28.2, 31.6, 32.0, 33.8, 38.3 (CH$_2$), 56.3 (OCH$_3$), 68.1 (CH$_2$), 80.2 (CH), 173.0, 204.6 (C=O); *m/z* 340 (M$^+$), accurate mass C$_{20}$H$_{36}$O$_4$ requires 340.26136, found 340.26245.

Preparation of 16-methoxy-1,4,9-trioxa*spiro*[4.13]octadecane-8,11-dione (90ce)

2-(Methoxy)cyclohexane-1-*spiro*-3'-(1',2',4'-trioxane)-5'-*spiro*-1''-2''-1''',4'''-dioxa*spiro*[4.5]decane (**86ce**) (80 mg; 2.55 mmol) was dissolved in decane (15 mL) and pipetted into a thermolysis tube. The solutions were then degassed and the tubes sealed, as stated, before being immersed in a silicone oil bath at 180 °C for 16 hours.

$C_{16}H_{26}O_6$
314.38 g mol^{-1}
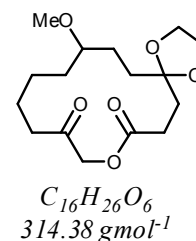
The product was isolated using flash column chromatography (1:3 ethyl acetate/ light petroleum) to afford the title compound R_f = 0.38 (34 mg; 1.08 mmol; 42.5%) as a white solid: m.p. 34-35°C from diethyl ether/ light petroleum, υ_{max} (CHCl$_3$) /cm^{-1} 1718, 1737; δ_H(400 MHz, CDCl$_3$) 1.32-1.82 (10 H, m), 2.00 (1 H, ddd, *J* 3.2, 6.4 and 12.2), 2.15 (1 H, ddd, *J* 3.2, 6.4 and 12.2), 2.36 (1 H, ddd, *J* 5.9, 9.2 and 14.9), 2.48 (2 H, m), 2.78 (1 H, ddd, *J* 6.1, 9.2 and 15.1), 3.29 (3 H, s, OCH$_3$), 3.36 (1 H, m, CH), 3.91 (4 H, m, OCH$_2$CH$_2$O), 4.31 (1 H, d, *J* 16.2, CH$_2$O), 4.66 (1 H, d, *J* 16.2, CH$_2$O) δc(100 MHz, CDCl$_3$) 22.3, 24.1, 25.8, 29.5, 30.4, 30.5, 31.1, 39.2 (CH$_2$), 56.3 (OCH$_3$), 64.9, 64.7 (OCH$_2$CH$_2$O), 68.6 (OCH$_2$), 78.7 (CH), 111.1 (qC), 172.5, 207.7 (C=O); *m/z* 314 (M$^+$), accurate mass C$_{20}$H$_{36}$O$_4$ requires 314.17266, found 314.17239.

Attempted preparation of 10-methoxy-6,7,8,9,10,11-hexahydrobenzo[d][1]oxacyclotridecine-2,5(1H,4H)-dione (90cg)

Indane-2-*spiro*-3'1(1',2',4'-trioxane)-6'-*spiro*-1''-2''-ethoxycyclohexane (**86cg**) (80 mg; 2.76 mmol) was dissolved in decane (15 mL) and pipetted into a thermolysis tube. The solutions were then degassed and the tubes sealed, as stated, before being immersed in a silicone oil bath at 180 °C for 16 hours. The crude product was purified by flash column chromatography (1:3 ethyl acetate/ light petroleum) to afford a complex mixture of compounds R_f = 0.25 (33 mg; 1.14 mmol; 41.2% yield): Observed signals for **90cg** δ_H (400MHz, CDCl$_3$) 1.2-1.7 (m, CH$_2$), 2.30 (1 H, m), 2.59(1H, dd, J 13.6, 8.9), 3.33(m, CH), 3.47 (s, OCH$_3$), 3.66 (2 H, m, CH$_2$), 3.82 (1 H, d, *J* 15.6, CH$_2$O), 3.88 (1 H, d, *J* 15.6, CH$_2$O), 4.42 (d, *J* 16.7, CH$_2$O), 4.84 (d, *J* 16.7, CH$_2$O), 7.18-7.40(m, Ar-CH); δ_C(100MHz, CDCl$_3$) 21.6, 22.5, 29.3, 36.5, 38.4, 38.5 (CH$_2$), 56.9 (OCH$_3$) , 68.0 (OCH$_2$), 76.7 (CH), 127.3, 127.8 (Ar-CH), 131.4, 132.0 (Ar-CH), 137.0 (Ar-qC), 170.8, 208.2 (C=O)
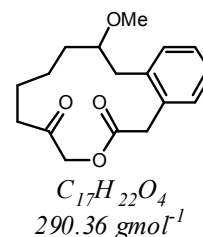
$C_{17}H_{22}O_4$
290.36 gmol^{-1}

Preparation of 8-ethoxyoxacyclotetradecane-2,13-dione (90da)

Cyclohexane-1-*spiro*-3'-(1'-2'-4'-trioxane)-6'-*spiro*-1'',2''-ethoxy cyclohexane (**86da**) (100 mg; 3.70 mmol) was dissolved in decane (15 mL) and pipetted into a thermolysis tube. The solutions were then degassed and the tubes sealed, as stated, before being immersed in a silicone oil bath at 180 °C for 16 hours. The crude product was purified by flash column chromatography (1:5 ethyl acetate/ light petroleum) to afford the title compound R_f = 0.30 (60 mg; 0.22 mmol; 60.0%) as a white solid: υ_{max} (CHCl$_3$) /cm^{-1} 1720, 1732; δ_H(400 MHz, CDCl$_3$) 1.15 (3 H, t, *J* 7.0, CH$_3$) 1.22-1.86 (16 H, m, CH$_2$), 2.21 (1 H, ddd, *J* 6.5, 8.9 and 15.3), 2.42 (1 H, ddd, *J* 3.7, 8.2 and 15.2), 2.55 (1 H, ddd, *J* 3.6, 9.4 and 15.2), 2.72 (1 H, ddd, *J* 6.9, 8.9 and 15.6), 3.23 (1 H, m, CH), 3.38 (1 H, dq, *J* 7.0, 7.0, 7.0 and 9.2, OCH$_2$CH$_3$), 3.48 (1 H, m, OCH$_2$CH$_3$), 4.30 (1 H, d, *J* 16.0, CH$_2$O), 4.73 (1 H, d, *J* 16.0, CH$_2$O), δ_C(100 MHz, CDCl$_3$); 15.6 (CH$_3$), 22.0, 23.5, 23.7, 24.3, 26.7, 30.5, 31.5, 33.0, 37.4 (CH$_2$), 64.0 (CH$_2$CH$_3$), 68.5 (OCH$_2$), 76.2 (CH), 172.9, 207.5 (C=O); *m/z* 270 (M$^+$), accurate mass [C$_{15}$H$_{24}$O$_4$NH$_4$]$^+$ requires 288.2169, found 288.2166.
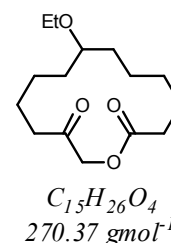
$C_{15}H_{26}O_4$
270.37 gmol^{-1}

Preparation of 7-ethoxyoxacyclotridecane-2,12-dione (90db)

Cyclohexane-1-*spiro*-3'-(1'-2'-4'-trioaxane)-6'-*spiro*-1'',2''-ethoxy cyclopentane (**90db**)(100 mg; 3.9 mmol) was dissolved in decane (15 mL) and pipetted into a thermolysis tube. The solutions were then degassed and the tubes sealed, as stated, before being immersed in a silicone oil bath at 180 °C for 16 hours. The crude product was purified by flash column chromatography (1:5 ethyl acetate/ light petroleum) to afford the title compound R_f = 0.42 (72 mg; 0.28 mmol; 72.0%) as a colourless oil: υ_{max} (CHCl$_3$) /cm^{-1} 1716, 1734; δ_H(400 MHz, CDCl$_3$) 1.14 (3 H, t, *J* 7.0, CH$_3$) 1.20-1.88 (14 H, m, CH$_2$), 2.24 (1 H, ddd, *J* 6.6, 9.4 and 13.6), 2.41 (1 H, m), 2.54 (2 H, m), 3.28 (1 H, m, CH), 3.40 (1 H, dq, *J* 7.1, 7.1, 7.1 and 9.3, OCH$_2$CH$_3$), 3.47 (1 H, dq, *J* 7.1, 7.1, 7.1 and 9.3, CH$_2$CH$_3$), 4.43 (1 H, d, *J* 15.4, CH$_2$O), 4.62 (1 H, d, *J* 15.4, CH$_2$O) δc(100 MHz, CDCl$_3$) 15.6 (CH$_3$), 22.9, 23.3, 23.4, 24.1, 29.5, 31.2, 33.7, 38.5 (CH$_2$), 63.7 (CH$_2$CH$_3$), 68.5 (OCH$_2$), 77.0 (CH), 172.7, 207.7 (C=O); *m/z* 256 (M$^+$), accurate mass [C$_{14}$H$_{22}$O$_4$NH$_4$]$^+$ requires 274.3013, found 274.2009.
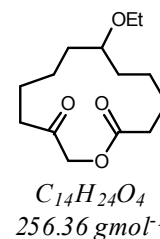
OEt

$C_{14}H_{24}O_4$
256.36 gmol^{-1}

Preparation of 9-ethoxyoxacyclopentadecane-2,14-dione (90dc)

Cyclohexane-1-*spiro*-3'-(1'-2'-4'-trioxane)-6'-*spiro*-1'',2''-ethoxy cycloheptane (**86dc**) (100 mg; 3.51 mmol) was dissolved in decane (15 mL) and pipetted into a thermolysis tube. The solutions were then degassed and the tubes sealed, as stated, before being immersed in a silicone oil bath at 180 °C for 16 hours. The crude product was purified by flash column chromatography (1:5 ethyl acetate/ light petroleum) to afford the title compound R_f = 0.57 (52 mg; 0.07 mmol; 52.0%) as a white solid: υ_{max} (CHCl$_3$) /cm^{-1} 1729, 1738; δ_H(400 MHz, CDCl$_3$) 1.16 (3 H, t, *J* 7.0, CH$_3$) 1.23-1.81 (18 H, m, CH$_2$), 2.35-2.58 (4 H, m, CH$_2$), 3.26 (1 H, m, CH), 3.45 (2 H, q, *J* 7.0, OCH$_2$CH$_3$), 4.50 (1 H, d, *J* 16.1, CH$_2$O), 4.59 (1 H, d, *J* 16.1, CH$_2$O), δc(100 MHz, CDCl$_3$) 15.7 (CH$_3$), 22.5, 23.4, 23.8, 24.0, 26.9, 27.6, 31.2, 31.5, 33.6, 39.0 (CH$_2$), 63.8 (CH$_2$CH$_3$), 68.4 (OCH$_2$), 77.1 (CH), 173.3, 207.1 (C=O); *m/z* 284 (M$^+$), accurate mass [C$_{15}$H$_{24}$-H]$^+$ requires 285.2060, found 285.2061.
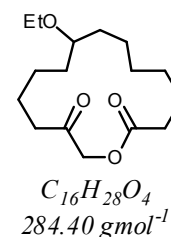
EtO

$C_{16}H_{28}O_4$
284.40 gmol^{-1}

Preparation of 14-ethoxyoxacycloicosane-2,19-dione (90dd)

Cyclohexane-1-*spiro*-3'-(1'-2'-4'-trioxane)-6'-*spiro*-1'',2''-ethoxy cyclododecane (**86dd**) (100 mg; 2.82 mmol) was dissolved in decane (15 mL) and pipetted into a thermolysis tube. The solutions were then degassed and the tubes sealed, as stated, before being immersed in a silicone oil bath at 180 °C for 16 hours. The crude product was purified by flash column chromatography (1:5 ethyl acetate/ light petroleum) to afford the title compound R_f= 0.35 (26 mg; 0.07 mmol; 26.0%) as a colourless oil: υ_{max} (CHCl$_3$) /cm^{-1} 1729, 1741; δ_H(400 MHz, CDCl$_3$) 1.15 (3 H, t, J 7.0, CH$_3$) 1.19-1.75 (30 H, m, CH$_2$), 2.41 (4 H, m, CH$_2$), 3.23 (1 H, m, CH), 3.45 (2 H, m, OCH$_2$CH$_3$), 4.56 (1 H, d, J 16.6, CH$_2$O), 4.61 (1 H, d, J 16.6, CH$_2$O), δ_c(100 MHz, CDCl$_3$) 15.7 (CH$_3$), 23.1, 24.4, 27.6, 27.9, 28.0, 28.1, 28.2, 32.2, 32.7, 33.8, 38.3 (CH$_2$), 63.8 (CH$_2$CH$_3$), 68.1 (OCH$_2$), 78.5 (CH), 173.1, 204.7 (C=O); m/z 256 (M$^+$), accurate mass [C$_{14}$H$_{22}$O$_4$NH$_4$]$^+$ requires 274.3013, found 274.2009.
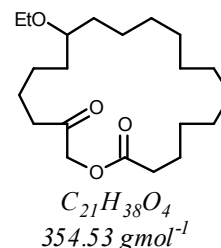
Preparation of 8-ethoxyoxacyclotetradecane-2,5,13-trione (90df)

Cyclohexane-4-one-1-*spiro*-3'-(1',2',4'-trioxane)-6'-*spiro*-1''-(2''-ethoxycyclohexaneone (**86df**) (72 mg; 2.53 mmol) was dissolved in decane (15 mL) and pipetted into a thermolysis tube. The solutions were then degassed and the tubes sealed, as stated, before being immersed in a silicon oil bath at 180 °C for 16 hours. The crude product was purified by flash column chromatography (1:1 ethyl acetate/ light petroleum) to afford the title compound R_f = 0.42 (15 mg; 0.053 mmol; 20.8%) as a white solid: m.p. 36-38°C from diethyl ether/ light petroleum, υ_{max} (CHCl$_3$) /cm^{-1} 1718, 1737; δ_H(400 MHz, CDCl$_3$) 1.16 (3 H, t, J 7.0, CH$_3$) 1.24 (2H, m), 1.40 (2H, m), 1.60 (2H, m), 1.75 (1H, m), 1.99 (1H, m), 2.24 (1 H, dt, J 7.1 and 16.8), 2.41 (1 H, dt, J 7.3 and 16.8), 2.49 (1 H, ddd, J 2.9, 8.4 and 18.4), 2.62-2.92 (5 H, m), 3.21 (1 H, m, CH), 3.41 (1 H, dq, J 7.0 and 9.2, CH$_2$CH$_3$), 3.51 (1 H, dq, J 7.0, 7.0, 7.0 and 9.3, CH$_2$CH$_3$), 4.37 (1 H, d, J 15.6, CH$_2$O), 4.56 (1 H, d, J 15.6, CH$_2$O), δ_c(100 MHz, CDCl$_3$) 15.6 (CH$_3$), 21.3, 23.1, 25.4, 28.6, 30.8, 36.7, 37.4, 37.9 (CH$_2$), 63.9 (CH$_2$CH$_3$), 69.0 (OCH$_2$), 76.7 (CH), 172.2, 207.2, 209.0 (C=O); m/z 284 (M$^+$), accurate mass C$_{15}$H$_{24}$O$_5$ requires 284.16181, found 284.16183.
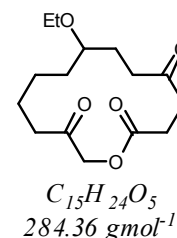
Attempted preparation of 10-ethoxy-6,7,8,9,10,11-hexahydrobenzo[d][1]oxacyclotridecine-2,5(1H,4H)-dione (90dg)

Indane-2-*spiro*-3'1(1',2',4'-trioxane)-6'-*spiro*-1''-2''-ethoxycyclohexane (**86dg**) (35 mg; 1.15 mmol) was dissolved in decane (10 mL) and pipetted into a thermolysis tube. The solutions were then degassed and the tubes sealed, as stated, before being immersed in a silicone oil bath at 180 °C for 16 hours. The crude product was purified by flash column chromatography (1:5 ethyl acetate/ light petroleum) to afford the title compound with some impurities R_f = 0.21 (10 mg; 0.33 mmol; 28.7% yield): δ_H (400MHz, CDCl$_3$) 1.23 (3 H, t, *J* 7.0, CH$_3$) 1.26-1.90 (6H, m, CH$_2$), 1.65 (s, unknown) 2.33 (1H, m, CH$_2$, CH$_2$), 2.63 (1H, m, CH$_2$), 2.72 (s, unknown), 3.26 (1H, dd, *J* 13.5 5.9, CH), 3.51 (2 H, dq, *J* 9.1 7.0, OCH$_2$CH$_3$), 3.71 (2 H, m, CH$_2$), 3.82 (1 H, d, *J* 15.8, CH$_2$O), 3.86 (1 H, d, *J* 15.8, CH$_2$O), 4.39 (1 H, d, *J* 16.7, CH$_2$O), 4.87 (1 H, d, *J* 16.7, CH$_2$O), 7.25-7.37 (4H, m, Ph-H), 8.41 (s, unknown); δ_C(100MHz, CDCl$_3$) 14.1 (unknown CH$_3$), 15.7 (CH$_3$), 17.6 (unknown CH$_3$), 21.5, 22.6, 29.6, 36.4, 38.4, 39.4 (CH$_2$), 22.7, 29.3, 29.7, 31.9, 51.2 (unknown CH$_2$), 64.8 (OCH$_2$CH$_3$), 68.0 (OCH$_2$), 75.4 (CH), δ112.9 (unknown *q*C), 127.1, 127.7 (Ar-CH), 131.3 (Ar-qC), 131.3, 132.0 (Ar-CH), 137.3 (Ar-qC), 170.8, 208.3 (C=O)
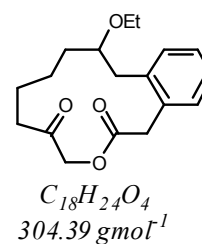
$C_{18}H_{24}O_4$
304.39 gmol^{-1}

[1] S. Li, X. Xiao, X. Yan, X. Lui, R. Xu and D. Bai, *Tetrahedron*, 2005, **61**, 11291-11298

[2] B. Atrash, T. S. Cooper, P. Sheldrake, P Workman and E. McDonald, *Tetrahedron Lett.*, 2006, **47**, 2237-2240

[3] B. Brockman and Henkel W., *Naturwissenschaften*, 1950, **37**, 138

[4] S. Pal, *Tetrahedron*, 2006, **62**, 3171-3200

[5] K.S. Yeung and I. Paterson, *Chem. Rev.*, 2005, **105**, 4237-4313

[6] J. Kang and E. Lee, *Chem. Rev.,* 2005, **105**, 4348-4378

[7] A. S. Williams, *Synthesis,* 1999, 1707-1723

[8] M. Gautschi, J. A. Bajgrowicz, P. Kraft, *Chimia,* 2001, **55**, 379-387

[9] K. C. Nicolaou, *Tetrahedron*, 1977, **33**, 683-710

[10] T. G. Back, *Tetrahedron*, 1977, **33**, 3041-3059

[11] C. J. Roxburgh, *Tetrahedron*, 1995, **51**, 9767-9822

[12] E. J. Corey and K.C. Nicolaou, *J. Am. Chem. Soc.*, **1974**, *96*, 5614–5616

[13] T. Mukaiyama, M. Usui, and K. Saigo, *Chem. Lett*, 1976, **5**, 49-50

[14] T. Kurihara, Y. Nakajima, O. Mitsunobu, *Tetrahedron Lett.,* 1976, **28**, 2455-2458

[15] J. Inanaga, K. Hirata, H. Saeki, T. Katsuki, and M. Yamaguchi, *Bull. Chem. Soc. Jpn.*, 1979, **7**, 1989-1993

[16] I. Shiina, and T. Mukaiyama, *Chem. Lett.*, 1994, **23**, 677-680

[17] K. Ishihara, M. Kubota, H. Kurihara, H. Yamamoto, *J. Org. Chem.*, 1996, **61**, 4560-4567

[18] Y. Oohashi, K. Kuumoto and T. Mukaiyama, *Chem. Lett.*, 2005, **34**, 72-73

[19] K. C. Majumdar, H. Rahaman, and B. Roy, *Curr. Org. Chem.*, 2007, **11**, 1339-1365

[20] A. Fuerstner and K. J. Langemann, *Synthesis*, 1997, 792-803

[21] A. Fuerstner and K. J. Langemann, *J. Org. Chem.* 1996, **61**, 3942-3943

[22] A.K. Ghosh and G.L. Gong, *J. Org. Chem.*, 2006, **71**, 1085-1093

[23] T. Haack, K.L. Haack, W. E. Diederich, B. Blackman, S. Roy, S. Pusuluri and G. I. George, *J. Org. Chem.*, 2005, **70**, 7592-7604

[24] S. J. Bailey, E. J. Thomas, S. M. Vather, and J. Wallis, *J. Chem. Soc, Perkin Trans. 1*, 1983, 851-859

[25] J–T. Shin, S. Shin, and C-G Cho, *Tetrahedron Lett.,* 2004, **45**, 5857-5860

[26] J–T. Shin, S-C. Hong, S. Shin, and C-G Cho, *Org. Lett.,* 2006, **8**, 3339-3341

[27] A. A. Nagal, W. D. Celmer, M. T. Jefferson, L. A. Vincent, and E. B. Whipple, *J. Org. Chem*, 1986, **51**, 5397-5400

[28] H. A. Kirst, J. A. Wind, and J. W. Paschal, *J. Org. Chem*, 1987, **52**, 4359-4362

[29] L. I. Tsuetelina, S. M. Binet, H. V. Nha, J. S. Chen, Ly T. Phan and Yat Sun Or, *Org. Lett*., 2003, **5**, 443-445

[30] P. Schwab, R.H. Grubbs, J.W Ziller, *J. Am. Chem. Soc*., 1996, **118**, 100-110

[31] D. Crich, A. L. J. Beckwith, G. F. Filzen, and R. W. Longmore, *J. Am. Chem. Soc*., 1996, **118**, 7422-7423

[32] W. R. Roush, K. Koyama, M. L. Curtin and K. J. Moriarty, *J. Am. Chem. Soc*., 1996, **118**, 7502-7512

[33] M. Tortosa, N. A. Yakelis, and W. R. Roush, *J. Am. Chem. Soc*., 2008, **130**, 2722-2723

[34] S. M. Winbush, D. J. Mergott, and W. R. Roush*, J. Org. Chem.,* 2008, **73**, 1818-1829

[35] P. Scafato, A. Larocca, and C. Rosini, *Tett. Asymm*., 2006, **17**, 2511-2515

[36] J. Ju, S-K. Lim, H. Jaing, J-W. Seo, Y. Her, and B. Shen, *Org. Lett.*, 2006, **8**, 5865-5868

[37] G. H. Posner, M. A. Hatcher and W. A. Maio, *Org. Lett*. 2005, **7**, 4301-4303

[38] B.Seyberlich, P. Laackmann, E-M. Peters, K. Peters, H. G. v. Schnering, W. Tochtermann, *Tetrahedron*, 2000, **56**, 4129-4137

[39] K. J. McCullough, Y. Motomura, A. Musuyama, and M. Nojima, *J. Chem. Soc. Chem. Commun.*, 1998, 1173-1174

[40] M. T. Arencibia, R. Freire, A. Perales, M. S. Rodriguez, and E. Suárez, *J. Chem. Soc., Perkin Trans. 1*, 1991, 3349-3360

[41] T. Arencibia, J. A. Salazar, E. Suárez, *Tetrahedron Lett.*, 1994, **35**, 7463-7466

[42] P.R Story, D. D. Denson, C. E. Bishop, B. C. Clark, J-C. Farine, *J. Org. Chem*.,1976, **41**, 214-215

[43] P. R. Story, B. Lee, C. E. Bishop, D. D. Denson, and P. Busch, *J. Org. Chem*., 1970, **35**, 3059-3062

[44] P. R. Story, D. D. Denson, C. E. Bishop, B. C. Clark, J-C. Farine, *J. Am. Chem. Soc.*, 1968, **90**, 817-818

[45] J. R. Sanderson, K. Paul, P. R. Story, D. D. Denson, and J. A. Alford, *Synthesis*, 1975, **3**, 159-161

[46] J. R. Sanderson, K. Paul, P. R. Story, *Synthesis*, 1975, **4**, 275-276

[47] P. R. Story and P. Busch, *Adv. Org. Chem.*, 1972, **8**, 67-95

[48] B. Kerr and K. J. McCullough, *J. Chem. Soc. Chem. Commun..*, 1985, 590-591

[49] A. Haq, B. Kerr and K. J. McCullough, *J. Chem. Soc. Chem. Commun.*, 1993, 1076-1078

[50] E. L. Eliel, S. H. Wilen, L. N. Mander, *Stereochemistry of Organic Compounds, John Wiley & Sons Inc., NY*, 1994, 768-769

[51] G. Borgen, and J. Dales, *J. Chem. Soc. Chem. Commun.*, 1970, 1340-1342

[52] J. Dale, *J. Chem. Soc.*, 1963, 93-111

[53] F. A. L. Anet, A. K. Cheng, J. J. Wagner, *J. Am. Chem. Soc*, 1972, **94**, 1251-1253

[54] J. Dale, *Acta Chem. Scand.*, 1973, **27**, 1115-1129

[55] P. Groth, *Acta. Chem. Scand*, 1976, **30**, 155-156

[56] P. Groth, *Acta. Chem. Scand*, 1975, **29**, 374-380

[57] J. Dale, *Top. Stereochem.*, 1976, *Multi-Step conformational interconversion mechanism*, 199-270

[58] F. A. L. Anet, and T. N. Rawdah, *J. Am. Chem. Soc.*, 1978, **100**, 7810-7814

[59] B. H. Rubin, M. Williams, M. Takeshita, F. M. Menger, F. A. L. Anet, B. Bacon, and N. L. Allinger, *J. Am. Chem. Soc.*, 1984, **106**, 2088-2092

[60] P. Groth, *Acta Chem. Scand.*, 1979, **33**, 503-513

[61] P. Groth, *Acta Chem. Scand.*, 1980, **34**, 609-620

[62] E. J. Valente, D. M. Pawar, F. R. Fronczek, and E. A. Nowe, *Acta Cryst. Sec. C.,* 2008, **64**, o447-o449

[63] W. G. M. Van Den. Hoek, H. A. J. Oonk, and J. Kroon, *Acta Cryst.,* **B35***,* 1979*, 1858-1861

[64] E. A. Noe, D. M. Pawar, and F. R. Fronczek, *Acta Cryst. Sec. C,* 2008*, **64**, o67-o68

[65] E. A. Noe, D. M. Pawar, and F. R. Fronczek, *Acta Cryst. Sec. C,* 2008, **64**, o139-o141

[66] F. A. L. Anet, A. K. Cheng, and J. Krane, *J. Am. Chem. Soc.*, 1973, **95**, 7877-7878

[67] N. L. Allinger, B. Gordon, and S. Profeta Jr., *Tetrahedron*, 1980, **36**, 859-864

[68] I. W. Bassi, R. Scordamaglia, and L. Fiore, *J. Chem. Soc., Perkin Trans. 2*, 1972, 1726-1729

[69] D. S. Clyne, and L Weiller, *Tetrahedron,* 2000, **56**, 1281-1297

[70] J. Dale, *Stereochemistry and Conformational Analysis*; Verlag Chemie: NY , 1978, 206

[71] J. Dale, *Acta Chem. Scand.*, 1973, **27**, 1149-1158

[72] S. L. Björnstad, G. Borgen, J. Dale, and G. Gaupset, *Acta Chem. Scand.*, 1975, **29B**, 320-324

[73] D. S. Clyne, and L Weiller, *Tetrahedron,* 2000, **56**, 1281-1297

[74] P. Kraft, and R. Cadalbert, *Chem. Eur. J.*, 2001, **7**, 3254-3261

[75] K. Savill, Heriot-Watt University, PhD Thesis, 1993

[76] G. M. Sheldrick, ShelXTL PC (vers. 5.1); Bruker AXS: Madison, WI, 1997

[77] G. R. Disiraju and T. Steiner, *The Weak Hydrogen Bond in structural chemistry and biology, IUCr Monographs on Crystallography*, 1999, **9**, 13

[78] B Kerr, Heriot-Watt University, PhD Thesis, 1989

[79] L. Kaisalo, T. Hase, *Synthesis*, 2001, **11**, 1619-1622

[80] K. L. Erikson, J. A. Beutler, J. H. Cardellina II, and M. R. Boyd, *J. Org. Chem.*, 1997, **62**, 8188-8192

[81] T. Fujisaka, M. Miura, M. Nojima, and S. Kusabayashi, *J. Chem. Soc., Perkin Trans. 1.*, 1989, 1031- 1039

[82] C. W. Jefford, and G. H. Vicente, *Heterocycles*, 1993, **2**, 725-729

[83] D. J. Henry, C. J. Parkinson, P. M. Meyer, and L. Radom, *J. Phys. Chem. A*, 2001, **105**, 6750-6756

[84] H. Zipse, *Top. Curr. Chem.,* 2006, **263**, 163-189

Chapter Three

DFT studies for the thermal rearrangement
of *dispiro*-1,2,4-trioxanes

β-Scission of alkoxyl radicals

In this section previous literature on the reactivity of alkoxyl radicals will be reviewed along with relevant computational studies of artemisinin and related compounds. The review will first concentrate on the reaction of simple alkoxyl radicals and discuss (i) how an α-substituent can stabilise the β-scission of alkoxyl radicals and (ii) the opening of ring systems concentrating on the fine balance between a β-scission process releasing ring strain and cleaving the molecule. The review will go onto detail some of the computational studies involving artemisinin and related model compounds. This section will cover both the formation of the alkoxyl radicals via iron-mediated decomposition and the chemistry of the alkoxyl radicals formed.

The cleavage of a C-C bond in a radical β-scission reaction leading to the formation of a carbonyl and release of an alkyl radical is one of the most important reactions of alkoxyl radicals. The chemistry of alkoxyl radicals has a number of important applications for example synthesis of pharmaceutically active natural products,[1] the formation of medium and large ringed structures[2] and as models for intermediates in atmospheric chemistry[3] and biological systems.[4] The alkoxyl radical has been shown to exhibit a number of other synthetically useful transformations including cyclization and 1,5-hydrogen transfer reactions.[5,6]

The β-scission of an alkoxyl radical in a ring expansion or fragmentation depends on the stability of the alkoxyl radical and the potential for competitive reactions like 1,5-hydrogen transfer to occur. Other competitive reactions include hydrogen transfer from a second molecule *(Scheme 1 (1))*, intramolecular hydrogen abstraction *(2)* and addition to double bonds *(3)*. The nature of the substrate dictates whether the β-scission cleaves the molecule in two *(4)*, performs a radical-mediated fragmentation *(5)*, or a radical-mediated ring expansion *(6)*. The order of rates for β-scission of alkoxyl radicals have clearly been shown to be primary < secondary < tertiary[7] with the β-scission of a tertiary alkoxyl radical being shown to occur 100 times faster than primary radicals.[8]
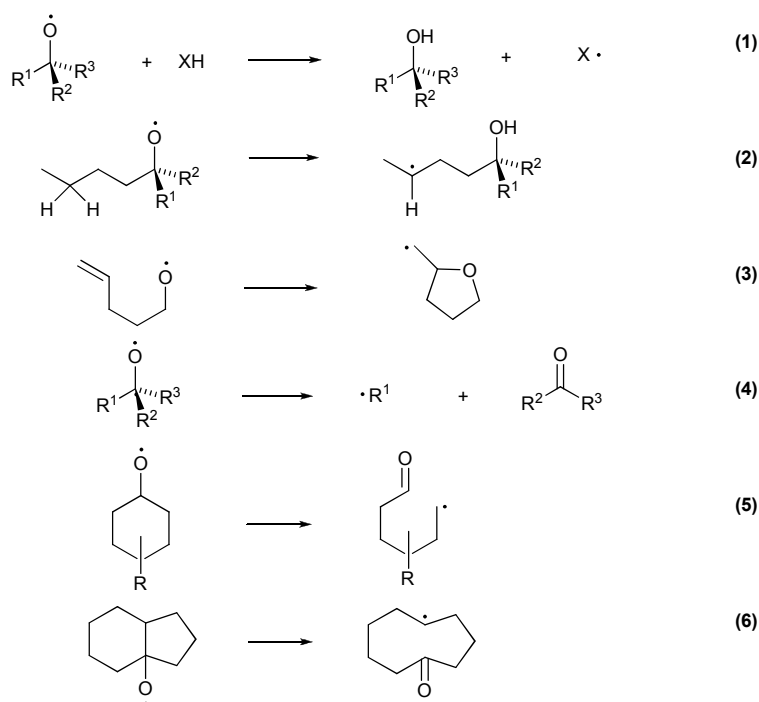
Scheme 1

In highly substituted unsymmetrical tertiary alkoxyl radicals it is possible for three different β-scissions to occur, forming three different products *(Scheme 2)*.[9] In general it is expected that the preferred β-scission is the one which produces the most substituted and/or most thermodynamically stable alkyl radical, normally in the order methyl < primary alkyl < secondary < tertiary.[10] Lower activation energies and greater exothermicities have been calculated from the formation of more substituted alkyl radicals.[11,12]
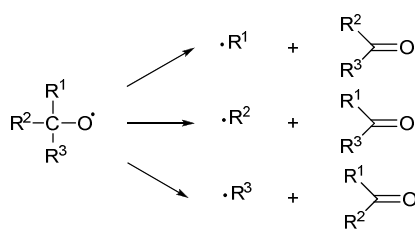
Scheme 2

The length and electronic population of the bonds *alpha* to the alkoxyl radical have further been shown to be linked to the site of the β-scission. Using DFT calculations the optimised geometry of the alkoxyl radical **1b** shows that one of the C-C bonds is 1.564 Å whilst the other are shorter at 1.542 Å. Further to this, NBO calculations have shown that the longer bond has a lower electronic population of 1.892 than the other shorter C-C bonds *(Figure 1)*. Similar results have also been obtained from alkoxyl

radical **1b** where the preferred site of β-scission is to release the more substituted ethyl radical.[13]

1.542 Pop= 1.937   1.564 Pop= 1.892

1.541 Pop= 1.937

1a

1.543 Pop= 1.934   1.585 Pop= 1.865

1.543 Pop= 1.934

1b
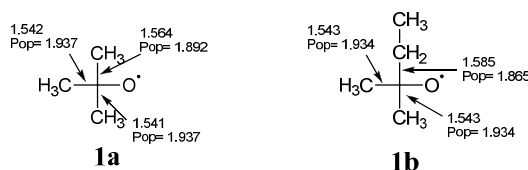
Figure 1

(i) Effect of α-substituents on radical stability

The nature of the group (or atom) in the α-position can have a stabilizing effect on the carbon radical. The so called 'α-effect' has been shown to be prominent for all but a few substituents tested. Particular stabilizing effects have been noted for unsaturated α-substituents and those bearing lone pairs.

Computed radical stabilization energies (RSE) have been used as a measure of the stabilization of the α-substituent relative to a methyl radical. The RSE is the difference between the C-H bond dissociation energies (BDE) of a methane molecule **(3)** and a substituted methane molecule **(2)**. The RSE will be negative for all radicals, which are more stable than the methyl radical *(Scheme 3)*.[14]

2   **3**
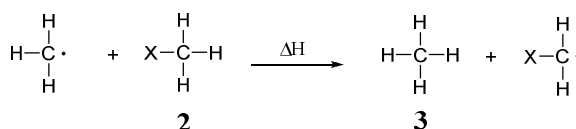
Scheme 3

The stabilization of radicals has been shown to occur due to interactions between the orbital carrying the unpaired electron and energetically and spatially adjacent orbitals on the substituent. The effect of a vinyl substituent involves the delocalization of the unpaired spin into an adjacent π-system in a three-centre three-electron stabilization *(Figure 2a)*. The orbital diagram describes how the stabilization is caused by the unpaired electron located in a p-orbital of the carbon interacting with the π- and π^*-orbitals of the substituent. The result of this interaction is a doubly occupied bonding orbital, a singly occupied approximately non-bonding orbital and an unoccupied anti-

bonding orbital *(Figure 2a)*. A RSE of -77.5 kJ mol^{-1} has been calculated for an allyl radical.[15]
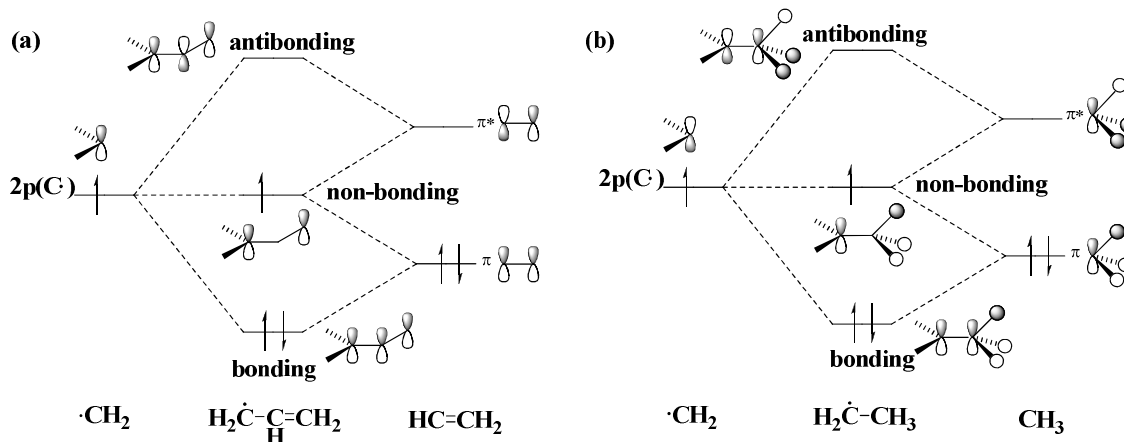
Figure 2: MO diagram showing π- interactions between CH$_2$ and vinyl (a) or alkyl (b) α-substituent

A related situation occurs for the stabilization of carbon-centred radicals by alkyl substituents *(Figure 2b)*. The π-orbitals are constructed through combination of individual C-H bonds and interact in a similar way as that seen for vinyl radicals. The stabilization is much smaller than vinyl radicals with RSE of -13.8 kJ mol^{-1} for an ethyl radical. Although the RSE is not significantly affected by the length of the alkyl chain, the addition of a more strained group like cyclopropyl provides π-type orbitals from more strained C-C bonds that interact more efficiently with the radical centre resulting in a RSE of -23.2 kJ mol^{-1}.[15,16]

A further type of stabilizing interaction can occur where the carbon-centred radical interacts with an adjacent lone pair in a two-centre three-electron interaction. This creates a low-lying doubly occupied bonding orbital and a singly occupied anti-bonding orbital *(Figure 3)*. For first row elements, the greatest RSE is seen with amino groups and the smallest with fluorine (NH$_2$ = -45.8 kJ mol^{-1}, OH = -32.3 kJ mol^{-1} and F = -12.9 kJ mol^{-1}) demonstrating a link between the electronegativity of the substituent and the size of the stabilization.[15] A similar effect however, is not seen for second row substituents.[15] In each case, the stabilization of the carbon-centred radical by an α-substituent is accompanied by a contraction in the bond between these two centres. For example, the C-O bond length in methanol is 1.419 Å and the same bond in hydroxymethyl radical is 1.370 Å.[17]
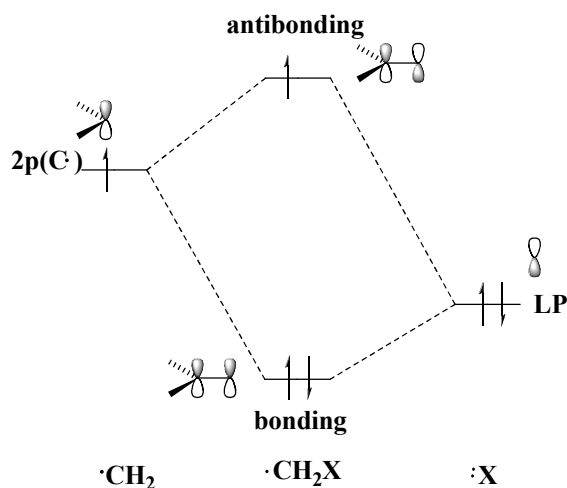
Figure 3: MO diagram showing interaction between a ·CH₂ and a α-substituent containing a lone pair

In some cases, the α-effect provides considerable stabilisation to the reaction allowing β-scission reactions to occur even when intramolecular hydrogen abstraction looks more likely. Primary alkoxyl radical **4** is ideally set up for intramolecular hydrogen abstraction with a ·O···5H distance of 2.8 Å. Despite this, the β-scission of **4** to form **6** is the preferred reaction with no trace of the intramolecular hydrogen-abstraction product **5** being isolated *(Scheme 4)*.[18,19] Similar findings were found for the reaction of carbohydrate-derived alkoxyl radicals.[20,21]

Z= acyl, carbamate
X= O-alkyl, alkyl, H
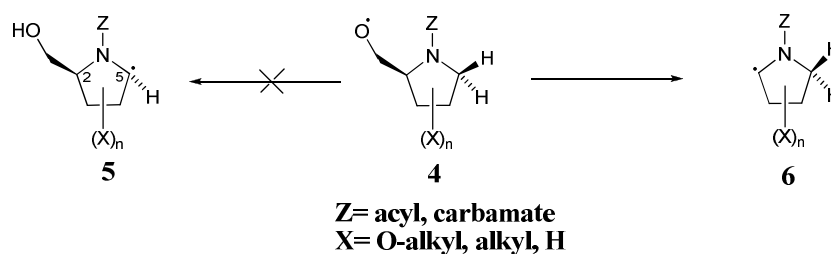
Scheme 4

A similar result from the reaction of primary alkoxy radicals **7a (R=H)** and **7b (R=Me)** was studied computationally *(Scheme 5)*. The reaction of **7a** produced exclusive β-scission to form **8**. In contrast, the preferred reaction of **7b** was a 1,5-hydrogen abstraction forming **9**. It was proposed that the half-filled p-orbital (SOMO) of **7a** was interacting with the hydrogen atom of the hydroxyl group forming a stabilising six-membered interaction which is not possible in **7b**. Computational models confirm the presence of the ·O···HO non-bonding interaction measuring 2.22 Å (**7aa**) and 2.37 Å (**7ab**) in the two studied conformations of **7a** *(Scheme 5)*. The ·O···HO non-bonding interaction appears to elongate the C-C bond distance to 1.585 Å (**7aa**) and 1.576 Å (**7ab**) at the site of β-scission suggesting a lowering in the transition state barrier. With

no close-range interaction, **7b** contains a longer C-C bond distance of 1.529 Å implying the β-scission would be more difficult.[22]
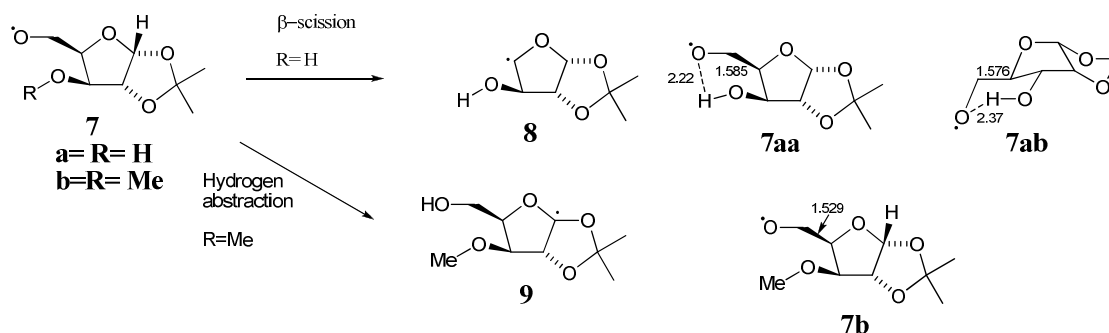
Scheme 5

(ii) Release of ring strain

The β-scission of an alkoxyl radical which subsequently causes a ring opening is also important in determining the preferred reaction of alkoxyl radicals. Computed energies for ring opening β-scission reactions of monocyclic alkoxyl radicals show increased activation barriers with increased ring size *(Table 1)*. The ring openings also become less exothermic with the increased ring size, with the opening of a six-membered alkoxyl radical actually computed to be slightly endothermic. Additionally the C-C bond distance at the transition state becomes longer as the ring size increases indicating a later transition state.[11] This follows the Hammond postulate that assumes the more endothermic the reaction the more closely will the transition state resemble the products.[23] These energy barriers are consistent with experimental results which determined the rate constants for the ring openings of cyclopentoxyl and cyclohexyloxy radicals to be $k_o = 4.7 \times 10^8$ s^{-1} and $k_o = 1.1 \times 10^7$ s^{-1} respectively.[24]

Reactant	Product	E_a	ΔE	R
		2.8	-23.1	1.742
		7.7	-23.7	1.900
		15.4	-4.3	2.030
		20.7	1.9	2.052

Table 1: Energy barriers and overall reaction energy (kcal mol^{-1}) for the β-scission of different ring sizes.
R= C···C bond distance in transition state.

For the alkoxyl radicals **10, 12** and **13**, the ring opening is in competition with the fragmentation of the molecule releasing either isopropyl or ethyl radicals. In **10**, a 700-fold increase for the β-scission of bond **A** was observed compared to bond **A** in **11** where an ethyl radical is released *(Figure 4)*. Consistent with lower ring strain in a six-membered ring, a smaller four-fold increase in β-scission within the ring was evident for the ring opening of **12**, compared to **11**, with the cleavage of bond **B** causing the release of a isopropyl radical still being favoured **11:1**. The replacement of the isopropyl group in **12** with an ethyl group in **13** does change the preference heavily in the favour of the opening of the six-membered ring.[25]

| **A:B 14:1** | **A:B 1:50** | **A:B 1:11** | **A:B 7:1** |
| **10** | **11** | **12** | **13** |
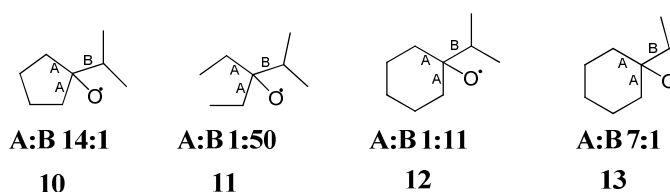
Figure 4

In another example of competitive β-scission reactions, 1-alkylcycloalkoxyl radicals such as **15** *(Scheme 6)* exhibit a fine balance between the β-scission within the ring or of the C-alkyl bond. Thus, where R= H or Me β-scission of the 5-membered ring consistent with the release of ring strain has been shown to occur forming **14**. However, when R= Et, the formation of 1-indanone **(16)** is observed consistent with release of an ethyl radical.[26]
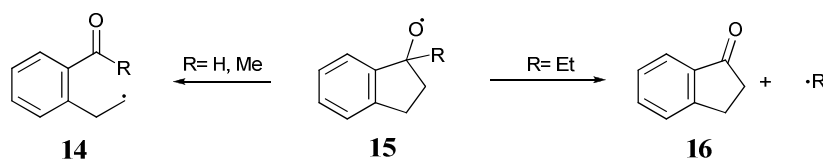
Scheme 6

In the examples outlined in *Figure 4* and *Scheme 6,* where competition exists between two different β-scission pathways, the release of ring strain loses out in each case to the release of alkyl radicals when more substituted alkyl radicals can be formed.

In a further competitive β-scission reaction, alkoxyl radical **17** has a choice to break either bond **A** or **B**. The cleavage of bond **A** was expected to be the preferred reaction mechanism as it would release the ring strain associated with the four-membered ring and generate an intermediate allylic radical **19** which would be resonance stabilised. In a

surprising result, however, β-scission of alkoxyl radical **17** formed the seven membered product **18** in 80% yield from β-scission of bond **B** and **19** from the opening of bond **A** in only 11% yield *(Scheme 7)*. Although both processes release ring strain from the cyclobutane ring, the breaking of bond **B** also opens the 5-membered ring therefore releasing the ring stain of both rings in one process. The replacement of the methyl at the position 5 with a hydrogen in **17** also resulted in the formation of the seven membered product in the higher yield despite the formation of a secondary radical centre. Furthermore, the reaction in the absence of the double bond in **17** actually achieved an increased yield of 22% from the opening of ring **A** with 69% of the alternative product from opening of **B**, despite the lack of the stabilization effect of the allylic group. This indicated that the stability of the intermediate **19** was having no effect on the overall reaction and that the energy barrier for the opening of bond **A** was more important.[27]
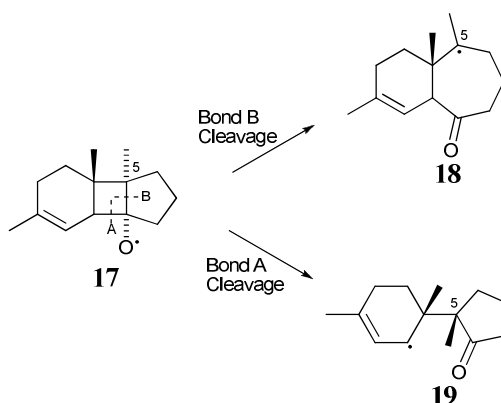
Scheme 7

To delineate the factors controlling the cleavage of bond **A** over bond **B**, model calculations using **20-23** were carried out. For each model studied, the opening of bond **B** was consistently favoured over bond **A** *(Table 2)*. The results for the opening of **20** show that the simultaneous cleavage of the fused four- and five-membered rings to form a 7-membered ring leads to a reduction in the activation energy, relative to the cleavage of a four-membered ring alone. The addition of the allylic group in **21** and **23** reduces the bond **A** cleavage barrier significantly but not enough for it to be less than that of bond **B**. The cleavage of bond **B** has a consistently smaller C···C distance in the transition state demonstrating an earlier transition state than that of the cleavage of bond **A** *(Table 2)*. As expected, the intermediate radical from the opening of bond **A** in **21** and **23** is stabilised by resonance to give a more exothermic reaction. The fact that the opening of bond **B** and formation of the seven membered ring product is observed

experimentally confirms the stability of the intermediate has little effect on the outcome of the reaction. The lower barrier associated with the release of ring strain of a 4-membered and 5-membered ring suggests the reaction is operating under kinetic control.[11]
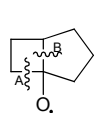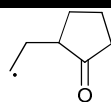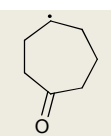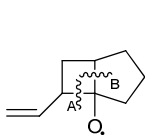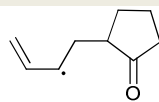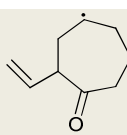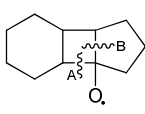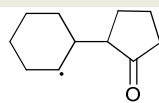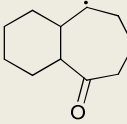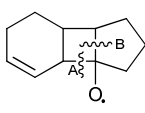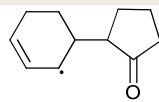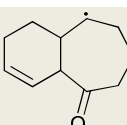
Reactant		Product	E_a	ΔE	R
20	A		10.1	-20.5	1.921
	B		5.5	-21.4	1.878
21	A		6.5	-35.6	1.882
	B		4.9	-20.6	1.880
22	A		7.3	-24.4	1.900
	B		5.0	-23.2	1.871
23	A		6.7	-32.4	1.979
	B		5.4	-20.6	1.878

*Table 2: Energy barriers and overall reaction energy (kcal mol^{-1}) for the β-scission at positions **A** and **B***

R= C···C bond distance in transition state

Computational studies into the decomposition of Artemisinin

Although in earlier work semi-empirical methods were used to study 1,2,4-trioxanes computationally,[28,29] it was after the advent of DFT methods the geometry of the 1,2,4-trioxane ring could be reproduced accurately.[30,31]   The structural and spectroscopic properties of artemisinin (**24**) and its derivatives have since been extensively studied using DFT calculations.[32]

Due to the computational expense of modelling the reaction mechanism for the full artemisinin molecule (**24**), initial theoretical studies were carried out on 6,7,8-trioxybicyclo[3.2.2]nonane (**25**) which provides a good mimic of the geometry of the 1,2,4-trioxane ring in artemisinin (**24**).[33]

24 Artemisinin   **25 6,7,8-trioxybicyclo[3.2.2]nonane**
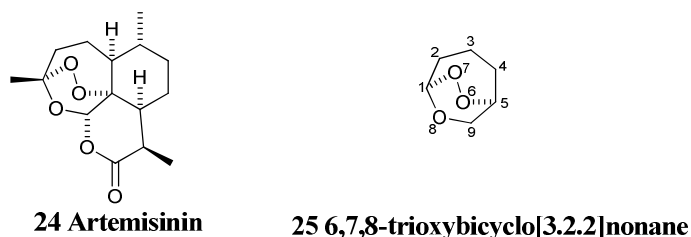
One such calculation explored the mechanism for cleavage of the peroxide bond by metal ions to give alkoxyl radicals. This process is regarded as the initial decomposition reaction of 1,2,4-trioxanes and crucial to antimalarial activity. The exact route for the opening of the peroxide was investigated by interaction of a number of iron, copper and zinc species with the peroxide bond of **25**. The metal ions can interact with the peroxide bond in different ways depending on the angle of approach. In the case of bare Fe^{2+} both the quintet and triplet spin states were investigated with the results for the triplet electrons reported. The approach of bare Fe^{2+} to O1 (**26**) or O2 (**27**) or both (**28**), each caused the opening of the peroxide bond with the lowest energy species shown to be where the iron is bound to both O1 and O2 in **28** *(Figure 5)*. Although the use of Fe^{2+} is not biologically realistic, related ring openings by complexes containing Fe^{2+}, Fe^{3+} and Cu^+ species with varying spin states demonstrated a similar O-O bond breaking. However in these a preference for the formation of a Fe-O1 bond in **26** over a Fe-O2 bond in **27** and **28** was apparent. No change in the O-O bond length was evident with Zn^{2+}.[34]

     26   **27**   **28**
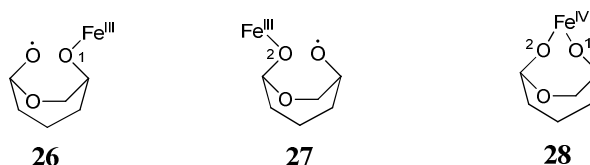
Figure 5

One possible source of iron in the human body is heme. The interaction of **25** with heme showed the preferential formation of a Fe-O1 bond (this was 10.6 kJ mol^{-1} lower in

energy than the alternative Fe-O2 bond) with an oxygen radical positioned at O2. This radical reacts to form a more stable carbon-centred radical via a β-scission reaction which further reacts to form a bond between itself and one of the *meso*-position of the heme *(Figure 6)*. The cleavage of the Fe-O bond in the heme complex results in the formation of a stable covalent product with no antimalarial activity.[35] Further studies into the nature of the Fe-O bond between artemisinin and heme have been reported.[36]
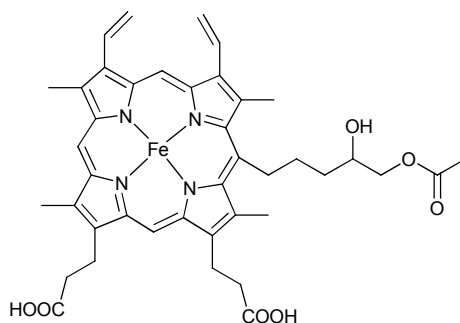
Figure 6

The reactions of the alkoxyl radicals **29** and **31** have been further investigated by comparing the β-scission and 1,5-hydrogen abstraction processes *(Scheme 8)*. A transition state energy of 7.2 kcal mol^{-1} was calculated for the 1,5-hydrogen abstraction of the hydrogen in the 2 position of **29** to the oxygen radical in the 6 position of **30**. Overall the formation of **30** is exothermic by 5.2 kcal mol^{-1} from **29** and therefore deemed to be irreversible. The expected β-scission reaction of **31** has similar, but higher, activation energy of 7.8 kcal mol^{-1} with the formation of **32** being exothermic by 10.1 kcal mol^{-1} from **31**. The resulting carbon-centred radical from the β-scission is therefore substantially lower in energy than that derived from 1,5-H abstraction.
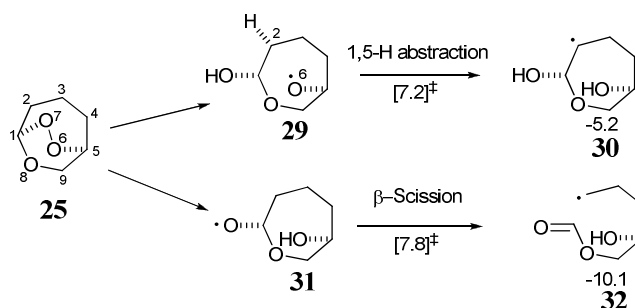
Scheme 8

Arguments put forward by Haynes *et. al. (Chapter 1)* invoke the formation of a carbocation during the artemisinin mechanism which accounts for the antimalarial

activity. However computational studies into the preferred Lewis acid protonation site of artemisinin (**24**) and arteether **33** both show that the protonation is very unlikely to occur at either oxygen of the peroxide bond *(Table 3)*; indeed protonation is more likely to occur at O5 in artemisinin (**24**) and O4 in arteether **33**.[37] In contrast, calculations on deoxyartethers **34** and **35**, where the oxygens at the 3- or 4-positions, respectively, are replaced by a methylene, demonstrate more accessible energies associated with protonation of O2 indicating that protonation of the peroxide bond is more likely to occur. Interestingly when O4 is replaced with a methylene group in **35** the protonation of O2 results in a low energy species and additionally promotes the cleavage of the O2-C bond leading to the formation of a carbocation as suggested by Haynes.[38]

24 Artemisinin   **33 Arteether**   **34 Deoxyartether**   **35 Deoxyartether**
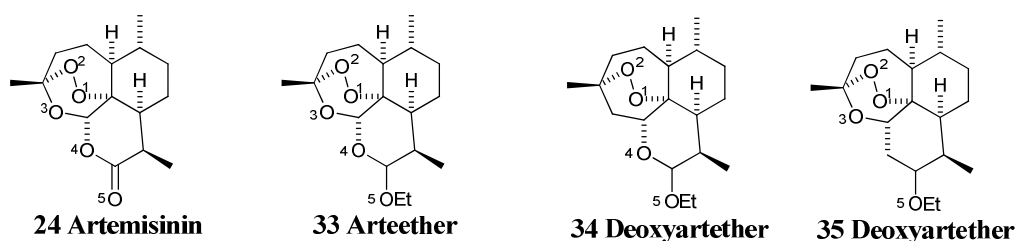
| Proton Site | Relative Energy/ kcal mol^{-1} | | | |
| | Artemisinin | Arteether | Arteether- O3 replaced with CH$_2$ | Arteether- O4 replaced with CH$_2$ |
	24	33	34	35
1	31.4	16.7	10.8	12.1
2	17.8	10.4	5.2 (14.1)	6.6 (6.6)
3	13.1	1.8	-	0.0
4	12.0	0	0.0	-
5	0	2.4	3.2	6.5

Table 3: Protonation energies for different oxygen sites in artemisinin and related compounds

A very extensive study mapping all proposed intermediates in the decomposition of **24** and **25**[39] has illustrated the stability of the various radical intermediates proposed during their iron-mediated decomposition *(Schemes 9, 10 and 11)*. The initial ring opening of the peroxide bond was modelled using a hydrogen atom which mimics the ring opening using Fe(II). On approach to the peroxide bond at either O1 or O2, the O1-O2 bond distance steadily increases to form low energy transition states (**TS[24-37]**= 5.1 kcal mol^{-1} and **TS[24-38]**= 4.2 kcal mol^{-1}) which relax to form low energy intermediates **37** and **38** in exothermic processes *(Scheme 9)*.[40]
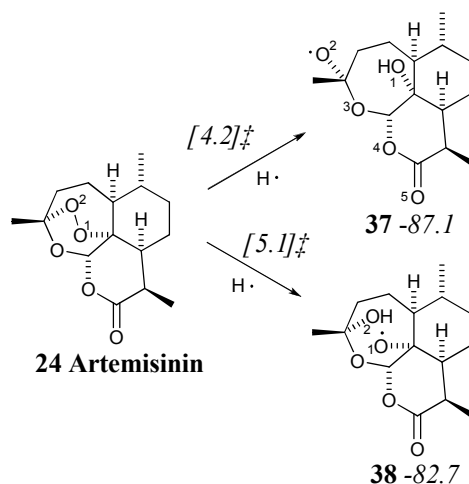
Scheme 9: Scheme 10: Reaction intermediates in the computed decomposition of Artemisinin. Energies are in kcal mol^{-1}

From intermediate **38,** the O1-centred radical has been shown to undergo 1,5-hydrogen abstraction reaction through a transition state of *ca*. 5.5 kcal mol^{-1}, forming the carbon centred radical **39** in a mildly exothermic reaction *(Scheme 10)*. Compounds **41** and **44** are known metabolites from artemisinin and various routes have been suggested for their formation. The route studied for the formation of **41** is via epoxide **40** and involves a large increase in energy for its formation suggesting a slow reaction. The other route suggested for the formation of **40** was by epoxidation of **42** by Fe(IV)=O and subsequent release of Fe(II)[41] but was not investigated in this study. The formation of **44** was investigated by two routes, first the addition of hydrogen atom followed by the release of water. Although this route looks favourable with low energy barriers and intermediates, the reaction relies on a source of hydrogen atoms. Therefore, in the absence of hydrogen atoms, the loss of ·OH followed by ring closure was considered. Despite the formation of **42** from **39** requiring a lower barrier than **40** from **39** the barrier is still *ca*. 27 kcal mol^{-1} and suggests that radical **39** may have a long lifetime.[40]
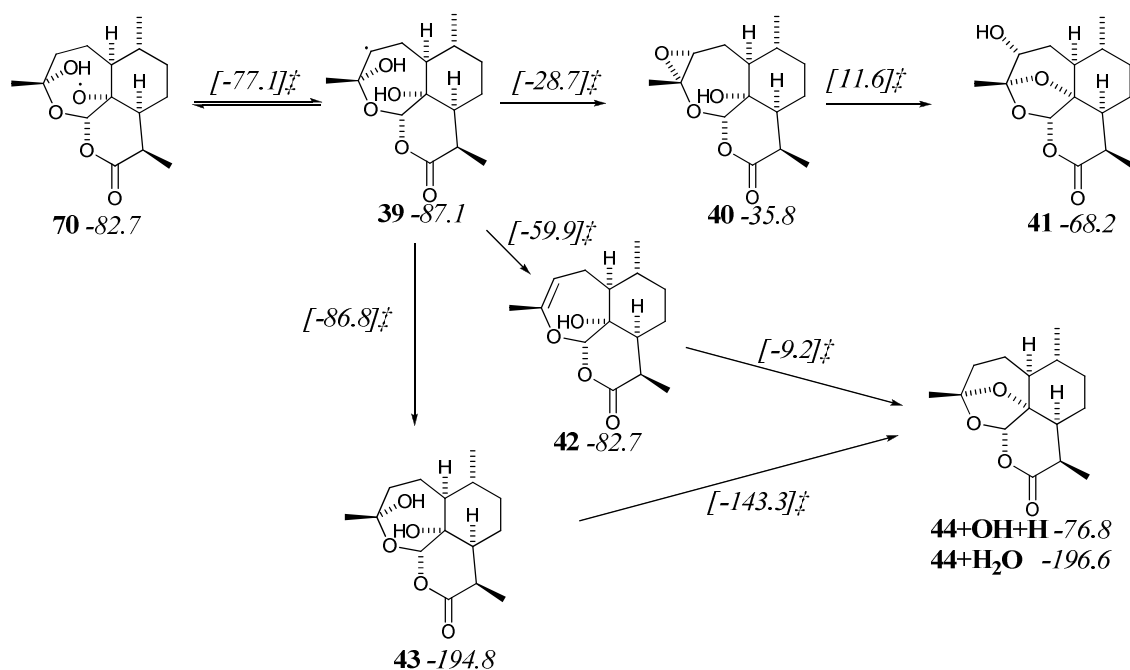
Scheme 10: Reaction intermediates in the computed decomposition of Artemisinin.

Energies are in kcal mol^{-1}

The formation of the radical at O2 leads on to a number of competitive β-scission reactions via intermediate **45** (Scheme 11). In particular, **46** is a low energy intermediate that is thought to be responsible for the biological activity of artemisinin and is easily formed. Subsequent reaction to **47** (which would stop activity due to **46**) is calculated to have a high barrier (~50 kcal mol^{-1}). This suggests the lifetime of the radical may be long enough to give an antimalarial effect. The further reaction of oxygen-centred radical **48** can follow a number of different steps. The formation of **49** through the β-scission of the C-O bond looks unlikely as a large barrier is computed. The alternative reactions, involving β-scission of C-C bonds and hydrogen transfer, both form the same low energy intermediate **52** through two different mechanisms. Similar to the transformation of **46** to **47** a large barrier has to be overcome in the formation of the product **53**. The final stage of each of the processes studied to produce artemisinin metabolites **41**, **44**, **47** and **53** involve large activation energies. This suggests that the radical intermediates may have a long enough lifetime to provide the antimalarial activity observed for artemisinin.[40]
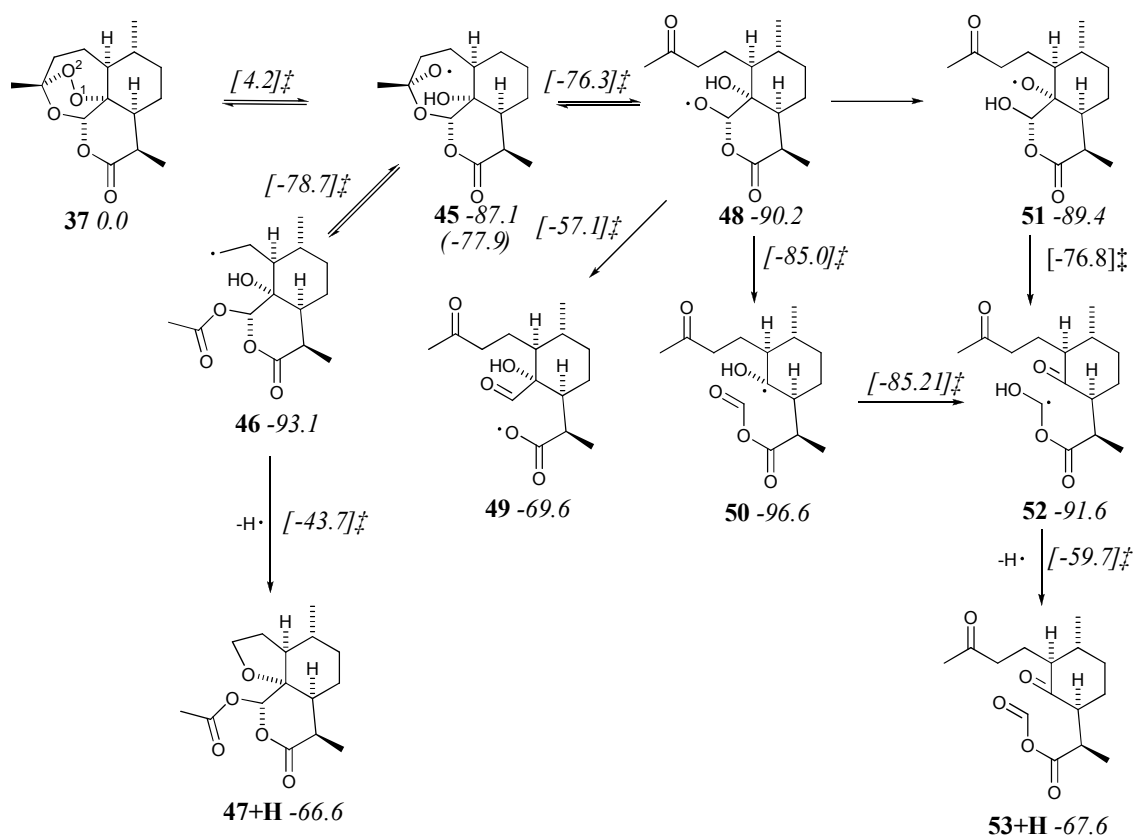
Scheme 11: Reaction intermediates in the computed decomposition of Artemisinin

Energies are in kcal mol⁻¹

Computational study of β-scission reactions during the thermolysis of *dispiro*-**1,2,4-trioxanes**

Experimental results have shown that the products obtained through the thermolysis of *dispiro*-1,2,4-trioxanes **54a-d** vary with the nature of the substituent in the α-position of ring **A**. In general, the thermolysis of the unsubstituted *dispiro*-1,2,4-trioxane **54a** results in the selective formation of oxalactone **56a**.[42,43] The observed product is consistent with initial opening of the 1,2,4-trioxane ring (ring **B**) by O-O homolysis giving **55a**, followed by selective β-scission in ring **C** before that in ring **A** *(Scheme 12)*.

54 a= H
b= Me
c= OMe
d= OEt

55

56 Oxalactone
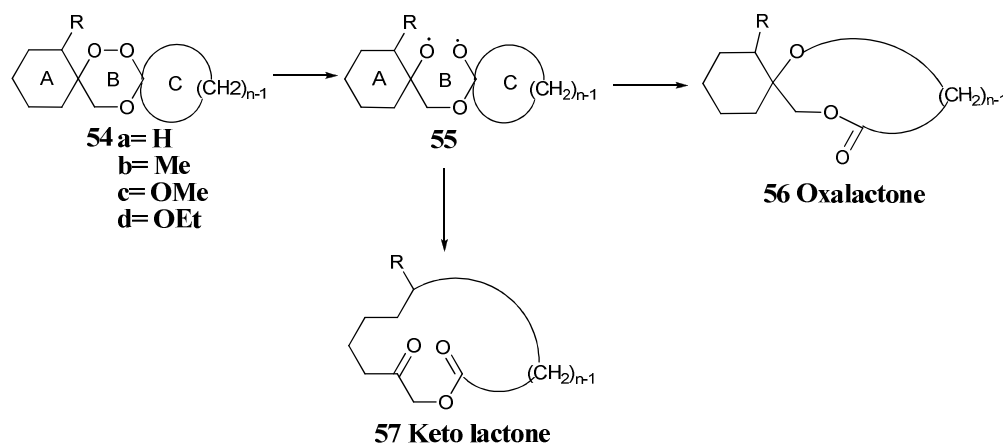
57 Keto lactone

Scheme 12

Although the thermolysis of the methyl-substituted *dispiro*-1,2,4-trioxane **54b** again resulted in oxalactone **56b**, the fully ring expanded keto lactone **57b** is also isolated in low yield.[43,44] The formation of **57b** suggests that different energetic conditions make the energy barrier associated with the β-scission of ring **A** more competitive with the barrier for the β-scission of ring **C**.

The results reported in *Chapter 2* for the thermolysis of methoxy- and ethoxy-substituted *dispiro*-1,2,4-trioxane **54c** and **54d** have shown the selective formation of the fully ring expanded keto lactones **57c** and **57d** in high yield without the formation of any oxalactone **56c** or **57c** in isolable amounts. This suggests that the introduction of an alkoxy-substituent results in the energy barrier for the β-scission of ring **A** being directly competitive with the barrier for the β-scission of ring **C**.

It was clear from these experimental results that there is a change in the products isolated from the thermolysis of different *dispiro*-1,2,4-trioxanes. Since there was no

definitive explanation for this observation it was appropriate to investigate the reaction mechanism through density functional theory (DFT) calculations. In order to investigate the mechanism this study was separated into two sections.

(i) Firstly, small models were studied to investigate the opening of both rings **A** and **C** individually. To do this the calculations were carried out on simplified oxy radicals **58** and **59** which were used to model rings **A** and **C** respectively *(Figure 7)*.
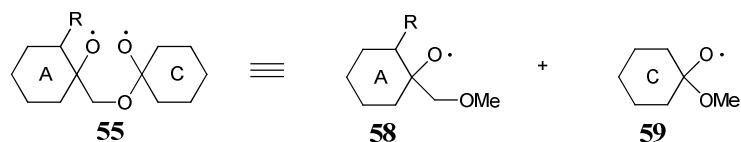
Figure 7

In adopting this approach it is assumed that the oxy-radicals formed during the thermolysis of a *dispiro*-1,2,4-trioxane act independently of each other. The aim of this study was first to prove that ring **C** opens significantly faster than ring **A** when R=H and then by changing R to Me or OMe investigate their influence on the barrier associated with the opening of ring **A**. A number of different ring sizes and substituents have been considered to establish what influence these have on the energy barriers involved in the reaction. Although the investigation concentrated on examples with experimental results, DFT calculations provided the opportunity to study hypothetical α-substituents as a predictive tool for selective formation of keto lactones **57** from *dispiro*-1,2,4-trioxanes **54**.

(ii) A full model study mapping out the intermediates involved in the radical rearrangement reactions of *dispiro*-1,2,4-trioxanes **54a-c** which aimed to further analyse the competitive β-scission reactions. Analysis of the bi radical system allows the radicals to recombine at any point during the reaction making the system more realistic. In addition, the use of the *dispiro*-1,2,4-trioxane as the starting point allowed for the homolytic cleavage of the peroxide bond giving the two alkoxy-radicals to be studied.

Computational Details

The calculations contained within this chapter have been carried out using density functional theory (DFT) methods using Gaussian 98[45] and Gaussian 03[46] with the

hybrid functional B3LYP deploying a 6-31G** basis set. All bond lengths contained within this chapter are displayed in Angstrom (Å) with energies containing a zero-point correction factor displayed in kcal mol^{-1}.

Calculations on the full *dispiro*-1,2,4-trioxane were carried out as open shell singlet calculations. A general approach to optimise open shell singlet calculations is to use an unrestricted DFT method and the 'guess=mix' option in Gaussian 98 and Gaussian 03. In such a calculation the $<S^2>$ term becomes close to 1.0 rather than the expected value of 0.0. In nearly every case the values of $<S^2>$ was *ca.* 1.0 and any deviations from 1.0 will be discussed in the text. Further checks that the models represent the open shelled singlet were carried out by calculating natural spin densities and the elimination of the possible wavefunction corresponding to the $O^+ \cdots O^-$ by checking the ionic charge distribution.

In an effect regularly observed with zero-point corrected energies' the transition-state energy in some cases is actually lower than one of the minima to which it is linked. If the pure electronic SCF energies of the reactant and the transition state are compared, the transition state is the less stable. However, when the zero-point correction is applied, the relative energy of the transition state is destabilised by less than that of reactant, resulting in transition state being more stable than the reactant. This happens because a transition state, as a turning point with one imaginary frequency, is considered in a frequency calculation as run in the Gaussian program to have one less vibrational mode than a minimum (with 3N-7 rather than 3N-6 vibrational modes). This results in transition states being less destabilised by zero-point energy corrections than minimum structures are. If a minimum and a transition state are close in energy, this difference in the degree of destabilisation can lead to the transition state having a lower energy than the minimum.

From the transition states, intrinsic reaction coordinate (IRC) calculations were used to find a local minimum. In each case the straight-chain product was also calculated with energies regularly being higher in energy than the intermediate calculated from the IRC calculation. Despite this, the overall thermodynamics of the reaction remained unchanged therefore throughout this study the intermediates from the IRC calculations will be discussed.

Theoretical studies into the ring opening of cyclohexyloxyl radicals 58a and 59

The oxy radicals used in the small model study, **58a** and **59**, were both orientated and optimised into a classic chair conformation. From the crystal structures of the *dispiro*-1,2,4-trioxanes discussed in *Chapter 1* it was noted that the configuration of the peroxide oxygens are axial with respect to both ring **A** and **C**. The configuration of the reactant models **58a** and **59** was therefore set up so that the oxygen radical is positioned in an axial arrangement. As a consequence, the methoxy group in **59** and the ether group in **58a** were equatorial with respect to rings **C** and **A** respectively *(Figure 8)*.
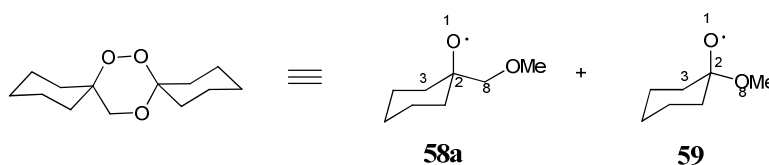
Figure 8

A comparison between the opening of the ring **A** (**58a**) and **C** (**59**) models shows a clear preference for the opening of ring **C**. The barrier associated with the opening of ring **C** at C(2)-C(3) via **TS[59-59′]**, is 7 kcal mol^{-1} lower in energy than the barrier for the ring opening of **A** at C(2)-C(3) via **TS[58a-58a′]** *(Figure 9)*. Additionally the opening of ring **C** results in a intermediate **59′** which is 5.6 kcal mol^{-1} lower in energy than the reactant, whilst the opening of ring **A** to form **58a′** is endothermic by 4.9 kcalmol^{-1}. This demonstrates the presence of the adjacent exocyclic O(8) strongly promotes the ring opening and is consistent with experimental results showing the preferential formation of oxalactone **56a** from the thermolysis of unsubstituted *dispiro*-1,2,4-trioxanes **54a**. In both cases the β-scission is accompanied by the expected shortening of the carbonyl C(2)-O(1) distances and increased planarity of the incipient terminal C(3) due to a build up of radical character. In fact a shortening of the C(2)-O(1) bond in reactant **59** suggests the oxy radical is already delocalised. A shorter C(2)-C(3) distance in **TS[59-59′]** compared to **TS[58a-58a′]** implies an earlier transition state for the former and is consistent with the lower activation energy seen for the opening of ring **C**. The complete transfer of radical character is confirmed by the short carbonyl bond distance in the intermediate.
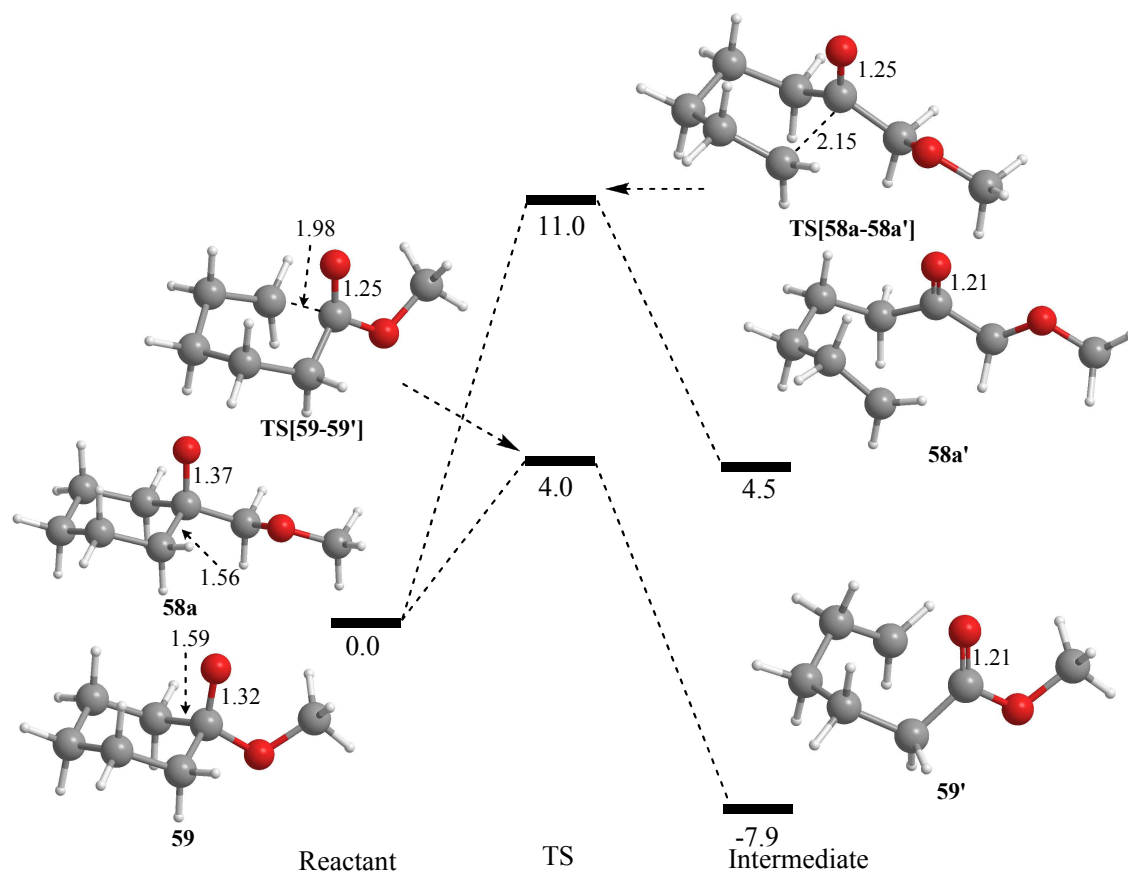
*Figure 9: The reaction profile for ring opening of oxy radical **58a** and **59**/ kcal mol^{-1}*
with molecular bond lengths/ Å

As previously shown in *Chapter 2*, the complete fragmentation of the *dispiro*-1,2,4-trioxanes during the thermolysis has been observed by GC analysis of the crude product mixture to form ketones and formaldehyde (not seen by GC). To investigate the energies involved in these processes the barriers associated with the cleavage of C(2)-C(8) in **58** and C(2)-O(8) in **59** were calculated (*Scheme 13*).
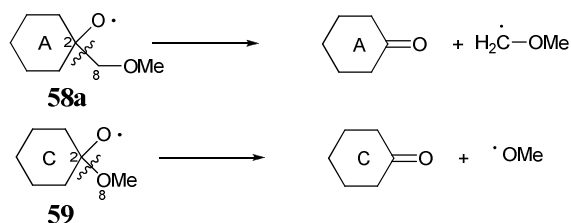
Scheme 13

Modelling studies to cleave the C(2)-C(8) bond in radicals **58a** found a transition state at 4.4 kcal mol^{-1}. Although this energy is competitive with the activation energy for the ring opening of ring **C** the nature of the model allows for a close range interaction of *ca.* 2.27 Å between hydrogens on the methoxy group and O(8) as illustrated in

TS[58a-58a‴] *(Figure 10) (Tables 4 and 5)*. This stabilising interaction would lower the energy of the transition state unrealistically as the interaction could not occur in the full system, where the hydrogens would be replaced by carbons of ring **C**. The close range interaction was artificially prevented by fixing the dihedral angle of the leaving group and quaternary carbon to 180°. In this arrangement the energy associated with **TS[58a-58a‴]** was *ca.* 12 kcal mol^{-1} higher in energy than the unrestricted transition state. Although neither transition state can be considered to model the true situation, the actual transition state is expected to be between the two energies. The transition states associated with the cleavage of C(2)-C(8) have been calculated for each small model contained within this chapter and all contain the additional close-range interaction and vary slightly in energy. Although these values are quoted in this chapter, the barriers are expected to be lower than the 'real' value. The transition states associated with the complete fragmentation of the molecule are further investigated in the full model systems.
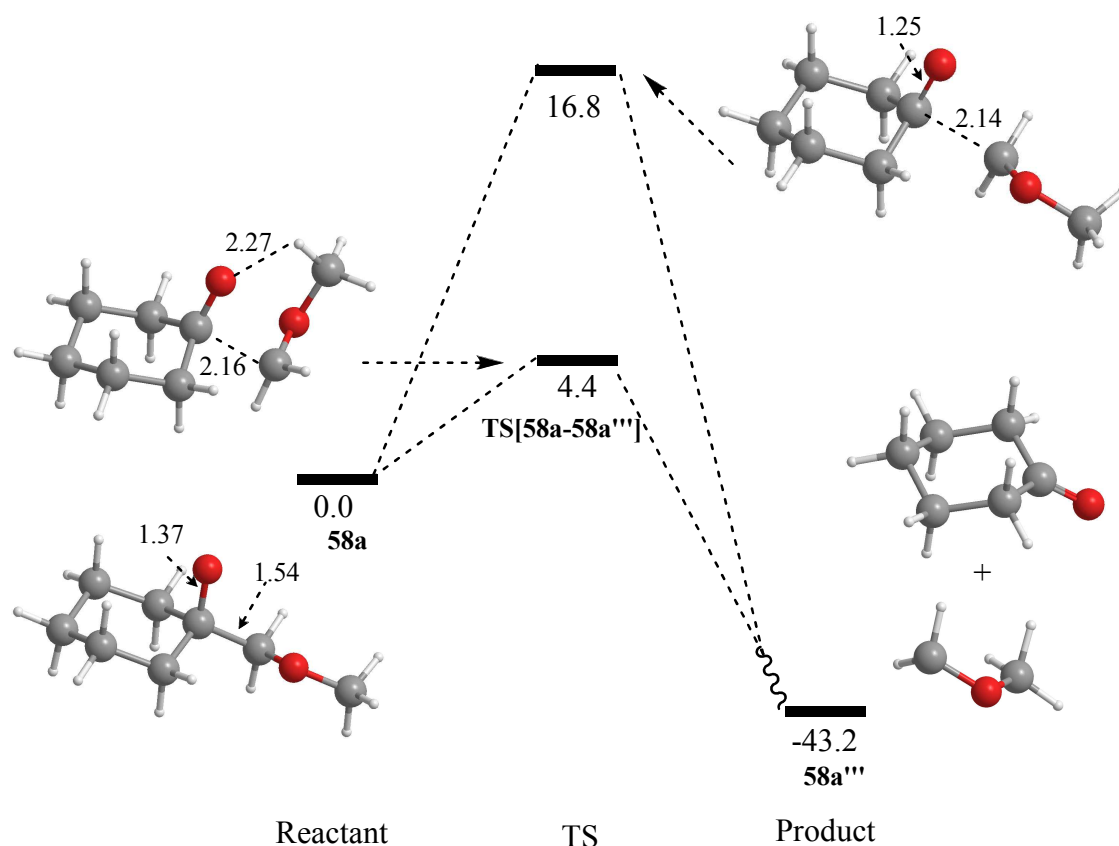
*Figure 10: The reaction profile C(2)-C(8) bond cleavage in **58a**/ kcal mol^{-1} with bond lengths in Å*
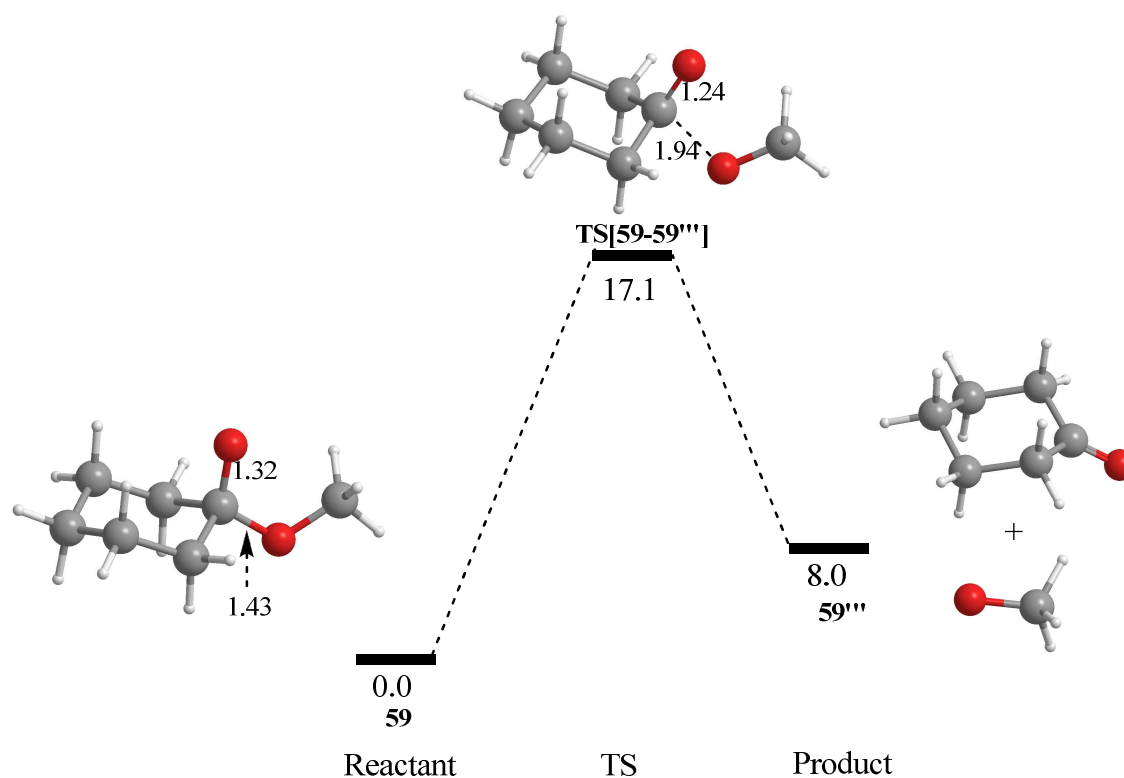
Figure 11: The reaction profile for C(2)-O(8) bond cleavage in 59/ kcal mol⁻¹ with bond lengths in Å

Modelling studies for the cleave of C(2)-O(8) in **59** showed the barrier to β-scission to be 17.1 kcal mol⁻¹, with the overall reaction being endothermic by 8.0 kcal mol⁻¹ *(Figure 11)*. This is in contrast to the cleavage of C(2)-C(3) which was substantially lower in energy and exothermic *(Tables 4 and 5)*. These processes are also further investigated in the large model systems.

	Reactant		TS		Intermediate	Product
	Bond lengths	energy	bond lengths	energy	bond lengths	energy
58a	C(2)-C(3)= 1.58 C(2)-O(1)= 1.37	11.0 *4.4	C(2)-C(3)= 2.15 C(2)-O(1)= 1.25	4.5	C(2)-O(1)= 1.22	2.7
59	C(2)-C(3)= 1.59 C(2)-O(1)= 1.32	4.0 #17.1	C(2)-C(3)= 1.98 C(2)-O(1)= 1.25	-7.9	C(2)-O(1)= 1.21	-9.0

Table 4: All energies given are related to reactant energy in each case

* TS of β-scission of other ring C(2)-C(8) bond # TS of β-scission of C(2)-O(8) bond

The product from the reaction is from the straight-chain open system

	Reactant	TS	Intermediate
	O(1)= 0.89	O(1)= 0.35	O(1)= 0
58a	C(2)= -0.03	C(2)= -0.08	C(2)= 0
	C(3)= 0.09	C(3)= 0.69	C(3)= 1.00
	O(1)= 0.72	O(1)= 0.37	O(1)= 0
59	C(2)= -0.03	C(2)= -0.05	C(2)= 0
	C(3)= 0.12	C(3)= 0.57	C(3)= 1.02

*Table 5: Natural spin densities at selected positions for the ring opening of ring **C***

The effect of α-Me and α-OMe substituents on β-scission of ring A

The change in the products obtained from different *dispiro*-1,2,4-trioxanes highlighted above indicate that the barrier associated with opening of ring **A** is changing with varying substituents. This study is designed to access the effect of α-substituents, R, has on the opening of ring **A**, where R= Me or OMe *(Scheme 14)*.

Through analysis of X-ray crystal structures of substituted *dispiro*-1,2,4-trioxanes discussed in *Chapter 1,* the α-substituent was shown to be positioned *trans* with respect to the peroxide oxygens and in an axial orientation with respect to ring **A**. Although the alternative regioisomer where the α-substituent is *cis* with respect to the peroxide oxygens has also been considered, more emphasis will be given to the results obtained with the α-substituent in a *trans* position.

The addition of an α-substituent makes the model unsymmetrical meaning there are potentially two competing β-scission sites which can initiate ring opening *(Scheme 14)*. Due to the formation of a secondary carbon-centred radical (**58b,c′**) from cleaving C(2)-C(3) compared to a primary carbon-centred radical (**58b,c″**) from the cleaving of C(2)-C(3′), it was expected that the transition state associated with the later process would be substantially higher in energy.
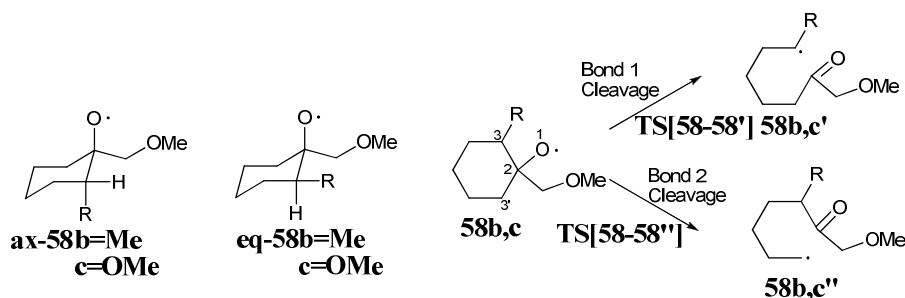
Scheme 14

The calculated activation barrier for the ring opening of methyl-substituted radical **ax-58b** at C(2)-C(3) show a reduction in energy of 5.5 kcal mol^{-1} compared to the unsubstituted model **58a** *(Figure 11)*. There is a clear preference for the opening of the substituted C(2)-C(3) bond over the alternative C(2)-C(3′) cleavage. The shorter C(2)···C(3) distance of 2.11 Å and the longer C(2)-O(1) bond of 1.26 Å in the transition state for C(2)-C(3) cleavage demonstrates an earlier transition state than that of the cleavage of C(2)-C(3′). The opening of **ax-58b** to form **ax-58b'** is also mildly exothermic by 0.4 kcal mol^{-1} which is in contrast to the opening of **58a** which was endothermic by 4.9 kcal mol^{-1}. Although the barrier has decreased by 5.5 kcal mol^{-1} from the unsubstituted model **58** the transition state is still 2.5 kcal mol^{-1} higher in energy than the opening of C(2)-C(3) for ring **C** in model **59**. The lowering of the barrier for the opening of ring **A** is consistent with the isolation of keto lactone from the thermolysis of methyl-substituted *dispiro*-1,2,4-trioxane **54b**. However, as oxalactone is still the major product from the thermolysis this suggests that the two separate ring opening reactions do not occur equally, and that the opening of ring **C** followed by the recombination to make a new C-O bond is still favoured.
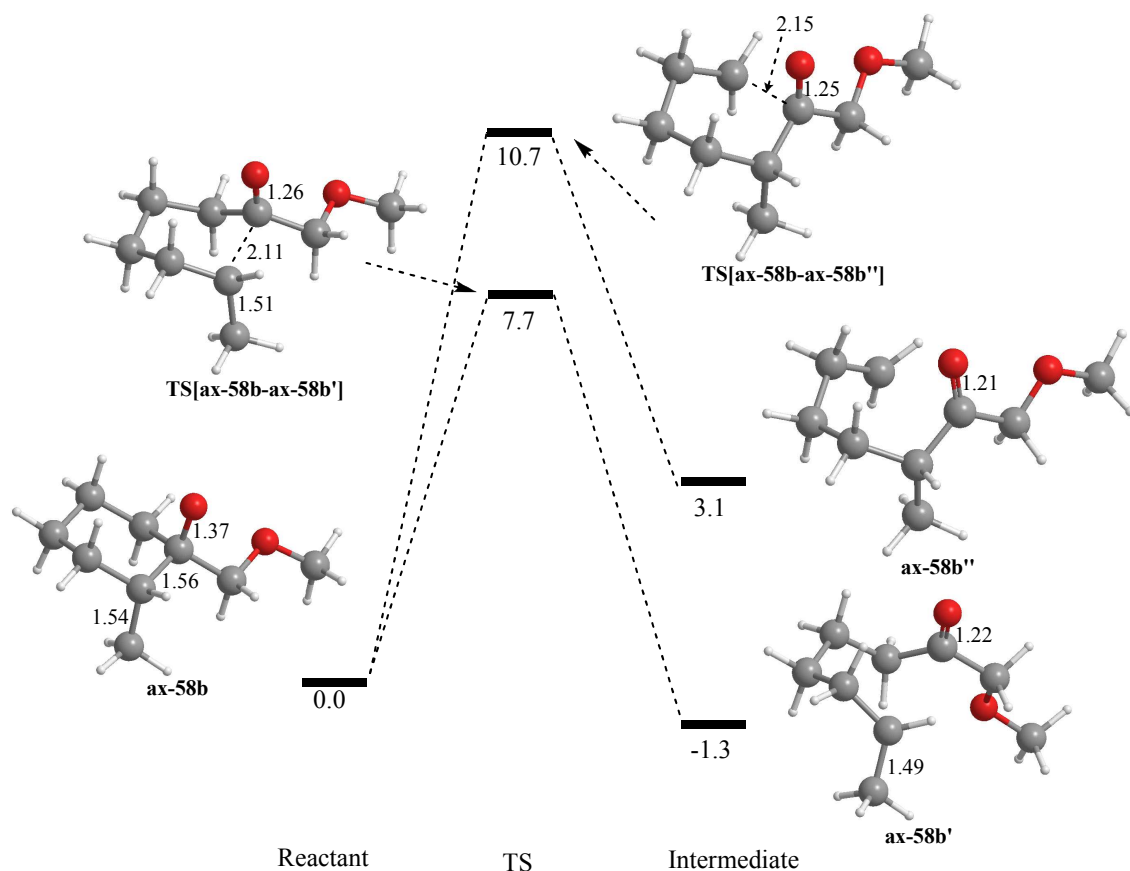
*Figure 11: The reaction profile for ring opening of oxy radical **ax-58b**/ kcal mol^{-1}*
with molecular bond lengths/ Å

Calculated activation barriers for the ring opening of methoxy-substituted radicals **ax-58c** also show a reduction in energy of 8.7 kcal mol^{-1} compared to the unsubstituted model **58a**. There is again clear preference for the opening of the substituted C(2)-C(3) bond over the alternative C(2)-C(3′) bond *(Figure 12)*. Interestingly, the barrier via **TS[ax-58c- ax-58c′]** for the opening of the C(2)-C(3) bond is now 0.7 kcal mol^{-1} lower in energy than the opening of C(2)-C(3) in ring **C** in **59**. This suggests a change in the preferred site of β-scission towards the opening of ring **A**. In addition to the low transition state barrier of 4.5 kcal mol^{-1} the overall ring opening step to form **ax-58c′** is exothermic by 5.0 kcal mol^{-1}. The shorter C(2)···C(3) bond of 2.06 Å in **TS[ax-58c- ax-58c′]** compared to 2.11 Å in **TS[ax-58b- ax-58b′]** suggests an earlier more accessible transition state. **TS[ax-58c-ax-58c′]** also shows a shortening of the C(3)-Sub bond distance from 1.43 Å in **ax-58c** to 1.37 Å consistent with the developing radical character being shared by the substituent itself.
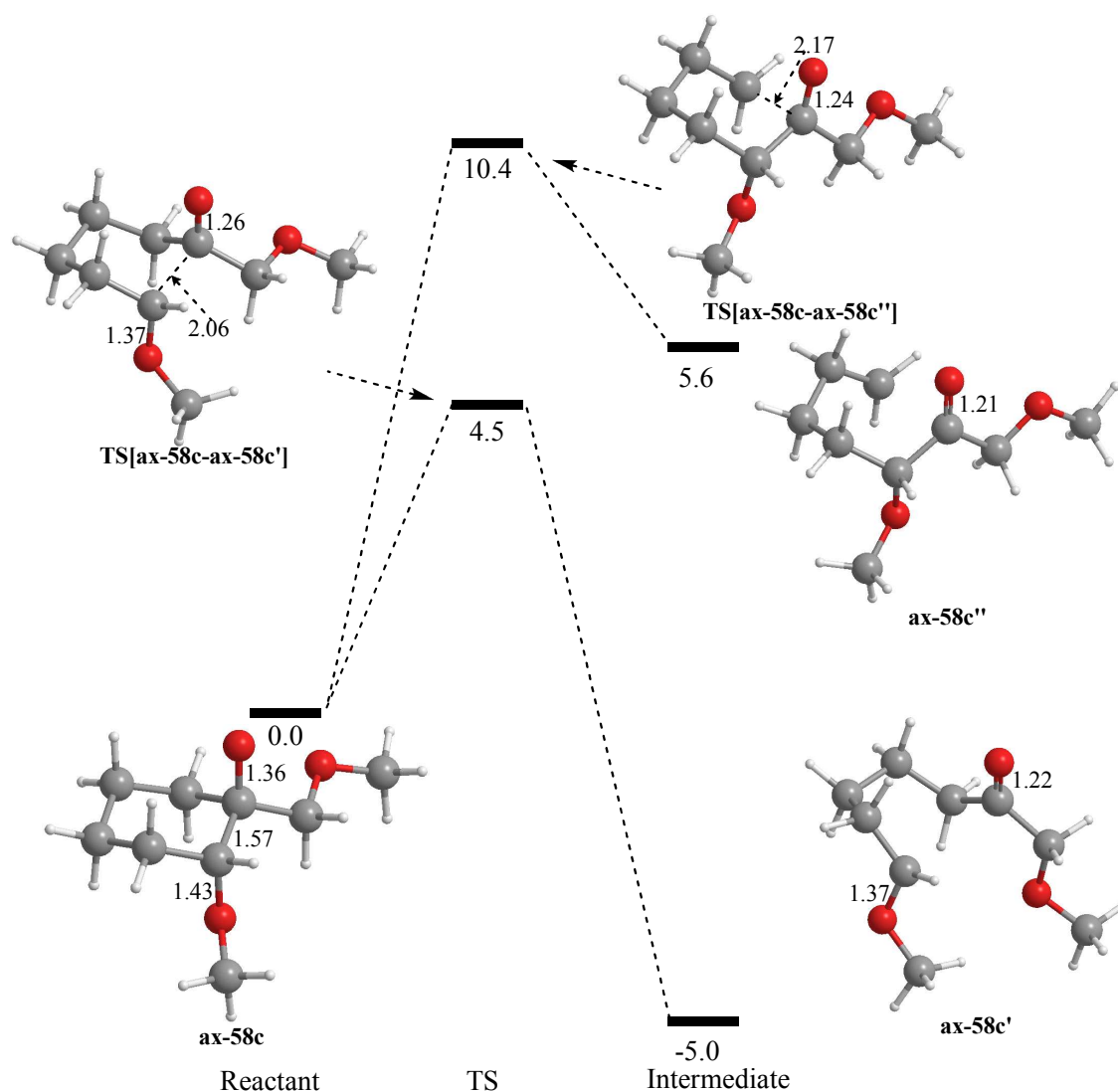
*Figure 12: The reaction profile for ring opening of oxy radical **ax-58c**/ kcal mol^{-1} with molecular bond lengths/ Å*

Although the energy barrier for the opening of the C(2)-C(3′) bond varies for the different R groups discussed, it remains consistently higher in energy than the substituted C(2)-C(3) bond. Therefore the barriers will be included in future tables but will not be discussed. Moreover, when the position of the substituent is equatorial and *cis* to the oxy radical in **eq-58b** and **eq-58c**, the energies associated with the reactions do not change significantly. Also the same trends in bond lengths and angles seen in cases where the substituent is *trans* to the oxy radical are repeated in the *cis* models.

The energies associated with the various β-scission reactions are illustrated in *Table 6* and show a systematic lowering of the transition state energy and overall reaction energy as the substituent is changed from R=H to R=Me to R=OMe. This finding is consistent with the increase isolated yields of keto lactone and lower isolated yield of oxalactone as you move from hydrogen to methyl to methoxy.

	R	Reactant		TS		Intermediate	Product
		Bond lengths	energy	bond lengths	energy	bond lengths	energy
58a	H	C(2)-C(3)= 1.58 C(2)-O(1)= 1.37	11.0 *4.4	C(2)-C(3)= 2.15 C(2)-O(1)= 1.25	4.5	C(2)-O(1)= 1.22	2.7
ax-58b	Me (ax)	C(2)-C(3)= 1.56 C(2)-O(1)= 1.37 C(3)-Sub= 1.54	7.7 *10.7 # 9.6	C(2)-C(3)= 2.11 C(2)-O(1)= 1.26 C(3)-Sub= 1.51	-1.3	C(2)-O(1)= 1.22 C(3)-Sub= 1.49	-4.3
ax-58c	OMe (ax)	C(2)-C(3)= 1.57 C(2)-O(1)= 1.36 C(3)-Sub= 1.43	4.5 *10.4 # 3.5	C(2)-C(3)= 2.06 C(2)-O(1)= 1.26 C(3)-Sub= 1.37	-5.0	C(2)-O(1)= 1.22 C(3)-Sub= 1.37	-3.6
eq-58b	Me (eq)	C(2)-C(3)= 1.57 C(2)-O(1)= 1.37 C(3)-Sub= 1.54	7.1 *10.5 # 2.9	C(2)-C(3)= 2.10 C(2)-O(1)= 1.25 C(3)-Sub= 1.50	-2.5	C(2)-O(1)= 1.22 C(3)-Sub= 1.49	-2.3
eq-58c	OMe (eq)	C(2)-C(3)= 1.56 C(2)-O(1)= 1.37 C(3)-Sub= 1.42	5.4 *12.0 # 5.4	C(2)-C(3)= 2.04 C(2)-O(1)= 1.26 C(3)-Sub= 1.36	-4.4	C(2)-O(1)= 1.22 C(3)-Sub= 1.36	-4.3

Table 6: All energies given are related to reactant energy in each case

* TS of β-scission of other ring C(2)-C(3') bond # TS of β-scission of C(2)-C(8) bond

The product from the reaction is from the straight-chain open system

Initial calculations of the full model systems indicated that a further close range interaction exists between the methoxy substituent and the ether oxygen of the 1,2,4-trioxane ring, as illustrated in **60**. To facilitate this interaction in the small model systems the ether group in oxy radical **ax-58c** was rotated to bring the interacting parts close together as illustrated in *Figure 13*. This close range interaction between the ether oxygen and one methoxy hydrogen (O···H **=** 2.46 Å) initiates a *pseudo* seven-membered ring within the molecule. The length of the substituted C(2)-C(3) bond increases from 1.57 Å to 1.62 Å indicating substantial delocalisation of the radical character from the oxy radical. Further evidence of this is the shorter C(2)-O(1) bond of 1.35 Å. Additionally the shorter C(3)-O bond of 1.41 Å indicates the radical character is further delocalised onto the methoxy substituent. The structural changes within the reactant suggested the barrier for the cleavage of C(2)-C(3) would be affected.
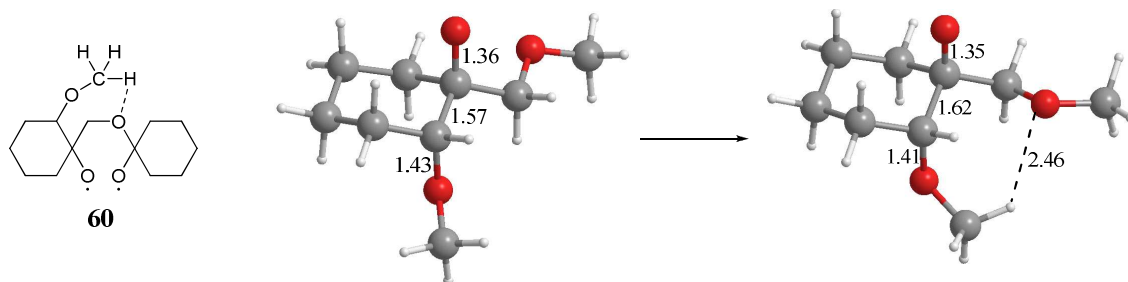
Figure 13

Although the transition state for the cleavage of C(2)-C(3) gives a shortening of the close range interaction between the ether oxygen and one methoxy hydrogen (O···H**=** 2.35 Å) the other bond lengths within the molecule remain approximately the same as the model with no close range interaction. The barrier for **TS[ax-58c-ax-58c′]** has however reduced by 2.7 kcal mol^{-1} to 1.8 kcal mol^{-1} *(Figure 14)*. The transition state relaxes to form **ax-58c′** at -2.2 kcal mol^{-1} giving an overall exothermic process. Although the close interaction between the ether oxygen and one methoxy hydrogen (O···H**=** 2.70 Å) has lengthened it is still present in **ax-58c′**.
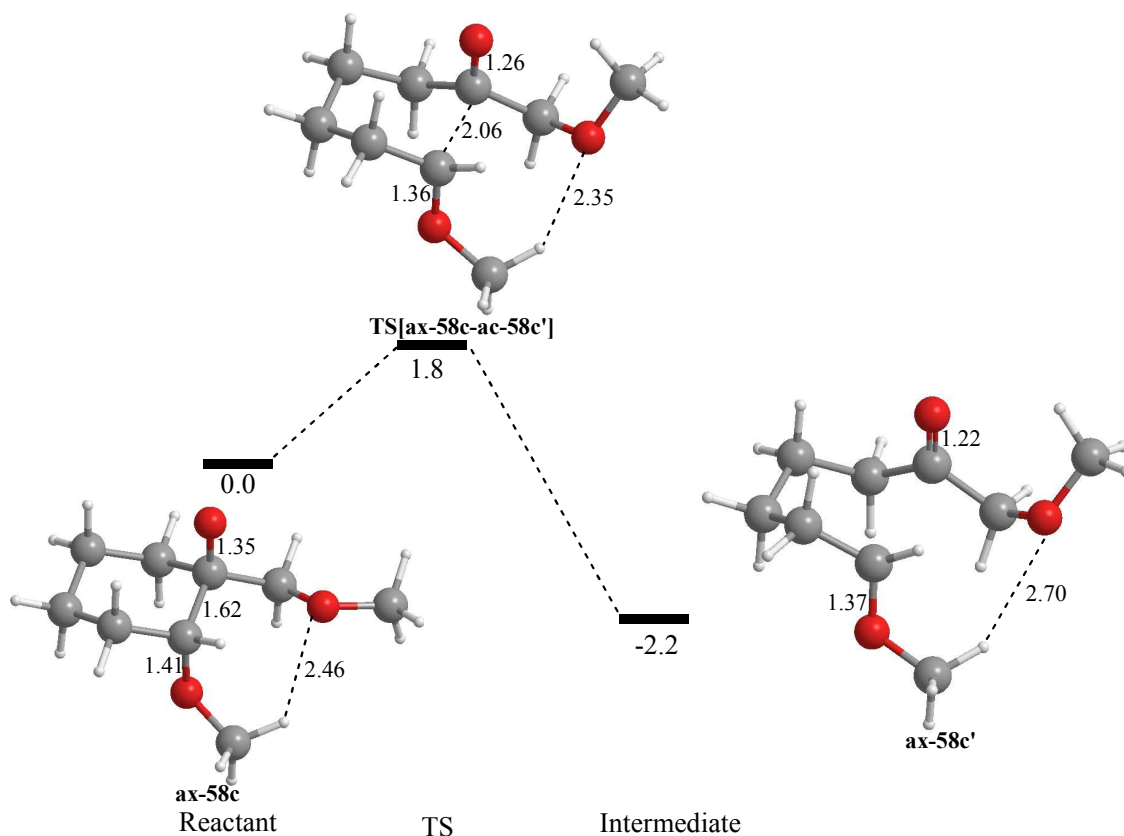
*Figure 14: The reaction profile for ring opening of oxy radical **ax-58c**/ kcal mol^{-1}*
with molecular bond lengths/ Å

Similarly in the methyl model **ax-58b**, a rotation of the ether group can facilitate a close range interaction between the ether oxygen and one methyl hydrogen (O···H= 2.63 Å) as illustrated in *Figure 15*. The interaction within **ax-58b** is 0.17 Å longer than the corresponding methoxy-substituted **ax-58c** because there is no flexibility in the position of the methyl carbon meaning the close range interaction cannot be optimised. Methyl substituted **ax-58c** has a lengthened substituted C(2)-C(3) bond of 1.60 Å whilst no other bond lengths have changed significantly.
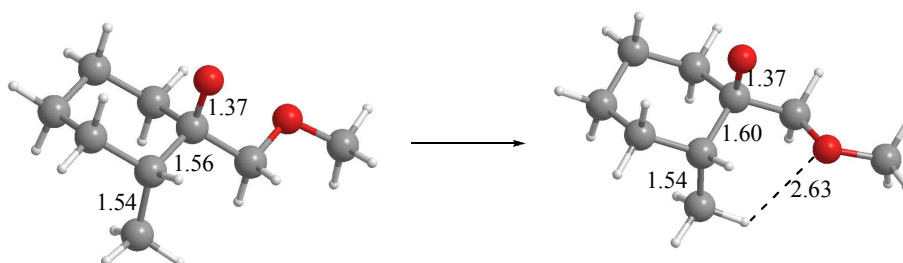
Figure 15

Despite the lengthening of the C(2)-C(3) to 1.60 Å, the energy associated with **TS[ax-58b-ax-58b′]** energy is not affected by the close range interaction *(Figure 16)*. In

TS[ax-58b-ax-58b′] the close range interaction has increased in length from 2.63 Å in **ax-58b** to 2.76 Å. The fixed position nature of the methyl group means that as the length of the C-C bond is increased the close range interaction between the ether oxygen and one methyl hydrogen automatically has to increase as well. Although the intermediate **ax-58b′** is exothermic with respect to the reactant the reaction has also interrupted the interaction between the ether oxygen and methyl hydrogen.
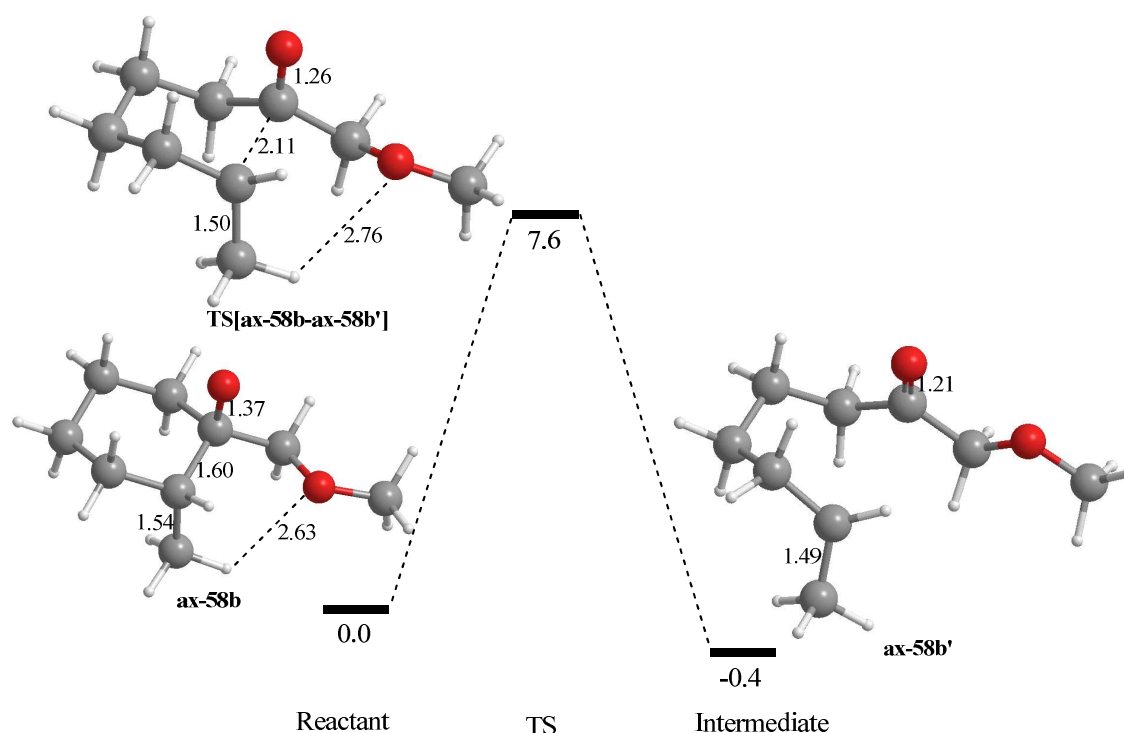
*Figure 16: The reaction profile for ring opening of oxy radical **ax-58b**/ kcal mol^{-1} with bond lengths in Å*

The energies associated with the β-scission reactions which contain the additional close interaction are illustrated in *Table 7* and continue to show a systematic lowering of the transition state energy and overall reaction energy as the substituent is changed from R= H to R=Me to R=OMe. Additionally they show how an additional close range interaction further reduces the transition state barrier where there is a methoxy substituent. This important observation indicates that the additional close range interaction facilitates the lowering of the barrier to be directly competitive with the opening of ring **C**. Moreover, the results correlate well with the experimental results for the thermolysis of alkoxy-substituted *dispiro*-1,2,4-trioxanes which showed exclusive isolation of the fully ring expanded product.

	R	Reactant		TS		Intermediate	Product
		Bond lengths	energy	bond lengths	energy	bond lengths	energy
ax-58b	Me (ax)	C(2)-C(3)= 1.60 C(2)-O(1)= 1.37 C(3)-Sub= 1.54 H Bond= 2.63	7.6 *11.6 # 5.0	C(2)-C(3)= 2.11 C(2)-O(1)= 1.26 C(3)-Sub= 1.50 H Bond= 2.75	-0.4	C(2)-O(1)= 1.21 C(3)-Sub= 1.49 H Bond= 4.53	-3.4
ax-58c	OMe (ax)	C(2)-C(3)= 1.62 C(2)-O(1)= 1.35 C(3)-Sub= 1.41 H Bond= 2.46	1.8 *11.8 # 4.8	C(2)-C(3)= 2.06 C(2)-O(1)= 1.26 C(3)-Sub= 1.36 H Bond= 2.35	-2.2	C(2)-O(1)= 1.22 C(3)-Sub= 1.37 H Bond= 2.71	-2.2
eq-58b	Me (eq)	C(2)-C(3)= 1.57 C(2)-O(1)= 1.37 C(3)-Sub= 1.54 H Bond= 2.40	6.6 *10.1 # 1.9	C(2)-C(3)= 2.10 C(2)-O(1)= 1.26 C(3)-Sub= 1.50 H Bond= 2.36	-1.5	C(2)-O(1)= 1.21 C(3)-Sub= 1.49 H Bond= 3..62	-3.3
eq-58c	OMe (eq)	C(2)-C(3)= 1.64 C(2)-O(1)= 1.34 C(3)-Sub= 1.39 H Bond= 2.70	2.8 *13.6 # 8.7	C(2)-C(3)= 2.08 C(2)-O(1)= 1.26 C(3)-Sub= 1.35 H Bond= 2.75	-1.9	C(2)-O(1)= 1.22 C(3)-Sub= 1.37 H Bond= 2.78	-4.1

Table 7: All energies given are related to reactant energy in each case in each case

* TS of β-scission of other ring C(2)-C(3') bond # TS of β-scission of C(2)-C(8) bond

The product from the reaction is from the straight-chain open system

Analysis of the spin density distributions during the β-scission reactions of ax-58b and ax-58c

It is well-known that α-substituents, in particular those bearing lone pairs, stabilize C-centered radicals, the so-called "α-effect".[15,17] The effect of an oxygen atom on the stability of the adjacent carbon centred radical has been demonstrated in the above examples. A clear reduction in the barrier for the β-scission of a methoxy-substituted oxy radical **ax-58c** compared to an unsubstituted oxy radical **58** demonstrates the effect is enough to make the ring opening for **ax-58c** via **TS[ax-58c-ax-58c′]** competitive with the opening ring **C** in **59** via **TS[59-59′]**. To quantify this substituent effect on opening ring **A** we have performed a natural atomic orbital analysis[47] to obtain the spin density distributions for the stationary points associated with **58**, **58b**, and **58c** *(Table 7)*.

The results for each substituent show the anticipated transfer of spin density from O(1) in the reactants onto C(3) in the transition states and products. The reactants **58a**, **58b**

and **58c** have increasing spin densities on the substituent (0.06 for **ax-58c**) on progressing from the H to Me to OMe substituents, demonstrating a delocalisation of radical character onto that site. For **TS[58-58′]** the redistributed spin density is localized on C(3) however, in **TS[ax-58c-ax58c′]** a significant contribution (0.13) is localized on the methoxy substituent. This delocalization serves to stabilize **TS[ax-58c-ax58c′]** and thus significantly lowers the barrier to ring opening. For **TS[ax-58b-ax58b′]** the situation is intermediate between those of **TS[58-58′]** and **TS[ax-5c-ax58c′]**. The changes in spin density from reactant to transition state also show that **TS[ax-58c-ax58c′]** is more reactant-like than the others indicating an earlier transition state consistent with the Hammond Postulate[23] *(Table 8).* The α-substituent further stabilizes the radical character of the intermediate with increased spin density on the substituent along the series R= H, R=Me and R= OMe.

	R	Reactant	TS	Intermediate
58a	H	O(1)= 0.89 C(2)= -0.03 C(3)= 0.09 α-H= 0	O(1)= 0.35 C(2)= -0.08 C(3)= 0.69 α-H= -0.03	O(1)= 0 C(2)= 0 C(3)= 1.00 α-H= -0.03
ax-58b	Me	O(1)= 0.88 C(2)= -0.03 C(3)= 0.09 Sub= 0.01	O(1)= 0.40 C(2)= -0.06 C(3)= 0.58 Sub= 0.02	O(1)= 0.01 C(2)= 0 C(3)= 0.93 Sub= 0.03
ax-58c	OMe	O(1)= 0.80 C(2)= -0.03 C(3)= 0.11 Sub= 0.06	O(1)= 0.38 C(2)= -0.02 C(3)= 0.45 Sub= 0.13	O(1)= 0.06 C(2)= 0 C(3)= 0.76 Sub= 0.13
eq-58b	Me	O(1)= 0.88 C(2)= -0.03 C(3)= 0.09 Sub= 0.00	O(1)= 0.35 C(2)= -0.08 C(3)= 0.69 Sub= 0.01	O(1)= 0 C(2)= 0 C(3)= 1.00 Sub= 0.04
eq-58c	OMe	O(1)= 0.74 C(2)= -0.02 C(3)= 0.11 Sub= 0.09	O(1)= 0.36 C(2)= -0.02 C(3)= 0.64 Sub= 0.15	O(1)= 0 C(2)= 0 C(3)= 0.79 Sub= 0.16

*Table 8: Natural spin densities at selected positions for the ring opening of ring **C***

Investigation of oxy radical 61

It was clear that the significant lowering of the barrier towards β-scission of the methoxy-substituted oxy radical **58c**, is due to a combination of effects. Firstly, the oxygen substituent provides stabilisation of the radical character developing on the incipient carbon and, secondly, the CH_3 group of the methoxy substituent forms a close range interaction with the oxygen of the ether group. In order to further quantify the stabilisation effect of an oxygen in the α-position, β-scission reactions of **61** were investigated. Oxy radical **61** contains a pyranone ring with O(4) expected to provide a similar stabilisation effect seen for the methoxy substituent. Importantly, as the stabilising oxygen atom is contained within the ring, no short range interactions can be formed with the ether oxygen *(Figure 17)*. It is expected however that the energy for the β-scission will be slightly higher due to the formation of a primary radical centre.
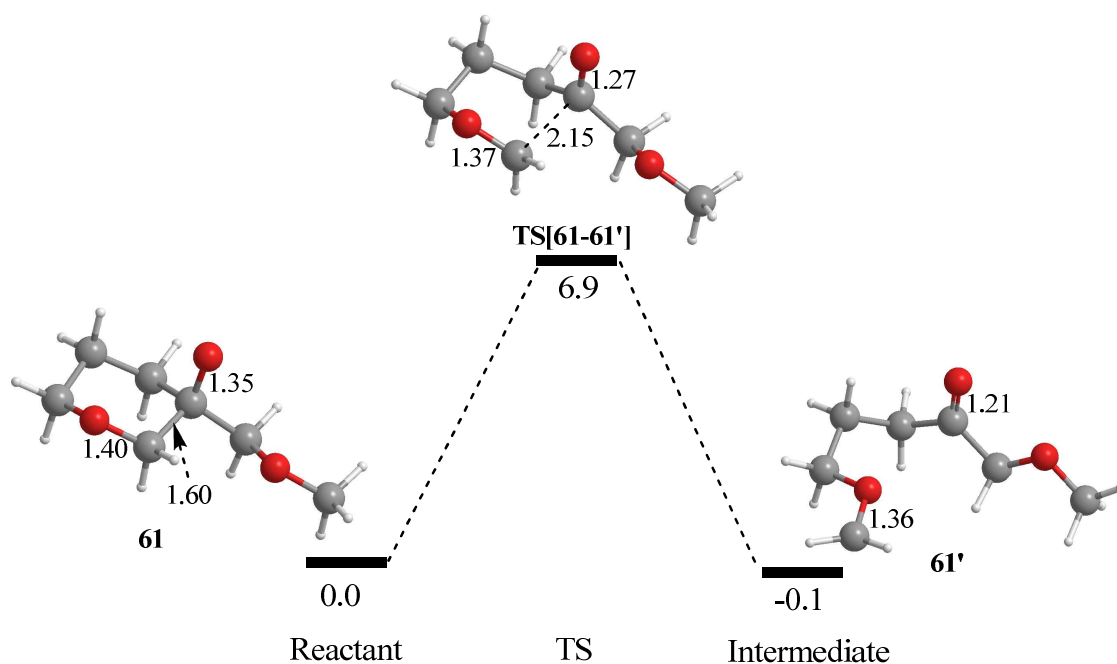
*Figure 17: The reaction profile for ring opening of oxy radical **14**/ kcal mol^{-1}*
with molecular bond lengths/ Å

The reactant oxy radical **61** shows an elongated C(2)-C(3) of 1.60 Å and a shortened C(2)-O(1) bond of 1.35 Å. The C(2)-C(3) bond however has not elongated as much as in **ax-58c** (1.62 Å) *(Table 9)*. The C(2)-C(3) bond cleaves to give a transition state at 6.9 kcal mol^{-1}, 6.2 kcal mol^{-1} lower in energy than the unsubstituted model **58** and 5.1 kcal mol^{-1} higher than the barrier for the methoxy model **ax-58c**. Additionally the reaction is nearly energetically neutral compared to the exothermic reaction observed for the

methoxy model. The spin density distributions for the stationary points associated with the β-scission show a transfer of character from O(1) to C(3), similar to that seen for the reaction of **ax-58c**. The pyranone model **61** however has a greater spin density on the terminal C(3) than was seen for **ax-58c** which is indicative of a later, less favourable transition state. O(4), which is expected to share the radical character with C(3), has a spin density of 0.14 in the transition state which is the approximately the same as was seen for the methoxy-oxygen in **ax-58c** *(Table 10)*. It is apparent therefore that despite the oxygen atom providing a major stabilising effect on the β-scission reaction without the additional close range interaction seen in the reaction of **ax-58c** the barrier remains higher than the β-scission of ring **C**.

		Reactant		TS		Intermediate	Product
		Bond lengths	energy	bond lengths	energy	bond lengths	energy
61		C(2)-C(3)= 1.60	6.9	C(2)-C(3)= 2.15	-0.1	C(2)-O(1)= 1.21	-0.1
		C(2)-O(1)= 1.35	*13.6	C(2)-O(1)= 1.27		C(3)-O(4)= 1.36	
		C(3)-O(4)= 1.40	# 6.7	C(3)-O(4)= 1.37			

Table 9: All energies given are related to reactant energy in each case in each case
* TS of β-scission of other ring C(2)-C(3') bond # TS of β-scission of C(2)-C(8) bond
The product from the reaction is from the straight-chain open system

		Reactant	TS	Intermediate
61		O(1)= 0.84	O(1)= 0.32	O(1)= 0
		C(2)= -0.03	C(2)= -0.04	C(2)= 0
		C(3)= 0.09	C(3)= 0.55	C(3)= 0.87
		O(4)= 0.03	O(4)= 0.14	O(4)= 0.24

*Table 10: Natural spin densities at selected positions for the ring opening of ring **C***

Conclusion

Calculations on the small model systems have provided good correlation between calculated transition state barriers for β-scission of the C(2)-C(3) bond and the observed experimental products. The calculation of the barriers for the opening of rings **A** and **C** of an unsubstituted *dispiro*-1,2,4-trioxane showed a significantly larger barrier for the opening of ring **C** over ring **A,** consistent with the formation of oxalactone and not the fully ring expanded keto lactone.

Furthermore, the presence of 2-Me and 2-OMe substituents on ring **A** significantly decreases the ring-opening barrier making the process directly competitive with the opening of ring **C** in the methoxy example. It is apparent a methoxy group accelerates the opening of ring **A** because of the so called 'α-effect' where the carbon centred radical is stabilised by the adjacent oxygen of the methoxy substituent. In addition to the α-effect an intramolecular close range interaction (C-H⋯O) forming a *pseudo* seven-membered ring helps facilitate the opening of the C-C bond by causing an elongation of the bond in the reactant species. These effects seem to make the formation of the fully expanded keto lactone **4** more likely for R=OMe.

The effect of alternative α-substituents, R

The effect of further R groups, which have not been investigated experimentally, has been considered computationally to predict how other substituents may provide a similar α-effect on the β-scission reaction. The R groups studied were NX_2, OH, F, SiX_3, PX_2, SX and Cl (X= H, Me) and the carbon-based substituents phenyl, CN and CO_2Me.

The model chosen for this study, **eq-58**, has the substituent equatorial with respect to the ring and *cis* to the oxygen radical. This conformation was chosen prior to the determination of X-ray crystal structures detailed in *Chapter 1* in which the substituent was shown to be axial *trans* to the oxygen radical. Although the barriers calculated are not on the expected conformation the stabilising α-effect of the substituent and subsequent trends are expected to be unaffected as seen for the R= Me and R= OMe models discussed above.

R=	e = NH$_2$	i = SiH$_3$	m = SiMe$_3$	p = Ph
	f = NMe$_2$	j = PH$_2$	n = PMe$_2$	q = CN
	g = OH	k = SH	o = SMe	r = COOMe
	h = F	l = Cl		

eq-58
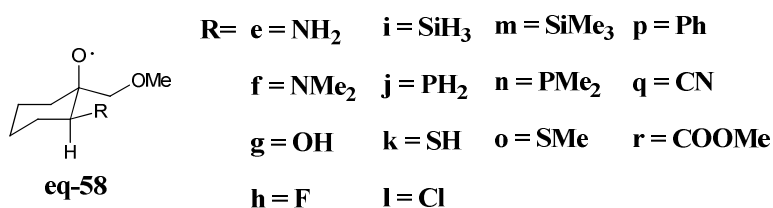
As seen above the manipulation of the model to facilitate a close range interaction between the external exocyclic oxygen and the substituent can help to cleave the C(2)-C(3) bond. As this important additional interaction has been seen in the initial calculations on the full model system, it has been further investigated with these

additional R groups. The results are reported in *Tables 11* to *18*. In all cases, reaction profiles have also been calculated without this beneficial interaction, but these generally have higher barriers and will not be discussed further in this section. Energies and geometries for these models are contained in *Table 1, Appendix 3*.

NX_2, OH, F (X= H, Me)

Amino (NH_2, NMe_2), hydroxy and fluorine substituents all provide lone pairs which can stabilise the carbon centred radicals, as described above.[15] Previous studies on carbon centred radicals with heteroatom α-substituents showed increased stability with decreased electronegativity of the substituent.[15] Thus the most stable radical contained a NMe_2 substituent whilst the least stable contained fluorine. Calculated activation barriers for the ring opening of first row element substituted radicals **58e** to **58h** at C(2)-C(3) show a similar trend with $NMe_2 \approx NH_2 <$ OH $<$ F *(Table 11)*.

The geometry and spin densities of the reactant species show a clear link between the delocalisation of the radical character towards the substituent and the barrier for ring opening *(Table 11)*. Ring opening via C(2)-C(3) bond cleavage where R = NH_2 (**58e**) or NMe_2 (**58f**) has been shown to be effectively a barrierless process. The nitrogen-based oxy radicals **58e** and **58f** contain elongated C(2)-C(3) bonds of 1.73 Å and 1.79 Å respectively, whilst both contain shortened C(2)-O(1) bonds of 1.31 Å. The lengthening of the C(2)-C(3) bond is accompanied by increased radical character on the C(3)-NH_2 and C(3)-NMe_2 groups of 0.28 and 0.42 respectively, with the C(3)-NMe_2 having a shorter C(3)-N bond by 0.02 Å *(Table 11)*.

In contrast the oxy radicals containing OH (**58g**) or F (**58h**) substituents have successively shorter C(2)-C(3) bonds of 1.64 Å and 1.55 Å and longer C(2)-O(1) bonds of 1.34 Å and 1.37 Å respectively. The changes in the geometry of the oxy radicals indicate less delocalisation of the radical character from O(1). The radical spin densities further prove this with the C(3)-OH and C(3)-F groups having natural spin densities of 0.15 and 0.06 respectively.

The C(2)⋯C(3) bond distances in the β-scission transition state are shorter in the reactions with a lower activation barrier consistent with the Hammond Postulate[23] *(Table 11)*. In each transition state the β-scission is accompanied by the expected

shortening of the carbonyl C(2)-O(1) distance and increased planarity at C(3) due to the further build-up of radical character. The radical character on the carbon is increasingly shared by the substituent in generally the same order as the activation barrier, i.e NH_2 > NMe_2 > OH > F. Although NMe_2 shows less radical character on C(3) than NH_2 there is more radical character on the NMe_2 group than NH_2. Interestingly **TS[58f-58f′]** has a greater spin density on the nitrogen than on C(3) demonstrating a major stabilisation of radical character. Upon complete cleavage of C(2)-C(3) the radical centre C(3) continues to be delocalised to varying degrees onto the heteroatom *(Table 12)*. The β-scission of nitrogen-substituted oxy radicals seem to be barrierless suggesting that if a nitrogen substituted *dispiro*-1,2,4-trioxane was thermolysed the β-scission of the C(2)-C(3) bond would occur spontaneously after the homolytic cleavage of the peroxide bond.

	R	Reactant		TS		Intermediate		Product
		Bond lengths	energy	bond lengths	energy	bond lengths		energy
58e	NH_2	C(2)-C(3)= 1.73 C(2)-O(1)= 1.31 C(3)-Sub= 1.42 H Bond= 2.08	-0.1 *13.6 # 5.2	C(2)-C(3)= 1.97 C(2)-O(1)= 1.27 C(3)-Sub= 1.39 H Bond= 2.09	-3.4	C(2)-O(1)= 1.22 C(3)-Sub= 1.39 H Bond= 2.36		-1.5
58f	NMe_2	C(2)-C(3)= 1.79 C(2)-O(1)= 1.31 C(3)-Sub= 1.40 H Bond= 2.31	-0.2 *15.7 # 11.0	C(2)-C(3)= 1.96 C(2)-O(1)= 1.28 C(3)-Sub= 1.38 H Bond= 2.28	-4.3	C(2)-O(1)= 1.22 C(3)-Sub= 1.39 H Bond= 2.55		-2.7
58g	OH	C(2)-C(3)= 1.64 C(2)-O(1)= 1.34 C(3)-Sub= 1.39 H Bond= 1.86	2.8 *13.2 # 6.0	C(2)-C(3)= 2.09 C(2)-O(1)= 1.25 C(3)-Sub= 1.35 H Bond= 1.83	0.5	C(2)-O(1)= 1.22 C(3)-Sub= 1.36 H Bond= 1.91		0.7
58h	F	C(2)-C(3)= 1.55 C(2)-O(1)= 1.37 C(3)-Sub= 1.39 H Bond= 2.78	8.7 *12.1 # 1.6	C(2)-C(3)= 2.10 C(2)-O(1)= 1.25 C(3)-Sub= 1.34 H Bond= 2.88	1.8	C(2)-O(1)= 1.20 C(3)-Sub= 1.39 H Bond= 3.75		-0.5

Table 11: All energies given are related to reactant energy in each case

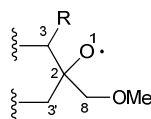** TS of β-scission of other ring C(2)-C(3') bond # TS of β-scission of C(2)-C(8) bond*

The product from the reaction is from the straight-chain open system

	R	Reactant	TS	Intermediate
58e	NH$_2$	O(1)= 0.65 C(2)= 0 C(3)= 0.17 Sub= 0.11	O(1)= 0.43 C(2)= 0 C(3)= 0.33 Sub= 0.16	O(1)= 0.06 C(2)= 0.03 C(3)= 0.68 Sub= 0.24
58f	NMe$_2$	O(1)= 0.47 C(2)= 0 C(3)= 0.15 Sub= 0.27	O(1)= 0.37 C(2)= 0.03 C(3)= 0.24 Sub= 0.27	O(1)= 0.05 C(2)= 0.02 C(3)= 0.66 Sub= 0.23
58g	OH	O(1)= 0.81 C(2)= -0.03 C(3)= 0.12 Sub= 0.03	O(1)= 0.37 C(2)= -0.05 C(3)= 0.46 Sub= 0.11	O(1)= 0.08 C(2)= 0.01 C(3)= 0.74 Sub=0.13
58h	F	O(1)= 0.90 C(2)= -0.04 C(3)= 0.06 Sub= 0	O(1)= 0.38 C(2)= -0.07 C(3)= 0.56 Sub= 0.07	O(1)= 0.03 C(2)= 0 C(3)= 0.86 Sub= 0.08

*Table 12: Natural spin densities at selected positions for the ring opening of ring **C***

SiX$_3$, PX$_2$, SX and Cl (X= H, Me)

The incorporation of silyl (SiH$_3$, SiMe$_3$), phosphino (PH$_2$, PMe$_2$), thiol (SH, SMe) and Cl based R groups has also been considered in this study. With the exception of the silyl groups each substituent should provide a stabilising effect from a lone pair of electrons, as described above. Each of the substituents studied has a lower barrier than the unsubstituted model **58** and β-scission is overall moderately exothermic in each case.

Unlike the geometries and spin densites shown in *Tables 11* and *12* for NX$_2$, OH, F (X= H, Me) the reactants do not show a clear link between the delocalisation of the radical character towards the substituent and the transition state energy barrier for ring opening *(Table 14)*. In general there is less elongation of C(2)-C(3), a longer C(2)-O(1) bond distance and less radical character on C(3), all indicative of the higher transition states seen for models with silyl, phosphorus, thiol and Cl R groups.

Calculated ring opening activation energies show the highest energy barriers for **58i**, (R=SiH$_3$ 8.3 kcal mol^{-1}) and **58l**, (R=Cl 8.7 kcalmol^{-1}) and these correspond loosely to the substituents with the lowest spin density in the transition state. Although chlorine in **58l** has a spin density similar to that of PH$_2$ there is no short range interaction between the chlorine and the ether oxygen in the transition state (Cl···O= 3.23, P-H···O= 2.33 Å).

The addition of a silyl α-substituent in oxy radical **58i** produces an activation energy higher than that seen in the methyl model **ax-58b**. The close range interaction in **58i** (Si-H···O = 2.78 Å) is 0.15 Å longer than that seen for **ax-58b**. In addition **58i** has a shorter C(2)-C(3) bond of 1.56 Å indicative a more difficult cleavage *(Table 13)*.

In contrast, where the R= PH$_2$ (**58j**) or R= SH (**58k**) the transition state barriers are lower at 5.7 kcal mol^{-1} and 3.8 kcal mol^{-1} respectively. The SH substituent in **58k** induces a longer C(2)-C(3) bond of 1.61Å compared to 1.57 Å in **58j** R= PH$_2$. Consistent with this is the larger natural spin density on the thiol substituent throughout the reaction of **58k** indicative of a more favourable process. The order of the barrier heights for second row substituents was therefore SH < PH$_2$ < SiH$_3$ ≈ Cl which does not follow the pattern of electronegativity seen for first row substituents but is consistent with previously studied α-effects.[15]
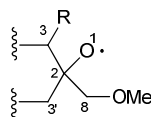
		Reactant		TS		Intermediate	Product
	R	Bond lengths	energy	bond lengths	energy	bond lengths	energy
58i	SiH$_3$	C(2)-C(3)= 1.56 C(2)-O(1)= 1.37 C(3)-Sub= 1.92 H Bond= 2.78	8.3 *9.5 # 5.5	C(2)-C(3)= 2.08 C(2)-O(1) 1.26 C(3)-Sub= 1.90 H Bond= 2.77	-2.5	C(2)-O(1) 1.21 C(3)-Sub= 1.86 H Bond= 3.31	-4.9
58j	PH$_2$	C(2)-C(3)= 1.57 C(2)-O(1)= 1.36 C(3)-Sub= 1.90 H Bond= 2.34	5.7 *8.4 # 1.4	C(2)-C(3)= 2.03 C(2)-O(1)= 1.26 C(3)-Sub= 1.84 H Bond= 2.33	-5.6	C(2)-O(1)= 1.21 C(3)-Sub= 1.80 H Bond= 2.96	-7.5
58k	SH	C(2)-C(3)= 1.61 C(2)-O(1)= 1.36 C(3)-Sub= 1.84 H Bond= 2.95	3.8 *8.5 # 2.9	C(2)-C(3)= 1.99 C(2)-O(1)= 1.27 C(3)-Sub= 1.77 H Bond= 3.34	-8.1	C(2)-O(1)= 1.22 C(3)-Sub= 1.75 H Bond= 3.15	-8.5
58l	Cl	C(2)-C(3)= 1.56 C(2)-O(1)= 1.36 C(3)-Sub= 1.83 H Bond= 3.10	8.7 *10.4 # -0.1	C(2)-C(3)= 2.03 C(2)-O(1)= 1.26 C(3)-Sub= 1.75 H Bond= 3.23	-2.8	C(2)-O(1)= 1.21 C(3)-Sub= 1.74 H Bond= 4.42	-5.4

Table 13: All energies given are related to reactant energy in each case

* TS of β-scission of other ring C(2)-C(3') bond # TS of β-scission of C(2)-C(8) bond

The product from the reaction is from the straight-chain open system

	R	Reactant	TS	Intermediate
5i	SiH$_3$	O(1)= 0.86 C(2)= -0.03 C(3)= 0 Sub= 0	O(1)= 0.43 C(2)= -0.08 C(3)= 0.60 Sub= 0.01	O(1)= 0 C(2)= 0 C(3)= 0.94 Sub= 0.03
5j	PH$_2$	O(1)= 0.88 C(2)= -0.04 C(3)= 0.01 Sub= 0	O(1)= 0.44 C(2)= -0.07 C(3)= 0.48 Sub= 0.07	O(1)= 0 C(2)= 0 C(3)= 0.87 Sub= 0.07
5k	SH	O(1)= 0.84 C(2)= -0.04 C(3)= 0.11 Sub= 0.03	O(1)= 0.44 C(2)= -0.06 C(3)= 0.43 Sub= 0.13	O(1)= 0 C(2)= 0 C(3)= 0.82 Sub= 0.15
5l	Cl	O(1)= 0.89 C(2)= -0.04 C(3)= 0.02 Sub= 0	O(1)= 0.45 C(2)= -0.09 C(3)= 0.52 Sub= 0.07	O(1)= 0 C(2)= 0 C(3)= 0.88 Sub= 0.09

*Table 14: Natural spin densities at selected positions for the ring opening of ring **C***

The introduction of methyl groups to each of the second row substituents lowers the activation barrier for β-scission of C(2)-C(3) without dramatically changing the geometries of the reactant or transition state. The one change that does occur is a shortening of the close range interaction between the substituent and the ether oxygen. This is because introduced methyl group makes the overall substituent bigger and therefore able to access a closer Sub-H···O(ether) interaction. Indeed, in **58n** (R= PMe$_2$) there are two interactions of less than 2.4 Å in the reactant *(Figure 18)*.

| **58n** | **TS[eq-58n-eq-58n′]** |
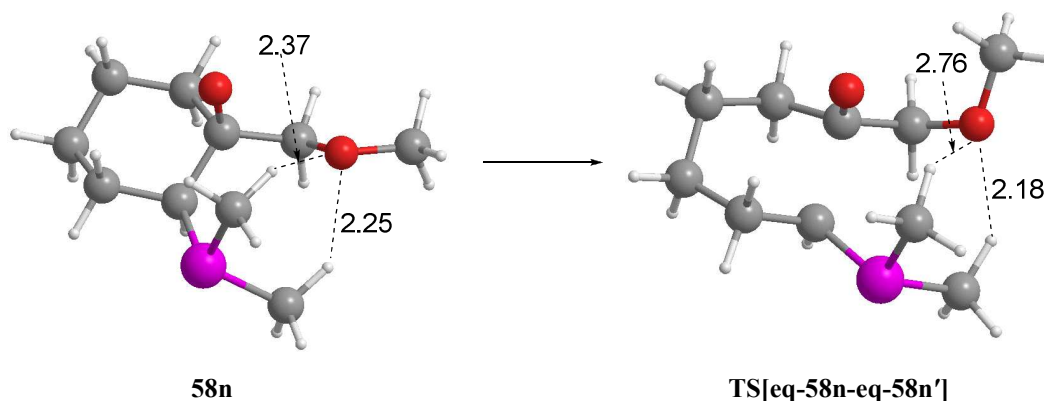
Figure 18

In general the additional methyl group gives lower activation barriers and further stabilisation of the radical character on C(3). Activation barriers for the opening of **58n**

(R=PMe$_2$) and **58o** (R=SMe) decrease with the barrier of **58n** falling significantly lower than **58o** *(Table 15)*. In **TS[eq-58n-eq-58n′]** one of the PMe···O(ether) close range interactions bonds shortens to 2.18 Å whilst the spin density on the PMe$_2$ substituent has increased to 0.18, which is 0.12 higher than in PH$_2$ *(Table 16)*. In **TS[eq-58o-eq-58o′]** the SMe···O(ether) close range interactions bond lengthens to 2.86 Å whilst the spin density on the SMe substituent has increased to 0.19, only 0.06 higher than for SH *(Table 16)*. This suggests that the larger decrease in the energy for β-scission in **58n** compared to **58o** is due to the PMe$_2$ group being able to accommodate more spin density in **TS[eq-58n-eq-58n′]** than can the SMe group in **TS[eq-58o-eq-58o′]** whilst also being able to maintain a shorter close range interaction. Therefore the order of activation barrier has changed from SH < PH$_2$ < SiH$_3$ to PMe$_2$ < SMe < SiMe$_3$ when methyl groups replace the hydrogens.
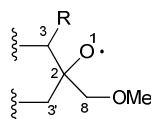
	R	Reactant		TS		Intermediate	Product
		Bond lengths	energy	bond lengths	energy	bond lengths	energy
58m	SiMe$_3$	C(2)-C(3)= 1.57 C(2)-O(1)= 1.37 C(3)-Sub= 1.94 H Bond= 2.48	6.7 *8.0 # 3.5	C(2)-C(3)= 2.07 C(2)-O(1)= 1.26 C(3)-Sub= 1.92 H Bond= 2.50	-5.7	C(2)-O(1)= 1.21 C(3)-Sub= 1.87 H Bond= 2.59	-7.6
58n	PMe$_2$	C(2)-C(3)= 1.58 C(2)-O(1)= 1.36 C(3)-Sub= 1.90 H Bond= 2.25	1.5 *7.6 # 4.5	C(2)-C(3)= 2.00 C(2)-O(1)= 1.27 C(3)-Sub= 1.82 H Bond= 2.18	-10.2	C(2)-O(1)= 1.22 C(3)-Sub= 1.79 H Bond=2.54	-9.8
58o	SMe	C(2)-C(3)= 1.59 C(2)-O(1)= 1.35 C(3)-Sub= 1.83 H Bond= 2.56	2.9 *9.8 # 2.9	C(2)-C(3)= 2.00 C(2)-O(1)= 1.27 C(3)-Sub= 1.76 H Bond= 2.86	-7.3	C(2)-O(1)= 1.22 C(3)-Sub= 1.74 H Bond= 2.75	-7.9

Table 15: All energies given are related to reactant energy in each case

* TS of β-scission of other ring C(2)-C(3') bond # TS of β-scission of C(2)-C(8) bond

The product from the reaction is from the straight-chain open system

	R	Reactant	TS	Intermediate
58m	SiMe$_3$	O(1)= 0.88 C(2)= -0.04 C(3)= 0.01 Sub= 0	O(1)= 0.45 C(2)= -0.08 C(3)= 0.45 Sub= 0.01	O(1)= 0 C(2)= 0 C(3)= 0.94 Sub= 0.02
58n	PMe$_2$	O(1)= 0.82 C(2)= -0.03 C(3)= 0.03 Sub= 0.03	O(1)= 0.41 C(2)= -0.04 C(3)= 0.38 Sub= 0.18	O(1)= 0.10 C(2)= 0 C(3)= 0.81 Sub= 0.05
58o	SMe	O(1)= 0.80 C(2)= -0.03 C(3)= 0.04 Sub= 0.07	O(1)= 0.41 C(2)= -0.05 C(3)= 0.38 Sub= 0.19	O(1)= 0.01 C(2)= 0 C(3)= 0.78 Sub= 0.17

*Table 16: Natural spin densities at selected positions for the ring opening of ring **C***

Phenyl, CN and COOMe

The introduction of further carbon-based substituents as in **58p** (R= Ph), **58q** (R= CN) and **58r** (R= COOMe) has also been considered. Previous studies demonstrated that unsaturated groups provide the greatest stabilisation for carbon centred radicals.[15] The presence of an unsaturated α-carbon was therefore expected to stabilise the product of β-scission, however it was not known what effect it would have on the transition state. Consistent with this expectation, the β-scission of C(2)-C(3) in models **58p-58r** is very exothermic with the radical character of the terminal carbon delocalised onto the substituent *(Table 17)*. As predicted by earlier studies[15] the greatest stability exists with the phenyl substituent with the product being 14.9 kcal mol^{-1} more stable than the reactant and the radical character on the aromatic ring in **58p′** being 0.33 *(Table 18)*.

Unlike the substituents discussed above model oxy radicals **58p-58r** show consistently short C(2)-C(3) bond distances of 1.57 Å and long C(2)-O(1) distances of 1.37 Å. This suggests the radical is localised on the oxygen atom and computed spin densities for **58p-58r** show virtually no radical character situated on C(3) or the substituent. The calculated activation barrier from oxy radical **58p** was calculated to be 3.8 kcal mol^{-1}. This low barrier is consistent with the increased stabilisation of C(3) by the aromatic substituent. In contrast with **58q** and **58r** calculated barriers of 7.6 kcal mol^{-1} and 7.9 kcal mol^{-1} respectively are found similar to that of **ax-58b**. The higher barriers are in line with the lower spin densities associated with the substituents in the transition state.

The results demonstrate that despite the stabilisation of the intermediate **58q′** and **58r′** by the unsaturated groups the barrier for cleaving the C(2)-C(3) bond is still high.
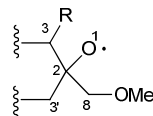
	R	Reactant		TS		Intermediate	Product
		Bond lengths	energy	bond lengths	energy	bond lengths	energy
58p	Ph	C(2)-C(3)= 1.57 C(2)-O(1)= 1.37 C(3)-Sub= 1.52	3.8 *10.1 # 0.8	C(2)-C(3)= 1.98 C(2)-O(1)= 1.27 C(3)-Sub= 1.47	-12.8	C(2)-O(1)= 1.21 C(3)-Sub= 1.42	-14.9
58q	CN	C(2)-C(3)= 1.57 C(2)-O(1)= 1.37 C(3)-Sub= 1.47	7.6 *11.3 # 0.8	C(2)-C(3)= 2.00 C(2)-O(1)= 1.27 C(3)-Sub= 1.43	-9.3	C(2)-O(1)= 1.24 C(3)-Sub= 1.40	-12.1
58r	COOMe	C(2)-C(3)= 1.57 C(2)-O(1)= 1.37 C(3)-Sub= 1.52 H Bond= 3.34	7.9 *11.1 # 5.1	C(2)-C(3)= 2.02 C(2)-O(1)= 1.26 C(3)-Sub= 1.49 H Bond= 3.07	-6.8	C(2)-O(1)= 1.21 C(3)-Sub= 1.45 H Bond= 2.90	-9.7

Table 17: All energies given are related to reactant energy in each case

* TS of β-scission of other ring C(2)-C(3′) bond # TS of β-scission of C(2)-C(8) bond

The product from the reaction is from the straight-chain open system

	R	Reactant	TS	Intermediate
58p	Ph	O(1)= 0.87 C(2)= -0.03 C(3)= 0.02 Sub= 0	O(1)= 0.47 C(2)= -0.06 C(3)= 0.43 Sub= 0.10	O(1)= 0.02 C(2)= 0 C(3)= 0.68 Sub= 0.33
58q	CN	O(1)= 0.79 C(2)= -0.04 C(3)= 0 Sub= 0	O(1)= 0.50 C(2)= -0.10 C(3)= 0.48 Sub= 0.08	O(1)= 0 C(2)= 0 C(3)= 0.75 Sub= 0.22
58r	COOMe	O(1)= 0.88 C(2)= -0.03 C(3)= 0.01 Sub= 0.02	O(1)= 0.49 C(2)= -0.10 C(3)= 0.51 Sub= 0.06	O(1)= 0.01 C(2)= 0 C(3)= 0.81 Sub= 0.16

*Table 18: Natural spin densities at selected positions for the ring opening of ring **C***

Varying the size of ring C

Experimentally changing the size of ring **C** from six- to five- or seven-membered has little effect on the overall reaction products. For both the unsubstituted **54a** and methyl-substituted *dispiro*-1,2,4-trioxanes **54b** the yields of the keto lactone **57** and oxalactone **56** vary only slightly with ring size. Likewise the yield of keto lactone **57c** and 57d from the thermolysis of methoxy- and ethoxy-substituted *dispiro*-1,2,4-trioxanes **54c** and **54d** shows no significant difference. The addition of extra functionality to ring **C** does however give different experimental results where an indanylidene ring is present. A methyl-substituted *dispiro*-1,2,4-trioxane **54b** containing a indanylidene ring **C** has been shown to form the oxalactone **56b** exclusively in high yield without any sign of keto lactone **57b**.[43] Although the thermolysis of the indanylidene containing methoxy- and ethoxy-substituted *dispiro*-1,2,4-trioxanes reactions seems to form the fully ring expanded keto lactone, other unidentified products were also formed suggesting the indanylidene ring was behaving differently *(Chapter 2)*. In this section a variety of ring C like models have been investigated to establish the effect of the indanylidene ring.

However, the modelling of different ring sizes show that changing the size of ring **C** has an effect on the energy barrier associated with β-scission. The barrier for β-scission of a five-membered oxy radical **62** at C(2)-C(3) is only 2.0 kcal mol^{-1}, half of that associated with the six-membered ring **59** *(Table 19)*. The β-scission of the five membered oxy radical **62** is accompanied by a slightly longer C(2)-O(1) bond of 1.27 Å and a shorter C(2)-C(3) bond distance of 1.93 Å in the transition state, implying an earlier transition state than **59** consistent with the lower activation energy. This is further supported by the increase in radical character on O(1) of 0.47 and smaller radical character on C(3) of 0.57 *(Table 20)*. The low activation barrier for the opening of the five-membered oxy radical 62 is consistent with the additional ring strain associated with a five-membered ring.[11]

The ring strain associated with the opening of a seven-membered ring **63** is similar to that of a six-membered ring **59**.[11] This is shown in the barrier for β-scission in the seven-membered oxy radical **63** being 4.1 kcal mol^{-1}, exactly the same as the six-membered ring **59** *(Table 19)*. Consistent with this, the key bond lengths and spin

densities associated with the β-scission of the seven-membered ring oxy-radical are similar to those computed for **59** *(Tables 19 and 20)*.

Like the six-membered oxy radical **59,** the five-membered (**62**) and seven-membered (**63**) oxy radicals open the C(2)-C(3) bond in an exothermic reaction (-4.3 kcal mol^{-1} and -1.2 kcal mol^{-1} respectively) and each form even lower energy products when in a straight-chain conformation. These findings further demonstrate that the opening of ring **C** by β-scission is a favourable process and are consistent with experimental results showing the preferential formation of oxalactone **56** from the thermolysis of selected *dispiro*-1,2,4-trioxanes **54a** and **54b**.

Modelling studies for the cleavage of the C(2)-C(3) bond of indanylidene oxy radical **64** gave a barrier for β-scission of 3.3 kcal mol^{-1}. Although the transition state is lower than the corresponding six-membered ring in **59** by 0.8 kcal mol^{-1} the transition state is 1.3 kcal mol^{-1} higher in energy than the cleavage of the five-membered ring in **62**. This is not consistent with the experimental results for the thermolysis of cyclopentylidene containing *dispiro*-1,2,4-trioxanes which produced some keto lactone whilst the indanylidene *dispiro*-1,2,4-trioxanes formed exclusively the oxalactone. The answer to this may lie in the thermodynamics of the two reactions. Whilst the ring opening of the five membered ring in **62** is mildly exothermic at -4.3 kcal mol^{-1} the intermediate linked to the transition state of the β-scission of the indanylidene oxy radical in **64** is more exothermic at -22.5 kcal mol^{-1}. The β-scission of C(2)-C(3) in **64** therefore looks irreversible and intermediate formed then goes on to forming the oxalactone. The stability of the intermediate is typical of the radical character on the C(3) being stabilised by the π-orbitals of the aromatic group.[17] This is seen by the total spin density over the aromatic ring being 0.33 in the intermediate **64'**. The stabilisation effect of the aromatic group is less pronounced in the transition state with a total spin density on the aromatic ring of 0.05.

The addition of a ketone functionality into ring **C** of *dispiro*-1,2,4-trioxane **54d** has been shown experimentally to form the keto lactone **57d** exclusively. With the barrier of β-scission of C(2)-C(3) being 4.0 kcal mol^{-1} for **65** the modelling study shows the ketone has no effect on the overall energy of the cleavage. Bond lengths and spin densities involved in the reaction are also similar to those seen for the corresponding six-membered oxy radical example.
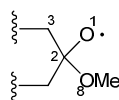
Model	Reactant		TS		Intermediate	Product
	Bond lengths	energy	bond lengths	energy	bond lengths	energy
62	C(2)-C(3)= 1.58 C(2)-O(1)= 1.31	2.0 #15.3	C(2)-C(3)= 1.93 C(2)-O(1)= 1.27	-4.3	C(2)-O(1)= 1.21	-14.3
63	C(2)-C(3)= 1.58 C(2)-O(1)= 1.32	4.1 #15.3	C(2)-C(3)= 1.98 C(2)-O(1)= 1.25	-1.2	C(2)-O(1)= 1.21	-22.9
64	C(2)-C(3)= 1.61 C(2)-O(1)= 1.33	3.3 #14.6	C(2)-C(3)= 1.92 C(2)-O(1)= 1.26	-23.6	C(2)-O(1)= 1.21	-22.5
65	C(2)-C(3)= 1.58 C(2)-O(1)= 1.32	4.0 #17.3	C(2)-C(3)= 1.97 C(2)-O(1)= 1.25	-9.51	C(2)-O(1)= 1.21	-12.0

Table 19: All energies given are related to reactant energy in each case

 # TS of β-scission of C(2)-O(8) bond

The product from the reaction is from the straight-chain open system

	Reactant	TS	Intermediate
62	O(1)= 0.72 C(2)= -0.04 C(3)= 0.13	O(1)= 0.47 C(2)= -0.06 C(3)= 0.51	O(1)= 0 C(2)= 0 C(3)= 1.00
63	O(1)= 0.74 C(2)= -0.03 C(3)= 0.11	O(1)= 0.38 C(2)= -0.05 C(3)= 0.57	O(1)= 0 C(2)= 0 C(3)= 1.00
64	O(1)= 0.81 C(2)= -0.04 C(3)= 0.07 Aromatic= 0	O(1)= 0.46 C(2)= -0.06 C(3)= 0.51 Aromatic= 0.05	O(1)= 0 C(2)= 0 C(3)= 0.71 Aromatic= 0.33
65	O(1)= 0.72 C(2)= -0.03 C(3)= 0.11	O(1)= 0.37 C(2)= -0.05 C(3)=0.57	O(1)= 0 C(2)= 0 C(3)= 0.97

*Table 20: Natural spin densities at selected positions for the ring opening of ring **C***

Varying the size of ring A

For completeness the influence of the size of ring **A** has also been considered for five and seven-membered rings.

The ring opening of five-membered oxy radical **66** has a lower barrier than the six-membered **58** by *ca.* 2 kcal mol^{-1}. This difference is approximately the same seen for the opening of oxy radicals **59** and **62** in ring **C**. The C(2)···C(3) bond distance in the ring opening transition state was 2.11 Å in **66** compared to 2.15 Å in **58** consistent with an earlier transition state. Additionally in the transition state for the β-scission of **66** the spin density on the O(1) is 0.42 and C(3) is 0.64 which is different than for the **58** which was 0.35 on O(4) and 0.69 on C(3). This again is consistent with an early transition state and low activation energy. Similar to the opening of ring **C**, changing the size of the ring **A** to seven gives only small differences in energy (ca. 0.6 kcal mol^{-1}) *(Table 21 and 22)*. Unlike the ring opening of the six-membered oxy radical **58**, the β-scissions of five- and seven-membered oxy radicals **66** and **67** are mildly exothermic. This suggests the apparent lack of β-scission of ring **A** and subsequent formation of oxalactone due to the large barrier and not the overall energy of the reaction.

The small differences in the activation barrier for the opening of different ring **A** sizes is consistent with experimental results which suggest the ring size does not make the opening of ring **A** competitive with ring **C**.[48]

Model	Reactant		TS		Intermediate		Product
	Bond lengths	energy	bond lengths	energy	bond lengths		energy
66	C(2)-C(3)= 1.59 C(2)-O(1)= 1.37	8.7 *3.5	C(2)-C(3)= 2.11 C(2)-O(1)= 1.25	-1.1	C(2)-O(1)= 1.21		-1.40
67	C(2)-C(3)= 1.58 C(2)-O(1)= 1.37	10.4 *2.6	C(2)-C(3)= 2.11 C(2)-O(1)= 1.25	-3.3	C(2)-O(1)= 1.21		-4.95

Table 21: All energies given are related to reactant energy in each case

* TS of β-scission of other ring C(2)-C(8) bond

The product from the reaction is from the straight-chain open system

	Reactant	TS	Intermediate
66	O(1)= 0.89 C(2)= -0.04 C(3)= 0.10 α-H= 0	O(1)= 0.42 C(2)= -0.09 C(3)= 0.64 α-H= -0.03	O(1)= 0 C(2)= 0 C(3)= 1.00 α-H= -0.03
67	O(1)= 0.90 C(2)= -0.03 C(3)= 0.10 α-H = 0	O(1)= 0.39 C(2)= -0.07 C(3)= 0.64 α-H = 0	O(1)= 0 C(2)= 0 C(3)= 1.01 α-H = 0

*Table 22: Natural spin densities at selected positions for the ring opening of ring **C***

Computational study of the thermolysed rearrangement of *dispiro*-1,2,4-trioxanes

It was clear from the small model calculations that in isolation the opening of ring **C** is lower in energy than ring **A** for the unsubstituted models. The addition of a substituent onto the α-position of ring **A** affects the energy barrier for the ring opening, making the process more competitive with that of ring **C**. To further investigate the outcomes of the small model calculations on a real system, full model studies were undertaken. The models chosen to investigate initially were *dispiro*-1,2,4-trioxanes **54aa**, **54ba** and **54ca** which cover the rearrangement reactions of unsubstituted, methyl- and methoxy-substituted *dispiro*-1,2,4-trioxanes respectively. In addition, models **54cb** and **54cc** were also studied to investigate the change in the size of ring **C** *(Figure 19)*. The full model studies sought to map out all the transition states and intermediates involved in the rearrangement process.
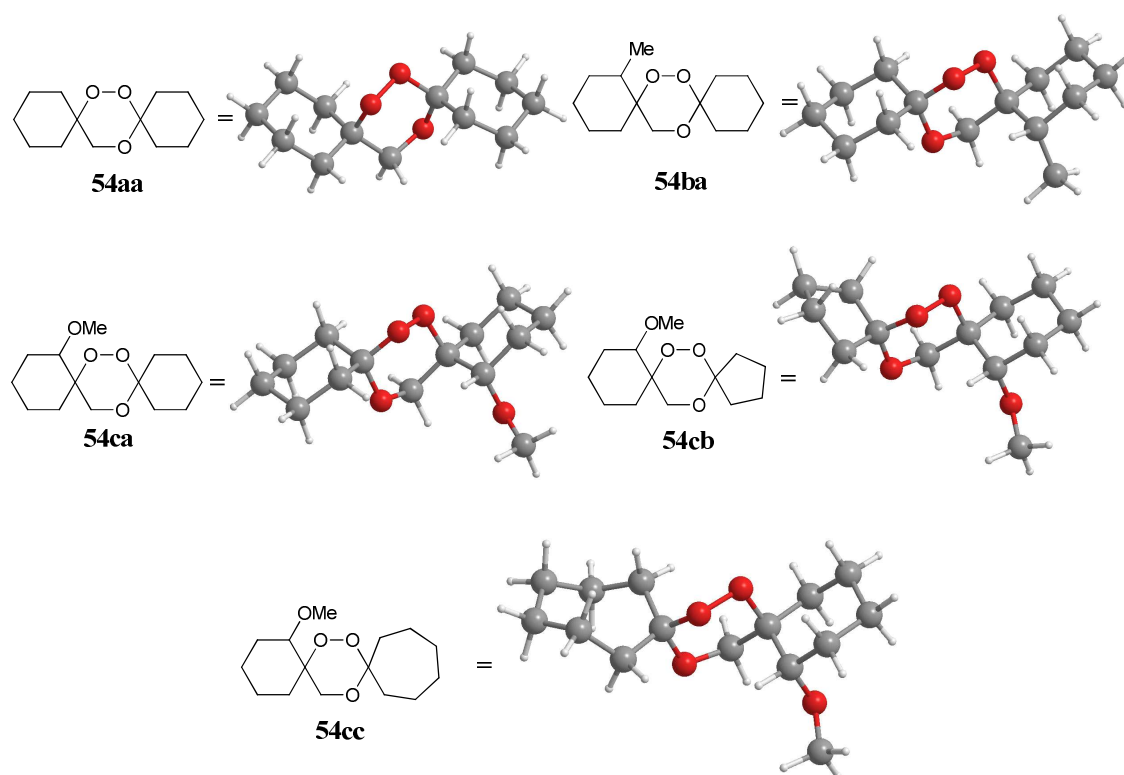
*Figure 19: Optimised structures of **54aa, 54ba, 54ca, 54cb** and **54cc***

The geometries of each *dispiro*-1,2,4-trioxanes studied are related directly to the crystal structures, outlined in *Chapter 1*, with each of the *spiro* six-membered rings optimised into a chair conformation with the peroxide oxygens axial with respect to both rings **A** and **C**. The addition of the substituent (where appropriate) was positioned axial with respect to ring **A** and *trans* to the peroxide oxygens *(Figure 19)*. Upon optimisation, the computed geometry of the 1,2,4-trioxane ring related favourably with the related crystal structures reported in *Chapter 1* demonstrating the accuracy of the method in replicating the structure (full geometry comparisons are in *Appendix 3*, *Tables 2 and 3*).

Following the homolytic cleavage of the peroxide bond, the model systems would have six competing β-scission sites. Four sites can initiate ring opening of ring **A** or **C** (C(2)-C(3), C(2)-C(7), C(2′)-C(3′) and C(2′)-C(7′)) and two which promote the fragmentation to component ketones (C(2)-C(8) and C(2′)-O(8′)). In this section, each of the β-scission reactions has been investigated individually and compared. Once the most favoured β-scission reaction(s) were established, the second β-scission of the unopened ring could be investigated in a similar way *(Scheme 15)*.
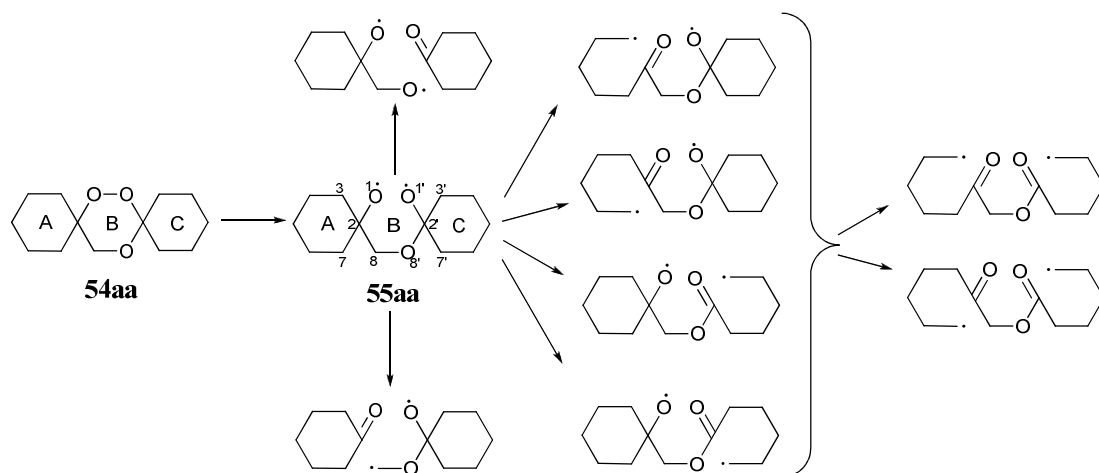
Scheme 15

The relaxation through IRC calculations of the transition states for each of the β-scission reactions included no restrictions and therefore allowed possible radical recombination to take place. On occasion, the transition states for the β-scission reactions were calculated initially using a triplet spin state. This allowed the correct position of the radicals to be established and prevented the oxygen radicals recombining to reform the 1,2,4-trioxane ring. Once the transition state was located the geometry was optimised using a open shell singlet spin state with no change to the geometry apparent. Each model discussed in this section is in the open shell singlet spin state.

Dispiro-1,2,4-trioxane 54aa

Opening of the peroxide bond of *dispiro*-1,2,4-trioxane 54aa

The thermolysis of 1,2,4-trioxanes proceeds through the homolytic cleavage of the peroxide bond to give two oxy radicals. In order to model this, the distance between O(1) and O(1′) were routinely increased stepwise and optimised. The energy of the system increased steadily along with the O(1)···O(1′) bond distance until the energy levelled out at *ca.* 2.20 Å. Attempts to optimise this geometry resulted in the recombination of oxy radicals reforming the 1,2,4-trioxane ring. Although further increases in the O(1)···O(1′) resulted in only minimal increases in energy, a local

minimum, **55aa**, was found from optimisation of the structure with an O(1)···O(1′) 2.80 Å *(Figure 20)*. Upon optimisation, the molecule twists O(1) and O(1′) apart by making ring **C** almost perpendicular to ring **A**. Attempts to find a transition state for this process were unsuccessful. Any transition state therefore is expected to be very close in energy to the intermediate.

54aa
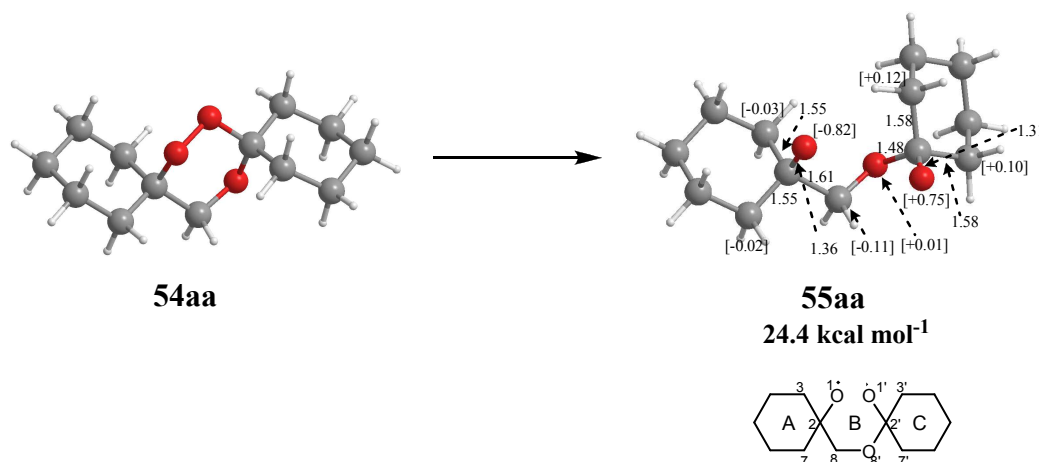
55aa
24.4 kcal mol⁻¹

*Figure 20: Optimised geometries of **54aa** and **55aa** highlighting bond lengths/ Å*
Here and throughout the spin densities are shown in square brackets

Intermediate **55aa** contains a short C(2′)-O(1′) bond of 1.31 Å and elongated C(2′)-C(3′) and C(2′)-C(7′) bond lengths indicative of the radical character of O(1′) being delocalised onto ring **C**. This is supported by the moderate build-up of radical character on C(3′) and C(7′) (+0.12 and +0.10 respectively). In contrast the C(2)-O(1) bond length is substantially longer than C(2′)-O(1′) at 1.36 Å whilst the C(2)-C(3) and the C(2)-C(7) bond distances are shorter (1.55 Å) than those seen in ring **C.** This suggests β-scission may be more difficult for the opening of ring **A**. Interestingly, there is an elongated C(2)-C(8) bond (1.61 Å) and a delocalisation of radical character from O(1) onto C(8) consistent with favourable β-scission at this site.

Further increases in the O(1)···O(1′) distance beyond 2.80 Å during the scan resulted firstly in the cleavage of the C(2)-C(8) bond followed by the C(2′)-O(8′) bond resulting in the formation of two molecules of cyclohexanone and a molecule of formaldehyde. The formation of ketones from the thermolysis of 1,2,4-trioxanes is expected and regularly reported.[49] In fact, cyclohexanone has been observed in the thermolysis of **54aa** reaction using gas chromatography.[50] A transition state **TS[55aa-frag]** for this process was found at 27.1 kcal mol⁻¹, only 2.5 kcal mol⁻¹ above the intermediate **55aa** *(Figure 21)*. **TS[55aa-frag]** contains a shortened C(2)-O(1) bond of 1.28 Å and a

shortened C(8)-O(8′) bond of 1.34 Å indicative of the build-up of radical character on C(8). **TS[55aa-frag]** contains an $<S^2>$ value of *ca.* 0.82 highlighting a deviation away from 1.0, seen for other open shell singlet calculations. It is suspected that this is due the reaction being asynchronous, the breaking of the C(2)-C(8) bond also breaking the C(2′)-O(8′) upon relaxation, resulting in a small proportion of closed shell singlet character in **TS[55aa-frag]**. This is repeated in the fragmentation reactions of **55ba** and **55ca** discussed later.

Attempts to find a transition state for the cleavage of C(2′)-O(8′) alone failed and instead converges on **TS[55aa-frag]**. The same result for the opening of C(2′)-O(8′) occurs in each model discussed in this chapter.

Figure 21: The reaction profile for the fragmentation of **55aa** */ kcal mol*[-1]
with molecular bond lengths/ Å and spin densities

β-Scission reactions of oxy radicals derived from 55aa

In addition to the formation of cyclohexanone, the thermolysis of *dispiro*-1,2,4-trioxane **54aa** also produces oxalactone **56aa** during the thermolysis reaction. This indicates that the cleavage of ring **C** will be substantially lower than that of ring **A**.

A comparison between the opening of rings **A** and **C** from intermediate **55aa** showed a *ca.* 5 kcal mol^{-1} preference for the opening of C(2′)-C(3′) and C(2′)-C(7′) in ring **C** over C(2)-C(3) and C(2)-C(7) in ring **A** *(Figure 22)*. Additionally, like the small model calculations, opening of ring **A** via **TS[55aa-68]** and **TS[55aa-69]** is endothermic whilst the opening of ring **C** via **TS[55aa-70]** and **TS[55aa-56aa]** is exothermic. This again demonstrates the presence of the adjacent exocyclic O(8′) strongly promotes the opening of ring **C** consistent with experimental results showing the preferential formation of oxalactone **56aa**. Interestingly, the opening of C(2′)-C(3′) via **TS[54aa-56aa]** has the lowest energy barrier of 29.0 kcal mol^{-1} and relaxes to form the oxalactone **56aa** (-51.3 kcal mol^{-1}), seen in the experiment, directly.

In all cases, the β-scission is accompanied by the expected shortening of the carbonyl C(2)-O(1) or C(2′)-O(1′) distances and increased planarity of the incipient terminal carbon due to a build up of radical character. A shorter C(2′)-C(3′) and C(2′)-C(7′) distance in **TS[55aa-70]** and **TS[55aa-56a]** and less spin density on C(3′) and C(7′) than seen for C(3) and C(7) in **TS[55aa-68]** and **TS[55aa-69]** demonstrates an earlier transition state for the opening of ring **C,** consistent with the lower activation energy. In general, the complete transfer of radical character is confirmed by the short carbonyl bond distance in the intermediates and the planarity of the terminal carbon.

The opening of C(2′)-C(3′) via **TS[55aa-56aa]** brings the developing carbon-centred radical at C(3′) into close proximity with the oxy radical (O1) meaning little reorganisation was required by the model to form the oxalactone **56aa**. It is expected that the solvent cage in this case would provide sufficient external pressure to force two closely residing radicals together quickly forming the oxalactone. This is an important observation as it suggests the lifetime of the radical on C(3′) is very short and confirms the formation of oxalactone via the lowest energy process.

*Figure 22: The reaction profile for the competitive β-scission reactions of **55aa** / kcal mol⁻¹*

with molecular bond lengths/ Å and spin densities

Although the transition state energy for the formation of **70** is higher than **TS[55aa-56aa]** the difference in the energy is only 0.6 kcal mol^{-1} meaning both transition states could potentially be accessible. **TS[55aa-70]** relaxes to form an intermediate **70** at 18.6 kcal mol^{-1} and contains the carbon-centred radical C(7′) situated away from the oxy radical at O(1). To access the oxalactone **70** would require a large degree of reorganisation meaning that the intermediate may have enough time to undergo further β-scission reactions on ring **A** and form the fully ring expanded keto lactone.

Intermediate **70** contains a slightly elongated C(2)-C(3) bond of 1.58 Å with +0.10 spin density on C(3), compared to 1.55 Å for C(2)-C(7) and +0.02 spin density on C(7). This suggests the opening of C(2)-C(3) will be easier than C(2)-C(7).

A comparison between the β-scission at C(2)-C(3) via **TS[70-72]** and C(2)-C(7) via **TS[70-71]** does show a preference for the cleavage of C(2)-C(3) by 2.0 kcal mol^{-1} however the barriers lie *ca*. 10-12 kcal mol^{-1} higher than intermediate **70** *(Figure 23)*. As oxalactone is the only product other than cyclohexanone observed during the thermolysis of *dispiro*-1,2,4-trioxane **54aa**, it is suggested that these barriers are higher than the energy required to rearrange to form the oxalactone **56aa**. If, however, the barriers for **TS[70-72]** and **TS[70-71]** were achievable the formation of keto lactone **57aa** (E= -58.5 kcal mol^{-1}) via radical recombination is thermodynamically favourable.

Although **TS[55aa-68]** and **TS[55aa-69]** relaxes to form intermediates **68** and **69** (29.9 kcal mol^{-1} and 26.3 kcal mol^{-1} respectively) these β-scission reactions have much higher activation barriers than **TS[55aa-70]** and **TS[55aa-56aa]** so further reactions from intermediates **68** and **69** were not investigated.

The reaction profile shows a clear preference for the formation of oxalactone **56aa** rather than keto lactone **57aa**. It is apparent that the oxalactone is formed through two subtly different reaction mechanisms: (i) directly from **TS[54aa-56aa]** occurs because the radical is formed in close proximity to O(1) meaning only minimum rearrangement is required for recombination; (ii) alternatively via the formation of **70** followed by the reorganisation of the system. The latter case looks more favourable than the β-scission reactions via **TS[70-71]** and **TS[70-72]**.

*Figure 23: The reaction profile for the competitive β-scission reactions of **70** / kcal mol⁻¹*

with molecular bond lengths/ Å and spin densities

Dispiro-1,2,4-trioxane 55ba

Opening of the peroxide bond for *dispiro*-1,2,4-trioxane 54ba

Like the modelling of the unsubstituted *dispiro*-1,2,4-trioxane **54aa,** the peroxide bond in **54ba** opens in the absence of a transition state to form an intermediate where ring **C** has twisted to facilitate the lengthening of the O(1)···O(1′) distance *(Figure 24)*. Additionally the opening of the O(1)···(O1′) bond distance has introduced a long range integration (2.86 Å) between the C(9)-H and C(8′) creating the same *pseudo* six-membered ring seen in the small model investigations.
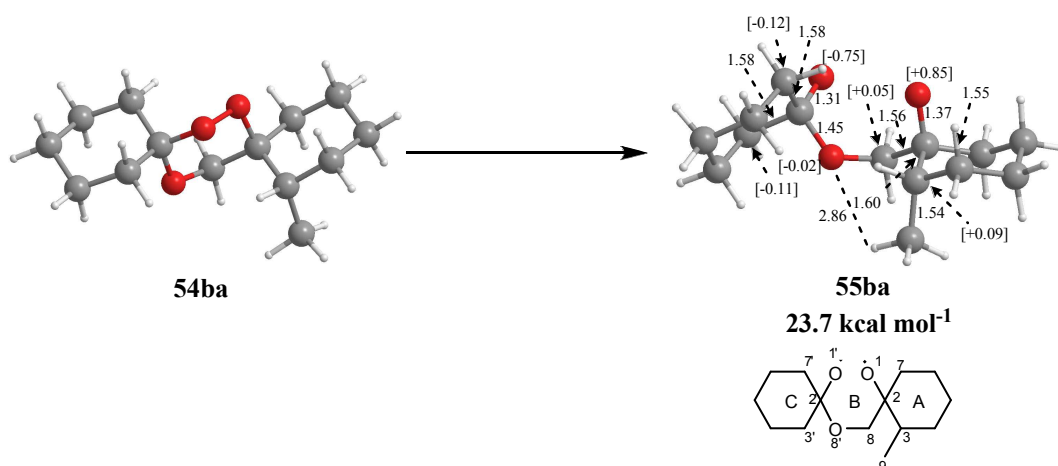
*Figure 24: Optimised geometries of **54ba** and **55ba** highlighting bond lengths/ Å and spin densities*

This additional interaction combined with an increased spin density on the methyl-substituted C(3) (+0.09) has lengthened the C(2)-C(3) bond in **55ba** to 1.60 Å thus suggesting an easier cleavage. This increase in radical character on C(3) is accompanied by a shortening of the C(2)-C(8) bond to 1.56 Å compared to **54aa** and a decreased radical character on C(8). The transition state **TS[55ba-frag]** for the fragmentation process was found at 26.6 kcal mol^{-1}, 2.9 kcal mol^{-1} above the intermediate **55ba** *(Figure 24)*. The other bond lengths associated with rings **A** and **C** in **55ba** remain similar to intermediate **55aa** with delocalisation of the radical character in ring **C** from O(1′) to C(3′) and C(7′).
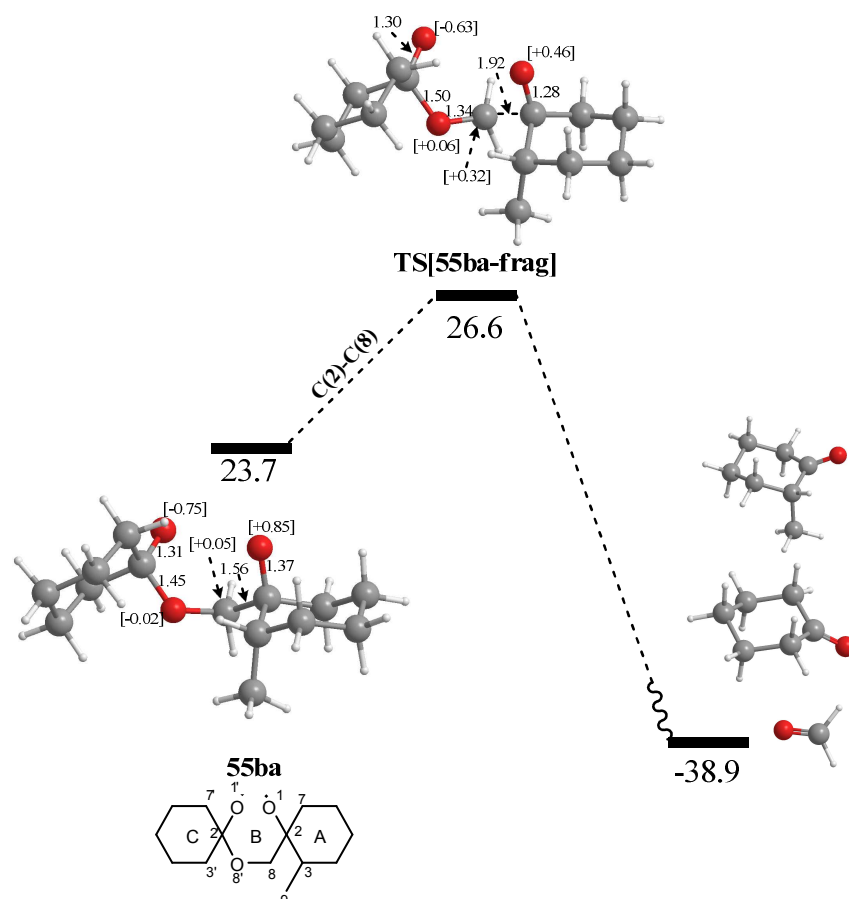
*Figure 25: The reaction profile for the fragmentation of **55ba** / kcal mol*[-1]

with molecular bond lengths/ Å and spin densities

β-Scission reactions of oxy radicals derived from 55ba

In addition to the formation of component cyclic ketones, the thermolysis of *dispiro*-1,2,4-trioxane **54ba** produces both oxalactone **56ba,** as the major product, and keto lactone **57ba**. This suggests the cleavage of ring **C** will still be lower in energy than ring **A** but the difference will be smaller than that for **55aa**.

A comparison between the opening of rings **A** and **C** from intermediate **55ba** show similar energies to those of **55aa** except for a reduction in the transition state energy for the opening of C(2)-C(3) via **TS[55ba-74]** to 29.9 kcal mol^{-1} and the formation of **74** being exothermic from **55ba** *(Figure 26)*. **TS[55ba-74]** shows a shortening of the C(2)-O(1) bond and lengthening C(2)-C(3) bond along with a transfer of radical character from O(1) to C(3) as expected for a β-scission reaction. In addition, **TS[55ba-74]** has a shortened C(3)-C(9) bond of 1.50 Å along with increased spin density on the methyl substituent. The C(3)-(9) bond distance is further decreased and spin density on the methyl substituent increased in **74** illustrating further delocalisation of the C(3) radical.

254
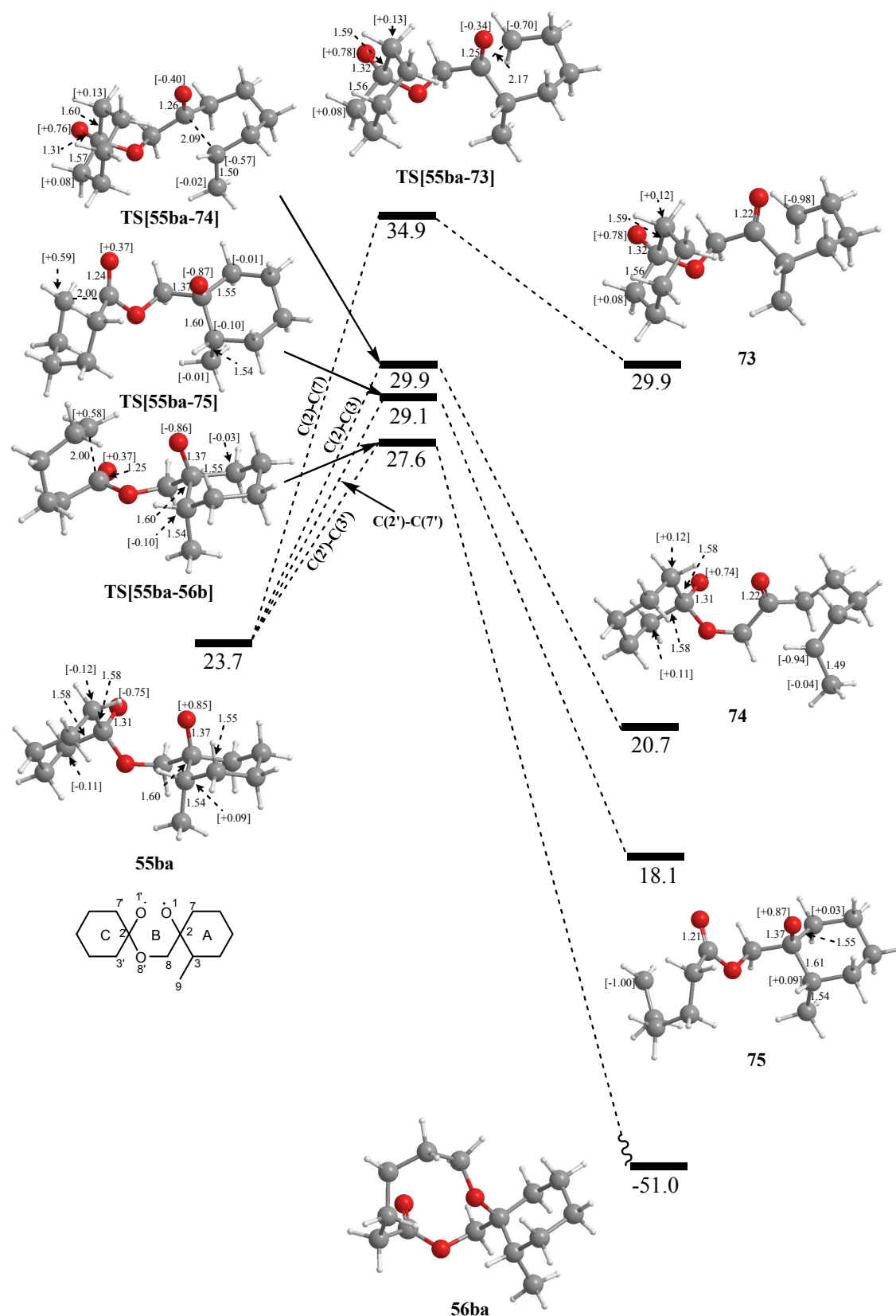
*Figure 26: The reaction profile for the competitive β-scission reactions of **55ba** / kcal mol^{-1}*

with molecular bond lengths/ Å and spin densities where the spin density quoted is for

all the centres on the methyl group

The opening of C(2′)-C(3′) via **TS[55ba-56ba]** again has the lowest transition state barrier (27.6 kcal mol^{-1}) and relaxes to form the oxalactone **56ba** (-51.0 kcal mol^{-1}) consistent with experimental results.

As the experiment also forms keto lactone **57ba** in low yield, it is suggested that the barriers associated with **TS[55ba-75]** may also be accessible. **TS[55ba-75]** lies 1.5 kcal mol^{-1} higher in energy than **TS[54ba-56ba]** and relaxes to form an intermediate **75** at 18.1 kcal mol^{-1}. Intermediate **75** contains an elongated C(2)-C(3) bond of 1.61 Å with +0.09 spin density on C(3) compared to 1.55 Å for C(2)-C(7) and +0.03 spin density on C(7) *(Figure 27)*. A comparison between the β-scission at C(2)-C(3) via **TS[75-77]** and C(2)-C(7) via **TS[75-76]** shows a preference for the cleavage of C(2)-C(3) by 5.0 kcal mol^{-1}. **TS[75-77]** lies 6.4 kcal mol^{-1} higher in energy than **75** and must be accessible for the formation of keto lactone **57ba** via this route. Like **TS[55aa-74]**, **TS[75-77]** shows the developing radical character on C(3) being delocalised onto the methyl group stabilising the transition state energy. Overall the formation of **77** is exothermic from **75** and is an expected intermediate in the formation of keto lactone **57ba**. **TS[75-76]** from the cleavage of C(2)-C(7) lies 5.5 kcal mol^{-1} higher in energy than **TS[75-77]** and relaxes to form **77** in an endothermic reaction, from **75**, not expected to occur in the rearrangement.

Therefore the reaction from intermediate **75** potentially accesses two different routes: (i) β-scission of the C(2′)-C(3′) bond via **TS[75-77]** followed by recombination of the carbon-centred radicals giving the keto lactone **57ba** or/and (ii) the recombination of the C(7′) radical with the O(1) radical giving more of the oxalactone **56ba**.

For completeness, the reaction profile from **74** has also been investigated as illustrated in *Appendix 3 Figure 1*. The formation of **74** through **TS[55ba-74]** lies 2.3 kcal mol^{-1} higher in energy than the lowest transition state. It is therefore deemed unlikely that a significant proportion of substrate would reach this barrier to account for the yield of keto lactone.
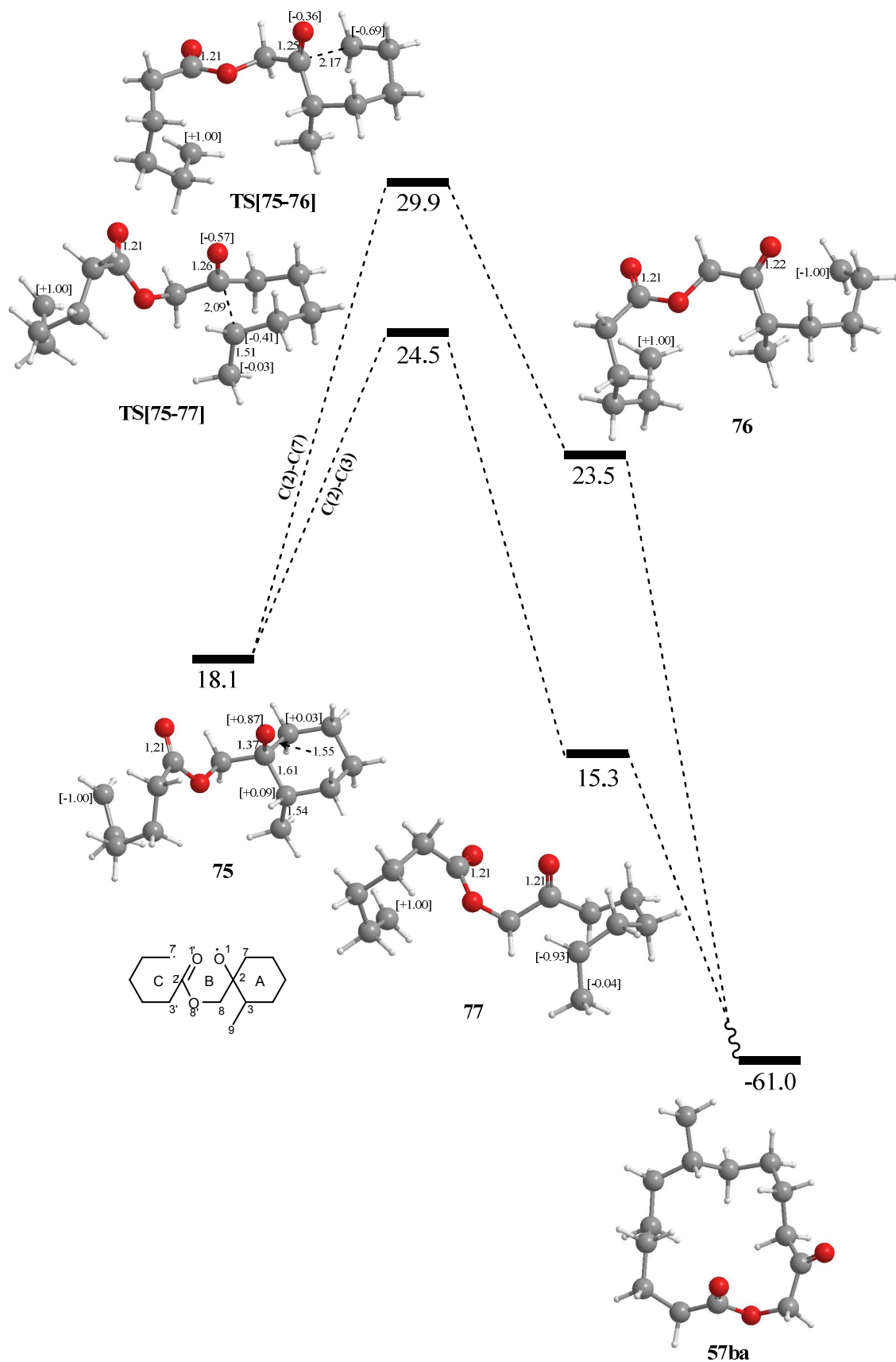
Figure 27: The reaction profile for the competitive β-scission reactions of 75 / kcal mol^{-1}

with molecular bond lengths/ Å and spin densities where the spin density quoted is for

all the centres on the methyl group

Dispiro-1,2,4-trioxane 55ca

Opening of the peroxide bond for *dispiro*-1,2,4-trioxane 54ca

Like the modelling of the other *dispiro*-1,2,4-trioxanes **54aa** and **54ba,** the peroxide bond in **54ca** opens in the absence of a transition state to form an intermediate where ring **C** has twisted to be almost perpendicular to ring **A** *(Figure 28)*. In the optimised geometry of **54ca** the methoxy group is situated away from the rest of the structure but during the step-wise increase of the O(1)⋯O(1′) distance, the C(3)-O(9) bond rotates the methyl group at C(10) towards O(8′). Upon optimisation, this facilitates a short contact (2.50 Å) between C(10)-H and O(8′) creating the same *pseudo* seven-membered ring discussed in the small models. The size and flexibility of the methoxy group over a methyl group has allowed this interaction to be considerably shorter than that in **55ba**.
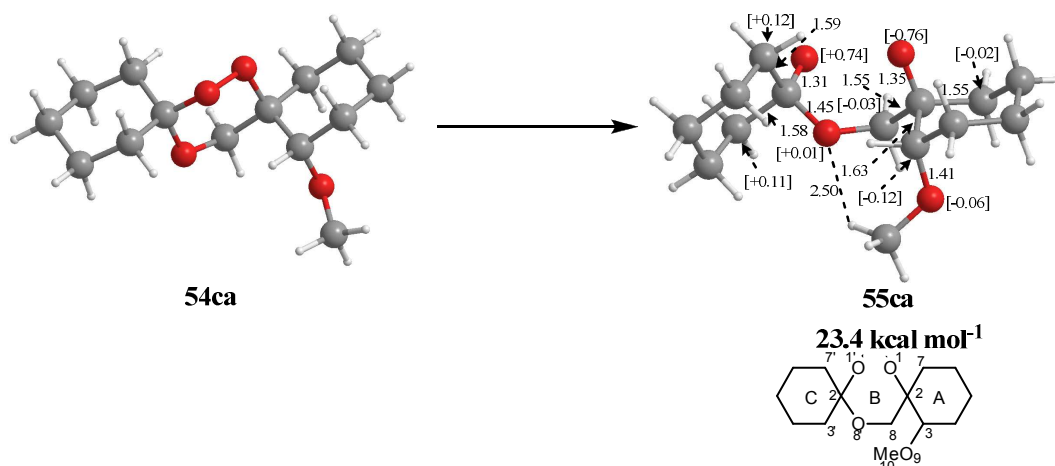
*Figure 28: Optimised geometries of **54ca** and **55ca** highlighting bond lengths/ Å and spin densities*

Unlike **55ba**, intermediate **55ca** exhibits some spin density (-0.06) on O(9) signifying further delocalisation of radical character on O(1) and hence the larger stabilising influence of a methoxy group. This effect in addition to the spin density on C(3) (-0.12) and the short range interaction, C(10)-H⋯O(8′) leads to an elongation of the C(2)-C(3) bond distance to 1.63 Å and a short C(3)-O(9) bond of 1.41 Å.

This increase in radical character on C(3) and O(9) is accompanied by a shortening of the C(2)-C(8) bond to 1.55 Å compared to **54aa** (1.60 Å) and a decreased radical character on C(8). The transition state **TS[55ca-frag]** for the fragmentation process was found at 26.0 kcal mol⁻¹, 2.6 kcal mol⁻¹ above the intermediate **55ca** *(Figure 29)*. The other bond lengths associated with rings **A** and **C** in **55ca** remain similar to those in

intermediate **55aa** and **55ba** with delocalisation of the radical character in ring **C** from O(1′) to C(3′) and C(7′) again being seen.
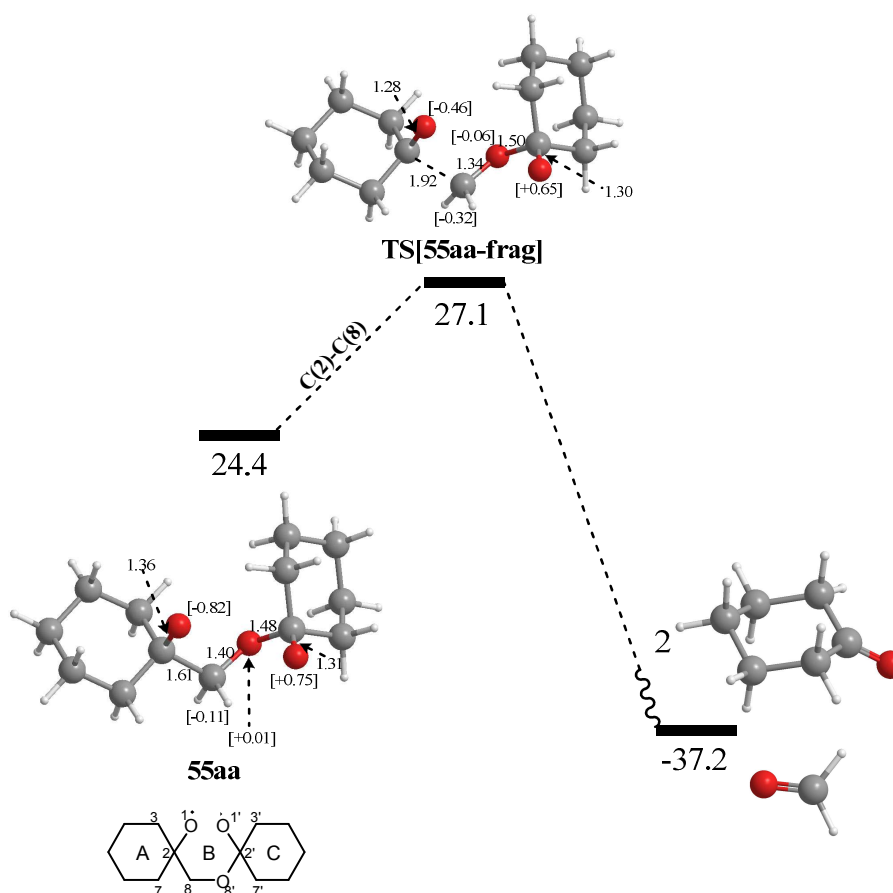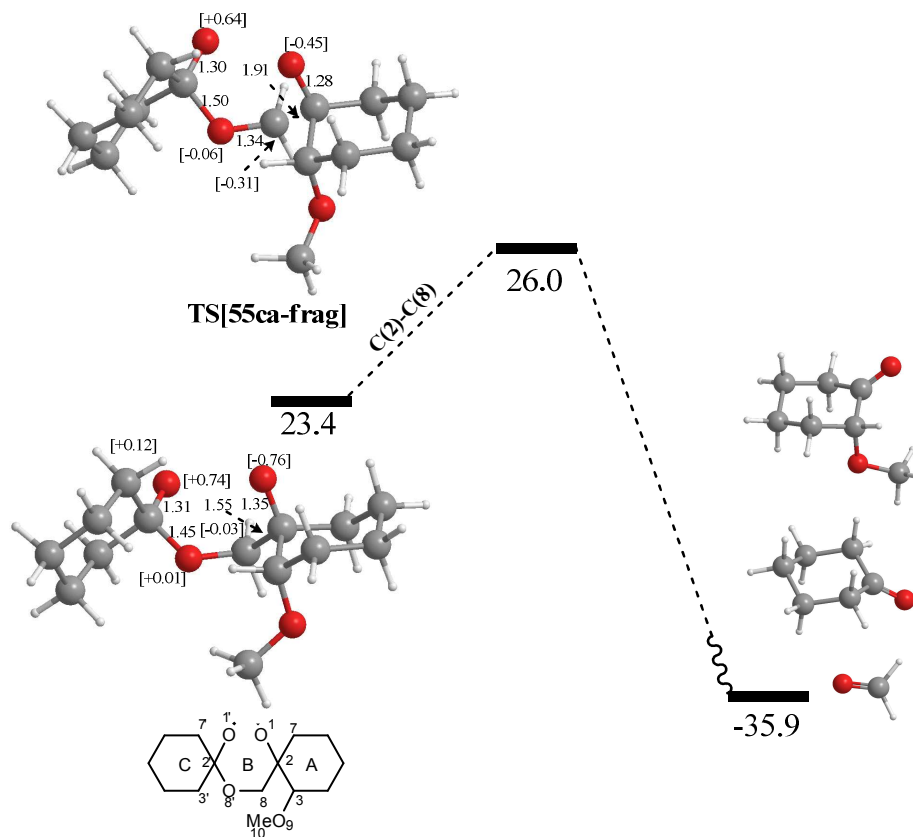

*Figure 29: The reaction profile for the fragmentation of **55ca** / kcal mol⁻¹*

with molecular bond lengths/ Å and spin densities

β-Scission reactions of oxy radicals derived from 55ca

In addition to the fragmentation products, the thermolysis of methoxy-substituted *dispiro*-1,2,4-trioxane **54ca** formed the fully ring expanded keto lactone **57ca** in high yield. This suggests that the β-scission of ring **A** must be directly competitive with ring **C** thus preventing the synthesis of oxalactone **56ca**.

A comparison between opening rings **A** and **C** from intermediate **55ca** show similar energies to those of **55aa** and **55ba** except for a reduction in the transition state energy for the opening of C(2)-C(3) via **TS[55ca-81]** to 25.4 kcal mol⁻¹ *(Figure 30)*. This brings the barrier for opening of the C(2)-C(3) bond 1.7 kcal mol⁻¹ lower in energy than those for the opening of ring **C** via **TS[55ca-56ca]** and the fragmentation pathway via **TS[55ca-frag]**. This is a significant observation as it confirms that the formation of keto lactone **57ca** occurs because ring **A** opens faster than ring **C** meaning that oxalactone **56ca** is prevented from being formed.
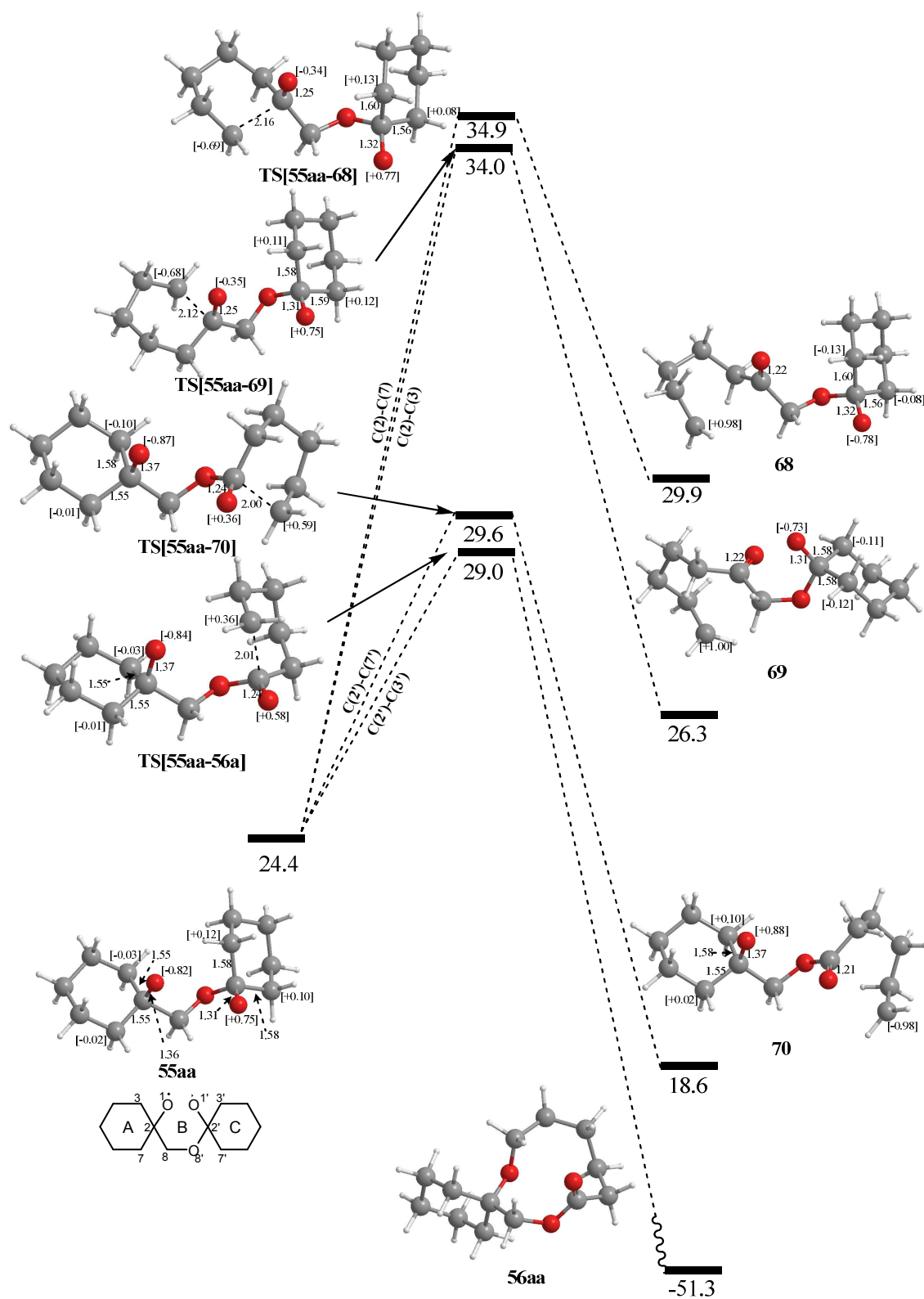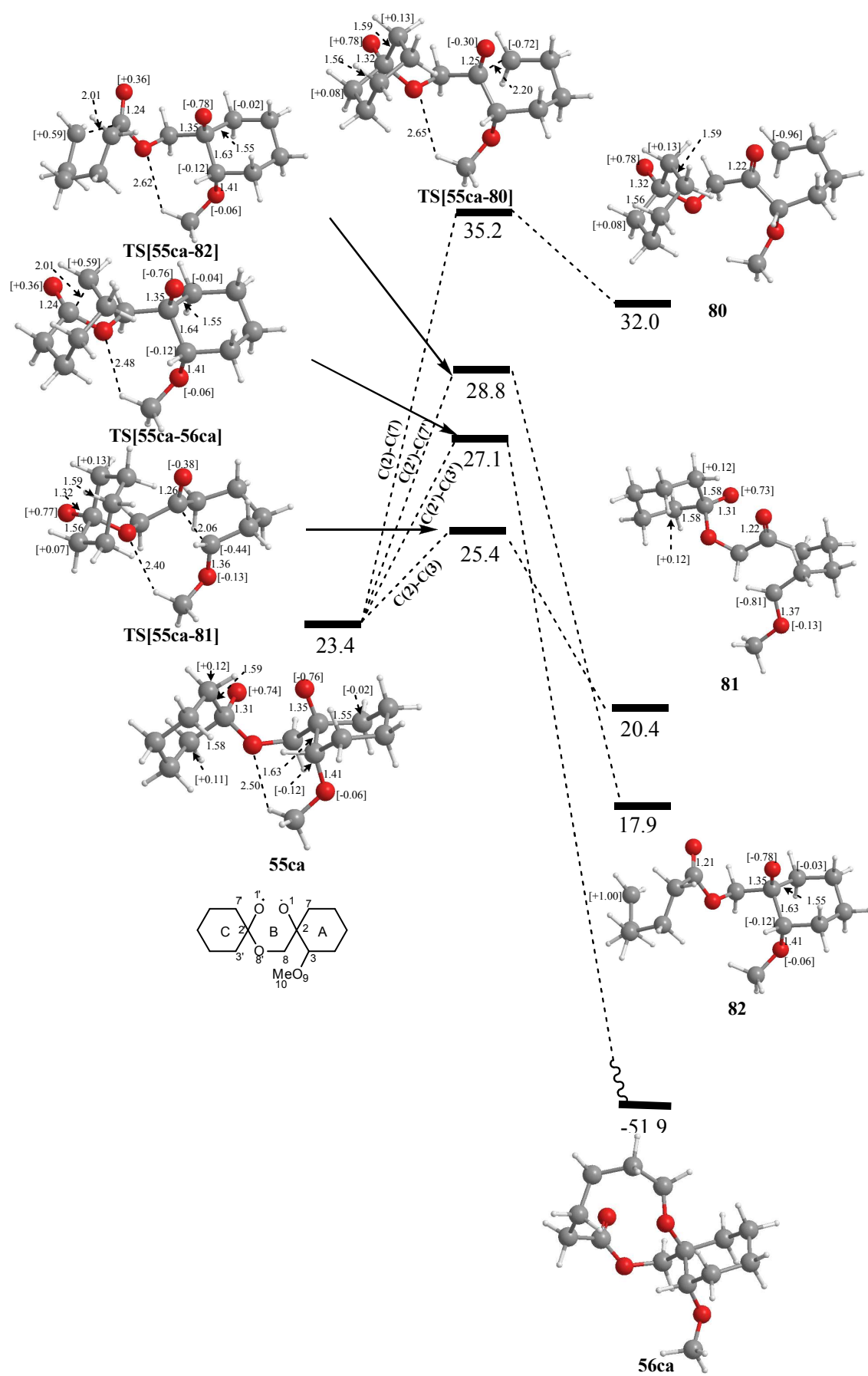
*Figure 30: The reaction profile for the competitive β-scission reactions of **55ca** / kcal mol⁻¹*
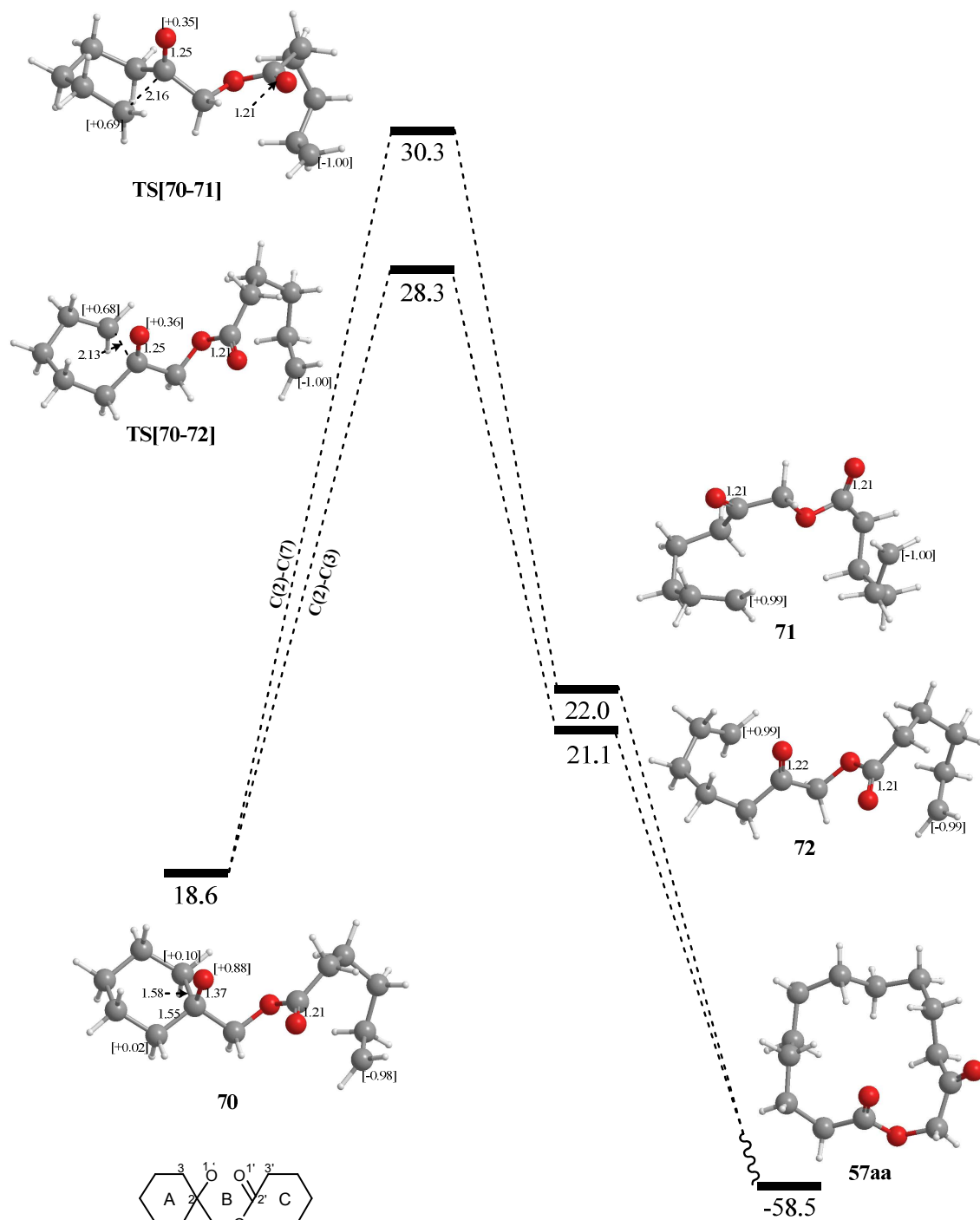
with molecular bond lengths/ Å and spin densities

TS[55ca-81] is more reactant like than the other competing transition states consistent with the Hammond postulate.[23] The oxygen of the methoxy group continues to stabilise the spin density on C(3) resulting in increased spin density on O(9) (**TS[55ca-81]**= -0.13, **81**= 0.13) and a shortening C(3)-O bond (**TS[55ca-81]**= 1.37 Å, **81**= 1.37 Å). The newly formed carbon-centred radical at C(3) is positioned away from the other radical at O(1′) in **81** meaning that significant rearrangement would be required to give the recombined product. Instead, β-scission of ring **C** may occur.

Intermediate **81** contains the opened ring **A** and a delocalisation of spin density from O(1′) to C(3′) and C(7′) in ring **C**. **TS[81-83]** and **TS[81-84]** for the β-scission of ring **C** show barriers of *ca.* 5 kcal mol^{-1} for both the opening of the C(2′)-C(3′) and C(2′)-C(7′) bonds, consistent with the analogous processes in **55ca** and the small model systems *(Figure 31)*. Both **TS[81-83]** and **TS[81-84]** show relatively short C⋯C interatomic distances of 2.01 Å. Throughout the reaction, the radical character on C(3) continues to be delocalised onto O(9). These processes form intermediates **83** and **84** respectively at 15.0 kcal mol^{-1} in exothermic reactions from **81**. From **83** and **84** recombination of the carbon-centred radicals would form the experimentally observed keto lactone.

For completeness, a reaction profile forming the fully ring expanded ketolactone **57ca** from **82** has also been considered with the results illustrated in *Appendix 3 Figure 2*.
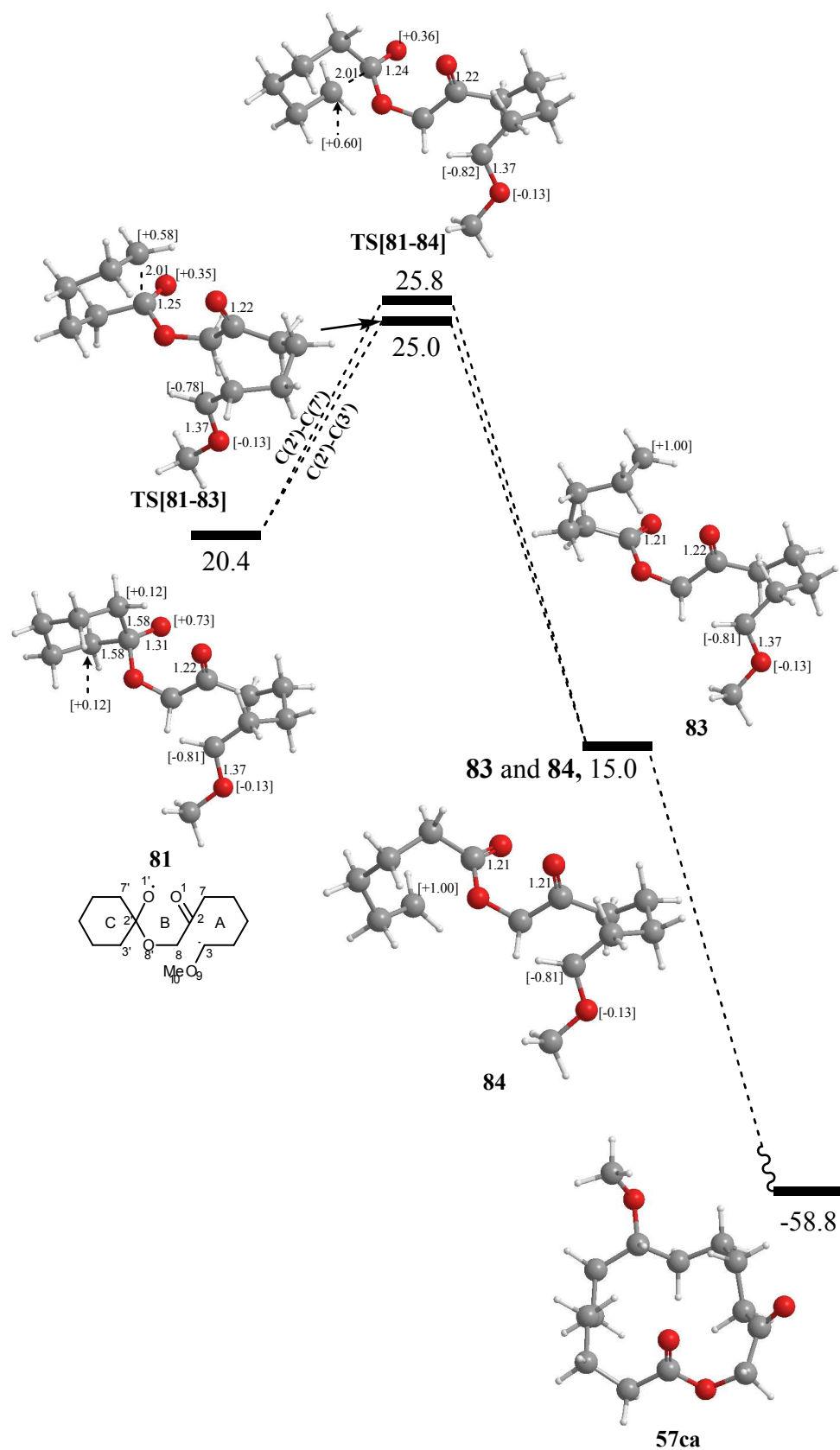
*Figure 31: The reaction profile for the competitive β-scission reactions of **55ca** / kcal mol⁻¹*

with molecular bond lengths/ Å and spin densities

Conclusion

Calculations on the full model systems have provided a good explanation for the observed products in the thermolysis of *dispiro*-1,2,4-trioxanes **54aa**, **54ba** and **54ca**. Additionally the transition state barriers for β-scission have shown a very good correlation with the small model systems signifying that the models chosen were representative of the full system. The results further reveal that the assumption made in the small models, which was that rings **A** and **C** were acting independently of each other, was valid.

The calculation of the various β-scission reactions for the opening of rings **A** and **C** of a unsubstituted *dispiro*-1,2,4-trioxane **54aa** confirm a significantly larger barrier for the opening of ring **A** over ring **C**, consistent with the formation of oxalactone **56aa** and not the fully ring-expanded keto lactone **57aa**. In fact, the lowest transition state found for **55aa** linked directly to the oxalactone **56aa** itself.

The introduction of methyl- or methoxy-substituents into the α-position of ring **A** delivers a systematic stabilisation of radical character from C(3) onto the substituent consistent with the step-wise increase in the 'α-effect' provided by the methyl and methoxy groups.

Although the methyl substituent provides a moderate α-effect, the transition state for the C(2)-C(3) bond is lowered significantly from **54aa**, however not low enough to compete directly with the transition state for the opening of ring **C**. Like **54aa,** the lowest energy β-scission transition state links directly to the formation of oxalactone **56ba**. The opening of ring **C** in this example would occur first resulting in the oxalactone being the major product formed. The formation of keto lactone **57ba** would therefore occur via the small proportion of species which open via the β-scission of the C(2′)-C(7′) bond.

The greater α-effect provided by the methoxy group delivers a relatively low transition state barrier for the opening of the C(2)-C(3) bond which significantly is the lowest energy β-scission reaction. It would be suggested that the opening of ring **A** in this example would occur first closely followed by ring **C** thus preventing oxalactone **56ca** from being formed in substantial quantities.

Dispiro-**1,2,4-trioxanes 54cb and 54cc**

For completeness the various β-scission reactions of *dispiro*-1,2,4-trioxanes **54cb** and **54cc** were also investigated with the results contained within *Appendix 3 Figures 3-8* The results almost mirror those reported for **54ca** with the formation of the corresponding keto lactone **56cb** explained through low energy pathways in each case. However, in a slight change to the results, the opening of ring **C** via β-scission of the C(2′)-C(3′) bond in **54cb** was slightly lower than the opening of the methoxy-substituted C(2)-C(3) bond. This is consistent with the greater amount of ring strain released from a 5-membered ring compared to a 6- or 7- membered ring.[11] Despite the change in energy for the opening of ring **C** in **55cb** resulting in the energy barriers for the opening of rings **A** and **C** being similar, the fact that experimentally only keto lactone **57cb** is observed suggests both rings open in rapid succession.

Computational background

Introduction

This section contains a brief explanation of density functional theory (DFT), the computational method used within this chapter.[51,52] An explanation of the fundamental quantum mechanics and methods such as Hartree-Fock (HF) will also be discussed as this provides a framework in which practical systems for DFT, as applied for molecular systems, has been developed.

Background Quantum Mechanics

The Schrödinger Equation

A major goal of quantum chemistry is to find a solution to the time-independent Schrödinger equation:

$$\hat{H}\Psi = E\Psi \qquad (\mathbf{1})$$

Here $\hat{H}$ is the Hamiltonian, a differential operator representing the total energy, which acts on the wave function, Ψ, to produce an eigenvalue, E, the total energy of the system.

In the Schrödinger equation the Hamiltonian operator, $\hat{H}$, is used:

$$\hat{H} = \frac{1}{2}\sum_{i=1}^{N}\nabla^2 - \frac{1}{2}\sum_{A=1}^{M}\frac{1}{M_A}\nabla_A{}^2 - \sum_{i=1}^{N}\sum_{A=1}^{M}\frac{Z_A}{r_{iA}} + \sum_{i=1}^{N}\sum_{j>i}^{N}\frac{1}{r_{ij}} + \sum_{A=1}^{M}\sum_{B>A}^{M}\frac{Z_A Z_B}{R_{AB}} \qquad (\mathbf{2})$$

The first two terms in $\hat{H}$ describe the kinetic energies of N electrons and M nuclei within a molecule, where M_A is the mass of the nucleus A. The Laplacian operator ∇^2, which is contained in these two terms, is defined in equation **3** where x,y and z are Cartesian coordinates.

$$\nabla^2 = \frac{\partial^2}{\partial x_q^2} + \frac{\partial^2}{\partial y_q^2} + \frac{\partial^2}{\partial z_q^2} \qquad (3)$$

The third term of equation **2** describes the attractive electrostatic interaction between the electrons and nuclei in the molecule and the final two terms represent the repulsive potential which arises from electron-electron and nucleus-nucleus interactions respectively. In total, the final three terms of the operator describe the potential energy part of the system.

Exact solutions to the Schrödinger equation are not possible and therefore some approximations have to be made in order to simplify it.

The Born-Oppenheimer Approximation

The large difference in the mass of a nucleus compared with an electron provides the basis behind the Born-Oppenheimer approximation. With the nuclei being at least 1800 times heavier than an electron the nuclei moves relatively much more slowly than their associated electrons. The approximation makes the assumption that the nuclei are effectively static compared to electrons.

Based on this assumption the Schrödinger equation can be greatly simplified. The kinetic energy term associated with the nuclei is considered to be zero and the nucleus-nucleus repulsion term, contained within the potential energy part of the operator, can be replaced with a constant. This results in the 'electronic Hamiltonian operator', $\hat{H}_{elec}$.

$$\hat{H}_{elec} = \frac{1}{2}\sum_{i=1}^{N}\nabla^2 - \sum_{i=1}^{N}\sum_{A=1}^{M}\frac{Z_A}{r_{iA}} + \sum_{i=1}^{N}\sum_{j>i}^{N}\frac{1}{r_{ij}} = T + V_{eN} + V_{ee} \qquad (4)$$

Here T is the kinetic operator, V_{eN} is the attractive electron-electron potential and V_{ee} is the repulsive electron-electron potential. Often V_{eN} is referred to as V_{ext}, as it describes the external potential of a set of nuclei attracting the electrons.

Changing the nature of the operator, $\hat{H}$, to being an electronic operator, $\hat{H}_{elec}$, changes the solution of the Schrödinger equation to an electronic wave function, Ψ_{elec}, and the corresponding electronic energy, E_{elec}.

Variation Principle

In principle, the variation principle provides a method from which the ground state energy of the system can be derived.

The expectation value of a particular property (in this case the energy of a molecule) represented by an appropriate operator (such as $\hat{H}$) acting on any possible normalized wave function (Ψ_{trial}) is given by the following equation:

$$\langle \Psi_{trial} | \hat{H} | \Psi_{trial} \rangle = E_{trial} \geq E_0 = \langle \Psi_0 | \hat{H} | \Psi_0 \rangle \qquad \textbf{(5)}$$

The variation principle means that the energy E_{trial} will always be greater than or equal to the lowest possible energy, i.e. ground state E_0.

The Hartree-Fock Approximation

In practice, a search for all possible wave-functions to find E_0 is impossible. An alternative approach is to limit the search to a subset of wave functions which should allow the best wave-function to be identified by applying the variation principle.

The Hartree-Fock method assumes that the wave function of a chemical system can be described by a single Slater determinant, Φ_{SD}, composed as a combination of one electron spin orbitals comprised of a special part and a spin component which can either be α or β spin.[53] The Φ_{SD} approximates the wave function by use of an antisymmetrized product of the one electron spin orbitals, $\chi_N(\mathbf{x}_N)$.

$$\Psi \approx \Phi_{SD} = \frac{1}{\sqrt{N!}} \begin{vmatrix} \chi_1(\mathbf{x}_1) & \chi_2(\mathbf{x}_1) & \cdots & \chi_N(\mathbf{x}_1) \\ \chi_1(\mathbf{x}_2) & \chi_2(\mathbf{x}_2) & \cdots & \chi_N(\mathbf{x}_2) \\ \vdots & \vdots & \ddots & \vdots \\ \chi_1(\mathbf{x}_N) & \chi_2(\mathbf{x}_N) & \cdots & \chi_N(\mathbf{x}_N) \end{vmatrix} \qquad \textbf{(6)}$$

and can be abbreviated as:

$$\Phi_{SD} = \frac{1}{\sqrt{N!}} det\{\chi_1(\pmb{x}_1)\chi_2(\pmb{x}_2)\cdots\chi_N(\pmb{x}_N)\} \qquad (7)$$

A Φ_{SD} must be antisymmetric with respect to the interchange of two electrons, resulting in the interchange of two rows changing the sign of Φ_{SD}. If two columns are the same, corresponding to two electrons occupying the same spin orbital, the Φ_{SD} equals zero thus obeying the Pauli exclusion principle.

The HF method is a self-consistent field (SCF) approach which calculates the electronic structure of a given molecule/system iteratively. The method starts with a set of guess orbitals which are solved using equation **8** which contains the Fock operator (**9**). Using this method a new set of orbitals are formed which are compared to the previous set. The cycle continues until the orbitals do not change and the lowest energy is found.

$$f\chi = E\chi \qquad\qquad (8)$$

$$f = -\frac{1}{2}\nabla_i^2 - \sum_A^M \frac{Z_A}{r_{iA}} + V_{HF}(i) \qquad (9)$$

This one electron operator in equation **9** is comparable with the electronic Hamiltonian operator. The first two terms represent the kinetic and potential energy due to electron-nucleus attraction and the V_{HF} term is the Hartree-Fock potential of one electron in the presence of the remaining electrons. The V_{HF} term consists of two components, the Coulomb and exchange operators, shown below:

$$V_{HF}(\pmb{x}_1) = \sum_j^N (\hat{J}_j(\pmb{x}_1) - K_j(\pmb{x}_1)) \qquad (10)$$

The Coulomb operator is defined as the potential that an electron at position ($\pmb{x}_1$) experiences due to the average charge distribution from another spin orbital χ_j (summed for all electrons).

$$\hat{J}_j(\boldsymbol{x}_1) = \int |\chi_j(\boldsymbol{x}_2)|^2 \frac{1}{r_{12}} d\boldsymbol{x}_2 \qquad (11)$$

The second term, for the exchange operator, has no classical interpretation and can only be defined through its effect when operating on a spin orbital.

$$K_j(\boldsymbol{x}_1)\chi_i(\boldsymbol{x}_1) = \int \chi_j^*(\boldsymbol{x}_2) \frac{1}{r_{12}} \chi_i(\boldsymbol{x}_2) d\boldsymbol{x}_2 \chi_j(\boldsymbol{x}_1) \qquad (12)$$

The major problem with the Hartree-Fock approximation is it doesn't take account for the dynamic nature of the electron-electron interactions, or electron correlation. The approximation uses an average of electron-electron interactions across all the electrons resulting in the E_{HF} always being higher than the real energy. The difference between the real energy and the E_{HF} is defined as the electron correlation energy, E_C.

Density Functional Theory

The central concept behind density functional theory is use of electron density, $\rho(\boldsymbol{x}_1)$, to calculate the electronic energy of the system. The electron density is a physically observable property which can in principle be measured experimentally via X-ray crystallography and can be used to calculate E without using approximations. $\rho(\boldsymbol{x}_1)$ measures the probability of finding any of the electrons (of arbitrary spin) within the volume element $d\boldsymbol{x}_1$ while the other electrons have arbitrary spin and positions in the state represented by Ψ. This is shown mathematically in equation **13** where the integral is over all spin coordinates of the electrons and all spatial coordinates

$$\rho(\boldsymbol{x}_1) = N \int \cdots \int |\Psi(\boldsymbol{x}_1, \boldsymbol{x}_2, \dots \boldsymbol{x}_N)|^2 d\boldsymbol{x}_1 \, d\boldsymbol{x}_2 \dots d\boldsymbol{x}_N \qquad (13)$$

$\rho(\boldsymbol{x}_1)$ has some interesting properties, which are useful in understanding of density functional theory (DFT). Namely, the electron density tends to zero as the three spacial coordinates tend to infinity, which can be written as:

$$\rho(\boldsymbol{x}_1 \to \infty) = 0 \qquad (14)$$

Secondly, the electron density integrates to give the total number of electrons in the molecule, N:

$$\int \rho(\boldsymbol{x}_1) d\boldsymbol{x}_1 = N \qquad (\mathbf{15})$$

And thirdly, due to the attractive charge exerted by the positive charge of the nucleus in an atom on an electron, the electron density at the position of a nucleus exhibits a maximum with a finite value. The gradient of the electron density at these positions is zero, leading to a discontinuity called a 'cusp'. The properties of the cusp are related to the nuclear charge of the nucleus.

The Hohenberg-Kohn Theorems

The two Hohenberg-Kohn theorems produced the starting point for modern DFT and provided a mathematical proof that the molecular properties of a molecule can, in principle, be found from the electron density of the molecule.[54]

The first of Hohenberg-Kohn theorems shows that the external potential of the molecule, $V_{ext}(\boldsymbol{x})$ is a unique functional of the electron density $\rho(\boldsymbol{x})$. As $V_{ext}(\boldsymbol{x})$ determines the operator, $\hat{H}$, the full many particle ground state energies must also be a unique functional of $\rho(x)$.

This theorem was demonstrated by considering two different external potentials, V_{ext} and V'_{ext} which give rise to the same electron density $\rho(\boldsymbol{x})$. The external potentials are part of two distinct Hamiltonian operators, $\hat{H}$ and $\hat{H}'$ respectively, which differ only by the fact that they have different external potentials, i.e. $\hat{H} = T + V_{ee} + V_{ext}$ and $\hat{H}' = T + V_{ee} + V'_{ext}$. These two Hamiltonian operators correspond to different ground state wave functions, Ψ and Ψ' and the associated energies, E_0 and E_0', which are non-equivalent.

As the wave functions, Ψ and Ψ', are different they can be used as trial wave functions for the $\hat{H}$ and $\hat{H}'$ operators. The variation principle can then be applied as illustrated below for Ψ' and $\hat{H}$.

$$E_0 < \langle \Psi' | \hat{H} | \Psi' \rangle = \langle \Psi' | \hat{H}' | \Psi' \rangle + \langle \Psi' | \hat{H} - \hat{H}' | \Psi' \rangle \qquad (16)$$

As the Hamiltonians differ only because of their respective external potentials, this can be written as:

$$E_0 < E'_0 + \langle \Psi' | T + V_{ee} - T - V_{ee} - V'_{ext} | \Psi' \rangle \qquad (17)$$

Which simplifies to:

$$E'_0 < E_0 + \int \rho(\mathbf{r}) \{V_{ext} - V'_{ext}\} d\mathbf{r} \qquad (18)$$

The corresponding equation for the trial combining Ψ and $\hat{H}'$ is:

$$E'_0 < E_0 - \int \rho(\mathbf{r}) \{V_{ext} - V'_{ext}\} d\mathbf{r} \qquad (19)$$

Upon addition, these equations reduce to:

$$E_0 + E'_0 = E'_0 - E_0 \qquad (20)$$

This is clearly inconsistent therefore showing that two different external potentials cannot give the same electronic ground state and further confirming that the ground state energy is a unique functional of the ground state electron density.

The expression linking the ground state energy with the ground state electron density can be further broken down into the following contributions:

$$E_0[\rho] = T[\rho_0] + E_{ee}[\rho_0] + V_{ext} d\mathbf{x} \qquad (21)$$

The first two terms, the kinetic energy $T[\rho_0]$ and the electron-electron repulsion $E_{ee}[\rho_0]$, are independent of N, R_A and Z_A and are therefore not specific to one system. These terms are collectively known as the Hohenberg-Kohn functional, $F_{HK}[\rho_0]$. Effectively, if

the Hohenberg-Kohn functional is given a particular density then it generates the expectation value for the ground state kinetic energy and the ground state electron-electron repulsion energy.

$$F_{HK}[\rho] = T[\rho] + E_{ee}[\rho] = \langle \Psi | T + V_{ee} | \Psi \rangle \qquad (22)$$

The second of Hohenberg-Koln theorems is related to the variation principle detailed in equation **5**. It states that a trial density ρ_{trial} gives an energy equal to or higher than the ground state electron density ρ ($E_{trial} \geq E(\rho)$).

The Kohn-Sham Method

It was a paper by Kohn and Sham in 1965 which provided the basis of modern density functional theory by finding a description of a molecule's energy based upon electron density.[55] By introducing one-electron orbitals into DFT they realised that using a system of non-interacting electrons they can calculate very accurately the majority of the kinetic energy.

The system of non-interacting electrons is constructed from a Slater determinant similar to that used in Hartree-Fock theory:

$$\Psi_s = \frac{1}{\sqrt{N!}} \det [\varphi_1 \varphi_2 \cdots \varphi_N] \qquad (23)$$

The kinetic energy for non-interacting electrons, T_s, can then be expressed using equation **24**:

$$T_s = -\frac{1}{2} \sum_i^N \langle \varphi_i | \nabla^2 | \varphi_i \rangle \qquad (24)$$

In reality the electrons are interacting and **24** does not provide the total kinetic energy, T. However the difference, T_C between the exact kinetic energy and that calculated, T_S, by assuming non-interacting electrons is small. The remaining kinetic energy, T_C is

absorbed into an exchange–correlation functional, E_{XC}, and a general DFT energy expression can be written:

$$E[\rho] = T_s[\rho] + E_{Ne}[\rho] + J[\rho] + E_{xc}[\rho] \qquad (25)$$

Where E_{XC} can be defined as:

$$E_{xc}[\rho] = T_c[\rho] + E_{ncl}[\rho] \qquad (26)$$

Where the E_{ncl} is made up of the non-classical electrostatic contributions and the potential energy (self interaction, exchange and electron-electron correlation).

Unfortunately E_{XC} cannot be calculated accurately so some approximations have to be made.

The Local Density Approximation (LDA)

One such approximation is to use a uniform electron gas model. A uniform electron gas is a volume (V) with *n* electrons uniformly distributed, which consequently has an electron density $\rho = n/V$ making it structurally similar to a metal. It is obtained when *n* and V approach infinity, and has uniformly distributed positive changes, which neutralise the system. The local density approximation (LDA), $E_{XC}[\rho]$ takes the form:

$$E_{XC}^{LDA}[\rho] = \int \rho(\boldsymbol{x}) \varepsilon_{XC}(\rho(\boldsymbol{x})) dr \qquad (27)$$

This is the electron-exchange correlation energy per particle of a uniform-electron-gas with the density $\rho(\boldsymbol{x})$. The exchange-correlation term can be split into two components, exchange, $\varepsilon_x(\rho(\boldsymbol{x}))$ and correlation $\varepsilon_c(\rho(\boldsymbol{x}))$. The exchange part can be calculated using the Slater exchange (S):

$$S = \varepsilon_x(\rho(\boldsymbol{x})) = -\frac{3}{4}\left(\frac{3\rho(\boldsymbol{x})}{\pi}\right)^{\frac{1}{3}} \qquad (28)$$

No such equation exists for the correlation part. However highly accurate quantum Monte-Carlo simulations of the homogeneous electron gas are often used to approximate $\varepsilon_c(\rho(\mathbf{x}))$.

The Generalised Gradient Approximation (GGA)

The LDA does not accurately approximate the exchange-correlation energy for real molecular systems very well, as they do not generally have a uniform electron density. One way of improving the LDA is to use a correction which uses the gradient of change in the electron density. One such method is the Generalised Gradient Approximation (GGA) which can be expressed as:

$$E_{XC}^{GGA}[\rho_\alpha, \rho_\beta] = \int f\left(\rho_\alpha, \rho_\beta, \nabla\rho_\alpha \nabla\rho_\beta\right)dr \qquad (29)$$

Here, the exchange correlation term is often split into explicit exchange and correlation terms, and the two terms are approximated separately:

$$E_{XC}^{GGA} = E_X^{GGA} + E_C^{GGA} \qquad (30)$$

The gradient corrected exchange functional, E_X^{GGA}, can be expressed as:

$$E_X^{GGA} = E_X^{LDA} - \sum_\sigma F(s_\sigma)\,\rho_\sigma^{4/3}(\mathbf{x})d\mathbf{x} \qquad (31)$$

Where the first term is the local density approximation of the exchange functional and the second term involves the reduced density gradient, which is the GGA term, F, and a local inhomogenity parameter, s_σ.

The function F used in this work was described by Becke and often referred to as B.[56] The B exchange functional contains an empirical parameter, β, which originates from the experimentally determined values of exchange energies of the six noble gases.

$$F^B = \frac{\beta s_\sigma^2}{1 + 6\beta s_\sigma sinh^{-1} s_\sigma} \qquad (32)$$

The Becke exchange functional can be combined with correlation functions such as P86[57] (Perdew 1986), LYP[58] (Lee, Yang and Parr 1988) and PW91[59] (Perdew and Wang 1991) to give commonly used functionals like BLYP, BP86 and BPW91.

Exchange functionals can be further improved by including some exchange energy, calculated using HF theory, in a so-called hybrid functional. From HF theory the exchange energy from the Slater determinant can be solved exactly. Some DFT methods have been developed to include a proportion of Hartree-Fock exchange. An example of a hybrid functional is B3 which when combined with a correlation functional e.g LYP gives the B3LYP hybrid functional:

$$E_{xc}^{B3LYP} = (1-a)E_x^{LDA} + aE_X^{HF} + b\Delta E_x^B + (1-c)E_c^{LDA} + cE_c^{LYP} \qquad (33)$$

Basis Sets

In molecular orbital theory molecular orbitals are constructed by using a linear combination of atomic orbitals. In molecular calculations the atomic orbitals are represented in a basis set as a series of basis functions. In theory, each MO would be perfectly described using an infinite number of basis functions, a so-called complete basis set. However this is not computationally practical meaning that there is required to be an approximation.

There are two types of basis function which are commonly used in electronic structure calculations: Slater Type Orbitals (STO); and Gaussian Type Orbitals (GTO). Although STOs provide a better approximation of the AO, particularly close to and far away from the nucleus, they are more computationally demanding than GTOs. Therefore basis sets using GTOs were developed where a number of GTOs are combined to give a good approximation of an STO.

Basis sets are selected based on accuracy verses computational expense. The most popular are the basis sets designed by J. A. Pople and coworkers.[60] The so-called

'minimal basis sets' are the simplest, but least accurate, and contain one basis function for each atomic orbital. A common minimal basis set is STO-3G where three GTO is used to represent each STO.

These 'minimal basis sets' can be improved by varying the number of basis functions used to describe the different atomic orbitals. This can be achieved using *Double Zeta* basis sets in which there are two basis functions for each AO. Given that chemical reactivity uses the valence rather than the core electrons it is reasonable to assume that if valence orbitals are described via two basis functions whilst the core orbitals are described by one, the accuracy will not be affected significantly whilst computational time would be saved. Such basis sets are termed 'Split Valence' basis sets with one of the most popular examples being 6-31G. 6-31G represents the core electrons by a fixed combination of 6 GTOs whilst the valence electrons are represented by 3 GTOs contracted together plus 1 GTO.

The basis set can be further improved by introducing polarization functions onto heavy atoms, by adding d-orbital polarization, and hydrogens, by adding p-orbital polarization. The 6-31G* (6-31G + d-functions for first row atoms) and 6-31G** (6-31G + d for first row and p for hydrogen) basis sets allows for an accurate representation of geometries without great computational expense.

Benchmarking Calculations

To test the efficiency of different functionals a series of benchmarking calculations were undertaken. The two reactions investigated were the β-scission reactions of **90** and **59** which model rings **A** and **C** of the *dispiro*-1,2,4-trioxane ring respectively (Scheme 16). The functionals chosen to test include B3LYP, BLYP, BP86 and BPW91 with the results illustrated in *Tables 23-25*. A 6-31G** basis set was used throughout.

The results show that the activation barriers for ring opening of **90** through **TS[90-90′]** are consistently higher in energy than the opening of **59** through **TS[59-59′]**. These are all consistent with the rate of β-scission in ring **C** being much faster than that of ring **A**. Although the choice of functional makes some difference to the absolute values of ΔE_a only a small difference to the difference in activation energy, $\Delta\Delta E_a$, between the two

reactions. Additionally the formation of **90′** and **59′** are consistently endothermic and exothermic respectively.
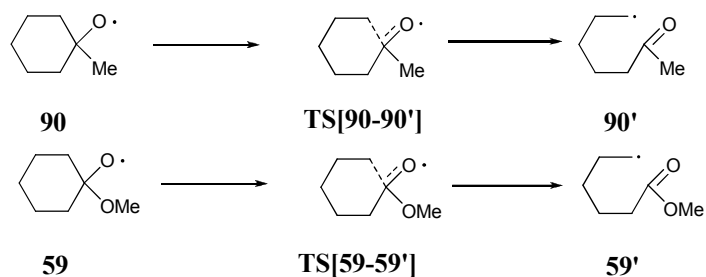
Scheme 16

	B3LYP	BLYP	BP86	BPW91
TS[90-90′]	10.3	8.0	9.4	9.6
90′	2.9	2.1	5.6	5.1

*Table 23 Energies for the β-scission reaction of **90** using different functionals*

All calculations used 6-31G** basis set / kcal mol^{-1}

	B3LYP	BLYP	BP86	BPW91
TS[59-59′]	4.0	3.1	4.0	4.1
59′	-7.9	-6.5	-3.3	-4.0

*Table 24 Energies for the β-scission reaction of **59** using different functionals*

All calculations used 6-31G** basis set / kcal mol^{-1}

Functional	$\Delta\Delta E_a$
B3LYP	6.3
BLYP	4.9
BP86	5.4
BPW91	5.5

Table 25: Differences in activation energies, $\Delta\Delta E_a$, for the β-scission reaction of

***90** and **59** using different functionals*

All calculations used 6-31G** basis set / kcal mol^{-1}

To test the efficiency of different basis sets a series of benchmarking calculations were undertaken using the reaction highlighted in *Scheme 16*. The basis sets chosen to test include 6-31G, 6-31G*, 6-31G** and 6-311G** with the results illustrated in *Tables 26-28*. A B3LYP functional was used throughout.

The overall energies calculated for the different basis sets remain constant and suggest a significantly faster β-scission reaction in ring **C** over ring **A**. Calculations using a basis set without polarization e.g. 6-31G show significantly higher activation barriers and ΔΔEa energies than those with polarization. The basis sets with polarization show similar energies and $\Delta\Delta E_a$ energies with smaller differences apparent between 6-31G* and 6-31G** than between 6-31G and 6-31G*. Although 6-311G** will provide a slightly better energy than 6-31G** the calculations take twice as long to complete. As large model systems would be required to be calculated the 6-31G** basis set was used throughout.

	6-31G	6-31G*	6-31G**	6-311G**
TS[90-90′]	13.9	10.4	10.3	11.0
90′	7.8	3.3	2.9	0.6

*Table 26: Energies for the β-scission reaction of **90** using different basis sets*

All calculations used the B3LYP functional / kcal mol^{-1}

	6-31G	6-31G*	6-31G**	6-311G**
TS[59-59′]	6.7	4.1	4.0	3.0
59′	-2.9	-7.6	-7.9	-10.34

*Table 26: Energies for the β-scission reaction of **59** using different basis sets*

All calculations used the B3LYP functional / kcal mol^{-1}

Basis Set	$\Delta\Delta E_a$
6-31G	7.2
6-31G*	6.3
6-31G*	6.3
6-311G*	7.0

Table 28: Differences in activation energies, ΔΔEa, for the β-scission reaction of

***90** and **59** using different basis sets*

All calculations used the B3LYP functional / kcal mol^{-1}

[1] T. Yoshimitsu, S. Sasaki, Y. Arano, H. Nagaoka, *J. Org. Chem,* 2004, **69**, 9262-9268

[2] W. Xu, J-P., Zou, X-J. Mu, and W. Zhang, *Tetrahedron Lett.*, 2008, **49**, 7311-7314

[3] E. S. C. Kwok, J. Arey, and R, Atkinson, *J. Phys. Chem.*, 1996, **100**, 214-219

[4] P. M. O'Neill, G. H. Posner, *J. Med. Chem.*, 2004, **46**, 2945-2964

[5] P. Grey, and A. Williams, *Chem. Rev.*, 1959, **59**, 239-328

[6] C. Walling, *Pure Appl. Chem.*, 1967, **15**, 69-80

[7] C. Walling, and A. Padwa, *J. Am. Chem. Soc.*, 1963, **85**, 1593-1597

[8] C. Walling, and R. T. Clark, *J. Am. Chem. Soc.*, 1974, **96**, 4530-4534

[9] J. K. Kochi, *J. Am. Chem. Soc.*, 1962, **84**, 1193-1197

[10] J. D. Bacha, and J. K. Kochi, *J. Org. Chem.*, 1965, **30**, 3272-3278

[11] S. Wilsey, P. Dowd, and K. N. Houk, *J. Org. Chem.*, 1999, **64**, 8801-8811

[12] M. Bubeck, M. Kling, and S. Schmatz, *Z. Phys. Chem.*, 2005, **219**, 1205-1222

[13] M. Leblanc, D. Siri, S. R. A. Marque, S. Grimaldi, D. Bertin, and P. Tardo, *Int. J. Quant. Chem.*, 2006, **106**, 676-685

[14] D. J. Henry, C. J. Parkinson, P. M. Meyer, and L. Radom, *J. Chem. Soc., Perkin Trans. A*, 1999, 2305-2313

[15] D. J. Henry, C. J. Parkinson, P. M. Meyer, and L. Radom, *J. Phys. Chem. A*, 2001, **105**, 6750-6756

[16] A. Rauk, R. J. Boyd, S. L. Boyd, D. J. Henry, and L. Radom, *Can. J. Chem.*, 2003, **81**, 431-442

[17] H. Zipse, *Top. Curr. Chem.,* 2006, **263**, 163-189

[18] A. Boto, R. Hernández, A. Montoya and E. Suárez, *Tetrahedron Lett.,* 2003, **45**, 1559-1563

[19] A. Boto, D. Hernández, R. Hernández, A. Montoya and E. Suárez, *Eur. J. Org. Chem.,* 2007, 325-334

[20] A. Boto, R. Hernández, and E. Suárez, *Tetrahedron Lett.,* 2002, **43**, 1821-1824

[21] A. Boto, R. Hernández, and E. Suárez, *J. Org. Chem.*, 2003, **68**, 5310-5319

[22] L. Hernndez-Garca, L. Quintero, M. Sanchez, and F. Sartillo-Piscil, *J. Org. Chem.*, 2007, **72**, 8196-8201

[23] G. S. Hammond, *J. Am. Chem. Soc.*, 1955, **77**, 334-338

[24] A. L. J. Beckwith, B. P. Hay, *J. Am. Chem. Soc.*, 1989, **111**, 230-234

[25] F. D. Greene, M. L. Savitz, F. D. Oserholtz, H. H. Lau, W. N. Smith, and P. M. Zanet, *J. Org. Chem.*, 1963, **28**, 55-64

[26] M. Bietti, O. Lanzulunga, and M. Salamone, *J. Org. Chem.*, 2005, **70**, 1417-1422

[27] W. Zhang, and P. Dowd, *Tetrahedron*, 1993, **49**, 1965-1978

[28] C. Thomson, M. Cory, M. Zerner, *Int. J. Quant. Chem.*, 1991, **40**, S18, 231-245

[29] G. Bernardinelli, C W Jefford, D. Maric, *Int. J. Quant. Chem.*, 1994, **52**, S21, 117-131

[30] J-D. Gu, K-X. Chen, H-L. Jiang, W-L. Zhu, J-Z. Chen, and R-Y. Ji, *Chem. Phys. Lett.,* 1997, **277**, 234-238

[31] J. Gu, K. Chen, H. Jiang, R. Ji*, J. Mol. Struct. (Theochem)*, 1999, **459**, 103-111

[32] V. Galasso, B. Kovaĉ, A. Modelli, *Chem. Phys.*, 2007, **335**, 141-154

[33] J. Gu, K. Chen, H. Jiang, and J. Leszczynski, *J. Phys. Chem. A*, 1999, **103**, 9364-9369

[34] M. G. B. Drew, J. Metcalfe, F. M. D. Ismail, *J. Mol. Struct. (Theochem),* 2004, **711**, 94-105

[35] M. G. B. Drew, J. Metcalfe, F. M. D. Ismail, *J. Mol. Struct. (Theochem),* 2005, **756**, 87-95

[36] J. Q. Araújo, J. W. de M. Carneiro, M. T. de Araujo, F. H. A. Leite, and A. G. Taranto*, Bioorg. Med. Chem.*, 2008, **16**, 5021-5029 and references there in

[37] M. G. B. Drew, J. Metcalfe, M. J. Descombe, and F. M. D. Ismail, *J. Med. Chem.* 2006, **49**, 6065-6073

[38] M. G. B. Drew, J. Metcalfe, M. J. Descombe, and F. M. D. Ismail, *J. Mol. Struct. (Theochem),* 2007, **823**, 34-46

[39] P. Moles, M. Oliva, V. S. Safont, *J. Phys. Chem. A.*, 2006, **110**, 7144-7158

[40] P. Moles, M. Oliva, V. S. Safont, *Tetrahedron*, 2008, **64**, 9448-9463

[41] W-M Wu, Y. Wu, Y-L. Wu, Z-J Yao, C-M. Zhou, Y. Li, and F. Shan, *J. Am. Chem. Soc.*, 1998, **120**, 3316-3325

[42] B. Kerr and K. J. McCullough, *J. Chem. Soc. Chem. Commun.*, 1985, 590-591

[43] A. Haq, B. Kerr and K. J. McCullough, *J. Chem. Soc. Chem. Commun.*, 1993, 1076-1078

[44] B. Kerr and K. J. McCullough, *J. Chem. Soc. Chem. Commun.*, 1985, 590-591

[45] Gaussian 98, Revision A.11.4, M. J. Frisch, G. W. Trucks, H. B. Schlegel, G. E. Scuseria, M. A. Robb, J. R. Cheeseman, V. G. Zakrzewski, J. A. Montgomery, Jr., R. E. Stratmann, J. C. Burant, S. Dapprich, J. M. Millam, A. D. Daniels, K. N. Kudin, M. C.

Strain, O. Farkas, J. Tomasi, V. Barone, M. Cossi, R. Cammi, B. Mennucci, C. Pomelli, C. Adamo, S. Clifford, J. Ochterski, G. A. Petersson, P. Y. Ayala, Q. Cui, K. Morokuma, N. Rega, P. Salvador, J. J. Dannenberg, D. K. Malick, A. D. Rabuck, K. Raghavachari, J. B. Foresman, J. Cioslowski, J. V. Ortiz, A. G.   Baboul, B.   B. Stefanov, G. Liu, A. Liashenko, P. Piskorz, I. Komaromi, R. Gomperts, R. L. Martin, D. J. Fox, T. Keith, M. A. Al-Laham, C. Y. Peng, A. Nanayakkara, M. Challacombe, P. M. W. Gill, B. Johnson, W. Chen, M. W. Wong, J. L. Andres, C. Gonzalez, M. Head-Gordon, E. S. Replogle, and J. A. Pople, Gaussian, Inc., Pittsburgh PA, 2002.

[46] Gaussian 03, Revision C.02, M. J. Frisch, G. W. Trucks, H. B. Schlegel, G. E. Scuseria, M. A. Robb, J. R. Cheeseman, J. A. Montgomery, Jr., T. Vreven, K.   N. Kudin, J. C. Burant, J. M. Millam, S. S. Iyengar, J. Tomasi, V. Barone, B. Mennucci, M. Cossi, G. Scalmani, N. Rega, G. A. Petersson, H. Nakatsuji, M. Hada, M. Ehara, K. Toyota, R. Fukuda, J. Hasegawa, M. Ishida, T. Nakajima, Y. Honda, O. Kitao, H. Nakai, M. Klene, X. Li, J. E. Knox, H. P. Hratchian, J. B. Cross, C. Adamo, J. Jaramillo, R. Gomperts, R. E. Stratmann, O. Yazyev, A. J. Austin, R. Cammi, C. Pomelli, J. W. Ochterski, P. Y. Ayala, K. Morokuma, G. A. Voth, P. Salvador, J. J. Dannenberg, V. G. Zakrzewski, S. Dapprich, A. D. Daniels, M. C. Strain, O. Farkas, D. K. Malick, A. D. Rabuck, K. Raghavachari, J. B. Foresman, J. V. Ortiz, Q. Cui, A. G. Baboul, S. Clifford, J. Cioslowski, B. B. Stefanov, G. Liu, A. Liashenko, P. Piskorz, I. Komaromi, R. L. Martin, D. J. Fox, T. Keith, M. A. Al-Laham, C. Y. Peng, A. Nanayakkara, M. Challacombe, P. M. W. Gill, B. Johnson, W. Chen, M. W. Wong, C. Gonzalez, and J. A. Pople, Gaussian, Inc., Wallingford CT, 2004

[47] E. D. Glendening, A. E. Reed, J. E. Carpenter, F. Weinhold, *QCPE Bull.*, 1990, **10**, 58

[48] A. A. Patel, Heriot-Watt University, MPhil thesis, 2002

[49] G. B. Schuster, and L. A. Bryant, *J. Org. Chem*, 1978, **43**, 521-522

[50] B. Kerr, Heriot-Watt University PhD thesis, 1989

[51] W. Koch, M. C. Holthausen, *A Chemists Guide to Density Functional Theory*, 2002, Wiley-VCH

[52] C. J. Cramer, *Essentials of Computational Chemistry*, 2004, Wiley

[53] J. C. Slater, *Phys. Rev.*, 1951, **81**, 385

[54] P. Hohenberg, W. Kohn, *Phys. Rev.,* 1964, **136**, B864

[55] W. Kohn, L. J. Sham, *Phys. Rev.*, 1965, **140**, A1133

[56] A. D. Becke, *Phys. Rev. A,* 1988, **38**, 3098

[57] J. P. Perdew, *Phys. Rev. B*, 1986, **33**, 8822

[58] C. Lee, W. Yang and R. G. Parr, *Phys. Rev. B*, 1988, **37**, 785

[59] J. P. Perdew and Y. Wang, *Phys. Rev. B*, 1992, **45**, 13244

[60] W. J. Hehre, L. Radom, P. V. R. Schleyer and J. A. Pople, *Ab initio molecular orbital theory*, Wiley, 1986

Chapter One

Appendix

X-Ray Crystal data for 153

Table 1. Crystal data and structure refinement for **153**

Empirical formula	C5 H10 O6
Formula weight	166.13
Temperature	100(2) K
Wavelength	0.71073 Å
Crystal system	Monoclinic
Space group	P2(1)/n
Unit cell dimensions	a = 5.548(5) Å α= 90°.
	b = 15.315(14) Å β= 92.83(3)°.
	c = 8.813(8) Å γ = 90°.
Volume	747.9(12) Å^3
Z	4
Density (calculated)	1.475 Mg/m^3
Absorption coefficient	0.138 mm^{-1}
F(000)	352
Crystal size	0.6 x 0.40 x 0.15 mm^3
Theta range for data collection	2.66 to 30.74°.
Index ranges	$-7 \le h \le 7, 0 \le k \le 21, 0 \le l \le 12$
Reflections collected	2855
Independent reflections	2855 [R(int) = 0.0000]
Completeness to theta = 25.00°	100.0 %
Absorption correction	Semi-empirical from equivalents
Max. and min. transmission	0.9729 and 0.8515
Refinement method	Full-matrix least-squares on F^2
Data / restraints / parameters	2855 / 0 / 105
Goodness-of-fit on F^2	0.905
Final R indices [I>2sigma(I)]	R1 = 0.0365, wR2 = 0.1143
R indices (all data)	R1 = 0.0485, wR2 = 0.1238
Largest diff. peak and hole	0.307 and -0.315 e.Å^{-3}

Table 2. Atomic coordinates (x 10^4) and equivalent isotropic displacement parameters (Å^2x 10^3) for compound **153**. U(eq) is defined as one third of the trace of the orthogonalized U^{ij} tensor.

	x	y	z	U(eq)
O(1)	1591(2)	4360(1)	-1758(1)	28(1)
O(2)	3160(1)	3608(1)	-1503(1)	23(1)
O(3)	724(1)	2981(1)	266(1)	19(1)
O(4)	792(1)	2122(1)	-473(1)	19(1)
O(5)	2994(1)	1479(1)	1546(1)	22(1)
O(6)	1451(2)	709(1)	1558(1)	28(1)
C(1)	3446(2)	4063(1)	1150(1)	25(1)
C(2)	3034(2)	3332(1)	33(1)	18(1)
C(3)	4758(2)	2562(1)	155(1)	24(1)
C(4)	3065(2)	1782(1)	25(1)	18(1)
C(5)	3682(2)	1074(1)	-1065(1)	26(1)

X-Ray Crystal data for 155

Table 1. Crystal data and structure refinement for compound **155**

Empirical formula	C7 H13 Cl O
Formula weight	148.62
Temperature	100(2) K
Wavelength	0.71073 Å
Crystal system	Tetragonal
Space group	I-4
Unit cell dimensions	a = 14.1037(12) Å $\alpha = 90°$.
	b = 14.1037(12) Å $\beta = 90°$.
	c = 7.5957(8) Å $\gamma = 90°$.
Volume	1510.9(2) Å^3
Z	8
Density (calculated)	1.333 Mg/m^3
Absorption coefficient	0.434 mm^{-1}
F(000)	648
Crystal size	0.60 x 0.50 x 0.40 mm^3
Theta range for data collection	2.04 to 36.37°.
Index ranges	$-23 \leq h \leq 23, -23 \leq k \leq 23, -12 \leq l \leq 12$
Reflections collected	19375
Independent reflections	3090 [R(int) = 0.0555]
Completeness to theta = 25.00°	79.9 %
Absorption correction	Semi-empirical from equivalents
Max. and min. transmission	0.8456 and 0.7808
Refinement method	Full-matrix least-squares on F^2
Data / restraints / parameters	3090 / 0 / 83
Goodness-of-fit on F^2	0.747
Final R indices [I>2sigma(I)]	R1 = 0.0325, wR2 = 0.0881
R indices (all data)	R1 = 0.0370, wR2 = 0.0979
Absolute structure parameter	1.01(5)
Largest diff. peak and hole	0.263 and -0.396 e.Å^{-3}

Table 2.   Atomic coordinates (x 10^4) and equivalent isotropic displacement parameters ($Å^2$x 10^3) for compound **155**. U(eq) is defined as one third of the trace of the orthogonalized U^{ij} tensor.

	x	y	z	U(eq)
Cl(1)	5689(1)	2986(1)	10168(1)	21(1)
O(1)	5446(1)	3703(1)	5061(1)	14(1)
C(1)	5539(1)	3035(1)	6493(1)	10(1)
C(2)	4695(1)	2349(1)	6469(2)	13(1)
C(3)	4690(1)	1727(1)	4811(2)	16(1)
C(4)	5625(1)	1183(1)	4638(2)	17(1)
C(5)	6470(1)	1866(1)	4611(2)	15(1)
C(6)	6476(1)	2508(1)	6240(2)	12(1)
C(7)	5541(1)	3650(1)	8156(2)	15(1)

X-Ray Crystal data for 148c

Table 1. Crystal data and structure refinement for **148c**.

Empirical formula	C8 H16 O3
Formula weight	160.21
Temperature	100(2) K
Wavelength	0.71073 Å
Crystal system	Trigonal
Space group	P3(2)
Unit cell dimensions	a = 10.8807(10) Å $\quad$ α= 90°.
	b = 10.8807(10) Å $\quad$ β= 90°.
	c = 6.2353(13) Å $\quad$ γ = 120°.
Volume	639.30(16) Å^3
Z	3
Density (calculated)	1.233 Mg/m^3
Absorption coefficient	0.093 mm^{-1}
F(000)	258
Crystal size	0.4 x 0.3 x 0.2 mm^3
Theta range for data collection	2.16 to 22.86°.
Index ranges	$-11 \leq h \leq 10, -10 \leq k \leq 11, -6 \leq l \leq 6$
Reflections collected	1438
Independent reflections	837 [R(int) = 0.0255]
Completeness to theta = 22.86°	100.0 %
Absorption correction	Semi-empirical from equivalents
Max. and min. transmission	0.982 and 0.967
Refinement method	Full-matrix least-squares on F^2
Data / restraints / parameters	837 / 1 / 103
Goodness-of-fit on F^2	0.907
Final R indices [I>2sigma(I)]	R1 = 0.0394, wR2 = 0.1071
R indices (all data)	R1 = 0.0551, wR2 = 0.1221
Absolute structure parameter	0(3)
Largest diff. peak and hole	0.207 and -0.218 e.Å^{-3}

Table 2. Atomic coordinates (x 10^4) and equivalent isotropic displacement parameters (Å^2x 10^3)

for **148c**. U(eq) is defined as one third of the trace of the orthogonalized U^{ij} tensor.

	x	y	z	U(eq)
O(1)	2260(3)	10537(3)	10679(5)	20(1)
O(2)	2573(3)	11982(3)	11260(6)	29(1)
O(3)	1005(3)	10072(3)	6431(4)	21(1)
C(1)	3064(5)	10664(5)	8741(7)	16(1)
C(2)	2787(5)	9140(5)	8485(7)	20(1)
C(3)	3416(5)	8743(5)	10355(7)	24(1)
C(4)	4982(5)	9814(5)	10737(8)	28(1)
C(5)	5222(5)	11311(5)	10984(8)	29(1)
C(6)	4624(5)	11730(5)	9091(8)	22(1)
C(7)	3345(6)	8949(6)	6333(8)	31(1)
C(8)	2462(4)	11125(5)	6914(8)	20(1)

X-Ray Crystal data for 160aa

Table 1. Crystal data and structure refinement for compound **160aa**

Empirical formula	$C_{14} H_{24} O_4$
Formula weight	256.33
Temperature	100(2) K
Wavelength	0.71073 Å
Crystal system	Monoclinic
Space group	C(2)/c
Unit cell dimensions	a = 22.7198(15) Å α= 90°.
	b = 6.0596(4) Å β= 117.027(3)°.
	c = 22.0700(14) Å γ = 90°.
Volume	2706.6(3) Å^3
Z	8
Density (calculated)	1.258 Mg/m^3
Absorption coefficient	0.090 mm^{-1}
F(000)	1120
Crystal size	0.45 x 0.40 x 0.30 mm^3
Theta range for data collection	3.48 to 36.65°.
Index ranges	-37 ≤ h ≤ 37, -10 ≤ k ≤ 8, -37 ≤ l ≤ 32
Reflections collected	17287
Independent reflections	6358 [R(int) = 0.0305]
Completeness to theta = 25.00°	99.8 %
Absorption correction	Semi-empirical from equivalents
Max. and min. transmission	0.973 and 0.959
Refinement method	Full-matrix least-squares on F^2
Data / restraints / parameters	6358 / 0 / 164
Goodness-of-fit on F^2	0.928
Final R indices [I>2sigma(I)]	R1 = 0.0435, wR2 = 0.1263
R indices (all data)	R1 = 0.0686, wR2 = 0.1483
Largest diff. peak and hole	0.477 and -0.242 e.Å^{-3}

Table 2. Atomic coordinates (x 10^4) and equivalent isotropic displacement parameters (Å^2x 10^3)for compound **160aa**. U(eq) is defined as one third of the trace of the orthogonalized U^{ij} tensor.

	x	y	z	U(eq)
O(1)	2489(1)	840(1)	3975(1)	13(1)
O(2)	3390(1)	-1562(1)	4473(1)	20(1)
O(3)	3030(1)	-3141(1)	3921(1)	23(1)
O(4)	1028(1)	-2438(1)	3363(1)	24(1)
C(1)	3181(1)	592(1)	4203(1)	13(1)
C(2)	3383(1)	1162(1)	3651(1)	15(1)
C(3)	3514(1)	2097(2)	4818(1)	17(1)
C(4)	4132(1)	1233(2)	3928(1)	19(1)
C(5)	4262(1)	2236(2)	5082(1)	21(1)
C(6)	4442(1)	2858(2)	4517(1)	20(1)
C(7)	2375(1)	-3123(1)	3854(1)	21(1)
C(8)	2053(1)	-901(1)	3575(1)	15(1)
C(9)	1441(1)	-587(1)	3686(1)	16(1)
C(10)	1105(1)	1609(2)	3398(1)	19(1)
C(11)	1852(1)	-705(2)	2815(1)	20(1)
C(12)	1528(1)	1503(2)	2521(1)	23(1)
C(13)	928(1)	1881(2)	2647(1)	24(1)
C(14)	534(1)	-2787(2)	3574(1)	26(1)

X-Ray Crystal data for 160ab

Table 1. Crystal data and structure refinement for compound **160ab**

Empirical formula	C13 H22 O4
Formula weight	242.31
Temperature	100(2) K
Wavelength	0.71073 Å
Crystal system	Triclinic
Space group	P-1
Unit cell dimensions	a = 6.250(3) Å α = 72.439(15)°.
	b = 10.204(6) Å β = 89.901(19)°.
	c = 10.248(5) Å γ = 84.455(17)°.
Volume	619.9(6) Å^3
Z	2
Density (calculated)	1.298 Mg/m^3
Absorption coefficient	0.095 mm^{-1}
F(000)	264
Crystal size	0.60 x 0.42 x 0.10 mm^3
Theta range for data collection	2.09 to 35.32°.
Index ranges	-9 $\leq$ h $\leq$ 9, -15 $\leq$ k $\leq$ 16, 0 $\leq$ l $\leq$ 16
Reflections collected	21516
Independent reflections	7060 [R(int) = 0.0000]
Completeness to theta = 25.00°	98.8 %
Absorption correction	Semi-empirical from equivalents
Max. and min. transmission	0.9906 and 0.9454
Refinement method	Full-matrix least-squares on F^2
Data / restraints / parameters	7060 / 0 / 156
Goodness-of-fit on F^2	1.039
Final R indices [I>2sigma(I)]	R1 = 0.0713, wR2 = 0.1976
R indices (all data)	R1 = 0.1115, wR2 = 0.2256
Largest diff. peak and hole	0.359 and -0.372 e.Å^{-3}

Table 2.   Atomic coordinates (x 10^4) and equivalent isotropic displacement parameters ($Å^2$x 10^3) for compound **160ab**. U(eq) is defined as one third of the trace of the orthogonalized U^{ij} tensor.

	x	y	z	U(eq)
O(1)	2509(2)	8059(1)	762(1)	14(1)
O(2)	4560(2)	8280(1)	-1184(1)	19(1)
O(3)	6255(2)	7282(1)	-341(1)	22(1)
O(4)	6179(2)	7776(1)	3524(1)	22(1)
C(1)	2551(2)	7933(2)	-576(2)	16(1)
C(2)	1952(2)	6576(2)	-739(2)	20(1)
C(3)	918(2)	9039(2)	-1485(2)	18(1)
C(4)	1304(3)	6981(2)	-2253(2)	29(1)
C(5)	130(2)	8432(2)	-2581(2)	21(1)
C(6)	6391(2)	7708(2)	865(2)	21(1)
C(7)	4355(2)	7427(2)	1668(2)	15(1)
C(8)	4263(2)	5891(2)	2350(2)	19(1)
C(9)	4206(2)	8206(2)	2740(2)	16(1)
C(10)	2313(3)	5572(2)	3240(2)	22(1)
C(11)	2228(2)	7892(2)	3604(2)	18(1)
C(12)	2212(3)	6358(2)	4300(2)	21(1)
C(13)	6441(3)	8493(2)	4491(2)	26(1)

X-Ray Crystal data for 161

Table 1. Crystal data and structure refinement for compound **161**

Empirical formula	C12 H22 O6
Formula weight	262.30
Temperature	100(2) K
Wavelength	0.71073 Å
Crystal system	Monoclinic
Space group	P2(1)/n
Unit cell dimensions	a = 10.4152(5) Å $\alpha = 90°$.
	b = 6.9136(3) Å $\beta = 104.978(2)°$.
	c = 18.5092(9) Å $\gamma = 90°$.
Volume	1287.50(10) Å^3
Z	4
Density (calculated)	1.353 Mg/m^3
Absorption coefficient	0.108 mm^{-1}
F(000)	568
Crystal size	0.50 x 0.40 x 0.35 mm^3
Theta range for data collection	2.28 to 37.66°.
Index ranges	$-15 \leq h \leq 17$, $-11 \leq k \leq 11$, $-30 \leq l \leq 30$
Reflections collected	25258
Independent reflections	6266 [R(int) = 0.0336]
Completeness to theta = 25.00°	99.9 %
Absorption correction	Multi_scans
Max. and min. transmission	0.9633 and 0.9481
Refinement method	Full-matrix least-squares on F^2
Data / restraints / parameters	6266 / 0 / 165
Goodness-of-fit on F^2	1.186
Final R indices [I>2sigma(I)]	R1 = 0.0452, wR2 = 0.1565
R indices (all data)	R1 = 0.0595, wR2 = 0.1656
Largest diff. peak and hole	0.539 and -0.350 e.Å^{-3}

Table 2. Atomic coordinates (x 10^4) and equivalent isotropic displacement parameters (Å^2x 10^3) for compound **161**. U(eq) is defined as one third of the trace of the orthogonalized U^{ij} tensor.

	x	y	z	U(eq)
O(1)	2904(1)	3196(1)	2328(1)	15(1)
O(2)	2302(1)	1531(1)	1881(1)	12(1)
O(3)	1201(1)	3494(1)	885(1)	12(1)
O(4)	-131(1)	2825(1)	926(1)	12(1)
O(5)	149(1)	3926(1)	2152(1)	12(1)
O(6)	-38(1)	1989(1)	2424(1)	17(1)
C(1)	2112(1)	1947(1)	1104(1)	10(1)
C(2)	1608(1)	50(1)	712(1)	12(1)
C(3)	2684(1)	-1498(1)	826(1)	14(1)
C(4)	3904(1)	-735(2)	604(1)	17(1)
C(5)	4432(1)	1087(2)	1049(1)	16(1)
C(6)	3374(1)	2675(1)	921(1)	14(1)
C(7)	-601(1)	4127(1)	1392(1)	11(1)
C(8)	-2060(1)	3569(1)	1274(1)	14(1)
C(9)	-2769(1)	4963(2)	1685(1)	16(1)
C(10)	-2644(1)	7041(2)	1440(1)	16(1)
C(11)	-1187(1)	7620(1)	1588(1)	16(1)
C(12)	-412(1)	6242(1)	1212(1)	13(1)

X-Ray Crystal data for 162

Table 1. Crystal data and structure refinement for compound **162**

Empirical formula	C10 H16 O6
Formula weight	232.23
Temperature	100(2) K
Wavelength	0.71073 Å
Crystal system	Monoclinic
Space group	P2(1)/n
Unit cell dimensions	a = 9.3084(4) Å α= 90°.
	b = 12.0062(5) Å β= 102.410(2)°.
	c = 20.5828(9) Å γ = 90°.
Volume	2246.56(17) Å^3
Z	8
Density (calculated)	1.373 Mg/m^3
Absorption coefficient	0.114 mm^{-1}
F(000)	992
Crystal size	0.60 x 0.40 x 0.30 mm^3
Theta range for data collection	1.98 to 36.29°.
Index ranges	$-15 \le h \le 15, -19 \le k \le 19, -33 \le l \le 33$
Reflections collected	63188
Independent reflections	10609 [R(int) = 0.0276]
Completeness to theta = 25.00°	99.9 %
Absorption correction	Semi-empirical from equivalents
Max. and min. transmission	0.9666 and 0.9348
Refinement method	Full-matrix least-squares on F^2
Data / restraints / parameters	10609 / 0 / 293
Goodness-of-fit on F^2	1.502
Final R indices [I>2sigma(I)]	R1 = 0.0503, wR2 = 0.1928
R indices (all data)	R1 = 0.0676, wR2 = 0.2035
Largest diff. peak and hole	0.736 and -0.445 e.Å^{-3}

Table 2. Atomic coordinates (x 10^4) and equivalent isotropic displacement parameters (Å^2x 10^3) for compound **162**. U(eq) is defined as one third of the trace of the orthogonalized U^{ij} tensor.

	x	y	z	U(eq)
O(1)	3333(1)	-140(1)	1008(1)	18(1)
O(2)	3368(1)	731(1)	1509(1)	14(1)
O(3)	1217(1)	1572(1)	911(1)	12(1)
O(4)	433(1)	1443(1)	1460(1)	13(1)
O(5)	725(1)	-485(1)	1510(1)	14(1)
O(6)	1514(1)	-413(1)	2205(1)	19(1)
O(7)	968(1)	7508(1)	234(1)	19(1)
O(8)	1812(1)	7657(1)	915(1)	14(1)
O(9)	2058(1)	5737(1)	1069(1)	13(1)
O(10)	1294(1)	5750(1)	1629(1)	14(1)
O(11)	-872(1)	6492(1)	980(1)	16(1)
O(12)	-875(1)	7441(1)	1427(1)	25(1)
C(1)	2731(1)	1724(1)	1190(1)	11(1)
C(2)	3406(1)	2091(1)	604(1)	14(1)
C(3)	3900(1)	3294(1)	770(1)	21(1)
C(4)	4332(1)	3299(1)	1530(1)	21(1)
C(5)	3099(1)	2622(1)	1729(1)	14(1)
C(6)	-309(1)	404(1)	1376(1)	12(1)
C(7)	-1387(1)	436(1)	1846(1)	17(1)
C(8)	-2893(1)	593(1)	1387(1)	20(1)
C(9)	-2778(1)	-84(1)	773(1)	20(1)
C(10)	-1227(1)	182(1)	672(1)	15(1)
C(11)	2820(1)	6757(1)	1072(1)	12(1)
C(12)	3823(1)	7076(1)	1741(1)	15(1)
C(13)	5293(1)	7363(1)	1568(1)	16(1)
C(14)	5373(1)	6550(1)	1002(1)	18(1)
C(15)	3812(1)	6598(1)	571(1)	16(1)
C(16)	-224(1)	5564(1)	1362(1)	12(1)
C(17)	-561(1)	4563(1)	886(1)	15(1)
C(18)	-1707(1)	3889(1)	1150(1)	19(1)
C(19)	-1255(1)	4062(1)	1902(1)	21(1)
C(20)	-893(1)	5306(1)	1965(1)	17(1)

X-Ray Crystal data for 163

Table 1. Crystal data and structure refinement for compound **163**

Empirical formula	C14 H24 O4
Formula weight	256.33
Temperature	100(2) K
Wavelength	0.71073 Å
Crystal system	Monoclinic
Space group	P2(1)/c
Unit cell dimensions	$a = 9.261(2)$ Å $\quad \alpha = 90°.$
	$b = 6.3293(13)$ Å $\quad \beta = 103.287(8)°.$
	$c = 11.453(3)$ Å $\quad \gamma = 90°.$
Volume	653.4(3) Å^3
Z	2
Density (calculated)	1.303 Mg/m^3
Absorption coefficient	0.094 mm^{-1}
F(000)	280
Crystal size	0.80 x 0.30 x 0.04 mm^3
Theta range for data collection	3.66 to 24.65°.
Index ranges	$-10 \leq h \leq 9, -4 \leq k \leq 7, -13 \leq l \leq 13$
Reflections collected	2379
Independent reflections	1073 [R(int) = 0.0487]
Completeness to theta = 24.65°	97.2 %
Absorption correction	Semi-empirical from equivalents
Max. and min. transmission	0.9963 and 0.9288
Refinement method	Full-matrix least-squares on F^2
Data / restraints / parameters	1073 / 0 / 82
Goodness-of-fit on F^2	1.135
Final R indices [I>2sigma(I)]	R1 = 0.0629, wR2 = 0.1577
R indices (all data)	R1 = 0.0825, wR2 = 0.1735
Largest diff. peak and hole	0.285 and -0.538 e.Å^{-3}

Table 2.   Atomic coordinates (x 10^4) and equivalent isotropic displacement parameters (Å^2x 10^3) for compound **163**. U(eq) is defined as one third of the trace of the orthogonalized U^{ij} tensor.

	x	y	z	U(eq)
O(1)	6421(2)	5615(3)	546(2)	20(1)
O(2)	5414(2)	4601(3)	1204(2)	20(1)
C(1)	3930(3)	5223(4)	656(2)	17(1)
C(2)	2970(3)	3893(4)	1286(2)	23(1)
C(3)	2420(3)	4938(5)	2305(2)	23(1)
C(4)	1055(3)	6335(5)	1883(2)	24(1)
C(5)	1351(3)	8463(4)	1345(2)	22(1)
C(6)	2126(3)	8320(4)	310(2)	22(1)
C(7)	3733(3)	7603(4)	675(2)	19(1)

X-Ray Crystal data for 149bc

Table 1. Crystal data and structure refinement for compound **149bc**

Empirical formula	C16 H28 O4
Formula weight	284.38
Temperature	100(2) K
Wavelength	0.71073 Å
Crystal system	Monoclinic
Space group	P2(1)/c
Unit cell dimensions	a = 13.256(2) Å $\alpha = 90°$.
	b = 10.9154(16) Å $\beta = 106.642(7)°$.
	c = 11.0803(16) Å $\gamma = 90°$.
Volume	1536.1(4) Å^3
Z	4
Density (calculated)	1.230 Mg/m^3
Absorption coefficient	0.086 mm^{-1}
F(000)	624
Crystal size	0.90 x 0.60 x 0.60 mm^3
Theta range for data collection	1.60 to 34.20°.
Index ranges	$-20 \leq h \leq 20, -17 \leq k \leq 17, -17 \leq l \leq 17$
Reflections collected	52929
Independent reflections	6321 [R(int) = 0.0371]
Completeness to theta = 25.00°	100.0 %
Max. and min. transmission	0.9500 and 0.9264
Refinement method	Full-matrix least-squares on F^2
Data / restraints / parameters	6321 / 0 / 182
Goodness-of-fit on F^2	1.236
Final R indices [I>2sigma(I)]	R1 = 0.0408, wR2 = 0.1455
R indices (all data)	R1 = 0.0547, wR2 = 0.1622
Largest diff. peak and hole	0.582 and -0.226 e.Å^{-3}

Table 2.   Atomic coordinates (x 10^4) and equivalent isotropic displacement parameters ($Å^2$x 10^3) for compound **149bc**. U(eq) is defined as one third of the trace of the orthogonalized U^{ij} tensor.

	x	y	z	U(eq)
O(1)	2268(1)	-1154(1)	10118(1)	16(1)
O(2)	3356(1)	-687(1)	10542(1)	16(1)
O(3)	2775(1)	1283(1)	9876(1)	16(1)
O(4)	1571(1)	-108(1)	6851(1)	17(1)
C(1)	1706(1)	-505(1)	8984(1)	13(1)
C(2)	2201(1)	-779(1)	7914(1)	14(1)
C(3)	2183(1)	-2158(1)	7647(1)	18(1)
C(4)	1064(1)	-2674(1)	7336(1)	21(1)
C(5)	561(1)	-2402(1)	8385(1)	21(1)
C(6)	594(1)	-1028(1)	8685(1)	18(1)
C(7)	1724(1)	861(1)	9302(1)	15(1)
C(8)	3328(1)	567(1)	10938(1)	14(1)
C(9)	4486(1)	940(1)	11255(1)	19(1)
C(10)	4821(1)	2022(1)	12162(1)	22(1)
C(11)	5126(1)	1663(1)	13558(1)	24(1)
C(12)	4216(1)	1262(1)	14052(1)	21(1)
C(13)	3527(1)	239(1)	13296(1)	18(1)
C(14)	2822(1)	672(1)	12014(1)	17(1)
C(15)	2095(1)	161(1)	5927(1)	22(1)
C(16)	1345(1)	880(1)	4883(1)	24(1)

X-Ray Crystal data for 149bg

Table 1. Crystal data and structure refinement for compound **149bg**

Empirical formula	C18 H24 O4
Formula weight	304.37
Temperature	100(2) K
Wavelength	0.71073 Å
Crystal system	Monoclinic
Space group	P2(1)/c
Unit cell dimensions	a = 12.7162(12) Å α= 90°.
	b = 21.3047(19) Å β= 100.008(3)°.
	c = 11.9605(10) Å γ = 90°.
Volume	3191.0(5) Å^3
Z	8
Density (calculated)	1.267 Mg/m^3
Absorption coefficient	0.088 mm^{-1}
F(000)	1312
Crystal size	0.55 x 0.45 x 0.30 mm^3
Theta range for data collection	1.63 to 26.51°.
Index ranges	$0 \leq h \leq 15$, $-26 \leq k \leq 0$, $-14 \leq l \leq 14$
Reflections collected	6546
Independent reflections	6546 [R(int) = 0.0000]
Completeness to theta = 25.00°	99.9 %
Absorption correction	Semi-empirical from equivalents
Max. and min. transmission	0.9740 and 0.8281
Refinement method	Full-matrix least-squares on F^2
Data / restraints / parameters	6546 / 0 / 399
Goodness-of-fit on F^2	1.073
Final R indices [I>2sigma(I)]	R1 = 0.0620, wR2 = 0.1539
R indices (all data)	R1 = 0.1493, wR2 = 0.2064
Largest diff. peak and hole	0.369 and -0.441 e.Å^{-3}

X-Ray Crystal data for 149bg

Table 2. Atomic coordinates (x 10^4) and equivalent isotropic displacement parameters ($Å^2$x 10^3) for compound **149bg**. U(eq) is defined as one third of the trace of the orthogonalized U^{ij} tensor.

	x	y	z	U(eq)
O(1A)	4282(2)	1504(1)	2102(2)	17(1)
O(2A)	4682(2)	1413(1)	3336(2)	17(1)
O(3A)	4469(2)	2473(1)	3668(2)	16(1)
O(4A)	1754(2)	2252(1)	2364(2)	18(1)
C(1A)	3459(3)	1983(1)	1979(3)	15(1)
C(2A)	3146(3)	2069(2)	698(3)	18(1)
C(3A)	2632(3)	1486(2)	90(3)	19(1)
C(4A)	1691(3)	1260(2)	626(3)	20(1)
C(5A)	2035(3)	1153(2)	1898(3)	18(1)
C(6A)	2507(3)	1747(1)	2503(3)	15(1)
C(7A)	3954(3)	2578(2)	2523(3)	18(1)
C(8A)	5217(3)	1980(2)	3751(3)	17(1)
C(9A)	6196(3)	2106(2)	3182(3)	19(1)
C(10A)	7101(3)	1813(2)	3999(3)	20(1)
C(11A)	8118(3)	1672(2)	3828(3)	25(1)
C(12A)	8843(3)	1409(2)	4706(3)	29(1)
C(13A)	8539(3)	1294(2)	5752(3)	30(1)
C(14A)	7521(3)	1431(2)	5922(3)	24(1)
C(15A)	6796(3)	1686(2)	5040(3)	21(1)
C(16A)	5640(3)	1849(2)	5006(3)	20(1)
C(17A)	951(3)	2196(2)	3051(3)	23(1)
C(18A)	223(3)	2751(2)	2819(3)	29(1)
O(1B)	4388(2)	669(1)	6599(2)	18(1)
O(2B)	4689(2)	1039(1)	7655(2)	17(1)
O(3B)	4225(2)	217(1)	8748(2)	16(1)
O(4B)	1685(2)	230(1)	7002(2)	20(1)
C(1B)	3500(3)	265(2)	6731(3)	16(1)
C(2B)	3294(3)	-113(2)	5632(3)	21(1)
C(3B)	2858(3)	284(2)	4590(3)	22(1)
C(4B)	1872(3)	644(2)	4775(3)	22(1)
C(5B)	2131(3)	1059(2)	5821(3)	22(1)
C(6B)	2520(3)	662(2)	6867(3)	19(1)
C(7B)	3851(3)	-153(2)	7752(3)	18(1)
C(8B)	5064(3)	615(2)	8565(3)	16(1)
C(9B)	5403(3)	1055(2)	9583(3)	17(1)

303

C(10B)	6587(3)	1140(2)	9609(3)	17(1)
C(11B)	7275(3)	1580(2)	10184(3)	23(1)
C(12B)	8340(3)	1573(2)	10061(3)	28(1)
C(13B)	8712(3)	1127(2)	9379(3)	28(1)
C(14B)	8020(3)	682(2)	8805(3)	23(1)
C(15B)	6964(3)	691(2)	8917(3)	17(1)
C(16B)	6077(3)	266(2)	8372(3)	19(1)
C(17B)	1311(3)	278(2)	8056(3)	21(1)
C(18B)	430(3)	-198(2)	8034(3)	30(1)

X-Ray Crystal data for 149cd

Table 1. Crystal data and structure refinement for compound **149cd**

Empirical formula	C20 H36 O3
Formula weight	324.49
Temperature	100(2) K
Wavelength	0.71073 Å
Crystal system	Orthorhombic
Space group	Pbcn
Unit cell dimensions	a = 12.6243(8) Å α= 90°.
	b = 11.2695(8) Å β= 90°.
	c = 26.6915(18) Å γ = 90°.
Volume	3797.4(4) Å^3
Z	8
Density (calculated)	1.135 Mg/m^3
Absorption coefficient	0.074 mm^{-1}
F(000)	1440
Crystal size	0.58 x 0.21 x 0.12 mm^3
Theta range for data collection	1.53 to 23.30°.
Index ranges	$-13 \le h \le 14, -12 \le k \le 12, -29 \le l \le 29$
Reflections collected	48697
Independent reflections	2729 [R(int) = 0.0736]
Completeness to theta = 23.30°	99.6 %
Absorption correction	Semi-empirical from equivalents
Max. and min. transmission	0.9912 and 0.9543
Refinement method	Full-matrix least-squares on F^2
Data / restraints / parameters	2729 / 0 / 209
Goodness-of-fit on F^2	1.171
Final R indices [I>2sigma(I)]	R1 = 0.0405, wR2 = 0.1083
R indices (all data)	R1 = 0.0754, wR2 = 0.1462
Largest diff. peak and hole	0.311 and -0.239 e.Å^{-3}

Table 2. Atomic coordinates (x 10^4) and equivalent isotropic displacement parameters (Å^2x 10^3) for compound **149cd**. U(eq) is defined as one third of the trace of the orthogonalized U^{ij} tensor.

	x	y	z	U(eq)
O(1)	2497(1)	10052(1)	2486(1)	22(1)
O(2)	1824(1)	9931(2)	2937(1)	22(1)
O(3)	2652(1)	11570(1)	3299(1)	22(1)
C(1)	2638(2)	11319(2)	2390(1)	20(1)
C(2)	1569(2)	11934(2)	2293(1)	26(1)
C(3)	987(2)	11388(3)	1849(1)	30(1)
C(4)	1677(2)	11400(3)	1377(1)	33(1)
C(5)	2742(2)	10784(3)	1473(1)	28(1)
C(6)	3342(2)	11307(2)	1921(1)	25(1)
C(7)	3201(2)	11829(2)	2845(1)	25(1)
C(8)	2423(2)	10336(2)	3362(1)	22(1)
C(9)	1626(2)	10267(2)	3793(1)	22(1)
C(10)	1111(2)	9052(2)	3869(1)	25(1)
C(11)	643(2)	8897(2)	4392(1)	28(1)
C(12)	1472(2)	8787(2)	4811(1)	28(1)
C(13)	2097(2)	7630(2)	4795(1)	28(1)
C(14)	3150(2)	7660(2)	5080(1)	31(1)
C(15)	3982(2)	8521(2)	4859(1)	27(1)
C(16)	4402(2)	8140(2)	4348(1)	27(1)
C(17)	4932(2)	9135(2)	4054(1)	28(1)
C(18)	4154(2)	10074(2)	3851(1)	25(1)
C(19)	3428(2)	9603(2)	3438(1)	23(1)
C(20)	3798(2)	12541(2)	1805(1)	34(1)

Chapter Two

Appendix

X-Ray Crystal data for 90ca

Table 1. Crystal data and structure refinement for **90ca**.

Empirical formula	C14 H24 O4
Formula weight	256.33
Temperature	273(2) K
Wavelength	0.71073 Å
Crystal system	Monoclinic
Space group	P2(1)
Unit cell dimensions	a = 5.9569(12) Å α= 90°.
	b = 27.197(5) Å β= 100.74(3)°.
	c = 8.9521(18) Å γ = 90°.
Volume	424.9(5) Å^3
Z	4
Density (calculated)	1.195 Mg/m^3
Absorption coefficient	0.086 mm^{-1}
F(000)	560
Crystal size	0.55 x 0.35 x 0.15 mm^3
Theta range for data collection	1.50 to 30.48°.
Index ranges	-8 ≤ h ≤ 8, 0 ≤ k ≤ 38, 0 ≤ l ≤ 12
Reflections collected	6617
Independent reflections	6617 [R(int) = 0.0000]
Completeness to theta = 30.48°	92.3 %
Absorption correction	None
Refinement method	Full-matrix least-squares on F2
Data / restraints / parameters	6617 / 1 / 328
Goodness-of-fit on F^2	0.807
Final R indices [I>2sigma(I)]	R1 = 0.0574, wR2 = 0.1181
R indices (all data)	R1 = 0.1751, wR2 = 0.1656
Absolute structure parameter	0(2)
Largest diff. peak and hole	0.254 and -0.282 e.Å^{-3}

Table 2. Atomic coordinates (x 10^4) and equivalent isotropic displacement parameters ($Å^2$x 10^3)

for **90ca**. U(eq) is defined as one third of the trace of the orthogonalized U^{ij} tensor.

	x	y	z	U(eq)
O(1A)	5396(7)	9343(2)	4170(4)	28(1)
O(2A)	1820(7)	10305(1)	3117(4)	25(1)
O(3A)	7386(6)	10011(1)	5175(3)	23(1)
O(4A)	6298(7)	9227(1)	-2251(3)	27(1)
C(1A)	7231(10)	9530(2)	4727(5)	20(1)
C(2A)	9545(10)	9281(2)	4956(5)	25(1)
C(3A)	9525(11)	8771(2)	4247(6)	30(1)
C(4A)	8763(10)	8762(2)	2511(5)	28(1)
C(5A)	10269(10)	9064(2)	1639(5)	24(1)
C(6A)	9461(10)	9050(2)	-97(6)	28(1)
C(7A)	7199(9)	9330(2)	-660(5)	20(1)
C(8A)	7481(10)	9888(2)	-559(5)	22(1)
C(9A)	5262(10)	10182(2)	-750(5)	24(1)
C(10A)	3971(10)	10132(2)	589(5)	25(1)
C(11A)	5243(10)	10353(2)	2082(5)	21(1)
C(12A)	3917(10)	10295(2)	3383(5)	18(1)
C(13A)	5184(11)	10249(2)	5005(5)	23(1)
C(14A)	5109(12)	8775(2)	-2491(6)	32(2)
O(1B)	474(7)	7122(1)	4460(3)	23(1)
O(2B)	-3141(7)	6172(2)	3350(3)	24(1)
O(3B)	2417(6)	6448(1)	5451(3)	21(1)
O(4B)	1520(7)	7296(1)	-1974(3)	26(1)
C(1B)	2264(10)	6926(2)	5021(5)	20(1)
C(2B)	4595(10)	7163(2)	5278(5)	22(1)
C(3B)	4600(11)	7685(2)	4606(6)	27(1)
C(4B)	3859(11)	7730(2)	2865(5)	26(1)
C(5B)	5363(10)	7440(2)	1951(5)	25(1)
C(6B)	4571(10)	7466(2)	217(6)	24(1)
C(7B)	2356(9)	7188(2)	-383(5)	21(1)
C(8B)	2590(9)	6629(2)	-281(5)	20(1)
C(9B)	318(10)	6344(2)	-496(5)	26(1)
C(10B)	-930(9)	6386(2)	838(5)	19(1)
C(11B)	311(10)	6143(2)	2324(5)	20(1)

C(12B)	-1064(10)	6184(2)	3587(5)	19(1)
C(13B)	195(10)	6200(2)	5244(5)	23(1)
C(14B)	279(11)	7747(2)	-2239(6)	29(1)

X-Ray Crystal data for 90cb

Table 1. Crystal data and structure refinement for compound **90cb**

Empirical formula	C15 H26 O4
Formula weight	270.36
Temperature	100(2) K
Wavelength	0.71073 Å
Crystal system	Monoclinic
Space group	P2(1)
Unit cell dimensions	a = 8.9217(7) Å α = 90°.
	b = 5.3270(5) Å β = 97.197(4)°.
	c = 15.8597(12) Å γ = 90°.
Volume	747.81(11) Å^3
Z	2
Density (calculated)	1.201 Mg/m^3
Absorption coefficient	0.085 mm^{-1}
F(000)	296
Crystal size	0.52 x 0.32 x 0.25 mm^3
Theta range for data collection	1.29 to 32.40°.
Index ranges	$-13 \leq h \leq 10, -7 \leq k \leq 8, -22 \leq l \leq 23$
Reflections collected	15394
Independent reflections	4667 [R(int) = 0.0251]
Completeness to theta = 25.00°	97.2 %
Absorption correction	Semi-empirical from equivalents
Max. and min. transmission	0.979 and 0.928
Refinement method	Full-matrix least-squares on F^2
Data / restraints / parameters	4667 / 1 / 173
Goodness-of-fit on F^2	0.841
Final R indices [I>2sigma(I)]	R1 = 0.0399, wR2 = 0.1112
R indices (all data)	R1 = 0.0474, wR2 = 0.1219
Absolute structure parameter	1.9(7)
Largest diff. peak and hole	0.323 and -0.235 e.Å^{-3}

Table 2. Atomic coordinates (x 10^4) and equivalent isotropic displacement parameters (Å^2x 10^3) for compound **90cb**. U(eq) is defined as one third of the trace of the orthogonalized U^{ij} tensor.

	x	y	z	U(eq)
O(1)	1101(1)	11037(2)	3700(1)	22(1)
O(2)	5165(1)	8813(2)	4323(1)	19(1)
O(3)	1300(1)	7827(2)	4624(1)	15(1)
O(4)	3793(1)	5656(2)	847(1)	20(1)
C(1)	531(1)	9288(2)	4017(1)	15(1)
C(2)	-1082(1)	8412(3)	3830(1)	16(1)
C(3)	-1980(2)	9604(3)	3044(1)	20(1)
C(4)	-1950(2)	8064(3)	2230(1)	21(1)
C(5)	-408(1)	7914(3)	1914(1)	18(1)
C(6)	-385(2)	6079(3)	1175(1)	19(1)
C(7)	1067(2)	6161(3)	745(1)	20(1)
C(8)	2551(1)	5814(3)	1334(1)	15(1)
C(9)	2596(2)	3423(3)	1860(1)	16(1)
C(10)	4103(2)	2991(3)	2415(1)	18(1)
C(11)	4610(1)	5165(3)	3018(1)	16(1)
C(12)	3457(1)	5793(3)	3619(1)	16(1)
C(13)	3930(1)	7809(3)	4253(1)	14(1)
C(14)	2844(1)	8553(3)	4879(1)	16(1)
C(15)	4189(2)	7970(3)	493(1)	25(1)

X-Ray Crystal data for 90da

Table 1. Crystal data and structure refinement for compound **90da**.

Empirical formula	C15 H26 O4
Formula weight	270.36
Temperature	100(2) K
Wavelength	0.71073 Å
Crystal system	Monoclinic
Space group	P2(1)/c
Unit cell dimensions	a = 8.9041(9) Å $\quad$ α= 90°.
	b = 5.5036(5) Å $\quad$ β= 95.3650(10)°.
	c = 31.153(3) Å $\quad$ γ = 90°.
Volume	1520.0(3) Å^3
Z	4
Density (calculated)	1.181 Mg/m^3
Absorption coefficient	0.084 mm^{-1}
F(000)	592
Crystal size	0.60 x 0.60 x 0.30 mm^3
Theta range for data collection	1.31 to 29.23°.
Index ranges	$-12 \leq h \leq 12, 0 \leq k \leq 7, 0 \leq l \leq 42$
Reflections collected	4072
Independent reflections	4072 [R(int) = 0.0000]
Completeness to theta = 25.00°	99.6 %
Absorption correction	Semi-empirical from equivalents
Max. and min. transmission	0.975 and 0.855
Refinement method	Full-matrix least-squares on F^2
Data / restraints / parameters	4072 / 0 / 173
Goodness-of-fit on F^2	1.067
Final R indices [I>2sigma(I)]	R1 = 0.0485, wR2 = 0.1377
R indices (all data)	R1 = 0.0844, wR2 = 0.1664
Largest diff. peak and hole	0.455 and -0.497 e.Å^{-3}

X-Ray Crystal data for 90da

Table 2. Atomic coordinates (x 10^4) and equivalent isotropic displacement parameters (Å^2x 10^3) for compound **90da**. U(eq) is defined as one third of the trace of the orthogonalized U^{ij} tensor.

|	x	y	z	U(eq)
O(1)	1148(1)	12017(2)	1951(1)	24(1)
O(2)	1391(1)	8696(2)	2374(1)	20(1)
O(3)	5177(1)	9802(2)	2150(1)	26(1)
O(4)	2604(1)	6080(2)	336(1)	26(1)
C(1)	2934(2)	9397(3)	2489(1)	21(1)
C(2)	3478(2)	6813(3)	1821(1)	22(1)
C(3)	4500(2)	6472(3)	1463(1)	23(1)
C(4)	4091(2)	4255(3)	1179(1)	29(1)
C(5)	2427(2)	4096(3)	1003(1)	29(1)
C(6)	1849(2)	6220(3)	721(1)	25(1)
C(7)	130(2)	6150(3)	619(1)	32(1)
C(8)	-770(2)	6797(3)	1001(1)	31(1)
C(9)	-677(2)	9484(3)	1126(1)	24(1)
C(10)	-1567(2)	10179(3)	1505(1)	24(1)
C(11)	-908(2)	9139(3)	1938(1)	20(1)
C(12)	620(2)	10156(3)	2079(1)	18(1)
C(13)	2718(2)	8340(3)	120(1)	29(1)
C(14)	3630(2)	7928(3)	-259(1)	31(1)
C(15)	3966(2)	8769(3)	2142(1)	19(1)
C(15)	3966(2)	8769(3)	2142(1)	19(1)

314

Chapter Three

Appendix

R	Reactant		TS		Intermediate	Product
	Bond lengths	energy	bond lengths	energy	bond lengths	energy
NH$_2$	C(2)-C(3)= 1.57 C(2)-O(1)= 1.37 C(3)-Sub= 1.47	0.6 *13.1 # 4.4	C(2)-C(3)= 2.00 C(2)-O(1)= 1.27 C(3)-Sub= 1.39	-6.2	C(2)-O(1)= 1.23 C(3)-Sub= 1.39	-30.9
NMe$_2$	C(2)-C(3)= 1.64 C(2)-O(1)= 1.34 C(3)-Sub= 1.43	-0.6 *12.9 # 5.8	C(2)-C(3)= 2.01 C(2)-O(1)=1.27 C(3)-Sub= 1.39	-7.0	C(2)-O(1)= 1.22 C(3)-Sub= 1.39	-5.6
OH	C(2)-C(3)= 1.56 C(2)-O(1)= 1.37 C(3)-Sub= 1.43	0.6 *9.3 # -0.2	C(2)-C(3)= 2.06 C(2)-O(1)= 1.26 C(3)-Sub= 1.36	-6.4	C(2)-O(1)= 1.23 C(3)-Sub= 1.37	-2.9
Cl	C(2)-C(3)= 1.55 C(2)-O(1)= 1.37 C(3)-Sub=1.84	10.2 *10.6 # 3.6	C(2)-C(3)= 2.06 C(2)-O(1)= 1.25 C(3)-Sub= 1.76	7.2	C(2)-O(1)= 1.22 C(3)-Sub= 1.74	-1.7
SiH$_3$	C(2)-C(3)= 1.57 C(2)-O(1)= 1.37 C(3)-Sub= 1.91	7.7 *8.8 # 1.5	C(2)-C(3)= 2.09 C(2)-O(1)= 1.26 C(3)-Sub= 1.89	-5.4	C(2)-O(1)= 1.22 C(3)-Sub= 1.86	-5.5
SiMe$_3$	C(2)-C(3)= 1.58 C(2)-O(1)= 1.37 C(3)-Sub= 1.93	7.0 *8.4 # 2.6	C(2)-C(3)= 2.09 C(2)-O(1)= 1.26 C(3)-Sub= 1.91	-6.9	C(2)-O(1)= 1.22 C(3)-Sub= 1.88	-7.1
PH$_2$	C(2)-C(3)= 1.57 C(2)-O(1)= 1.36 C(3)-Sub= 1.89	7.4 *8.8 # 7.7	C(2)-C(3)= 2.03 C(2)-O(1)= 1.26 C(3)-Sub= 1.84	-3.9	C(2)-O(1)= 1.21 C(3)-Sub= 1.80	-5.9
PMe$_2$	C(2)-C(3)= 1.60 C(2)-O(1)= 1.37 C(3)-Sub= 1.90	4.9 *7.0 # -0.3	C(2)-C(3)= 2.07 C(2)-O(1)= 1.26 C(3)-Sub= 1.85	-9.1	C(2)-O(1)= 1.22 C(3)-Sub= 1.79	-8.8
SH	C(2)-C(3)= 1.56 C(2)-O(1)= 1.37 C(3)-Sub= 1.86	6.7 *10.0 # 1.9	C(2)-C(3)= 2.02 C(2)-O(1)= 1.26 C(3)-Sub= 1.78	-6.1	C(2)-O(1)= 1.22 C(3)-Sub= 1.76	-6.0
SMe	C(2)-C(3)= 1.56 C(2)-O(1)= 1.37 C(3)-Sub= 1.86	5.2 *6.0 # 1.5	C(2)-C(3)= 2.01 C(2)-O(1)= 1.27 C(3)-Sub= 1.77	0.6	C(2)-O(1)= 1.22 C(3)-Sub= 1.74	-8.3
F	C(2)-C(3)= 1.55 C(2)-O(1)= 1.37 C(3)-Sub= 1.40	9.8 *12.2 # 4.4	C(2)-C(3)= 2.12 C(2)-O(1)= 1.25 C(3)-Sub= 1.35	1.7	C(2)-O(1)= 1.22 C(3)-Sub= 1.35	-2.3
Ph	C(2)-C(3)= 1.58 C(2)-O(1)= 1.37 C(3)-Sub=1.52	4.5 *10.3 # 3.4	C(2)-C(3)= 2.00 C(2)-O(1)= 1.27 C(3)-Sub= 1.47	-12.8	C(2)-O(1)= 1.22 C(3)-Sub= 1.42	-12.4
CN	C(2)-C(3)= 1.58 C(2)-O(1)= 1.36 C(3)-Sub= 1.47	7.8 *11.2 # 2.8	C(2)-C(3)= 2.01 C(2)-O(1)= 1.27 C(3)-Sub= 1.43	-11.0	C(2)-O(1)= 1.21 C(3)-Sub= 1.39	-10.2
COOMe	C(2)-C(3)= 1.56 C(2)-O(1)= 1.37 C(3)-Sub= 1.52	6.6 *10.2 # 1.7	C(2)-C(3)= 2.03 C(2)-O(1)= 1.27 C(3)-Sub= 1.49	-9.4	C(2)-O(1)= 1.22 C(3)-Sub= 1.45	-9.2

Table 1: Energies of β-scission reactions of substituted cyclohexoyloxy radicals without additional close range interaction

*All energies given are related to reactant energy in each case * TS of β-scission of other ring C(2)-C(3) bond # TS of β-scission of C(2)-C(8) bond. The product from the reaction is from the straight-chain open system*
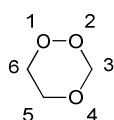
	Compound	O1–O2	O2–C3	C3–O4	O4–C5	C5–C6	C6–O1
1		1.47480(8)	1.4410(9)	1.4271(9)	1.4325(9)	1.5303(10)	1.4492(9)
2		1.481(3)	1.431(4)	1.410(4)	1.438(4)	1.515(4)	1.449(4)
3		1.487(3)	1.432(4)	1.409(4)	1.429(4)	1.513(4)	1.450(4)
4		1.479(2)	1.438(3)	1.430(3)	1.427(3)	1.520(4)	1.462(3)
5		1.47	1.42	1.43	1.42	1.54	1.45
6		1.46	1.43	1.43	1.43	1.54	1.46
7		1.47	1.43	1.42	1.43	1.53	1.45
8		1.46	1.43	1.41	1.43	1.53	1.45
9		1.47	1.43	1.43	1.43	1.53	1.45

*Table 2: Comparison of Bond lengths of the 1,2,4-trioxane ring from X-ray crystal structures (**1-4**) and computed geometries (**5-9**)/ Å*
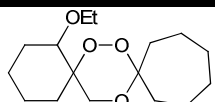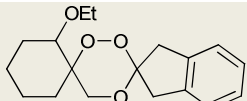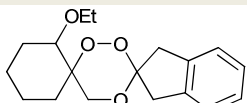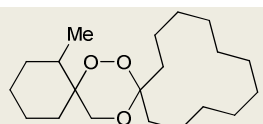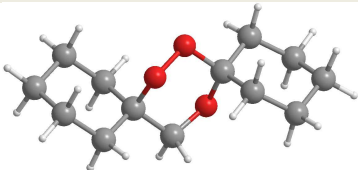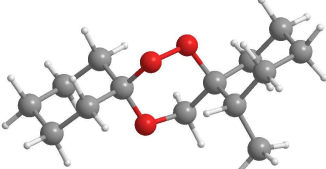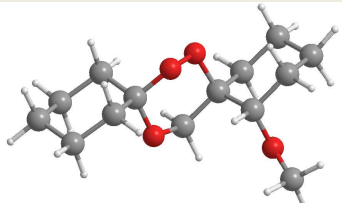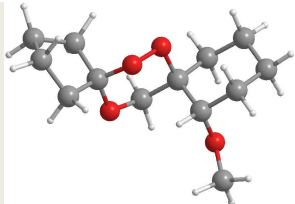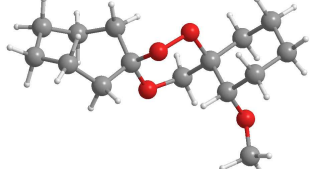
	Compound	6-1-2	1-2-3	2-3-4	3-4-5	4-5-6	5-6-1	6123
1		108.67(5)	108.55(5)	108.74(6)	113.26(6)	111.34(6)	107.84(6)	66.76(6)
2		108.3(2)	108.4(2)	109.6(3)	110.5(2)	110.8(3)	108.1(3)	64.17(3)
3		108.0(2)	107.1(2)	109.2(3)	112.1(2)	111.5(3)	107.9(3)	-66.90(3)
4		107.71(16)	108.02(16)	108.83(19)	113.35(18)	112.0(2)	106.54(19)	-68.7(2)
5		108.1	108.2	109.4	114.3	111.4	106.1	-69.5
6		108.5	108.4	109.6	114.1	111.5	105.4	-69.1
7		108.5	108.3	109.4	114.4	111.5	107.3	-68.4
8		108.2	108.0	109.4	113.3	111.4	107.2	-68.2
9		108.0	108.4	109.0	115.0	112.0	107.5	-69.6

*Table 3: Comparison of Bond angles of the 1,2,4-trioxane ring from X-ray crystal structures (**1-4**)*

*and computed geometries (**5-9**)/ Å*
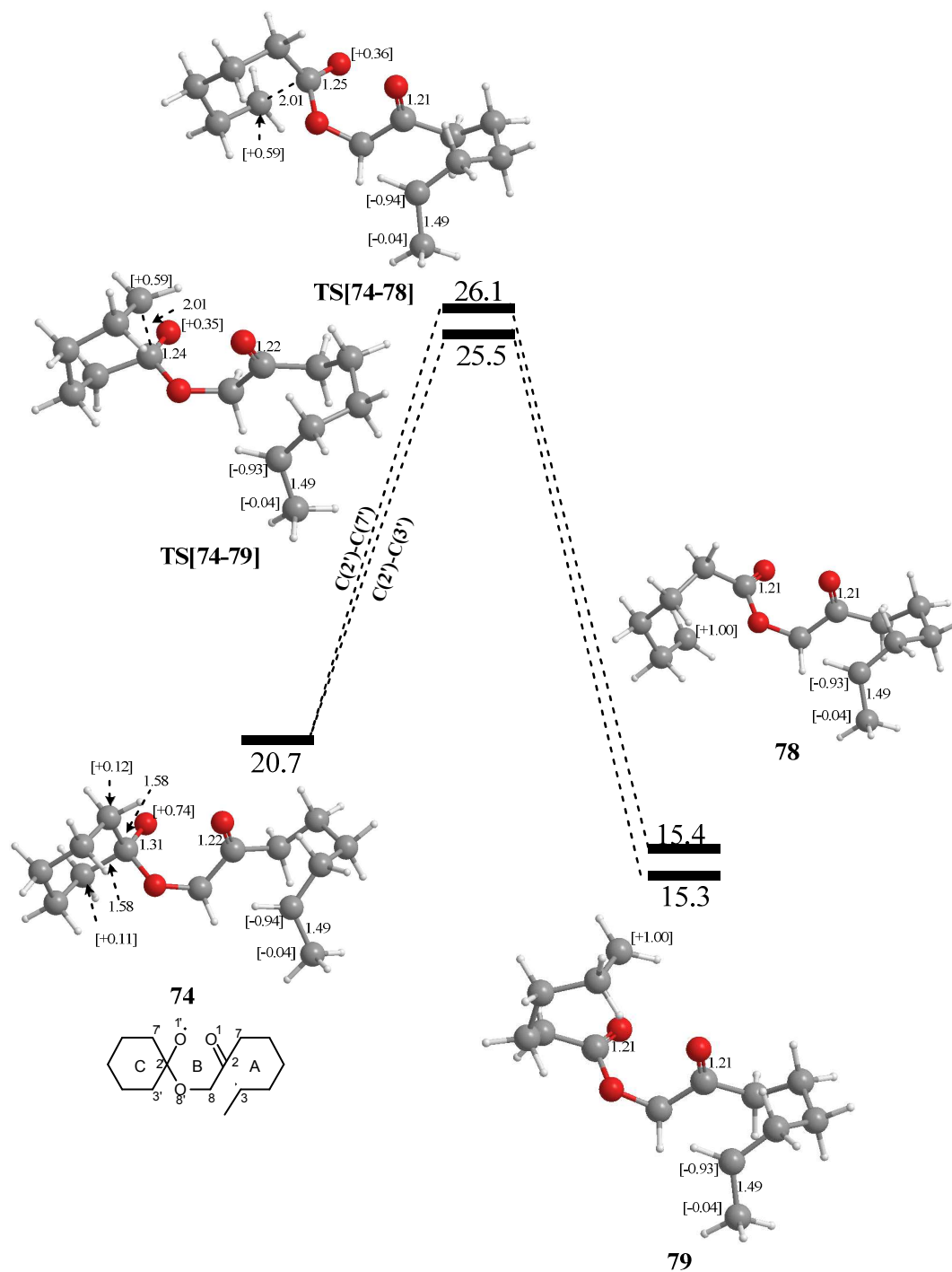
*Figure 1: The reaction profile for the competitive β-scission reactions of **74** / kcal mol⁻¹*

with molecular bond lengths/ Å and spin densities where the spin density quoted is for
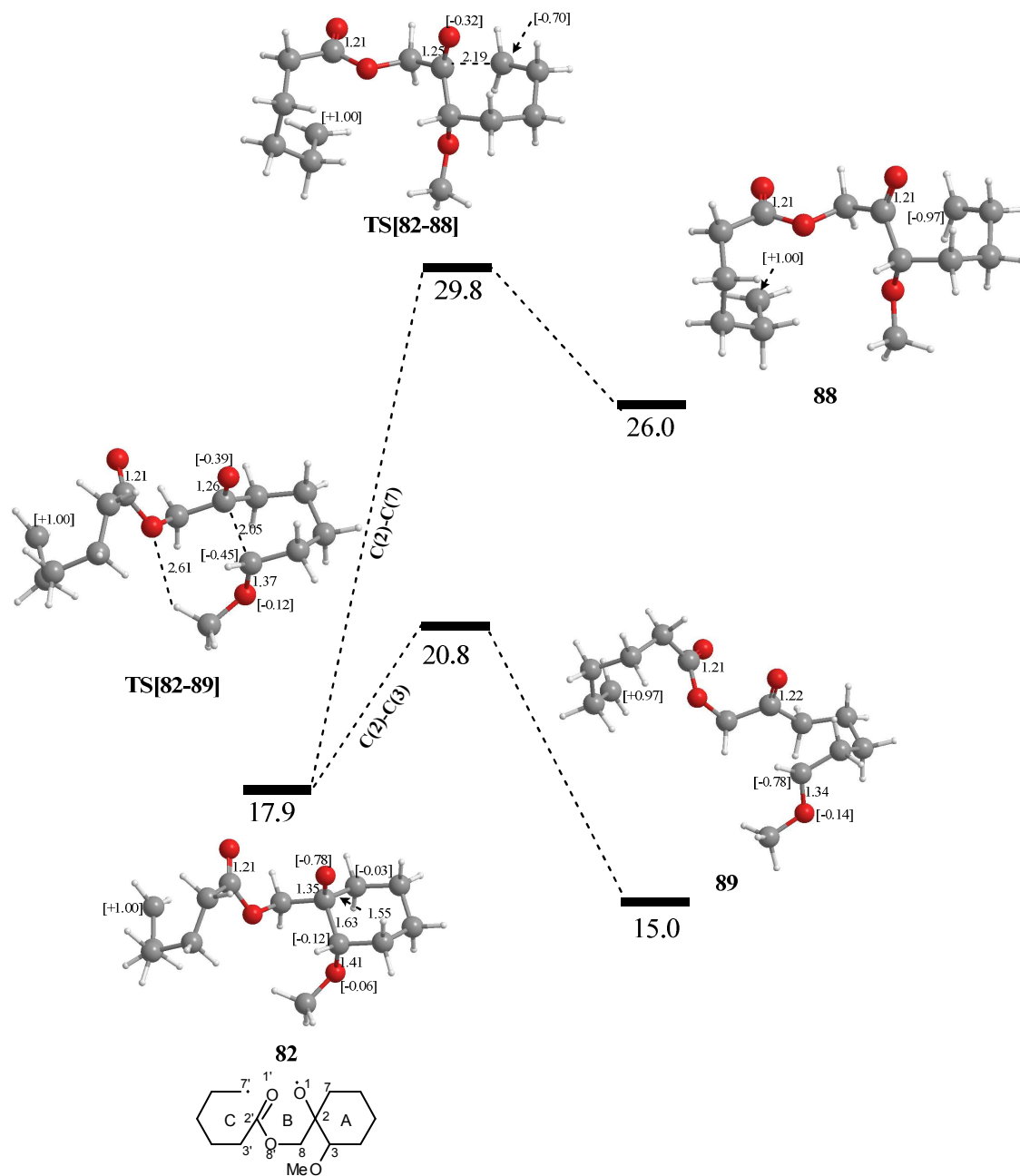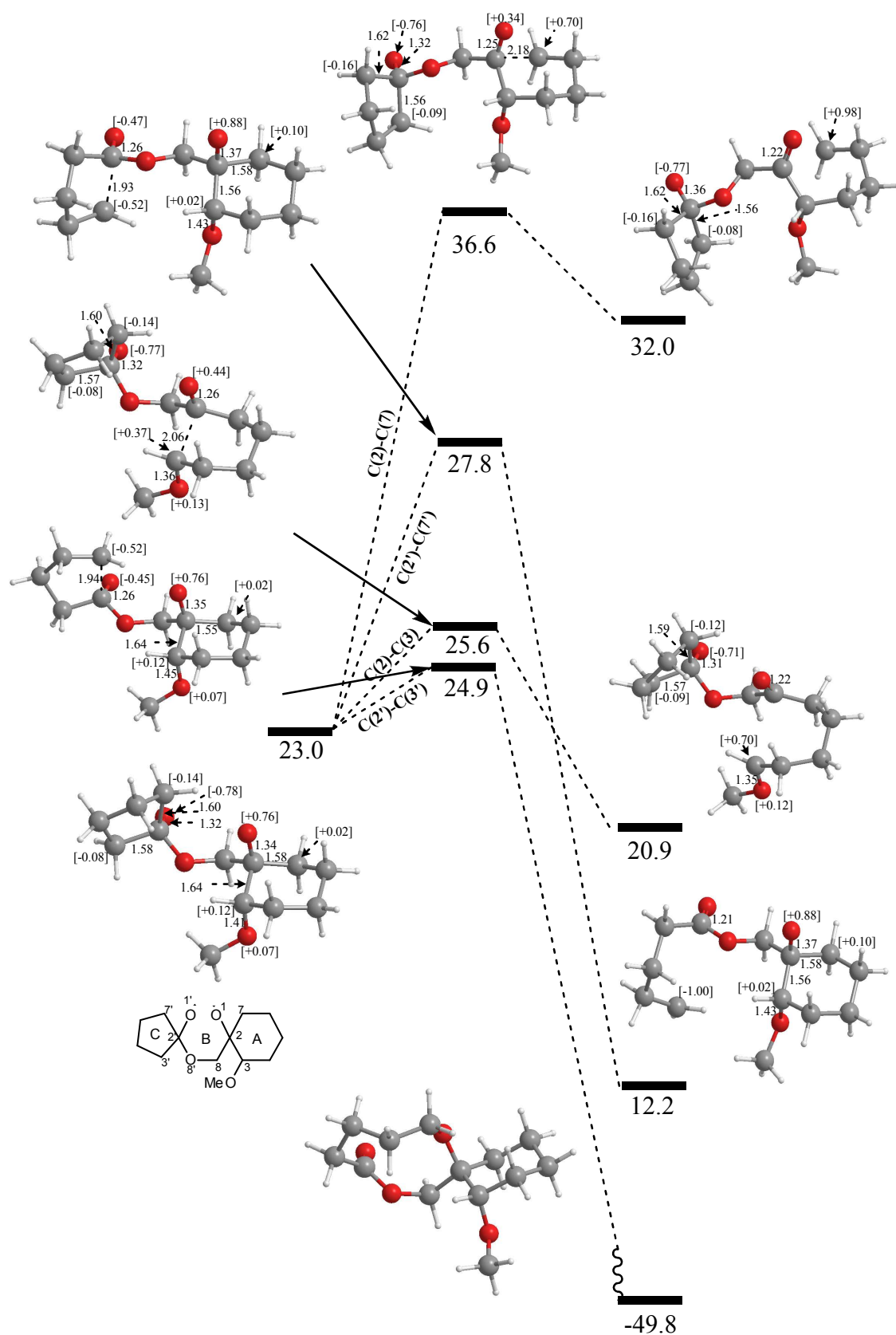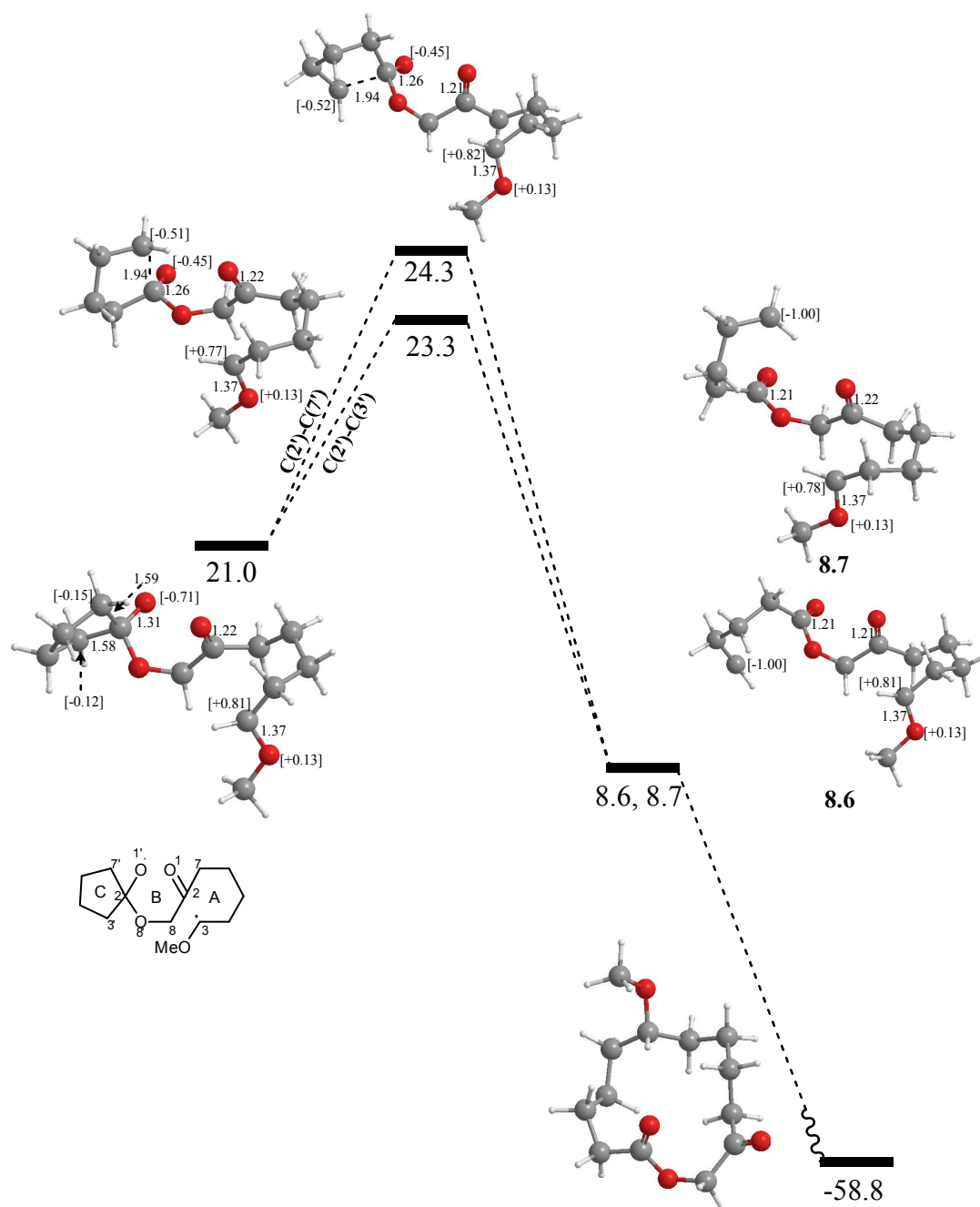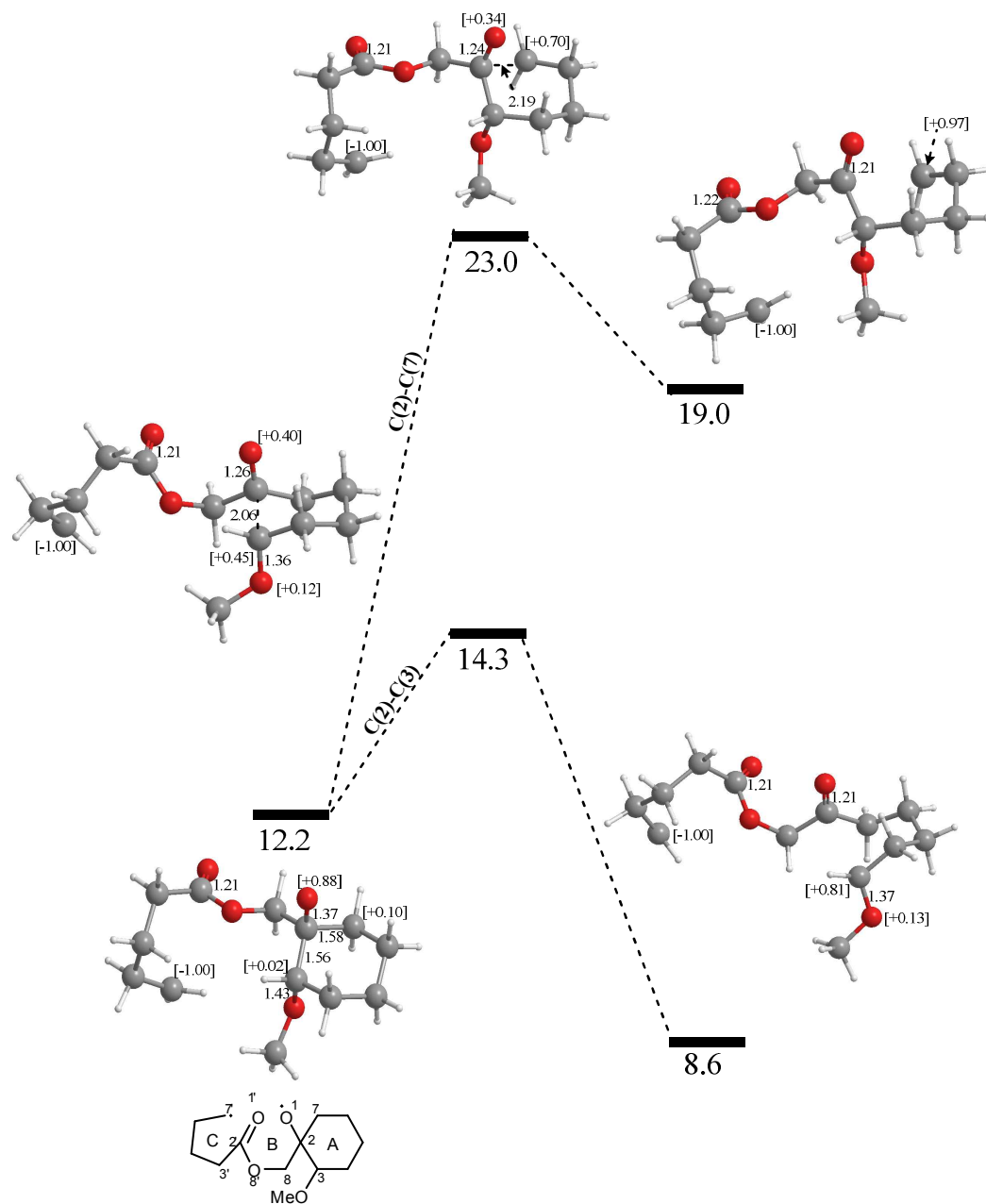
all the centres on the methyl group

*Figure 2: The reaction profile for the competitive β-scission reactions of **82** / kcal mol⁻¹*
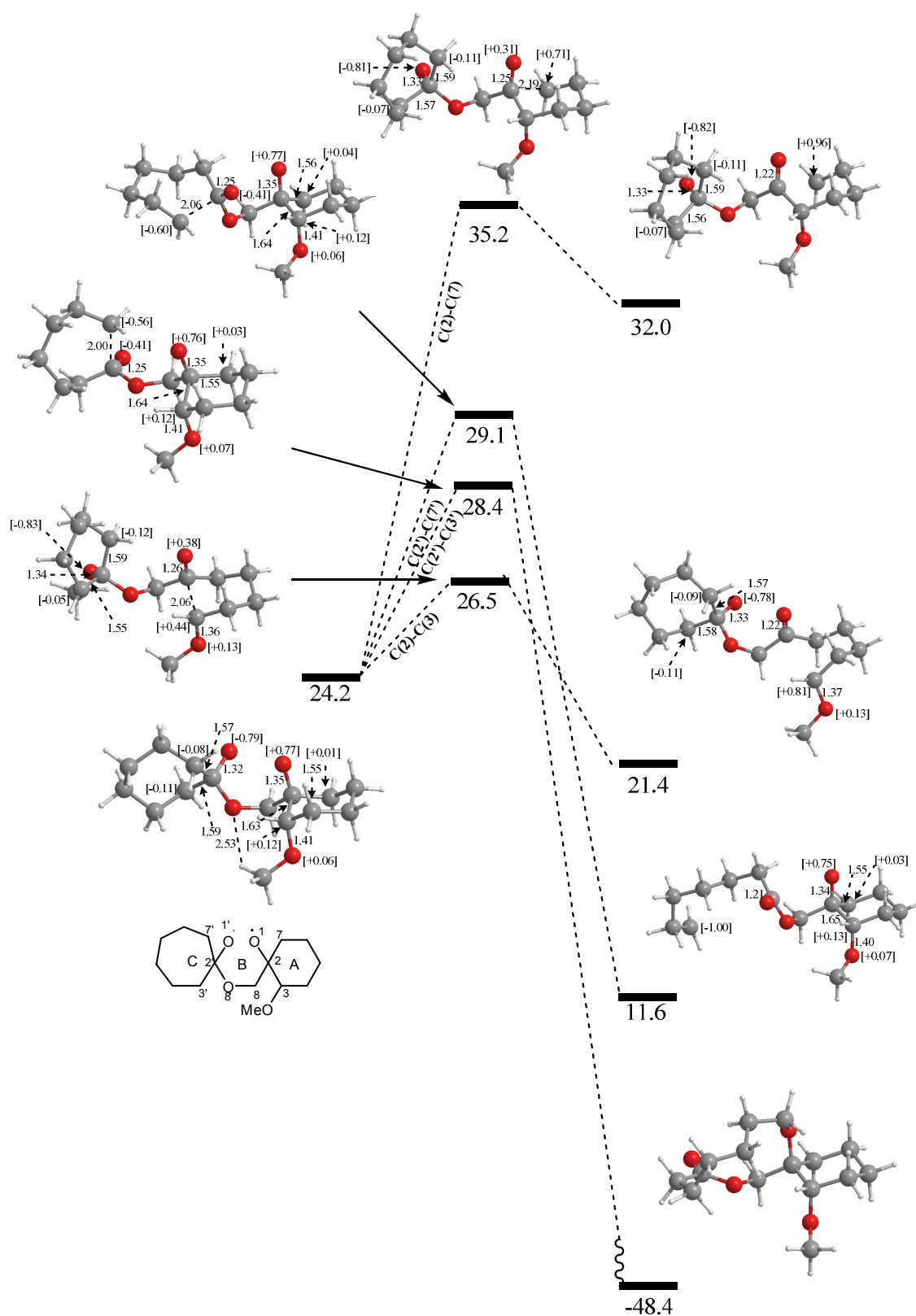
with molecular bond lengths/ Å and spin densities

*Figure 3: The reaction profile for the competitive β-scission reactions of **55cb** / kcal mol^{-1} with molecular bond lengths/ Å and spin densities*

*Figure 4: The reaction profile for the competitive β-scission reactions of **55cb** / kcal mol⁻¹*

with molecular bond lengths/ Å and spin densities

*Figure 5: The reaction profile for the competitive β-scission reactions of **55cb** / kcal mol⁻¹ with molecular bond lengths/ Å and spin densities*

*Figure 6: The reaction profile for the competitive β-scission reactions of **55cc** / kcal mol⁻¹ with molecular bond lengths/ Å and spin densities*
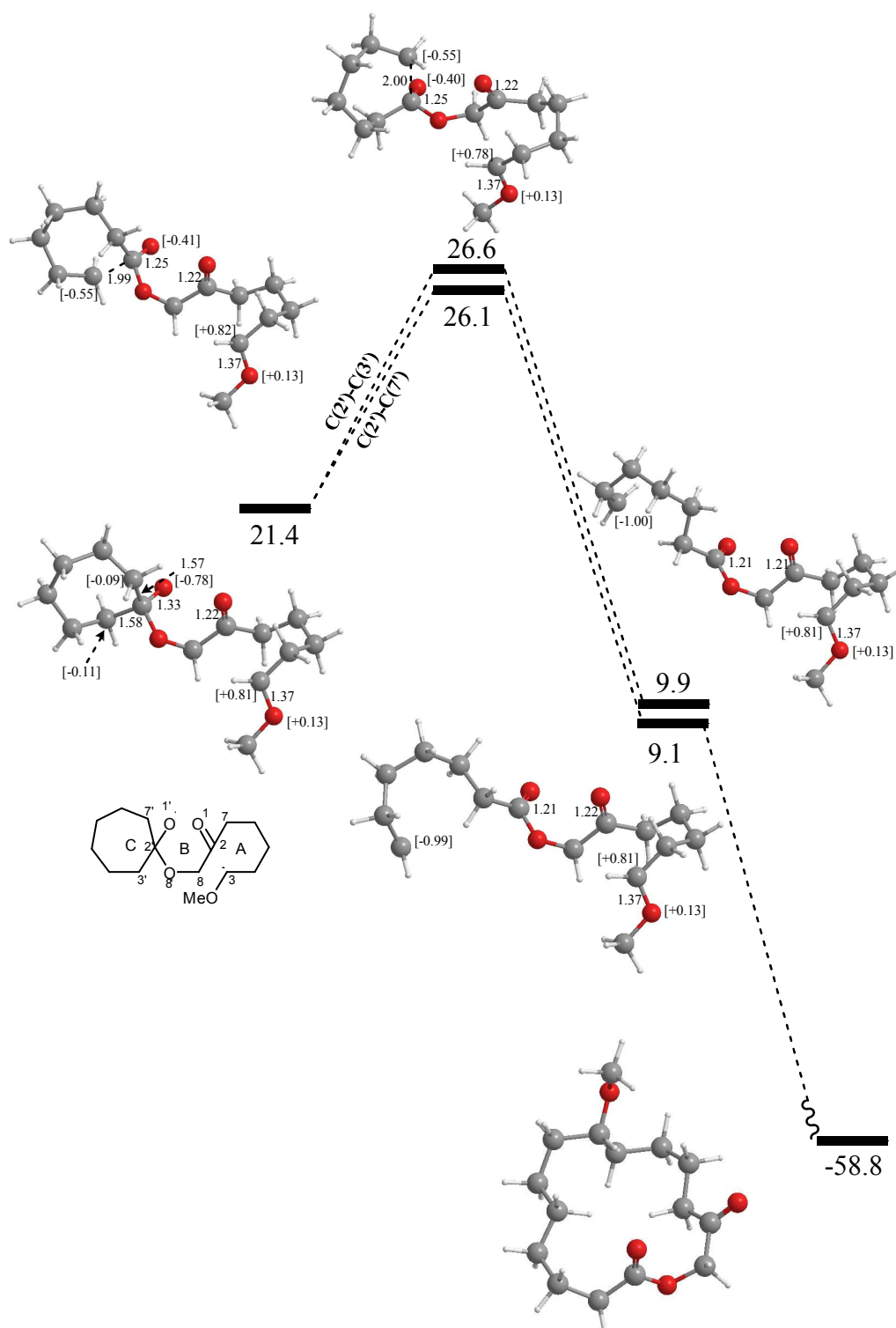
*Figure 7: The reaction profile for the competitive β-scission reactions of **55cc** / kcal mol⁻¹*
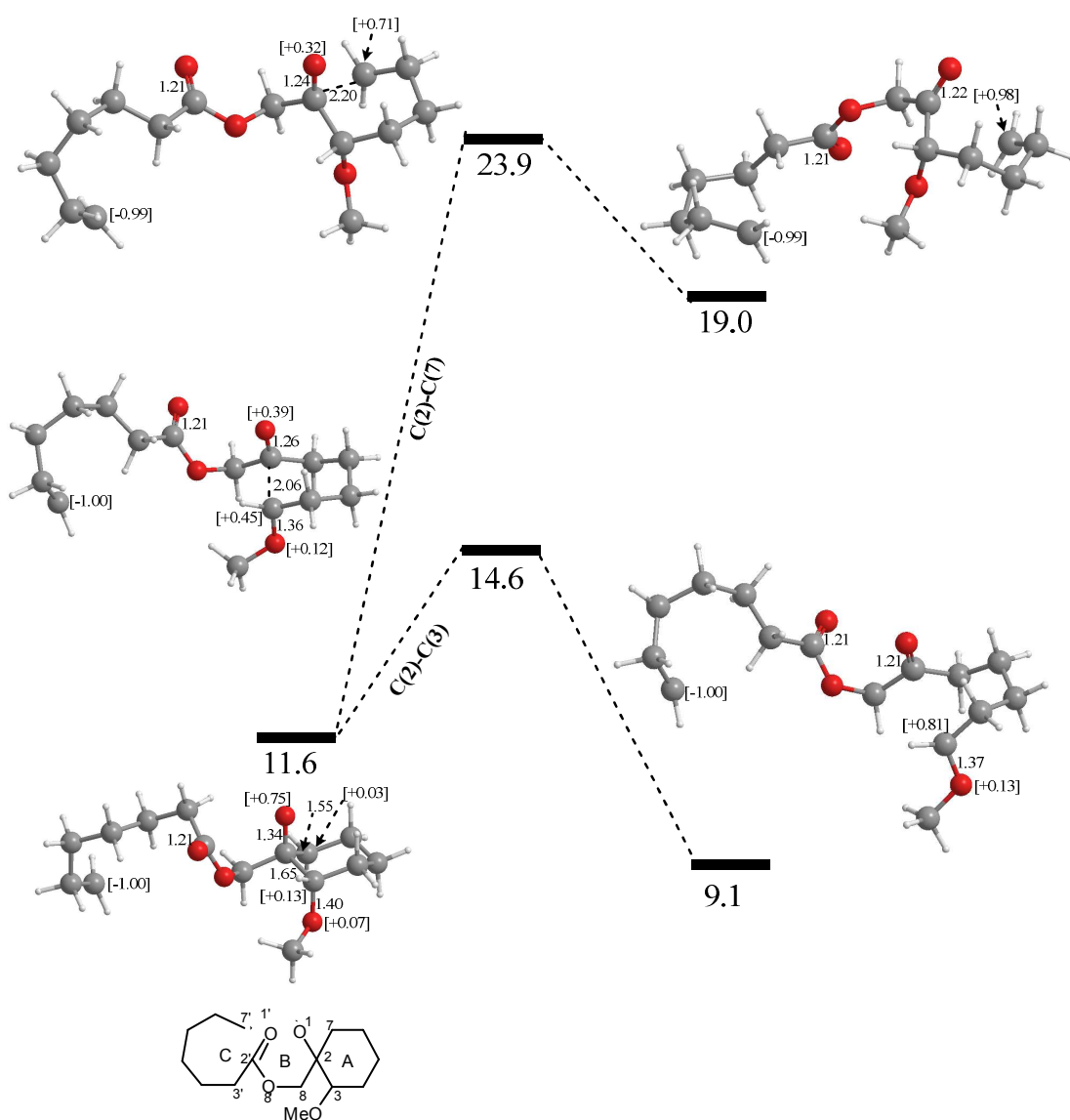
with molecular bond lengths/ Å and spin densities

*Figure 8: The reaction profile for the competitive β-scission reactions of **55cc** / kcal mol⁻¹*

with molecular bond lengths/ Å and spin densities

Model Studies of β-Scission Ring-Opening Reactions of Cyclohexyloxy Radicals: Application to Thermal Rearrangements of Dispiro-1,2,4-trioxanes
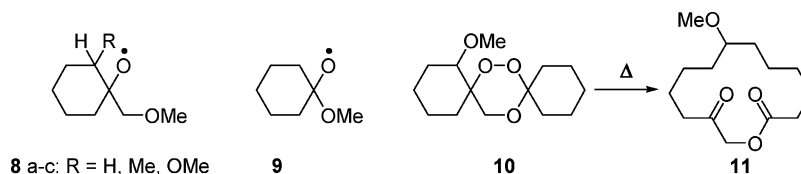
Stefan Erhardt, Stuart A. Macgregor,* Kevin J. McCullough,* Karen Savill, and Benjamin J. Taylor

Department of Chemistry, School of Engineering and Physical Sciences, Heriot-Watt University, Riccarton, Edinburgh EH14 4AS, U.K.

k.j.mccullough@hw.ac.uk

ABSTRACT

A DFT study of model cyclohexyloxy radicals (8a–c, 9) show that (a) the presence of an adjacent oxygen atom, and (b) α-substituents on the cyclohexyl ring, particularly methoxy, accelerate the rate of β-scission ring-opening reactions. Consistent with theoretical results, thermolysis of the methoxy-substituted dispiro-1,2,4-trioxane 10 afforded the structurally novel, 14-membered macrocyclic keto lactone 11 as the major isolable product.

Several naturally occurring and synthetic organic cyclic peroxides have been found to exhibit useful antimalarial and anticancer properties.[1,2] In particular, the 1,2,4-trioxane substructural unit has been identified as an essential pharmacophore in the antimalarial activity of artemisinin and related analogues.[3] It has been proposed that the antimalarial activity of artemisinin and other cyclic peroxides is related to iron(II)-induced cleavage of the peroxide bond followed by radical rearrangement to generate reactive carbon-centered radicals.[1a−d,4,5]

We have previously reported that, on thermolysis, dispiro-1,2,4-trioxanes **1** rearrange in a stepwise fashion to give oxalactones **4** and/or unsaturated hydroxy esters **5** by partial ring expansion. Alternatively, depending on the nature of the substituent on ring A, total ring expansion can yield macrocyclic keto lactones **7** (Scheme 1).[6] The observed products are consistent with an initial opening of the 1,2,4-trioxane ring (ring B) by O−O bond homolysis, followed by selective β-scission in ring C before that in ring A.[7] Since analogous symmetrical dispiro-1,2,4,5-tetroxanes are known to give macrocyclic products,[8] the presence of an adjacent oxygen atom may activate oxy radicals to undergo β-scission

(1) (a) Jefford, C. W. *Drug Discovery Today* **2007**, *12*, 487. (b) O'Neill, P. M.; Posner, G. H. *Acc. Chem. Res.* **2004**, *37*, 397. (c) Robert, A.; Dechy-Cabaret, O.; Cazelles, J.; Meunier, B. *Acc. Chem. Res.* **2002**, *35*, 167. (d) McCullough, K. J.; Nojima, M. *Curr. Org. Chem.* **2001**, *5*, 601. (e) Jefford, C. W. *Adv. Drug Res.* **1997**, *29*, 271.

(2) (a) Dembitsky, V. M.; Gloriozova, T. A.; Poroikov, V. V. *Mini-Rev. Med Chem.*, **2007**, *7*, 571. (b) Capon, R. J. *Eur. J. Org. Chem.* **2001**, 633. (c) Faulkner, D. J. *Nat. Prod. Rep.* **2000**, 1 and previous reviews in series. (d) Casteel, D. A. *Nat. Prod. Rep.* **1999**, *16*, 55.
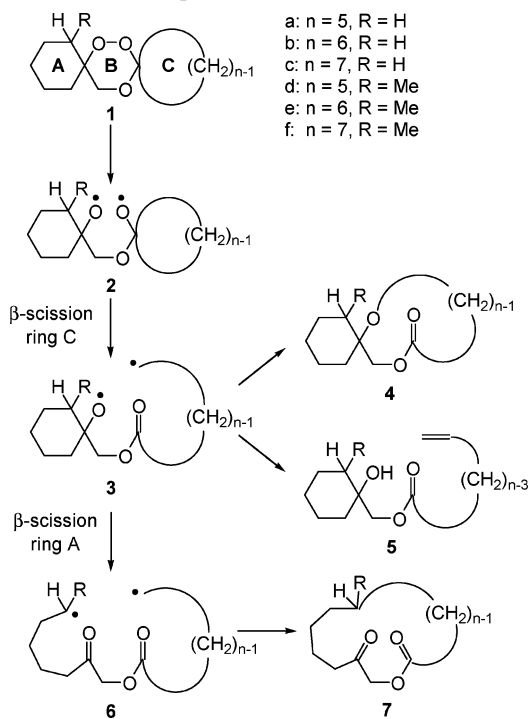
(3) Klayman, D. L. *Science* **1985**, *228*, 1049.

(4) (a) Robert, A.; Benoit-Vical, F.; Meunier, B. *Coord. Chem. Rev.* **2005**, *249*, 1927. (b) O'Neill, P. M.; Posner, G. H. *J. Med. Chem.* **2004**, *47*, 2945.

(5) Tang, Y.; Dong, Y.; Wang, W.; Sriraghavan, K.; Wood, J. K.; Vennerstrom, J. L. *J. Org. Chem.* **2005**, *70*, 5103.

(6) (a) Kerr, B.; McCullough, K. J. *J. Chem. Soc., Chem. Commun.* **1985**, 590. (b) Haq, A.; Kerr, B.; McCullough, K. J. *J. Chem. Soc. Chem. Commun.* **1993**, 1076.

Scheme 1. Radical Rearrangement Reactions of Dispiro-1,2,4-trioxanes 1

a: n = 5, R = H
b: n = 6, R = H
c: n = 7, R = H
d: n = 5, R = Me
e: n = 6, R = Me
f: n = 7, R = Me

in the thermal rearrangement of trioxanes **1**. We aim, first, to account for the fact that ring C of intermediate oxy biradical **2** opens faster than ring A and, second, to investigate how α-substituents might activate the opening of ring A and hence provide a higher proportion of macrocyclic lactones **7** from dispiro-1,2,4-trioxanes **1**.

In order to probe the relative rates of ring opening in species such as intermediate **2** calculations were carried out on the putative oxy radicals **8** and **9** (Scheme 2), model

Scheme 2. Model Species Used in the Calculations

8 a: R = H
b: R = Me
c: R = OMe

9
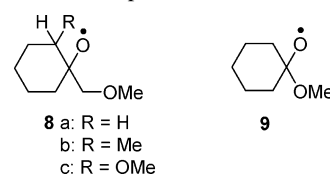
species for rings A and C, respectively.[13] In adopting this approach we assume the oxy radical centers in **2** will behave independently. The computed energy profiles are presented in Figure 1 and show a clear preference for opening ring C, with this process having a barrier of only 4 kcal/mol, 7 kcal/mol less than that for opening ring A. In both cases β-scission is accompanied by the expected shortening of the carbonyl C−O distances and a buildup of radical character at the incipient terminal carbon, evidenced through an increase in planarity. The breaking C−C bond is shorter in **TS 9** than in **TS 8a**, implying an earlier transition state in the former. This is consistent with the lower activation barrier for ring opening in **9** and the fact that this process is significantly exothermic compared to the endothermic ring opening in **8a**.[14] Therefore, for unsubstituted models the presence of an adjacent exocyclic oxygen strongly promotes ring opening, and this is consistent with the experimental observation of oxalactones **4** and hydroxyl esters **5** as the major products in the ring-opening reactions of **1b**.[6]

A second set of calculations was then performed to assess the effect of α-substituents, R, on the opening of ring A, where R = Me (**8b**) or OMe (**8c**). In the following we focus on isomers with R in an axial position, although analogous calculations on the equatorial-substituted species show similar trends (see Supporting Information). Computed activation barriers for ring opening in **8b** and **8c** show a clear preference for cleavage of the substituted C−C bond (see Figure 2). Moreover, the presence of Me and OMe substituents

processes. In this respect, it is noteworthy that treatment of trioxane **1b** with iron(II) bromide results in the formation of a bromoester derived exclusively from β-scission in ring C as a major component of the product mixture; no species relating to β-scission in ring A were reported.[5] In addition, it is known that 3-methoxy-1,2-dioxanes also readily undergo iron(II)-mediated β-scission processes to give methyl esters.[9] In a more general synthetic sense, oxy radicals have been exploited as key intermediates in ring-expansion reactions,[10] and in ring-cleavage reactions of carbohydrates.[11]

In this paper, we report the results of a density functional theory (DFT) study[12] of β-scission ring-opening reactions of model cyclohexyloxy radicals analogous to those proposed

(7) Thermolyses of artemisinin and other polycyclic 1,2,4-trioxanes generally result in extensive fragmentation of the trioxane ring and/or intramolecular H-abstraction processes after the initial O−O bond homolysis. See for example: (a) Luo, X.-D; Yeh, H. J. C.; Brossi, A.; Flippen-Anderson, J. L.; Gilardi, R. *Heterocycles* **1985**, *23*, 881. (b) Lin, A. J.; Theoharides, A. D.; Klayman, D. L. *Tetrahedron* **1986**, *42*, 2181. (c) Lin, A. J.; Klayman, D. L.; Hoch, J. M.; Silverton, J. V.; George, C. F. *J. Org. Chem.* **1985**, *50*, 4504. (d) Cafferata, L. F. R.; Jeandupeux, R.; Romanelli, G. P.; Mateo, C. M.; Jefford, C. W. *Afinidad* **2003**, *60*, 206. (e) Cafferata, L. F. R.; Rimada, R. S. *Molecules* **2003**, *8*, 655.

(8) Story, P. R.; Busch, P. *Adv. Org. Chem.* **1972**, *8*, 67.

(9) (a) Murakami, M.; Kawanishi, M.; Itagaki, S.; Horii, T.; Kobayashi, M. *Bioorg. Med. Chem. Lett.* **2004**, *14*, 3513. (b) Kawanishi, M.; Kotoku, N.; Itagaki, S.; Horii, T.; Kobayashi, M. *Bioorg. Med. Chem.* **2004**, *12*, 5297.

(10) Sugimone, H. In *Handbook of Organic Photochemistry and Photobiology*; Horspool, W. M., Song, P.-S., Eds.; CRC Press: London, 1994; pp 1229−1253 and references therein.

(11) Recent examples include: (a) Alonso-Cruz, C. R.; Kennedy, A. R.; Rodriguez, M. S.; Suarez, E. *Tetrahedron Lett.* **2007**, *48*, 7207. (b) Alonso-Cruz, C. R.; Leon, E. I.; Ortiz-Lopez, F. J.; Rodriguez, M. S.; Suarez, E. *Tetrahedron Lett.* **2005**, *46*, 5265. (c) Alonso-Cruz, C. R.; Kennedy, A. R.; Rodriguez, M. S.; Suarez, E. *Org. Lett.* **2003**, *5*, 3729. (d) Francisco, C. G.; Gonzalez, C.; Paz, N. R.; Suarez, E. *Org. Lett.* **2003**, *5*, 4171.

(12) Frisch, M. J.; et al. *Gaussian 03*, Revision C.02; Gaussian, Inc.: Wallingford CT, 2004. Calculations used the B3LYP hybrid functional and 6-31G** basis sets. All energies include corrections for zero-point energy. See Supporting Information for full details.

(13) Recent theoretical treatments of β-scission in alkoxy radicals: (a) Thiriot, E.; Canneaux, S.; Hénon, E.; Bohr, F. *React. Kinet. Catal. Lett.* **2005**, *85*, 123. (b) Buback, M.; Kling, M.; Schmatz, S. *Z. Phys. Chem.* **2005**, *219*, 1205. (c) Leblanc, M.; Siri, D.; Marque, S. R. A.; Grimaldi, S.; Bertin, D.; Tordo, P. *Int. J. Quant. Chem.* **2006**, *106*, 676. (d) Suh, I.; Zhao, J.; Zhang, R. *Chem. Phys. Lett.* **2006**, *432*, 313.

(14) Straight-chain forms of products **P 8a** ($E = +2.7$ kcal/mol) and **P 9** ($E = −9.0$ kcal/mol) are slightly more stable than the initial intermediates shown in Figure 1 but retain the same thermodynamic preference for opening **9**.
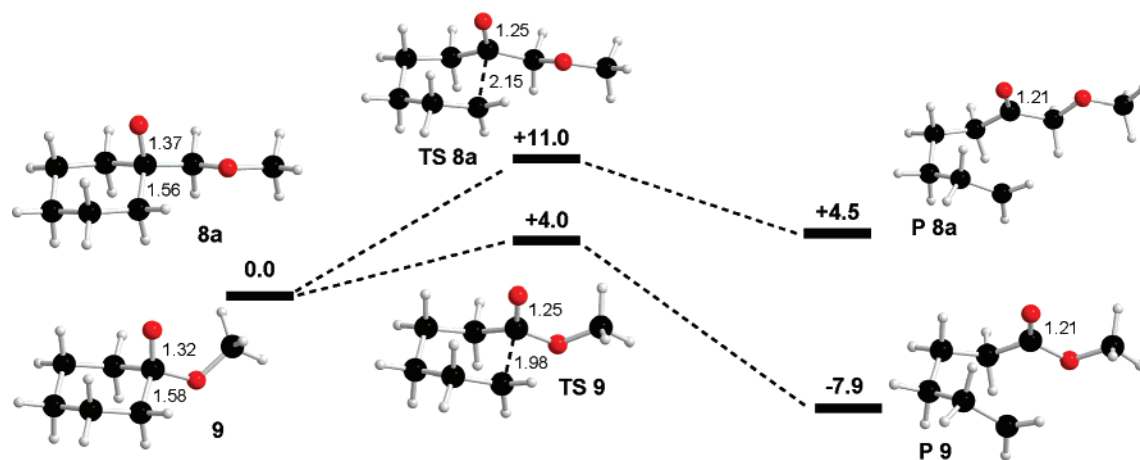
Figure 1. Computed ring-opening energy profiles in model species **8a** and **9** (kcal/mol; selected distances in Å).

significantly decrease the ring-opening barrier. For **8c** an important additional feature of the transition state, **TS 8c**, is
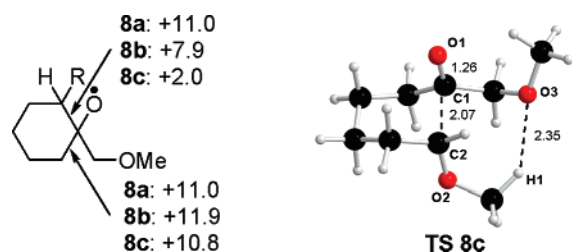

Figure 2. Computed activation barriers (kcal/mol) for ring opening in **8a** (R = H) and axially substituted **8b** (R = Me) and **8c** (R = OMe). **TS 8c** is also shown (selected distances in Å).

a short contact between the ether oxygen and one methoxy hydrogen (O3···H1 = 2.35 Å). This interaction is shown to facilitate ring opening, as an alternative transition state where the ether group is rotated to obviate this effect was found to be 2.5 kcal/mol higher in energy.[15]

It is well-known that α-substituents, in particular those bearing lone pairs, stabilize C-centered radicals, the so-called "α-effect".[16,17] In the present case this factor is already apparent in the β-scission transition states, and it is enough to make ring opening for **8c** via **TS 8c** a more accessible process than opening ring C in **9** via **TS 9**. To quantify this substituent effect on opening ring A we have performed a natural atomic orbital analysis[18] to obtain the spin density

distributions for the stationary points associated with **8a**, **8b**, and **8c** (see Table 1). The results show the anticipated transfer

Table 1. Computed Natural Spin Densities at Selected Positions for Ring-Opening of **8a** and the Axial Isomers of **8b** and **8c** (see Figure 2 for Numbering)

|	position	reactant	ts	product
8a (R = H)	O1	0.89	0.35	0.00
	C1	−0.03	−0.07	0.00
	C2	0.03	0.69	0.99
	R[a]	0.00	−0.02	−0.05
8b (R = Me)	O1	0.85	0.40	0.01
	C1	−0.03	−0.06	0.00
	C2	0.09	0.58	0.93
	R	0.02	0.03	0.03
8c (R = OMe)	O1	0.80	0.38	0.13
	C1	−0.03	−0.02	0.00
	C2	0.11	0.45	0.77
	R	0.06	0.13	0.14

[a] For R = Me and OMe the total spin on the substituent is indicated, although the major contribution comes from the α-atom.

of spin density from O1 in the reactants onto C2 in the transition states and products. For **TS 8a** the redistributed spin density is localized on C2; however, in **TS 8c** a significant contribution (0.13) is localized on the methoxy substituent. This delocalization serves to stabilize **TS 8c** and thus significantly lowers the barrier to ring opening. For **8b** the situation is intermediate between those of **8a** and **8c**.

Most importantly, the calculations allow us to predict that a methoxy substituent will make opening ring A competitive with that of ring C. This should enhance the possibility of both processes occurring to form fully expanded macrocycles such as **7** in preference to partially opened **4** and **5**. With this in mind we synthesized the methoxy-substituted dispiro-

(15) Preliminary calculations on the analogous OMe-substituted dispiro-1,2,4-trioxanes show this interaction is retained in the full systems; thus, this stabilization is not an artefact of our truncated models.

(16) Nelson, S. F. In *Free Radicals*; Kochi, J. K., Ed.; Wiley: New York, 1973; Vol. 2.

(17) For recent examples where the α-effect is highlighted see: (a) Rauk, A.; Boyd, R. J.; Boyd, S. L.; Henry, D. J.; Radom, L. *Can. J. Chem.* **2003**, *81*, 431. (b) Henry, D. J.; Parkinson, C. J.; Mayer, P. M.; Radom, L. *J. Chem. Phys. A* **2001**, *105*, 6750. (c) Zipse, H. *Top. Curr. Chem.* **2006**, *263*, 163.

(18) Glendening, E. D.; Reed, A. E.; Carpenter, J. E.; Weinhold, F. *QCPE Bull.* **1990**, *10*, 58.
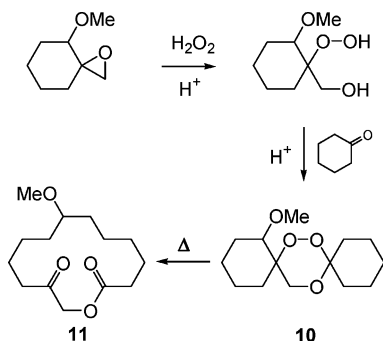
1,2,4-trioxane **10** as outlined in Scheme 3. Thermolysis of a solution of **10** in decane (1% w/v) at 180 °C afforded a relatively clean thermolysate, the major component of which was isolated in 67% yield as a low-melting solid.[19] This was subsequently identified by spectroscopic and X-ray crystallographic analysis as the structurally novel 14-membered macrocyclic lactone **11** (Figure 3).

From the thermolysis results it is therefore clear that the α-methoxy group accelerates the opening of ring A in the dioxy diradical derived from **10**, as predicted from the calculations on the model systems **8c** and **9**. The preponderance of keto lactone **11** suggests that the rates of opening rings A and C must be comparable, with the resulting carbon-centered radicals being in relative close proximity to enable efficient in-cage coupling. Further studies of substituent effects on β-scission processes of oxy radicals are in progress to design systems that will readily undergo radical cyclization reactions.

Figure 3. X-ray crystal structure of 14-membered methoxy substituted lactone **11** (ORTEP, 50% probability ellipsoids for non-hydrogen atoms).[20]

Supporting Information Available: Experimental procedures for the synthesis of **10** and related compounds, copies of ¹H and ¹³C NMR spectra, tables of atomic coordinates and derived crystallographic data. Tables of computed Cartesian coordinates and energies for all species, full reference 12. This material is available free of charge via the Internet at http://pubs.acs.org.

OL702534D

(19) Trace quantities of the ring B fragmentation products cyclohexanone and methoxycyclohexanone were also identified by gas chromatography.

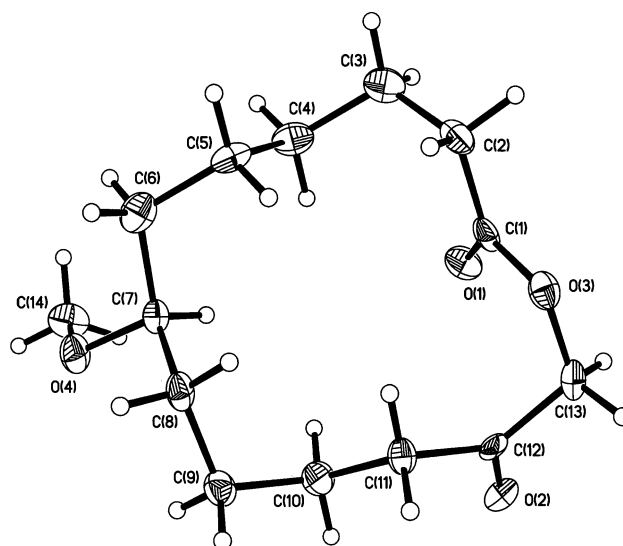(20) Sheldrick, G. M. *SHELXTL PC* (vers. 5.1); Brucker AXS: Madison, WI, 1997.